

IRIDIUM CATALYZED C-H ACTIVATION BORYLATIONS OF FLUORINE
BEARING ARENES AND RELATED STUDIES

By

Chathurika Ruwanthi Kumarihami Jayasundara

A DISSERTATION

Submitted to
Michigan State University
in partial fulfillment of the requirements
for the degree of

Chemistry – Doctor of Philosophy

2018

ABSTRACT

IRIDIUM CATALYZED C-H ACTIVATION BORYLATIONS OF FLUORINE BEARING ARENES AND RELATED STUDIES

By

Chathurika Ruwanthi Kumarihami Jayasundara

During the last two decades, iridium catalyzed aromatic borylation has emerged as one of the most convenient methodologies for functionalizing arenes and heteroarenes. The regioselectivity of Ir-catalyzed borylations are typically governed by sterics, therefore it complements the regioselectivity found in electrophilic aromatic substitution or directed *ortho* metalation. This unique regioselectivity and broad functional group tolerance (ester, amide, halogen, etc.) allows for synthesis of novel synthetic intermediates, many of which were previously either unknown or difficult to make.

Since these reactions are mainly driven by sterics, it is possible to install boronic ester group (Bpin) next to small substituents like hydrogen, cyano, or fluorine. This feature is helpful but can also create challenges, specially in cases like borylation of fluoro arenes. These fluoro arenes tend give 1:1 mixture of steric (*meta* to fluorine) and electronic (*ortho* to fluorine) products. Therefore, to overcome this problem, we introduced a two-step Ir-catalyzed borylation/Pd-catalyzed dehalogenation sequence that allows one to synthesize fluoroarenes where the boronic ester is *ortho* to fluorine (electronic). Here, a halogen *para* to the fluorine is used as a sacrificial blocking group allowing the Ir-catalyzed borylation to favor the electronic product exclusively. Then the chemoselective Pd-catalyzed dehalogenation by KF activated polymethylhydrosiloxane (PMHS) is used to remove the halogen without compromising the Bpin group.

Halosubstituted aryl boronates have the potential for orthogonal reactivity in cross-coupling reactions. We began exploring cross-coupling of triorganoindiums with these arylhalides bearing boronic esters in collaboration with Prof. P. Sestelo at University of da Coruña, Spain. We were able to synthesize borylated biaryls by merging Ir-catalyzed C–H borylations with Pd-catalyzed organoindium cross-couplings.

As a part of the Dow–MSU-GOALI collaborations, we were able to synthesize a cobalt catalyst for C–H borylations of alkyl arenes and heteroarenes. This catalyst enables selective monoborylation of the benzylic position of alkyl arenes using pinacolborane (HBpin) as the boron source. In 2016, an internship opportunity led to the screening of ligands for C–H borylations at the Dow chemicals company in Midland, MI. From this internship opportunity, we discovered the first ligand controlled synthesis of 1,2-di and 1,2,3-tri borylated arenes. Also, I investigated a recyclable iridium heterogeneous catalyst for borylations during the internship. Finally, a bulky terphenyl incorporated bipyridine ligand is synthesized for selective iridium catalyzed *para* C–H borylations.

*To my beloved mother, Indra Kumarihami Bandara
For her patience and her faith in me*

ACKNOWLEDGMENTS

I am grateful to Prof. Robert Maleczka for taking me into his group and guiding me through the Ph.D. This work would not have been possible without all the assistance and encouragement I have received from him during my Ph.D. I am also very thankful to him for his patience and giving me time to recover after my car accident.

I am thankful to Prof. Milton R Smith III for his valuable suggestions during boron group meetings. I would also like to thank Prof. Xuefei Huang, Prof. Babak Borhan and Prof. Gary Blanchard for serving on my guidance committee.

During my time as a graduate student, I also had the opportunity to do an internship at The Dow Chemical Company in Midland. I am thankful to Rob, Mitch and Jossian for this amazing experience.

I owe a great many thanks to Heidi Wardin for being there for me during my difficult times. It is always fun to talk to you about everything. I would also like to thank Dr. Staples for all the amazing work with crystal structures; specially the di- and tri-borylated compounds. I like to thank Dr. Holmes for all the help with NMR at MSU.

My special thanks go to Dr. Sean Preshlock and Dr. Hao Li. I learned many great techniques from Dr. Li, which helped me to do well in my Ph.D. I am very thankful to all my group members; Rosario, Susan, Damith, Aaron, Fangyi, Jonathan, Pepe, Barry and Emmanuel. I am so grateful to Barry for being a good friend and a great lab partner.

I would like to thank my apartment mate Dr. Daria Shamrova and also the Sri Lankans who helped me through the PhD. Special thanks go to Dilini, Punsisi, Gayanthi, Nalin, Thilani, Dhanushka and Viva. I would also like to thank my Starbucks matcha

buddies Yuling and Oliva. Thank you for all the advice and guidance Yuling, I really appreciate it.

Finally, I would like to thank the most important people in my life, My Family, for everything. A very special thank you goes to my mom for supporting all my decisions and being there for me every step of the way.

TABLE OF CONTENTS

LIST OF TABLES	ix
LIST OF FIGURES	xiii
LIST OF SCHEMES	xix
KEY TO ABBREVIATIONS	xxiii
Chapter 1. Introduction	1
1.1 Arylboronic Esters	1
1.2 Methods of Synthesizing Arylboronic Esters	2
1.3 Direct C–H activation borylations	2
1.4 Mechanism for direct C–H activation borylations	8
1.5 Regioselectivity in Ir-catalyzed CHBs	11
REFERENCES	14
Chapter 2. A Catalytic Borylation / Dehalogenation Route to <i>ortho</i>-Fluoro Arylboronates	18
2.1 Introduction	18
2.2 Alternate approach to <i>o</i> -fluoro arylboronates	20
2.3 Borylation of fluoroarenes	20
2.4 Dehydrohalogenation of fluoroarenes	21
2.5 One-pot borylation/dehalogenation	25
2.6 Recent advancements in selective <i>o</i> -fluoro arylboronic esters	25
2.7 Conclusions	27
2.8 Experimental	27
REFERENCES	46
Chapter 3. Merging Iridium Catalyzed C-H Borylations with Organoindium Cross-Couplings	48
3.1 Introduction	48
3.2 Organoindium cross coupling	49
3.3 Investigations and optimizations	50
3.4 Cross-couplings of R ₃ In with borylated haloarenes	52
3.5 One-pot borylations/cross-couplings of haloarenes	55
3.6 Experimental	56
REFERENCES	74
Chapter 4. Cobalt-Catalyzed C–H Borylations	78
4.1 C(sp ³)–H borylations	78
4.2 Cobalt catalyzed non-directed C(sp ³)–H borylations	78
4.3 Synthesis of a new cobalt catalyst	79
4.4 Testing cobalt catalyst A reactivity	81

4.5 C(sp ²)-H of heteroarenes vs. C(sp ²)-H and C(sp ³)-H bonds of alkylated arenes	88
4.6 Identifying the active catalyst species	89
4.7 Conclusions	92
4.8 Experimental.....	93
REFERENCES	104
Chapter 5. First, Ligand Controlled Synthesis of 1,2-di and 1,2,3-tri Borylated Arenes via Iridium Catalyzed C-H Borylations	107
5.1 Introduction to aromatic di- and poly-boronic esters (PBEs).....	107
5.2 Data and Discussion	108
5.3 Conclusions	126
5.4 Experimental.....	126
REFERENCES	135
Chapter 6: Ligand Screening for Ir-Catalyzed C-H Borylations.....	138
6.1 Introduction	138
6.2 Chelate-directed borylations.....	139
6.3 Relay-directed borylations.....	143
6.4 Outer sphere borylations.....	145
6.5 Monodentate Vs Bidentate ligands.....	150
6.6 Results and Discussion	152
6.7 Ligand synthesis	180
6.8 Different metal catalyst for C-H borylations.....	181
6.8 Conclusions	183
6.9 Experimental.....	183
REFERENCES	189
Chapter 7. Investigating Reactivity, Structure and Reusability of an Insoluble Iridium Catalyst for C-H Borylations.....	192
7.1 Introduction	192
7.2 Heterogeneous catalyst.....	194
7.3 Data and Discussion	196
7.4 Conclusions	203
7.5 Experimental.....	203
REFERENCES	208
Chapter 8. Selective <i>para</i>-CH Activation Borylations.....	210
8.1 Introduction	210
8.2 Sterically bulk ligand synthesis	211
8.3 Ligand synthesis for <i>para</i> selective C-H borylations	212
8.4 Synthesis of part A	213
8.5 Synthesis of part B.....	214
8.5 Synthesis of the bulky ligand	215
8.6 Iridium catalyzed selective <i>para</i> borylations	216
8.7 Experimental.....	216
REFERENCES	225

APPENDICES	229
APPENDIX A, crystal structures	230
APPENDIX B, nmr	Error! Bookmark not defined.

LIST OF TABLES

Table 1. Hydrodehalogenation with Ammonium Formate	44
Table 2. Solvent screening for L1	109
Table 3. Ir-catalyzed C-H borylation of 2, 6-CFA in THF.	153
Table 4. Ir-catalyzed C-H borylation of 2, 6-CFA in Hexane.....	154
Table 5. Ir-catalyzed C-H borylation of 2, 6-CFA in CPME.	155
Table 6. Ir-catalyzed C-H borylation of 2, 6-CFA in methyl cyclohexane.....	155
Table 7. Ir-catalyzed C-H borylation of 2, 6-CFA in Hunig's base.....	156
Table 8. Summary of Ir-catalyzed C-H borylation of 2, 6-CFA	157
Table 9. Ir-catalyzed C-H borylation of 2, 6-CFN in THF	162
Table 10. Ir-catalyzed C-H borylation of 2, 6-CFN in hexane	163
Table 11. Ir-catalyzed C-H borylation of 2, 6-CFN in CPME.....	164
Table 12. Ir-catalyzed C-H borylation of 2, 6-CFN in methyl cyclohexane.....	164
Table 13. Ir-catalyzed C-H borylation of 2, 6-CFN in Hunig's base.....	165
Table 14. Summary of Ir-catalyzed C-H borylation of 2, 6-CFN	166
Table 15. Ir-catalyzed C-H borylation of Cl-OMePy in THF.....	169
Table 16. Ir-catalyzed C-H borylation of 4-OMe-Py in THF.	172
Table 17. Ir-catalyzed C-H borylation of 4-OMe-Py in THF.	173
Table 18. Ir-catalyzed C-H borylation of F-OMe-Py in THF with no stirring.	174
Table 19. Ir-catalyzed C-H borylation of F-OMe-Py in hexane.	175
Table 20. Ir-catalyzed C-H borylation of 4-CN-2-OMe-Py in hexane.	178
Table 21. Ir-catalyzed C-H borylation of 4-CN-2-OMe-Py in hexane.	178
Table 22. Platinum catalyzed C-H borylation.....	183
Table 23. CHBs of benzene catalyzed by recyclable iridium catalyst.....	195

Table 24. NAA data for the black solid and the filtrate in hexane.....	198
Table 25. NAA data for the black solid and the filtrate in hexane.....	199
Table 26. Fractional Atomic Coordinates ($\times 10^4$) and Equivalent Isotropic Displacement Parameters ($\text{\AA}^2 \times 10^3$) for 67c.....	232
Table 27. Anisotropic Displacement Parameters ($\times 10^4$) 67c.....	232
Table 28. Bond Lengths in \AA for 67c.....	233
Table 29. Bond Angles in $^\circ$ for 67c.....	234
Table 30. Hydrogen Fractional Atomic Coordinates ($\times 10^4$) and Equivalent Isotropic Displacement Parameters ($\text{\AA}^2 \times 10^3$) for 67c.....	235
Table 31. Fractional Atomic Coordinates ($\times 10^4$) and Equivalent Isotropic Displacement Parameters ($\text{\AA}^2 \times 10^3$) for 68c.....	237
Table 32. Anisotropic Displacement Parameters ($\times 10^4$) 68c.....	237
Table 33. Bond Lengths in \AA for 68c.....	238
Table 34. Bond Angles in $^\circ$ for 68c.....	239
Table 35. Hydrogen Fractional Atomic Coordinates ($\times 10^4$) and Equivalent Isotropic Displacement Parameters ($\text{\AA}^2 \times 10^3$) for 68c.....	240
Table 36. Fractional Atomic Coordinates ($\times 10^4$) and Equivalent Isotropic Displacement Parameters ($\text{\AA}^2 \times 10^3$) for 68*.....	242
Table 37. Anisotropic Displacement Parameters ($\times 10^4$) 68*.....	243
Table 38. Bond Lengths in \AA for 68*.....	244
Table 39. Bond Angles in $^\circ$ for 68*.....	245
Table 40. Hydrogen Fractional Atomic Coordinates ($\times 10^4$) and Equivalent Isotropic Displacement Parameters ($\text{\AA}^2 \times 10^3$) for 68*.....	246
Table 41. Atomic Occupancies for all atoms that are not fully occupied in 68*.....	248
Table 42. Fractional Atomic Coordinates ($\times 10^4$) and Equivalent Isotropic Displacement Parameters ($\text{\AA}^2 \times 10^3$) for 69*.....	250
Table 43. Anisotropic Displacement Parameters ($\times 10^4$) 69*.....	251
Table 44. Bond Lengths in \AA for 69*.....	252

Table 45. Bond Angles in ° for 69*.....	253
Table 46. Hydrogen Fractional Atomic Coordinates ($\times 10^4$) and Equivalent Isotropic Displacement Parameters ($\text{\AA}^2 \times 10^3$) for 69*.....	254
Table 47. Atomic Occupancies for all atoms that are not fully occupied in 69*.....	256
Table 48. Fractional Atomic Coordinates ($\times 10^4$) and Equivalent Isotropic Displacement Parameters ($\text{\AA}^2 \times 10^3$) for 70c.....	258
Table 49. Anisotropic Displacement Parameters ($\times 10^4$) 70c.....	258
Table 50. Bond Lengths in \AA for 70c.....	259
Table 51. Bond Angles in ° for 70c.....	259
Table 52. Hydrogen Fractional Atomic Coordinates ($\times 10^4$) and Equivalent Isotropic Displacement Parameters ($\text{\AA}^2 \times 10^3$) for 70c.....	260
Table 53. Fractional Atomic Coordinates ($\times 10^4$) and Equivalent Isotropic Displacement Parameters ($\text{\AA}^2 \times 10^3$) for 71c'.....	263
Table 54. Anisotropic Displacement Parameters ($\times 10^4$) 71c'.....	263
Table 55. Bond Lengths in \AA for 71c'.....	263
Table 56. Bond Angles in ° for 71c'.....	264
Table 57. Hydrogen Fractional Atomic Coordinates ($\times 10^4$) and Equivalent Isotropic Displacement Parameters ($\text{\AA}^2 \times 10^3$) for 71c'.....	265
Table 58. Fractional Atomic Coordinates ($\times 10^4$) and Equivalent Isotropic Displacement Parameters ($\text{\AA}^2 \times 10^3$) for 72c'.....	267
Table 59. Anisotropic Displacement Parameters ($\times 10^4$) 72c'.....	267
Table 60. Bond Lengths in \AA for 72c'.....	268
Table 61. Bond Angles in ° for 72c'.....	268
Table 62. Hydrogen Fractional Atomic Coordinates ($\times 10^4$) and Equivalent Isotropic Displacement Parameters ($\text{\AA}^2 \times 10^3$) for 72c'.....	270
Table 63. Fractional Atomic Coordinates ($\times 10^4$) and Equivalent Isotropic Displacement Parameters ($\text{\AA}^2 \times 10^3$) for 73c'.....	272
Table 64. Anisotropic Displacement Parameters ($\times 10^4$) 73c'.....	272
Table 65. Bond Lengths in \AA for 73c'.....	273

Table 66. Bond Angles in ° for 73c'	273
Table 67. Hydrogen Fractional Atomic Coordinates ($\times 10^4$) and Equivalent Isotropic Displacement Parameters ($\text{\AA}^2 \times 10^3$) for 73c'	274
Table 68. Fractional Atomic Coordinates ($\times 10^4$) and Equivalent Isotropic Displacement Parameters ($\text{\AA}^2 \times 10^3$) for 103.	277
Table 69. Anisotropic Displacement Parameters ($\times 10^4$) 103.	278
Table 70. Bond Lengths in \AA for 103.	279
Table 71. Bond Angles in ° for 103.	280
Table 72. Hydrogen Fractional Atomic Coordinates ($\times 10^4$) and Equivalent Isotropic Displacement Parameters ($\text{\AA}^2 \times 10^3$) for 103.	281
Table 73. Fractional Atomic Coordinates ($\times 10^4$) and Equivalent Isotropic Displacement Parameters ($\text{\AA}^2 \times 10^3$) for L2*	284
Table 74. Anisotropic Displacement Parameters ($\times 10^4$) L2*	285
Table 75. Bond Lengths in \AA for L2*	286
Table 76. Bond Angles in ° for L2*	288
Table 77. Hydrogen Fractional Atomic Coordinates ($\times 10^4$) and Equivalent Isotropic Displacement Parameters ($\text{\AA}^2 \times 10^3$) for L2*	290

LIST OF FIGURES

Figure 1. Derivatization of the aryl boronic esters.	1
Figure 2. Transition state of proton transfer	11
Figure 3. General regioselectivity in Ir-catalyzed CHBs.....	12
Figure 4. a) Structures of <i>o</i> -fluoroaryl motifs in pharmaceuticals and agrochemicals. b) <i>o</i> -fluoroaryl motifs as building block.....	18
Figure 5. Borylation of fluoroarenes ^a	21
Figure 6. Dehalogenation with PMHS ^a	23
Figure 7. Different catalyst systems for selective <i>ortho</i> -fluoroarene borylation	26
Figure 8. Borylation of halo arenes. ^a	51
Figure 9. Pd-catalyzed cross-couplings of Ph ₃ In with borylated haloarenes ^a	53
Figure 10. Pd-catalyzed cross-couplings of various triorganoindium species with borylated haloarenes ^a	54
Figure 11. X-ray crystallography of complex A	81
Figure 12. Cobalt-Catalyzed CHBs ^a	82
Figure 13. Cobalt-Catalyzed CHBs of Heterocycles ^a	87
Figure 14. ¹ H NMR of complex A as HBpin concentration increases	90
.....	91
Figure 15. ¹¹ B NMR of complex A as HBpin concentration increases	91
Figure 16. ¹¹ B NMR of complex A at coupled and decoupled	92
Figure 17. Color difference after 18 h: (Right) with Hg, (Left) without Hg	94
.....	96
Figure 18. Spectra for Evans method calculations.....	96
Figure 19. ¹ H NMR of complex A in C ₆ D ₆	96
Figure 20. Preparation of <i>o</i> -Benzenediboronic Acids.....	107

Figure 21. Two possible regioisomers of di borylated arenes for 2,6-CFA	110
Figure 22. X-ray crystallographic structure of 67c.....	111
Figure 23. X-ray crystallographic structure of 68*.....	112
Figure 24. Synthesis of 1,2-di and 1,2,3-tri borylated arenes/heteroarenes.....	115
Figure 25. ^{19}F NMR for CHBs of 74a in hexane (top) Vs. dioxane (bottom)	118
Figure 26. ^{19}F NMR for CHBs of 74a with 76 (top) Vs. 74a without 76	121
Figure 27.....	123
1) ^1H NMR of 2,2'-bipyrazine (L1) in C_6D_{12}	123
2) ^1H NMR 2,2'-bipyrazine (L1) + $[\text{Ir}(\text{OMe})\text{COD}]_2$ in C_6D_{12}	123
3) ^1H NMR 2,2'-bipyrazine (L1) + B_2Pin_2 in C_6D_{12}	123
4) ^1H NMR 2,2'-bipyrazine (L1) + $[\text{Ir}(\text{OMe})\text{COD}]_2$ + B_2Pin_2 in C_6D_{12}	123
Figure 28. possible dearomatization structures for L1.....	124
Figure 29. CHBs with Ir-dtbpy system.....	125
Figure 30. Possible transition state for Ir-bypyrazine system.....	125
Figure 31. Substrate that did not give di or tri borylated compounds.....	133
Figure 32. Envisioned mechanism using hemi labile N, N-ligands.....	141
Figure 33. Proposed catalytic cycle for silicon-directed ortho-borylations.....	143
Figure 34. Catalytic cycle for outer-sphere directed borylation	145
Figure 35. Proposed transition states for ortho borylations of anilines	146
Figure 36. Hydrogen bond-directed meta borylation with an anionic ligand.....	147
Figure 37. 14 Vs 16 electron intermediates	151
Figure 38. Scope of substrates	152
Figure 39. Scope of the ligands.....	152
Figure 40. ^1H NMR of starting material 2,6-CFA	158
Figure 41. ^{19}F -NMR of	160

Figure 42. ¹ H NMR of crude reaction.....	161
Figure 43. ¹ H NMR of starting material 2,6-CFN.....	167
Figure 44. ¹ H NMR of starting material 2,6-CFN.....	168
Figure 45. ¹ H NMR of starting material Cl-OMePy.....	170
Figure 46. ¹ H NMR of	171
Figure 47. Comparing Table 16 (entry 5) with Table 17 (entry 7).	174
Figure 48. ¹ H NMR of starting material F-OMe-Py	176
Figure 49. ¹ H NMR of	177
Figure 50. Solid state ¹³ C NMR.....	202
Figure 51. Solid state ¹¹ B NMR.....	203
Figure 52. Discovery of selective <i>para</i> borylations.....	211
Figure 53. Selective iridium catalyzed C–H borylations.....	212
Figure 54. Sterically bulky ligand.....	212
Figure 55. Crude ¹ H NMR of the CHBs with 104.....	223
Figure 56. ¹ H NMR of 23	292
Figure 57. ¹³ C NMR of 23	293
Figure 58. ¹ H NMR of 24	294
Figure 59. ¹³ C NMR of 24	295
Figure 60. ¹ H NMR of 25	296
Figure 61. ¹³ C NMR of 25	297
Figure 62. ¹ H NMR of 26	298
Figure 63. ¹³ C NMR of 26	299
Figure 64. ¹ H NMR of 27	300
Figure 65. ¹³ C NMR of 27	301
Figure 66. ¹ H NMR of 28	302

Figure 67. ^{13}C NMR of 28	303
Figure 68. ^1H NMR of 29	304
Figure 69. ^{13}C NMR of 29	305
Figure 70. ^1H NMR of 31	306
Figure 71. ^{13}C NMR of 31	307
Figure 72. ^1H NMR of 32	308
Figure 73. ^{13}C NMR of 32	309
Figure 74. ^1H NMR of 35	310
Figure 75. ^{13}C NMR of 35	311
Figure 76. ^1H NMR of 36	312
Figure 77. ^{13}C NMR of 36	313
Figure 78. ^1H NMR of 38	314
Figure 79. ^{13}C NMR of 38	315
Figure 80. ^1H NMR of 41	316
Figure 81. ^{13}C NMR of 41	317
Figure 82. ^1H NMR of 42	318
Figure 83. ^{13}C NMR of 42	319
Figure 84. ^1H NMR of 43	320
Figure 85. ^{13}C NMR of 43	321
Figure 86. ^1H NMR of 47	322
Figure 87. ^{13}C NMR of 47	323
Figure 88. ^1H NMR of 52	324
Figure 89. ^{13}C NMR of 52	325
Figure 90. ^1H NMR of 67c.....	326
Figure 91. ^{13}C NMR of 67c.....	327

Figure 92. ^1H NMR of 68c.....	328
Figure 93. ^{13}C NMR of 68c.....	329
Figure 94. ^1H NMR of 68*	330
Figure 95. ^{13}C NMR of 68*	331
Figure 96. ^1H NMR of 69c.....	332
Figure 97. ^{13}C NMR of 69c.....	333
Figure 98. ^1H NMR of 69*	334
Figure 99. ^{13}C NMR of 69*	335
Figure 100. ^1H NMR of 70c.....	336
Figure 101. ^{13}C NMR of 70c.....	337
Figure 102. ^1H NMR of 71c'.....	338
Figure 103. ^{13}C NMR of 71c'.....	339
Figure 104. ^1H NMR of 72c'.....	340
Figure 105. ^{13}C NMR of 72c'.....	341
Figure 106. ^1H NMR of 73c'.....	342
Figure 107. ^{13}C NMR of 73c'.....	343
Figure 108. ^1H NMR of 98	344
Figure 109. ^{13}C NMR of 98	345
Figure 110. ^1H NMR of 100	346
Figure 111. ^{13}C NMR of 100	347
Figure 112. ^1H NMR of 102	348
Figure 113. ^{13}C NMR of 102	349
Figure 114. ^1H NMR of 103	350
Figure 115. ^{13}C NMR of 103	351
Figure 116. ^1H NMR of L2.....	352

Figure 117. ^{13}C NMR of L2 353

LIST OF SCHEMES

Scheme 1. Common synthesis of aryl boronate esters.....	2
Scheme 2. Reactions of the CpFe(CO) ₂ (Bcat) complex.....	3
Scheme 3. Reaction of the Cp*Ir(PMe ₃)(H)(Bpin) complex.....	4
Scheme 4. CHBs with combination of (Ind)Ir(COD) and phosphine ligands.....	5
Scheme 5. CHBs with combination of [Ir(COD)Cl] ₂ & 2,2'-bipyridine ligands.....	6
Scheme 6. CHBs with combination of catalyst and ligand.....	7
Scheme 7. Widely used catalyst and ligand combination for C–H borylations.....	8
Scheme 8. Proposed Mechanism for the Ir-Phosphine system.....	9
Scheme 9. Proposed Mechanism for the Ir-bpy system.....	10
Scheme 10. Typical C–H borylation of 3-substituted fluorobenzenes.....	19
Scheme 11. Alternate approach to o-fluoro arylboronates.....	20
Scheme 12. Patent example for dehalogenation with ammonium formate.....	22
Scheme 13. Dehalogenation with ammonium formate.....	22
Scheme 14. Protideborylation.....	24
Scheme 15. Selective debromination.....	24
Scheme 16. Hydrodehalogenation with Pd/C.....	24
Scheme 17. One-pot procedure.....	25
Scheme 18. Different type of cross-couplings for CC bond formation.....	48
Scheme 19. BF ₃ K Suzuki cross-couplings with a Bpin group present.....	49
Scheme 20. Suzuki cross-couplings with an unreactive boronate group present.....	49
Scheme 21. Organoindium cross-couplings.....	50
Scheme 22. Organoindium cross-couplings with a Bpin group present.....	50
Scheme 23. Synthesis of triorganoindiums.....	51

Scheme 24. Pd-catalyzed cross-couplings of Ph ₃ In with borylated haloarene 23	52
Scheme 25. Pd-catalyzed cross-coupling side reactions.....	53
Scheme 26. One pot borylation/cross-coupling reaction	56
Scheme 27. Polyborylation with a) Cobalt catalyst b) Nickel catalyst.....	78
Scheme 28. Polyborylation with a) cobalt catalyst b) MOF.....	79
Scheme 29. Synthesis of cobalt complex A.....	80
Scheme 30. Chirik's cobalt catalyst with ethylbenzene (58).....	84
Scheme 31. <i>m</i> -Fluorotoluene defluorinated in CHBs.....	86
Scheme 32. CHB of Toluene vs N-Methylpyrazole.....	89
Scheme 33. Hg test	89
Scheme 34. Directed o-C–H Functionalization by –Bpza group	108
Scheme 35. Ligand screening for CHBs.....	109
Scheme 36. CHBs of 67a.....	110
Scheme 37. C–H borylation of 68a.....	111
Scheme 38. Multiple catalyst loading in CHBs.....	113
Scheme 39. CHBs of 67a and 68a	113
Scheme 40. CHBs of 74a in hexane.....	117
Scheme 41. CHBs of 23 in dioxane.....	118
Scheme 42. CHBs of 75 in 1,4-dioxane.....	119
Scheme 43. Equal molar CHBs of 74a and 75.....	119
Scheme 44. a) CHBs of 76 b) Equal molar CHBs of 76 and 77.....	120
Scheme 45. CHBs of 74a with excess 76	121
Scheme 46. 1,4-Diboration of substituted pyrazines	124
Scheme 47. Analysis of regioselectivity in Ir-catalysed borylations.....	138
Scheme 48. Oxygen-directed Ir-catalyzed borylations.....	140

Scheme 49. Silica-SMAP- Ir-catalysed borylations.	140
Scheme 50. Selective borylation of 2-substituted indoles.	141
Scheme 51. Directed borylation of aryl pyridines.	142
Scheme 52. Ir-catalysed C–H borylation of benzylic amines.	142
Scheme 53. Silicon-directed ortho-borylations of arenes.	144
Scheme 54. Silicon-directed borylations at the 7-position of indoles.	144
Scheme 55. Outer-sphere directed borylation of Boc-protected anilines.	145
Scheme 56. Outer-sphere directed borylation of free anilines.	146
Scheme 57. Hydrogen bond-directed meta-selective borylation of aromatic amides. ...	147
Scheme 58. Aniline CHBs with B ₂ eg ₂	148
Scheme 59. Lewis acid-base interaction for ortho-selective borylation of aryl sulfides.	149
Scheme 60. B–N bond-directed meta-selective borylation of aromatic aldehydes.	149
Scheme 61. <i>ortho</i> -selective borylation of unprotected phenols using Beg as traceless directing group.	150
Scheme 62. CHBs of 2,6-CFA (67).	159
Scheme 63. Making boronic ester from boronic acid.	159
Scheme 64. CHBs of borylated 2,6-CFA (67a).	161
Scheme 65. CHBS of 2,6-CFN.	168
Scheme 66. Making boronic ester from boronic acid.	170
Scheme 67. Making boronic ester from boronic acid.	176
Scheme 68. CHBs of 2,6-CFA.	179
Scheme 69. CHBs of 2,6-CFA with extra ligand.	180
Scheme 70. Synthesis of DCE-bpy ligand.	180
Scheme 71. Synthesis of btf-DCA-bpy ligand.	181
Scheme 72. Platinum catalyzed CHBs.	181

Scheme 73. Platinum catalyzed CHBs of fluoroarenes	182
Scheme 74. Synthesis of platinum catalyst.....	182
Scheme 75. CHBs with Ir(0) nanoparticles	192
Scheme 76. CHBs with 2,2'-bipyridine-4,4'-dicarboxylic acid ligand	193
Scheme 77. CHBs with silica-SMAP-Ir	193
Scheme 78. CHBs with SBA-15-Ir(I).....	194
Scheme 79. CHBs of arenes and heteroarenes in an [IrCl(COD)] ₂ and 1 system	194
Scheme 80. CHBs without pre-generated active catalyst.....	196
Scheme 81. CHBs with pre-generated active catalyst	197
Scheme 82. Separation of the black solid	198
Scheme 83. Synthesis of the black solid.....	200
Scheme 84. Recycling of the black solid during CHBs.....	200
Scheme 85. CHBs of the black solid Vs. dtbpy	201
Scheme 86. Synthesis of 5,5'-dibromo-2,2'-bipyridine	213
Scheme 87. Miyaura coupling of 5,5'-dibromo-2,2'-bipyridine	213
Scheme 88. Synthesis of terphenyl halides.....	214
Scheme 89. Mechanism for synthesis of terphenyl halides	215
Scheme 90. Synthesis of bulky ligand.....	215
Scheme 91. C–H activation borylation.....	216

KEY TO ABBREVIATIONS

BDAN	1,8-diaminonaphthalene
B ₂ pin ₂	Bis(pinacolato)diboron
Bpin	4,4,5,5-Tetramethyl-1,3,2-dioxaborolane
BMIDA	N-methyliminodiacetic
Bpg	propane-1,2-diol
Beg	ethane-1,2-diol
Bn	Benzyl
Boc	tert-butyloxycarbonyl
Bpy(CF ₃) ₂	4,4'-bis(trifluoromethyl)-2,2'-bipyridine
bpy	2,2'-bipyridine
Cat	Catecholate
CHBs	C–H activation borylations
Cp	Cyclopentadienyl
COD	Cyclooctadiene
COE	Cyclooctene
2,6-CFA	2-Chloro-6-fluoroanisole
CPME	Cyclopentylmethyl ether
CFN	1-Chloro-3-fluoro-2-methoxybenzotrile
dmpe	Bis(dimethylphosphino)ethane
dppe	1,2-Bis(diphenylphosphino)ethane
dtbpy	4,4'-di- <i>tert</i> -butyl-2,2'-bipyridine

DCA-bpy	2,2'-Bipyridine-5,5'-dicarboxylic acid
DCE-bpy	Dimethyl 2,2'-bipyridine-4,4'-dicarboxylate
DoM	directed ortho metalation
EtOAc	Ethyl acetate
GC	Gas chromatography
GCMS	Gas chromatography–mass spectrometry
HBpin	Pinacoleborane
ICP	Induction Coupled Plasma
In	Indium
Ir	Iridium
ipcADI	N,N'-di(-)isopinocampheyl)butane-2,3-diimine
KF	Potassium fluoride
KO ^t Bu	Potassium tert-butoxide
L1	2,2'-Bipyrazine
MOF	metal-organic framework
Me	Methyl
MgSO ₄	Magnesium sulphate
NAA	Neutron Atomic Absorption
NMR	Nuclear magnetic resonance
NHC	N-heterocyclic carbene
Pt	Platinum
Pd	Palladium
PMHS	Polymethylhydrosiloxane

Pd(OAc) ₂	Palladium(II) acetate
Pd(PPh ₃) ₂ Cl ₂	Bis(triphenylphosphine)palladium(II) dichloride
Pd(dppf)Cl ₂	[1,1'-Bis(diphenylphosphino)ferrocene]palladium(II) dichloride
PBEs	Poly-boronic esters
PBAs	Poly-boronic acids
Pza	Pyrazolylaniline
THF	Tetrahydrofuran
tmp	3,4,7,8-tetramethylphenanthroline
R ₃ In	Triorganoindium
XRD	X-ray powder diffraction

Chapter 1. Introduction

1.1 Arylboronic Esters

Arylboronic esters are valuable synthetic intermediates in organic synthesis.¹ Owing to their low toxicity, stability, ease of handling and their ultimate degradation into boric acid, boronic acids can be regarded as “green” compounds.² Environmentally benign and user friendly characteristics make them more attractive than the other toxic, sensitive organometallic reagents. Also, versatile reactivity of arylboronic acid analogues makes derivatization easy (Figure 1).^{3,4} It has been well documented that these boronic esters/acids are mainly used in metal catalyzed cross-coupling reactions to form C–C bonds (e.g. Suzuki–Miyaura) or C-heteroatom bonds (e.g. Chan–Lam coupling).^{5,6}

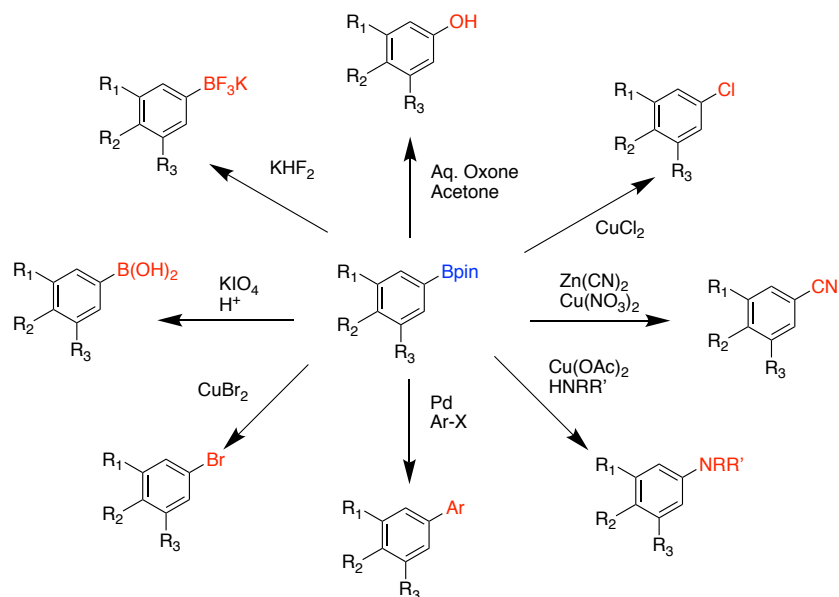
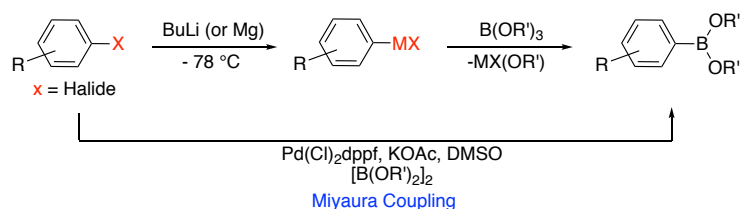


Figure 1. Derivatization of the aryl boronic esters.

1.2 Methods of Synthesizing Arylboronic Esters

Boron compounds are accessed mainly by two general methods starting from organic halides (Scheme 1). The first method involves making organometallic intermediates via metal–halogen exchange using arylmagnesium or aryllithium, followed by the reaction with trialkylboronates.^{7–9} Another widely used route for making boronate esters is Pd- or Cu-catalyzed borylations of aryl halides using a boron source such as bis(pinacolato)diboron (B_2pin_2) or pinacoleborane (HBpin).^{6,10} Also, Lewis acid catalyzed electrophilic borylations of electron-rich arenes,^{11–14} and Sandmeyer-type borylation of arylamines or diazonium salts with B_2pin_2 ,^{15–18} $B_2(OH)_4$,¹⁹ or R_2N-BH_2 ²⁰ are reported. However, most of these methods relies heavily on the availability of preceding organic halides



Scheme 1. Common synthesis of aryl boronate esters

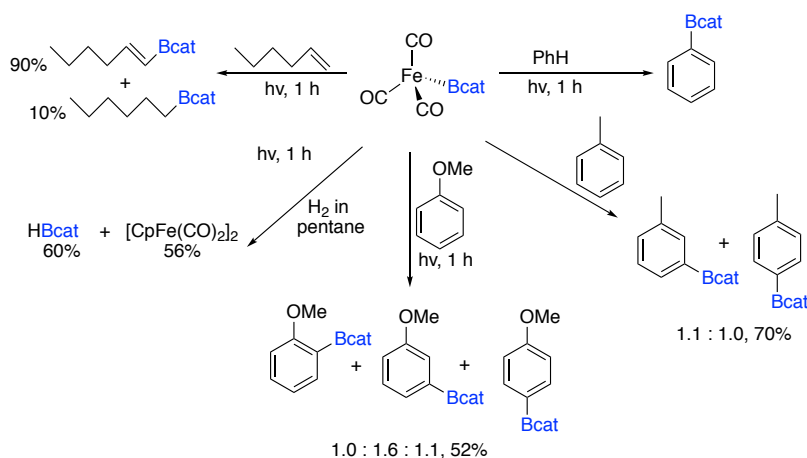
1.3 Direct C–H activation borylations

A long-standing challenge in synthetic chemistry is the direct, selective functionalization of various C–H bonds. Many research groups have made great progress towards functionalizing alkyl and aryl C–H bonds to C–C, C–O, C–N, C–X (X = F, Cl, Br and I) and etc. However, the direct conversion of C–H to C–B bonds is a more recent discovery and significant progress has been made by several research groups toward the development of this C–H bond functionalization in high yields and high

selectivity. Among these methods, iridium catalyzed C–H bond activation borylations (CHBs) is the most widely used route to synthesize organoboron compounds.^{2,21–23} This method reduces the number of steps and allows simple access to complementary regioselectivity.

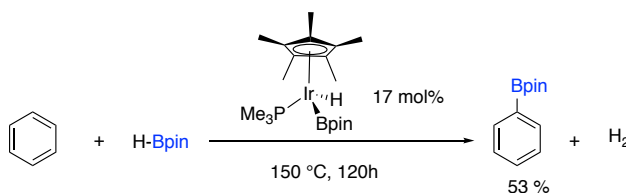
In 1993, Marder and co-workers reported the first synthesis of trisboryl iridium complexes and in supporting information GC/MS data indicated the formation of a small amount (<1%) of two isomers of toylboronate ester as side product arising from borylation of the toluene. However, the formation of this product was not discussed in the paper or further studies were done.²⁴

In 1995, Hartwig and co-workers developed the first stoichiometric route to functionalized arenes and alkenes by irradiation of $\text{CpFe}(\text{CO})_2(\text{Bcat})$ (Cp = cyclopentadienyl, cat = 1,2- $\text{O}_2\text{C}_6\text{H}_4$ =catecholate) (Scheme 2). In addition to the photochemical borylation of arenes by $\text{CpFe}(\text{CO})_2(\text{Bcat})$, similar borylations by $\text{Mn}(\text{CO})_5(\text{Bcat})$ and $\text{Re}(\text{CO})_5(\text{Bcat})$ were reported by the same group.²⁵



Scheme 2. Reactions of the $\text{CpFe}(\text{CO})_2(\text{Bcat})$ complex

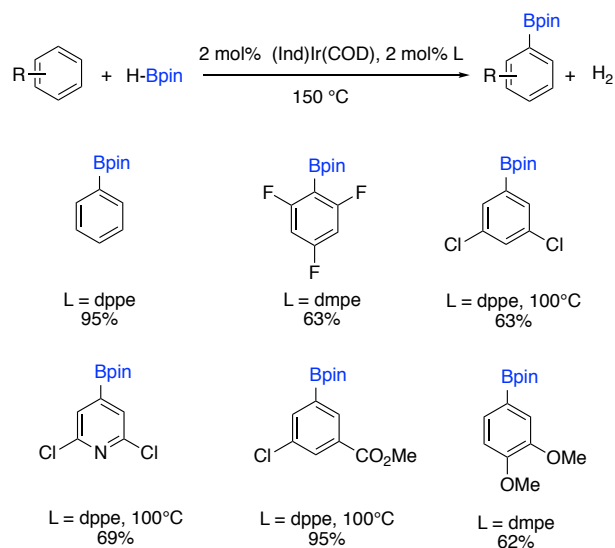
In 1999, Smith and co-workers developed the first thermal catalytic route to functionalized arenes using a Cp*Ir(PMe₃)(H)(Bpin) catalyst (Scheme 3).²¹ Low turnover numbers were observed with 5 equiv of HBpin in deuterated benzene at 150 °C catalyzed by 17 mol % of Cp*Ir(PMe₃)(H)(Bpin) to form C₆D₅Bpin in 53% yield (ca. 3 turnovers). Later the scope of the borylations of arenes was investigated by the same group.²⁶ The borylation of mono substituted arenes provided a mixture of arylboronate esters, and the borylation of 1,3-disubstituted arenes exclusively gave the 3,5-disubstituted arylboronate esters. However, no studies on arenes containing amines, esters, amides, or of heteroarenes catalyzed by Cp*Ir(PMe₃)(H)(Bpin) were reported.



Scheme 3. Reaction of the Cp*Ir(PMe₃)(H)(Bpin) complex

Later studies reported that iridium systems containing phosphine- and nitrogen-based ligands could catalyze the borylation of arenes with faster rates and higher yields than those containing Cp* ligands. In 2002, Smith, Maleczka and co-workers tested the reactivity of (Ind)Ir(COD) and trimethylphosphine, 1,2-bis(dimethylphosphino)ethane (dmpe), or 1,2-bis(diphenylphosphino)ethane (dppe) as catalysts for the borylation of arenes with HBpin (Scheme 4).²

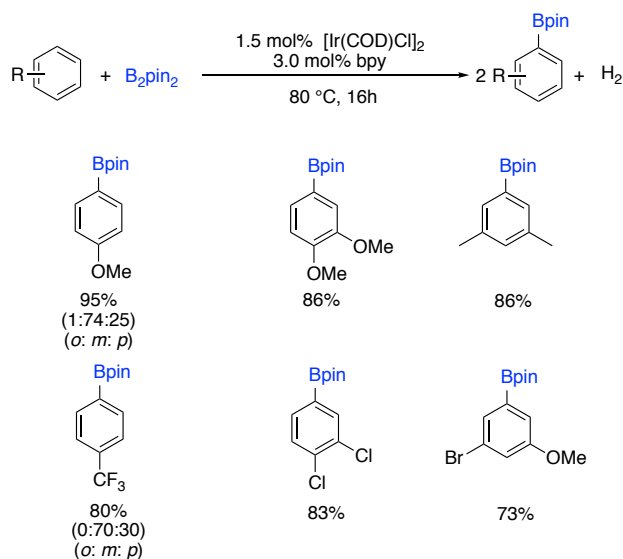
The highest yields of arylboronate esters was generated from a 2:1 ratio of PMe₃ to (Ind)Ir(COD) or a 1:1 ratio of dmpe or dppe to (Ind)Ir(COD). Also, this system tolerated halogens, ethers, and esters. Borylations of pyridine was also reported.



Scheme 4. CHBs with combination of (Ind)Ir(COD) and phosphine ligands

Also in 2002, Ishiyama, Miyaura, Hartwig, and co-workers reported the borylation of arenes catalyzed by iridium complexes of bipyridine and di-*tert*-butylbipyridine.²⁷ They reported the borylation of arenes with B_2pin_2 in the presence of catalytic amounts of $[\text{Ir}(\text{COD})\text{Cl}]_2$ and 2,2'-bipyridine (bpy) or 4,4'-di-*tert*-butyl-2,2'-bipyridine (dtbpy) occurred at $80 \text{ }^\circ\text{C}$. Moderate to good yields were observed for different arenes with B_2pin_2 catalyzed by 1.5 mol % $[\text{Ir}(\text{COD})\text{Cl}]_2$ and 3 mol % bpy (again regioselectivity was controlled by sterics).

Monosubstituted arenes, such as anisole, and trifluoromethylbenzene gave an approximately statistical mixture of (2:1) products arising from *meta*- and *para*-borylation, with the product from *ortho*-borylation being observed (1%) only from the reaction of anisole (Scheme 5).

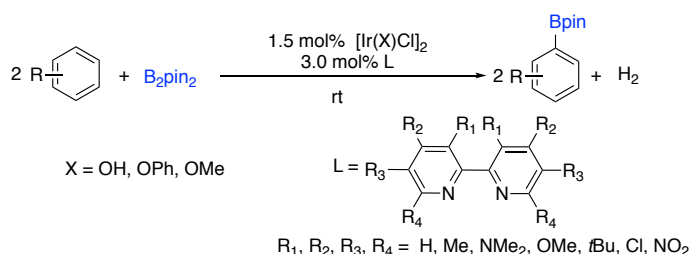


Scheme 5. CHBs with combination of $[\text{Ir}(\text{COD})\text{Cl}]_2$ & 2,2'-bipyridine ligands

The borylation of 1,3-disubstituted arenes formed 3,5-disubstituted arylboronate esters exclusively. Reactions catalyzed by the iridium catalyst containing the bipyridine derivative occur at room temperature to 80 °C, in many cases with turnover numbers between 500 and 1000. In contrast, the reactions catalyzed by the phosphine-ligated iridium complexes gave few turnover numbers.

Ishiyama, Miyaura, Hartwig, and co-workers then developed similar catalyst systems that were more active at lower temperatures and that reacted with higher turnover numbers than the initial system. An induction period was observed with the borylation of benzene-*d*6 with B_2pin_2 in a combination of $[\text{Ir}(\text{COD})\text{Cl}]_2$ and bpy. During this induction period, the cyclooctadiene ligand was reduced to cyclooctene-*d*2. Therefore, $[\text{Ir}(\text{COE})_2\text{Cl}]_2$ (COE = cyclooctene) was investigated as the iridium precursor, and dtbpy as the ligand. Borylation of benzene and yielded 80% PhBpin at room temperature with no observable induction period. This reaction was the first example of a metal-catalyzed borylation of an arene that occurred at room temperature. Furthermore,

they tested different Ir(I)-cyclooctadiene precursors such as $[\text{Ir}(\text{COD})\text{Cl}]_2$, $[\text{Ir}(\text{COD})_2]\text{BF}_4$, $[\text{Ir}(\text{COD})(\text{OH})]_2$, $[\text{Ir}(\text{COD})(\text{OPh})]_2$, $[\text{Ir}(\text{COD})(\text{OMe})]_2$, and $[\text{Ir}(\text{COD})(\text{OAc})]_2$ for CHBs of benzene and found that $[\text{Ir}(\text{OMe})\text{COD}]_2$ is the most active catalyst for borylations.²⁷ They also studied the borylation of arenes catalyzed by iridium complexes of a series of disubstituted 2,2'-bipyridines to investigate the importance of electronic and steric properties of the 2,2'-bipyridine ligand (Scheme 6).

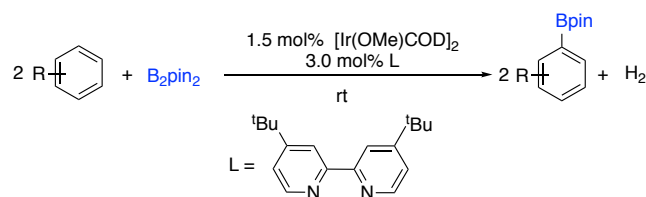


Scheme 6. CHBs with combination of catalyst and ligand

Electronic properties: They studied borylations catalyzed by iridium complexes of a series of 4,4'-disubstituted-2,2'-bipyridine ligands and found that electron donating substituents, such as NMe_2 , OMe , or $t\text{Bu}$, catalyzed the borylation benzene with B_2pin_2 with higher yields. However, bipyridine ligands containing electron-withdrawing groups, such as Cl and NO_2 , did not catalyze the borylations of benzene with B_2pin_2 .

Steric properties: 4,4'-Dimethyl-2,2'-bipyridine or 5,5'-dimethyl-2,2'-bipyridine ligands facilitated the reaction of benzene with B_2pin_2 to form PhBpin in good yields. However, the use of 3,3'-dimethyl-2,2'-bipyridine as ligand yielded only 60% PhBpin , because of steric hindrance. However, the Ir-catalyzed reaction of benzene with B_2pin_2 catalyzed by 3,3'-dimethyl-2,2'-bipyridine as the ligand gave only moderate yields of arylboronic esters. Methyl groups in the 3- and 3'-positions prevents the pyridine rings

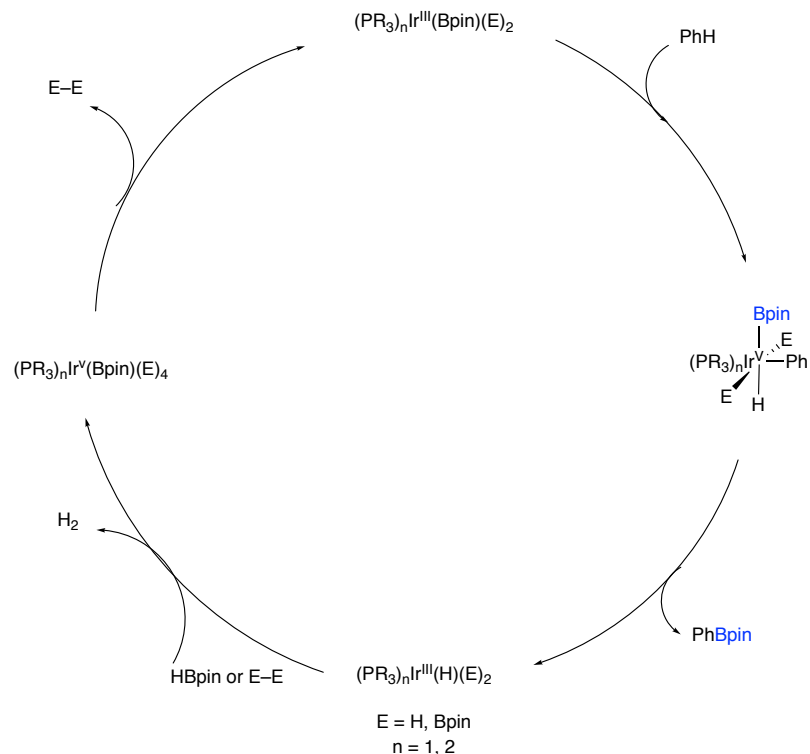
from adopting a coplanar arrangement, and this structural change was proposed to be responsible for the lower yields. Also, 6,6'-dimethyl-2,2'-bipyridine was not an effective ligand in the reaction of benzene and B₂pin₂, due to proposed steric hindrance around the nitrogen atoms in 6,6'-dimethyl-2,2'-bipyridine preventing binding to the iridium complex. All these studies lead to discovery of the most reactive iridium catalyst and ligand system for C–H activation borylations (Scheme 7).



Scheme 7. Widely used catalyst and ligand combination for C–H borylations

1.4 Mechanism for direct C–H activation borylations

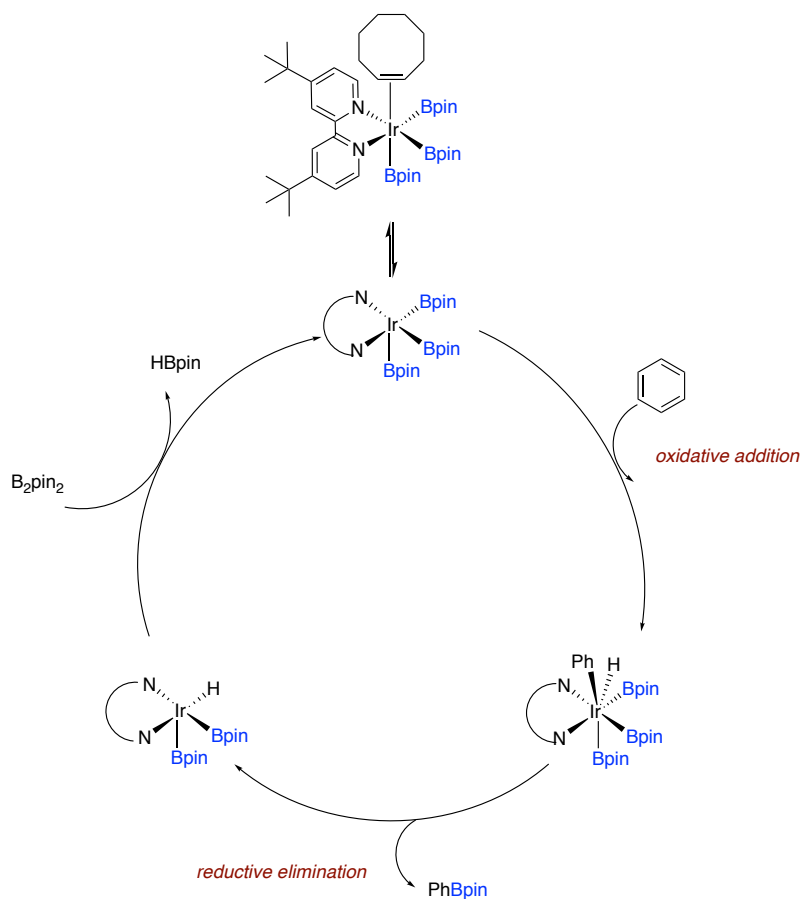
Smith and co-workers obtained data to distinguish between a catalytic cycle involving Ir(I) and Ir(III) intermediates and a cycle involving Ir(III) and Ir(V) intermediates. They prepared the Ir(I)-boryl complex Ir(Bpin)(PMe₃)₄ and the Ir(III)-boryl complex *fac*-Ir(Bpin)₃(PMe₃)₃. Both Ir(Bpin)(PMe₃)₄ and *fac*-Ir(Bpin)₃(PMe₃)₃ reacted with benzene to produce PhBpin.²¹ However, the reaction of Ir(Bpin)(PMe₃)₄ with iodobenzene did not produce the iodophenylboronic ester, whereas the reaction of Ir(III) complex with iodobenzene yielded a mixture of *meta*- and *para*-borylated iodobenzene in 54% yield and PhBpin in 45% yield. The authors did not rule out a pathway involving Ir(I) and Ir(III) intermediates but favored a catalytic cycle involving Ir(III) and Ir(V) species (Scheme 8).



Scheme 8. Proposed Mechanism for the Ir-Phosphine system

Further studies related to iridium catalyzed C–H borylations with bipyridine ligands were carried out by Hartwig and coworkers. In 2005, they reported some extensive mechanistic details about iridium catalyzed C–H borylations.²⁸ Studies were based on the functionalization of arenes with the diboron reagent B_2pin_2 catalyzed by the combination of dtbpy and olefin-ligated iridium halide or olefin-ligated iridium alkoxide complexes. The catalyst resting state was identified as $[\text{Ir}(\text{dtbpy})(\text{COE})(\text{Bpin})_3]$. Comparing the kinetic isotope effects of the catalytic and stoichiometric reactions indicated that the reactive intermediate $[\text{Ir}(\text{dtbpy})(\text{Bpin})_3]$ cleaves the arene C–H bond. Synthesis of $[\text{Ir}(\text{dtbpy})(\text{COE})(\text{Bpin})_3]$ was more facile with $[\text{Ir}(\text{COD})(\text{OMe})_2]$, dtbpy, COE, and HBpin and less yield with B_2pin_2 .

Hartwig and co-workers also proposed a catalytic cycle similar to that of Smith and co-workers that goes through a Ir(III)/Ir(v) cycle (Scheme 9). Also, kinetic studies showed that $[\text{Ir}(\text{dtbpy})(\text{COE})(\text{Bpin})_3]$ complex reacts with arenes after reversible dissociation of COE. They also confirmed that an alternative mechanism in which the arene reacts with the Ir(I) complex $[\text{Ir}(\text{dtbpy})\text{Bpin}]$ after dissociation of COE and reductive elimination of B_2pin_2 does not occur to a measurable extent.



Scheme 9. Proposed Mechanism for the Ir-bpy system

The reaction of $[\text{Ir}(\text{dtbpy})(\text{COE})(\text{Bpin})_3]$ with arenes and the catalytic reaction of B_2pin_2 with arenes catalyzed by the combination of $[\text{Ir}(\text{COD})(\text{OMe})_2]$ and dtbpy occurs faster with electron-poor arenes than with electron-rich arenes. However, both the

stoichiometric and catalytic reactions also occur faster with the electron-rich heteroarenes thiophene and furan than with arenes, perhaps because η^2 -heteroarene complexes are more stable than the η^2 -arene complexes and the η^2 -heteroarene or arene complexes are intermediates that precede oxidative addition.

The presence of electronic effects on relative reactivities of arenes in Ir-catalyzed CHBs has been noted from the earliest studies.²⁶ Smith, Maleczka, Singleton and co-workers carried out experimental and computational investigation on the Ir-catalyzed CHBs arene and heteroarenes. Experiment and theory favor a model of C-H borylation where significant proton transfer character exists in the transition state (Figure 2).²⁹ This explains the accelerated borylation rates in pyrrole, thiophenes, furan and the selective functionalization of C-H positions next to the heteroatoms in indole, benzofuran, benzothiophene, whose pKas' are relatively low.

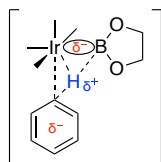


Figure 2. Transition state of proton transfer

1.5 Regioselectivity in Ir-catalyzed CHBs

In electrophilic aromatic substitution (EAS) reactions, steric effects can influence the substitution, however electronic effects typically dominate. Substituents on aromatic rings fall into two classes: ortho, para directors and meta directors and EAS does not always offer well-defined regiochemical outcomes. Ir-catalyzed CHBs are mainly governed by sterics. Figure 3 shows a summary of how CHBs work for arenes and heteroarenes.

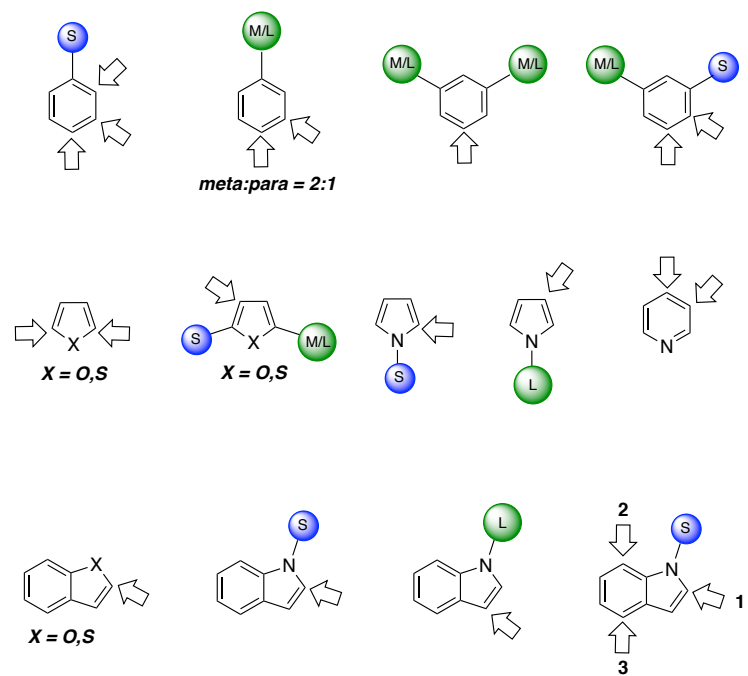


Figure 3. General regioselectivity in Ir-catalyzed CHBs

REFERENCES

REFERENCES

- (1) *Boronic Acids Preparation and Applications in Organic Synthesis, Medicine and Materials*, 2., vollständig überarbeitete Auflage.; Hall, D. G., Ed.; Wiley-VCH: Weinheim, Bergstr, 2011.
- (2) Maleczka, R. E., Jr.; Smith, M. R., III. Remarkably Selective Iridium Catalysts for the Elaboration of Aromatic C–H Bonds. *Science* **2002**, *295*.
- (3) Mkhaliid, I. A. I.; Barnard, J. H.; Marder, T. B.; Murphy, J. M.; Hartwig, J. F. C-H Activation for the Construction of C-B Bonds. *Chem. Rev.* **2010**, *110*, 890–931.
- (4) Hartwig, J. F. Borylation and Silylation of C-H Bonds: A Platform for Diverse C-H Bond Functionalizations. *Acc. Chem. Res.* **2012**, *45*, 864–873.
- (5) Miyaura, N. Organoboron Compounds. In *Cross-Coupling Reactions*; 2002; Vol. 219, pp 11–59.
- (6) Miyaura, N.; Suzuki, A. Palladium-Catalyzed Cross-Coupling Reactions of Organoboron Compounds. *Chem. Rev.* **1995**, *95*, 2457–2483.
- (7) Brown, H. C.; Srebnik, M.; Cole, T. E. Organoboranes. 48. Improved Procedures for the Preparation of Boronic and Borinic Esters. *Organometallics* **1986**, *5*, 2300–2303.
- (8) Brown, H. C.; Cole, T. E. Organoboranes. 31. A Simple Preparation of Boronic Esters from Organolithium Reagents and Selected Trialkoxyboranes. *Organometallics* **1983**, *2*, 1316–1319.
- (9) Kristensen, J.; Lysén, M.; Vedsø, P.; Begtrup, M. Synthesis of Ortho Substituted Arylboronic Esters by in Situ Trapping of Unstable Lithio Intermediates. *Org. Lett.* **2001**, *3*, 1435–1437.
- (10) Zhu, W.; Ma, D. Formation of Arylboronates by a CuI-Catalyzed Coupling Reaction of Pinacolborane with Aryl Iodides at Room Temperature. *Org. Lett.* **2006**, *8*,

261–263.

- (11) Ingleson, M. J. A Perspective on Direct Electrophilic Arene Borylation. *Synlett* **2012**, *23*, 1411–1415.
- (12) De Vries, T. S.; Prokofjevs, A.; Vedejs, E. Cationic Tricoordinate Boron Intermediates: Borenium Chemistry from the Organic Perspective. *Chem. Rev.* **2012**, *112*, 4246–4282.
- (13) Trinchera, P.; Corless, V. B.; Yudin, A. K. Synthesis of Previously Inaccessible Borylated Heterocycle Motifs Using Novel Boron-Containing Amphoteric Molecules. *Angew. Chem. Int. Ed Engl.* **2015**, *54*, 9038–9041.
- (14) Grosso, A. D.; Helm, M. D.; Solomon, S. A.; Caras-Quintero, D.; Ingleson, M. J. Simple Inexpensive Boron Electrophiles for Direct Arene Borylation. *Chem. Commun.* **2011**, *47*, 12459.
- (15) Ma, Y.; Song, C.; Jiang, W.; Xue, G.; Cannon, J. F.; Wang, X.; Andrus, M. B. Borylation of Aryldiazonium Ions with N-Heterocyclic Carbene-Palladium Catalysts Formed without Added Base. *Org. Lett.* **2003**, *5*, 4635–4638.
- (16) Mo, F.; Jiang, Y.; Qiu, D.; Zhang, Y.; Wang, J. Direct Conversion of Arylamines to Pinacol Boronates: A Metal-Free Borylation Process. *Angew. Chem. Int. Ed Engl.* **2010**, *49*, 1846–1849.
- (17) Zhang, J.; Wang, X.; Yu, H.; Ye, J. Sandmeyer-Type Reaction to Pinacol Arylboronates in Water Phase: A Green Borylation Process. *Synlett* **2012**, *23*, 1394–1396.
- (18) Yu, J.; Zhang, L.; Yan, G. Metal-Free, Visible Light-Induced Borylation of Aryldiazonium Salts: A Simple and Green Synthetic Route to Arylboronates. *Adv. Synth. Catal.* **2012**, *354*, 2625–2628.
- (19) Erb, W.; Hellal, A.; Albini, M.; Rouden, J.; Blanchet, J. An Easy Route to (hetero)arylboronic Acids. *Chemistry* **2014**, *20*, 6608–6612.

- (20) Guerrand, H. D. S.; Vaultier, M.; Pinet, S.; Pucheault, M. Amine-Borane Complexes: Air- and Moisture-Stable Partners for Palladium-Catalyzed Borylation of Aryl Bromides and Chlorides. *Adv. Synth. Catal.* **2015**, *357*, 1167–1174.
- (21) Iverson, C. N.; Smith, M. R. Stoichiometric and Catalytic B–C Bond Formation from Unactivated Hydrocarbons and Boranes. *J. Am. Chem. Soc.* **1999**, *121*, 7696–7697.
- (22) Chen, H.; Schlecht, S.; Semple, T. C.; Hartwig, J. F. Thermal, Catalytic, Regiospecific Functionalization of Alkanes. *Science* **2000**, *287*, 1995–1997.
- (23) Ishiyama, T.; Takagi, J.; Ishida, K.; Miyaura, N.; Anastasi, N. R.; Hartwig, J. F. Mild Iridium-Catalyzed Borylation of Arenes. High Turnover Numbers, Room Temperature Reactions, and Isolation of a Potential Intermediate. *J. Am. Chem. Soc.* **2002**, *124*, 390–391.
- (24) Nguyen, P.; Blom, H. P.; Westcott, S. A.; Taylor, N. J.; Marder, T. B. Synthesis and Structures of the First Transition-Metal Tris(boryl) Complexes: Iridium Complexes (η^6 -arene)Ir(BO₂C₆H₄)₃. *J. Am. Chem. Soc.* **1993**, *115*, 9329–9330.
- (25) Waltz, K. M.; He, X.; Muhoro, C.; Hartwig, J. F. *J. Am. Chem. Soc.* **1995**, *117*, 11357–11358.
- (26) Cho, J.-Y.; Iverson, C. N.; Smith, M. R. Steric and Chelate Directing Effects in Aromatic Borylation. *J. Am. Chem. Soc.* **2000**, *122*, 12868–12869.
- (27) Ishiyama, T.; Takagi, J.; Hartwig, J. F.; Miyaura, N. A Stoichiometric Aromatic C–H Borylation Catalyzed by Iridium(I)/2,2'-Bipyridine Complexes at Room Temperature. *Angew. Chem. Int. Ed.* **2002**, *41*, 3056–3058.
- (28) Boller, T. M.; Murphy, J. M.; Hapke, M.; Ishiyama, T.; Miyaura, N.; Hartwig, J. F. Mechanism of the Mild Functionalization of Arenes by Diboron Reagents Catalyzed by Iridium Complexes. Intermediacy and Chemistry of Bipyridine-Ligated Iridium Trisboryl Complexes. *J. Am. Chem. Soc.* **2005**, *127*, 14263–14278.
- (29) Vanchura, B. A., 2nd; Preshlock, S. M.; Roosen, P. C.; Kallepalli, V. A.; Staples, R. J.; Maleczka, R. E., Jr; Singleton, D. A.; Smith, M. R., 3rd. Electronic Effects in

Iridium C-H Borylations: Insights from Unencumbered Substrates and Variation of Boryl Ligand Substituents. *Chem. Commun.* **2010**, 46, 7724–7726.

Chapter 2. A Catalytic Borylation / Dehalogenation Route to *ortho*-Fluoro Arylboronates

2.1 Introduction

Fluorinated arenes regularly emerge as lead candidates for pharmaceutical,^{1,2} agrochemical,³ and materials applications.⁴ Drug candidates with one or more fluorine atoms have become conventional. The special nature of fluorine shows a variety of properties to certain medicines, including enhanced binding interactions, metabolic stability, changes in physical properties, and selective reactivities (Figure 4a).

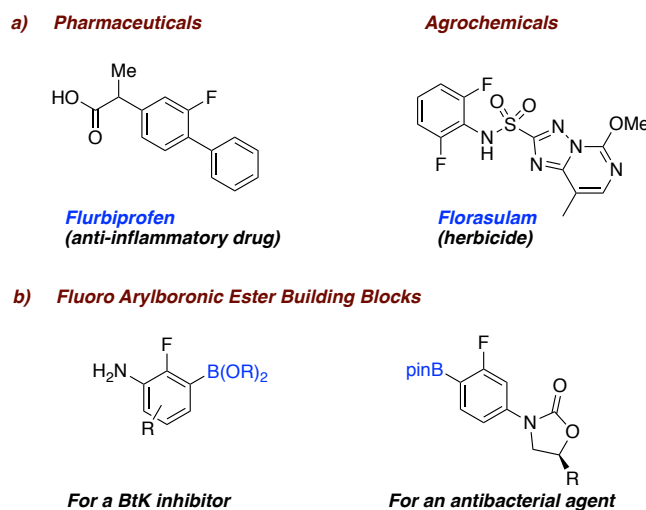


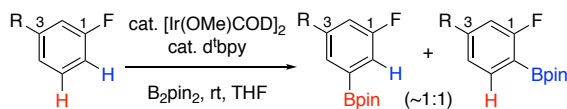
Figure 4. a) Structures of *o*-fluoroaryl motifs in pharmaceuticals and agrochemicals. b) *o*-fluoroaryl motifs as building block

Also, common to these fields is the use of arylboronic ester building blocks (Figure 4b).^{5,6} As such, preparations of arenes bearing both fluoro and boronate substituents are often sought after. Fluorobenzenes have been borylated via reactive intermediates generated by various methods including directed deprotonation and metal-halogen exchange.⁷ Such reactions typically demand the use of strong lithium bases

and/or cryogenic conditions. Activation of a properly positioned halogen by palladium⁸ represents a milder approach, but demands the regioselective installation of the halogen. Given the substrate dependence on aromatic halogenations, accessing suitable haloaromatic starting materials can be trivial or prohibitively difficult.

Ir-catalyzed CHBs avoid the need for strong bases, cold temperatures, and/or halogen pre-functionalization. They tolerate numerous functional groups, including fluorine and have thus been used to generate many fluorobenzenes bearing a 4,4,5,5-tetramethyl-1,3,2-dioxaborolane (Bpin) group.

Iridium catalyzed borylations are primarily driven by sterics, making it is relatively easy to install Bpin's ortho to hydrogen or fluorine vs. other aryl substituents.⁹ This feature can be very useful, but can also create challenges. Fluorine atom has been recognized as an unsuitable substituent for either steric or ortho-directing control of regioselectivity due to its small van der Waals radius and low coordination ability. Therefore, close competition between the sterics of the positions *ortho* (blue) to F vs. *meta* (red) to F has often made borylation via halogenated starting materials the preferred option for selective borylations of 3-substituted (or 2,3-disubstituted) fluorobenzenes. For example, under standard conditions, borylations of 3-substituted (or 2,3-disubstituted) fluorobenzenes typically afford ~1:1 mixtures of borylated arenes (Scheme 10).



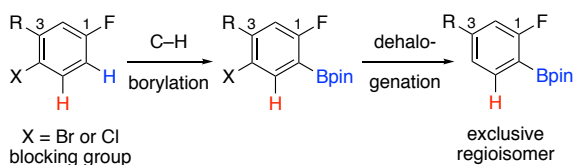
Scheme 10. Typical C–H borylation of 3-substituted fluorobenzenes

For selective borylations ortho to the fluorine this requires the acquisition of 6-halo-3-substituted-fluorobenzenes. The availability of arenes with such a substitution

pattern is highly dependent on the nature of the substituent C-3 (and that at C-2). In fact, in certain instances the availability and/or costs of arenes with a bromo or iodo substituent positioned ortho to the fluorine make them unattractive starting materials, while analogous arenes with halogens para to the fluorine are more readily available.

2.2 Alternate approach to o-fluoro arylboronates

We hypothesized that readily available 3-substituted fluoroarenes with a halo group *para* to the fluorine could serve as convenient starting materials for the generation of *ortho* borylated products. Specifically, in such cases the halogen would not serve as an activating group for metalation, but rather as a sacrificial blocking group in an Ir-catalyzed C–H borylation. In this way, borylation would only take place ortho to the fluorine and upon removal of the para positioned halogen the desired ortho borylated 3-substituted fluoroarene would be generated (Scheme 11).

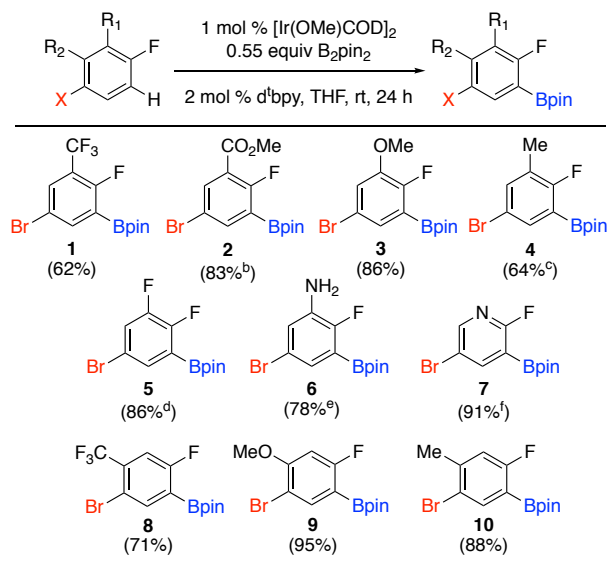


Scheme 11. Alternate approach to o-fluoro arylboronates

2.3 Borylation of fluoroarenes

To begin testing this hypothesis a variety of haloarenes were reacted with 1 mol % [Ir(OMe)(COD)]₂, 2 mol % 4,4'-di-*tert*-butyl-2,2'-dipyridyl ligand (d^tbpy) and 0.55 equiv of bis(pinacolato)diboron (B₂Pin₂) in THF at room temperature (Figure 5). Except where otherwise noted, all of these arenes selectively afforded the ortho borylated products in good yields.

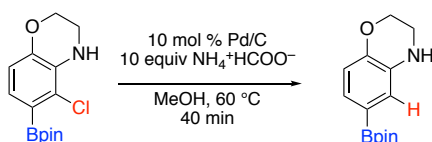
Figure 5. Borylation of fluoroarenes^a



^aIsolated yields. ^bBorylation run at 60 °C for 36 h; product contains 3% of the meta Bpin isomer. ^cProduct contains 1% of the meta Bpin isomer. ^dProduct contains 4% of the meta Bpin isomer. ^eBorylation run with 0.5 mol % [Ir(OMe)COD]₂, 1 mol % tmp, 3.0 equiv HBpin at 80 °C for 16 h. ^fBorylation run at 80 °C for 14 h after which 0.25 equiv HBpin was added and the reaction was allowed to continue at 80 °C for 10 h; product contains 9% of the meta Bpin isomer.

2.4 Dehydrohalogenation of fluoroarenes

The key goal was to dehalogenate the borylated arenes without compromising the Bpin group. Radical based methods are not suitable for that task, but, despite the potential for unwanted Suzuki couplings, a few such Pd-mediated reductions have been reported. Among these, Pd/C mediated transfer hydrogenation using ammonium formate as an in-situ hydrogen donor was attractive owing to the mild and low cost nature of the reagents.¹⁰ Another example from the patent literature involved removing a chloride group in presence of a Bpin (Scheme 12).



Scheme 12. Patent example for dehalogenation with ammonium formate

Unfortunately, in our hands, for fluoro aromatic systems except anisoles such reductions were almost always accompanied by 5-15% loss of the Bpin group as well as other unidentified impurities (Scheme 13).¹¹

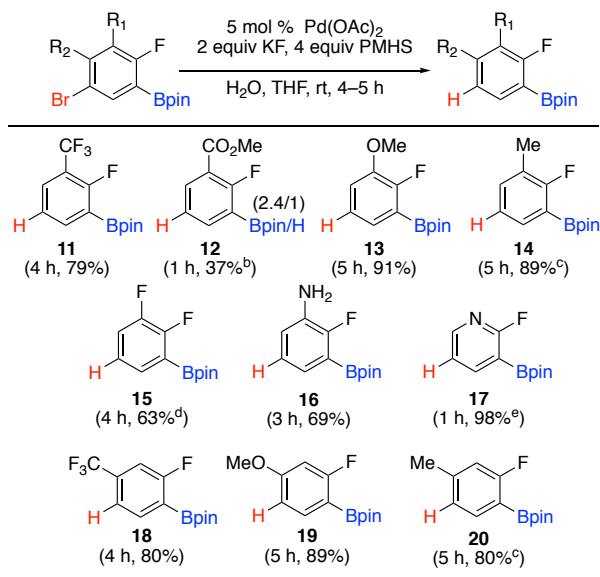


Scheme 13. Dehalogenation with ammonium formate

We next turned to our own experience with the hydrodehalogenation of 3-chloro-5-methylphenylpinacolborane using fluoride activated polymethylhydrosiloxane (PMHS)¹² in the presence of catalytic polysiloxane encapsulated Pd(0) nanoclusters.¹³ To see if we could build from this lone example, the borylated fluoroarenes were subjected to 4 equiv of PMHS, 2 equiv of aqueous KF, and 5 mol % Pd(OAc)₂ in THF (Figure 6).

Most substrates responded favorable to these reductions conditions, affording the desired products in 60–90% yield after 4-5 h reaction times and with no evidence of deborylation. Electron deficient arenes tended to undergo hydrodehalogenation slightly faster than electron rich arenes. The method was amenable to heterocycles as borylated 5-chloro-2-fluoropyridine underwent hydrodehalogenation in 1 h using only 2 equiv PHMS.

Figure 6. Dehalogenation with PMHS^a



^aIsolated yields of arylboronates. ^bCombined yield of the 2,4/1 borylated/deborylated material was 60%. ^cVia chlorinated starting material **4**; product contains 1% of the meta Bpin isomer per the starting material. ^dProduct contains 4% of the meta Bpin isomer per the starting material. ^eProduct included 9% of the meta Bpin isomer per the starting material, 1% of an unidentified fluorinated product and 2% starting material by ¹⁹F-NMR.

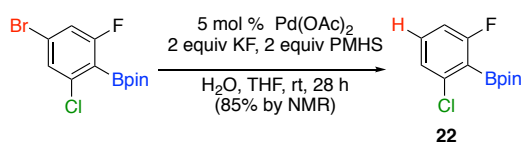
We were unable to completely eliminate protodeborylation as illustrated by the methylbenzoate example (compound **12**). In an attempt to overcome this problem, 18-crown-6/KF in a water free reaction was explored.¹⁴ This met with limited success as hydrodehalogenation times increased due to low KF solubility and other unidentified products were observed by ¹⁹F-NMR.

The dehalogenation shown in Scheme 14 indicates that the electronic influence of the fluorine is what heightens the propensity toward Protideborylation. Here the diborylated arene partially lost the Bpin group ortho to fluorine, while the meta Bpin remained completely intact.



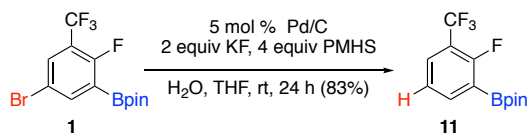
Scheme 14. Protodeborylation

Hydrodebrominations were generally more facile than hydrodechlorinations. We were able to exploit this differential reactivity and selectively remove a bromine in the presence of a chlorine by reducing the amount of PMHS to 2 equiv, which also resulted in increasing the reaction time (Scheme 15).



Scheme 15. Selective debromination

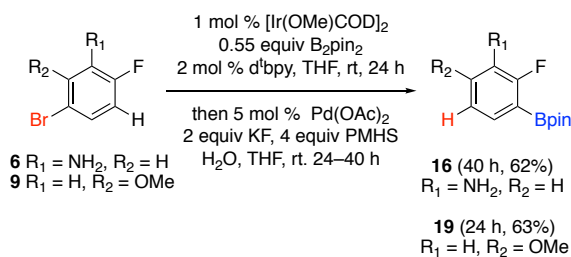
We also screened Pd/C (10% wt) as a palladium source (Scheme 16). Employing 5 mol % Pd/C (with respect to Pd weight) gave the corresponding hydrodehalogenated product, but required 24 h to reach full conversion vs. 4 h with Pd(OAc)₂. We attribute this time difference to the proficiency with which Pd(OAc)₂ forms polysiloxane encapsulated Pd(0) nanoclusters.¹⁰



Scheme 16. Hydrodehalogenation with Pd/C

2.5 One-pot borylation/dehalogenation

We investigated performing the Ir-catalyzed borylation and the Pd-catalyzed hydrodehalogenation in a single pot (Scheme 17). Again, longer reaction times were required to see full conversion during the dehalogenation step. This too is likely due to formation of the Pd(0) nanoparticles being slowed by the residuals from the borylation reaction. Nonetheless, the one-pot yields for the substrates tested, were comparable to the combined yields observed over two steps.

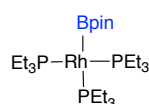


Scheme 17. One-pot procedure

2.6 Recent advancements in selective *ortho*-fluoro arylboronic esters

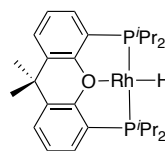
To the best of our knowledge and as indicated by a SciFinder Scholar (2014) search, fluorinations of arylboronic esters are unknown. Recently there have been several reports of introducing Bpin group to fluoroaromatic rings using precious or base metals. Such examples include the use of phosphine,¹⁵ and POP supported rhodium catalysts,¹⁶ NHC¹⁷ and PSiN ligated platinum catalysts,¹⁸ as well as a pincer ligated cobalt catalyst,¹⁹ for the selective *ortho*-fluoroarene borylation (Figure 7).

a) **Braun and Co-workers**



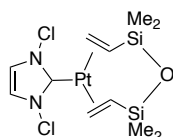
- Limited substrate scope (arenes with multiple fluorines)
- Excess material

b) **Esteruelas and Co-workers**



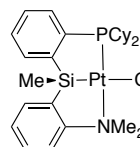
- Limited substrate scope
- Excess material
- Elevated temperatures

c) **Chatani and Co-workers**



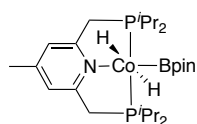
- Broad substrate scope
- Excess material
- C-H borylations at the sterically encumbered position

d) **Iwasawa and Co-workers**



- Broad substrate scope
- Excess material
- Elevated temperatures
- Electronically driven

e) **Chirik and Co-workers**



- Broad substrate scope
- Mild reaction conditions
- Halogens are not tolerated (except fluorine)
- No effect from directing groups (-NMe2 and -SiHMe2)

Example:

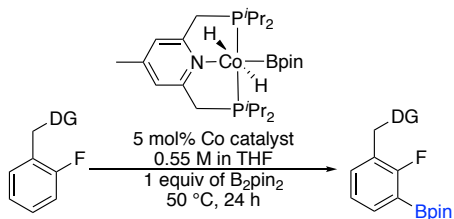


Figure 7. Different catalyst systems for selective *ortho*-fluoroarene borylation

These methods still suffer from excess use of substrate, limited functional group tolerance and expensive ligand synthesis. Selective borylation of fluoro arenes represent a new area that is still emerging and improved methods that can selectively generate either steric or electronic isomer exclusively without pre-functionalized arenes or without expensive ligand synthesis will be attractive.

2.7 Conclusions

We have demonstrated a solution to the problem of selectively generating arylboronic esters *ortho* to fluorine via Ir-catalyzed C–H borylations when both the *ortho* and *meta* positions are sterically accessible. Furthermore, as *para* halogenated fluorobenzenes are often more available and/or less expensive than their *ortho* counterparts, this protocol can be competitive with Pd-catalyzed borylations. Finally, telescoping the borylation and hydrodehalogenation into a single reaction flask is viable.

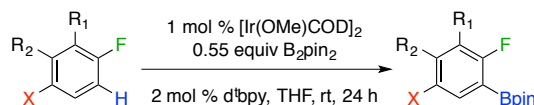
2.8 Experimental

Material and Methods

All reactions were carried out in oven-dried glassware under an atmosphere of nitrogen, with magnetic stirring, and monitored by ^1H -NMR and ^{19}F -NMR. Tetrahydrofuran was freshly distilled from sodium/benzophenone under nitrogen. Palladium (II) acetate purchased from Strem, anhydrous A. C. S grade potassium fluoride, and polymethylhydrosiloxane (PMHS) purchased from Aldrich were used. Column chromatography was performed with silica gel (230-400 mesh) purchased from Silicycle. ^1H , ^{13}C , ^{11}B , and ^{19}F NMR spectra were recorded on an Agilent DirectDrive2 500 MHz NMR spectrometer equipped with an OneProbe operating at 499.7 MHz for ^1H NMR, 125.7 MHz for ^{13}C NMR, 470.1 MHz for ^{19}F NMR and 160.3 MHz for ^{11}B NMR. Elemental composition was determined by accurate mass analysis using a Waters GCT Premier gas chromatograph / time-of-flight mass spectrometer at the Michigan State University Mass Spectrometry Service Center; the products were ionized using an electron ionization source operated in the positive mode. Infrared spectroscopy was

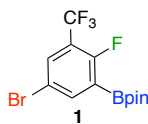
obtained at Michigan State University using an FT-IR Mattson spectrometer. Melting points were measured on a Thomas-Hoover capillary melting point apparatus.

General Procedure for Borylation:



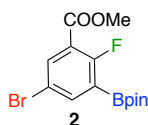
In a nitrogen atmosphere glove box bis(pinacolato)boron (B₂Pin₂) (140 mg, 0.55 mmol) was weighed into a 20 mL vial containing a magnetic stir bar. [Ir(OMe)COD]₂ (6.6 mg, 0.02 mmol) and 4,4'-di-tert-butyl-2,2'-dipyridyl ligand (5.4 mg, 0.02 mmol) were weighed into two test tubes separately, each being diluted with 2 mL of THF. The [Ir(OMe)COD]₂ solution was transferred into the 20 mL vial containing B₂Pin₂. This mixture was stirred until a golden yellow clear solution was obtained (~ 1 min). Next the solution containing ligand was transferred into the vial and upon stirring the resulting solution turned a dark brown color. Finally, the substrate (1 mmol) was added to the vial, which was then sealed. The reaction mixture stirred for 24 h at room temperature, after which the vial was taken out of the glove box. The reaction mixture was passed through a short plug of silica eluting with a 10:1 hexane/ethyl acetate solution (2 x 20 mL). The volatiles were removed by rotary evaporation.

Compound 1



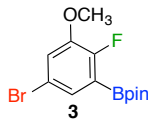
The general borylation procedure was carried out on 1.0 mmol of the starting arene. After workup 0.228 g of compound **1** were obtained as a white solid (mp 76–77 °C) in 62% yield. ¹H NMR (500 MHz, CDCl₃) δ 8.02 (dd, *J* = 2.5, 3.5 Hz, 1H), 7.78 (dd, *J* = 2.5, 6.5 Hz, 1H), 1.36 (s, 12H); ¹³C NMR (125 MHz, CDCl₃) δ 162.9 (dd, *J* = 1.9, 259.7 Hz), 143.1 (d, *J* = 8.5 Hz), 132.8 (qd, *J* = 1.9, 4.7 Hz), 121.7 (q, *J* = 270.3 Hz), 120.0 (qd, *J* = 33.1, 16.1 Hz), 116.3 (d, *J* = 3.5 Hz), 84.7, 24.8; ¹⁹F NMR (470 MHz, CDCl₃) δ -61.9, -106.4; ¹¹B NMR (160 MHz, CDCl₃) δ 29.3 (brs). MS EI+ *m/z* calculated for C₁₃H₁₄BBrF₄O₂ 368.0206, found 368.0178.

Compound 2



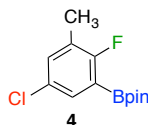
The general borylation procedure was carried out on 3.76 mmol of the starting arene. After workup 1.124 g of compound **2**, containing ~3% of the meta Bpin isomer, were obtained as a white solid (mp 99–101 °C) in 83% isolated yield. ¹H NMR (500 MHz, CDCl₃) δ 8.13 (dd, *J* = 3.0, 3.0 Hz, 1H), 8.00 (dd, *J* = 2.5, 3.0 Hz, 1H), 3.92 (s, 3H), 1.37 (s, 12H); ¹³C NMR (125 MHz, CDCl₃) δ 164.8 (d, *J* = 263.7 Hz), 163.9 (d, *J* = 4.6 Hz), 143.6 (d, *J* = 9.5 Hz), 137.7 (d, *J* = 1.9 Hz), 120.7 (d, *J* = 13.4 Hz), 116.3 (d, *J* = 3.7 Hz), 84.6, 52.6, 24.8; ¹⁹F NMR (470 MHz, CDCl₃) δ -101.5; ¹¹B NMR (160 MHz, CDCl₃) δ 29.4 (brs). FT-IR: 2978.7, 2928.4, 2843.1, 1740.5, 1722.0, 1602.7, 1438.3, 1408.2, 1357.4, 1235.9, 1211.1, 1142.6, 980.0, 849.4, 787.6, 672.1 cm⁻¹. MS EI+ *m/z* calculated for C₁₄H₁₇BBrFO₄ 358.0387, found 358.0422.

Compound 3



The general borylation procedure was carried out on 1 mmol of the starting arene. After workup 0.283 g of compound **3** were obtained as a white solid (mp 79–80 °C) in 86% isolated yield. ^1H NMR (500 MHz, CDCl_3) δ 7.37 (dd, $J = 2.5, 4.0$ Hz, 1H), 7.14 (dd, $J = 2.5, 7.5$ Hz, 1H), 3.85 (s, 3H), 1.34 (s, 12H); ^{13}C NMR (125 MHz, CDCl_3) δ 155.8 (d, $J = 251.2$ Hz), 148.3 (d, $J = 13.2$ Hz), 129.4 (d, $J = 7.6$ Hz), 119.6 (d, $J = 2.9$ Hz), 116.0 (d, $J = 3.7$ Hz), 84.3, 56.6, 24.8; ^{19}F NMR (470 MHz, CDCl_3) δ -126.6; ^{11}B NMR (160 MHz, CDCl_3) δ 29.7 (brs). MS EI+ m/z calculated for $\text{C}_{13}\text{H}_{17}\text{BBrFO}_3$ 330.0438, found 330.0467.

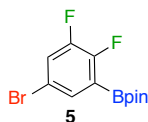
Compound 4



The general borylation procedure was carried out on 1 mmol of the starting arene. After workup 0.173 g of compound **4**, containing ~1% of the meta Bpin isomer, were obtained as a white solid (mp 64–65 °C) in 64% isolated yield. ^1H NMR (500 MHz, CDCl_3) δ 7.49 (dd, $J = 3.0, 6.5$ Hz, 1H), 7.22 (dd, $J = 2.0, 6.5$ Hz, 1H), 2.23 (d, $J = 2.0$ Hz, 3H), 1.34 (s, 12H); ^{13}C NMR (125 MHz, CDCl_3) δ 163.9 (d, $J = 247.5$ Hz), 134.2 (d, $J = 5.7$ Hz), 133.4 (d, $J = 8.5$ Hz), 128.4 (d, $J = 2.9$ Hz), 126.6 (d, $J = 21.9$ Hz), 84.1, 24.7, 14.5 (d, $J = 3.9$ Hz); ^{19}F NMR (470 MHz, CDCl_3) δ -109.9; ^{11}B NMR (160 MHz,

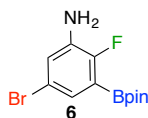
CDCl₃) δ 29.8 (brs). MS EI+ m/z calculated for C₁₃H₁₇BClFO₂ 270.0994, found 270.0984.

Compound 5



The general borylation procedure was carried out on 1 mmol of the starting arene. After the workup 0.274 g of compound **5**, containing ~4% of the meta Bpin isomer, were obtained as a white solid (mp 41–42 °C) in 86% isolated yield. ¹H NMR (500 MHz, CDCl₃) δ 7.57 (ddd, J = 2.0, 4.0, 5.0 Hz, 1H), 7.37 (ddd, J = 2.5, 7.0, 9.0 Hz, 1H), 1.34 (s, 12H); ¹³C NMR (125 MHz, CDCl₃) δ 153.7 (dd, J = 11.4, 252.2 Hz), 150.3 (dd, J = 16.1, 253.2 Hz), 133.7 (dd, J = 4.0, 7.0 Hz), 123.4 (d, J = 20.0 Hz), 115.6 (dd, J = 4.0, 7.0 Hz), 84.6, 24.7; ¹⁹F NMR (470 MHz, CDCl₃) δ -130.0, -134.9; ¹¹B NMR (160 MHz, CDCl₃) δ 29.3 (brs). MS EI+ m/z calculated for C₁₂H₁₄BBrF₂O₂ 318.0238, found 318.0251.

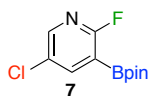
Compound 6



The borylation procedure¹ was carried out on 1 mmol of the starting arene, using 0.5 mol % [Ir(OMe)COD]₂, 1 mol % tmp (3,4,7,8-tetramethyl-1,10-phenanthroline) as the ligand, and 3.0 equiv of HBpin as the boron source at 80 °C for 16 h. The reaction mixture was stirred at 80 °C for 16 h. After the workup 0.246 g of compound **6** were obtained as a white solid (mp 99–100 °C) in 78% isolated yield. ¹H NMR (500 MHz,

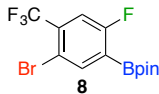
CDCl₃) δ 7.17 (dd, $J = 2.5, 4.0$ Hz, 1H), 6.99 (dd, $J = 2.5, 7.5$ Hz, 1H), 3.82 (brs, 2H (NH₂)), 1.36 (s, 12H); ¹³C NMR (125 MHz, CDCl₃) δ 154.6 (d, $J = 242.8$ Hz), 135.9 (d, $J = 16.1$ Hz), 126.9 (d, $J = 6.6$ Hz), 121.9 (d, $J = 3.7$ Hz), 116.6 (d, $J = 3.7$ Hz), 84.2, 24.8; ¹⁹F NMR (470 MHz, CDCl₃) δ -127.7; ¹¹B NMR (160 MHz, CDCl₃) δ 29.7 (brs). FT-IR: 3474.6, 3383.8, 2983.2, 2930.5, 1625.8, 1564.9, 1478.9, 1430.2, 1358.1, 1272.6, 1191.6, 1140.5, 972.9, 863.2, 846.0, 737.6, 675.0 cm⁻¹. MS EI+ m/z calculated for C₁₂H₁₆BBrFNO₂ 315.0441, found 315.0465.

Compound 7



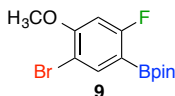
The general borylation procedure was carried out on 4 mmol of the starting arene and the reaction mixture was heated for 80 °C for 19 h. After 19 hr, 0.25 equiv of HBpin was added and the mixture stirred for an additional 10 h at 80 °C. After the workup 0.9328 g of compound 7, containing ~9% of the meta Bpin isomer (isomer ratio = 89:11), were obtained as a white solid (mp 46–47 °C) in 91% isolated yield. For 7 ¹H NMR (500 MHz, CDCl₃) δ 8.24 (d, $J = 2.0$ Hz, 1H), 8.12 (dd, $J = 3.0, 7.0$ Hz, 1H), 1.37 (s, 12H); ¹³C NMR (125 MHz, CDCl₃) δ 165.1 (d, $J = 243.8$ Hz), 148.9 (d, $J = 16.1$ Hz), 147.5 (d, $J = 8.5$ Hz), 128.6, 84.8, 24.8; ¹⁹F NMR (470 MHz, CDCl₃) δ -61.5; ¹¹B NMR (160 MHz, CDCl₃) δ 29.4 (brs). MS EI+ m/z calculated for C₁₁H₁₄BClFNO₂ 257.0790, found 257.0813.

Compound 8



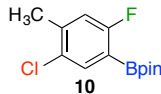
The general borylation procedure was carried out on 10 mmol of the starting arene. After workup 2.619 g of compound **8** were obtained as a white solid (mp 66–67 °C) in 71% isolated yield. ^1H NMR (500 MHz, CDCl_3) δ 8.03 (d, $J = 5.5$ Hz, 1H), 7.37 (d, $J = 8.5$ Hz, 1H), 1.37 (s, 12H); ^{13}C NMR (125 MHz, CDCl_3) δ 165.4 (d, $J = 253.1$ Hz), 142.8 (d, $J = 8.5$ Hz), 134.0 (qd, $J = 8.5, 32.2$ Hz), 121.9 (q, $J = 272.2$ Hz), 115.6 (m), 113.8, 84.8, 24.8; ^{19}F NMR (470 MHz, CDCl_3) δ -63.5, -102.9; ^{11}B NMR (160 MHz, CDCl_3) 29.5 (brs). MS EI+ m/z calculated for $\text{C}_{13}\text{H}_{14}\text{BBrF}_4\text{O}_2$ 368.0206, found 368.0220.

Compound 9



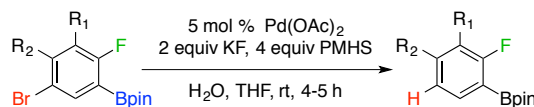
The general borylation procedure was carried out on 1 mmol of the starting arene. After workup 0.313 g of compound **9** were obtained as a white solid (mp 104–105 °C) in 95% isolated yield. ^1H NMR (500 MHz, CDCl_3) δ 7.89 (d, $J = 6.5$ Hz, 1H), 6.61 (d, $J = 11.0$ Hz, 1H), 3.72 (s, 3H), 1.35 (s, 12H); ^{13}C NMR (125 MHz, CDCl_3) δ 167.6 (d, $J = 251.2$ Hz), 159.5 (d, $J = 11.4$ Hz), 140.2 (d, $J = 10.4$ Hz), 108.3 (d, $J = 22.7$ Hz), 105.9 (d, $J = 2.9$ Hz), 83.9, 56.4, 24.8; ^{19}F NMR (470 MHz, CDCl_3) δ -100.4; ^{11}B NMR (160 MHz, CDCl_3) δ 29.5 (brs). MS EI+ m/z calculated for $\text{C}_{13}\text{H}_{17}\text{BBrFO}_3$ 330.0438, found 330.0411.

Compound 10



The general borylation procedure was carried out on 10 mmol of the starting arene. After workup 2.38 g of compound **10** were obtained as a white solid (mp 48–49 °C) in 88% isolated yield. ^1H NMR (500 MHz, CDCl_3) δ 7.66 (d, $J = 5.5$ Hz, 1H), 6.91 (d, $J = 9.5$ Hz, 1H), 2.35 (s, 3H), 1.34 (s, 12H); ^{13}C NMR (125 MHz, CDCl_3) δ 165.4 (d, $J = 249.4$ Hz), 141.7 (d, $J = 9.5$ Hz), 136.5 (d, $J = 8.5$ Hz), 129.1 (d, $J = 2.9$ Hz), 117.7 (d, $J = 25.6$ Hz), 84.1, 24.7, 20.4 (d, $J = 1.9$ Hz); ^{19}F NMR (470 MHz, CDCl_3) δ -106.5; ^{11}B NMR (160 MHz, CDCl_3) δ 29.8 (brs). MS EI+ m/z calculated for $\text{C}_{13}\text{H}_{17}\text{BClFO}_2$ 270.0994, found 270.0997.

General Procedure for the Hydrodehalogenation with PMHS:

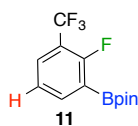


A round bottom flask was charged with the borylated arene (1 mmol), $\text{Pd}(\text{OAc})_2$ (0.05 mmol, 0.011g), and 5 mL of freshly distilled THF. The round bottom flask was fitted with a septum and flushed with nitrogen. While being flushed, KF (0.116 g, 2 mmol) in 2 mL of degassed water was then introduced by syringe. The nitrogen inlet was removed and a balloon filled with nitrogen was attached to the flask. PMHS (0.24 mL, 4 mmol) was then slowly injected dropwise (**Caution:** Gas evolution and an exothermic reaction occur upon the addition of PMHS).

The final reaction mixture was stirred until ^1H (and ^{19}F NMR) indicated the disappearance of starting material (~4 h unless otherwise noted). The reaction mixture

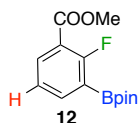
was then diluted with Et₂O and the layers separated. The ether layer was filtered through a plug of Celite contained in a 60 mL syringe. The Celite was flushed with EtOAc. Finally, the volatiles were removed by rotary evaporation. The product was redissolved in hexane/EtOAc and passed through a small plug of silica gel eluting with 20 mL hexane, followed by 40 mL EtOAc.

Compound 11



The general hydrodehalogenation procedure with PMHS was applied to 1 mmol of borylated arene **1**. After workup 0.229 g of compound **11**² were obtained as colorless oil in 79% yield. ¹H NMR (500 MHz, CDCl₃) δ 7.93 (ddd, *J* = 1.5, 5.5, 7.0 Hz, 1H), 7.70 (ddd, *J* = 1.5, 6.0, 7.5 Hz, 1H), 7.23 (dd, *J* = 6.5, 8.5 Hz, 1H), 1.37 (s, 12H); ¹³C NMR (125 MHz, CDCl₃) δ 164.0 (dd, *J* = 1.9, 260.3 Hz), 140.7 (d, *J* = 9.5 Hz), 130.8 (qd, *J* = 2.5, 4.7 Hz), 123.5 (d, *J* = 4.1 Hz), 122.7 (q, *J* = 271.0 Hz), 118.3 (m), 84.3, 24.8; ¹⁹F NMR (470 MHz, CDCl₃) δ -61.6, -104.2; ¹¹B NMR (160 MHz, CDCl₃) δ 29.8 (brs). MS EI+ *m/z* calculated for C₁₃H₁₅BF₄O₂ 290.1101, found 290.1089.

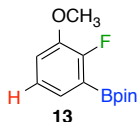
Compound 12



The general hydrodehalogenation procedure with PMHS was applied to 1 mmol of borylated arene **2**, with a reaction time of 1 h. After workup 0.286 g of a 2.4:1 ratio of

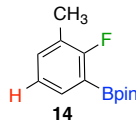
12 and methyl 2-fluorobenzoate containing was isolated in 60% combined yield. The mixture, which also contained a small amount of PMHS was subjected to column chromatography with hexane (50 mL) followed by hexane/ethyl acetate (4/1, 100 mL) to afford 0.1023 g of pure **12** as a white solid (mp 54–55 °C) in 37% isolated yield. (Note: Compounds were visualized using Alazarin TLC stain.) ^1H NMR (500 MHz, CDCl_3) δ 8.03 (ddd, $J = 2.0, 7.5, 7.5$ Hz, 1H), 7.92 (ddd, $J = 2.0, 5.5, 7.5$ Hz, 1H), 7.21 (dd, $J = 7.0, 7.5$ Hz, 1H), 3.92 (s, 3H), 1.37 (s, 12H); ^{13}C NMR (125 MHz, CDCl_3) δ 165.9 (d, $J = 263.7$ Hz), 165.3 (d, $J = 3.9$ Hz), 141.4 (d, $J = 9.5$ Hz), 135.3, 123.6 (d, $J = 3.7$ Hz), 118.5 (d, $J = 12.4$ Hz), 84.2, 52.3, 24.8 (d, $J = 4.75$); ^{19}F NMR (470 MHz, CDCl_3) δ -99.1; ^{11}B NMR (160 MHz, CDCl_3) δ 30.0 (brs).

Compound 13



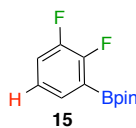
The general hydrodehalogenation procedure with PMHS was applied to 1 mmol of borylated arene **3**. The reaction ran for 5 h. After work up 0.228 g of **13** were obtained as a colorless oil in 91% isolated yield. ^1H NMR (500 MHz, CDCl_3) δ 7.27 (m, 1H), 7.06 (m, 2H), 3.87 (s, 3H), 1.36 (s, 12H); ^{13}C NMR (125 MHz, CDCl_3) δ 156.8 (d, $J = 249.5$ Hz), 147.5 (d, $J = 12.3$ Hz), 127.4 (d, $J = 7.6$ Hz), 123.8 (d, $J = 3.7$ Hz), 116.9 (d, $J = 1.9$ Hz), 83.9, 56.5, 24.8; ^{19}F NMR (470 MHz, CDCl_3) δ -125.1; ^{11}B NMR (160 MHz, CDCl_3) δ 30.2 (brs). MS EI+ m/z calculated for $\text{C}_{13}\text{H}_{18}\text{BFO}_3$ 252.1333, found 252.1337.

Compound 14



The general hydrodehalogenation procedure with PMHS was applied to 1 mmol of borylated arene **4**, which contained 1% of the meta Bpin isomer. The reaction ran for 5 h. After work up 0.211 g of **14**,² which contained 1% of the meta Bpin isomer, were obtained as a colorless oil in 89% isolated yield. ¹H NMR (500 MHz, CDCl₃) δ 7.56 (ddd, *J* = 1.5, 5.0, 7.5 Hz, 1H), 7.29 (ddd, *J* = 1.0, 6.0, 7.0 Hz, 1H), 7.04 (dd, *J* = 7.5, 7.5 Hz, 1H), 2.28 (d, *J* = 2.5 Hz, 3H), 1.37 (s, 12H); ¹³C NMR (125 MHz, CDCl₃) δ 165.6 (d, *J* = 248.4 Hz), 134.7 (d, *J* = 5.6 Hz), 134.1 (d, *J* = 8.6 Hz), 124.6 (d, *J* = 19.8 Hz), 123.4 (d, *J* = 2.9 Hz), 83.8, 24.8, 14.6; ¹⁹F NMR (470 MHz, CDCl₃) δ -106.9; ¹¹B NMR (160 MHz, CDCl₃) δ 30.4 (brs).¹ MS EI+ *m/z* calculated for C₁₃H₁₈BFO₂ 236.1384, found 236.1405.

Compound 15



The general hydrodehalogenation procedure with PMHS was applied to 1 mmol of borylated arene **5**, which contained 4% of the meta Bpin isomer. After work up 0.1512 g of **15**, which contained 1% of the meta Bpin isomer, were obtained as a colorless oil in 63% isolated yield. ¹H NMR (500 MHz, CDCl₃) δ 7.45 (m, 1H), 7.23 (m, 1H), 7.06 (m, 1H), 1.36 (s, 12H); ¹³C NMR (125 MHz, CDCl₃) δ 154.6 (dd, *J* = 11.5, 251.5 Hz), 150.5 (dd, *J* = 14.3, 247.6 Hz), 131.1 (dd, *J* = 3.7, 6.6 Hz), 124.1 (dd, *J* = 3.9,

5.7 Hz), 120.2 (d, $J = 17.1$ Hz), 84.2, 24.8; ^{19}F NMR (470 MHz, CDCl_3) δ -129.1, -139.1; ^{11}B NMR (160 MHz, CDCl_3) δ 29.8 (brs). MS EI+ m/z calculated for $\text{C}_{12}\text{H}_{15}\text{BF}_2\text{O}_2$ 240.1133, found 240.1142.

Compound 16



The general hydrodehalogenation procedure with PMHS was applied to 0.76 mmol of borylated arene **6**. The reaction ran for 3 h. After work up 0.143 g of **16** were obtained as a white solid (mp 92–93 °C) in 69% isolated yield. ^1H NMR (500 MHz, CDCl_3) δ 7.09 (m, 1H), 6.95 (dd, $J = 7.0, 8.0$ Hz, 1H), 6.89 (ddd, $J = 1.5, 6.5, 8.5$ Hz, 1H), 3.72 (s, 2H), 1.37 (s, 12H); ^{13}C NMR (125 MHz, CDCl_3) δ 155.7 (d, $J = 241.8$ Hz), 134.3 (d, $J = 14.2$ Hz), 125.3 (d, $J = 7.6$ Hz), 124.0 (d, $J = 3.9$ Hz), 119.9 (d, $J = 3.7$ Hz), 83.8, 24.8; ^{19}F NMR (470 MHz, CDCl_3) δ -125.6; ^{11}B NMR (160 MHz, CDCl_3) δ 30.3 (brs). MS EI+ m/z calculated for $\text{C}_{12}\text{H}_{17}\text{BFNO}_2$ 237.1336, found 237.1332.

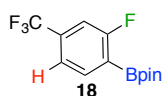
Compound 17



The general hydrodehalogenation procedure with PMHS was applied to 1 mmol of borylated arene **7**, which contained 9% of the meta Bpin isomer, using 2 equiv of PMHS. The reaction ran for 1 h. After workup ^{19}F NMR indicated an NMR yield of 88% **17**, 9% of the meta Bpin isomer per the starting material, 2% starting material, and

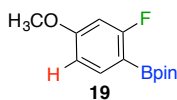
1% of an unidentified fluorinated product. For **17**³ ¹H NMR (500 MHz, CDCl₃) δ 8.28 (dd, *J* = 1.5, 4.5 Hz, 1H), 8.16 (ddd, *J* = 2.5, 7.0, 9.0 Hz, 1H), 7.17 (m, 1H) 1.35 (s, 12H); ¹³C NMR (125 MHz, CDCl₃) δ 166.8 (d, *J* = 243.7 Hz), 150.6 (d, *J* = 14.2 Hz), 148.4 (d, *J* = 7.5 Hz), 120.9 (d, *J* = 4.75 Hz), 84.4, 24.7; ¹⁹F NMR (470 MHz, CDCl₃) δ -57.8; ¹¹B NMR (160 MHz, CDCl₃) δ 29.7 (brs). MS EI+ *m/z* calculated for C₁₁H₁₅BFNO₂ 223.1180, found 223.1198.

Compound 18



The general hydrodehalogenation procedure with PMHS was applied to 1 mmol of borylated arene **8**. After workup 0.232 g of **18** were obtained as a colorless oil in 80% isolated yield. ¹H NMR (500 MHz, CDCl₃) δ 7.87 (dd, *J* = 6.5, 6.5 Hz, 1H), 7.40 (d, *J* = 8.0 Hz, 1H), 7.30 (d, *J* = 9.0 Hz, 1H), 1.38 (s, 12H); ¹³C NMR (125 MHz, CDCl₃) δ 166.7 (d, *J* = 251.4 Hz), 137.6 (d, *J* = 8.5 Hz), 135.1 (m), 123.2 (q, *J* = 271.2 Hz), 120.3 (m), 112.3 (m), 84.8, 24.8; ¹⁹F NMR (470 MHz, CDCl₃) δ -63.2, -100.6; ¹¹B NMR (160 MHz, CDCl₃) 30.1 (brs). MS EI+ *m/z* calculated for C₁₃H₁₅BF₄O₂ 290.1101, found 290.1102.

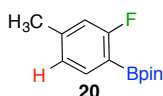
Compound 19



The general hydrodehalogenation procedure with PMHS was applied to 1 mmol of borylated arene **9**. The reaction ran for 5 h. After workup 0.152 g of **19** were obtained

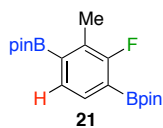
as a colorless oil in 61% isolated yield. ^1H NMR (500 MHz, CDCl_3) δ 7.66 (dd, $J = 7.5$, 7.5 Hz, 1H), 6.70 (dd, $J = 2.5$, 8.0 Hz, 1H), 6.58 (dd, $J = 2.5$, 12.0 Hz, 1H), 3.83 (s, 3H), 1.36 (s, 12H); ^{13}C NMR (125 MHz, CDCl_3) δ 168.6 (d, $J = 249.4$ Hz), 163.9 (d, $J = 11.2$ Hz), 137.7 (d, $J = 10.5$ Hz), 109.9 (d, $J = 2.9$ Hz), 101.1 (d, $J = 27.5$ Hz), 83.6, 55.4, 24.8; ^{19}F NMR (470 MHz, CDCl_3) δ -100.5; ^{11}B NMR (160 MHz, CDCl_3) δ 29.9 (brs). MS EI+ m/z calculated for $\text{C}_{13}\text{H}_{18}\text{BFO}_3$ 252.1333, found 252.1329.

Compound 20



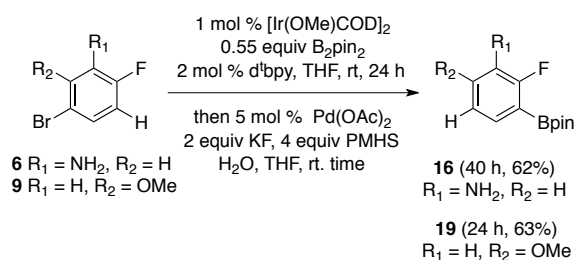
The general hydrodehalogenation procedure with PMHS was applied to 1 mmol of borylated arene **10**. The reaction ran for 5 h. After workup 0.189 g of **20**⁴ were obtained as a white solid (mp 58–60 °C) in 80% isolated yield. ^1H NMR (500 MHz, CDCl_3) δ 7.63 (dd, $J = 7.0$, 7.5 Hz, 1H), 6.96 (d, $J = 7.5$ Hz, 1H), 6.86 (d, $J = 10.5$ Hz, 1H), 2.37 (s, 3H), 1.37 (s, 12H); ^{13}C NMR (125 MHz, CDCl_3) δ 167.3 (d, $J = 249.4$ Hz), 144.4 (d, $J = 8.5$ Hz), 136.6 (d, $J = 8.6$ Hz), 124.5 (d, $J = 2.9$ Hz), 115.8 (d, $J = 23.7$ Hz), 83.7, 24.8, 21.5; ^{19}F NMR (470 MHz, CDCl_3) δ -103.8; ^{11}B NMR (160 MHz, CDCl_3) δ 30.3 (brs). MS EI+ m/z calculated for $\text{C}_{13}\text{H}_{18}\text{BFO}_2$ 236.1384, found 236.1391.

Compound 21



The general hydrodehalogenation procedure with PMHS was applied to 1 mmol of the starting borylated arene. The reaction ran for 24 h. After workup 0.324 g of a 3:1 ratio of 2,2'-(2-fluoro-3-methyl-1,4-phenylene)bis(4,4,5,5-tetramethyl-1,3,2-dioxaborolane) (**21**) and 2-(3-fluoro-2-methylphenyl)-4,4,5,5-tetramethyl-1,3,2-dioxaborolanein was isolated. The mixture was subjected to silica gel column chromatography eluting with hexane (100 mL) followed by hexane/ethyl acetate (9/1, 100 mL) to afford 0.135 g of **21** as a white solid (mp 163–165 °C) in 37% isolated yield. (Note: Compounds were visualized using Alazarin TLC stain.) ¹H NMR (500 MHz, CDCl₃) δ 7.50 (m, 2H), 2.45 (d, *J* = 3.0 Hz, 3H), 1.37 (s, 12H), 1.35 (s, 12H); ¹³C NMR (125 MHz, CDCl₃) δ 165.4 (d, *J* = 247.6 Hz), 132.9 (d, *J* = 8.5 Hz), 130.8 (d, *J* = 17.1 Hz), 130.4 (d, *J* = 3.8 Hz), 83.8, 83.7, 24.87, 24.83, 13.30, 13.25; ¹⁹F NMR (470MHz, CDCl₃) δ -107.2; ¹¹B NMR (160 MHz, CDCl₃) δ 30.4 (brs). Anal. Calcd for C₁₉H₂₉B₂FO₄: C, 63.0; H, 8.1. Found C, 61.6; H, 7.6.

One Pot Borylation and Hydrodehalogenation



The general borylation procedure was carried out on 1 mmol of starting arene **9** and the reaction was complete after 24 h as judged by NMR. The reaction solution was transferred to an oven dried round bottom flask, which was sealed by a rubber septum

and brought out of the nitrogen atmosphere glove box. The general hydrodehalogenation procedure was followed for 24 h.

The reaction mixture was then diluted with Et₂O and the layers separated. The ether layer was filtered through a plug of silica gel. The silica gel was flushed with hexane (2 x 10 mL) and then with a 1:1 hexane/ethyl acetate mixture (10 mL). The eluted solution was concentrated by rotary evaporation. The product was dissolved in 10:1 hexane/ethyl acetate and filtered through another plug of silica gel to remove the final traces of boron and Pd byproducts. The plug was flushed with hexane (4 x 10 mL). The volatiles were removed by rotary evaporation to afford 0.1597 g of **19** as a light orange oil in 63% isolated yield.

Hydrodehalogenation with NH₄⁺HCOO⁻:

Borylated arenes, 1–4, 6, and 8–10, were dehalogenated via Pd/C mediated transfer hydrogenation using ammonium formate as an in situ hydrogen donor.⁵ Unfortunately, in our hands, aside from anisoles such reductions were almost always accompanied by 5-15% loss of the Bpin group as well as other unidentified impurities. See Table 1 for details.

General Procedure for a One-pot Hydrodehalogenation with NH₄⁺HCOO⁻:

The general borylation procedure was carried out on 1 mmol of starting arene and the reaction was complete after 24 h as judged by NMR. The reaction solution transferred to an oven dried Schlenk flask, which was sealed by a rubber septum and brought out of the nitrogen atmosphere glove box. Palladium on activated charcoal (10%

Pd by weight, 0.108 g) and ammonium formate (0.64 g, 10.0 mmol) in MeOH (30 mL) were introduced under a nitrogen atmosphere. The mixture was heated at 60 °C for 30–40 min, cooled to RT and filtered through Celite®.

The filter cake was rinsed with MeOH. The filtrate was concentrated and sent through a short silica plug using 1:1 hexane/ethyl acetate to remove boron waste and palladium residues. Then the filtrate was concentrated to dryness and the residue partitioned between water (10 mL) and EtOAc (20 mL). The organic layer was washed with brine (20 mL), dried over anhydrous MgSO₄ and concentrated to obtain the boronic ester. (Note: This protocol led to partial protodeborylation when performed on electron poor arenes.)

Table 1. Hydrodehalogenation with Ammonium Formate

Entry	Starting Arene	Dehalogenation Product (rxn time, yield ^a)
1	<p>1</p>	<p>11 (40 min, 85:15)</p>
2	<p>2</p>	<p>12 (55 min, 87:13)</p>
3	<p>3</p>	<p>13 (40 min, 55%)</p>
4	<p>4</p>	<p>14 (60 min, 96:4)</p>
5	<p>6</p>	<p>16 (40 min, 93:6:1)</p>
6	<p>8</p>	<p>18 (40 min, 90:10)</p>
7	<p>9</p>	<p>19 (24 h, 78%)^b</p>
8	<p>10</p>	<p>20 (60 min, 87:7:6)</p>

^aIsolated yields. ^bOne pot reaction at room temperature.

REFERENCES

REFERENCES

- (1) (a) Hagmann, W. K. *J. Med. Chem.* **2008**, 51, 4359–4369. (b) Wang, J.; Sánchez-Roselló, M.; Aceña, J. L.; del Pozo, C.; Sorochinsky, A. E.; Fustero, S.; Soloshonok, V. A.; Liu, H. *Chem. Rev.* **2014**, 114, 2432–2506.
- (2) Purser, S.; Moore, P. R.; Swallow, S.; Gouverneur, V. *Chem. Soc. Rev.* **2008**, 37, 320–330.
- (3) (a) Jeschke, P. *Chembiochem.* **2004**, 5, 570–589. (b) Jeschke, P. *Pest Manag. Sci.* **2010**, 66, 10–27.
- (4) (a) Babudri, R.; Farinola, G. M.; Naso, F.; Ragni, R. *Chem. Commun.* **2007**, 1003–1022. (b) Berger, R.; Resnati, G.; Metrangolo, P.; Weber, E.; Hulliger, J. *Chem. Soc. Rev.* **2011**, 40, 3496–3508.
- (5) Zhichkin, P. E.; Krasutsky, S. G.; Beer, C. M.; Rennells, W. M.; Lee, S. H.; Xiong, J. M. *Synthesis* **2011**, 1604–1608.
- (6) Reck, F.; Zhou, F.; Eyermann, C. J.; Kem, G.; Carcanague, D.; Ioannidis, G.; Illingworth, R.; Poon, G.; Gravestock, M. B. *J. Med. Chem.* **2007**, 50, 4868–4881.
- (7) (a) Bouillon, A.; Lancelot, J. C.; Collot, V.; Bovy, P. R.; Rault, S. *Tetrahedron* **2002**, 58, 3323–3328. (b) Oppenheimer, J. M. Methods of Forming 4-Chloro-2-fluoro-3-substituted-phenylboronic Acid Pinacol Esters and Methods Using the Same U.S. Pat. Appl. 13/729,580, July 4, 2013. (c) Clary, J. W.; Rettenmaier, T. J.; Snelling, R.; Bryks, W.; Banwell, J.; Wipke, W. T.; Singaram, B. *J. Org. Chem.* **2011**, 76, 9602–9610.
- (8) Ishiyama, T.; Murata, M.; Miyaura, N. *J. Org. Chem.* **1995**, 60, 7508–7510.
- (9) (a) Cho, J. Y.; Tse, M. K.; Holmes, D.; Maleczka, R. E., Jr.; Smith, M. R., III, *Science* **2002**, 295, 305–308. (b) Chotana, G. A.; Rak, M. A.; Smith, M. R. *J. Am. Chem. Soc.* **2005**, 127, 10539–10544. (c) Mkhaliid, I. A. I.; Barnard, J. H.; Marder, T. B.; Murphy, J. M.; Hartwig, J. F. *Chem. Rev.* **2010**, 110, 890–931.

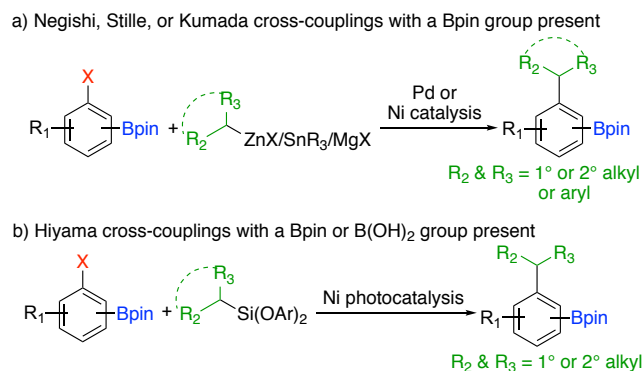
- (10) (a) Yoakim, C.; Bailey, M. D.; Bilodeau, F.; Carson, R. J.; Fader, L.; Kawai, S.; Simoneau, S. L. B.; Surprenant, S.; Thibeault, C.; Tsantrizos, Y. S. Inhibitors of human immunodeficiency virus replication U.S. Patent 8,338,441, December 25, 2012. (b) Rajagopal, S.; Spatola, A. F. *J. Org. Chem.* **1995**, *60*, 1347–1355. (c) Anwer, M. K.; Sherman, D. B.; Roney, J. G.; Spatola, A. F. *J. Org. Chem.* **1989**, *54*, 1284–1289.
- (11) For the versatile reducing ability of PMHS see: (a) Lawrence, N. J.; Drew, M. D.; Bushell, S. M. *J. Chem. Soc., Perkin Trans I.* **1999**, 3381–3391. (b) Lavis, J. M.; Maleczka, R. E., Jr. *Polymethylhydrosiloxane (PMHS)*, In *EROS-Electronic Encyclopedia of Reagents for Organic Synthesis*; Paquette, L. A.; Crich, D.; Fuchs, P. L.; Wipf, P., Eds.; Wiley: New York, 2003, Online.
- (12) (a) Maleczka, R. E., Jr.; Rahaim, R. J.; Teixeira, R. R. *Tetrahedron Lett.* **2002**, *43*, 7087–7090. (b) Rahaim, R. J.; Maleczka, R. E., Jr. *Tetrahedron Lett.* **2002**, *43*, 8823–8826.
- (13) Ghosh, B.; Maleczka, R. E., Jr. *Tetrahedron Lett.* **2011**, *52*, 5285–5287.
- (14) A one-pot Ir-catalyzed borylation/dehalogenation sequence using ammonium formate was also effective, but only when the arene was electron rich. See experimental section for details.
- (15) Kalläne, S. I.; Teltewskoi, M.; Braun, T.; Braun, B. *Organometallics* **2015**, *34*, 1156–1169.
- (16) Esteruelas, M. A.; Oliván, M.; Vélez, A. *Organometallics* **2015**, *34*, 1911–19924.
- (17) Furukawa, T.; Tobisu, M.; Chatani, N. *J. Am. Chem. Soc.* **2015**, *137*, 12211–12214.
- (18) Takaya, J.; Ito, S.; Nomoto, H.; Saito, N.; Kirai, N.; Iwasawa, N. *Chem. Commun.* **2015**, *51*, 17662–17665.
- (19) Obligacion, J. V.; Bezdek, M. J.; Chirik, P. J. *J. Am. Chem. Soc.* **2017**, *139*, 2825–2832.

Chapter 3. Merging Iridium Catalyzed C-H Borylations with Organoindium

Cross-Couplings

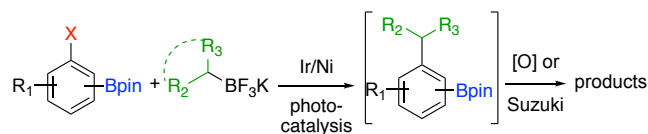
3.1 Introduction

Ir-catalyzed C-H borylation is a renowned method for making boronic esters of arene and heteroarenes.¹ This method tolerates many functional groups including halogens.² These halo boronic esters enables further orthogonal coupling reactions which leads to broad scope of diverse molecules. We and others have shown that halogen bearing arylboronic esters can undergo reactions to form C–C and C–N³ bonds leaving the boronic ester intact for future use. There are several reports for making C–C bonds, for example, some successes have also been realized for the Negishi,^{4–7} Stille,⁸ Kumada,⁹ and Hiyama¹⁰ couplings of Bpin substituted haloarenes (Scheme 18a–b)



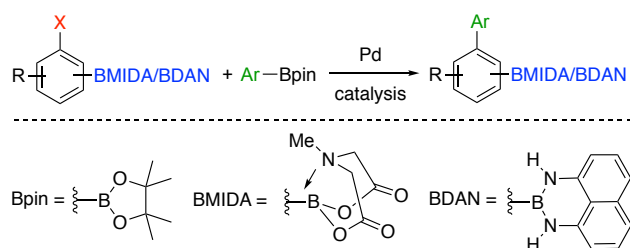
Scheme 18. Different type of cross-couplings for CC bond formation

Molander and co-workers have developed a complementary strategy whereby aryl-BF₃K salts selectively couple with Bpin bearing haloarenes to in situ form Bpin substituted arenes that can be subjected to subsequent chemical events such as oxidation and Suzuki coupling reactions (Scheme 19).¹¹



Scheme 19. BF_3K Suzuki cross-couplings with a Bpin group present

Cross coupling reactions of halo boronic esters occasionally suffer from unwanted polyphenyl formation or undergo hydrogen elimination which leads to other by-products. In cases where the borylation product bears a halide (e.g. Br) exposure to Suzuki conditions leads to the formation of hyperbranched polyphenyls.² Therefore, to avoid these hyperbranching palladium mediated reactions of haloarenes bearing N-methyliminodiacetic^{12–16} acid and 1,8-diaminonaphthalene^{17,18} boronic esters (BMIDA and BDAN respectively) have been reported. Here unwanted polyphenylene formation is avoided as BMIDA and BDAN are unreactive under certain Suzuki conditions, (Scheme 20). The produced borylated biaryls have been used in iterative palladium catalyzed Suzuki-Miyaura cross-couplings popularized by Burke and others.¹⁹

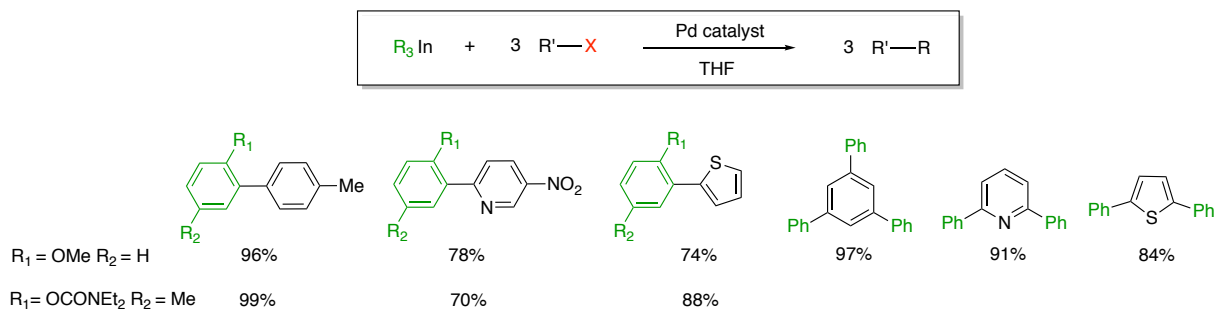


Scheme 20. Suzuki cross-couplings with an unreactive boronate group present

3.2 Organoindium cross coupling

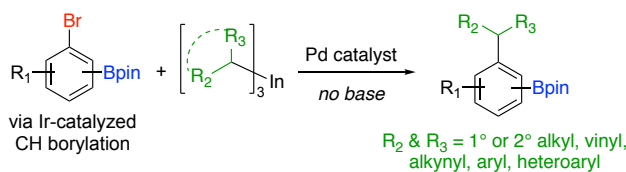
Seeking to build on our tandem Ir catalyzed borylations aminations, we sought cross-coupling conditions that would allow for C–C bond formation at the site of the halogen that would proceed without compromising the Bpin. The self-Suzuki reactions

are facilitated by the presence of aqueous base, and therefore should be minimized during base free Pd-catalyzed cross-coupling.³ Methodology that go close together with our need is Sarandeses–Sestelo couplings (Scheme 21). Here triorganoindium reagents possess the ability to transfer all three organic ligands; they are of low toxicity as compared to tin derivatives and they do not require the addition of base additives.



Scheme 21. Organoindium cross-couplings

Given these features, especially the ability to operate base-free and thereby minimize polyphenylene formation, we looked to merge Sarandeses–Sestelo cross-couplings with CHB's and establish a method for the cross-coupling of triorganoindiums with CHB derived arylhalides bearing a Bpin substituent (Scheme 22).^{20–26}



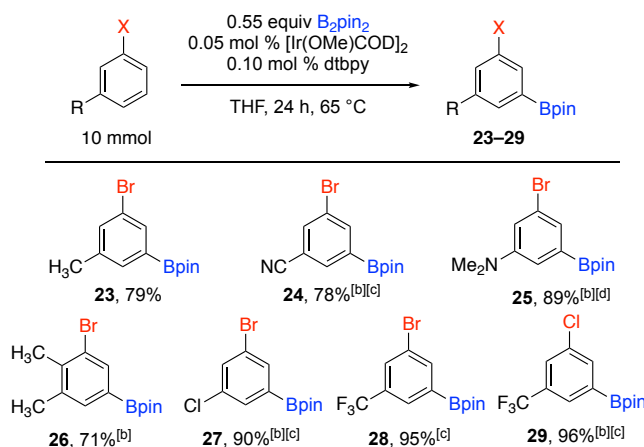
Scheme 22. Organoindium cross-couplings with a Bpin group present

3.3 Investigations and optimizations

To begin, a variety of haloarenes were reacted with 0.05 mol % [Ir(OMe)(COD)]₂, 0.10 mol % 4,4'-di-*tert*-butyl-2,2'-dipyridyl ligand (d^tbpy) and 0.55 equiv of

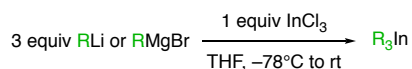
bis(pinacolato)diboron (B_2Pin_2) in THF at room temperature to isolate borylated haloarenes **23–29** (Figure 8).

Figure 8. Borylation of halo arenes.^a



[a] Yields are for isolated materials. [b] HBpin was the boron source. [c] run at room temperature for 48 h. See experimental section for details. [d] 72 h.

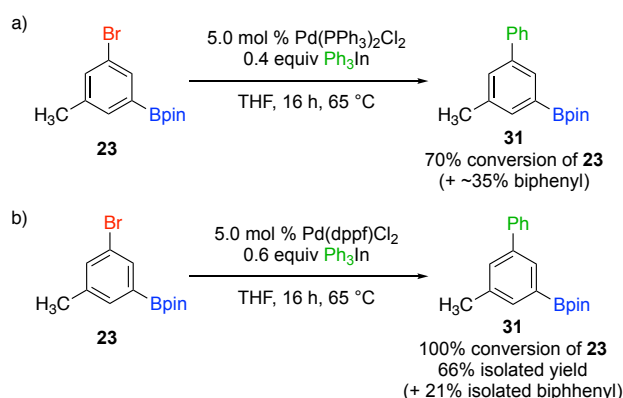
With our CHB produced borylated haloarenes in hand, the plan was to react them with in situ generated triorganoindiums. Triorganoindiums are typically prepared by combining dry $InCl_3$ with a organolithium or Grignard species (Scheme 23). We chose to begin the cross-coupling studies with Ph_3In prepares in this manner.



Scheme 23. Synthesis of triorganoindiums

To begin testing the capacity of borylated haloarenes to undergo Pd-catalyzed cross-couplings with triorganoindium reagents, we first cannula transferred 0.4 equiv of Ph_3In in THF to a THF solution of 5 mol % $Pd(PPh_3)_2Cl_2$ and 1 mmol of **23** (Scheme 24 a). This reaction stalled after 16 h affording at that time a 70:30 mixture of cross-coupled product **31**, unreacted **23**, along with ~35% biphenyl. Despite additional experimentation

and the potential for all three phenyl groups to transfer, elimination of biphenyl as a byproduct was never realized. Nonetheless, increasing the stoichiometry of the Ph_3In to 0.66 equiv and changing the catalyst to $\text{Pd}(\text{dppf})\text{Cl}_2$ resulted in the complete consumption of **23** after 16 h in refluxing THF (Scheme 24b). NMR and GC analyses of the crude reaction mixture indicated that aside from Ph–Ph formation, no other unwanted cross-couplings had occurred, nor was there loss of the Bpin group.

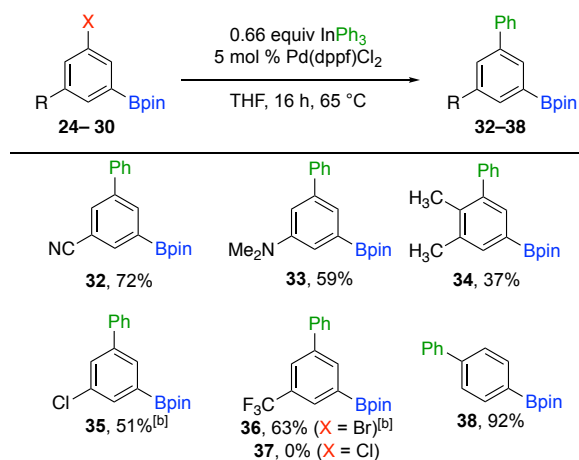


Scheme 24. Pd-catalyzed cross-couplings of Ph_3In with borylated haloarene **23**

3.4 Cross-couplings of R_3In with borylated haloarenes

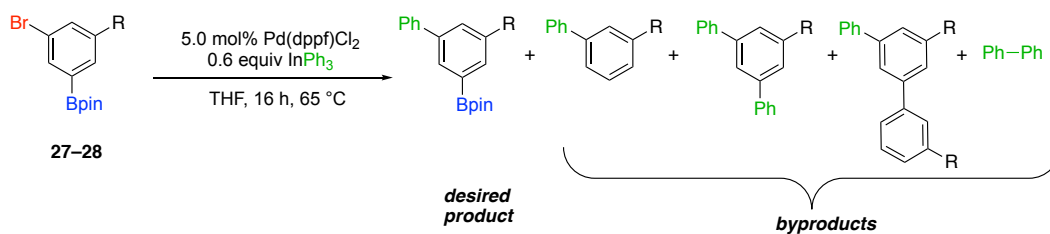
After these optimizations, we examined the reaction of Ph_3In with various borylated haloarenes (Figure 9). Similar to **23**, borylated 3-bromobenzonitrile (**24**) gave **32** in 72% isolated yield without any evidence of unreacted starting material, other cross-coupled products (aside from biphenyl), or deborylated materials in the crude product mixture. Likewise, aniline derivative **25** and 4-(Bpin)bromobenzene (**30**) coupled without incident affording **33** and **38** in 59% and 92% isolated yields respectively. NMR of the crude product mixture also indicated a clean reaction for **26**, but **34** was isolated in only 37% yield, presumably due to losses during chromatographic purification.

Figure 9. Pd-catalyzed cross-couplings of Ph₃In with borylated haloarenes^a



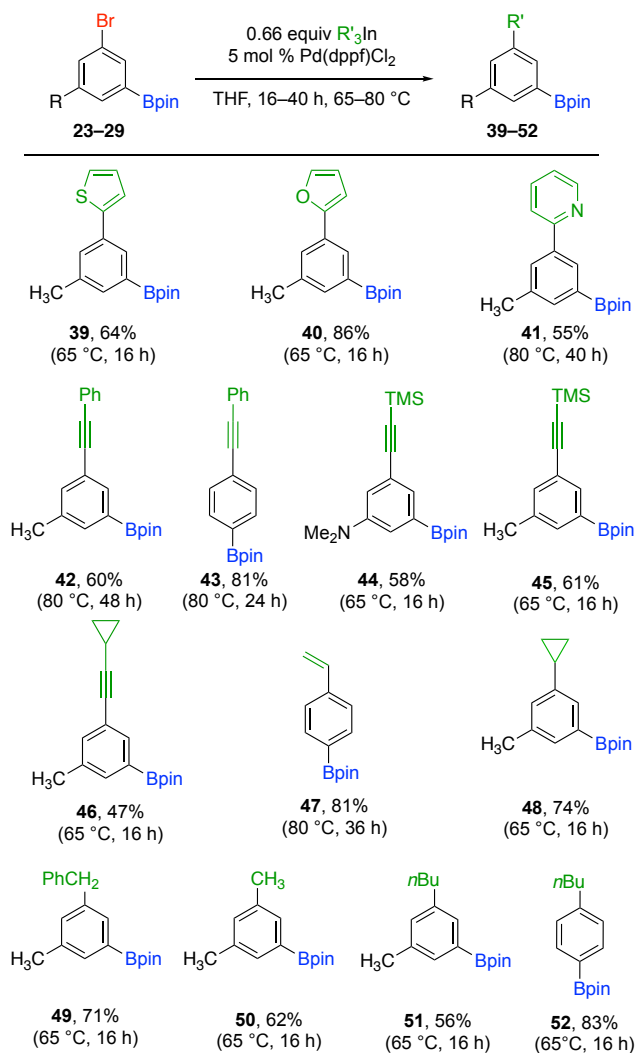
[a] Yields are for isolated materials. [b] Minor amounts of byproducts were also observed. See experimental section for details.

In contrast, while the cross-couplings of **35** and **36** gave desired products in 51% and 63% yields respectively, these reactions did show side products derived from the starting borylated haloarenes. Specifically, compounds stemming from ~10–20% deboronation of the cross-coupled products were observed for these substrates (Scheme 25). In addition, small amounts (1–4%) of over coupled products could also be seen in the crude reaction mixtures. Lastly, we were unable to affect the cross-coupling of chloroarene **29**.



Scheme 25. Pd-catalyzed cross-coupling side reactions

Figure 10. Pd-catalyzed cross-couplings of various triorganoindium species with borylated haloarenes^a



^a Yields are for isolated materials.

Other triorganoindium species were also tested (Figure 10). Triheteroarylindium reagents derived from 2-lithio forms of thiophene, furan, and pyridine afforded products **39**, **40**, and **41** in 64%, 86%, and 55% yields respectively. These results are notable since CHB of heteroarenes tend to be very facile.¹ As such, CHB's on 2-tolyl derivatives of thiophene, furan, or pyridines would borylate the heterocycle instead of generating **39–**

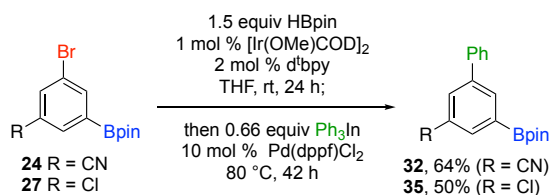
41.^{27–29}

Alkenes and alkynes are often problematic substituents in CHB's owing to their ability to be hydroborated and/or otherwise compromise the effectiveness of the catalyst. This incompatibility creates the need for methods that can incorporate unsaturated groups post-CHB. With this want in mind, we were gratified to see that three different trialkynylindium reagents successfully coupled with three different borylated haloarenes, affording compounds **42–46** in good (81%) to modest (47%) isolated yields. Of similar utility, trivinylindium cross-coupled with **30** to give **43** in 81% isolated yield.

The substrate scope was also extended to sp^3 organoindium reagents. Tricyclopropylindium, Bn_3In , and Me_3In coupled with boronic ester **23** giving products **48**, **49**, and **50** in synthetically useful yields (74–62%). Notably, even the *n*-butyl groups of $(n-Bu)_3In$ were transferable, with **23** and **30** leading to products **51** and **52** in 56% and 83% isolated yields respectively.

3.5 One-pot borylations/cross-couplings of haloarenes

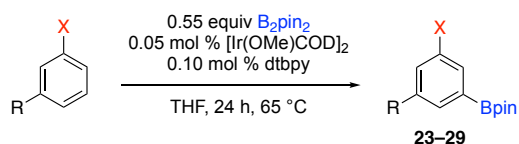
Next, we investigated performing the CHB and a Sarandeses–Sestelo cross-coupling in a single pot (Scheme 26). Following their respective generation to crude solutions **24** and **27** was added a THF solution of Ph_3In . For both substrates, the final products (**32** and **35**) were formed in yields comparable to the two-pot scheme. However, to achieve full conversion, longer reaction times and higher Pd loadings were required. We have observed the same phenomena in past efforts to telescope CHB's and subsequent Pd-catalyzed transformations.³⁰ We attribute this trend to residuals from the CHB causing a loss of catalytic activity.



Scheme 26. One pot borylation/cross-coupling reaction

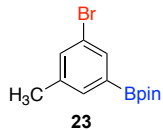
3.6 Experimental

General Borylation Procedure



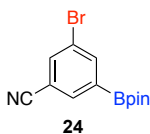
In a nitrogen atmosphere glove box, bis(pinacolato)boron (B₂Pin₂) (1.40 g, 5.5 mmol, 0.55 equiv) was weighed into a 20 mL vial containing a magnetic stir bar. [Ir(OMe)COD]₂ (3.3 mg, 0.005 mmol, 0.5 mol %) and 4,4'-di-tert-butyl-2,2'-dipyridyl ligand (2.7 mg, 0.010 mmol, 1.0 mol %) were weighed into two test tubes separately, each being diluted with 1 mL of THF. The [Ir(OMe)COD]₂ solution was transferred into the 20 mL vial containing B₂Pin₂. This mixture was stirred until a golden yellow clear solution was obtained (~ 1 min). Next the solution containing ligand was transferred into the vial and upon stirring the resulting solution turned a dark brown color. Finally, the substrate (10.0 mmol) was added to the vial, which was then sealed and was taken out of the glove box. The reaction mixture was stirred for 24 h at 65 °C. Then, the reaction mixture was passed through a plug of silica (BD 60 mL Syringe/Luer-Lok Tip-silica up to 50 mL mark) eluting with a 10:1 hexane/ethyl acetate solution (2 x 200 mL). The volatiles were removed by rotary evaporation.

Compound 23



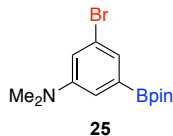
The general borylation procedure was carried out on the starting arene of 1-bromo-3-methylbenzene. After workup 2.356 g of compound **23** was obtained as a white solid (mp 74–76 °C, lit^{1a} 74 – 76 °C) in 7% yield. ¹H NMR (500 MHz, CDCl₃) δ 7.74 (s, 1H), 7.54 (s, 1H), 7.43 (s, 1H), 2.33 (s, 3H), 1.35 (s, 12H); ¹³C NMR (125 MHz, CDCl₃) δ 139.5, 134.7, 134.4, 133.8, 122.2, 84.3, 25.4, 20.6; ¹¹B NMR (160 MHz, CDCl₃) δ 30.5 (brs). MS EI+ m/z calculated for (M+H)⁺ C₁₃H₁₉BBro₂ 297.0661, found 297.0640.

Compound 24



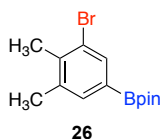
The general borylation procedure was carried out on 1.0 mmol of the starting arene at room temperature for 24h using HBpin (300 μL) as the boron source. After workup 0.238 g of compound **24** was obtained as a white solid (mp 87–88 °C, lit 83–86 °C) in 78% yield. ¹H NMR (500 MHz, CDCl₃) δ 8.14 (dd, *J* = 1.0, 2.0 Hz, 1H), 8.01 (dd, *J* = 1.0, 1.5 Hz, 1H), 7.85 (dd, *J* = 1.5, 2.0 Hz, 1H), 1.36 (s, 12H); ¹³C NMR (125 MHz, CDCl₃) δ 141.8, 136.8, 136.7, 122.6, 117.4, 113.8, 84.9, 24.8; ¹¹B NMR (160 MHz, CDCl₃) δ 29.5 (brs). MS EI+ m/z calculated for (M+H)⁺ C₁₃H₁₆BBrNO₂ 308.0457, found 308.0435.

Compound 25



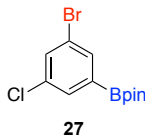
The general borylation procedure was carried out on 1.0 mmol of the starting arene at room temperature for 72 h using HBpin (300 μ L) as the boron source. After workup 0.291 g of compound **25** was obtained as a white solid (mp 121–123 $^{\circ}$ C) in 89% yield. ^1H NMR (500 MHz, Chloroform-*d*) δ 7.27 (s, 1H), 7.06 (dd, J = 2.6, 0.7 Hz, 1H), 6.93 (dd, J = 2.6, 1.8 Hz, 1H), 2.97 (s, 6H), 1.34 (s, 12H); ^{13}C NMR (126 MHz, Chloroform-*d*) δ 151.2, 125.0, 123.3, 117.7, 116.9, 83.9, 40.5, 24.8.; ^{11}B NMR (160 MHz, CDCl_3) δ 29.9 (brs). MS EI+ m/z calculated for $(\text{M}+\text{H})^+$ $\text{C}_{14}\text{H}_{22}\text{BBrNO}_2$ 326.0927, found 326.0963.

Compound 26



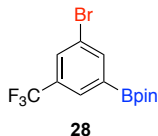
The general borylation procedure was carried out on 1.0 mmol of the starting arene at room temperature for 24 h using HBpin (300 μ L) as the boron source. After workup 0.220 g of compound **26** was obtained as a white solid (mp 103–105 $^{\circ}$ C) in 71% yield. ^1H NMR (500 MHz, Chloroform-*d*) δ 7.84 (d, J = 1.1 Hz, 1H), 7.50 (d, J = 1.1 Hz, 1H), 2.39 (s, 3H), 2.34 (s, 3H), 1.34 (s, 12H); ^{13}C NMR (126 MHz, Chloroform-*d*) δ 139.5, 137.9, 136.3, 134.9, 125.7, 83.9, 24.8, 21.0, 19.7; ^{11}B NMR (160 MHz, CDCl_3) δ 30.3 (brs). MS EI+ m/z calculated for $(\text{M}+\text{H})^+$ $\text{C}_{14}\text{H}_{21}\text{BBrO}_2$ 311.0818, found 311.0848.

Compound 27



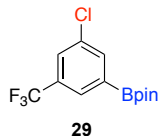
The general borylation procedure was carried out on 1.0 mmol of the starting arene at room temperature for 48 h using HBpin (300 μ L) as the boron source. After workup 0.287 g of compound **27** was obtained as a white solid (mp 51–53 $^{\circ}$ C) in 90% yield. ^1H NMR (500 MHz, CDCl_3) δ 7.80 (dd, $J = 1.0, 1.0$ Hz, 1H), 7.69 (dd, $J = 0.5, 2.0$ Hz, 1H), 7.59 (dd, $J = 2.0, 2.0$ Hz, 1H), 1.35 (s, 12H); ^{13}C NMR (125 MHz, CDCl_3) δ 135.6, 134.8, 133.8, 133.1, 122.6, 84.5, 24.9; ^{11}B NMR (160 MHz, CDCl_3) δ 29.9 (brs). MS EI+ m/z calculated for $(\text{M}+\text{H})^+$ $\text{C}_{12}\text{H}_{16}\text{BBrClO}_2$ 317.0115, found 317.0147.

Compound 28



The general borylation procedure was carried out on the starting arene at room temperature for 48h. After workup 3.312 g of compound **1f** was obtained as a white solid (mp 51–52 $^{\circ}$ C) in 95% yield. ^1H NMR (500 MHz, CDCl_3) δ 8.10 (s, 1H), 7.98 (s, 1H), 7.84 (s, 1H), 1.36 (s, 12H); ^{13}C NMR (125 MHz, CDCl_3) δ 140.8, 131.9 (q, $J = 32.3$ Hz), 130.8 (q, $J = 3.7$ Hz), 129.8 (q, $J = 3.3$ Hz), 124.3 (q, $J = 271.2$ Hz), 122.5, 84.7, 24.8; ^{19}F NMR (470 MHz, CDCl_3) δ -62.7; ^{11}B NMR (160 MHz, CDCl_3) δ 29.8 (brs). MS EI+ m/z calculated for $(\text{M}+\text{H})^+$ $\text{C}_{13}\text{H}_{16}\text{BBrF}_3\text{O}_2$ 351.0378, found 351.1444.

Compound 29



The general borylation procedure was carried out on the starting arene at room temperature for 48h. After workup 2.7 g of compound **1g** was obtained as a colorless oil in 96% yield. ^1H NMR (500 MHz, CDCl_3) δ 7.95 (dd, $J = 2.2, 0.7$ Hz, 1H), 7.93 (dd, $J = 1.7, 0.8$ Hz, 1H), 7.69 (dd, $J = 2.4, 0.7$ Hz, 1H), 1.36 (s, 12H). ^{13}C NMR (126 MHz, CDCl_3) δ 137.9, 134.5, 131.9(q, $J = 32.3$ Hz), 129.6 (q, $J = 3.6$ Hz), 127.9 (q, $J = 3.9$ Hz), 123.4 (q, $J = 272.9$ Hz), 84.6, 24.8. ^{11}B NMR (160 MHz, CDCl_3): δ 30.1(brs).

General Procedure for Preparation of Indium Organometallics

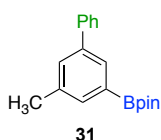
InCl_3 was dried under high vacuum at 80 °C. A 25 mL round-bottomed flask with a stirrer bar was charged with dry InCl_3 (0.6 mmol). A positive argon pressure was established and dry THF (3.0 mL) was added. The resulting solution was cooled to -78 °C, and a solution of RLi, or RMgBr (vinyl) (1.8 mmol) was slowly added (30-45 min). The mixture was stirred for 60 min, the cooling bath was removed, and the reaction mixture was warmed to room temperature. The resulting mixture was stirred at room temperature for 1-2 h.

General Procedure for the Palladium-Catalyzed Cross Coupling Reactions

A prepared solution of InR_3 (0.6 mmol in dry THF) was added to mixture of the electrophile (1 mmol, 1 equiv) and Pd catalyst (0.05 mmol, 5.0 mol%) in dry THF (6 mL). The resulting mixture was refluxed under argon until the starting material had been consumed (NMR or GC). The reaction was then quenched by the addition of few drops of

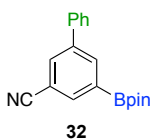
MeOH. The crude mixture was passed through a plug of silica (BD 60 mL Syringe/Luer-Lok Tip-silica up to 50 mL mark). Elution with hexane to remove the biphenyl by product followed by elution with hexane/ethyl acetate solution. The volatiles were removed by rotary evaporation. The residue was further purified by silica chromatography to afford the cross-coupled product.

Compound 31



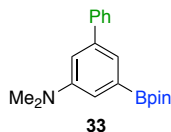
The general cross-coupling procedure was carried out on 1.0 mmol of **23** at 65 °C for 16 h. After purification by SiO₂ chromatography (8:2 hexane/ethyl acetate) 0.193 g of compound **31** was isolated as a white solid (mp 93–95 °C, lit⁵ 106–107 °C) in 66% yield. ¹H NMR (500 MHz, CDCl₃) δ 7.86 (dd, *J* = 1.9, 1.0 Hz, 1H), 7.65 – 7.61 (m, 3H), 7.52 (dd, *J* = 1.8, 0.9 Hz, 1H), 7.43 (dd, *J* = 7.7 Hz, 2H), 7.36 – 7.31 (m, 1H), 2.43 (s, 3H), 1.37 (s, 12H). ¹³C NMR (125 MHz, CDCl₃) δ 141.2, 140.6, 137.6, 134.3, 130.9, 130.7, 128.6, 127.3, 127.1, 83.8, 24.9, 21.3. ¹¹B NMR (160 MHz, CDCl₃) δ 30.8 (brs). The spectral data were in accordance with those reported in the literature.⁵ HRMS (EI+) *m/z* 295.1867 [(M+H)⁺ calcd for C₁₉H₂₄BO₂ 295.1869].

Compound 32



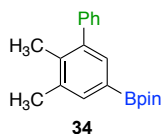
The general cross-coupling procedure was carried out on 1.0 mmol of **24** at 65 °C for 16 h. After purification by SiO₂ chromatography (from 9:1 to 8:2 hexane/ethyl acetate) 0.221 g of compound **32** was isolated as a white solid (mp 98–99 °C) in 72 % yield. ¹H NMR (500 MHz, CDCl₃) δ 8.23 (dd, *J* = 2.0, 1.0 Hz, 1H), 8.07 (dd, *J* = 1.6, 1.0 Hz, 1H), 7.94 (t, *J* = 1.8 Hz, 1H), 7.64–7.59 (m, 2H), 7.52–7.45 (m, 2H), 7.44–7.39 (m, 1H), 1.38 (s, 12H). ¹³C NMR (126 MHz, CDCl₃) δ 141.6, 138.9, 137.5, 136.9, 132.9, 129.0, 128.3, 127.2, 118.9, 109.9, 84.6, 24.9. ¹¹B NMR (160 MHz, CDCl₃) δ 30.0 (brs). HRMS EI+ *m/z* 306.1693 [(M+H)⁺ calcd for C₁₉H₂₁BNO₂ 306.1665].

Compound 33



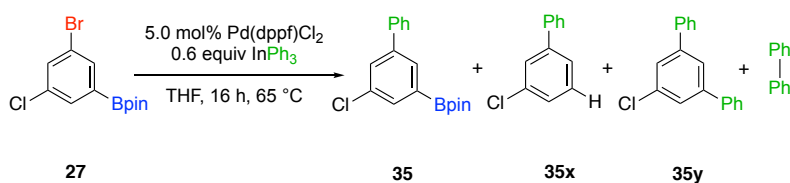
The general cross-coupling procedure was carried out on 0.34 mmol of **25** at 65 °C for 16 h. After purification 0.065 g of compound **33** was isolated as a white solid (mp 125–129 °C) in 59% yield. ¹H NMR (300 MHz, CDCl₃) δ 7.68–7.60 (m, 2H), 7.46–7.40 (m, 2H), 7.37–7.29 (m, 1H), 7.23–7.20 (m, 1H), 7.08–7.04 (m, 1H), 3.03 (s, 6H), 1.37 (s, 12H). ¹³C NMR (75 MHz, CDCl₃) δ 150.7, 142.2, 141.8, 128.6, 127.6, 127.1, 122.5, 117.9, 114.8, 83.8, 41.0, 25.0. ¹¹B NMR (128 MHz, CDCl₃) δ 31.3 (brs). HRMS (ESI+) *m/z* 324.2137 [(M+H)⁺ calcd for C₂₀H₂₇BNO₂ 324.2129].

Compound 34



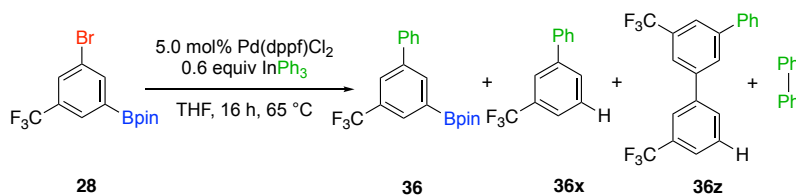
The general cross-coupling procedure was carried out on 0.34 mmol of **26** at 65 °C for 16 h. After purification 0.039 g of compound **34** was isolated as a white solid (mp 102–106 °C) in 37% yield. ¹H NMR (300 MHz, CDCl₃) δ 7.62 (s, 1H), 7.56 (s, 1H), 7.43–7.28 (m, 5H), 2.36 (s, 3H), 2.19 (s, 3H), 1.35 (s, 12H). ¹³C NMR (75 MHz, CDCl₃) δ 142.6, 142.0, 137.7, 136.7, 135.2, 134.3, 129.6, 128.0, 126.7, 83.8, 25.0, 20.6, 17.4. ¹¹B NMR (128 MHz, CDCl₃) δ 30.7 (brs). HRMS (ESI+) *m/z* 309.2020 [(M+H)⁺ calcd for C₂₀H₂₆BO₂ 309.2020].

Compound 35



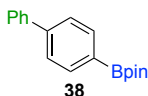
The general cross-coupling procedure was carried out on 1.0 mmol of **27** at 65 °C for 16 h. After 16 h a mixture of **35**, **35x** and **35y** in ratio of 85:11:4 (NMR/GCMS) was obtained. After purification by SiO₂ chromatography (hexane 100 mL then 9:1 hexane/ethyl acetate) 0.160 g of pure **35** was isolated as a white solid (mp 87–89 °C) in 51% yield. ¹H NMR (500 MHz, Chloroform-*d*) δ 7.90 (dd, *J* = 1.8, 1.0 Hz, 1H), 7.75 (dd, *J* = 2.2, 0.9 Hz, 1H), 7.66 (dd, *J* = 1.9 Hz, 1H), 7.60 (dd, *J* = 8.2, 1.2 Hz, 2H), 7.43 (dd, *J* = 7.0, 6.0 Hz, 2H), 7.38–7.33 (m, 1H), 1.36 (s, 12H). ¹³C NMR (126 MHz, Chloroform-*d*) δ 142.5, 139.7, 134.4, 133.2, 131.5, 129.8, 128.8, 127.7, 127.2, 84.21, 24.86. ¹¹B NMR (160 MHz, CDCl₃) δ 30.1 (brs). HRMS EI+ *m/z* 315.1302 [(M+H)⁺ calcd for C₁₈H₂₁BClO₂ 315.1323].

Compound 36



The general cross-coupling procedure was carried out on 1.0 mmol of **28** at 65 °C for 16 h. After 16 h a mixture of **36**, **36x** and **36z** in ratio of 72:20:8 (NMR/GCMS) was obtained. After purification by SiO₂ chromatography (Hexane 100 mL then from 9:1 to 8:2 hexane/ethyl acetate) 0.219 g of compound **36** was isolated as a white sticky solid as a mixture (**36:36z** = 90:1) in 63% yield. ¹H NMR (500 MHz, CDCl₃) 8.22 (s, 1H), 8.06 (s, 1H), 7.93 (d, *J* = 2.4 Hz, 1H), 7.65 (dd, *J* = 8.1, 2.2 Hz, 2H), 7.47 (dd, *J* = 8.3, 7.8 Hz, 2H), 7.43–7.36 (m, 1H), 1.39 (s, 12H). ¹³C NMR (126 MHz, CDCl₃) δ 141.3, 139.7, 136.7, 130.6 (d, *J* = 31.8 Hz), 130.1 (d, *J* = 3.7 Hz), 128.9, 128.2 (q, *J* = 216.2 Hz), 127.9, 127.3, 126.4 (d, *J* = 3.8 Hz), 84.4, 24.9. ¹⁹F NMR (470 MHz, CDCl₃) δ –62.5. ¹¹B NMR (160 MHz, CDCl₃) δ 30.1 (brs). The spectral data were in accordance with those reported in the literature.⁶ HRMS EI+ *m/z* 349.1561 [(M+H)⁺ calcd for C₁₉H₂₁BF₃O₂ 349.1587].

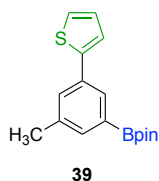
Compound 38



The general cross-coupling procedure was carried out on 1.0 mmol of 2-(4-bromophenyl)-4,4,5,5-tetramethyl-1,3,2-dioxaborolane (**30**) at 65 °C for 16 h. After purification by SiO₂ chromatography (9:1 hexane/ethyl acetate) 0.257 g of compound **38** was isolated as a white solid (mp 100–101 °C, lit^{7b} 111–112 °C) in 92% yield. ¹H NMR (500 MHz, Chloroform-*d*) δ 7.93 (d, *J* = 8.1 Hz, 2H), 7.67 – 7.64 (m, 4H), 7.48 (t, *J* = 7.6

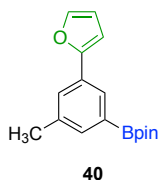
Hz, 2H), 7.41–7.36 (m, 1H), 1.40 (s, 12H). ¹³C NMR (126 MHz, Chloroform-*d*) δ 143.9, 141.0, 135.3, 128.8, 127.6, 127.3, 126.5, 83.8, 24.9. ¹¹B NMR (160 MHz, CDCl₃) δ 30.7 (brs). The spectral data were in accordance with those reported in the literature.⁷ (EI+) *m/z* 281.1708 [(M+H)⁺ calcd for C₁₈H₂₂BO₂ 281.1713]

Compound 39



The general cross-coupling procedure was carried out on 0.34 mmol of **23** at 65 °C for 16 h. After purification 0.065 g of compound **39** was isolated as a white solid (mp 95–98 °C) in 64% yield. ¹H NMR (300 MHz, CDCl₃) δ 7.88 (s, 1H), 7.57 (s, 1H), 7.53 (s, 1H), 7.36 (dd, *J* = 3.6, 1.2 Hz, 1H), 7.26 (dd, *J* = 5.1, 1.2 Hz, 1H), 7.07 (dd, *J* = 5.1, 3.6 Hz, 1H), 2.40 (s, 3H), 1.37 (s, 12H). ¹³C NMR (75 MHz, CDCl₃) δ 144.6, 137.9, 134.7, 134.0, 129.7, 129.5, 128.0, 124.7, 123.3, 84.0, 25.0, 21.4. ¹¹B NMR (128 MHz, CDCl₃) δ 31.0 (brs). HRMS (ESI+) *m/z* 301.1427 [(M+H)⁺ calcd for C₁₇H₂₂BO₂S 301.1428].

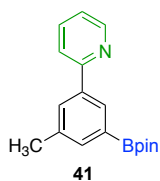
Compound 40



The general cross-coupling procedure was carried out on 0.34 mmol of **23** at 65 °C for 16 h. After purification 0.081 g of compound **40** was isolated as an orange oil in 86% yield. ¹H NMR (300 MHz, CDCl₃) δ 7.91 (s, 1H), 7.53 (s, 1H), 7.45 (s, 1H), 6.68 (d, *J* = 3.4

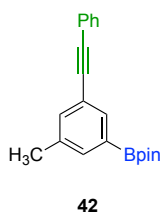
Hz, 1H), 6.49–6.43 (m, 1H), 2.39 (s, 3H), 1.36 (s, 12H); ^{13}C NMR (75 MHz, CDCl_3) δ 154.3, 142.0, 137.7, 134.6, 130.5, 127.6, 127.4, 111.7, 105.1, 84.0, 25.0, 21.4. ^{11}B NMR (128 MHz, CDCl_3) δ 30.1 (brs). HRMS (ESI+) m/z 285.1667 [$(\text{M}+\text{H})^+$ calcd for $\text{C}_{17}\text{H}_{22}\text{BO}_3$ 285.1656].

Compound 41



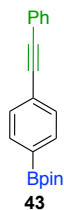
The general cross-coupling procedure was carried out on 1.0 mmol of **23** at 80 °C for 40 h. After purification by SiO_2 chromatography (from 9:1 to 7:3 hexane/ethyl acetate) 0.162 g of compound **41** was isolated as a white solid (mp 123–125 °C) in 55% yield. ^1H NMR (500 MHz, CDCl_3) δ 8.69 (d, $J = 4.5$ Hz, 1H), 8.15 (s, 1H), 7.99 (s, 1H), 7.80 (d, $J = 7.9$ Hz, 1H), 7.74 (dd, $J = 7.5, 7.7$ Hz, 1H), 7.69 (s, 1H), 7.22 (dd, $J = 5.5, 6.2$ Hz, 1H), 2.44 (s, 3H), 1.36 (s, 12H). ^{13}C NMR (126 MHz, CDCl_3) δ 157.6, 149.5, 138.7, 137.8, 136.6, 136.0, 130.6, 130.3, 121.9, 120.9, 83.8, 24.9, 21.3. ^{11}B NMR (160 MHz, CDCl_3) δ 30.4 (brs). (EI+) m/z 296.1839 [$(\text{M}+\text{H})^+$ calcd for $\text{C}_{18}\text{H}_{23}\text{BNO}_2$ 296.1822]

Compound 42



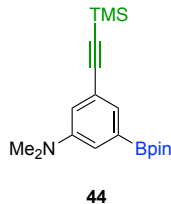
The general cross-coupling procedure was carried out on 1.0 mmol of **23** at 80 °C for 48 h. After purification by SiO₂ chromatography (8:2 hexane/ethyl acetate) 0.192 g of compound **42** was isolated as a yellow oil in 60% yield. ¹H NMR (500 MHz, CDCl₃) δ 7.83 (d, *J* = 1.6 Hz, 1H), 7.60 (dd, *J* = 1.8, 1.0 Hz, 1H), 7.55–7.49 (m, 2H), 7.46 (dd, *J* = 1.8, 0.9 Hz, 1H), 7.39–7.31 (m, 3H), 2.36 (d, *J* = 0.8 Hz, 3H), 1.36 (s, 12H). ¹³C NMR (126 MHz, CDCl₃) δ 137.3, 135.2, 135.2, 134.7, 131.5, 128.3, 128.1, 123.4, 122.7, 89.5, 89.1, 83.9, 24.9, 21.1. ¹¹B NMR (160 MHz, CDCl₃) δ 30.5 (brs). (EI+) *m/z* 319.1864 [(M+H)⁺ calcd for C₂₁H₂₄BO₂ 319.1869]

Compound 43



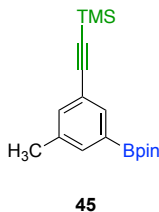
The general cross-coupling procedure was carried out on 1.0 mmol of 2-(4-bromophenyl)-4,4,5,5-tetramethyl-1,3,2-dioxaborolane (**30**) at 80 °C for 24 h. After purification by SiO₂ chromatography (9:1 hexane/ethyl acetate) 0.247 g of compound **43** was isolated as a brown solid (mp 88–89 °C, lit⁸ 93–95 °C) in 81% yield. ¹H NMR (500 MHz, CDCl₃) δ 7.80 (d, *J* = 8.1 Hz, 2H), 7.57–7.52 (m, 4H), 7.38–7.34 (m, 3H), 1.36 (s, 12H). ¹³C NMR (126 MHz, CDCl₃) δ 136.3, 134.6, 131.6, 130.8, 128.4, 125.9, 123.1, 90.7, 89.5, 83.9, 24.9. ¹¹B NMR (160 MHz, CDCl₃) δ 30.6 (brs). (EI+) *m/z* 305.1710 [(M+H)⁺ calcd for C₂₀H₂₂BO₂ 305.1713]. Spectral data were consistent with literature⁸ reported values except the ¹³C peak reported at 137.13 was not observed.⁸ Presumably this peak is that of the carbon bearing boron. Such carbons are often difficult to observe.

Compound 44



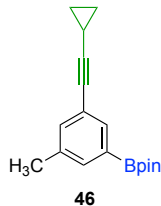
The general cross-coupling procedure was carried out on 0.34 mmol of **25** at 65 °C for 16 h. After purification 0.068 g of compound **44** was isolated as a yellow oil in 58% yield. ^1H NMR (300 MHz, CDCl_3) δ 7.31 (s, 1H), 7.14–7.10 (m, 1H), 6.93–6.89 (m, 1H), 2.95 (s, 6H), 1.33 (s, 12H), 0.23 (s, 9H). ^{13}C NMR (75 MHz, CDCl_3) δ 149.9, 127.1, 123.2, 119.1, 118.4, 106.3, 92.8, 83.9, 40.8, 25.0, 0.2. ^{11}B NMR (128 MHz, CDCl_3) δ 31.0 (brs). HRMS (ESI+) m/z 344.2226 [(M+H) $^+$ calcd for $\text{C}_{19}\text{H}_{31}\text{BNO}_2\text{Si}$ 344.2211].

Compound 45



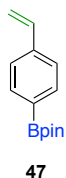
The general cross-coupling procedure was carried out on 0.34 mmol of **23** at 65 °C for 16 h. After purification 0.065 g of compound **45** was isolated as a white solid (mp 77–79 °C) in 61% yield. ^1H NMR (300 MHz, CDCl_3) δ 7.74 (s, 1H), 7.56 (s, 1H), 7.38 (s, 1H), 2.31 (s, 3H), 1.34 (s, 12H), 0.23 (s, 9H). ^{13}C NMR (75 MHz, CDCl_3) δ 137.3, 135.7, 135.5, 135.2, 122.7, 105.4, 93.8, 84.1, 25.0, 21.1, 0.2. ^{11}B NMR (128 MHz, CDCl_3) δ 30.6 (brs). HRMS (ESI+) m/z 315.1935 [(M+H) $^+$ calcd for $\text{C}_{18}\text{H}_{28}\text{BO}_2\text{Si}$ 315.1946].

Compound 46



The general cross-coupling procedure was carried out on 0.34 mmol of **23** at 65 °C for 16 h. After purification 0.045 g of compound **46** was isolated as a yellow solid (mp 68–70 °C) in 47% yield. ¹H NMR (300 MHz, CDCl₃) δ 7.65 (s, 1H), 7.50 (s, 1H), 7.29 (s, 1H), 2.30 (s, 3H), 1.48–1.37 (m, 1H), 1.33 (s, 12H), 0.87–0.73 (m, 4H). ¹³C NMR (75 MHz, CDCl₃) δ 137.2, 135.4, 134.9, 134.5, 123.5, 93.2, 84.0, 75.9, 25.0, 21.1, 8.7, 0.3. ¹¹B NMR (128 MHz, CDCl₃) δ 31.1 (brs). HRMS (ESI+) *m/z* 305.1672 [(M+Na)⁺ calcd for C₁₈H₂₃BO₂Na 305.1683].

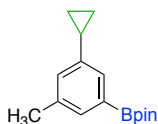
Compound 47



The general cross-coupling procedure was carried out on 1.0 mmol of 2-(4-bromophenyl)-4,4,5,5-tetramethyl-1,3,2-dioxaborolane (**30**) at 80 °C for 36 h. After purification by SiO₂ chromatography (9:1 hexane/ethyl acetate) 0.187 g of compound **47** was isolated as a colorless oil in 81% yield. ¹H NMR (500 MHz, CDCl₃) δ 7.78 (d, *J* = 8.0 Hz, 2H), 7.42 (d, *J* = 8.5 Hz, 2H), 6.74 (dd, *J* = 17.6, 10.9 Hz, 1H), 5.83 (dd, *J* = 17.6, 0.9 Hz, 1H), 5.30 (dd, *J* = 10.9, 1.0 Hz, 1H), 1.36 (s, 12H). ¹³C NMR (126 MHz, CDCl₃) δ 140.2, 136.9, 135.0, 125.5, 114.9, 83.8, 24.9. ¹¹B NMR (160 MHz, CDCl₃) δ 30.6 (brs).

The spectral data were in accordance with literature.⁹ HRMS (EI+) m/z 231.1546 [(M+H)⁺ calcd for C₁₄H₂₀BO₂ 231.1556].

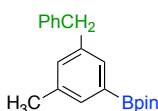
Compound 48



48

The general cross-coupling procedure was carried out on 0.34 mmol of **23** at 65 °C for 16 h. After purification 0.065 g of compound **48** was isolated as a yellow solid (mp 76–78 °C) in 74% yield. ¹H NMR (300 MHz, CDCl₃) δ 7.44 (s, 1H), 7.36 (s, 1H), 6.99 (s, 1H), 2.33 (s, 3H), 1.97–1.84 (m, 1H), 1.35 (s, 12H), 0.98–0.88 (m, 2H), 0.77–0.68 (m, 2H). ¹³C NMR (75 MHz, CDCl₃) δ 143.3, 137.2, 132.7, 129.6, 129.4, 83.8, 25.0, 21.3, 15.3, 9.0. ¹¹B NMR (128 MHz, CDCl₃) δ 30.7 (brs). HRMS (ESI+) m/z 281.1678 [(M+Na)⁺ calcd for C₁₆H₂₃BO₂Na 281.1683].

Compound 49



49

The general cross-coupling procedure was carried out on 0.34 mmol of **23** at 65 °C for 16 h. After purification 0.074 g of compound **49** was isolated as a white solid (mp 116–119 °C) in 71% yield. ¹H NMR (300 MHz, CDCl₃) δ 7.53–7.46 (m, 2H), 7.31–7.23 (m, 2H), 7.21–7.14 (m, 3H), 7.08 (s, 1H), 3.95 (s, 2H), 2.30 (s, 3H), 1.34 (s, 12H). ¹³C NMR (75 MHz, CDCl₃) δ 141.6, 140.5, 137.6, 133.5, 133.0, 132.6, 129.0, 128.5, 126.1, 83.9, 42.0,

25.0, 21.3. ^{11}B NMR (128 MHz, CDCl_3) δ 30.7 (brs). HRMS (ESI+) m/z 309.2035 [(M+H) $^+$ calcd for $\text{C}_{20}\text{H}_{26}\text{BO}_2$ 309.2020].

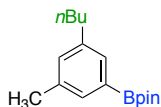
Compound 50



50

The general cross-coupling procedure was carried out on 0.34 mmol of **23** at 65 °C for 16 h. After purification 0.048 g of compound **50** was isolated as a white solid (mp 91–93 °C, lit¹⁰ 90–91 °C) in 62 % yield. ^1H NMR (300 MHz, CDCl_3) δ 7.46 (s, 2H), 7.12 (s, 1H), 2.34 (s, 6H), 1.36 (s, 12H). ^{13}C NMR (75 MHz, CDCl_3) δ 137.3, 133.1, 132.5, 83.8, 25.0, 21.3. ^{11}B NMR (128 MHz, CDCl_3) δ 31.1 (brs). The spectral data were in accordance with those reported in the literature.¹⁰ HRMS (ESI+) m/z 233.1715 [(M+H) $^+$ calcd for $\text{C}_{14}\text{H}_{22}\text{BO}_2$ 233.1707].

Compound 51

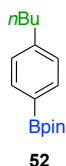


51

The general cross-coupling procedure was carried out on 0.34 mmol of **23** at 65 °C for 16 h. After purification 0.052 g of compound **51** was isolated as a yellow oil in 56% yield. ^1H NMR (300 MHz, CDCl_3) δ 7.46 (s, 1H), 7.44 (s, 1H), 7.10 (s, 1H), 2.62–2.54 (m, 2H), 2.33 (s, 3H), 1.66–1.53 (m, 2H), 1.43–1.36 (m, 2H), 1.35 (s, 12H), 0.92 (t, $J = 7.3$ Hz, 3H). ^{13}C NMR (75 MHz, CDCl_3) δ 142.4, 137.2, 132.9, 132.5, 132.0, 83.8, 35.7, 34.0,

25.0, 22.7, 21.3, 14.1. ^{11}B NMR (128 MHz, CDCl_3) δ 31.0 (brs). HRMS (ESI+) m/z 275.2168 [(M+H) $^+$ calcd for $\text{C}_{17}\text{H}_{28}\text{BO}_2$ 275.2176].

Compound 52



The general cross-coupling procedure was carried out on 1.0 mmol of 2-(4-bromophenyl)-4,4,5,5-tetramethyl-1,3,2-dioxaborolane (**30**) at 65 °C for 16 h. After purification by SiO_2 chromatography (9:1 hexane/ethyl acetate) 0.215 g of compound **52** was isolated as a colorless oil in 83% yield. ^1H NMR (500 MHz, CDCl_3) δ 7.75 (d, $J = 7.9$ Hz, 2H), 7.21 (d, $J = 7.8$ Hz, 2H), 2.64 (t, $J = 8.0$ Hz, 2H), 1.67–1.55 (m, 2H), 1.37 (m, 2H), 1.35 (s, 12H), 0.93 (t, $J = 7.4$ Hz, 3H). ^{13}C NMR (126 MHz, CDCl_3) δ 146.4, 134.8, 127.9, 83.6, 35.9, 33.5, 24.9, 22.4, 13.9. ^{11}B NMR (160 MHz, CDCl_3) δ 30.8 (brs). The spectral data were in accordance with those reported in the literature. 11 HRMS (EI+) m/z 261.1986 [(M+H) $^+$ calcd for $\text{C}_{16}\text{H}_{26}\text{BO}_2$ 261.2025].

REFERENCES

REFERENCES

- (1) Mkhaliid, I. A. I.; Barnard, J. H.; Marder, T. B.; Murphy, J. M.; Hartwig, J. F. C-H Activation for the Construction of C-B Bonds. *Chem. Rev.* **2010**, *110*, 890–931.
- (2) Maleczka, R. E., Jr.; Smith, M. R., III. Remarkably Selective Iridium Catalysts for the Elaboration of Aromatic C–H Bonds. *Science* **2002**, *295*.
- (3) Holmes, D.; Chotana, G. A.; Maleczka, R. E., Jr; Smith, M. R., 3rd. One-Pot Borylation/amination Reactions: Syntheses of Arylamine Boronate Esters from Halogenated Arenes. *Org. Lett.* **2006**, *8*, 1407–1410.
- (4) Kalvet, I.; Sperger, T.; Scattolin, T.; Magnin, G.; Schoenebeck, F. Palladium(I) Dimer Enabled Extremely Rapid and Chemoselective Alkylation of Aryl Bromides over Triflates and Chlorides in Air. *Angew. Chem. Int. Ed Engl.* **2017**, *129*, 7184–7188.
- (5) Dai, C.; Fu, G. C. The First General Method for Palladium-Catalyzed Negishi Cross-Coupling of Aryl and Vinyl Chlorides: Use of Commercially Available Pd(P(t-Bu)(3))(2) as a Catalyst. *J. Am. Chem. Soc.* **2001**, *123*, 2719–2724.
- (6) Joshi-Pangu, A.; Ganesh, M.; Biscoe, M. R. Nickel-Catalyzed Negishi Cross-Coupling Reactions of Secondary Alkylzinc Halides and Aryl Iodides. *Org. Lett.* **2011**, *13*, 1218–1221.
- (7) Çalimsiz, S.; Sayah, M.; Mallik, D.; Organ, M. G. Pd-PEPPSI-IPent: Low-Temperature Negishi Cross-Coupling for the Preparation of Highly Functionalized, Tetra-Ortho-Substituted Biaryls. *Angew. Chem. Int. Ed.* **2010**, *49*, 2014–2017.
- (8) Manickam, G.; Dieter Schlüter, A. New Parts for a Construction Set of Bifunctional Oligo(het)arylene Building Blocks for Modular Chemistry. *Synthesis* **2000**, *2000*, 442–446.
- (9) Hua, X.; Masson-Makdissi, J.; Sullivan, R. J.; Newman, S. G. Inherent vs Apparent Chemoselectivity in the Kumada-Corriu Cross-Coupling Reaction. *Org. Lett.* **2016**.
- (10) Vara, B. A.; Jouffroy, M.; Molander, G. A. C(sp³)-C(sp²) Cross-Coupling of Alkylsilicates with Borylated Aryl Bromides - an Iterative Platform to Alkylated Aryl-

and Heteroaryl Boronates. *Chem. Sci.* **2017**, *8*, 530–535.

- (11) Yamashita, Y.; Tellis, J. C.; Molander, G. A. Protecting Group-Free, Selective Cross-Coupling of Alkyltrifluoroborates with Borylated Aryl Bromides via Photoredox/nickel Dual Catalysis. *Proc. Natl. Acad. Sci. U. S. A.* **2015**, *112*, 12026–12029.
- (12) Seath, C. P.; Fyfe, J. W. B.; Molloy, J. J.; Watson, A. J. B. Tandem Chemoselective Suzuki-Miyaura Cross-Coupling Enabled by Nucleophile Speciation Control. *Angew. Chem. Int. Ed Engl.* **2015**, *54*, 9976–9979.
- (13) Fyfe, J. W. B.; Seath, C. P.; Watson, A. J. B. Chemoselective Boronic Ester Synthesis by Controlled Speciation. *Angew. Chem. Int. Ed Engl.* **2014**, *53*, 12077–12080.
- (14) Fyfe, J. W. B.; Valverde, E.; Seath, C. P.; Kennedy, A. R.; Redmond, J. M.; Anderson, N. A.; Watson, A. J. B. Speciation Control during Suzuki-Miyaura Cross-Coupling of Haloaryl and Haloalkenyl MIDA Boronic Esters. *Chemistry* **2015**, *21*, 8951–8964.
- (15) Molloy, J. J.; Law, R. P.; Fyfe, J. W. B.; Seath, C. P.; Hirst, D. J.; Watson, A. J. B. A Modular Synthesis of Functionalised Phenols Enabled by Controlled Boron Speciation. *Org. Biomol. Chem.* **2015**, *13*, 3093–3102.
- (16) Woerly, E. M.; Roy, J.; Burke, M. D. Synthesis of Most Polyene Natural Product Motifs Using Just 12 Building Blocks and One Coupling Reaction. *Nat. Chem.* **2014**, *6*, 484–491.
- (17) Noguchi, H.; Hojo, K.; Suginome, M. Boron-Masking Strategy for the Selective Synthesis of Oligoarenes via Iterative Suzuki-Miyaura Coupling. *J. Am. Chem. Soc.* **2007**, *129*, 758–759.
- (18) Noguchi, H.; Shioda, T.; Chou, C.-M.; Suginome, M. Differentially Protected Benzenediboronic Acids: Divalent Cross-Coupling Modules for the Efficient Synthesis of Boron-Substituted Oligoarenes. *Org. Lett.* **2008**, *10*, 377–380.
- (19) Li, J.; Ballmer, S. G.; Gillis, E. P.; Fujii, S.; Schmidt, M. J.; Palazzolo, A. M. E.; Lehmann, J. W.; Morehouse, G. F.; Burke, M. D. Synthesis of Many Different Types of Organic Small Molecules Using One Automated Process. *Science* **2015**, *347*, 1221–1226.

- (20) Takami, K.; Yorimitsu, H.; Shinokubo, H.; Matsubara, S.; Oshima, K. Palladium-Catalyzed Cross-Coupling Reaction of Organoindiums with Aryl Halides in Aqueous Media. *Org. Lett.* **2001**, *3*, 1997–1999.
- (21) Pérez, I.; Sestelo, J. P.; Sarandeses, L. A. Atom-Efficient Metal-Catalyzed Cross-Coupling Reaction of Indium Organometallics with Organic Electrophiles. *J. Am. Chem. Soc.* **2001**, *123*, 4155–4160.
- (22) Pena, M. A.; Sestelo, J. P.; Sarandeses, L. A. Palladium-Catalyzed Aryl-Aryl Cross-Coupling Reaction Using Ortho-Substituted Arylindium Reagents. *J. Org. Chem.* **2007**, *72*, 1271–1275.
- (23) Font-Sanchis, E.; Céspedes-Guirao, F. J.; Sastre-Santos, A.; Fernandez-Lazaro, F. Indium-Mediated Synthesis of Heterobiaryls. *J. Org. Chem.* **2007**, *72*, 3589–3591.
- (24) Jana, R.; Pathak, T. P.; Sigman, M. S. Advances in Transition Metal (Pd, Ni, Fe)-Catalyzed Cross-Coupling Reactions Using Alkyl-Organometallics as Reaction Partners. *Chem. Rev.* **2011**, *111*, 1417–1492.
- (25) Shen, Z.-L.; Wang, S.-Y.; Chok, Y.-K.; Xu, Y.-H.; Loh, T.-P. Organoindium Reagents: The Preparation and Application in Organic Synthesis. *Chem. Rev.* **2013**, *113*, 271–401.
- (26) Zhao, K.; Shen, L.; Shen, Z.-L.; Loh, T.-P. Transition Metal-Catalyzed Cross-Coupling Reactions Using Organoindium Reagents. *Chem. Soc. Rev.* **2017**, *46*, 586–602.
- (27) Maegawa, Y.; Inagaki, S. Iridium–bipyridine Periodic Mesoporous Organosilica Catalyzed Direct C–H Borylation Using a Pinacolborane. *Dalton Trans.* **2015**, *44*, 13007–13016.
- (28) Sadler, S. A.; Tajuddin, H.; Mkhaliid, I. A. I.; Batsanov, A. S.; Albesa-Jove, D.; Cheung, M. S.; Maxwell, A. C.; Shukla, L.; Roberts, B.; Blakemore, D. C.; et al. Iridium-Catalyzed C-H Borylation of Pyridines. *Org. Biomol. Chem.* **2014**, *12*, 7318–7327.
- (29) Mkhaliid, I. A. I.; Coventry, D. N.; Albesa-Jove, D.; Batsanov, A. S.; Howard, J. A. K.; Perutz, R. N.; Marder, T. B. Ir-Catalyzed Borylation of C–H Bonds in N-Containing Heterocycles: Regioselectivity in the Synthesis of Heteroaryl Boronate Esters. *Angew.*

Chem. Int. Ed. **2006**, *45*, 489–491.

- (30) Jayasundara, C. R. K.; Unold, J. M.; Oppenheimer, J.; Smith, M. R., 3rd; Maleczka, R. E., Jr. A Catalytic Borylation/dehalogenation Route to O-Fluoro Arylboronates. *Org. Lett.* **2014**, *16*, 6072–6075.

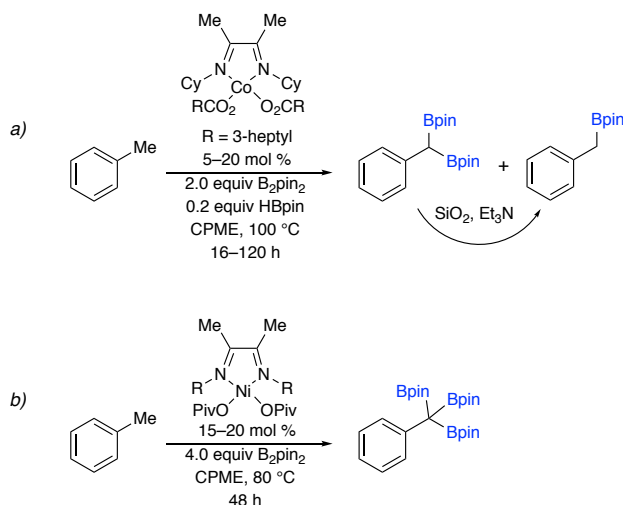
Chapter 4. Cobalt-Catalyzed C–H Borylations

4.1 C(sp³)-H borylations

Aryl/alkyl boronic acids and their derivatives find widespread utility as intermediates in organic synthesis. However, while borylations of C(sp²)-H has been well documented, whereas C–H borylations of unactivated C(sp³)-H bonds are still emerging. Pioneering work by the Hartwig group has shown that metal-boryl catalysts based on Re,¹ Rh,^{2–4} and Ru⁵ complexes allow the preparation of primary alkylboronates from alkanes through activation of terminal primary C–H bonds. Recently, a number of research groups have reported C–H borylations of C(sp³)-H bonds in arene systems using precious metals. However, these type of C–H borylations usually require directing groups,^{6–9} highly active substrates,^{10,11} and/or high temperatures.^{5,12} A handful of non-directed methods have been reported for selectively functionalize benzylic C–H bonds.^{13–}

15

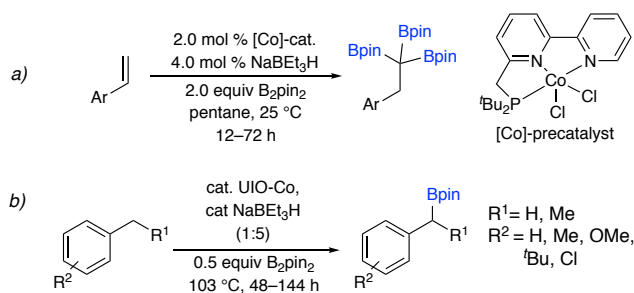
4.2 Cobalt catalyzed non-directed C(sp³)-H borylations



Scheme 27. Polyborylation with a) Cobalt catalyst b) Nickel catalyst

Chirik and co-workers have recently synthesized geminal diboronates and polyboronate compounds, via CHBs of both benzylic and unactivated C(sp³)–H bonds using 5–20 mol % of an air-stable α -diimine cobalt bis(carboxylate) catalyst (Scheme 27 a).¹⁶ They subsequently showed that an α -diimine nickel compounds can catalyze chemoselective triborylation of benzylic C(sp³)–H bonds by B₂pin₂ (Scheme 27b).¹⁷

Huang and co-workers have reported that 1,1,1-tris(boronates) substituted at homobenzylic carbons can be efficiently and selectively prepared from styrenes and B₂pin₂ with Co(I) precatalysts (Scheme 28a).¹⁸ These reactions proceed via Co-catalyzed double dehydrogenative borylation of vinylarenes, and subsequent hydroboration of 1,1-diborylalkene intermediates, with in situ generated HBpin. Benzylic CHBs have also been described by Lin and co-workers using a metal-organic framework (MOF) with catalytically active cobalt nodes (Scheme 28b).¹⁹

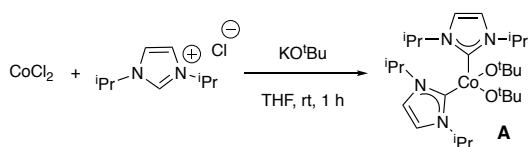


Scheme 28. Polyborylation with a) cobalt catalyst b) MOF

4.3 Synthesis of a new cobalt catalyst

The cobalt catalyzed processes are interesting but it is not widely used method due to lack of functional group tolerance (e.g. Cl, Br, I). Therefore, we decided to build a catalyst system that can overcome these limitations. Choice of Co complex **A** to explore

catalytic CHBs was motivated by Herrmann's Rh and Ir N-heterocyclic carbene complexes that facilitate CHBs of arene C(sp²)-H bonds.²⁰ They synthesized bridged and unbridged N-heterocyclic carbene (NHC) ligands that are metalated with [Ir/Rh(COD)₂Cl]₂ to give rhodium(I/III) and iridium(I) mono- and biscarbene substituted complexes. Given this precedent we wondered if NHC complexes of Co, the lightest Group 9 element, would behave like Herrmann's catalysts. Cobalt complex **A** was synthesized by reacting CoCl₂ with potassium *t*-butoxide and 1,3-diisopropyl-1H-imidazol-3-ium chloride in THF (Scheme 29).



Scheme 29. Synthesis of cobalt complex A

Recrystallization from pentane afforded single crystals suitable for X-ray diffraction studies (Figure 11). There are three broad resonances (41.70, 39.00, 8.76, 2.31 ppm) in the ¹H NMR spectrum (C₆D₆) of **A**. Assignments for the O-*t*-Bu and NHC ligand's methyl protons can be made based on integrations. The lowest intensity resonances (41.70 and 39.00) are due to the NHC ligand's isopropyl methine and imidazolyl ring protons. Application of the Evans method yields an $\text{eff} = 4.20 \text{ B}$ for **A**. Although **A** is air-sensitive, it has remained active for more than one year when stored at -35 °C.

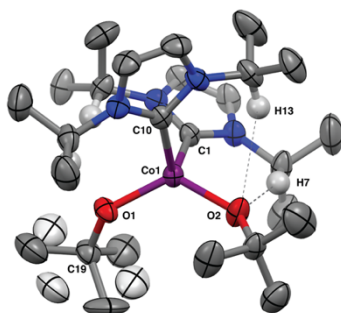


Figure 11. X-ray crystallography of complex A

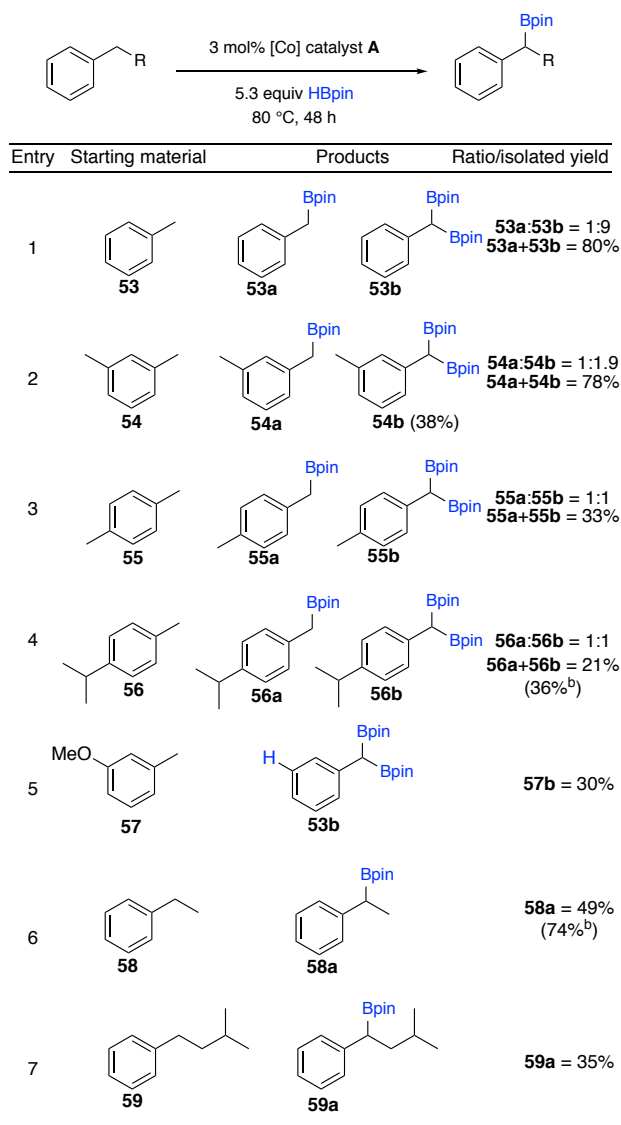
The structure of **A**, shown in Figure 6, reveals a distorted tetrahedral geometry with rotational disorder of the methyl group about the O1–C19 vector in one *O-t*-Bu ligand. The bond angles with Co at the vertex range from 102.6° for ∠O1–Co1–C10 and ∠O2–Co1–C1 to 123.4° for ∠O2–Co1–O1. There are close contacts between the *O-t*-Bu O atoms and the methine H atoms of the NHC isopropyl groups as represented by H13–O2 and H7–O2 distances of 2.698 and 2.112 Å, respectively. The latter O–H distance is typical for structures with O[⋯]H hydrogen bonding. However, the short O[⋯]H distances in **A** could simply be geometric consequences of the sterically most favored orientation of bulky *i*-Pr and *t*-Bu groups.

4.4 Testing cobalt catalyst **A** reactivity

With Co complex **A** in hand, we explored its proclivity for CHBs (Figure 12). A sealed tube reaction of toluene with 2 mol % Co precatalyst **A**, 2.6 equiv HBpin in THF at 80 °C for 48 h gave a 63% conversion (GC) of the starting material to a 2:3 mixture of mono (**53a**) and di (**53b**) benzylic CHB products. When activated with 0.05 equiv HBpin, B₂pin₂ could be used as the boron source, but the conversion was nearly identical to that obtained with HBpin. B₂pin₂ was less practical for isolating diborylated products since

chromatographic separation with silica gel of unreacted B₂pin₂ promotes the protodeboronation of PhCH(Bpin)₂.¹⁶

Figure 12. Cobalt-Catalyzed CHBs^a



^aIsolated yields. ^bBorylation with 20 mol % of **A**.

Since HBpin is a liquid, we explored CHBs in neat HBpin (2.6 equiv). This gave a modest improvement in conversion (70%). Increasing the reaction temperature to 150 °C decreased conversion (52% at 4 h), with no further conversion at longer reaction times.

As depicted in entry 1 of Figure 12, an excellent isolated yield with high selectivity for the PhCH(Bpin)₂ was obtained at 80 °C with 5.3 equiv of HBpin and 3 mol % **A** (97% conversion, mono:di = 1:9). These optimized conditions established an efficiency for Co precatalyst **A** that was on par with Chirik's best conditions for the diborylation of toluene.¹⁶

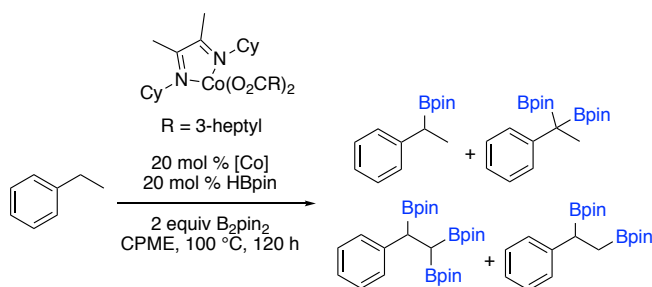
CHBs of *m*-xylene, *p*-xylene, and cymene were examined in neat HBpin (5.3 equiv per arene) with 2 mol % **A**. All three compounds were selectively borylated at their benzylic positions. Nonetheless, there were differences between substrates. *m*-Xylene afforded a 1:1 mixture of the mono (**54a**) and geminally diborylated (**54b**) products (74% conversion). Increasing the HBpin stoichiometry to 6.7 equiv improved conversion and selectivity for **54b** (81% conversion, **54a:54b** = 1:2). The borylated products were isolated as a mixture in 78% yield after workup, and the diborylated (**54b**) material could be separated by column chromatography with recovery of only 38% of **54b** that was present in mixture, presumably due to protodeboronation. Surprisingly, CHB of *p*-xylene with 6.7 equiv of HBpin ceased after 40% conversion, giving 33% isolated yield of a 1:1 mixture of mono (**55a**) to geminally substituted diborylation (**55b**) products. Cymene was the least reactive substrate giving only 33% conversion and 21% isolated yield of the mono (**56a**) and geminally substituted diborylation (**56b**) products in a 1:1 ratio.

Despite *m*-xylene being more reactive than *p*-xylene, the Co precatalyst system appears to be very sensitive to sterics at the benzylic position as indicated by the borylation of methyl vs. isopropyl substituents on cymene. The inert nature of the isopropyl group was studied further through the attempted borylations of isopropylbenzene, as well as 1,3-di- and 1,3,4-trisopropylbenzene. All three compounds

failed to borylate at any position, including the benzylic and C(sp²)-H bonds. Chirik and co-workers showed that the isopropyl methyl groups of cymene (**56**) can be borylated, albeit more slowly than the aryl methyl site.¹⁶ Empirically, the more reactive the substrate, the more likely it undergoes di-borylation.

We tested CHBs of ethylbenzene and isopentylbenzene (entries 6 and 7). Under our standard conditions using 2 mol % **A**, ethylbenzene gave the monoborylated benzyl-Bpin product (**58a**) as the exclusive product, but with a modest 42% conversion. Interestingly, reducing HBpin to 2.6 equiv gave 51% conversion and **58a** was isolated in 49% yield. Increasing the loading of **A** to 20 mol % and HBpin to 3.3 equiv improved the yield of **58a** to 74% (77% conversion). CHB of isopentylbenzene using 2 mol % **A**, and 5.3 equiv of HBpin gave **59a** exclusively (35% isolated yield, 44% conversion).

The ability of solutions of HBpin and **A** to catalyze the selective production of monoborylated **58a** from ethylbenzene stands in contrast to the use of Chirik's Co catalyst and conditions, which in our hands afforded a mixture of polyborylated products (Scheme 30).



Scheme 30. Chirik's cobalt catalyst with ethylbenzene (58)

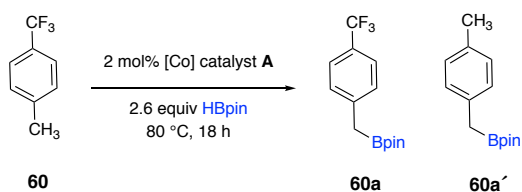
Furthermore, Lin's Co-MOF catalysts gave a 4:1 mixture of benzylic and aryl borylation products. While Ni(cod)₂/Icy-catalyzed (Icy=1,3-bis(cyclohexyl) imidazolium-

2-ylidene) CHBs of arenes (arene:HBpin=9-7.5:1) can generate monoborylated products at primary and secondary benzylic positions, functionalization of C(sp²)-H sites is favored. Monoborylations of toluene and meta-xylene have been reported using the UiO-Co MOF catalysts in Scheme 28b. For these substrates the selectivity for C(sp³)-H borylation is high, but the use of excess arene ([substrate]:[B₂pin₂] ≥ 90) potentially biases selectivities for monoborylation as compared to our chemistry where the arene is the limiting reagent. For substrates with secondary and tertiary C-H bonds, the selectivity for C(sp³)-H vs. C(sp²)-H borylation drops to 4:1 with the UiO-Co MOF catalysts. Entries 6 and 7 of Figure 12 indicate that selective monoborylation for substrates that exhibit poor selectivity with other catalysts is achievable with precatalyst **A**.

We subjected 1-methoxy-3-methylbenzene (entry 5) to the CHB conditions in Figure 12. Unfortunately, the OMe substituent was cleaved giving diborylated toluene **53b** in 30% isolated yield. Chirik saw minor amounts (13%) of C-OMe cleavage with his cobalt catalyst,¹⁶ but methoxy substituents were tolerated in his benzylic borylations catalyzed by (ipcADI)Ni(OPiv)₂ (ipcADI = N,N'-di(-)isopinocampheyl)butane-2,3-diimine).¹⁷ Chatani did observe PhBpin as a byproduct of C-OMe cleavage in Ni(cod)₂/Icy-catalyzed borylations of anisole, where C(sp²)-H borylation predominated to produce a mixture of monoborylated anisoles.²¹

m-Fluorotoluene defluorinated in CHBs with precatalyst **A**, as judged from ¹⁹F-NMR and ¹¹B-NMR. The NMR data pointed to trace amounts of unidentified species where C-B or B-F bond formation had occurred. When 1-methyl-4-(trifluoromethyl)benzene (**60**) was subjected to our standard CHB conditions, only 6% conversion of **60** was observed. GCMS indicated the formation of compound **60a**,

defluorinated **60a'** (**60a**:**60a'** = 5:1), and two additional unidentified compounds both with $m/z = 277$ (Scheme 31). The reduction of C(sp²)-F and C(sp³)-F bonds by precatalyst **A**, contrasts C(sp²)-F compatibility for 5-fluoro-N-methylindole^{5a} and C(sp³)-F compatibility for trifluoromethylbenzene^{5b} in Ni-catalyzed CHBs. It should be noted that C-F bonds were problematic when CHBs of arenes containing C(sp²)-F bonds or CF₃ groups were attempted using Ni(cod)₂/Icy catalysts.²¹ The UiO-Co MOF catalysts tolerate Cl and OMe groups, in contrast to CHBs catalyzed by precatalyst **A**.¹⁹



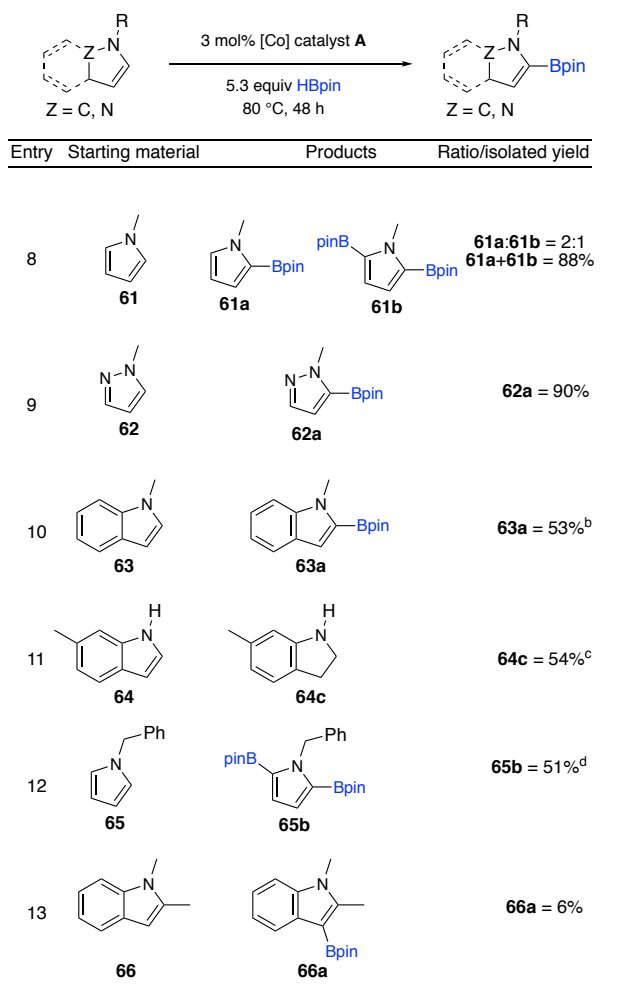
Scheme 31. *m*-Fluorotoluene defluorinated in CHBs

The reaction scope for Co precatalyst **A** can be extended to certain heteroarenes (Figure 13). N-Methylpyrrole was exceptionally reactive and formed the 2-borylated product **61a** and its 2,5-diborylated counterpart, **61b**. Although **61a** is prone to protodeboronation during purification, we managed to obtain a crystal structure of the product, which confirmed the assigned regiochemistry (see experimental section). With HBpin as the limiting reagent, good yields of **61a** have been reported with the Ni(cod)₂/Icy CHB catalyst.²¹

Both N-methylpyrazole and N-methylindole also borylate primarily at the position alpha to the formally sp³ N, affording **62a** and **63a**, respectively. N-Methylpyrazole is efficiently borylated under these conditions giving 5-borylated pyrazole (**62a**) in 90% yield, representing the first CHB of N-methylpyrazole catalyzed by a 3d metal.²² For N-methylindole, minor amounts of diborylated indole and N-methyl-

4,5,6,7-tetrahydro-1H-indole were also detected in addition to **63a**. It is noteworthy that 6-methyl-1H-indole (**64**) itself undergoes C2–C3 hydrogenation under these conditions to give 6-methylindoline (**64c**) as the major product (54% conversion). Quantitative yields of **63a** have been reported for CHBs mediated by the Ni(OAc)₂/Icy precatalyst/ligand combination with N-methylindole being the limiting reagent.²¹

Figure 13. Cobalt-Catalyzed CHBs of Heterocycles^a



^aIsolated yields. ^b88% isolated material with the monoborylated, diborylated, and hydrogenated products present in a 5:2:1 ratio. The monoborylated product was isolated in 53% yield. ^cBased on NMR yield. ^dAfter 48 h another 3 mol % of **A** and 0.4 equiv of HBpin were added and the mixture was heated at 80 °C for 24 h.

To compare C(sp³)-H vs. C(sp²)-H CHB selectivity between arenes and heteroarenes, we examined CHB of N-benzylpyrrole (**65**) with precatalyst A. Exclusive C(sp²)-H CHB occurred at the 2-position. The general borylation conditions with 6.7 equiv of HBpin gave 95% conversion, affording a mixture of mono and diborylated products (mono:di = 1.3:1). After 48 h, more precatalyst A (3 mol %) and HBpin (2.7 equiv) were added to the reaction mixture, which was heated at 80 °C for an additional 24 h. Compound **65b** was isolated as a white solid in 51% yield (X-ray crystal structure CCDC 1576846).

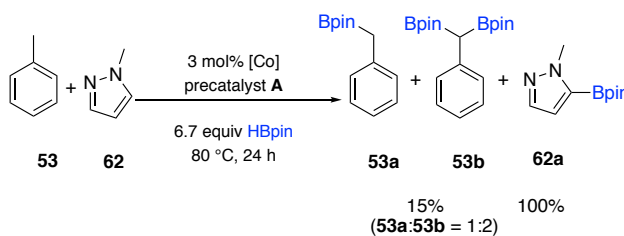
To test whether alkyl groups attached to heteroarenes are similarly disposed towards C(sp³)-H CHBs with precatalyst A like arenes are, we subjected indole **66** to identical borylation conditions using precatalyst A. Since the 2-position of indole preferentially borylates with Ir and other Co CHB catalysts, we selected a 2-methyl substrate to favor C(sp³)-H CHB. Only 9% of **66** was converted (based on NMR) with borylation exclusively at the 3-position affording **66a**.

As with arenes, Co precatalyst A appears to be narrowly tuned to certain classes of heterocycles. Thiophenes, pyridines and their benzo-fused derivatives were not borylated under these conditions. When borylation of equimolar amounts of m-xylene and 2-methylthiophene was attempted under standard conditions no reaction proceeded presumably due to poisoning of the Co precatalyst by thiophenes.

4.5 C(sp²)-H of heteroarenes vs. C(sp²)-H and C(sp³)-H bonds of alkylated arenes

To investigate how fast CHB of C(sp²)-H of heteroarenes vs. C(sp²)-H and C(sp³)-H bonds of alkylated arenes, the CHB of a toluene/N-methylpyrazole mixture was performed (Scheme 32). The preference for C(sp²)-H CHB at C5 of N-methylpyrazole

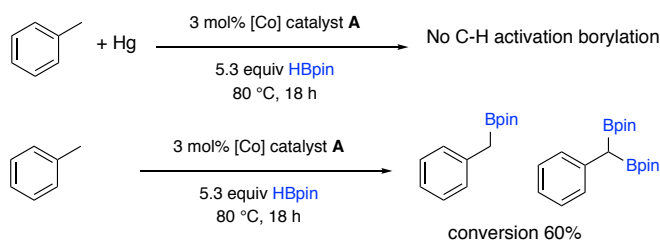
further validates that CHBs of heterocycle C(sp²)-H bonds with precatalyst **A** are favored over C(sp³)-H CHBs of alkyl groups in substituted arenes and heteroarenes.



Scheme 32. CHB of Toluene vs N-Methylpyrazole

4.6 Identifying the active catalyst species

The identity of the catalytically active species is presently unknown. The addition of one drop of mercury to a borylation reaction completely inhibited the reaction (Scheme 33). This likely indicates that the true catalysts generated from **A** are heterogeneous.²³ Notably, similar mercury poisoning has been reported for CHBs catalyzed by species generated from combinations of *N*-heterocyclic carbene ligands and Ni precatalysts.²¹



Scheme 33. Hg test

When HBpin is added to solutions of **A**, the chemical shifts for the paramagnetically shifted proton resonances assigned to **A** remain constant, but the intensities for decrease and vanish when $[\text{HBpin}]_0 \sim 3 [\text{A}]_0$ (Figure 14).

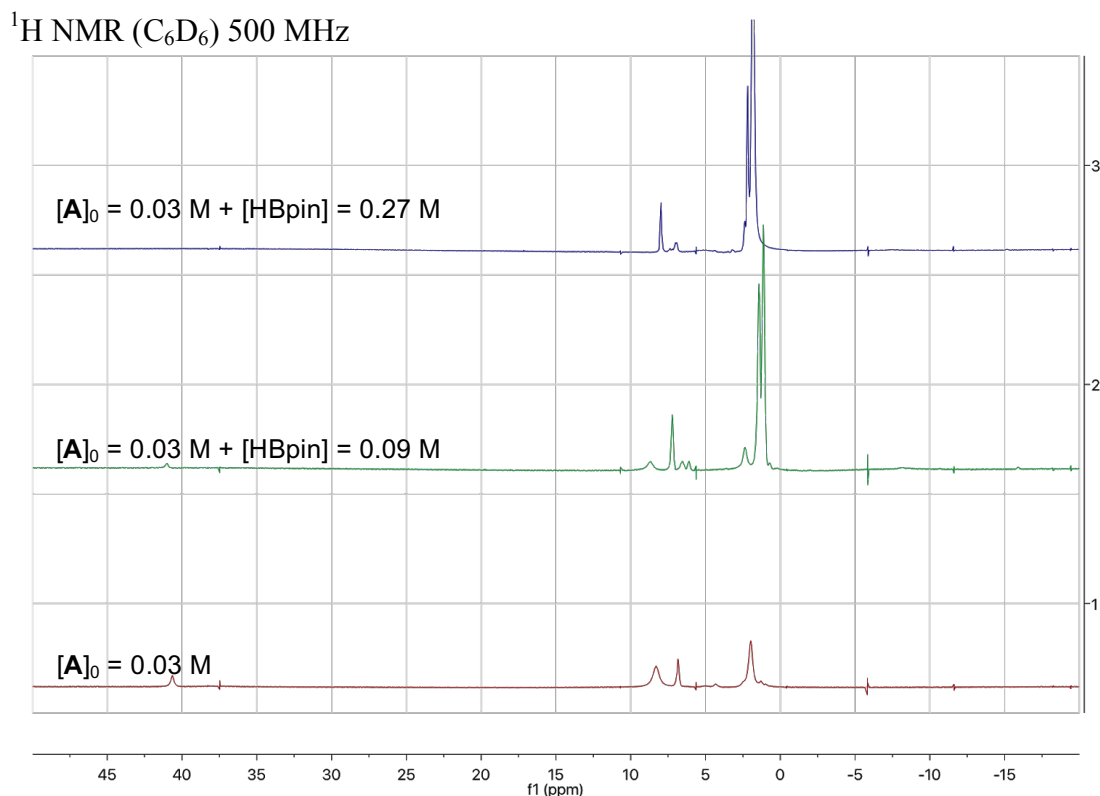


Figure 14. ¹H NMR of complex A as HBpin concentration increases

The ¹¹B NMR spectra initially show one sharp resonance at δ 22.5. The chemical shift and line width are virtually identical to those reported for *t*-BuOBpin. When $[\text{HBpin}]_0 > 3 [\text{A}]_0$, a broader resonance appears at δ 29.5, which is close to the chemical shift for HBpin (¹¹B{¹H} NMR, C₆D₆, δ 28.5, ¹J_{H-B} = 179 Hz). In the ¹¹B NMR spectrum when $[\text{A}]_0 = 0.03$ M and $[\text{HBpin}]_0 = 0.27$ M, the full width at half maximum (FWHM) is 450 Hz for the resonance at δ 29.5 (Figure 15).

^{11}B NMR (C_6D_6) 165 MHz

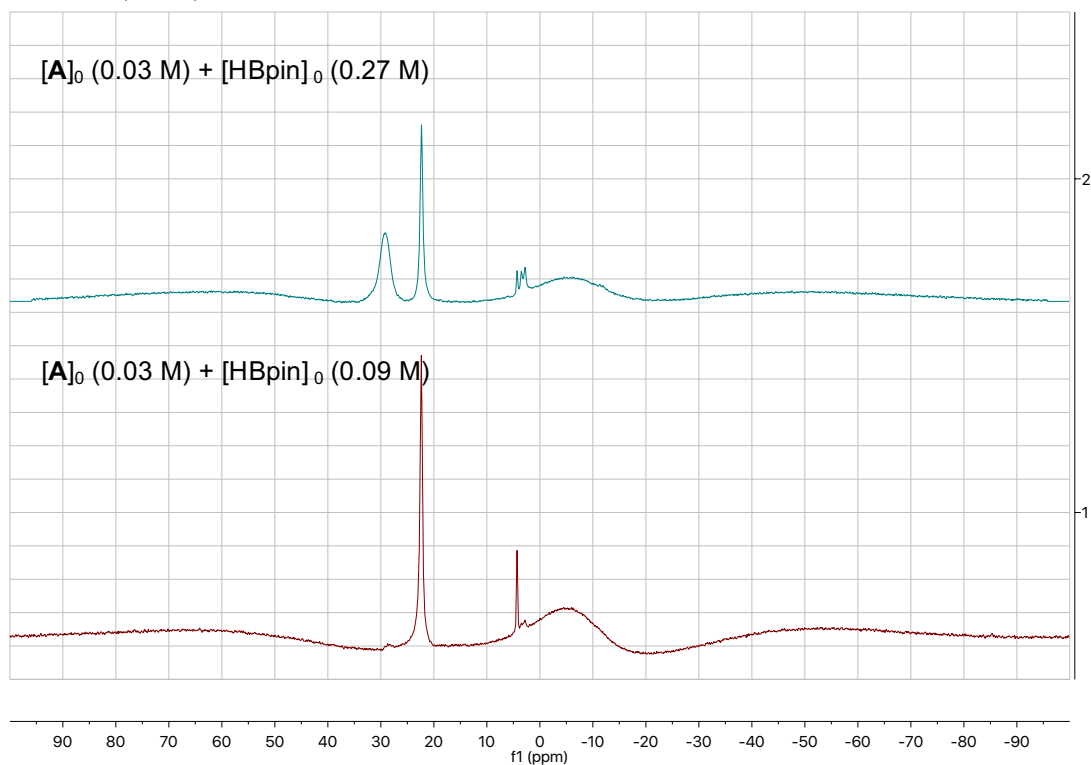


Figure 15. ^{11}B NMR of complex A as HBpin concentration increases

The broadening and 1.1 ppm upfield shift for the HBpin ^{11}B resonances is due to interaction of HBpin with unidentified paramagnetic or diamagnetic species. For $[\text{A}]_0 = 0.03 \text{ M}$, $[\text{HBpin}]_0 = 0.27 \text{ M}$, resonances for precatalyst **A** are undetected in ^1H NMR spectra, and no other ^{11}B resonances are observed, aside from those noted above. Thus, **A** is converted to unidentified species before catalysis ensues.

Coupled: Line width at half maximum for 29.5 ppm is 449.77 Hz and for 22.5 ppm is 91.84 Hz (Figure 16)

Decoupled: Line width at half maximum for 29.5 ppm is 297.71 Hz and for 22.5 ppm is 92.26 H (Figure 16)

^{11}B NMR (C_6D_6) 165 MHz

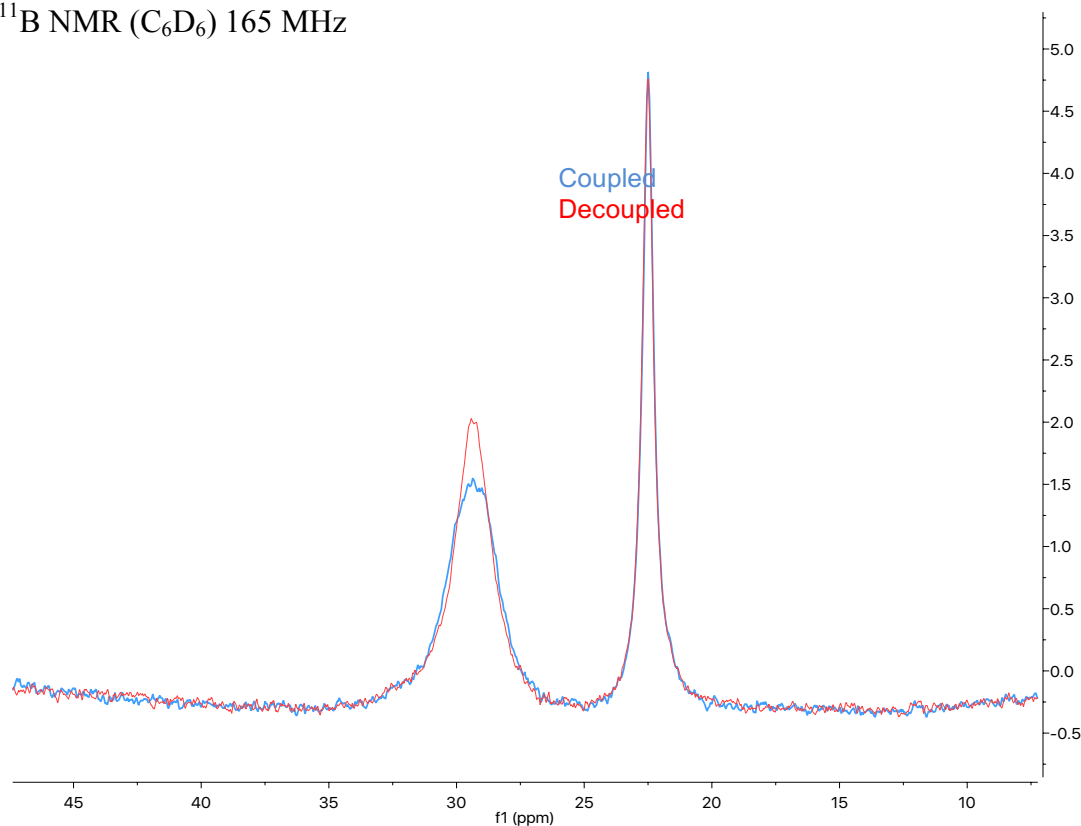


Figure 16. ^{11}B NMR of complex A at coupled and decoupled

4.7 Conclusions

Co compound **A** is the first 3d transition metal precatalyst that can monoborylate primary and secondary benzylic C–H bonds with high selectivity. Compound **A** is also the first Co precatalyst capable of borylating both $\text{C}(\text{sp}^3)\text{--H}$ bonds of alkyl benzenes and $\text{C}(\text{sp}^2)\text{--H}$ bonds in heterocycles. For diborylations, Co precatalyst **A** is generally more selective for the geminally diborylated products than previously described Co catalysts. Like $\text{Ni}(\text{cod})_2/\text{Icy}$ -catalyzed CHBs, catalysis with compound **A** is completely inhibited by adding elemental Hg.

4.8 Experimental

General Procedures

In a nitrogen-filled glovebox, a 5 mL vial was charged with cobalt complex A (15.3 mg, 0.03 mmol, 3 mol %) followed by addition of HBpin (0.8 mL, 5.3 mmol). The reaction mixture was stirred at room temperature until its color changed from purple to brown (~5 min). Next, the substrate (1 mmol) was then introduced by syringe. The vial was capped, taken out of the glovebox, and placed in an oil bath that was preheated to 80 °C. The reaction was allowed to proceed at this temperature for 48 h. At that time, the mixture was cooled to room temperature and analyzed by GC and NMR. The crude mixture was transferred into a 20 mL vial, and any excess HBpin was removed by rotary evaporation. A black-blue residue was obtained. To that residue was added deionized water, and the resultant mixture was stirred until the black-blue color had disappeared. The aqueous layer was extracted with dichloromethane (2 × 5 mL). The combined organics were dried over MgSO₄, concentrated, and passed through a short silica plug with hexane or hexane/EtOAc (9/1) as eluent. This plug step removed boronate byproducts from the reaction mixture.

Hg Test

In a nitrogen-filled glovebox, a 5 mL vial was charged with cobalt complex A (15.3 mg, 0.03 mmol, 3 mol %) followed by addition of HBpin (0.8 mL, 5.3 mmol). The reaction mixture was stirred at room temperature until its color changed from purple to brown (~5 min). Next, toluene (1 mmol) was introduced. Finally, 1 drop of Hg was placed in the vial (dark brown reaction mixture) (Scheme 33). The vial was capped, taken

out of the glovebox, and placed in an oil bath that was preheated to 80 °C. The reaction was allowed to proceed at this temperature for 18 h. A transparent (green in color) reaction mixture was observed after 18 h. ¹H NMR confirmed no CHB (Figure 17).



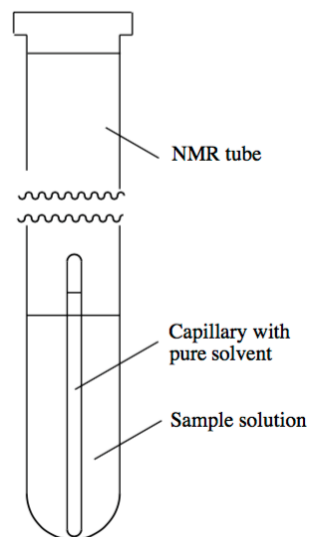
Figure 17. Color difference after 18 h: (Right) with Hg, (Left) without Hg

Preparation of Precatalyst A

Inside a nitrogen-filled glovebox, an oven-dried flask was charged with CoCl₂ (344 mg, 2.65 mmol) and 1,3-diisopropyl-1H-imidazol-3-ium chloride (1.010 g, 5.3 mmol). THF (16 mL) was added followed by addition of KO^tBu (1.19 g, 10.6 mmol) in one portion. The resulting mixture was stirred inside the glovebox for 1 h. Then, solvent was removed under vacuum. The residue was suspended in toluene and filtered through a pad of Celite. The filtrate was collected, and solvent was removed under vacuum, providing a dark purple crystalline material that was dried under vacuum. Recrystallization from pentane at -35 °C afforded 1.140 g (84%) of crystalline complex **A** (mp 165 °C dec). Single crystals suitable for X-ray diffraction studies were selected from the recrystallization, and such analysis confirmed the structure. ¹H NMR (500 MHz, C₆D₆, ppm): δ 41.70 (s, 4 H), 39.00 (br s, 4 H), 8.76 (br s, 18 H), 2.31 (br s, 24 H). Complex **A** is stable on storage in the glovebox at -35 °C but quickly decomposes on exposure to ambient atmospheric conditions.

Calculating magnetic moment

A 2% (0.0094M) standard solution of hexamethyldisiloxane in benzene- d_6 was prepared. This solution was added into a capillary and the capillary was sealed. Inside a glove box, pre-catalyst **A** (15.3 mg, 0.03 mmol) was dissolved in 1.00 mL of the standard solution and then transferred to an NMR tube. The sealed capillary was then inserted into the tube containing the sample solution and the ^1H NMR spectrum was acquired. The difference between the two hexamethyldisiloxane signals was measured (in Hz).



The experimental $\Delta\nu$ value was 453.5 Hz. Using this value, the magnetic susceptibility (χ_m) was determined using equation 1, where ν is the proton frequency for the spectrometer (500 MHz) and $[C]$ is the concentration of the precatalyst in the standard solution (0.03 M). The effective magnetic moment (μ_{eff}) was then determined using equation 2, at $T = 294.2$ K. This yielded an experimental magnetic moment of 4.20 μB ., which is slightly higher than the theoretical spin-only magnetic moment of 3.88 μB for a pseudotetrahedral d^7 , high-spin configuration.²⁴ The effective magnetic moment for precatalyst **A** calculated by the Evans method is 4.29 μB .

$$\chi_m = \frac{3000\Delta\nu}{4\pi\nu[C]} - \chi_{dia} = \frac{3000(453.5)}{4\pi(500)[0.03]} - (-268.7 \times 10^{-6})$$

$$= 7483.4 \times 10^{-6} \text{M}^{-1}$$

$$\mu_{\text{eff}} = 2.828\sqrt{\chi_m T} = 2.828\sqrt{7214.7 \times 10^{-6} \text{M}^{-1}(294.2)} = 4.20 \mu\text{B}$$

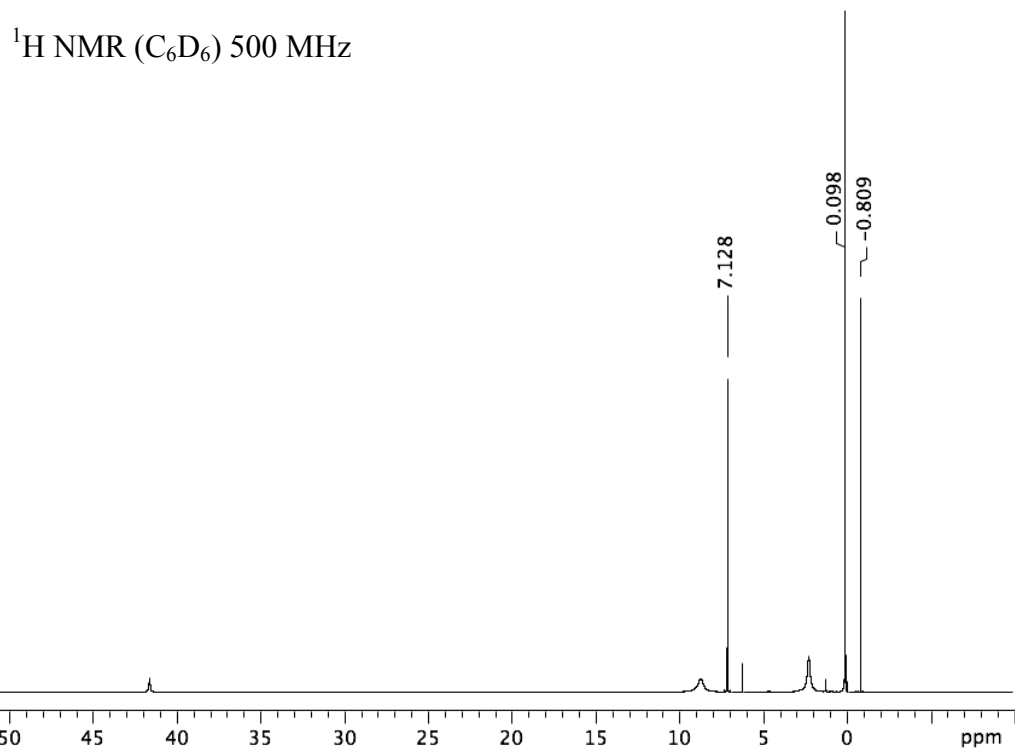


Figure 18. Spectra for Evans method calculations

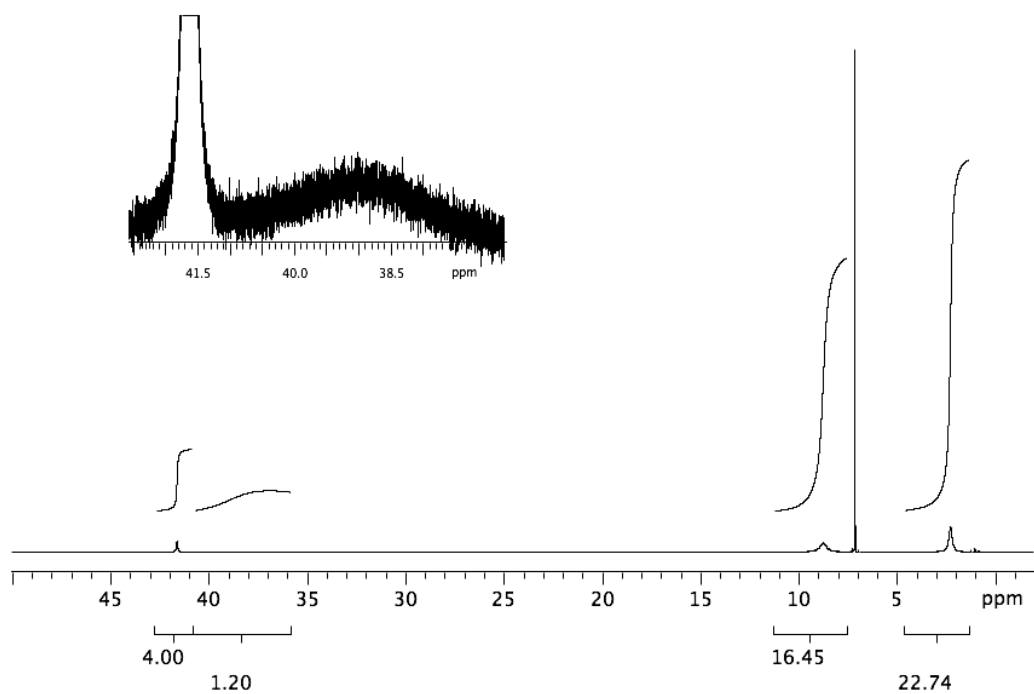
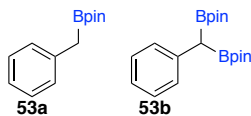


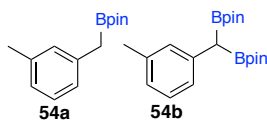
Figure 19. ^1H NMR of complex A in C_6D_6

Compound 53a & 53b



The general borylation procedure was carried out on toluene to afford 0.265 g of the products as a white solid (**53a**:**53b** = 1:9) in 80% yield. For **53b**: ^1H NMR (500 MHz, CDCl_3 , ppm) δ 7.27 (d, $J = 6.5$ Hz, 2 H), 7.22 (t, $J = 7.5$ Hz, 2 H), 7.08 (t, $J = 7.0$ Hz, 1 H), 2.30 (s, 1 H), 1.23 (s, 12 H), 1.21 (s, 12 H). ^{13}C NMR (125 MHz, CDCl_3 , ppm) δ 139.49, 129.13, 127.92, 124.15, 83.34, 24.68, 24.59. ^{11}B NMR (160 MHz, CDCl_3 , ppm) δ 33.3.¹⁶

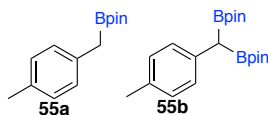
Compound 54a & 54b



The general borylation procedure was carried out on *m*-xylene using 1.0 mL HBpin (6.7 equiv). This modified procedure afforded 0.248 g of the products (**54a**:**54b** = 1:1.9) in 78% yield. SiO_2 column chromatography, eluting with hexane/EtOAc (5:1) afforded 0.136 g of the diborylated product (**54b**) as a white sticky solid in 38% yield. ^1H NMR (500 MHz, CDCl_3 , ppm) δ 7.13–7.09 (m, 2 H), 7.05 (s, 1 H), 6.89 (d, $J = 6.5$ Hz, 1 H), 2.29 (s, 3 H), 2.26 (s, 1 H), 1.23 (s, 12 H), 1.22 (s, 12 H). ^{13}C NMR (125 MHz, CDCl_3 , ppm) δ 139.26, 137.26, 129.94, 127.78, 126.23, 125.01, 83.30, 24.69, 24.60. ^{11}B NMR (160 MHz, CDCl_3 , ppm) δ 32.9. For **54a**: ^1H NMR (500 MHz, CDCl_3 , ppm) δ 7.13 (t, $J = 7.5$ Hz, 1 H), 7.00 (s, 1 H), 6.98 (s, 1 H), 6.94 (d, $J = 7.5$ Hz, 1 H), 2.31 (s, 3 H),

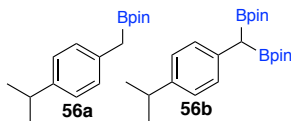
2.26 (s, 2 H), 1.24 (s, 12 H). ^{13}C NMR (125 MHz, CDCl_3 , ppm) δ 138.46, 137.72, 129.86, 128.13, 125.96, 125.60, 83.37, 24.72, 21.52. ^{11}B NMR (160 MHz, CDCl_3 , ppm) δ 33.1.

Compound 55a & 55b



The general borylation procedure was carried out on *p*-xylene using 1.0 mL HBpin (6.7 equiv). This modified procedure afforded 0.098 g of the products as an oil (**55a**:**55b** = 1:1) in 33% yield. Diborylated product (**55b**): ^1H NMR (500 MHz, CDCl_3 , ppm) δ 7.15 (d, J = 7.5 Hz, 2 H), 7.02 (d, J = 7.5 Hz, 2 H), 2.28 (s, 3 H), 2.25 (s, 1 H), 1.23–1.22 (overlapping peaks, 24 H). ^{11}B NMR (160 MHz, CDCl_3 , ppm) δ 33.0. Monoborylated product (**55a**): ^1H NMR (500 MHz, CDCl_3 , ppm) δ 7.07 (m, 4 H), 2.29 (s, 3 H), 2.25 (s, 2 H), 1.21 (s, 12 H). 7.07 (m, 4 H), 2.29 (s, 3 H), 2.25 (s, 2 H), 1.21 (s, 12 H).

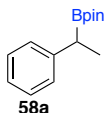
Compound 56a & 56b



The general borylation procedure was carried out on cymene and afforded 0.091 g of the products as an oil mixture (**56a**:**56b** = 1:1) in 21% yield. Monoborylated product (**56a**): ^1H NMR (500 MHz, CDCl_3 , ppm) δ 7.11 (s, 4 H), 2.85 (m, 1 H), 2.27 (s, 2 H), 1.21 (s, 12 H). Diborylated product (**56b**): ^1H NMR (500 MHz, CDCl_3 , ppm) δ 7.19 (d, J

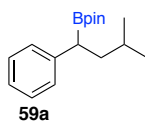
= 8.5 Hz, 2 H), 7.07 (d, $J = 8.5$ Hz, 2 H), 2.85 (m, 1 H), 2.29 (s, 1 H), 1.24 (s, 12 H), 1.23 (s, 12 H).

Compound 58a



The general borylation procedure was carried out on ethylbenzene with 2 mol % Co precatalyst (10.2 mg, 0.02 mmol) and HBpin (0.4 mL, 2.6 mmol). This modified procedure afforded 0.106 g of the product was isolated as colorless oil in 49% yield. ¹H NMR (500 MHz, CDCl₃, ppm) δ 7.27–7.21 (m, 4 H), 7.14–7.12 (m, 1 H), 2.43 (q, $J = 7.5$ Hz, 1 H), 1.33 (d, $J = 7.5$ Hz, 3 H), 1.21 (s, 6 H), 1.20 (s, 6 H). ¹³C NMR (125 MHz, CDCl₃, ppm) δ 144.95, 128.29, 127.78, 125.08, 83.27, 24.62, 24.58, 17.06. ¹¹B NMR (160 MHz, CDCl₃, ppm) δ 33.3.

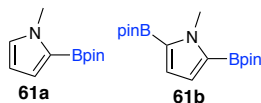
Compound 59a



The general borylation procedure was carried out on isopentylbenzene with 2 mol % Co precatalyst (10.2 mg, 0.02 mmol). After workup 0.097 g of the product were isolated as a colorless oil in 35% yield. ¹H NMR (500 MHz, CDCl₃, ppm) δ 7.27–7.21 (m, 4 H), 7.14–7.12 (m, 1 H), 2.43 (t, $J = 8.0$ Hz, 1 H), 1.72–1.58 (m, 2 H), 1.52–1.45 (m, 1 H), 1.20 (s, 6 H), 1.18 (s, 6 H), 0.90 (d, $J = 7.0$ Hz, 3 H), 0.88 (d, $J = 6.5$ Hz, 3 H). ¹³C

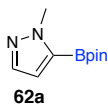
NMR (125 MHz, CDCl₃, ppm) δ 143.45, 128.34, 128.23, 125.02, 83.19, 41.46, 29.72 (C–B), 26.87, 24.57, 22.99, 22.17. ¹¹B NMR (160 MHz, CDCl₃, ppm) δ 33.2.

Compound 61a & 61b



The general borylation procedure was carried out on *N*-methylpyrrole with 2 mol % Co precatalyst (10.2 mg, 0.02 mmol). This modified procedure afforded 0.211 g of the products as a solid mixture (**61a**:**61b** = 2:1) in 88% yield. 2-Borylated *N*-methylpyrrole is not stable and deboronates back to starting material. Monoborylated product (**61a**): ¹H NMR (500 MHz, CDCl₃, ppm) δ 6.81–6.80 (m, 2 H), 6.15 (dd, *J* = 2.5, 3.5 Hz, 1 H), 3.85 (s, 3 H), 1.27 (s, 12 H). ¹³C NMR (125 MHz, CDCl₃, ppm) δ 128.2, 121.8, 108.3, 83.0, 36.6, 24.8. ¹¹B NMR (160 MHz, CDCl₃, ppm) δ 28.9. Diborylated product (**61b**): ¹H NMR (500 MHz, CDCl₃, ppm) δ 6.77 (s, 2 H), 4.01 (s, 3 H), 1.30 (s, 24 H). ¹³C NMR (125 MHz, CDCl₃, ppm) δ 121.6, 108.1, 83.1, 24.5. ¹¹B NMR (160 MHz, CDCl₃, ppm) δ 28.9.

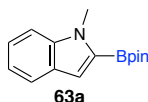
Compound 62a



The general borylation procedure was carried out on *N*-methylpyrazole with 2 mol % Co precatalyst (10.2 mg, 0.02 mmol). This modified procedure afforded 0.185 g of **62a** as white solid (mp = 59–60 °C; lit. 74–75 °C) in 90% yield. ¹H NMR (500 MHz, CDCl₃,

ppm) δ 7.49 (d, $J = 2.0$ Hz, 1 H), 6.71 (d, $J = 2.0$ Hz, 1 H), 4.09 (s, 3 H), 1.34 (s, 12 H). ^{13}C NMR (125 MHz, CDCl_3 , ppm) δ 138.3, 115.8, 84.1, 39.3, 24.8. ^{11}B NMR (160 MHz, CDCl_3 , ppm) δ 27.7. HRMS (EI+) m/z 209.1452 [(M+H $^+$) calcd for $\text{C}_{10}\text{H}_{18}\text{BN}_2\text{O}_2$ 209.1461].

Compound 63a



The general borylation procedure was carried out on *N*-methylindole and afforded 0.227 g of a mixture of products. SiO_2 column chromatography, eluting with hexane/ CH_2Cl_2 (3:1) afforded 0.133 g of the 2-borylated product was isolated as a white solid (mp = 82–84 °C) in 53% yield. Over time in a refrigerator **63a** developed a brownish color. ^1H NMR (500 MHz, CDCl_3 , ppm) δ 7.65 (d, $J = 8.0$ Hz, 1 H), 7.35 (d, $J = 8.0$ Hz, 1 H), 7.28–7.25 (m, 1 H), 7.13 (s, 1 H), 7.09 (t, $J = 7.5$ Hz, 1 H), 3.98 (s, 3 H), 1.37 (s, 12 H). ^{13}C NMR (125 MHz, CDCl_3 , ppm) δ 140.1, 127.8, 123.2, 121.6, 119.3, 114.2, 109.7, 83.7, 32.2, 24.8. ^{11}B NMR (160 MHz, CDCl_3 , ppm) δ 28.4. HRMS (EI+) m/z 258.1662 [(M+H $^+$) calcd for $\text{C}_{15}\text{H}_{21}\text{BNO}_2$ 258.1665].

Compound 65b



The general borylation procedure was carried out on 1-benzyl-1*H*-pyrrole and after 48 h another 3 mol % Co precatalyst and HBpin (0.4 mL) was added and heated at 80 °C for

another 48 h. This modified procedure afforded 0.207 g of the product as white solid (mp = 107–108 °C) in 51 % yield. ^1H NMR (500 MHz, CDCl_3 , ppm) δ 7.23–7.16 (m, 2H), 7.16–7.11 (m, 1H), 7.04–6.99 (m, 2H), 6.85 (s, 2H), 5.73 (s, 2H), 1.22 (s, 24H). ^{13}C NMR (126 MHz, CDCl_3 , ppm) δ 141.2, 127.8, 126.5, 126.3, 121.9, 83.3, 51.7, 24.6. ^{11}B NMR (160 MHz, CDCl_3 , ppm) δ 27.8. HRMS (EI+) m/z 410.2708 [(M+H⁺) calcd for $\text{C}_{23}\text{H}_{34}\text{B}_2\text{NO}_4$ 410.2674].

Compound 66a



The general borylation procedure was carried out on 1,2-dimethylindole and afforded 0.016 g of product as a sticky white solid in 6% yield. ^1H NMR (500 MHz, CDCl_3) δ 8.03–7.97 (m, 1H), 7.25 (dt, J = 8.0, 0.9 Hz, 1H), 7.18–7.04 (m, 2H), 3.67 (s, 3H), 2.64 (s, 3H), 1.36 (s, 12H). ^{13}C NMR (126 MHz, Chloroform-*d*) δ 147.5, 137.9, 132.4, 121.8, 120.8, 120.1, 108.5, 82.3, 24.9.

REFERENCES

REFERENCES

- (1) Chen, H.; Hartwig, J. F. Catalytic, Regiospecific End-Functionalization of Alkanes: Rhenium-Catalyzed Borylation under Photochemical Conditions. *Angew. Chem. Int. Ed Engl.* **1999**, *38*, 3391–3393.
- (2) Chen, H.; Schlecht, S.; Semple, T. C.; Hartwig, J. F. Thermal, Catalytic, Regiospecific Functionalization of Alkanes. *Science* **2000**, *287*, 1995–1997.
- (3) Lawrence, J. D.; Takahashi, M.; Bae, C.; Hartwig, J. F. Regiospecific Functionalization of Methyl C-H Bonds of Alkyl Groups in Reagents with Heteroatom Functionality. *J. Am. Chem. Soc.* **2004**, *126*, 15334–15335.
- (4) Wei, C. S.; Jiménez-Hoyos, C. A.; Videa, M. F.; Hartwig, J. F.; Hall, M. B. Origins of the Selectivity for Borylation of Primary over Secondary C-H Bonds Catalyzed by Cp*-Rhodium Complexes. *J. Am. Chem. Soc.* **2010**, *132*, 3078–3091.
- (5) Murphy, J. M.; Lawrence, J. D.; Kawamura, K.; Incarvito, C.; Hartwig, J. F. Ruthenium-Catalyzed Regiospecific Borylation of Methyl C-H Bonds. *J. Am. Chem. Soc.* **2006**, *128*, 13684–13685.
- (6) Kawamorita, S.; Murakami, R.; Iwai, T.; Sawamura, M. Synthesis of Primary and Secondary Alkylboronates through Site-Selective C(sp³)-H Activation with Silica-Supported Monophosphine-Ir Catalysts. *J. Am. Chem. Soc.* **2013**, *135*, 2947–2950.
- (7) Mita, T.; Ikeda, Y.; Michigami, K.; Sato, Y. Iridium-Catalyzed Triple C(sp³)-H Borylations: Construction of Triborylated sp³-Carbon Centers. *Chem. Commun.* **2013**, *49*, 5601.
- (8) Zhang, L.-S.; Chen, G.; Wang, X.; Guo, Q.-Y.; Zhang, X.-S.; Pan, F.; Chen, K.; Shi, Z.-J. Direct Borylation of Primary C-H Bonds in Functionalized Molecules by Palladium Catalysis. *Angew. Chem. Int. Ed Engl.* **2014**, *126*, 3980–3984.
- (9) Kawamorita, S.; Miyazaki, T.; Iwai, T.; Ohmiya, H.; Sawamura, M. Rh-Catalyzed Borylation of N-Adjacent C(sp³)-H Bonds with a Silica-Supported Triarylphosphine

Ligand. *J. Am. Chem. Soc.* **2012**, *134*, 12924–12927.

- (10) Ohmura, T.; Torigoe, T.; Suginome, M. Functionalization of Tetraorganosilanes and Permethyloligosilanes at a Methyl Group on Silicon via Iridium-Catalyzed C(sp³)-H Borylation. *Organometallics* **2013**, *32*, 6170–6173.
- (11) Liskey, C. W.; Hartwig, J. F. Iridium-Catalyzed C-H Borylation of Cyclopropanes. *J. Am. Chem. Soc.* **2013**, *135*, 3375–3378.
- (12) Li, Q.; Liskey, C. W.; Hartwig, J. F. Regioselective Borylation of the C-H Bonds in Alkylamines and Alkyl Ethers. Observation and Origin of High Reactivity of Primary C-H Bonds Beta to Nitrogen and Oxygen. *J. Am. Chem. Soc.* **2014**, *136*, 8755–8765.
- (13) Shimada, S.; Batsanov, A. S.; Howard, J. A. K.; Marder, T. B. Formation of Aryl- and Benzylboronate Esters by Rhodium-Catalyzed C-H Bond Functionalization with Pinacolborane. *Angew. Chem. Int. Ed Engl.* **2001**, *113*, 2226–2229.
- (14) Ishiyama, T.; Ishida, K.; Takagi, J.; Miyaura, N. Palladium-Catalyzed Benzylic C-H Borylation of Alkylbenzenes with Bis(pinacolato)diboron or Pinacolborane. *Chem. Lett.* **2001**, *30*, 1082–1083.
- (15) Larsen, M. A.; Wilson, C. V.; Hartwig, J. F. Iridium-Catalyzed Borylation of Primary Benzylic C-H Bonds without a Directing Group: Scope, Mechanism, and Origins of Selectivity. *J. Am. Chem. Soc.* **2015**, *137*, 8633–8643.
- (16) Palmer, W. N.; Obligacion, J. V.; Pappas, I.; Chirik, P. J. Cobalt-Catalyzed Benzylic Borylation: Enabling Polyborylation and Functionalization of Remote, Unactivated C(sp³)-H Bonds. *J. Am. Chem. Soc.* **2016**, *138*, 766–769.
- (17) Palmer, W. N.; Zarate, C.; Chirik, P. J. Benzyltriboronates: Building Blocks for Diastereoselective Carbon-Carbon Bond Formation. *J. Am. Chem. Soc.* **2017**, *139*, 2589–2592.
- (18) Zhang, L.; Huang, Z. Synthesis of 1,1,1-Tris(boronates) from Vinylarenes by Co-Catalyzed Dehydrogenative Borylations-Hydroboration. *J. Am. Chem. Soc.* **2015**, *137*, 15600–15603.

- (19) Manna, K.; Ji, P.; Lin, Z.; Greene, F. X.; Urban, A.; Thacker, N. C.; Lin, W. Chemoselective Single-Site Earth-Abundant Metal Catalysts at Metal-Organic Framework Nodes. *Nat. Commun.* **2016**, *7*, 12610.
- (20) Frey, G. D.; Rentzsch, C. F.; von Preysing, D.; Scherg, T.; Mühlhofer, M.; Herdtweck, E.; Herrmann, W. A. Rhodium and Iridium Complexes of N-Heterocyclic Carbenes: Structural Investigations and Their Catalytic Properties in the Borylation Reaction. *J. Organomet. Chem.* **2006**, *691*, 5725–5738.
- (21) Furukawa, T.; Tobisu, M.; Chatani, N. Nickel-Catalyzed Borylation of Arenes and Indoles via C-H Bond Cleavage. *Chem. Commun.* **2015**, *51*, 6508–6511.
- (22) Ivachtchenko, A. V.; Kravchenko, D. V.; Zheludeva, V. I.; Pershin, D. G. Synthesis of Pinacol Esters of 1-Alkyl-1 H -Pyrazol-5-Yl- and 1-Alkyl-1 H -Pyrazol-4-Ylboronic Acids. *J. Heterocycl. Chem.* **2004**, *41*, 931–939.
- (23) (a) Paal, C.; Hartmann, W. *Ber. Dtsch. Chem. Ges.* **1918**, *51*, 711–737. (b) Widegren, J. A.; Finke, R. G. A Review of the Problem of Distinguishing True Homogeneous Catalysis from Soluble or Other Metal-Particle Heterogeneous Catalysis under Reducing Conditions. *J. Mol. Catal. A: Chem.* **2003**, *198*, 317–341.
- (24) Crawford, T. H.; Swanson, J. *J. Chem. Educ.* **1971**, *48*, 328–386.

Chapter 5. First, Ligand Controlled Synthesis of 1,2-di and 1,2,3-tri Borylated Arenes *via* Iridium Catalyzed C-H Borylations

5.1 Introduction to aromatic di- and poly-boronic esters (PBEs)

Aromatic di and polyboronic acids(PBAs)/esters (PBEs) are valuable synthetic intermediates in organic synthesis^{1,2} for formation of transition metal catalyzed C-C and carbon-heteroatom bond formation.³⁻⁵ However, installing two or three boryl groups in the aromatic ring is challenging.

Traditionally, installing two boryl groups (**E**) on aromatic ring relied on pre-functionalized mono or 1,2-dihalobenzene (**A**) compounds (Figure 20). These undergo metal-halogen⁶⁻⁹ (Mg or Li) exchange or Pd-catalyzed Miyaura coupling¹⁰⁻¹² to give *o*-benzenediboronic acids. Recently, Pt- and Cu-catalyzed 1,2-diborylation of in situ generated arynes has attracted attention as a convenient method to form *o*-benzenediboronic acids.¹³⁻¹⁵ Other methods include high yielding 1,2-selective dual C-H/C-X borylation starting with mono halobenzene (**B**).^{16,17}

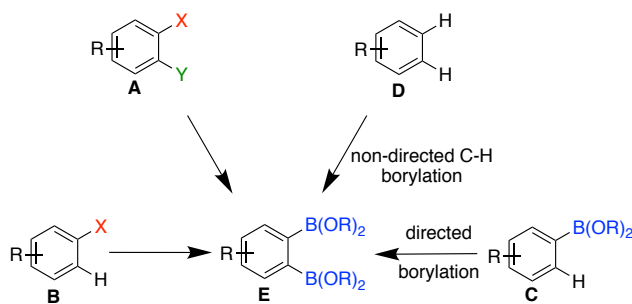
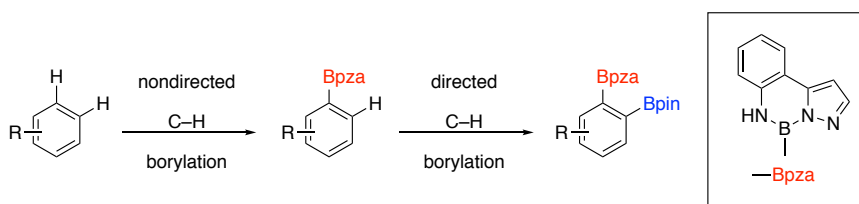


Figure 20. Preparation of *o*-Benzenediboronic Acids

Given the substrate dependence on aromatic halogenations, accessing suitable haloaromatic starting materials can be trivial or prohibitively difficult. Installing, two or

three boryl groups on an aromatic ring starting from unfunctionalized arenes would be attractive. Recently, Yoshida and co-workers reported formation of *o*-benzenediboronic acid via Ir catalyzed *ortho* C-H borylation directed by pyrazolylaniline modified boronyl group (C).¹⁸

This is the first report achieving *o*-C-H borylation directed by a boronyl group using Ir as the catalyst. First, non-functionalized arenes are borylated using non-directed C-H activation borylation using Ir catalyst. Then the boronyl group is modified by pyrazolylaniline, which leads to the formation of the Bpza group. This PZA-modified boronyl group behave as a temporary directing group in Ir-catalyzed *o*-C-H borylations yielding 1,2-benzenediboronic acid derivatives (Scheme 34).



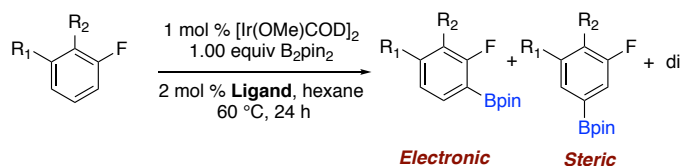
Scheme 34. Directed *o*-C-H Functionalization by -Bpza group

It would be an attractive method if we could achieve 1,2-benzenediboronic acid derivatives without any directing groups. Up to date there have been no report of non-directed iridium catalyzed C-H borylation to give 1,2-diborylated arenes without using any prefunctionalized starting arenes (D).

5.2 Data and Discussion

In 2014, we reported selectively generating arylboronic esters *ortho* to fluorine via Ir-catalyzed C-H borylations followed by hydrodehalogenations (Chapter 2).¹⁹ However, a more attractive method would be the selective Ir-catalyzed C-H borylations *ortho* to

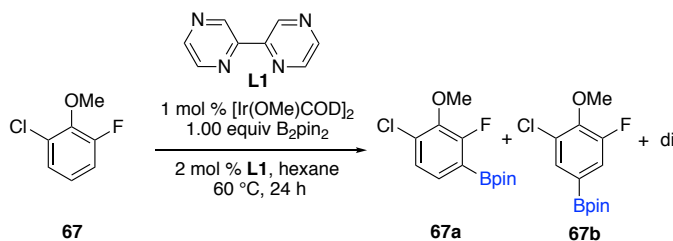
fluorine via ligand control. Therefore, our group continued studies on selective Ir-catalyzed C–H borylations with various ligand systems. These ligands were reacted with 1 mol % [Ir(OMe)(COD)]₂, 2 mol % ligand and 1.00 equiv of B₂Pin₂ in hexane at 60 °C (more in detail about ligand screening in Chapter 6) (Scheme 35).



Scheme 35. Ligand screening for CHBs

We were interested in any ligand system that favored exclusively one of the isomers (steric or electronics) over the other one. However, among these ligands 2,2'-bipyrazine (**L1**) stood out for resulting in significant amounts of diborylated arenes when screening against 1-chloro-3-fluoro-2-methoxybenzene (2,6-CFA). Diborylation was enhanced when reactions were run in non-polar solvents such as hexane and methylcyclohexane (Table 2).

Table 2. Solvent screening for L1



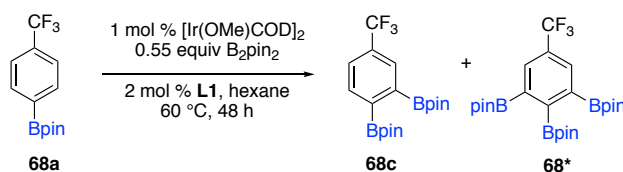
Entry	Solvent	Conversion(GC)	67a/67b/Di
1	THF	49%	44/52/4
2	Hexane	77%	35/40/25
3	CPME	77%	39/49/12
4	Me-cyclohexane	82%	35/44/21
5	Hunig's Base	84%	41/43/16
6	1,4-dioxane	34%	54/31/15

CHBs of **67a** was carried out and after 48 h 65% of the diborylated product was formed. We thought the best way to identify the correct regioisomer of the diborylated product was through X-ray crystallography. Indeed, after isolation, and X-ray crystallography confirmed that the correct structure was that of **67c**. (Figure 22).



Figure 22. X-ray crystallographic structure of 67c.

This is the first Ir catalyzed non-directed CHBs that forms 1,2- diborylated arenes. Intrigued by this unusual reactivity of ligand **L1**, we set out to see if we could synthesize more 1,2 diborylated arenes. We started with mono borylated arenes and performed Ir-catalyzed borylations to obtain diborylated arenes.



Scheme 37. C–H borylation of 68a

One such example is the borylation of 4,4,5,5-tetramethyl-2-(4-(trifluoromethyl)phenyl)-1,3,2-dioxaborolane (**68a**) (Scheme 37). After 48 h, an off white fine powder crashed out of the crude reaction mixture. This fine powder was separated from the reaction mixture by simple gravity filtration. ¹H NMR of this fine white powder

suggested the presence of 12xCH₃ groups { δ 1.48 (12H), 1.33 (24H)}. Astonished by this result, we were determined to get an X-ray crystal structure. After growing crystals and subjecting them to X-ray, we finally confirmed that it is triborylated arene (**68***) (Figure 23). In 2017, Suginome and co-workers reported isolation of 1,2,3-benzenetriboronic acid pinacol ester (5%) using the PZA directing group.

Up to date no one had ever directly installed three Bpin group next to each other in an arene system. We and others have showed that it is possible to directly install several Bpin groups in Sp³ carbons^{22,23} but not in Sp² arene system.²⁴ Therefore, this is the first report, where direct iridium catalyzed CHBs were able to install multiple boryl groups next to each other without any directing groups.

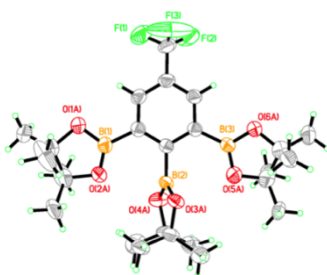
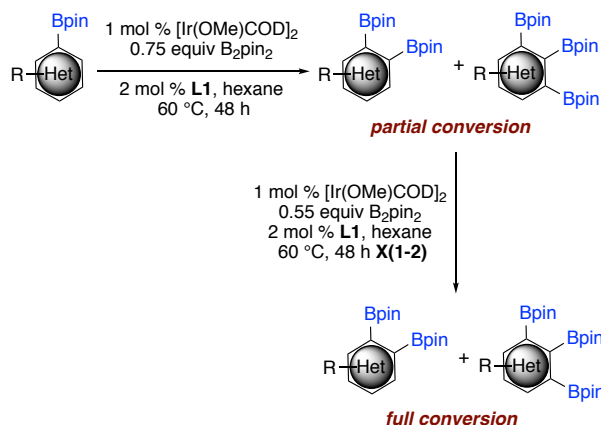


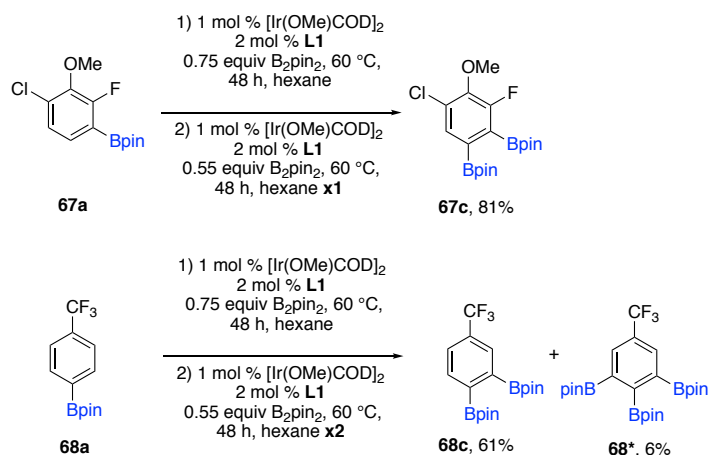
Figure 23. X-ray crystallographic structure of 68*.

However, this catalyst system is not reactive as the most commonly used [Ir(OMe)COD]₂ and dtbpy system. After 48 h only 45% conversion was observed. Therefore, to have a better conversion to polyborylated compounds, we increased the catalyst loading to 3 mol % of [Ir(OMe)COD]₂, 6 mol % of 1 and 1.00 equiv of B₂pin₂ in hexane 60 °C for 48 h. However, this did not help to improve product formation. Next, we tried introducing a new catalyst loading after every 48 h (1–2 times) after the first addition. This helped to consume all the starting material (Scheme 38).



Scheme 38. Multiple catalyst loading in CHBs

With this new finding in hand we set out to investigate our previously described substrates (**67a** and **68a**) as well as new substrates for making 1,2-di or 1,2,3-tri borylated compounds (Scheme 39). CHBs of **67a** with only two catalyst loadings, was able to afford full conversion to **67c**, which was isolated in 81% yield. In this case, no tri borylation was observed. On the other hand, **68a** used up 3 loadings and was able to isolate **68c** (61%) and **68*** (6%).



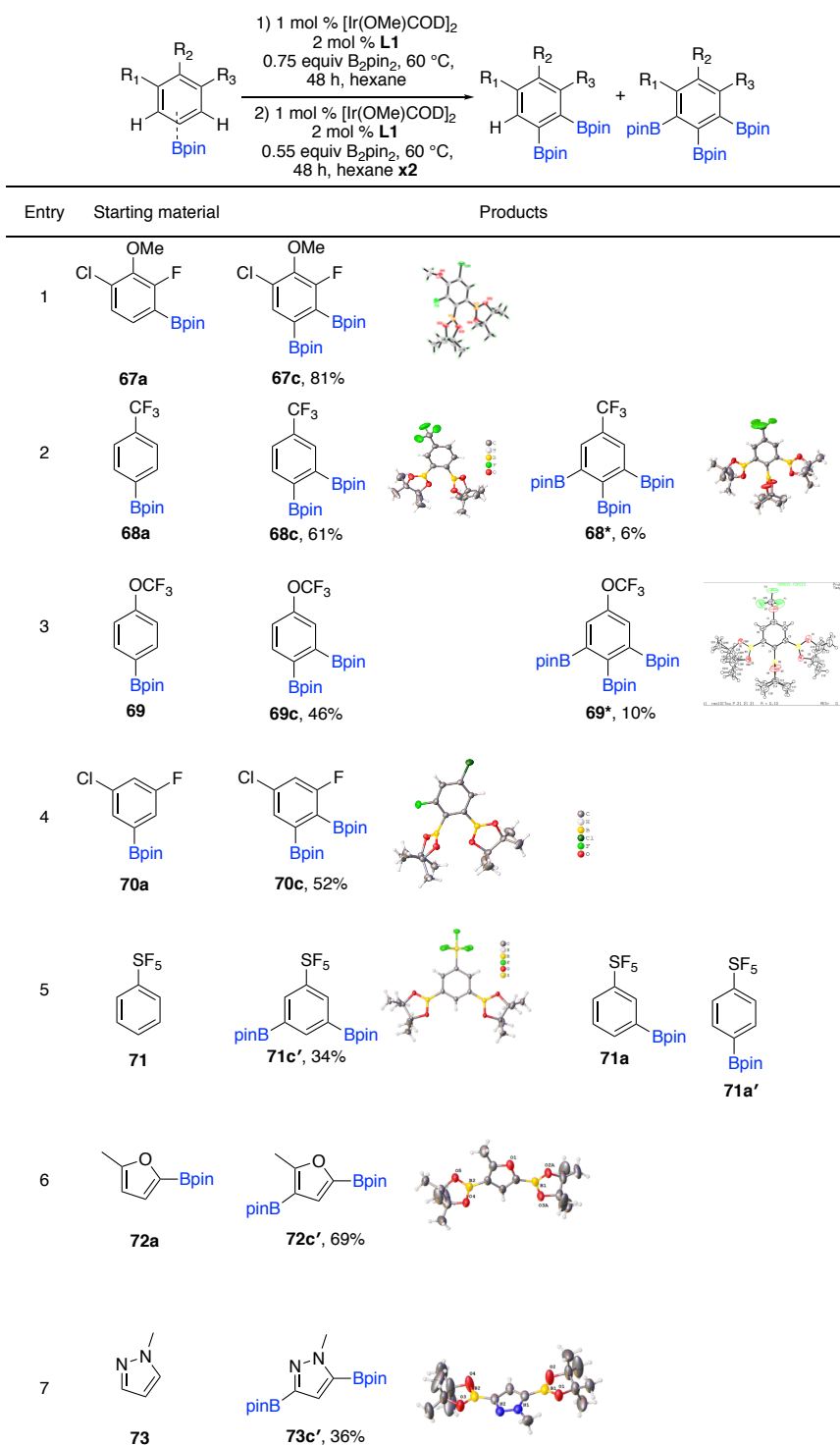
Scheme 39. CHBs of 67a and 68a

Intrigued by these data, we started screening C-H borylations of mono borylated compounds. Our main goal was to make sterically demanding 1,2-di and 1,2,3-tri borylated compounds (Figure 24). Thus, we purchased commercially available boronic acids and converted them to corresponding boronic esters or unless otherwise noted.

CHBs of 4,4,5,5-tetramethyl-2-(4-(trifluoromethoxy)phenyl)-1,3,2-dioxaborolane (**69a**) resulted in a similar borylation pattern like (**68a**). After three catalyst loadings, 1,2-di (**69c**) was formed in 46 % and 1,2,3-tri (**69***) in 10% yields. Next, we tried the CHB of 2-(3-chloro-5-fluorophenyl)-4,4,5,5-tetramethyl-1,3,2-dioxaborolane (**70**). This substrate was synthesized in our lab, as part of an on-going project. After reacting with three catalyst loadings ~92% product formation was observed. (**70c**: tri = 97:3). The 1,2-diborylated (**70c**) was isolated in 46% yield, however, we were unable to isolate the tri borylated product (Figure 24).

Next, we investigated CHB of pentafluorosulfanylbenzene (**71**). After the first catalyst loading, two mono borylated products *meta* borylated **71a**, *para* borylated **71a'** and a single diborylated product (**71c'**) were generated in a ratio of 63: 31: 6. Introduction of the second catalyst loading, formation of **71c'** was enhanced. During the course of the reaction diborylated compound **71c'** crashes out from the reaction mixture and 32% was isolated after a simple filtration. Surprisingly, pentafluorosulfanylbenzene gave 1,3-diborylated product **17c'** and not the 1,2-di borylated product as before. compound **71a'** was unreactive for further CHBs.

Figure 24. Synthesis of 1,2-di and 1,2,3-tri borylated arenes/heteroarenes

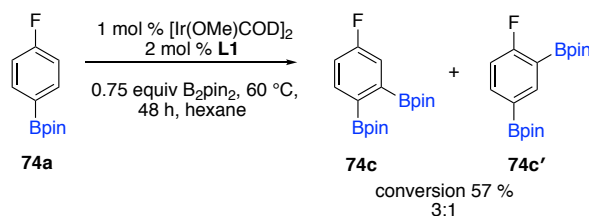


We also investigated CHBs of mono borylated 1,4 substitution of bromo, toluene, isopropyl, chloro and cyano. Surprisingly, these compounds did not show any CHBs. We also tried CHBs of 1,3-dicyanobenzene and 2-bromothiophene. 1,3-Dicyanobenzene showed no CHBs, but 2-bromothiophene progressed half way through to the 5-mono borylated species. However, borylation of the species didn't progress any further even after adding a second loading of catalyst and a black film was formed around the wall of the vial. Nevertheless, this was a promising result for catalytic activity of this ligand system and motivated us to investigate more into heteroarenes.

C-H borylation of 2-methyl furan resulted in a mixture of 5-mono and diborylated compounds. For the ease of isolation and characterization of the diborylated product, a CHB was carried out with compound **72a**. Two diborylated regioisomers {1,3-di (**72c'**) and 1,2-di (**72c**)} and one tri borylated isomer were observed in a ratio of 78: 17: 5 (confirmed by GCMS and ¹HNMR). The favored regioisomer was 1,3-diborylated methyl furan (**72c'**) which was isolated in 69% yield. C-H borylation next to the methyl group was favored over the Bpin group in **72a**. We also investigated CHB of N-methyl pyrazole (**73**). We were able to isolate 1,3-diborylated N-methylpyrazole (**73c'**) in 36% yield. Surprisingly, only one regioisomer was observed with borylation next to nitrogen favored. CHBs of N-methylindole gave a mixture of 2- and 3- mono borylated products, where 2-borylated N-methylindole is the more favored regioisomer for mono borylation and also several di- borylated isomers (GCMS).

Even though this ligand system gives unprecedented chemistry, it is reactive towards limited substrate scope. This system shows an intriguing bias towards fluoro containing arenes. However, the fluorine need not be directly attached to the arene. To

understand more about how this system work in CHBs we carried out further investigations. As we know from chapter 2, fluoro arenes often gives a mixture of products (steric and electronic). A hydrogen next to fluorine is more susceptible for CHBs due to its acidity. Therefore, CHBs of 2-(4-fluorophenyl)-4,4,5,5-tetramethyl-1,3,2-dioxaborolane (**74a**) should favor C–H activation next to fluorine (Scheme 40).

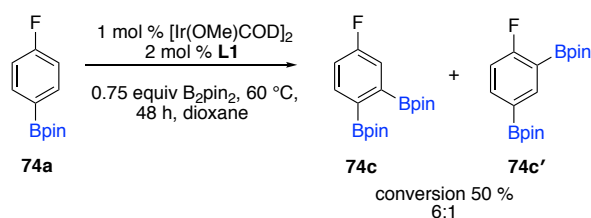


Scheme 40. CHBs of 74a in hexane

Surprisingly, CHBs of **74a** favors borylation next to Bpin group. This CHB activation catalyst system going against fundamentals of iridium catalyzed CHBs, which is borylation is sterically driven. Several regioisomers of di and tri borylated products were observed by ^{19}F NMR and GCMS.

Intrigued by the results in Scheme 41, we wanted to investigate the outcome if we used different type of boron derivatives, such as, propane-1,2-diol (Bpg), ethane-1,2-diol (Beg), *N*-methyliminodiacetic acid (BMIDA) and 1,8-diaminonaphthalene (BDAN) boronic esters. These different boron derivatives vary with sterics and electronic properties. Unfortunately, synthesis of the Bpg derivative starting from (4-fluorophenyl)boronic acid was unsuccessful. Nevertheless, we were able to buy the BMIDA of fluorobenzene (**75**).

BMIDA compounds are not soluble in hexane, which led us to change the solvent for the CHBs. Initial solvent screening suggested that this catalyst system gives lower conversions to the diborylated product in relatively polar solvents, such as THF and 1,4-dioxane (Figure 23). As BMIDA arenes readily dissolve in 1,4-dioxane at elevated temperatures, we repeated the reaction in Scheme 41 in 1,4-dioxane to see if the same selectivity observed in hexane repeated (Scheme 41).



Scheme 41. CHBs of 23 in dioxane

Remarkably, in dioxane a significant bias towards 1,2-diborylation (**74c**) was observed. In hexane only a 3:1 ratio was observed for **74c**:**74c'**, but with dioxane as the solvent the selectivity raised to 6:1. This shows that not only the substrate electronics, but also the solvent electronics influence selectivity (Figure 25).

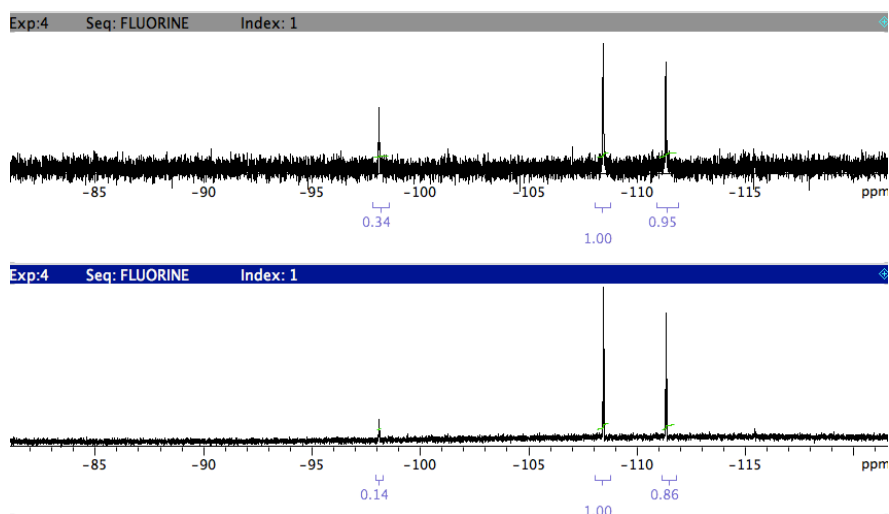
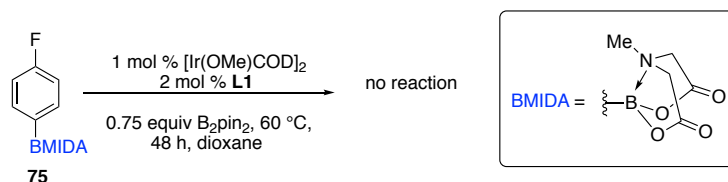


Figure 25. ¹⁹F NMR for CHBs of 74a in hexane (top) Vs. dioxane (bottom)

We proceed to investigate to this remarkable catalyst system further. CHB of **75** in 1,4-dioxane was attempted (Scheme 42), unfortunately no C–H borylation was observed and only starting material was present in the crude reaction mixture.

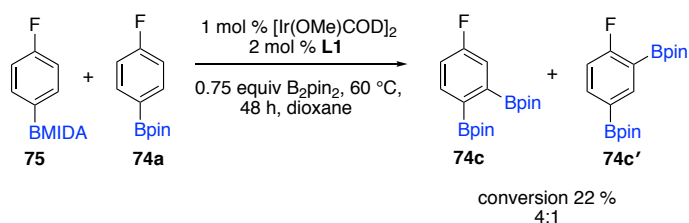


Scheme 42. CHBs of **75 in 1,4-dioxane**

We hypothesized that we did not see CHBs due to several possible reasons:

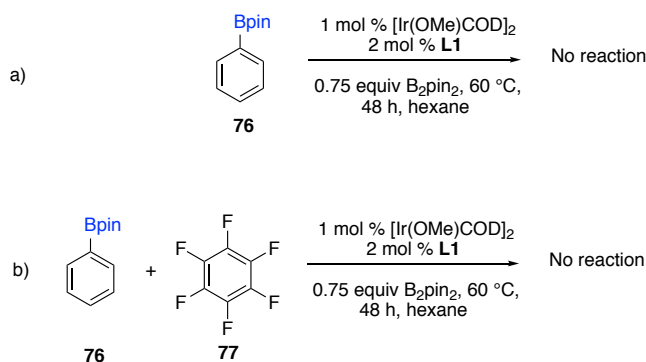
1. BMIDA is more sterically hindered compared to Bpin group
2. Boron has an empty p-orbital in a Bpin group but not in a BMIDA group
3. BMIDA ability to coordinate to the catalyst and shut down the CHB

To test these hypothesis, we set up a CHB with equal molar amount of **74a** and **75** in 1,4-dioxane (Scheme 43). After 48 h, only 22% product formation (**74c** and **74c'**) was observed compared to the 50% (Scheme 41) resulted in absence of **75**. Selectivity decreased to 4:1 from 6:1. This shows that, changing Bpin group has an effect, but we cannot clearly indicate that this is a “boron directed” CHBs without additional evidence.



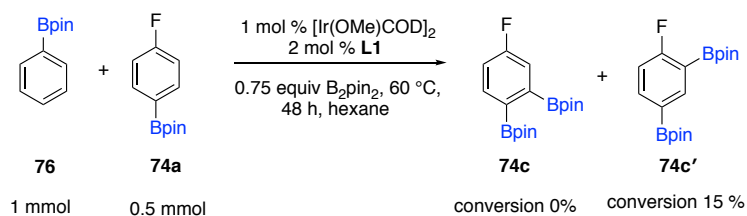
Scheme 43. Equal molar CHBs of **74a and **75****

Another unanswered question is what is the role of fluorine? To answer that question, we investigated CHBs of borylated benzene (**76**) (Scheme 44 a). Even though, there are many available hydrogens, no CHBs were observed. Next, we added hexafluorobenzene (**77**) as an external fluorine source to see whether it will promote any CHBs of **76** (Scheme 44 b). Unfortunately, no evidence for any kind of CHBs were observed.



Scheme 44. a) CHBs of 76 b) Equal molar CHBs of 76 and 77

We also investigated CHBs of **76** (1 mmol) with **74a** (0.5 mmol). The outcome of this reaction was astonishing (Scheme 45). In presence of excess **76**, after 48 h only 15% product formation was observed for **74a** and no CHBs were observed from **76**. This shows that conversion has significantly decreased in presence of an excess external Bpin-arene. We also know that catalyst activity diminishes as the reaction progress and when we use B_2pin_2 as the boron source. Maybe there is some kind of deactivation is coming from boron source itself. NMR studies will help to get more information regarding this deactivation by monitoring catalyst behavior as reaction progresses.



Scheme 45. CHBs of 74a with excess 76

Furthermore, only one regioisomer **74c'** was observed in contrast to Scheme 41, (Figure 26). This suggests that an excess external Bpin source changes the selectivity for CHBs.

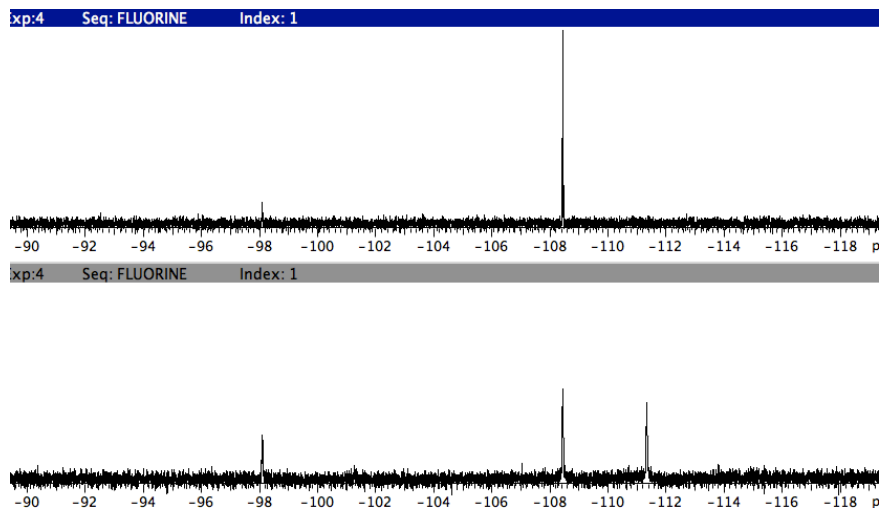


Figure 26. ¹⁹F NMR for CHBs of 74a with 76 (top) Vs. 74a without 76

NMR Experiments

All reactions were run in C₆D₁₂ at 900 MHz.

1) (0.02 mmol) 2,2'-bipyrazine (**L1**) in (1.0 mL) C₆D₁₂

Ligand **L1** is sparingly soluble in C₆D₁₂ at room temperature. By proton NMR three major peaks were observed in the aromatic region of the spectrum. ¹H NMR

(900 MHz, C₆D₁₂) δ 9.61 (s, 1H), 8.48 (d, *J* = 2.1 Hz, 1H), 8.44 (d, *J* = 2.2 Hz, 1H)
(Figure 27.1).

2) (0.02 mmol) 2,2'-bipyrazine (L1) + (0.01 mmol) [Ir(OMe)COD]₂ in (1.0 mL) C₆D₁₂

No significant color change or changes to the ligand proton signals and the catalyst proton signals were observed. Therefore, at room temperature there is not a rapid reaction between the ligand and the Ir pre-catalyst (Figure 27.2).

¹H NMR (900 MHz, C₆D₁₂) δ 9.61 (s, 1H), 8.48 (d, *J* = 2.1 Hz, 1H), 8.44 (d, *J* = 2.2 Hz, 1H), 3.45 (d, *J* = 4.1 Hz, 8H), 3.17 (s, 6H), 2.23 – 2.12 (m, 8H), 1.33 (d, *J* = 7.8 Hz, 8H).

3) (0.02 mmol) 2,2'-bipyrazine (L1) + (0.04 mmol) B₂Pin₂ in (1.0 mL) C₆D₁₂

Next, the ligand was combined with B₂pin₂. It is noteworthy that B₂pin₂ is only sparingly soluble in C₆D₁₂. As soon as the ligand is combined with B₂pin₂ the solution turned green. Bipyrazine proton peaks in the aromatic region did not completely disappear, however new three up field shifted peaks were observed {δ 7.13 (s, 1H), 6.83 (d, *J* = 5.3 Hz, 1H), 6.35 (d, *J* = 5.4 Hz, 1H)}. Also ¹H-NMR spectrum became messier with this combination. Therefore, there is a rapid reaction between the ligand and B₂pin₂ (Figure 27.3).

4) (0.02 mmol) 2,2'-bipyrazine (L1) +(0.01 mmol) [Ir(OMe)COD]₂ + (0.12 mmol) B₂Pin₂ in (1.0 mL) C₆D₁₂

After combining the ligand, Ir-precatalyst and B₂pin₂, a green solution was observed and in the ¹H NMR spectrum, the bipyrazine proton peaks in the aromatic region completely disappeared. We did not observe a messy proton NMR spectrum like in the previous case. However, we did observe the three up-field shifted peaks {δ 7.92 (s, 1H), 6.81 (s, 1H), 6.33 (s, 1H)} with slightly different chemical shifts than in the previous case (Figure 19.4). When all three species are combined together an immediate degradation of the ligand is not observed. However, after 24 h the proton NMR spectrum of this mixture is messy and we were unable to detect the three up field shifted proton signals.

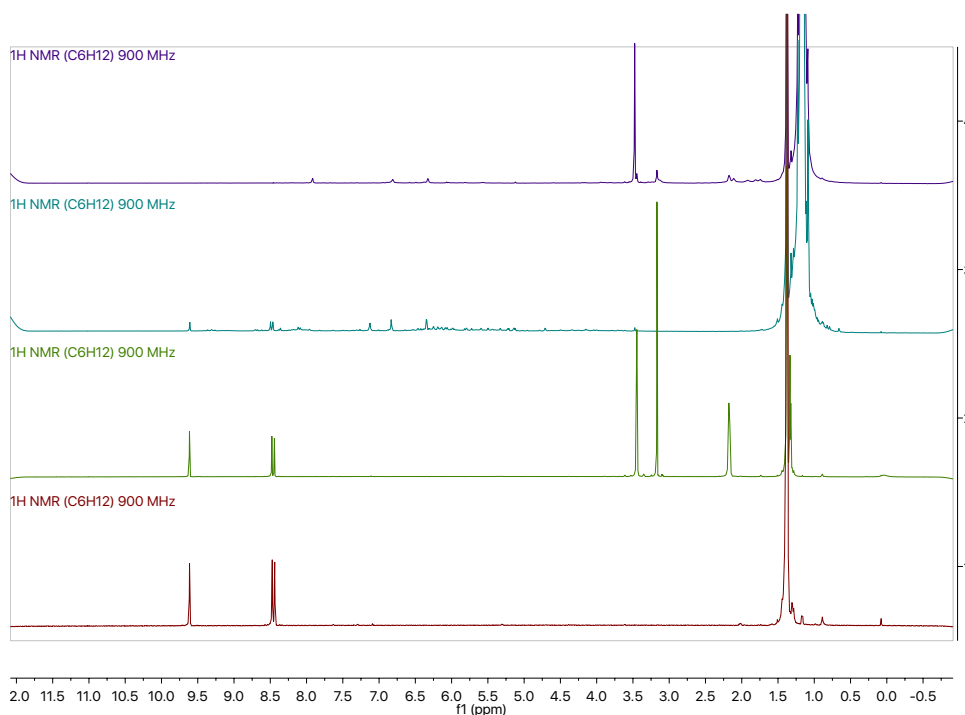
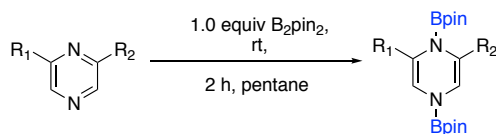


Figure 27.

- 1) ¹H NMR of 2,2'-bipyrazine (L1) in C₆D₁₂
- 2) ¹H NMR 2,2'-bipyrazine (L1) + [Ir(OMe)COD]₂ in C₆D₁₂
- 3) ¹H NMR 2,2'-bipyrazine (L1) + B₂Pin₂ in C₆D₁₂
- 4) ¹H NMR 2,2'-bipyrazine (L1) + [Ir(OMe)COD]₂ + B₂Pin₂ in C₆D₁₂

Usually CHBs with this catalyst system are run at 60 °C, therefore future investigations of NMR studies should be run at that temperature. This will help to avoid any unambiguous data due to solubility issues. Moreover, investigating changes in the ^{11}B NMR spectra may also be important for a clearer understanding of the chemical reactions between the ligand, Ir pre-catalyst and B_2pin_2 .

In 2012, Suginome and co-workers reported an efficient dearomatizing of pyrazines to 1,4-dihydropyrazines and 1,2,3,4-tetrahydropyrazine via transition-metal-free addition of boron reagents (Scheme 46).²⁵ Dearomatization is facile with B-B, B-Si, and B-H boron reagents. The authors suggest that high reactivities of pyrazines in the dearomatizing addition reactions may due to the formation of B–N bonds.



Scheme 46. 1,4-Diboration of substituted pyrazines

Up-field shifted proton signals in the presence of B_2pin_2 may suggest there is some kind of dearomatization taking place via the addition of B_2pin_2 to the 2,2'-bipyrazine ligand (**L1**). This may lead to rapid degradation or polymerization of (**L1**) {messy proton NMR}. Possible dearomatized structures of **L1** are shown in Figure 28.

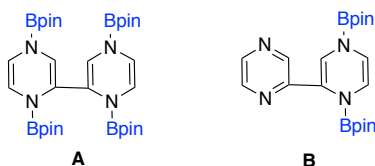


Figure 28. possible dearomatization structures for L1

The most commonly used iridium catalyst system for CHBs is $[\text{Ir}(\text{OMe})\text{COD}]_2$, dtbpy and B_2pin_2 and these CHBs are sterically driven (Figure 29). From previous reports, we know the active catalyst of the Ir-dtbpy system is a $16e^-$ trisBpin Ir complex.

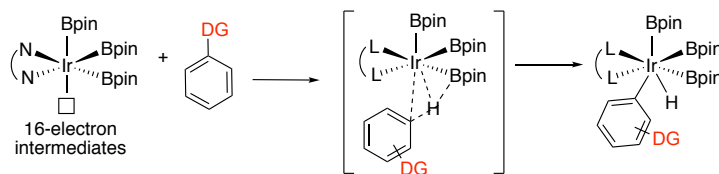


Figure 29. CHBs with Ir-dtbpy system

Clearly, we do not have a solid explanation for these results and more work has to be done to understand how this system works during CHBs. As for future work, repeating the CHBs in Scheme 45b with pentafluorobenzene or 1,3,5-trifluorobenzene would be worth exploring. This system (Ir-bypyrazine) is favoring CHBs next to a Bpin group, giving rise to sterically demanding 1,2-di and 1,2,3-tri borylated compounds. Therefore, we can hypothesize several scenarios;

- 1) 2,2'-Bipyrazine behaves as a hemi labile ligand and a $14e^-$ system might be involved.
- 2) A nitrogen of one of the bipyrazine rings coordinates to a Bpin group of the substrate and directs CHBs next to that Bpin group (Figure 30).

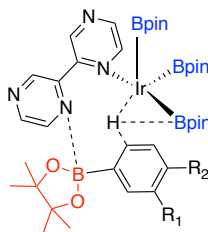


Figure 30. Possible transition state for Ir-bypyrazine system

5.3 Conclusions

This is the first ligand controlled synthesis of 1,2-di and 1,2,3-triborylated arenes via direct Ir-catalyzed borylation. Also, unprecedented, synthesis of 1,2,3-triborylated arenes via non-directed Ir-catalyzed borylation. This system shows an intriguing bias towards fluoro containing arenes. However, the fluorine need not be directly attached to the arene. Works with heteroarenes to give 1,3-diborylated heteroarenes.

5.4 Experimental

All commercially available chemicals were used as received unless otherwise indicated. Solvents were degassed. All experiments were assembled in a glovebox under a nitrogen atmosphere.

Analytical Methods. ^1H NMR spectra were recorded on a Varian VXR-500 or Varian Unity-500-Plus spectrometer (499.74 MHz) and referenced to residual solvent signals. ^{11}B NMR spectra were recorded on a Varian VXR-500 spectrometer operating at 160.41 MHz, 125.7 MHz for ^{13}C NMR and 470.1 MHz for ^{19}F NMR. All coupling constants are apparent J values measured at the indicated field strengths. Melting points were measured on a MEL-TEMP or Thomas-Hoover capillary melting apparatus and are uncorrected.

Elemental composition was determined by high resolution/accurate mass spectrometry analysis using a Thermo Scientific LTQ-Orbitrap Velos mass spectrometer at the Molecular Metabolism and Disease Collaborative Mass Spectrometry Core facility at Michigan State University. Samples were introduced to the mass spectrometer by direct infusion electrospray ionization in positive ionization mode, and data was acquired

at a resolution of 100,000 defined at m/z 400. Melting points were measured on Stuart Scientific capillary melting point apparatus.

General Procedure for Borylation

In a nitrogen atmosphere glove box bis(pinacolato)boron (B_2Pin_2) (0.192 g, 0.75 mmol) was weighed into a 20 mL vial containing a magnetic stir bar. $[Ir(OMe)COD]_2$ (6.6 mg, 0.01 mmol) and 2,2'-bipyrazine ligand (3.3 mg, 0.02 mmol) were weighed into two test tubes separately, each being diluted with 0.5 mL of hexane. The $[Ir(OMe)COD]_2$ solution was transferred into the 20 mL vial containing B_2Pin_2 . This mixture was stirred until a golden yellow solution was obtained (~ 1 min). Next the solution containing ligand was transferred into the vial and upon stirring the resulting solution turned a dark green color. Finally, the substrate (1.0 mmol) was added to the vial. 0.5 mL of hexane was used to rinse the test tubes and transfer any remaining catalyst/ligand/substrate. Then sealed the vial and mixture was stirred for 48 h at 60 °C. After, 48 h GC and NMR data were collected. If reaction is not completed added another loading of catalyst {Ir (0.01 mmol), ligand (0.02 mmol), B_2Pin_2 (0.55 mmol) and 1.5 mL hexane}.

Work up procedure A:

Part 1

The reaction mixture was passed through a plug of silica (BD 60 mL Syringe/Luer-Lok Tip-silica up to 50 mL mark) eluting with a 4:1 hexane/ethyl acetate solution (2 x 200 mL) and fractions were collected. The volatiles were removed by rotary evaporation (from this step, most of the excess B_2pin_2 was removed). The collected fractions were re-

dissolved in a minimum amount of hexane and kept inside the refrigerator for crystal formation. After crystals were formed, these fractions were washed with cold hexane (1 mL*2) to remove any residual B₂pin₂. The left-over crystals were collected and dried.

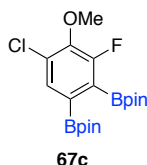
Part 2

If the crystallization did not work, the material was purified using a SiO₂ column chromatography. eluting with hexane (B₂pin₂ will elute with hexane) and then with hexane/ethyl acetate (4:1).

Work up procedure B:

Tri-borylated compounds usually crash out from the crude reaction mixture. In these cases, the solid is filter using a disposable filter cone. CH₂Cl₂ is then added and collect the solution. Volatiles are removed by rotary evaporation and pure tri borylated product is obtained as solid.

Compound 67c



The general borylation procedure was carried out on the starting arene of 2-(4-chloro-2-fluoro-3-methoxyphenyl)-4,4,5,5-tetramethyl-1,3,2-dioxaborolane. After work up procedure **A**, 0.412 g of compound **67c** was obtained as a white solid (mp > 200°C) in 86% yield. ¹H NMR (500 MHz, Chloroform-*d*) δ 7.60 (d, *J* = 1.1 Hz, 1H), 3.97 (d, *J* = 1.8 Hz, 3H), 1.42 (s, 12H), 1.33 (s, 12H). ¹³C NMR (126 MHz, Chloroform-*d*) δ 158.1 (d, *J* = 245.0 Hz), 145.7 (d, *J* = 15.3 Hz), 132.5 (d, *J* = 2.8 Hz), 128.5, 84.6, 84.5, 61.4 (d, *J*

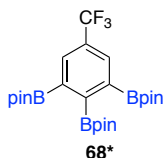
= 5.3 Hz), 24.9, 24.8. ^{19}F NMR (470 MHz, Chloroform-*d*) δ -121.69. ^{11}B NMR (160 MHz, Chloroform-*d*) δ 30.2. MS EI+ m/z calculated for $(\text{M}+\text{H})^+$ $\text{C}_{19}\text{H}_{29}\text{B}_2\text{ClFO}_5$ 413.1874, found 413.1887.

Compound 68c



The general borylation procedure was carried out on the starting arene of 4,4,5,5-tetramethyl-2-(4-(trifluoromethyl)phenyl)-1,3,2-dioxaborolane with 3 loading of catalyst. After work up procedure **A**, 0.244 g of compound **68c** was obtained as a waxy solid in 61% yield. ^1H NMR (500 MHz, Chloroform-*d*) δ 7.90 (dd, $J = 1.9, 1.0$ Hz, 1H), 7.73 (dd, $J = 8.0, 1.9$, 1H), 7.61 (ddd, $J = 7.8, 1.0$ Hz, 1H), 1.38 (s, 12H), 1.38 (s, 12H). ^{13}C NMR (126 MHz, Chloroform-*d*) δ 133.5, 130.9 (q, $J = 32.0$ Hz), 129.9 (q, $J = 3.7$ Hz), 125.6 (q, $J = 3.8$ Hz), 124.3 (d, $J = 272.4$ Hz), 84.3, 84.3, 24.9. ^{19}F NMR (470 MHz, Chloroform-*d*) δ -62.95. ^{11}B NMR (160 MHz, Chloroform-*d*) δ 30.9. MS EI+ m/z calculated for $(\text{M}+\text{H})^+$ $\text{C}_{19}\text{H}_{28}\text{B}_2\text{F}_3\text{O}_4$ 399.2126, found 399.2133.

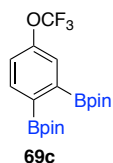
Compound 68*



The general borylation procedure was carried out on the starting arene of 4,4,5,5-tetramethyl-2-(4-(trifluoromethyl)phenyl)-1,3,2-dioxaborolane with 3 loading of catalyst.

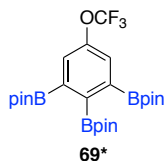
After work up procedure **B**, 0.0310 g of compound **68*** was obtained as a white solid in 6% yield. ^1H NMR (500 MHz, Chloroform-*d*) δ 8.17 (q, $J = 0.7$ Hz, 2H), 1.50 (s, 12H), 1.35 (s, 24H). C NMR (126 MHz, Chloroform-*d*) δ 133.85 (q, $J = 3.7$ Hz), 129.06 (q, $J = 32.2$ Hz), 124.43 (d, $J = 272.7$ Hz), 84.44, 84.31, 25.82, 24.75. ^{19}F NMR (470 MHz, Chloroform-*d*) δ -62.78. ^{11}B NMR (160 MHz, Chloroform-*d*) δ 30.4. MS EI+ m/z calculated for $(\text{M}+\text{H})^+$ $\text{C}_{25}\text{H}_{39}\text{B}_3\text{F}_3\text{O}_6$ 525.2977, found 399.2136. (decomposing during ESI to give similar products as 399-di)

Compound 69c



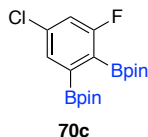
The general borylation procedure was carried out on the starting arene of 4,4,5,5-tetramethyl-2-(4-(trifluoromethoxy)phenyl)-1,3,2-dioxaborolane. After work up procedure **A**, 0.190 g of compound **69c** was obtained as an oil in 46% yield. ^1H NMR (500 MHz, Chloroform-*d*) δ 7.69 (d, $J = 8.2$ Hz, 1H), 7.45 (s, 1H), 7.21 (dd, $J = 8.2, 2.6$ Hz, 1H), 1.37 (s, 12H), 1.36 (s, 12H). ^{13}C NMR (126 MHz, Chloroform-*d*) δ 150.2 (d, $J = 1.7$ Hz), 135.5, 125.4, 121.24, 120.4 (d, $J = 257.1$ Hz), 84.3, 84.2, 24.9. ^{19}F NMR (470 MHz, Chloroform-*d*) δ -57.47. ^{11}B NMR (160 MHz, Chloroform-*d*) δ 30.9.

Compound 69*



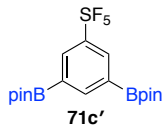
The general borylation procedure was carried out on the starting arene of 4,4,5,5-tetramethyl-2-(4-(trifluoromethoxy)phenyl)-1,3,2-dioxaborolane. After work up procedure **B**, 0.056 g of compound **69*** was obtained as a white solid (mp > 200°C) in 10% yield. ¹H NMR (500 MHz, Chloroform-*d*) δ 7.75 (d, *J* = 1.0 Hz, 2H), 1.48 (s, 12H), 1.33 (s, 24H). ¹³C NMR (900 MHz, Chloroform-*d*) δ 148.95, 142.87(C-B), 135.10(C-B), 129.86, 120.66 (q, *J* = 256.7 Hz), 84.43 (d, *J* = 9.5 Hz), 25.97, 24.90. ¹⁹F NMR (470 MHz, Chloroform-*d*) δ -57.35. ¹¹B NMR (160 MHz, Chloroform-*d*) δ 30.9. MS EI+ *m/z* calculated for (M+H)⁺ C₂₅H₃₉B₃F₃O₇ 541.2927, found 541.2940.

Compound 70c



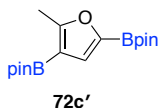
The general borylation procedure was carried out on the starting arene of 2-(3-chloro-5-fluorophenyl)-4,4,5,5-tetramethyl-1,3,2-dioxaborolane. After work up procedure **A**, 0.198 g of compound **70c** was obtained as a white solid in 52% yield. ¹H NMR (500 MHz, Chloroform-*d*) δ 7.55 (d, *J* = 1.9 Hz, 1H), 7.09 (dd, *J* = 8.6, 1.9 Hz, 1H), 1.41 (s, 12H), 1.33 (s, 12H). ¹³C NMR (126 MHz, Chloroform-*d*) δ 135.8 (d, *J* = 9.6 Hz), 130.6 (d, *J* = 2.9 Hz), 117.8, 117.6, 84.5 (d, *J* = 7.7 Hz), 24.94, 24.82. ¹⁹F NMR (470 MHz, Chloroform-*d*) δ -103.99 (d, *J* = 8.9 Hz). ¹¹B NMR (160 MHz, Chloroform-*d*) δ 30.0. MS EI+ *m/z* calculated for (M+H)⁺ C₁₈H₂₇B₂ClFO₄ 383.1768, found 383.1782.

Compound 71c'



The general borylation procedure was carried out on the starting arene of pentafluoro(phenyl)-λ₆-sulfane. Final crude mixture contained mixture of products in ratio of 38: 34: 28 for di: 4-mono: 3-mono. After work up procedure **B**, 0.1532 g of compound **71c'** was obtained as a white solid in 34% yield. ¹H NMR (500 MHz, Chloroform-*d*) δ 8.36 (s, 1H), 8.23 (d, *J* = 1.1 Hz, 2H), 1.36 (s, 24H). ¹³C NMR (126 MHz, Chloroform-*d*) δ 153.6, 143.9, 134.3 (m), 84.4, 24.9. ¹⁹F NMR (470 MHz, Chloroform-*d*) δ 84.75 (p, *J* = 150.5 Hz), 62.80 (d, *J* = 150.0 Hz). ¹¹B NMR (160 MHz, Chloroform-*d*) δ 29.7. MS EI+ *m/z* calculated for (M+H)⁺ C₁₇H₂₈B₂F₅O₄S 457.1814, found 457.1902.

Compound 72c'



The general borylation procedure was carried out on the starting arene of 4,4,5,5-tetramethyl-2-(5-methylfuran-2-yl)-1,3,2-dioxaborolane. Final crude mixture contained mixture of products in ratio of 78: 17: 5 for 2,4di: 2,3di: tri. 2,4-diborylated compound was isolated by passing the concentrated crude reaction mixture through a celite/silica (3:1) plug and collecting fractions using hexane. After further purification using another Celite/silica (2:1) plug with hexane, 0.2314 g of compound **72c'** was obtained as a sticky white solid in 69% yield (mp: 96–98 °C). ¹H NMR (500 MHz, Chloroform-*d*) δ 7.22 (s,

1H), 2.51 (s, 3H), 1.32 (s, 12H), 1.29 (s, 12H). ¹³C NMR (126 MHz, Chloroform-*d*) δ 167.2, 129.4, 83.9, 83.1, 24.8, 24.7, 14.4. ¹¹B NMR (160 MHz, Chloroform-*d*) δ 29.6, 27.1. MS EI+ m/z calculated for (M+H)⁺ C₁₇H₂₉B₂O₅ 335.2201, found 335.2264.

Compound 73c'



The general borylation procedure was carried out on the starting arene of 1-methyl-1H-pyrazole. After work procedure A 0.120 g of compound 73c' white solid in 36% yield. ¹H NMR (500 MHz, Chloroform-*d*) δ 7.15 (d, *J* = 0.8 Hz, 1H), 4.12 (s, 3H), 1.32 (s, 12H), 1.30 (s, 12H). ¹³C NMR (126 MHz, Chloroform-*d*) δ 124.4, 84.0, 83.8, 24.79, 24.77. ¹¹B NMR (160 MHz, CDCl₃) δ 28.2. MS EI+ m/z calculated for (M+H)⁺ C₁₄H₂₉B₂N₂O₄ 335.2313, found 335.2369.

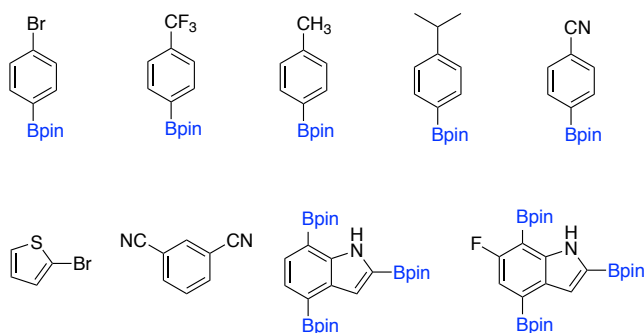


Figure 31. Substrate that did not give di or tri borylated compounds

REFERENCES

REFERENCES

- (1) *Boronic Acids Preparation and Applications in Organic Synthesis, Medicine and Materials*, 2., vollständig überarbeitete Auflage.; Hall, D. G., Ed.; Wiley-VCH: Weinheim, Bergstr, 2011.
- (2) Ghosh, A. K.; Cheng, X.; Zhou, B. Enantioselective Total Synthesis of (+)-Lithospermic Acid. *Org. Lett.* **2012**, *14*, 5046–5049.
- (3) Miyaura, N.; Suzuki, A. Palladium-Catalyzed Cross-Coupling Reactions of Organoboron Compounds. *Chem. Rev.* **1995**, *95*, 2457–2483.
- (4) Shimizu, M.; Tomioka, Y.; Nagao, I.; Hiyama, T. Palladium-Catalyzed Double Cross-Coupling Reaction of Vic-Diborylalkenes and -Arenes with Vic-Bromo(bromomethyl)arenes. *Synlett* **2009**, *2009*, 3147–3150.
- (5) Shimizu, M.; Hiyama, T. Palladium-Catalyzed Double Cross-Coupling Reactions of Organodimetallic Reagents Leading to Polycyclic Aromatic Hydrocarbons: Synthesis of Polycyclic Aromatic Hydrocarbons. *Eur. J. Org. Chem.* **2013**, *2013*, 8069–8081.
- (6) Seven, Ö.; Bolte, M.; Lerner, H.-W.; Wagner, M. High-Yield Syntheses and Reactivity Studies of 1,2-Diborylated and 1,2,4,5-Tetraborylated Benzenes. *Organometallics* **2014**, *33*, 1291–1299.
- (7) Durka, K.; Luliński, S.; Serwatowski, J.; Woźniak, K. Influence of Fluorination and Boronic Group Synergy on the Acidity and Structural Behavior of O-Phenylenediboronic Acids. *Organometallics* **2014**, *33*, 1608–1616.
- (8) Seven, Ö.; Qu, Z.-W.; Zhu, H.; Bolte, M.; Lerner, H.-W.; Holthausen, M. C.; Wagner, M. Synthesis, Coupling, and Condensation Reactions of 1,2-Diborylated Benzenes: An Experimental and Quantum-Chemical Study. *Chemistry* **2012**, *18*, 11284–11295.
- (9) Durka, K.; Luliński, S.; Smętek, J.; Dąbrowski, M.; Serwatowski, J.; Woźniak, K. The Influence of Boronate Groups on the Selectivity of the Br-Li Exchange in Model Dibromoaryl Boronates: Selectivity of the Br-Li Exchange in Model Dibromoaryl

Boronates. *Eur. J. Org. Chem.* **2013**, 2013, 3023–3032.

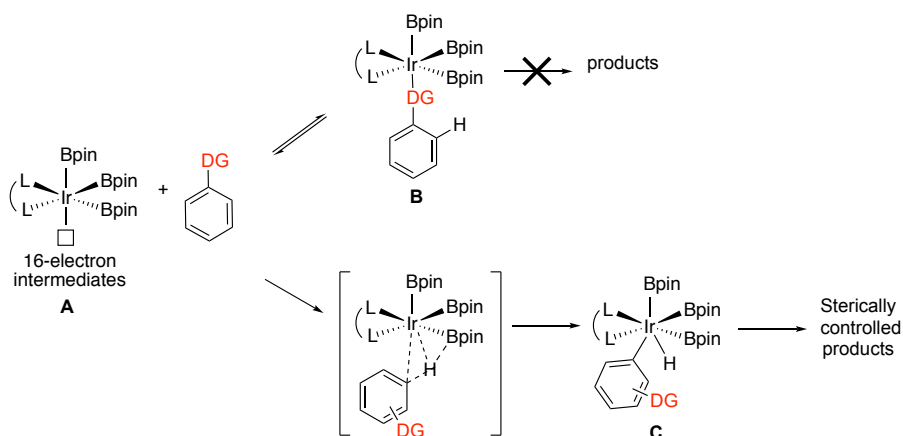
- (10) Noguchi, H.; Shioda, T.; Chou, C.-M.; Suginome, M. Differentially Protected Benzenediboronic Acids: Divalent Cross-Coupling Modules for the Efficient Synthesis of Boron-Substituted Oligoarenes. *Org. Lett.* **2008**, 10, 377–380.
- (11) Shimizu, M.; Nagao, I.; Tomioka, Y.; Kadowaki, T.; Hiyama, T. Palladium-Catalyzed Double Cross-Coupling Reaction of 1,2-Bis(pinacolatoboryl)alkenes and -Arenes with 2,2'-Dibromobiaryls: Annulative Approach to Functionalized Polycyclic Aromatic Hydrocarbons. *Tetrahedron* **2011**, 67, 8014–8026.
- (12) Togashi, K.; Nomura, S.; Yokoyama, N.; Yasuda, T.; Adachi, C. Low Driving Voltage Characteristics of Triphenylene Derivatives as Electron Transport Materials in Organic Light-Emitting Diodes. *J. Mater. Chem.* **2012**, 22, 20689–20695.
- (13) Yoshida, H.; Kawashima, S.; Takemoto, Y.; Okada, K.; Ohshita, J.; Takaki, K. Copper-Catalyzed Borylation Reactions of Alkynes and Arynes. *Angew. Chem. Int. Ed Engl.* **2012**, 124, 239–242.
- (14) Yoshida, H.; Okada, K.; Kawashima, S.; Tanino, K.; Ohshita, J. Platinum-Catalysed Diborylation of Arynes: Synthesis and Reaction of 1,2-Diborylarenes. *Chem. Commun.* **2010**, 46, 1763–1765.
- (15) Pareek, M.; Fallon, T.; Oestreich, M. Platinum(0)-Catalyzed Indolyne Insertion into Bis(pinacolato)diboron Followed by Site-Selective Suzuki-Miyaura Cross-Coupling. *Org. Lett.* **2015**, 17, 2082–2085.
- (16) Mfuh, A. M.; Nguyen, V. T.; Chhetri, B.; Burch, J. E.; Doyle, J. D.; Nesterov, V. N.; Arman, H. D.; Larionov, O. V. Additive- and Metal-Free, Predictably 1,2- and 1,3-Regioselective, Photoinduced Dual C-H/C-X Borylation of Haloarenes. *J. Am. Chem. Soc.* **2016**, 138, 8408–8411.
- (17) Bose, S. K.; Deißberger, A.; Eichhorn, A.; Steel, P. G.; Lin, Z.; Marder, T. B. Zinc-Catalyzed Dual C-X and C-H Borylation of Aryl Halides. *Angew. Chem. Int. Ed Engl.* **2015**, 54, 11843–11847.

- (18) Yamamoto, T.; Ishibashi, A.; Suginome, M. Regioselective Synthesis of O-Benzenediboronic Acids via Ir-Catalyzed O-C-H Borylation Directed by a Pyrazolylaniline-Modified Boronyl Group. *Org. Lett.* **2017**, *19*, 886–889.
- (19) Jayasundara, C. R. K.; Unold, J. M.; Oppenheimer, J.; Smith, M. R., 3rd; Maleczka, R. E., Jr. A Catalytic Borylation/dehalogenation Route to O-Fluoro Arylboronates. *Org. Lett.* **2014**, *16*, 6072–6075.
- (20) Mkhaliid, I. A. I.; Barnard, J. H.; Marder, T. B.; Murphy, J. M.; Hartwig, J. F. C-H Activation for the Construction of C-B Bonds. *Chem. Rev.* **2010**, *110*, 890–931.
- (21) Maleczka, R. E., Jr.; Smith, M. R., III. Remarkably Selective Iridium Catalysts for the Elaboration of Aromatic C–H Bonds. *Science* **2002**, *295*.
- (22) Jayasundara, C. R. K.; Sabasovs, D.; Staples, R. J.; Oppenheimer, J.; Smith, M. R.; Maleczka, R. E. Cobalt-Catalyzed C–H Borylation of Alkyl Arenes and Heteroarenes Including the First Selective Borylations of Secondary Benzylic C–H Bonds. *Organometallics* **2018**, *37*, 1567–1574.
- (23) Palmer, W. N.; Obligacion, J. V.; Pappas, I.; Chirik, P. J. Cobalt-Catalyzed Benzylic Borylation: Enabling Polyborylation and Functionalization of Remote, Unactivated C(sp³)-H Bonds. *J. Am. Chem. Soc.* **2016**, *138*, 766–769.
- (24) Zhang, L.; Huang, Z. Synthesis of 1,1,1-Tris(boronates) from Vinylarenes by Co-Catalyzed Dehydrogenative Borylations-Hydroboration. *J. Am. Chem. Soc.* **2015**, *137* (50), 15600–15603.
- (25) Oshima, K.; Ohmura, T.; Suginome, M. Dearomatizing Conversion of Pyrazines to 1,4-Dihydropyrazine Derivatives via Transition-Metal-Free Diboration, Silaboration, and Hydroboration. *Chem. Commun.* **2012**, *48*, 8571.

Chapter 6: Ligand Screening for Ir–Catalyzed C–H Borylations

6.1 Introduction

The regioselectivity in most of the catalysts developed for the borylation of alkanes and arenes is mainly governed by steric factors. Complementary regioselectivity is obtained by directed ortho metalation (DoM) methodologies using aryl/alkyl metals and cryogenic temperatures. The development of site-selective directed borylations provides a very attractive alternative to the directed ortho metalation (DoM) methodologies, not only because of their higher versatility in cross-coupling applications, but also because of the specific transformations developed for organoboranes, including oxidation, halogenation, amination, etherification (known as the Chan–Lam–Evans), etc.



Scheme 47. Analysis of regioselectivity in Ir-catalysed borylations.

The direct borylation catalyzed by the 1:2 $[\text{Ir}(\text{OMe})(\text{COD})]_2/\text{dtbpy}$ system takes place through a $[\text{Ir}(\text{dtbpy})(\text{Bpin})_3]$ $16e^-$ catalytically active species (A) (Scheme 47).^{1,2} In sensitivity of this process towards any directing effects is due to the lack of an additional vacant coordination sites in complex B formed upon coordination of directing

functionalities. Therefore, the reaction can only proceed via intermediate (C) and thus the regioselectivity is driven by sterics.

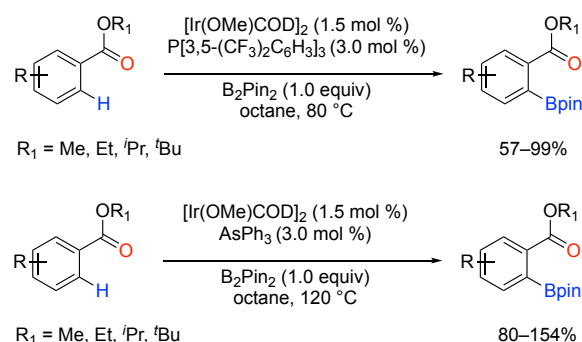
Recently, in order to enable directing group effects in these reactions, different strategies based on catalyst or substrate modification have been developed. These afford attractive site-selective borylation methodologies for the synthesis of ortho-substituted arylboronic esters. Three types of approaches have been designed:

1. Chelate-directed borylations
2. Relay-directed borylations
3. Outer sphere H-bond-directed borylations.

6.2 Chelate-directed borylations

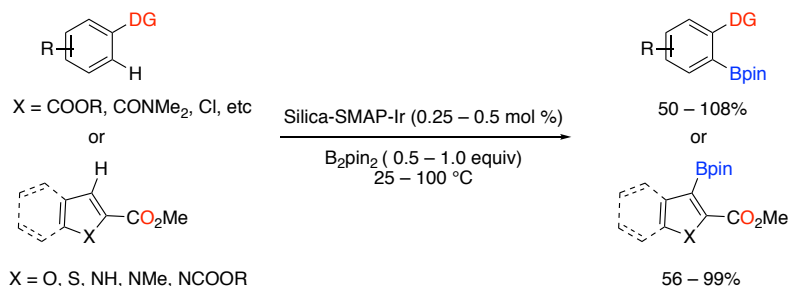
The first strategy consists of modification of the ligand to the Ir catalyst so as to enable an additional vacant coordination site in the catalyst–substrate complex. Ishiyama, Miyaura et al. developed a catalytic system based on the use of $[\text{Ir}(\text{OMe})(\text{COD})]_2$, and an electron-poor phosphine such as $\text{P}[3,5-(\text{CF}_3)_2\text{C}_6\text{H}_3]_3$ ³ as the ligand. This enabled the site-selective borylation of several substrates containing oxygen-based directing groups (Scheme 48).

The method was first applied to the ortho-regioselective borylation of benzoates using B_2pin_2 in octane at 80 °C for 16 h. However, excess of arene (5 equiv.) was needed to avoid partial ortho, ortho'-diborylations. Later, by using AsPh_3 instead of phosphine ligand increased the catalyst activity (Scheme 48). These reactions take place at 120 °C for 16 h, with a broad family of ketones containing different functional groups.⁴



Scheme 48. Oxygen-directed Ir-catalyzed borylations.

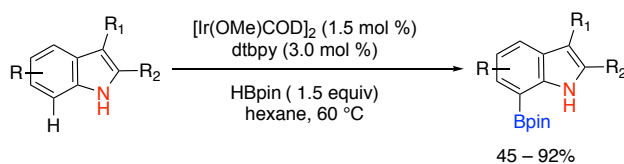
Sawamura et al reported a different approach using a solid-supported monophosphine–Ir system (Silica-SMAP–Ir) for the directed ortho-borylation of functionalized arenes in a very efficient manner (Scheme 49).⁵ This reaction is successful with different oxygenated directing groups. It is noteworthy that the chlorine atom of aryl chlorides can behave as a directing group. Presumably, the supported catalyst assists the formation of 14-electron intermediates for the successive coordination/CH activation. Unfortunately, this heterogeneous catalyst cannot be recovered for recycling. Later, the method was extended to phenol derivatives bearing oxygenated protecting/directing groups and also to heteroarenes bearing 2-methoxycarbonyl as the directing group.^{6,7}



Scheme 49. Silica-SMAP- Ir-catalyzed borylations.

Maleczka, Smith and co-workers reported selective borylation at the 7-position of 2-substituted indoles (Scheme 50).⁸ Control experiments and labelling studies performed

support a mechanism where N-chelation to the iridium center (or the boron atom of a boryl ligand) directs the borylation.



Scheme 50. Selective borylation of 2-substituted indoles.

Lassalate and co-workers introduced a more general nitrogen directed Ir-catalyzed arene ortho-borylations.⁹ Here, they replaced the dtbpy ligand with a hemi labile N,N ligand that facilitates the temporary generation of a coordinatively unsaturated intermediate **C** from the established catalytic species **A** via complex **B** (Figure 32). Complex **C** is pre-organized for the intramolecular activation of C(*ortho*)–H bonds (**D**), from which reductive elimination (**E**) and re-coordination of the hemi labile ligand (**F**) lead to the product and regenerates catalyst **A** after reaction with B₂pin₂.

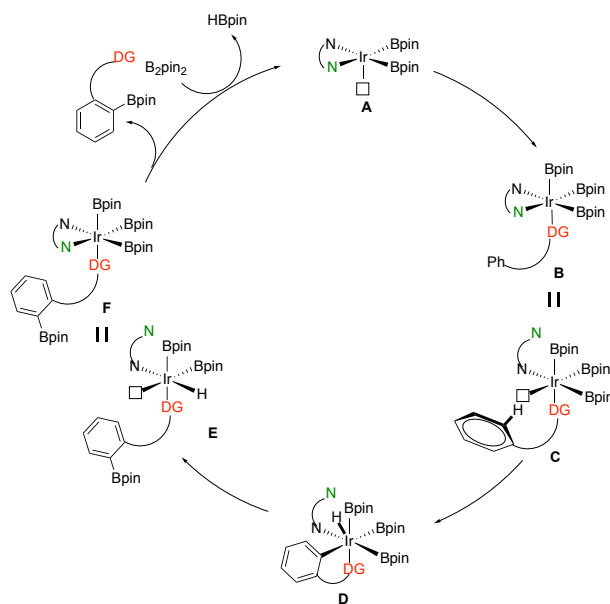
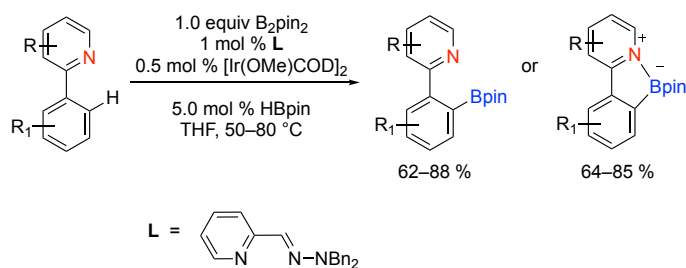


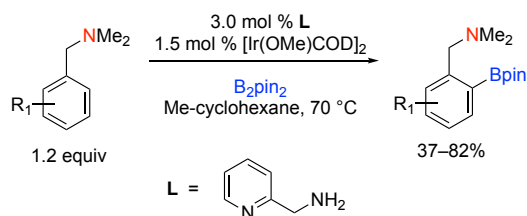
Figure 32. Envisioned mechanism using hemi labile N, N-ligands.

$[\text{Ir}(\text{OMe})(\text{COD})]_2$ combined with picolinaldehyde N, N-dibenzylhydrazone (**L**) used for the borylation of 2-arylpyridines under mild conditions (Scheme 51). Depending on the steric hindrance around the biaryl axis, two types of products were observed. Hindered products revealed no internal N–B interactions, and the (hetero)aromatic rings arrange in a perpendicular fashion. However, less hindered products present intramolecular N–B bonds in planar structures.



Scheme 51. Directed borylation of aryl pyridines.

Clark and co-workers reported a similar idea where nitrogen-directed ortho-C–H borylation of benzylic amines using the picolylamine ligand with $[\text{Ir}(\text{OMe})(\text{COD})]_2$ as the catalyst (Scheme 52).¹⁰ The origin of the ortho-regioselectivity seems to lie in the hemilability of the ligand, instead of a hydrogen bonding directing effect as it was originally proposed.



Scheme 52. Ir-catalysed C–H borylation of benzylic amines.

6.3 Relay-directed borylations

Hartwig and co-workers developed a strategy for the site-selective Ir(III) catalyzed borylation of arenes based on the use of silanes as traceless directing groups.¹¹ Benzyl dimethylsilanes substrates, undergoes Si–H/Ir–B σ -bond metathesis between the catalytically active species **A** to form a silyl bis boryl Ir complex **B** (Figure 33). With complex **B**, the intramolecular activation of the ortho CH bonds takes place preferentially to afford intermediate **C**, which after reductive elimination to give **D** and then reaction with B_2pin_2 releases the product and regenerates the catalyst.

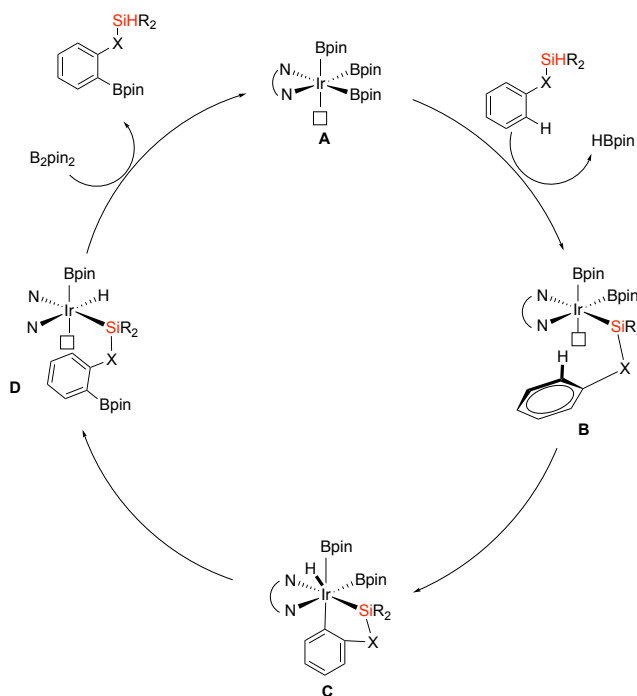
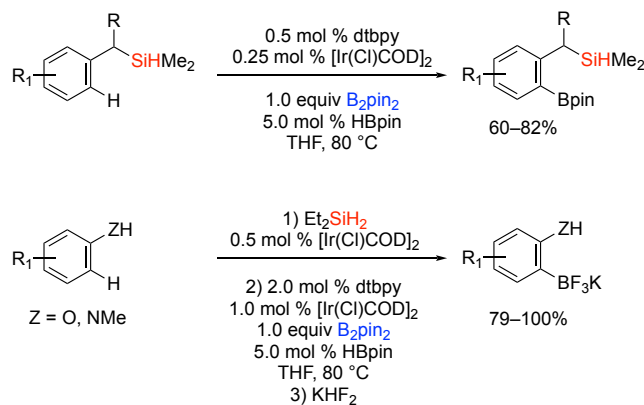


Figure 33. Proposed catalytic cycle for silicon-directed ortho-borylations.

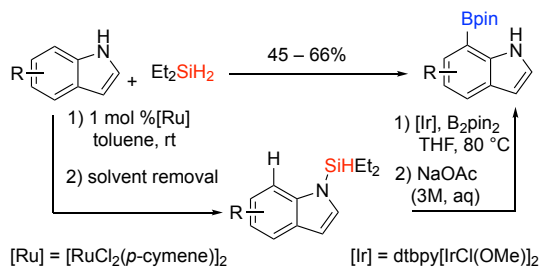
This approach affords the corresponding ortho-borylated products in good to excellent yields. Formation of small amounts of ortho, ortho'- diborylated arylboronic esters is observed in some cases. The methodology has been applied to interesting

substrates, such as silyl ethers and silyl amines, formed in situ by iridium-catalyzed silylation of the corresponding phenols and anilines (Scheme 53).



Scheme 53. Silicon-directed ortho-borylations of arenes.

This method has been extended for the regioselective borylation at the 7-position of indoles (Scheme 54).¹² Usually indoles are borylated at the most reactive 2-position by direct borylation. This procedure tolerates the use of unsubstituted substrates, in contrast, to the previously mentioned methods based on chelating effects.^{7,8} The Ru-catalyzed N-silylation followed by Ir-catalyzed borylation affords the corresponding 7-borylated indoles with complete regioselectivity in moderate yields.

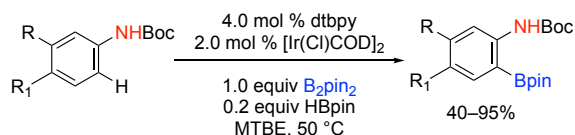


Scheme 54. Silicon-directed borylations at the 7-position of indoles.

6.4 Outer sphere borylations

H-bond-directed:

Outer sphere director refers to the recognition of a functionality in the substrate by a ligand on the catalyst. Smith, Maleczka, Singleton et al.¹³ studied the directing effect of acidic NH groups in monoprotected anilines, finding out that Boc protecting groups provide significant ortho selectivity in the borylations performed with B₂pin₂ as the reagent and [Ir(OMe)(COD)]₂/dtbpy catalytic system (Scheme 55).



Scheme 55. Outer-sphere directed borylation of Boc-protected anilines.

Control experiments and computational studies support an outer sphere mechanism initiated by the formation of a (Boc)NH–O hydrogen bond between the NH group of the substrate and the basic oxygen atom of one of the catalyst boryl groups (Figure 34).

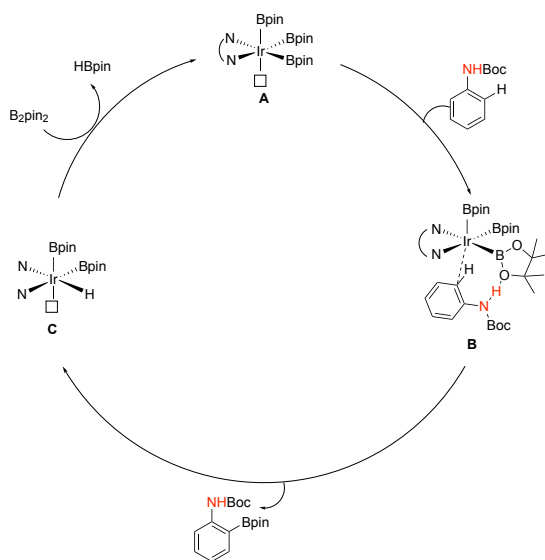
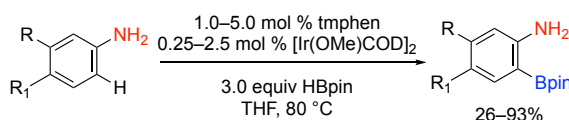


Figure 34. Catalytic cycle for outer-sphere directed borylation

We also reported that Bpin can be used as a traceless directing group for the ortho borylation of a variety of anilines (Scheme 56).¹⁴ Here, 3,4,7,8-tetramethyl-1,10-phenanthroline (tmphen) serves as the ligand and HBpin (2–3 equiv.) as the protecting group as well as the borylating reagent. The NBpin directing group can be installed and removed in situ. The products were isolated in better yields compared with those observed by using the NBoc protecting group. However, the scope of the method is again limited to para-substituted substrates.



Scheme 56. Outer-sphere directed borylation of free anilines.

The previously reported traceless CHBs of primary anilines consistent with an outer-sphere mechanism involving N–H···O hydrogen bonding between the aniline substrate (NH–Boc or NH–Bpin) and a Ir–Bpin ligand (Figure 35).^{13,14} These required C4 substituents larger than H to achieve high ortho selectivity. Furthermore, substitution at C-2 position is not allowed.

Poor regioselectivity

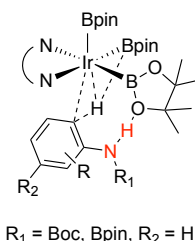
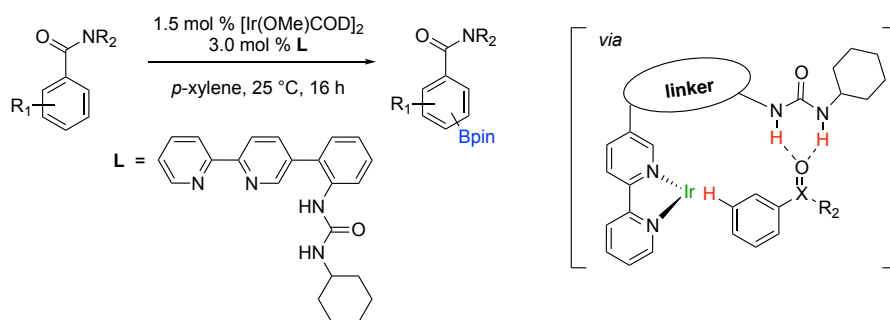


Figure 35. Proposed transition states for ortho borylations of anilines

Kanai, Kuninobu and co-workers reported an elegant use of H-bonding interaction for remote C–H borylations (Scheme 57).¹⁵ A pendant urea moiety covalently linked to bipyridine core unit shows secondary H-bonding interaction with an H-bond acceptor group present on aromatic amides, aryl phosphonates, phosphonic diamides and phosphine oxides. This secondary interaction facilitates high selectivity for meta-C–H activation borylations.



Scheme 57. Hydrogen bond-directed meta-selective borylation of aromatic amides.

In 2017, Phipps and co-workers introduced a single anionic bipyridine ligand containing a remote sulfonate unit that allows meta-selective borylation of a range of aromatic trifluoroamide substrates. They proposed that meta selectivity is due to hydrogen-bonding interaction between the substrate and the anionic ligand present in the catalyst (Figure 36).^{16,17}

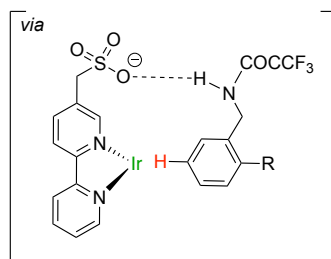
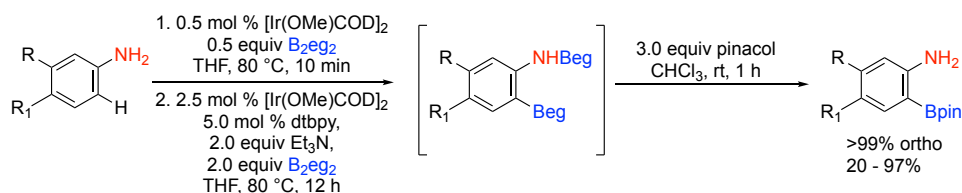


Figure 36. Hydrogen bond-directed meta borylation with an anionic ligand

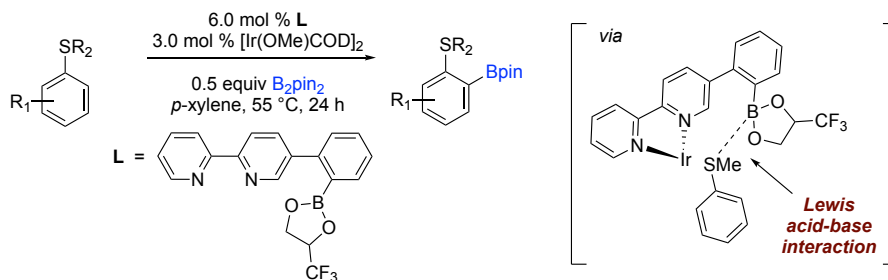
Very recently, Smith, Maleczka, Chattopadhyay and co-workers reported high ortho selectivity for CHBs of aniline using B_2eg_2 (eg = ethylene glycolate) as the boron source.¹⁸ Here, they reported that by changing the boron reagent from HBpin or B_2pin_2 to bis(ethylene glycolato)diboron (B_2eg_2), ortho CHBs can be accomplished with a wide variety of anilines including anilines with no substituents at the 4-position and 2-substituted anilines (Scheme 58). Computational results show that Beg outperforms Bpin because the N(H)Beg substituent and Beg ligands can adopt optimal hydrogen-bonding configurations with minimal steric interference.



Scheme 58. Aniline CHBs with B_2eg_2

Lewis acid-base controlled:

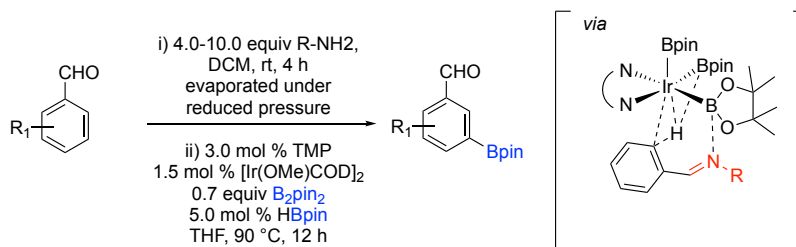
Kuninobu, Kanai and co-workers recently reported a novel Lewis acid-base controlled ortho-selective CHBs of aryl sulfides.¹⁹ The noncovalent interaction in the form of a Lewis acid-base interaction between the S-atom of the substrate and boryl group of ligands facilitate the ortho-borylation of aryl sulfides (Scheme 59). Here electronic properties of boryl ligand affects the ortho-selectivity. Therefore, the boryl ligand is made electron-deficient by introducing a trifluoromethyl group on the ligand, which increases the selectivity (ortho/others) up to 30/1. However, this method is limited to only methyl substituted for aryl sulfides.



Scheme 59. Lewis acid-base interaction for ortho-selective borylation of aryl sulfides.

They extended the same strategy for the ortho-selective borylation of phenols and anilines by introducing an electron-withdrawing group at the bipyridine ligand system.²⁰ The authors expect a similar mechanism as their previous report is operative, where an outer-sphere directed Lewis acid-base interaction exists between a boryl ligand of the iridium metal center and a sulfur atom of the substrate.

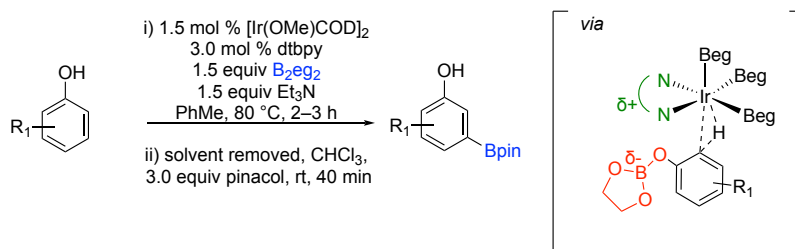
In 2016, Chattopadhyay and co-workers reported an efficient method for the meta-selective borylation of aromatic aldehydes using an electrostatic interaction and boron-nitrogen non-covalent interaction (Scheme 60).²¹ In-situ generated imines from the corresponding aromatic aldehydes are utilized for a B–N noncovalent interaction, which results in high meta selectivity. Imines together with the electron-rich 3,4,7,8-tetramethylphenanthroline (TMP) as ligand exhibited very high selectivity for the meta-position.



Scheme 60. B–N bond-directed meta-selective borylation of aromatic aldehydes.

Electrostatic interactions:

In 2018, Malezcka, Singleton, Smith and co-workers reported a novel approach for *ortho* CHBs of phenols based on the electrostatic interaction between the partial negatively charged OBpin group and partial positively charged bipyridine ring of the ligand (Scheme 61).²² Like previous aniline borylations, 4-substituents larger than H were necessary to achieve high *ortho* selectivity. This indicates that the OBpin directing effect is not strong enough to override the steric control. Computational studies predicted that the *ortho* CHB transition state could be significantly stabilized if the Bpin groups on Ir and the phenol boronate ester were replaced with Beg (eg = ethylene glycolate). This led to exquisite *ortho* selectivities for Ir-catalyzed CHBs of phenols with B₂eg₂ as the diboron reagent.



Scheme 61. *ortho*-selective borylation of unprotected phenols using Beg as traceless directing group.

6.5 Monodentate Vs Bidentate ligands

From previous reported work, it is obvious that bipyridine borylation catalysts are more reactive than their chelating phosphine counterparts. Furthermore, monophosphine ligated catalysts can be effective for *ortho* borylations.²³ It is surprising that pyridines have not gained much attention as monodentate ligands for borylations.

Therefore, in collaboration with Dow Chemical Company, we began screening iridium catalyst systems with different substrates, ligands and solvent in order to understand how electronics affect the C-H activation-borylation of different functionalized arenes and heterocycles. Importantly, we decided to look at bidentate ligands that are not commonly used and also monodentate pyridines as potential ligands in borylation for directing group containing substrates.

During non-directed borylation, the metal center is coordinated by a bidentate pyridine ligand, thus leaving one open coordination site for the substrate to bind and undergo the C-H activation step. However, with monodentate pyridines as ligands, an additional free coordination site on the metal center may be open. We hypothesized that appropriate monopyridine ligands might favor a 14 electron intermediate **1** over 16 electron intermediate **2** and allow for directed borylation (Figure 37). In particular, pyridines that are electron-poor or sterically hindered were considered to be likely candidates.

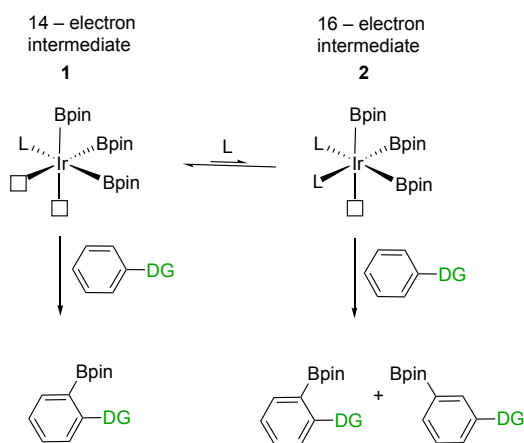


Figure 37. 14 Vs 16 electron intermediates

First, we selected a set of substrates that included fluoro arenes as well as pyridine substrates (Figure 38). We anticipate that some of the pyridine substrates would also behave as the ligand.

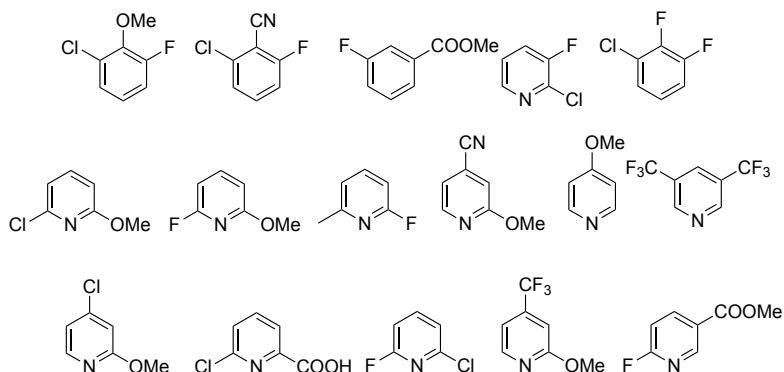


Figure 38. Scope of substrates

Then we selected several bidentate and monodentate ligands for screening (Figure 39). Each substrate (1mmol) was screened with 1 mol % $[\text{Ir}(\text{OMe})\text{COD}]_2$ as the the pre-catalyst, 2 mol % of ligand, 1 equiv of B_2pin_2 as the boron source and different solvent at 60°C for 24h.

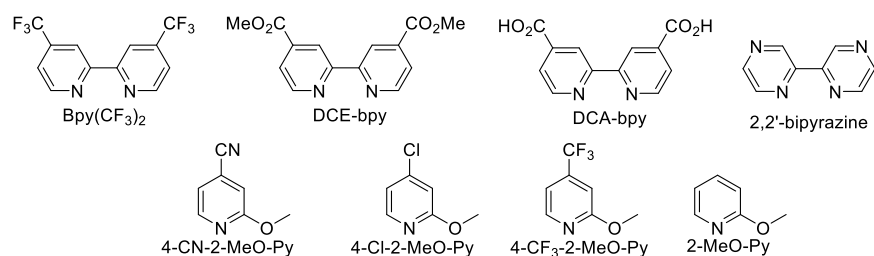


Figure 39. Scope of the ligands

6.6 Results and Discussion

1) Iridium catalyzed C-H borylation of 1-chloro-3-fluoro-2-methoxybenzene (2,6-CFA)

Iridium catalyzed C-H borylation for CFA with different solvent, ligands and boron sources were screened.

a) Tetrahydrofuran (THF)

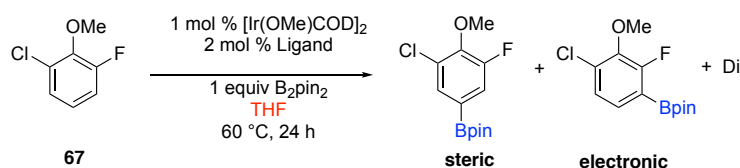


Table 3. Ir-catalyzed C-H borylation of 2, 6-CFA in THF.

	Ligand	Pre-catalyst Stirring time	Reaction time	Conversion (%)	St/Ele/di
1	Bpy(CF3)2	No stirring	16 h	100%	39/58/3
2	4-CN-2-MeO-Py		24 h	85%	20/57/23
3	4-Cl-2-MeO-Py		24 h	82%	20/70/10
4	4-CF3-2-MeO-Py		24 h	71%	19/73/8
5	2-MeO-Py		24 h	83%	25/67/8
6	DCE-bpy		24 h	100%	47/46/7
7	DCA-bpy		15 h	100%	44/50/6
8	Bipyrazine		24 h	49%	44/52/4

Bidentate ligands showed the highest reactivity and the least selectivity. These ligands gave 1:1 mixture of the steric and the electronic products. However, monodentate ligands showed more selectivity towards the electronic product (>4:1). These monodentate ligands were less reactive than bidentate ligands. High temperature and longer reaction time could help the reaction to progress.

b) Hexane

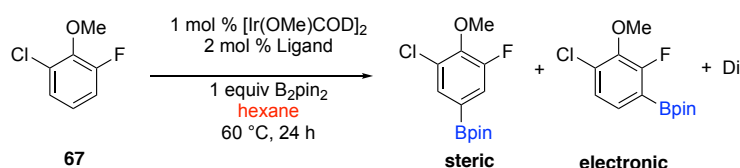


Table 4. Ir-catalyzed C-H borylation of 2, 6-CFA in Hexane.

Entry	Ligand	ligand loading	Pre-catalyst Stirring time	Reaction time	Conversion (%)	St/Ele/di
1	Bpy(CF ₃) ₂	2 mol%	No stirring	24 h	92%	36/54/10
2	4-CN-2-MeO-Py			24 h	93%	21/60/19
3	4-Cl-2-MeO-Py			24 h	77%	18/77/5
4	4-CF ₃ -2-MeO-Py			24 h	51%	18/79/3
5	2-MeO-Py			24 h	78%	24/69/7
6	DCE-bpy			24 h	100%	46/48/6
7	DCA-bpy			15 h	100%	39/58/3
8	Bipyrazine			24 h	77%	35/40/25
9	4-CN-2-MeO-Py	5 mol%		24 h	0%	
10	4-Cl-2-MeO-Py			24 h	8%	34/66

Entry 2, showed the best result that is close to our target. Conversion > 90% and selectivity > 4:1 favoring the electronic product. Bipyrazine ligand in hexane gave better conversion than THF and significant amount of diborylation product was observed. Entry 9, 10 indicated that excess amount of monodentate ligands may shut down the catalyst system.

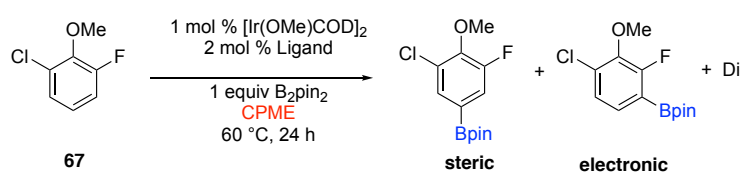
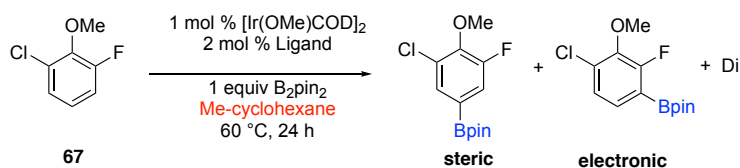
c) Cyclopentylmethyl ether (CPME-50 ppm BHT as the inhibitor)

Table 5. Ir-catalyzed C-H borylation of 2, 6-CFA in CPME.

Entry	Ligand	Pre-catalyst Stirring time	Reaction time	Conversion (%)	St/Ele/di
1	Bpy(CF ₃) ₂	No stirring	24 h	98%	37/59/4
2	4-CN-2-MeO-Py		24 h	61%	25/65/10
3	4-Cl-2-MeO-Py		24 h	54%	20/77/3
4	4-CF ₃ -2-MeO-Py		24 h	41%	19/77/4
5	2-MeO-Py		24 h	73%	24/70/6
6	DCE-bpy		6 h	100%	46/46/8
7	DCA-bpy		22 h	100%	43/54/3
8	Bipyrazine		24 h	77%	39/49/12

Monodentate ligands gave better selectivity favoring the electronic product than the bidentate ligands. However, these monodentate ligands were less reactivity than bidentate ligands.

d) Methyl Cyclohexane

**Table 6. Ir-catalyzed C-H borylation of 2, 6-CFA in methyl cyclohexane.**

Entry	Ligand	Pre-catalyst Stirring time	Reaction time	Conversion (%)	St/Ele/di
1	Bpy(CF ₃) ₂	No stirring	24 h	93%	35/55/10
2	4-CN-2-MeO-Py		24 h	85%	22/64/14
3	4-Cl-2-MeO-Py		24 h	59%	18/79/3
4	4-CF ₃ -2-MeO-Py		24 h	42%	18/82/0
5	2-MeO-Py		24 h	54%	25/70/5
6	DCE-bpy		24 h	100%	43/46/11
7	DCA-bpy		7 h	100%	38/60/2
8	Bipyrazine		24 h	82%	35/44/21

In entry 2, no borylated products were observed after 7 h. However, after 24 h 83% product formation was observed. This indicates a possibility of an induction period.

e) **Hunig's base**

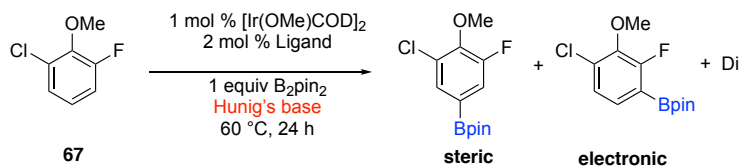


Table 7. Ir-catalyzed C-H borylation of 2, 6-CFA in Hunig's base.

Entry	Ligand	Pre-catalyst Stirring time	Reaction time	Conversion (%)	St/Ele
1	Bpy(CF3)2	No stirring	24 h	80%	37/58/5
2	4-CN-2-MeO-Py		24 h	36%	34/66/0
3	4-Cl-2-MeO-Py		24 h	3%	
4	4-CF3-2-MeO-Py		24 h	0%	
5	2-MeO-Py		24 h	34%	29/71/0
6	DCE-bpy		24 h	100%	44/53/3
7	DCA-bpy		24 h	100%	37/58/5
8	Bipyrazine		24 h	84%	41/43/16

Pyridine ligands showed less reactivity in Hunig's base as the solvent. One possibility is due to the coordinating ability of the solvent itself to the catalyst system. However bidentate ligands showed good reactivity in Hunig's base. Moreover, electron deficient bidentate ligands in Hunig's base favored the electronic borylated product.

f) **Summary of 2, 6-CFA C-H borylation**

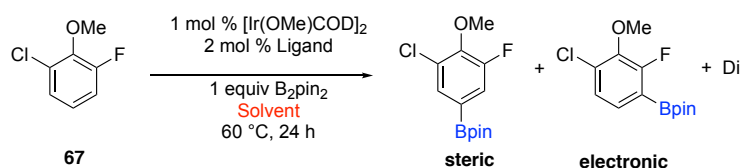


Table 8. Summary of Ir-catalyzed C-H borylation of 2, 6-CFA

Ligand	THF		Hexane		CPME		Hunig's Base		Me-cyclohexane	
	Conv (%)	St/Ele/di	Conv (%)	St/Ele/di	Conv (%)	St/Ele/di	Conv (%)	St/Ele/di	Conv (%)	St/Ele/di
Bpy(CF ₃) ₂	100%	39/58/3	92%	36/54/10	98%	37/59/4	80%	37/58/5	93%	35/55/10
4-CN-2-MeO-Py	85%	20/57/23	93%	21/60/19	61%	25/65/10	36%	34/66/0	85%	22/64/14
4-Cl-2-MeO-Py	82%	20/70/10	77%	18/77/5	54%	20/77/3	3%		59%	18/79/3
4-CF ₃ -2-MeO-Py	71%	19/73/8	51%	18/79/3	41%	19/77/4	0%		42%	18/82/0
2-MeO-Py	83%	25/67/8	78%	24/69/7	73%	24/70/6	34%	29/71/0	54%	25/70/5
DCE-bpy	100%	47/46/7	100%	46/48/6	100%	46/46/8	100%	44/53/3	100%	43/46/11
DCA-bpy	100%	44/50/6	100%	39/58/3	100%	43/54/3	100%	37/58/5	100%	38/60/2
Bipyrazine	49%	44/52/4	77%	35/40/25	77%	39/49/12	84%	41/43/16	82%	35/44/21

Several different monodentate and bidentate ligands were screened. Best results obtain did not meet the target of >90% yield and >6:1 favoring electronic product. Fastest reactivity in all the solvents for 2,6-CFA was observed with DCABpy and DCEbpy bidentate ligands. Moreover, best selectivity for the electronic product was observed with 4-Cl-2-OMepy and 4-CN-2-OMepy monodentate ligands. Pyridine ligands, more electron deficient the ligand is favor the electronic product in non- polar solvent but less conversion.

g) Discussion

From the above data we see that bidentate ligands are very reactive compared to monodentate ligands. Bpy(CF₃)₂ gave the best selectivity towards electronic product where as other bidentate ligands gave a 1:1 mixture of steric and electronic products. In contrast, monodentate pyridine ligands favored the electronic product, but was less reactive than bipyridine ligands.

Bipyrazine showed different reactivity and selectivity compared to mono- and bidentate ligands. Significant amounts of diborylations were observed, especially in nonpolar solvents. To understand the reactivity and selectivity, we fully characterize the starting material by NMR. Furthermore, we prepared authentic materials from alternative routes and compared spectral data with the crude reaction mixture.

2,6-CFA has three different protons. In ^1H NMR the most down field peak corresponds to the proton close to chlorine (H1) (Figure 40). Sterically favored hydrogen (H2) and the hydrogen close to fluorine (H3) are overlapping with each other and up field in the spectrum.

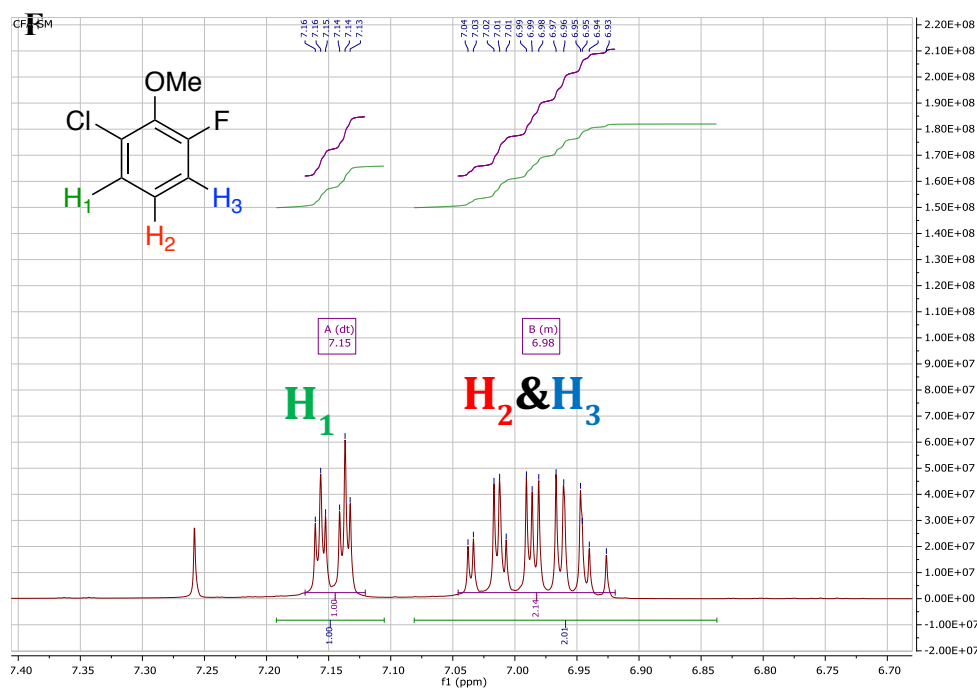
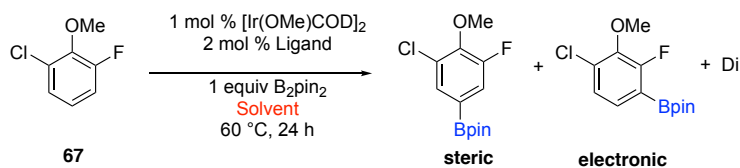


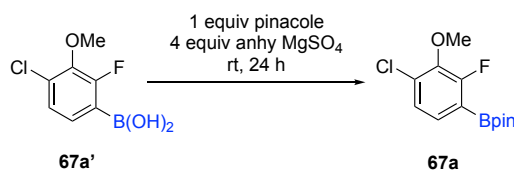
Figure 40. ^1H NMR of starting material 2,6-CFA

C-H borylations of 2,6-CFA gives three products, including two mono (electronic and steric) and one diborylated product (Scheme 62). From previous studies, we know that it is easier to borylate next to fluorine (Chapter 2) than a chlorine.



Scheme 62. CHBs of 2,6-CFA (67)

However, to prove borylation is favored at H3 over H1, and also to get NMR data on the electronic product we synthesized the boronic ester from the previously made (4-chloro-2-fluoro-3-methoxyphenyl) boronic acid (**67a'**) (Scheme 63).



Scheme 63. Making boronic ester from boronic acid

We compared the ^{19}F -NMR of starting material 2,6-CFA (**67**), **67a** and the crude reaction mixture from the C-H borylation of 2,6-CFA to get a picture of the products formed during the C-H borylation (Figure 41).

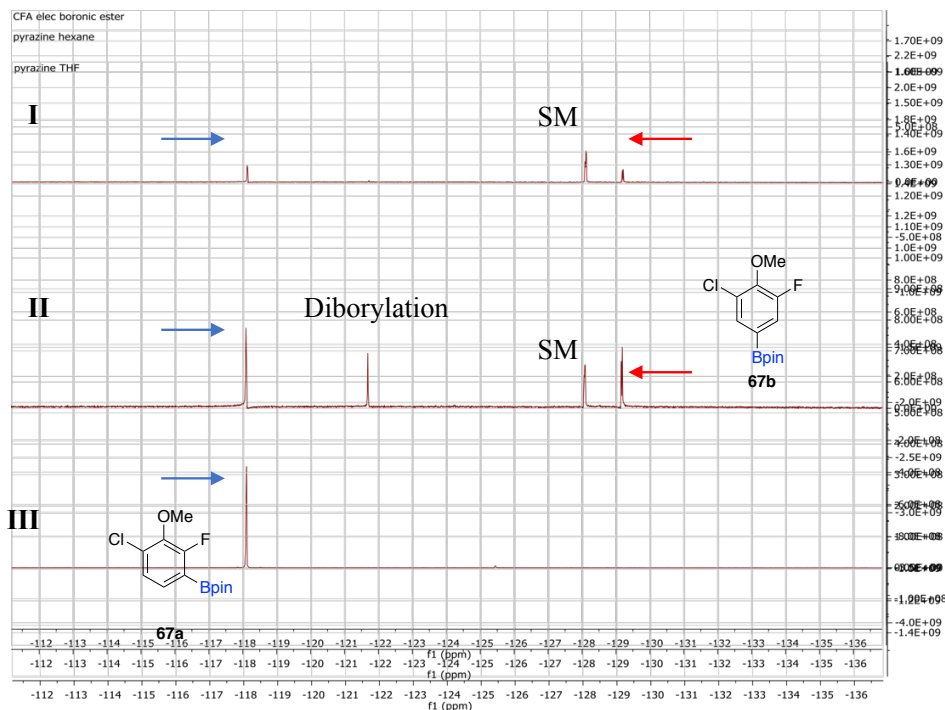
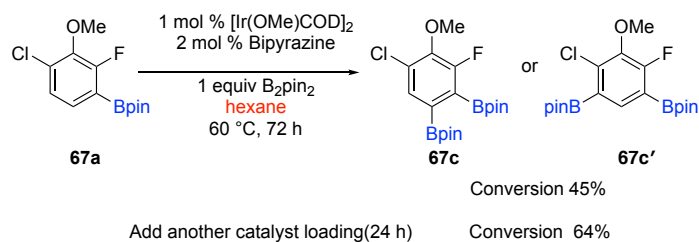


Figure 41. ^{19}F -NMR of

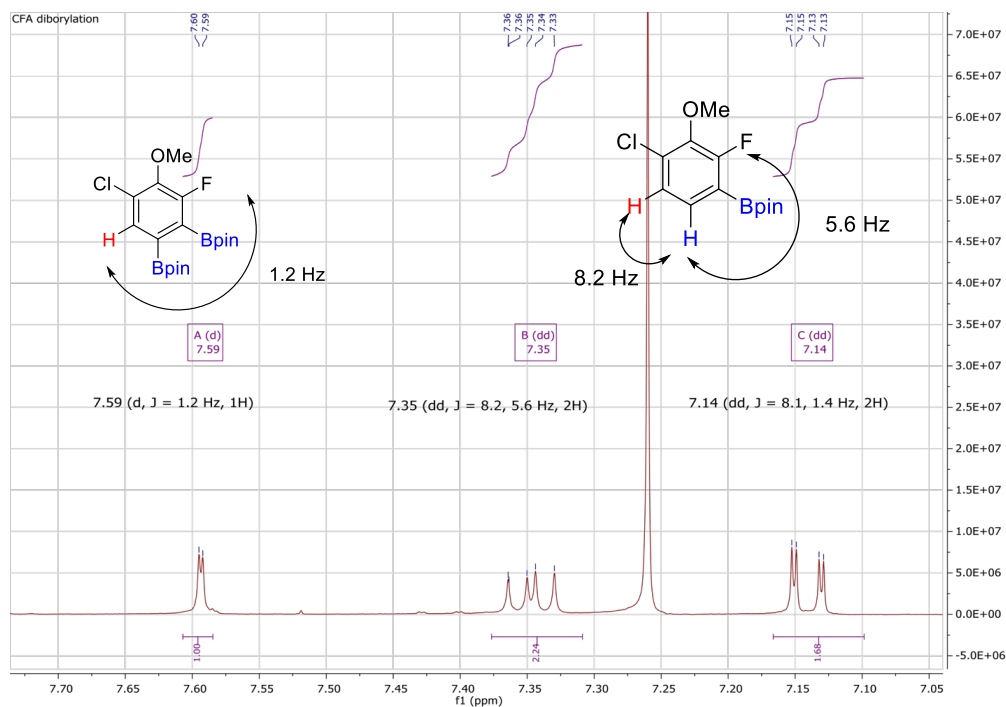
- I) C–H borylation crude reaction of CFA in THF
- II) C–H borylation crude reaction of CFA in hexane
- III) Pure compound (**67a**)

Spectrum (III) correlates with spectra I and II, confirming that the borylation takes place ortho to fluorine (**67a**) over chlorine. Significant amounts of diborylations of CFA were observed with the bipyrazine ligand in hexane as the solvent. ^{19}F -NMR of the crude reaction mixture shows a broad single peak (small coupling) for the diborylation product. This suggests that it is a 1,2-diborylation product (**67c**) vs the 1,3-diborylation product (**67c'**). However, forming (**67c**) would be considered unfavored under iridium-catalyzed C–H activation borylation. In order to confirm the structure of the CFA diborylation product, C–H activation borylation of compound (**67a**) was carried out (Scheme 64).



Scheme 64. CHBs of borylated 2,6-CFA (67a)

^1H NMR of the crude reaction mixture showed a single peak for the newly formed diborylated species. This had a coupling constant of $J=1.2$ Hz (Figure 42). This suggests that **67c** is the diborylated species and not **67c'** (for **67c'** proton we expect a larger coupling constant with fluorine since it is meta to fluorine). Further studies and results are discussed in Chapter 5.



2) Iridium catalyzed C-H borylation of 1-chloro-3-fluoro-2-methoxybenzonitrile (78, CFN)

Iridium catalyzed C-H borylation for CFN with different solvent, ligands and boron sources were screened.

a) Tetrahydrofuran (THF)

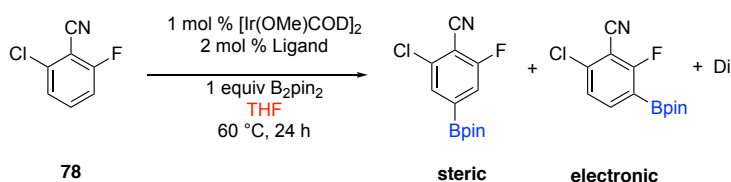


Table 9. Ir-catalyzed C-H borylation of 2, 6-CFN in THF

Entry	Ligand	ligand loading	Stirring time	Reaction time	Conversion (%)	St/Ele/di
1	Bpy(CF3) ₂	2 mol%	No stirring	24 h	100%	42/52/6
2	4-CN-2-MeO-Py	5 mol%		24 h	0%	-
3	4-Cl-2-MeO-Py			24 h	8%	70/30/0
4	4-CN-2-MeO-Py	2 mol%		24 h	0%	-
5	4-Cl-2-MeO-Py			24 h	24%	74/26/0
6	4-CF3-2-MeO-Py			24 h	23%	76/24/0
7	2-MeO-Py			24 h	22%	72/28/0
8	DME-bpy			7 h	100%	49/31/20
9	DCA-bpy			24 h	100%	47/36/17
12	Bipyrazine	24 h		100%	66/31/3	

Excess monodentate ligands showed no CHBs with CFN. In general, pyridine ligands indicated less reactivity with CFN. The steric product was the most favored borylated product with majority of the ligand systems (except entry 1) for CFN.

b) Hexane

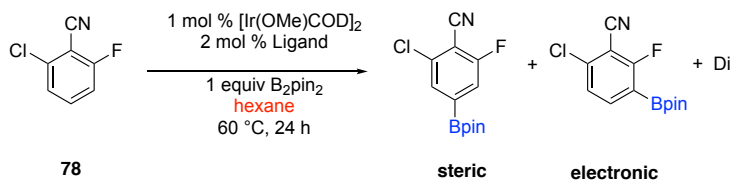


Table 10. Ir-catalyzed C-H borylation of 2, 6-CFN in hexane

Entry	Ligand	ligand loading	Stirring time before adding substrate	Reaction Time/h	Conversion (%)	St/Ele/di
1	Bpy(CF ₃) ₂	2 mol%	No stirring	22 h	100%	36/58/6
2	4-CN-2-MeO-Py	5 mol%		24 h	0%	
3	4-Cl-2-MeO-Py			24 h	8%	70/30/0
4	4-CN-2-MeO-Py	2 mol%		24 h	5%	one isomer
5	4-Cl-2-MeO-Py			24 h	23%	68/32/0
6	4-CF ₃ -2-MeO-Py			24 h	23%	67/33/0
7	DME-bpy			7 h	100%	49/43/8
8	2-OMepy		60 min	24 h	29%	68/32/0
9	DCA-bpy	5 h		100%	44/49/7	
10	Bipyrazine	17 h		100%	60/34/6	
11	2-OMepy	No stirring		24 h	15%	68/32/0
12	DCAbpy			5 h	100%	45/50/5

Pre-generating the active catalyst before introducing the substrate slightly enhanced the reactivity of the monodentate ligands. However, there were no significant change for bidentate ligands. These ligands showed high reactivity with or without pre-generating the active catalyst. Overall, monodentate ligands were less reactive for CFN and less amount of diborylated products were formed with these ligands.

c) **Cyclopentylmethyl ether (CPME-50 ppm BHT as the inhibitor)**

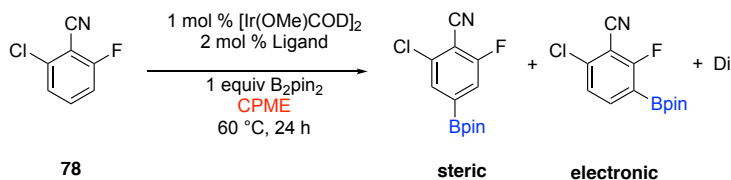


Table 11. Ir-catalyzed C-H borylation of 2, 6-CFN in CPME

Entry	Ligand	Stirring time before adding substrate	Reaction time	Conversion (%)	St/Ele/di
1	Bpy(CF ₃) ₂	60 min	20 h	100%	37/58/5
2	4-CN-2-MeO-Py		24 h	15%	63/37/0
3	4-Cl-2-MeO-Py		24 h	18%	68/32/0
4	DCE-bpy		1.5 h	100%	48/46/6
5	DCA-bpy		1.5 h	100%	50/44/6
6	Bipyrazine		20 h	100%	64/30/6

Similar trend of reactivity was observed for CFN as previous cases. Bpy(CF₃)₂ was the only ligand, that favored the electronic product.

d) **Methyl cyclohexane**

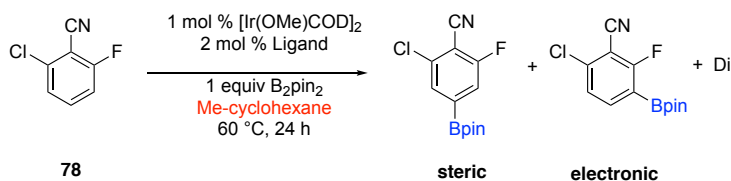


Table 12. Ir-catalyzed C-H borylation of 2, 6-CFN in methyl cyclohexane

Entry	Ligand	Stirring time	Reaction time	Conversion (%)	St/Ele/di
1	Bpy(CF ₃) ₂		19 h	100% (19h)	39/58/3
2	4-CN-2-MeO-Py		24 h	17%	66/34/0
3	4-Cl-2-MeO-Py		24 h	25%	64/36/0

Table 12 (cont'd)

4	4-CF ₃ -2-MeO-Py	60 min	24 h	28%	66/34/0
5	2-MeO-Py		24 h	30%	66/34/0
6	DCE-bpy		2 h	100%	47/43/10
7	DCA-bpy		2 h	100%	44/52/4
8	Bipyrazine		15 h	100%	60/35/5
9	2-CN-4-Ome-Py		24 h	65%	73/27/0

There were no significant deviations observed in Me-cyclohexane for CFN. Similar trend was observed as previous solvent systems.

e) Hunig's base

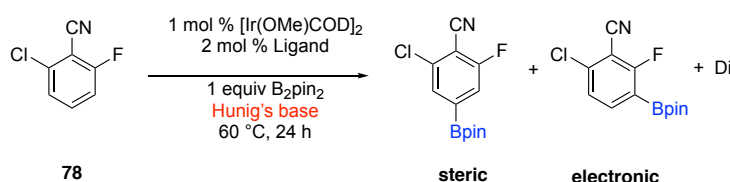


Table 13. Ir-catalyzed C-H borylation of 2, 6-CFN in Hunig's base

Entry	Ligand	Stirring time	Reaction time	Conversion (%)	St/Ele/di
1	Bpy(CF ₃) ₂	60 min	24 h	98%	36/60/4
2	4-CN-2-MeO-Py		24 h	7%	70/30/0
3	4-Cl-2-MeO-Py		24 h	8%	71/29/0
4	4-CF ₃ -2-MeO-Py		24 h	10%	55/45/0
5	2-MeO-Py		24 h	8%	69/31/0
6	DCE-bpy		24 h	98%	37/61/2
7	DCA-bpy		24 h	98%	36/61/3
8	Bipyrazine		17 h	100%	63/33/4

In previous solvent systems only Bpy(CF₃)₂ ligand favored the electronic product formation for CFN. However, in Hunig's base except bipyrazine, all the other bidentate ligands (DCAbpy, DCEbpy and Bpy(CF₃)₂) favored the electronic product over the steric product

Monodentate pyridine ligands showed less/or no reactivity in Hunig's base. If monodentate pyridine ligands go through a 14 electron intermediate, then there are several vacant coordination sites at the metal center and these ligands are less sterically hindered than bidentate ligands. As stated earlier Hunig's base solvent itself has the ability to coordinate to the catalyst system. This could be a reason for deactivation of the catalyst system.

f) Summary of 2, 6-CFN C-H borylation

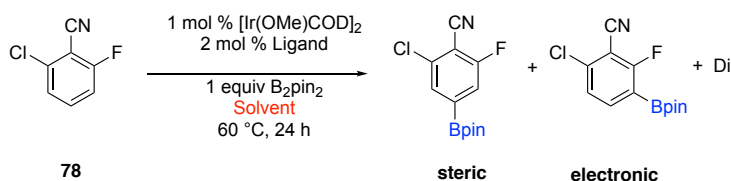


Table 14. Summary of Ir-catalyzed C-H borylation of 2, 6-CFN

Ligand	THF		Hexane		Hunig's base		Me-Cyclohexane		CPME	
	Conv (%)	St/Ele/di	Conv (%)	St/Ele/di	Conv (%)	St/Ele/di	Conv (%)	St/Ele/di	Conv (%)	St/Ele/di
Bpy(CF ₃) ₂	100%	42/52/6	100%	36/58/6	98%	36/60/4	100%	39/58/3	100%	37/58/5
4-CN-2-OMe-Py	0%	-	5%	one isomer	7%	70/30/0	17%	66/34/0	15%	63/37/0
4-Cl-2-OMe-Py	24%	74/26/0	23%	68/32/0	8%	71/29/0	25%	64/36/0	18%	68/32/0
4-CF ₃ -2-OMe-Py	23%	76/24/0	23%	67/33/0	10%	55/45/0	28%	66/34/0		
2-OMe-Py	22%	72/28/0	100%	49/43/8	8%	69/31/0	30%	66/34/0		
DCE-bpy	100%	49/31/20	29%	68/32/0	98%	37/61/2	100%	47/43/10	100%	48/46/6
DCA-bpy	100%	47/36/17	100%	44/49/7	98%	36/61/3	100%	44/52/4	100%	50/44/6
Bipyrazine	100%	66/31/3	100%	60/34/6	100%	63/33/4	100%	60/35/5	100%	64/30/6
2-CN-4-OMe							65%	73/27/0		

Bpy(CF₃)₂ ligand favored the electronic product of CFN in all the solvents. Generating the active catalyst before introducing the substrate was only important for the reactivity of the monodentate pyridine ligands. These ligands were less reactive in CHBs

for benzonitrile. All the monodentate ligands favored the steric product. However, Hunig's base was an ideal solvent for favoring the electronic product with electron deficient ligands.

g) Discussion

In 2,6-CFN (Figure 43) the most down field hydrogen (H2) is para to the cyano group and it is the most sterically and electronically favored hydrogen in this case. We assume that this is the reason for C-H borylation of 2, 6-CFN substrate favoring compound **74b** as the major product with a majority of ligands. Hydrogen (H1) is close to chlorine and more deshielded than the hydrogen close to fluorine (H3).

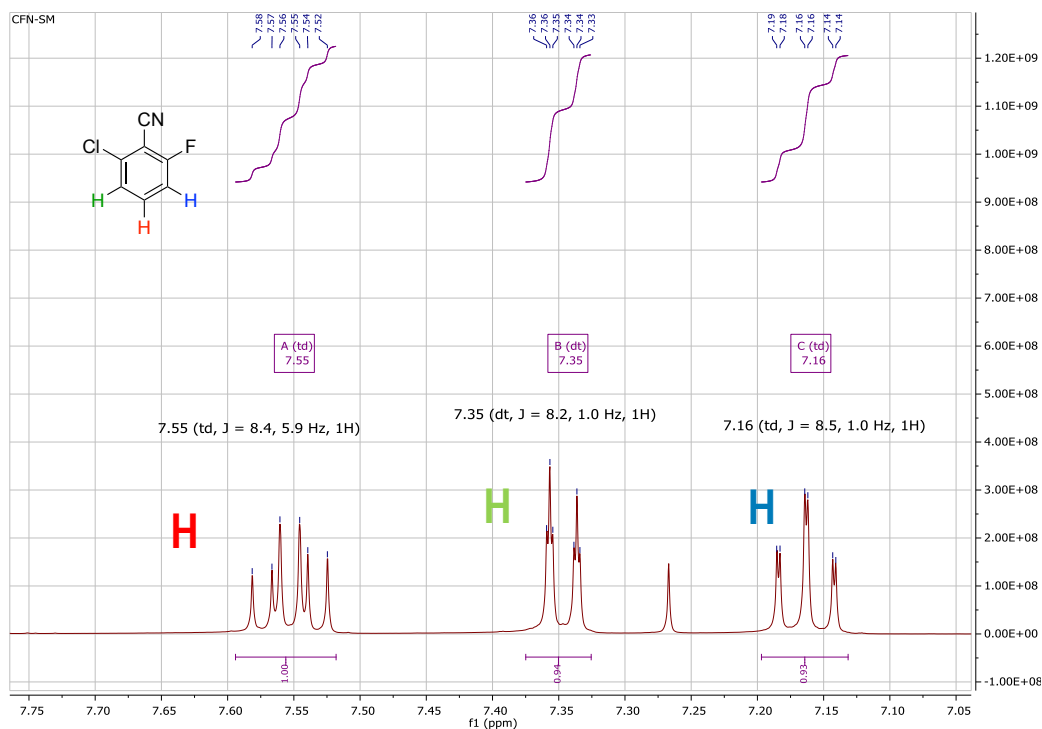


Figure 43. ¹H NMR of starting material 2,6-CFN

C–H activation borylation of 2,6-CFN with DCE-bpy as the ligand in THF gave significant amounts of diborylation. Therefore, to identify the diborylated species we did a thorough investigation on the ¹H-NMR of the crude reaction mixture (Figure 44).

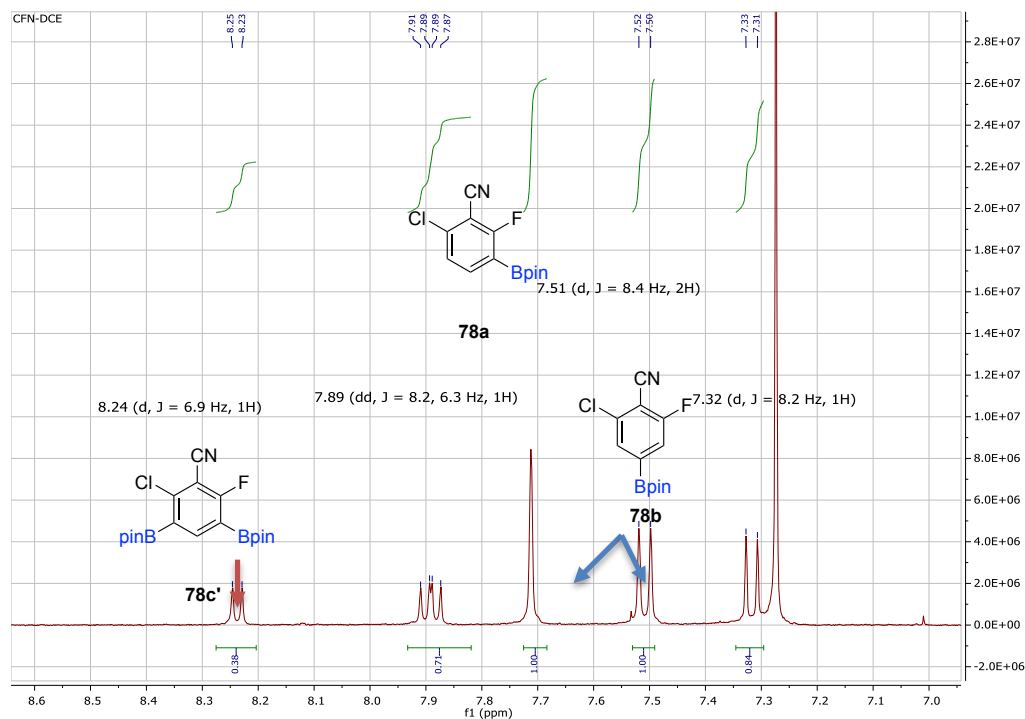
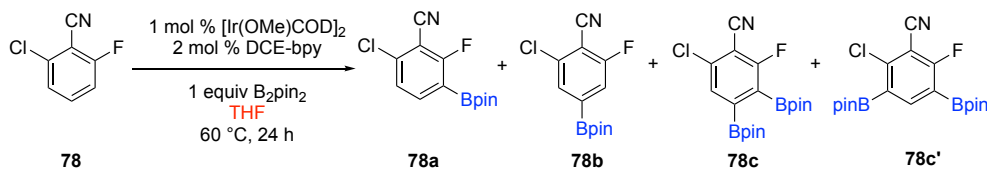


Figure 44. ¹H-NMR of starting material 2,6-CFN

There are two possibilities, either 1,2-diborylated product (**78c**) or 1,3-diborylated product (**78c'**) (Scheme 65). Based on coupling constants 1,3-diborylation (**78c'**) is the diborylated product and not **78c**. Substrate (**78a**) already known in literature.



Scheme 65. CHBS of 2,6-CFN

3) Iridium catalyzed C–H borylation of 2-chloro-6-methoxypyridine (Cl-OMepy)

Iridium catalyzed C-H borylation for Cl-OMepy with different solvent, ligands and boron sources were screened. Three mono borylated regioisomers are possible with this substrate.

a) Tetrahydrofuran (THF)

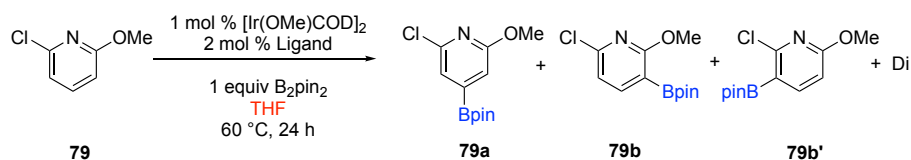


Table 15. Ir-catalyzed C-H borylation of Cl-OMePy in THF.

Entry	Ligand	Stirring time	Reaction time	Conversion (%)	(79a)/(79b)/(79c)/di
1	Bpy(CF ₃) ₂	No stirring	8 h	100%	82/14/0/4
2	4-CN-2-MeO-Py		24 h	55%	75/13/12/0
3	4-Cl-2-MeO-Py		24 h	58%	75/18/7/0
4	4-CF ₃ -2-MeO-Py		24 h	58%	72/20/8/0
5	2-MeO-Py		24 h	77%	79/17/4/0
6	DCE-bpy		3 h	100%	90/10/0/0
7	DCA-bpy		2 h	100%	88/10/0/2

Bipyridine ligands showed high reactivity (Entry 1,6,7) in CHBs of Cl-OMepy when compared to monodentate ligands. Bidentate ligands gave two mono and one diborylated products. However, monodentate pyridine ligands gave three mono borylated products but no diborylated products.

DCAbpy and DCEbpy ligands showed high reactivity in CHBs of Cl-OMepy. These two ligands gave full conversion to the desired borylated product within 2-3 h.

b) Discussion

Starting material of Cl-OMepyridine (Figure 45) has three different protons. The most down field hydrogen (H2) is para to the nitrogen group and it is the most sterically and electronically favored hydrogen in this case. Therefore, this is the main reason for obtaining **79a** as the major isomer with all ligands. (H1) and (H3) assignments are inconclusive.

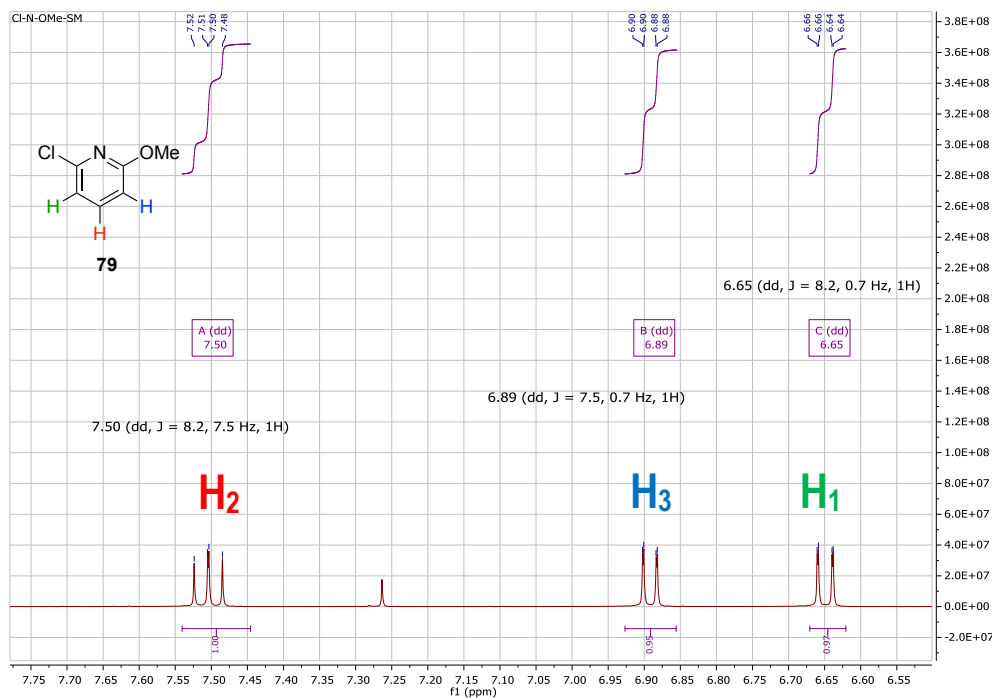
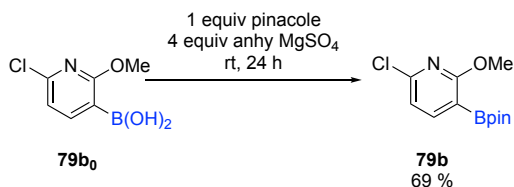


Figure 45. ¹H NMR of starting material Cl-OMePy

To confirm which isomer is major between **79b** and **79b'**, we purchased the boronic acid (**79b₀**) and converted it into the boronic ester (Scheme 66).



Scheme 66. Making boronic ester from boronic acid

Now by comparing $^1\text{H-NMR}$ of the crude reaction mixture for C-H borylation of Cl-OMe-pyridine with the $^1\text{H-NMR}$ of synthesized authentic sample **79b**, gives a clear indication about which isomer is made as the electronic product. Borylation ortho to methoxy group (**79b**) is favored over borylation ortho to chlorine (**79b'**) (Figure 46).

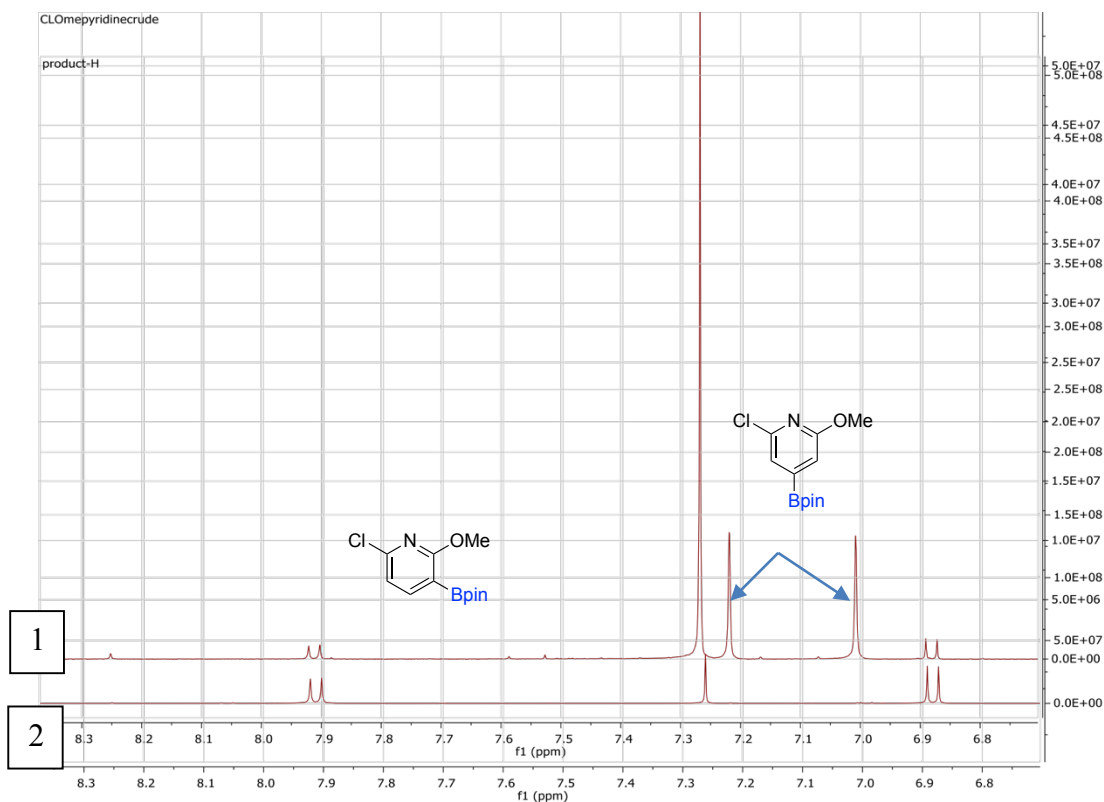


Figure 46. $^1\text{H NMR}$ of

- 1) Crude C-H borylation reaction mixture
- 2) Pure compound **79b**

Interestingly, this is a very good example to show how selectivity changes in different substrates. We expect C-H borylation to favor ortho to chlorine compared to a methoxy group due to sterics. However, the major electronic product here is borylation ortho to methoxy (**79b**). Not enough evidence exists to prove which diborylated product is made during this C-H borylation.

4) Iridium catalyzed C-H borylation of 4-methoxypyridine (4-OMe-pyridine)

a) Tetrahydrofuran (THF) – No active catalyst pregenerate

4-OMe pyridine was screened with several monodentate and bidentate ligands in THF as the solvent. Here the active catalyst was not formed prior to introducing the substrate.

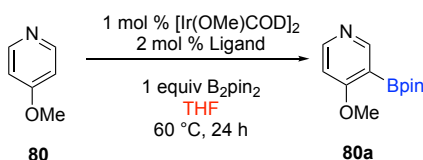


Table 16. Ir-catalyzed C-H borylation of 4-OMe-Py in THF.

Entry	Ligand	Stirring time	Reaction time	Conversion (%)
1	Bpy(CF ₃) ₂	No stirring	24 h	0%
2	4-CN-2-MeO-Py		24 h	0%
3	4-Cl-2-MeO-Py		24 h	0%
4	DCE-bpy		24 h	17%
5	DCA-bpy		24 h	0%

Monodentate or bidentate ligands did not show C-H borylations for 4-OMepy (except for entry 4). This is may be due to the strong coordinating ability of the substrate. We hypothesized that 4-OMepy coordinates to the metal center and deactivate the catalyst system. Therefore, by generating the active catalyst before introducing the substrate might help to carry out CHBs.

With DCABpy ligand a black solid was observed, however in this case no black solid was formed. This again confirmed that the active catalyst was not formed.

b) Tetrahydrofuran (THF) – pre-generate active catalyst

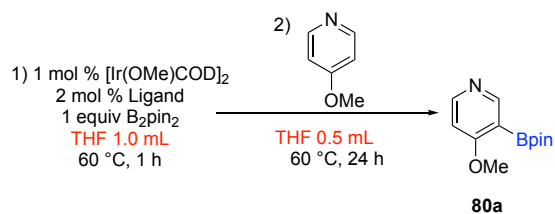


Table 17. Ir-catalyzed C-H borylation of 4-OMe-Py in THF.

Entry	Ligand	Stirring Time/min	Conversion (%)	Reaction time
1	Bpy(CF ₃) ₂	30	0%	24h
2	4-CN-2-MeO-Py	30	0%	24h
3	4-Cl-2-MeO-Py	30	0%	24h
4	4-CF ₃ -2-MeO-Py	60	0%	24h
5	2-MeO-Py	60	0%	24h
6	DCE-bpy	60	12%	24h
7	DCA-bpy	60	100%	5h
8	Dtbpy	20	15%	24h
9	Dtbpy	60	15%	24h

Generating the active catalyst first before introducing the substrate did not help with CHBs of 4-OMepy with most of the ligands except DCAbpy ligand. All monodentate ligands and Bpy(CF₃)₂ completely failed in CHB.

DCA-bpy ligand showed remarkable reactivity in CHBs throughout the ligand screening process. This is an example that shows the exceptional reactivity of DCAbpy compared to the most commonly used dtbpy ligand. In depth discussion about the reactivity of DCAbpy is discussed in Chapter 7.

In Table 16, entry 5 a black solid was not observed, however, in Table 17 for DCAbpy (entry 7) a black solid was observed (Figure 47) and complete conversion to the desired borylated product was observed in 5 h.

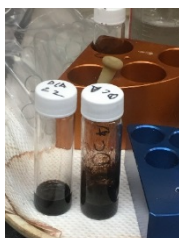


Figure 47. Comparing Table 16 (entry 5) with Table 17 (entry 7).

5) Iridium catalyzed C–H borylation of 2-Fluoro-6-methoxypyridine (F-OMe-py)

1) Tetrahydrofuran (THF)

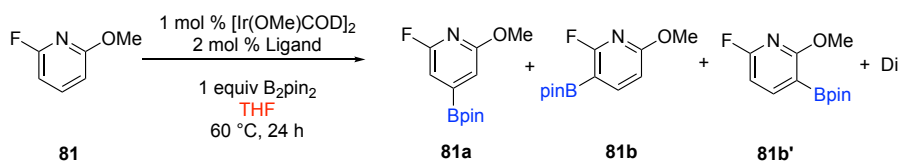


Table 18. Ir-catalyzed C-H borylation of F-OMe-Py in THF with no stirring.

Entry	Ligand	Substrate Source	Conversion (%)	Ste(81a) 7.55	Ele1(81b) 7.69	Ele2(81c) 7.30	Di1 9.92	Di2 9.97
1	DCA-bpy	Matrix Scientific Batch #041031	100%	50	25	N/A	25	N/A
2#	DCA-bpy	Combi-Block Batch #L30987	100%	53	33	3	10	N/A
3#	Bpy(CF ₃) ₂		99%	38	39	3	18	
4#	Bipyrazine		60%	30	11	36	14(9.3)	8
5*	No ligand		64%	13	8	40	33	6

*No PCl₃ issue

#PCl₃ issue

CHBs of F-OMepy gave several mono and di borylated products. CHB without any ligands progressed up to 64% and showed different selectivity. Since there was a PCl_3 contamination inside the box most of the the CHBs results of F-OMe-pyridine were inconclusive.

2) Hexane

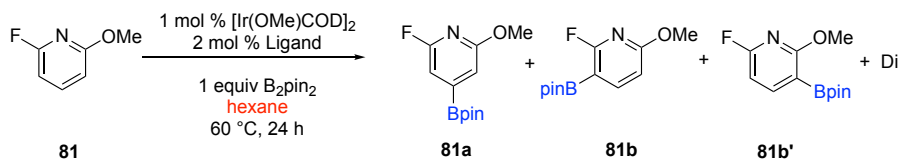


Table 19. Ir-catalyzed C-H borylation of F-OMe-Py in hexane.

Entry	Ligand	Substrate Source	Stirring time	Reaction time	Conversion (%)	Ste(81a) 7.55	Ele1(81b) 7.69	Ele2 7.30	Di1 9.92	Di2 9.97
1#	DCA-bpy	Matrix Scientific Batch #041031	No stirring	24 h	100%	47	33	2	17	1
2#	dtfbpy	Combi-Block Batch #L30987		24 h	94%	33	46	6	10	5
3#	Bipyrazine			24 h	96%	59	14	6	19	2(11.5)
4*	No ligands			24 h	45%	26	17	44	6	7

*No PCl_3 issue

PCl_3 issue

3) Discussion

Starting material of F-OMe-pyridine has three different protons (Figure 48). The most down field hydrogen (H2) is para to nitrogen group and it is the most sterically and electronically favored hydrogen. Therefore, the major isomer in C-H borylation is **81a** (steric product). (H1) and (H3) assignments are inconclusive.

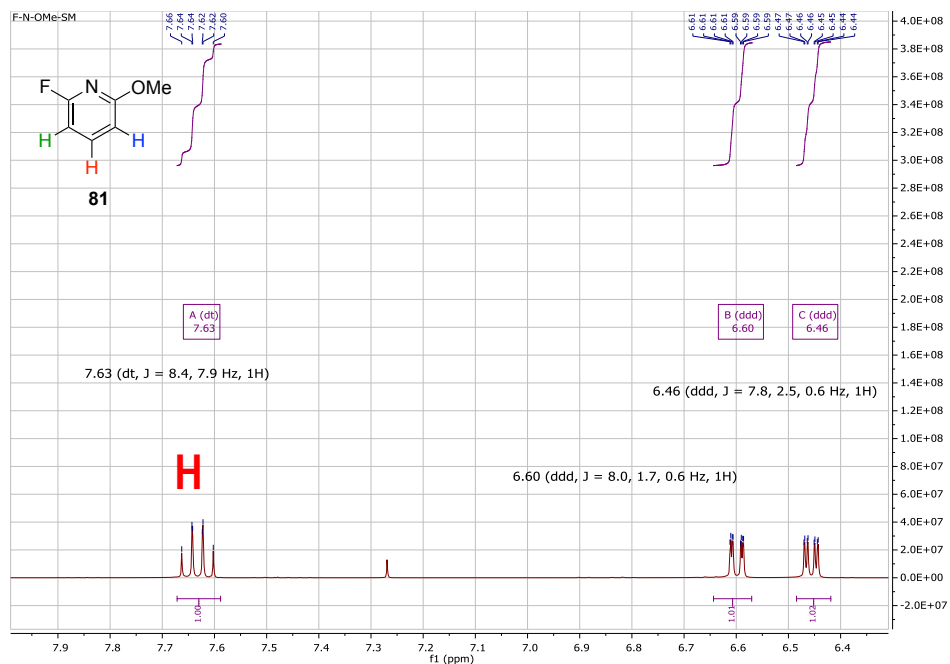
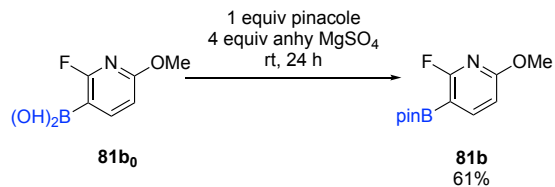


Figure 48. ^1H NMR of starting material F-OMe-Py

2-Fluoro pyridine substrates usually have unusual coupling patterns. In Figure 40, we don't see H-F coupling patterns in the starting material. This is a characteristic feature of 2-fluoropyridines. In Cl-OMe-pyridine, borylation ortho to methoxy (**79b**) was preferred over borylation ortho to chlorine. To confirm unambiguously the major electronic product for F-OMe-pyridine is compound (**81b**), we made an authentic sample starting from its boronic acid derivative (**81b₀**) (Scheme 67).



Scheme 67. Making boronic ester from boronic acid

Next, we compared the ^1H NMR of the crude reaction for C-H borylations of compound **81** with the authentic sample. This clearly shows that that major electronic

isomer is **81b**, that is borylation ortho to fluorine group (**81b**) is favored over borylation to ortho to methoxy group (Figure 49). This is favored sterically as well as electronically.

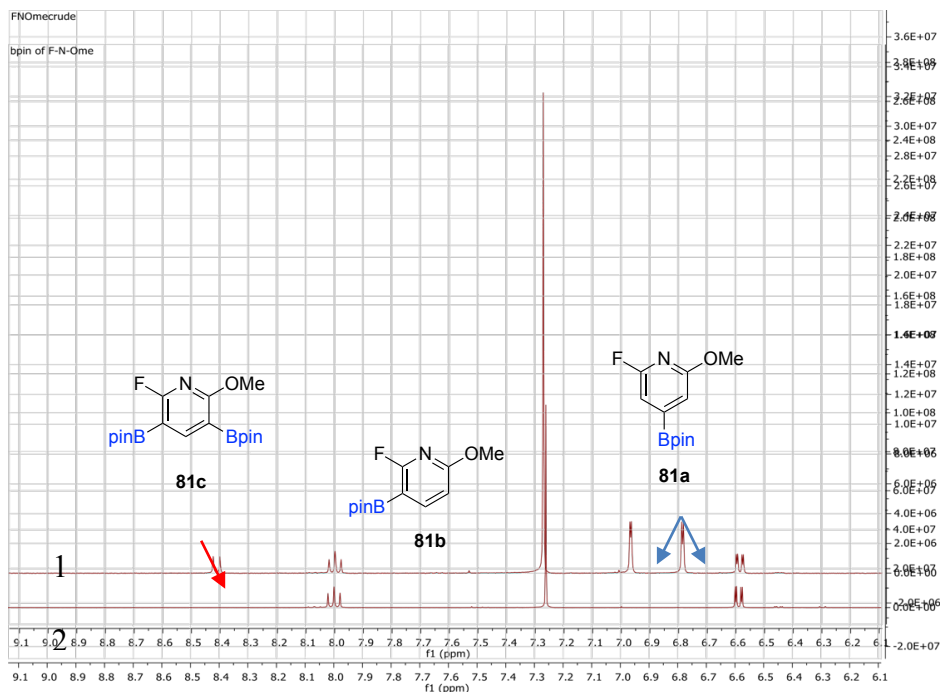


Figure 49. ^1H NMR of

- 1) Crude C-H borylation reaction mixture Table 18 (entry1)
- 2) Pure compound **81b**

Note that *meta* H-F coupling in 2-fluoropyridine is close to 8.7 Hz. It is unusually a large coupling constant. From this, we can confirm the structure of diborylation is to be 1, 3- diborylation (**81c**).

6) Iridium catalyzed C–H borylation of 2-methoxy-isonicotinonitrile (4-CN-2-OMe-pyridine)

Next, we investigated reactivity of ligands. Can the ligand itself be the substrate as well as the ligand for itself? To address this, we carried out following screenings.

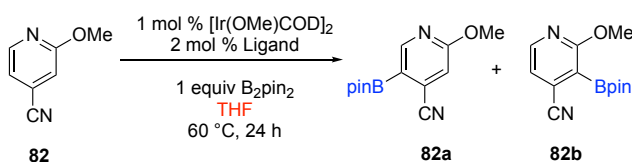
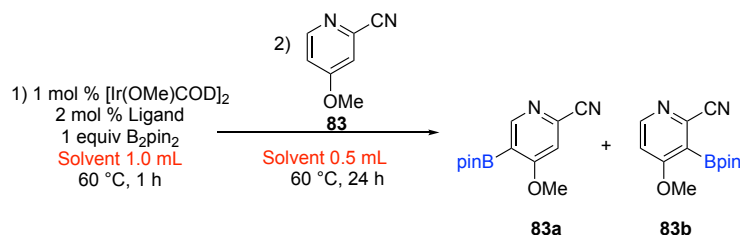


Table 20. Ir-catalyzed C-H borylation of 4-CN-2-OMe-Py in hexane.

Entry	Ligand	Conversion (%)	(82a)/(82b)/unknown	Reaction time
1	No ligand	0%	-	24h
2	dtbpy	65%	55/40/5	24h

- We have already encountered excess ligand of 4-CN-2-OMe-pyridine shuts down the Iridium catalyst system. There for entry 1 outcome is not surprising.
- Entry 2 with the most reactive ligand gave only 65% conversion. GC-MS confirms 3 monoborylated products (mass of 260). However, major isomer is **82a** as confirmed by NMR.

5) Iridium catalyzed C–H borylation of 4-methoxypicolinonitrile (2-CN-4-OMe-pyridine)

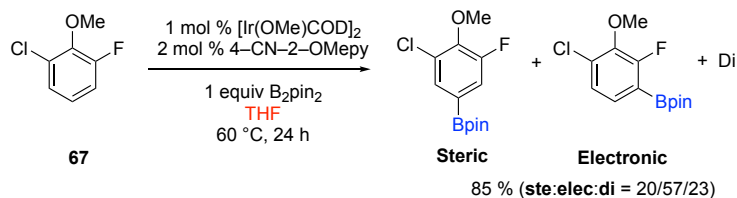
**Table 21. Ir-catalyzed C-H borylation of 4-CN-2-OMe-Py in hexane.**

Entry	Ligand	solvent	Conversion	(83a)/(83b)	Reaction time
1	Bpy(CF ₃) ₂	THF	58%	88/12	24h
2	DCA-bpy		100%	98/2	24h
3	Bipyrazine	Hexane	0%	-	24h
4	4-Cl-2-OMepy	Hexane + THF	0%	-	24h
5	Bipyrazine	THF	0%	-	24h
6	4-CN-2-OMepy		0%	-	24h
7	No ligand		0%	-	24h
8	dtbpy		100%	90/10	5h

Bidentate ligands showed high reactivity for CHBs in THF. Starting material was not soluble in hexane.

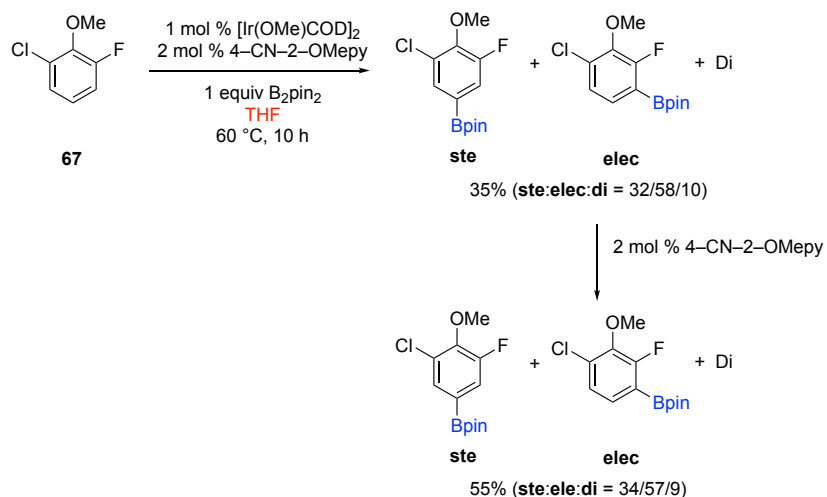
7) Investigating deactivating nature of 4-methoxypicolinonitrile (2-CN-4-OMe-pyridine)

Table 21 (entry 7) 2-CN-4-OMe-pyridine substrate could not act as the ligand or as the substrate. We hypothesized that, these 4-OMe pyridine ligands have a strong coordinating ability that will deactivate the catalyst system. In order to investigate further, we set up the reaction (Scheme 68) where CFA is borylated using Ir catalyst with the 4-CN-2-OMe pyridine as the ligand. After 24 h a mixture of products **ste**: **elec**: **di** in a ratio of 20:57:23 were observed (85% product formation). Surprisingly, this monodentate ligand favors electronic product (**elec**). This indicated the 4-CN-2-OMe pyridine is an excellent ligand for borylations and it favors electronic product in fluoro arenes.



Scheme 68. CHBs of 2,6-CFA

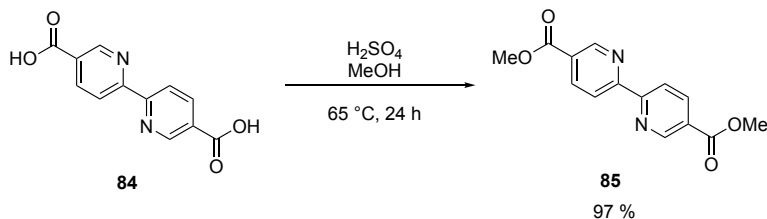
Next, we set up the same reaction and after 10 h, a mixture of products **ste**: **elec**: **di** in a ratio of 32:58:10 were observed (35% product formation). At 10 h mark we introduced another loading of the 4-CN-2-OMe pyridine ligand. Extra ligand diminishes the catalyst activity. After 24 h only 55% product formation was observed. This shows that in the presence of excess pyridine ligands the Iridium catalyst system slowly shuts down. However, more experiments are needed to make a solid conclusion about any coordination ability.



Scheme 69. CHBs of 2,6-CFA with extra ligand

6.7 Ligand synthesis

1) Synthesis of dimethyl [2,2'-bipyridine]-4,4'-dicarboxylate ligand (DME-bpy)

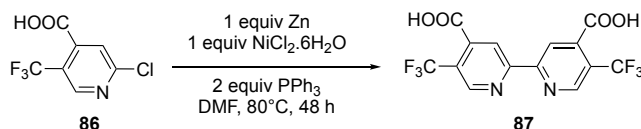


Scheme 70. Synthesis of DCE-bpy ligand

As a part of the Dow-MSU collaboration we envisioned that new ligand systems may result new regioselectivity in C–H borylations. Since the DCA-bpy ligand was extremely reactive, we were intrigued about the reactivity of ester version of this dicarboxylic ligand. Therefore, we esterified the dicarboxylic bipyridine ligand as follows (Scheme 71)

2) Synthesis of 5,5'-bis(trifluoromethyl)-[2,2'-bipyridine]-4,4'-dicarboxylic acid (Btf-DCA-bpy)

DCA-bpy (**84**) and DCE-bpy (**85**) ligands showed excellent reactivity in C-H activation borylation. Therefore, we challenged ourself with making more electron deficient dicarboxylic bipyridine ligands (Scheme 71).

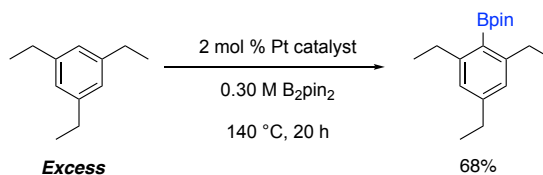


Scheme 71. Synthesis of btf-DCA-bpy ligand

Even though, these reaction conditions worked for synthesis of 4,4',5,5'-tetrakis(trifluoromethyl)-2,2'-bipyridine (dtfbpy), in our hands for synthesizing ligand (**87**) did not work. Major product of Scheme 71 was de-halogenated product of compound (**86**).

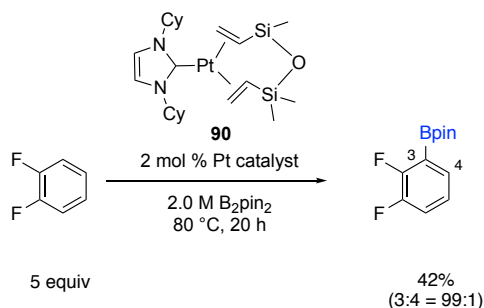
6.8 Different metal catalyst for C-H borylations

Iridium catalyzed borylation, the state-of-the-art method for the functionalization of simple arenes, is not capable of functionalizing the more hindered C(sp²)-H bonds found in 1,3,5-triethylbenzene. In 2015, Chatani and co-workers reported the first platinum catalyzed C-H borylation on sterically demanding substrates such as 1,3,5-triethylbenzene (Scheme 72).²⁴



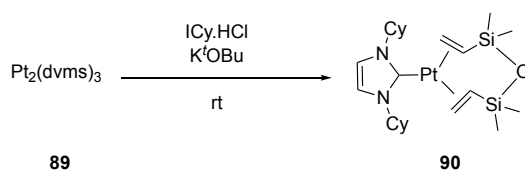
Scheme 72. Platinum catalyzed CHBs

The platinum/NHC catalyst system allowed the facile synthesis of ortho-fluorophenylboronic ester derivatives from fluoroarenes (Scheme 73). Inspired by this work, we tried using platinum chemistry to obtain the electronic product or borylation ortho to fluorine as the major product in our systems. We were also intrigued by the possibility of this catalyst to give diborylation products.



Scheme 73. Platinum catalyzed CHBs of fluoroarenes

Synthesis of platinum catalyst



Scheme 74. Synthesis of platinum catalyst

$Pt_2(dvms)_3$ precursor came in poly(dimethylsiloxane) vinyl terminated thick solution. Therefore the final catalyst (white solid) was contaminated with PDMS. This siloxane is insoluble in water and ethanol, but soluble in other organic solvents like the compound itself. Therefore, it was difficult to obtain this catalyst in pure form. However, we went ahead and screened some substrates for C-H borylation. In the future, when

making this catalyst, it will be crucial to avoid siloxanes (one can buy $\text{Pt}_2(\text{dvms})_3$ in xylene or synthesize **90** from H_2PtCl_6)

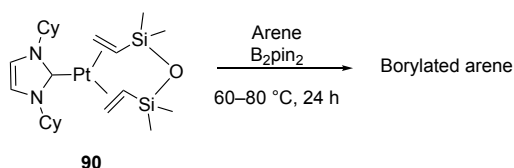


Table 22. Platinum catalyzed C-H borylation

Entry	Substrate	Substrate loading	B_2pin_2 loading	solvent	Catalyst loading	Tempe	Reaction time	Conversion	St/elec/di
1	2,6-CFA	2 mmol	0.3 equiv	neat	1.4 mol%	80 C	24h	50%	24/70/6
2	2-CN-4-OMepy	1 mmol	0.5 equiv	THF	2.2 mol%	60 C	24h	0%	-

Platinum catalyst favored the electronic product in CHBs of 2,6-CFA. However, Pt-catalyst did not show any borylation product for 2-CN-4-OMepy.

6.8 Conclusions

DCA-bpy and DCE-bpy are the most reactive ligands for CHBs. Bidentate ligands more reactive than mono dentate ligands. Furthermore, electron deficient bidentate ligand ($\text{Bpy}(\text{CF}_3)_2$) and mono dentate pyridine ligands favor electronic product of fluoro arenes. We also found that excess mono dentate ligands shut down the catalyst system and finally platinum catalyst also favor the electronic product of fluoro arenes.

6.9 Experimental

Material and Methods

All reactions were performed at the Dow chemical company at Midland, MI.

General procedure for Iridium catalyzed C-H borylation

In a nitrogen atmosphere glove box, bis(pinacolato)boron (B_2Pin_2) (256 mg, 1.0 mmol, 1.0 equiv) was weighed into a 16 mL vial containing a magnetic stir bar. $[Ir(OMe)COD]_2$ (6.6 mg, 0.01 mmol, 1.0 mol %) and the ligand (0.02 mmol, 2.0 mol %) were weighed into two test tubes separately, each being diluted with 0.5 mL of solvent. The $[Ir(OMe)COD]_2$ solution was transferred into the 16 mL vial containing B_2Pin_2 . This mixture was stirred until a golden yellow clear solution was obtained (~ 1 min). Next the solution containing ligand was transferred into the vial and upon stirring the resulting solution turned a dark brown color. Finally, the substrate (1.0 mmol) was added to the vial with the remaining solvent (0.5 mL). The reaction mixture was stirred for 24 h at 60 °C.

General procedure for Iridium catalyzed C-H borylation with pre-generated catalyst

In a nitrogen atmosphere glove box, bis(pinacolato)boron (B_2Pin_2) (256 mg, 1.0 mmol, 1.0 equiv) was weighed into a 16 mL vial containing a magnetic stir bar. $[Ir(OMe)COD]_2$ (6.6 mg, 0.01 mmol, 1.0 mol %) and the ligand (0.02 mmol, 2.0 mol %) were weighed into two test tubes separately, each being diluted with 0.5 mL of solvent. The $[Ir(OMe)COD]_2$ solution was transferred into the 16 mL vial containing B_2Pin_2 . This mixture was stirred until a golden yellow clear solution was obtained (~ 1 min). Next the solution containing ligand was transferred into the vial and upon stirring the resulting solution turned a dark brown color. The reaction mixture was stirred for 1 h at 60 °C.

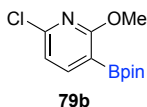
Finally, the substrate (1.0 mmol) was added to the vial with the remaining solvent (0.5 mL). Next the vial was closed and stirred for 24 h at 60 °C

Compound 67a



A mixture of boronic acid (9.8 mmol, 2.0g), pinacol (9.8 mmol) and anhydrous MgSO₄ (40.0 mmol) in MTBE (120 ml) was stirred at room temperature for 16 h (monitored using ¹H-NMR) . The solution was filtered and the filtrate was extracted with water (2 × 50 ml). Then, dried over MgSO₄, filtered, and concentrated *in vacuo* with no further purification to give the desired boronic ester in white solid of 2.30 g (82%). ¹H NMR (400 MHz, Chloroform-*d*) δ 7.35 (dd, *J* = 8.1, 5.6 Hz, 1H), 7.14 (dd, *J* = 8.1, 1.4 Hz, 1H), 3.96 (d, *J* = 1.4 Hz, 3H), 1.36 (s, 13H). ¹³C NMR (101 MHz, Chloroform-*d*) δ 160.35 (d, *J* = 254.5 Hz), 144.23 (d, *J* = 15.4 Hz), 131.76 (d, *J* = 4.0 Hz), 130.44 (d, *J* = 8.9 Hz), 125.17 (d, *J* = 3.6 Hz), 84.14, 61.45 (d, *J* = 5.0 Hz), 24.80. ¹⁹F NMR (376 MHz, Chloroform-*d*) δ -118.10 (d, *J* = 5.8 Hz).

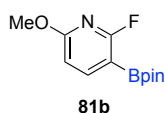
Compound 79b



A mixture of boronic acid (2.67 mmol, 0.5g), pinacol (2.67 mmol) and anhydrous MgSO₄ (10.0 mmol) in MTBE (40 ml) was stirred at room temperature for 16 h (monitored using ¹H-NMR) . The solution was filtered and the filtrate was extracted with water (2 × 50

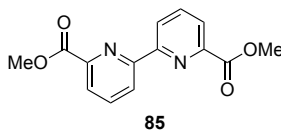
ml). Then, dried over MgSO_4 , filtered, and concentrated *in vacuo* with no further purification to give the desired boronic ester in white solid of 0.50 g (69%). ^1H NMR (400 MHz, Chloroform-*d*) δ 7.91 (d, $J = 7.5$ Hz, 1H), 6.88 (d, $J = 7.5$ Hz, 1H), 3.97 (s, 3H), 1.34 (s, 12H). ^{13}C NMR (101 MHz, Chloroform-*d*) δ 167.17, 151.41, 148.48, 115.96, 83.98, 54.44, 24.79.

Compound 81b



A mixture of boronic acid (2.93 mmol, 0.5g), pinacol (2.93 mmol) and anhydrous MgSO_4 (11.7 mmol) in MTBE (40 ml) was stirred at room temperature for 16 h (monitored using ^1H -NMR). The solution was filtered and the filtrate was extracted with water (2×50 ml). Then, dried over MgSO_4 , filtered, and concentrated *in vacuo* with no further purification to give the desired boronic ester in white solid of 0.45 g (61%). ^1H NMR (400 MHz, Chloroform-*d*) δ 8.00 (dd, $J = 8.8, 8.0$ Hz, 1H), 6.59 (dd, $J = 8.0, 2.1$ Hz, 1H), 3.94 (s, 3H), 1.34 (s, 12H). ^{19}F NMR (376 MHz, Chloroform-*d*) δ -58.92 (d, $J = 9.1$ Hz). ^{13}C NMR (101 MHz, Chloroform-*d*) δ 167.75, 165.86 (d, $J = 14.7$ Hz), 165.30, 149.41 (d, $J = 7.8$ Hz), 106.93 (d, $J = 4.9$ Hz), 83.85, 53.96, 24.73. ^{19}F NMR (376 MHz, Chloroform-*d*) δ -58.92 (d, $J = 9.1$ Hz).

Dimethyl [2,2'-bipyridine]-4,4'-dicarboxylate ligand



To a suspension of 4,4'-dicarboxy-2,2'-bipyridine (5.0 g, 20.47 mmol) in absolute methanol (200 mL) was added concentrated sulfuric acid (5 ml). The mixture was refluxed (65 °C) for 24 h to obtain a clear pink solution and then cooled to room temperature. Water was added (white slurry was formed) and the pH was adjusted to neutral with K₂CO₃ solution. Then the excess methanol was removed under vacuum. The resulting precipitate was extracted with ethyl acetate. The precipitate did not dissolve in EtOAc, therefore filter the white precipitate and wash with water. Finally dried under vacuum at 55 °C to remove excess water. ¹H NMR (400 MHz, Chloroform-*d*) δ 8.97 (dd, *J* = 1.6, 0.9 Hz, 1H), 8.87 (dd, *J* = 4.9, 0.9 Hz, 1H), 7.91 (dd, *J* = 5.0, 1.6 Hz, 1H), 4.00 (s, 3H). ¹³C NMR (101 MHz, Chloroform-*d*) δ 165.62, 156.51, 150.13, 138.60, 123.22, 120.56, 52.73.

Platinum catalyst synthesis

To a suspension of ICy.HCl and Pt catalyst in toluene under nitrogen was added tBuOK. The reaction mixture was stirred at room temperature for 3 h. The resulting mixture was filtered through a silica/celite (1:1) pad and it was washed with hexane/Et₂O (8:2). The filtrate was concentrated in vacuo to obtain a pale yellow solid.

REFERENCES

REFERENCES

- (1) Ishiyama, T.; Takagi, J.; Ishida, K.; Miyaura, N.; Anastasi, N. R.; Hartwig, J. F. Mild Iridium-Catalyzed Borylation of Arenes. High Turnover Numbers, Room Temperature Reactions, and Isolation of a Potential Intermediate. *J. Am. Chem. Soc.* **2002**, *124*, 390–391.
- (2) Boller, T. M.; Murphy, J. M.; Hapke, M.; Ishiyama, T.; Miyaura, N.; Hartwig, J. F. Mechanism of the Mild Functionalization of Arenes by Diboron Reagents Catalyzed by Iridium Complexes. Intermediacy and Chemistry of Bipyridine-Ligated Iridium Trisboryl Complexes. *J. Am. Chem. Soc.* **2005**, *127*, 14263–14278.
- (3) Ishiyama, T.; Isou, H.; Kikuchi, T.; Miyaura, N. Ortho-C–H Borylation of Benzoate Esters with Bis(pinacolato)diboron Catalyzed by Iridium–phosphine Complexes. *Chem. Commun.* **2010**, *46*, 159–161.
- (4) Sasaki, I.; Taguchi, J.; Doi, H.; Ito, H.; Ishiyama, T. Iridium(I)-Catalyzed C-H Borylation of α,β -Unsaturated Esters with Bis(pinacolato)diboron. *Chem. Asian J.* **2016**, *11*, 1400–1405.
- (5) Kawamorita, S.; Ohmiya, H.; Hara, K.; Fukuoka, A.; Sawamura, M. Directed Ortho Borylation of Functionalized Arenes Catalyzed by a Silica-Supported Compact Phosphine-Iridium System. *J. Am. Chem. Soc.* **2009**, *131*, 5058–5059.
- (6) Yamazaki, K.; Kawamorita, S.; Ohmiya, H.; Sawamura, M. Directed Ortho Borylation of Phenol Derivatives Catalyzed by a Silica-Supported Iridium Complex. *Org. Lett.* **2010**, *12*, 3978–3981.
- (7) Kawamorita, S.; Ohmiya, H.; Sawamura, M. Ester-Directed Regioselective Borylation of Heteroarenes Catalyzed by a Silica-Supported Iridium Complex. *J. Org. Chem.* **2010**, *75*, 3855–3858.
- (8) Paul, S.; Chotana, G. A.; Holmes, D.; Reichle, R. C.; Maleczka, R. E., Jr; Smith, M. R., 3rd. Ir-Catalyzed Functionalization of 2-Substituted Indoles at the 7-Position: Nitrogen-Directed Aromatic Borylation. *J. Am. Chem. Soc.* **2006**, *128*, 15552–15553.
- (9) Ros, A.; Estepa, B.; López-Rodríguez, R.; Álvarez, E.; Fernández, R.; Lassaletta, J. M. Use of Hemilabile N,N Ligands in Nitrogen-Directed Iridium-Catalyzed Borylations of

Arenes. *Angew. Chem. Int. Ed Engl.* **2011**, *50*, 11724–11728.

- (10) Roering, A. J.; Hale, L. V. A.; Squier, P. A.; Ringgold, M. A.; Wiederspan, E. R.; Clark, T. B. Iridium-Catalyzed, Substrate-Directed C-H Borylation Reactions of Benzylic Amines. *Org. Lett.* **2012**, *14*, 3558–3561.
- (11) Boebel, T. A.; Hartwig, J. F. Silyl-Directed, Iridium-Catalyzed Ortho-Borylation of Arenes. A One-Pot Ortho-Borylation of Phenols, Arylamines, and Alkylarenes. *J. Am. Chem. Soc.* **2008**, *130*, 7534–7535.
- (12) Robbins, D. W.; Boebel, T. A.; Hartwig, J. F. Iridium-Catalyzed, Silyl-Directed Borylation of Nitrogen-Containing Heterocycles. *J. Am. Chem. Soc.* **2010**, *132*, 4068–4069.
- (13) Roosen, P. C.; Kallepalli, V. A.; Chattopadhyay, B.; Singleton, D. A.; Maleczka, R. E., Jr; Smith, M. R., 3rd. Outer-Sphere Direction in Iridium C-H Borylation. *J. Am. Chem. Soc.* **2012**, *134*, 11350–11353.
- (14) Preshlock, S. M.; Plattner, D. L.; Maligres, P. E.; Krska, S. W.; Maleczka, R. E., Jr.; Smith, M. R., III. A Traceless Directing Group for C–H Borylation. *Angew. Chem. Int. Ed.* **2013**, *52*, 12915–12919.
- (15) Kuninobu, Y.; Ida, H.; Nishi, M.; Kanai, M. A *meta*-Selective C-H Borylation Directed by a Secondary Interaction between Ligand and Substrate. *Nat. Chem.* **2015**, *7*, 712–717.
- (16) Davis, H. J.; Genov, G. R.; Phipps, R. J. Meta -Selective C–H Borylation of Benzylamine-, Phenethylamine-, and Phenylpropylamine-Derived Amides Enabled by a Single Anionic Ligand. *Angew. Chem. Int. Ed.* **2017**, *56*, 13351–13355.
- (17) Davis, H. J.; Mihai, M. T.; Phipps, R. J. Ion Pair-Directed Regiocontrol in Transition-Metal Catalysis: A Meta-Selective C-H Borylation of Aromatic Quaternary Ammonium Salts. *J. Am. Chem. Soc.* **2016**, *138*, 12759–12762.
- (18) Smith, M. R.; Bisht, R.; Haldar, C.; Pandey, G.; Dannatt, J. E.; Ghaffari, B.; Maleczka, R. E.; Chattopadhyay, B. Achieving High Ortho Selectivity in Aniline C–H Borylations by Modifying Boron Substituents. *ACS Catal.* **2018**, 6216–6223.

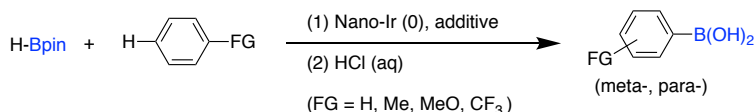
- (19) Li, H. L.; Kuninobu, Y.; Kanai, M. Lewis Acid-Base Interaction-Controlled Ortho - Selective C–H Borylation of Aryl Sulfides. *Angew. Chem. Int. Ed.* **2017**, *56*, 1495–1499.
- (20) Li, H.-L.; Kanai, M.; Kuninobu, Y. Iridium/Bipyridine-Catalyzed Ortho-Selective C-H Borylation of Phenol and Aniline Derivatives. *Org. Lett.* **2017**, *19*, 5944–5947.
- (21) Bisht, R.; Chattopadhyay, B. Formal Ir-Catalyzed Ligand-Enabled Ortho and Meta Borylation of Aromatic Aldehydes via in Situ-Generated Imines. *J. Am. Chem. Soc.* **2016**, *138*, 84–87.
- (22) Chattopadhyay, B.; Dannatt, J. E.; Andujar-De Sanctis, I. L.; Gore, K. A.; Maleczka, R. E., Jr; Singleton, D. A.; Smith, M. R., 3rd. Ir-Catalyzed Ortho-Borylation of Phenols Directed by Substrate-Ligand Electrostatic Interactions: A Combined Experimental/in Silico Strategy for Optimizing Weak Interactions. *J. Am. Chem. Soc.* **2017**, *139*, 7864–7871.
- (23) Ghaffari, B.; Preshlock, S. M.; Plattner, D. L.; Staples, R. J.; Maligres, P. E.; Krska, S. W.; Maleczka, R. E., Jr; Smith, M. R., 3rd. Silyl Phosphorus and Nitrogen Donor Chelates for Homogeneous Ortho Borylation Catalysis. *J. Am. Chem. Soc.* **2014**, *136*, 14345–14348.
- (24) Furukawa, T.; Tobisu, M.; Chatani, N. C-H Functionalization at Sterically Congested Positions by the Platinum-Catalyzed Borylation of Arenes. *J. Am. Chem. Soc.* **2015**, *137*, 12211–12214.

Chapter 7. Investigating Reactivity, Structure and Reusability of an Insoluble Iridium Catalyst for C-H Borylations

7.1 Introduction

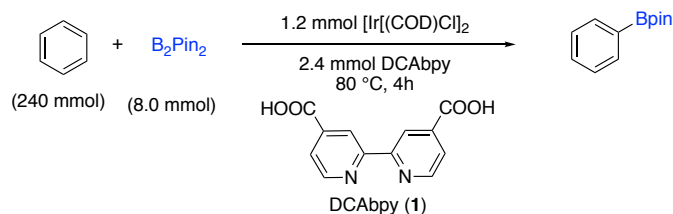
Since the first catalysts for the direct borylation of arenes based on Cp*Ir complexes were reported by Smith and co-workers,¹ various iridium systems containing phosphine- and nitrogen-based ligands have been studied. However, C–H borylation is usually catalyzed by homogeneous iridium complexes, which shares common drawbacks, that is, catalyst recovery and recycling is difficult. It is highly desirable to develop a new catalyst system that is stable, easy to recover and reuse.

In 2007, Zhu et al. synthesized ionic liquid-stabilized iridium (0) nanoparticles for the C–H borylation of arenes by pinacolborane (HBpin) (Scheme 75).^{2,3} This system could be reused at least six times. However, the catalyst was difficult to recover because the products had to be separated from the reaction mixture by distillation.



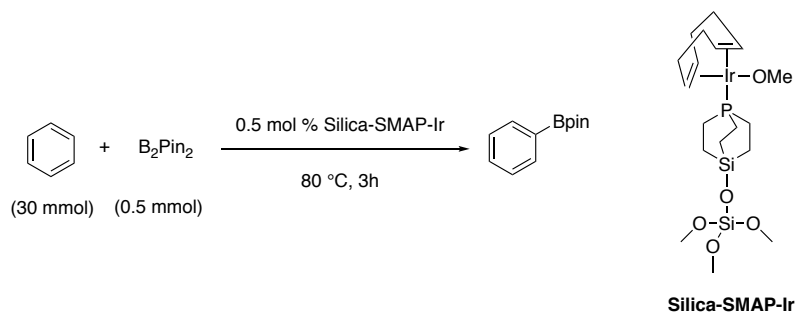
Scheme 75. CHBs with Ir(0) nanoparticles

In 2009, Nishida and co-workers obtained an insoluble iridium complex by filtration from the reaction mixtures of 2,2'-bipyridine-4,4'-dicarboxylic acid, [IrCl(COD)]₂ and B₂pin₂ (Scheme 76).^{4,5} This system could be reused 10 times over 1 week in C–H borylation reactions. However, the structure of this iridium complex was unknown due to its instability in air and insolubility in organic media.



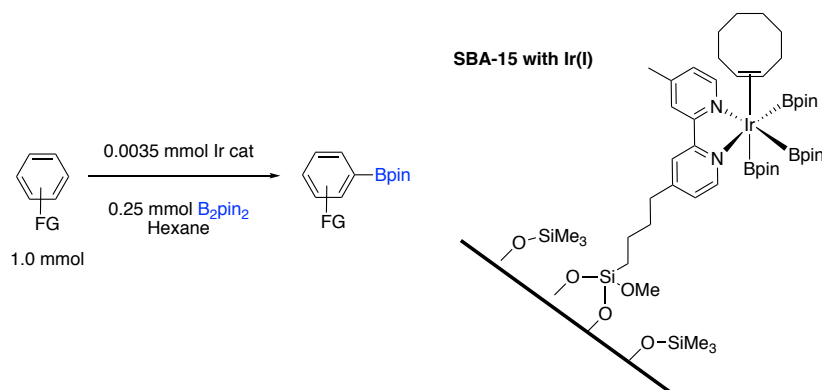
Scheme 76. CHBs with 2,2'-bipyridine-4,4'-dicarboxylic acid ligand

In the same year, Sawamura and co-workers reported a supported catalyst for aryl borylations.⁶ Their studies showed that reaction of Bpin with methylbenzoates catalyzed by the combination of $[Ir(COD)(OMe)]_2$ and a silica-supported phosphine ligand resulted in ortho-directed aromatic borylation in excellent yields (Scheme 77).^{6,7} However, the proposed Ir(I) complex formed during the reaction was not actually isolated because it is not air stable and is moisture sensitive.



Scheme 77. CHBs with silica-SMAP-Ir

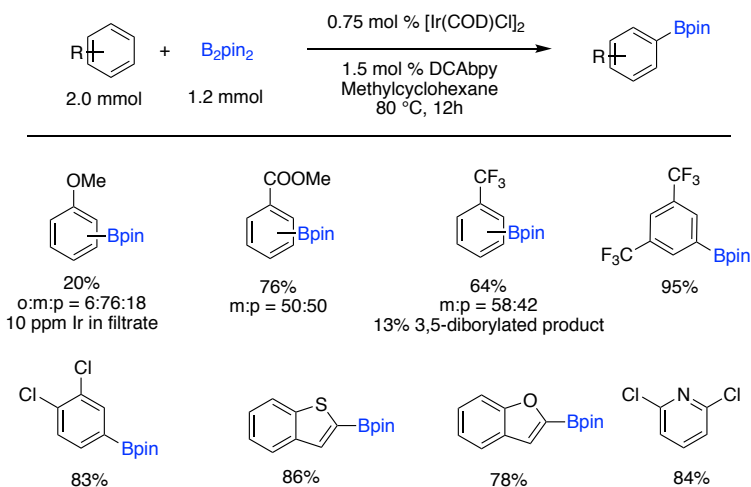
In 2014, Jones and co-workers developed an immobilized bipyridine-iridium system prepared from a silica-supported bipyridine ligand for C–H borylation (Scheme 78).⁸ They synthesized a mesoporous silica (SBA-15)-supported bipyridine iridium complex by grafting bipyridine onto the silica support, followed by complexation of an iridium(I) precursor in the presence of HBpin and cyclooctene. This heterogeneous catalyst system is highly air stable and can be reused several times without significantly affecting the structure or the texture of the catalyst.



Scheme 78. CHBs with SBA-15-Ir(I)

7.2 Heterogeneous catalyst

Nishida and co-workers⁴ investigated CHBs of different substrates with 0.75 mol % $[\text{Ir}(\text{COD})\text{Cl}]_2$ 1.5 mol% of **84** and 0.6 equiv of B_2pin_2 (Scheme 79). Surprisingly, in the reaction of anisole, the borylated product was obtained in low yield. The assumption was that the methoxy group may coordinate with the iridium catalyst because 10 ppm iridium was detected in the filtrate. However, reactions using other substrates proceeded smoothly and tolerated functionalities such as Cl, CO_2Me , and CF_3 .



Scheme 79. CHBs of arenes and heteroarenes in an $[\text{IrCl}(\text{COD})]_2$ and **1 system**

They also showed that this heterogeneous iridium complex (“black solid”) can easily filtered under nitrogen and could be reused more than 10 times for one week. No iridium was leached into the filtrates (Table 23).

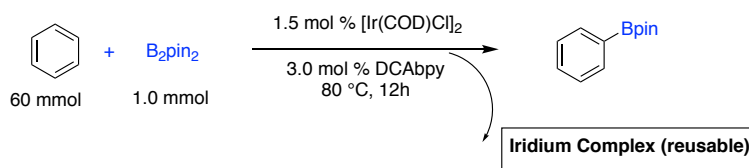


Table 23. CHBs of benzene catalyzed by recyclable iridium catalyst

Cycle	ICP Ir leaching (ppm)	Conversion %
1-10	<0.1	96-99

Unfortunately, few structural information about this reusable black solid was obtained because of its instability in air and its insolubility in organic solvents. However, ICP analysis of the complex showed that it contained both iridium and boron atoms in a molar ratio of 1:2.3-2.5. Therefore, they hypothesized that this complex may have a structure similar to that of the tris(boryl)iridium complex reported by Miyaura and co-workers.⁹ Also, not much information was offered about the regioselectivity of this heterogeneous catalyst with their limited substrate scope.

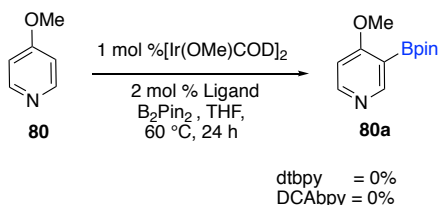
Even though, this is a very promising system for recycling iridium in CHBs, there are many questions to be answered. During ligand screening at the Dow Chemical Company (Chapter 6) we saw exceptional reactivity for CHBs with a 2,2'-bipyridine-4,4'-dicarboxylic (**84**) acid ligand. Inspired by previous work and our own curiosity as to how this heterogeneous system worked we began investigation into 2,2'-bipyridine-4,4'-dicarboxylic acid (**84**, DCAbpy) ligand. Our main objectives of this project were as follows:

- Ligand reactivity with $[\text{Ir}(\text{OMe})\text{COD}]_2$
- Regioselectivity during CHBs with their heterogeneous catalyst system
- Comparison with the dtbpy ligand system
- In depth structural analysis of the black solid

7.3 Data and Discussion

Reactivity

To begin investigating CHBs we chose $[\text{Ir}(\text{OMe})\text{COD}]_2$ as the pre-catalyst since this is the most active and widely used pre-catalyst for CHBs. We were intrigued by the results obtained during the ligand screening in Chapter 6. We saw contrasting reactivity and regioselectivity between dtbpy and DCAbpy ligands with the same pre-catalyst in CHBs of arenes. One such example is the borylation of 4-methoxy pyridine (**80**).

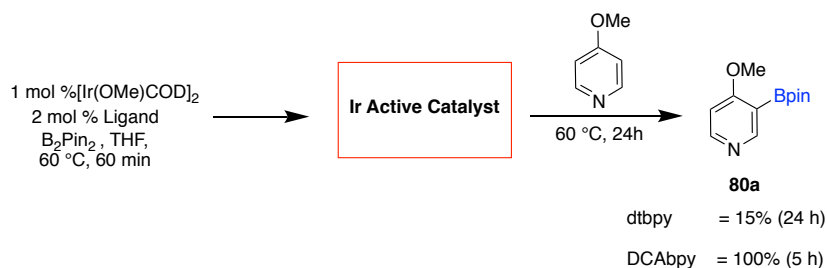


Scheme 80. CHBs without pre-generated active catalyst

Both ligands dtbpy and DCAbpy showed no C–H activation of **80** when the reaction was run without pre-generated active catalyst (Scheme 80). However, when CHBs of **80** was carried out with pre-generated active catalyst, the two ligands showed different reactivity (Scheme 81). First, 1.0 mol % of Ir catalyst, 2.0 mol % of ligand and 1.0 equiv of B_2pin_2 were combined in THF and heated at 60 °C for 30 min. After 60 min, the substrate (**80**) was introduced and the reaction mixture heated at 60 °C for 24 h. The

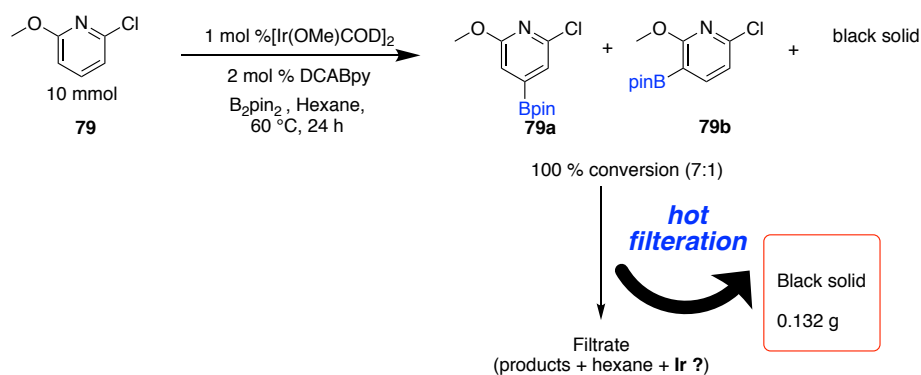
reaction mixture was monitored by NMR. After 5 h, full product (**80a**) formation was seen with the DCAbpy ligand, but only 15% product formation was observed with widely used ligand dtbpy even after 24 h. Scheme 82 is an example where dtbpy fails in CHBs.

As we discovered in Chapter 6, DCAbpy shows exceptional reactivity with wide range of substrates than dtbpy. However, it is noteworthy that pre-generating the catalyst is not necessary for non-coordinating substrates.



Scheme 81. CHBs with pre-generated active catalyst

Nishida and co-workers mentioned that CHBs of anisole resulted in lower yield and 10 ppm of Ir was observed due to coordination of the OMe group to Ir. To test this, we chose 2-chloro-6-methoxypyridine (**79**) for borylations. In a nitrogen filled glove box 10 mmol of **79** reacted with 1.0 mol% Ir catalyst (purchased from Johnson Matthey), 2.0 mol % ligand and 1.0 equiv of B₂pin₂ at 60°C for 24 h. After 24 h, all starting material was consumed and two mono borylated products (**79a** and **79b**) and a black solid (Scheme 82) were generated.



Scheme 82. Separation of the black solid

In the glove box the black solid was separated by filtration. Next, small samples in plastic containers were prepared from the filtrate and the black solid for NAA (Neutron Atomic Absorption) studies. This gives an idea about how much Ir is incorporated in the black solid as well as the filtrate (Table 24).

Table 24. NAA data for the black solid and the filtrate in hexane

Material-hexane	NAA study Ir (wt%)
Black solid	21.0 %
Filtrate	0.069 %

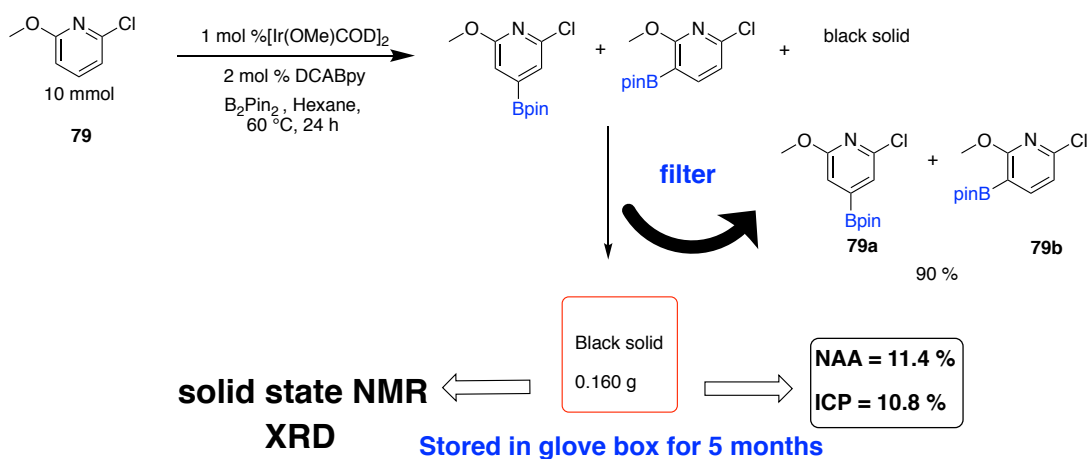
In contrast to Nishida's catalyst system, the amount of Ir leaking out (0.069%) was negligible even in the presence of an anisole group. We also observed that the best solvents for recovering the black solid are non-polar solvents such as hexane. When we repeated the same reaction in THF we had difficulties filtering the material out and the amount of Ir incorporated in black solid was less than what we observed where hexane was the solvent (Table 25).

Table 25. NAA data for the black solid and the filtrate in hexane

Material-THF	NAA study Ir (wt%)
Black solid	9.8 %
Filtrate	0.058 %

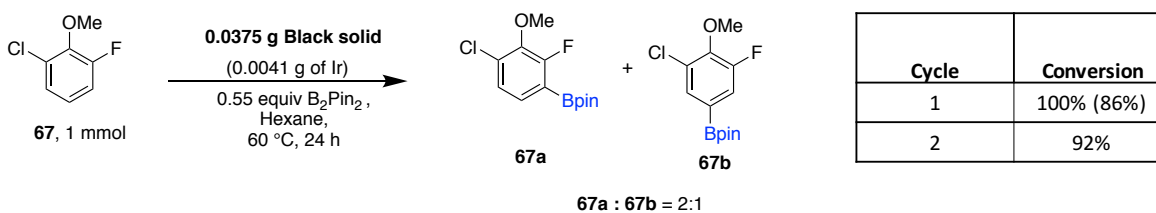
Recycling of the Black Solid

Our next goal was to investigate recycling the black solid. In a nitrogen filled glove box 10 mmol of **79** was reacted with 1.0 mol% Ir catalyst (made at MSU), 2.0 mol % ligand and 1.0 equiv of B₂pin₂ at 60°C for 24 h (Scheme 83). After 24 h, the black solid was separated by filtration. A portion of the black solid was used for solid state NMR/XRD (X-ray powder diffraction) and the other portion stored inside the glove box for 5 months. The filtrate was taken out of the glove box and was used to isolate monoborylated mixture (**79a** and **79b**) in 90%. NAA and ICP (Inductively Coupled Plasma) data suggested that incorporation of Ir in the black solid is about 10-11%. It is noteworthy that amount of Ir incorporation depends on the brand, batch of [Ir(OMe)COD]₂ used. This is not a surprising fact because, in our previous reports we have observed this phenomenon.



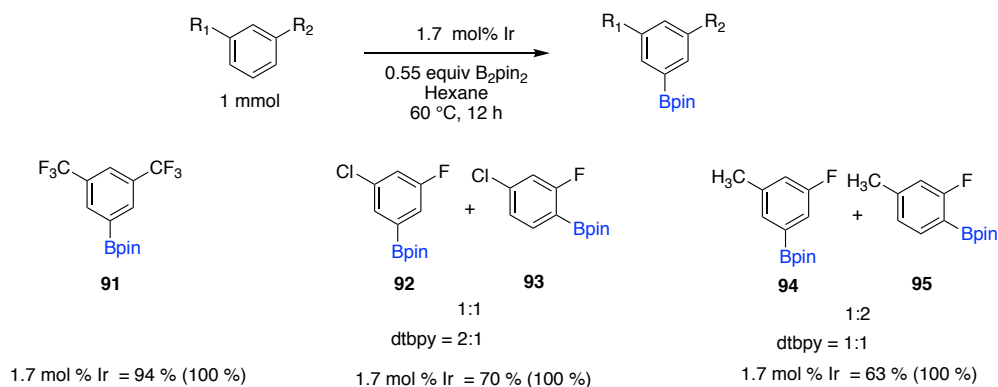
Scheme 83. Synthesis of the black solid

The black solid stored in the glove box under nitrogen for five months was used to run CHBs of 2,6-CFA (**67**) (Scheme 84). Compound **67** (1 mmol) was combined with 0.55 equiv of B_2pin_2 and 0.0375 g (0.0041 g of Ir) of the black solid in hexane at 60 °C for 24 h. After 24 h, the starting material was fully consumed and we separated out the black solid to reuse it in another CHBs cycle. From the filtrate mixture of monoborylates; electronic (**67a**) and steric (**67b**) products were isolated in 85% yield as a mixture (2:1 = **67a**:**67b**). For the second cycle, the same reaction conditions were used and after 24 h 92% of product formation was observed. This indicates that the black solid can be reuse even in small quantities to obtain high reactivity.



Scheme 84. Recycling of the black solid during CHBs

It is noteworthy that borylation of 2,6-CFA with the black solid favors regioselectivity next to fluorine (**67a**, electronic). We investigate CHBs using the black solid with several other fluorine containing compounds and compared the regioselectivity with dtbpy (Scheme 85). All three fluoro arenes showed full consumption of starting arene in 12 h. CHBs of 1,3-bis(trifluoromethyl)benzene gave the only one regioisomer, borylation at the C5 position (**91**) in 94% isolated yield.



Scheme 85. CHBs of the black solid Vs. dtbpy

CHBs of 1-chloro-3-fluorobenzene with the black solid gave a 1:1 mixture of **92** (steric) and **93** (electronic) mono borylated products in 70% yield. However, CHBs of 1-Chloro-3-fluorobenzene with dtbpy ligand gave a 2:1 ratio of **92** and **93** favoring the steric product. CHBs of 1-fluoro-3-methylbenzene with the black solid gave a mixture of **95** and **96** favoring the electronic product (2:1). In contrast, dtbpy ligand gave a 1:1 mixture of **95** and **96**. All these data indicate that CHBs with the black solid give a different region chemical outcome than does dtbpy and in fluoro arenes the electronic product is more favored over the sterics with the black solid catalyst. However, more in depth substrate screening is required to make a solid conclusion about regioselectivity of CHBs with this black solid catalyst.

Characterization of the Black Solid

The black solid catalyst was confirmed as an amorphous solid from X-ray powder diffraction. Also, since the solid is not soluble in any organic solvents, we carried out solid state NMR. ^{13}C solid state NMR indicated presence of C-O (84.5 ppm) and CH_3 (26.5 ppm) carbon bonds (Figure 50). ^{11}B solid state NMR shows a peak at 17 ppm (Figure 51). This is in contrast to the value we see in iridium trisbpin complex, which is 35 ppm (Ir-B). Furthermore, IR spectra indicated presence of a C=O (peak at 1710 cm^{-1}) bond.

Black solid $\{[\text{Ir}(\text{COD})\text{Cl}]_2 + \text{DCAbpy}\}$ was reported as an ignitable by Nishida and co-workers, however in our hands the black solid from $[\text{Ir}(\text{OMe})\text{COD}]_2$ and DCAbpy was not ignitable. However, we observed a color change from black to brown when the solid was exposed to the air.

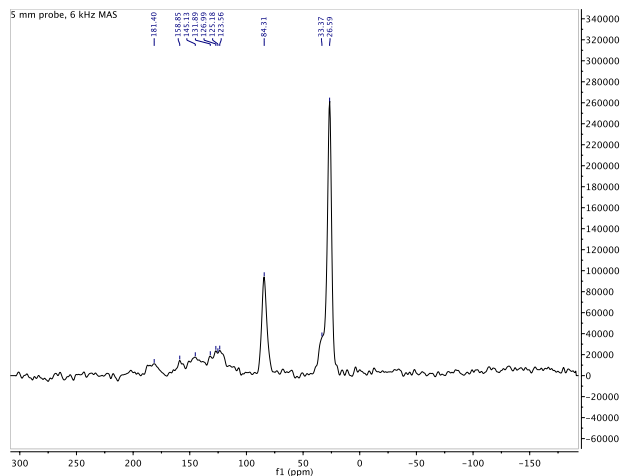


Figure 50. Solid state ^{13}C NMR

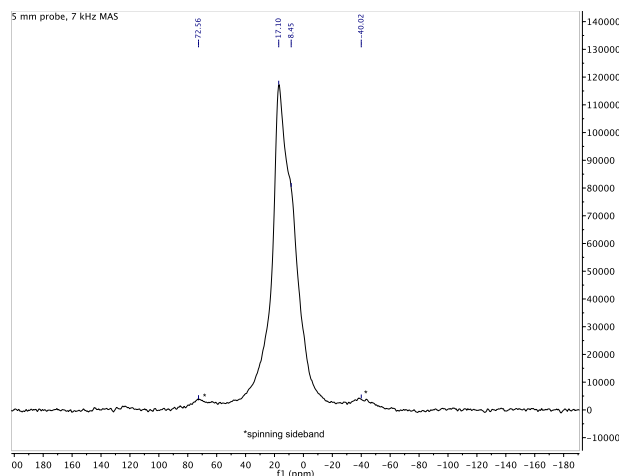


Figure 51. Solid state ^{11}B NMR

7.4 Conclusions

Nishida's black solid is a remarkable reusable heterogeneous catalyst for CHBs. It is easier to separate from the crude reaction mixture and can be reused several times without any Ir leaking or decrease in the reactivity. DCAbpy is an affordable ligand and also it is easy to use. Furthermore, DCAbpy showed exceptionally high reactivity than dtbpy and different region chemical preference than dtbpy.

7.5 Experimental

All reactions were run inside a nitrogen filled glove box at Dow Chemical company in Midland.

General procedure for Iridium catalyzed C-H borylation

In a nitrogen atmosphere glove box, bis(pinacolato)boron (B_2Pin_2) (256 mg, 1.0 mmol, 1.0 equiv) was weighed into a 16 mL vial containing a magnetic stir bar. $[\text{Ir}(\text{OMe})\text{COD}]_2$ (6.6 mg, 0.01 mmol, 1.0 mol %) and DCAbpy ligand (4.8 mg, 0.02

mmol, 2.0 mol %) were weighed into two test tubes separately, each being diluted with 0.5 mL of solvent. The $[\text{Ir}(\text{OMe})\text{COD}]_2$ solution was transferred into the 16 mL vial containing B_2Pin_2 . This mixture was stirred until a golden yellow clear solution was obtained (~ 1 min). Next the solution containing ligand was transferred into the vial and upon stirring the resulting solution turned a dark brown color. Finally, the substrate (1.0 mmol) was added to the vial with the remaining solvent (0.5 mL). The reaction mixture was stirred for 24 h at 60 °C.

General procedure for Iridium catalyzed C-H borylation with pre-generated catalyst

In a nitrogen atmosphere glove box, bis(pinacolato)boron (B_2Pin_2) (256 mg, 1.0 mmol, 1.0 equiv) was weighed into a 16 mL vial containing a magnetic stir bar. $[\text{Ir}(\text{OMe})\text{COD}]_2$ (6.6 mg, 0.01 mmol, 1.0 mol %) and DCAbpy ligand (4.8 mg, 0.02 mmol, 2.0 mol %) were weighed into two test tubes separately, each being diluted with 0.5 mL of solvent. The $[\text{Ir}(\text{OMe})\text{COD}]_2$ solution was transferred into the 16 mL vial containing B_2Pin_2 . This mixture was stirred until a golden yellow clear solution was obtained (~ 1 min). Next the solution containing ligand was transferred into the vial and upon stirring the resulting solution turned a dark brown color. The reaction mixture was stirred for 1 h at 60 °C. Finally, the substrate (1.0 mmol) was added to the vial with the remaining solvent (0.5 mL). Next the vial was closed and stirred for 24 h at 60 °C

Synthesis of the black solid

In a nitrogen atmosphere glove box, bis(pinacolato)boron (B_2Pin_2) (2.56 g, 1.0 mmol, 1.0 equiv) was weighed into a 50 mL vial containing a magnetic stir bar. $[Ir(OMe)COD]_2$ (66 mg, 0.1 mmol, 1.0 mol %) and DCAbpy ligand (48 mg, 0.2 mmol, 2.0 mol %) were weighed into two test tubes separately, each being diluted with 5.0 mL of solvent. The $[Ir(OMe)COD]_2$ solution was transferred into the 50 mL vial containing B_2Pin_2 . This mixture was stirred until a golden yellow clear solution was obtained (~ 3 min). Next the solution containing ligand was transferred into the vial and upon stirring the resulting solution turned a dark brown color. Finally, the substrate (10.0 mmol) was added to the vial with the remaining solvent (5.0 mL). The reaction mixture was stirred for 24 h at 60 °C. After 24 h, the reaction mixture was filtered through a plastic disposable filter cone inside the glove-box and the black solid obtained was washed twice with 10 mL solvent. The black solid was dried under over nitrogen atmosphere.

General procedure for Iridium catalyzed C-H borylation with the black solid

In a nitrogen atmosphere glove box, the black solid (0.0375 g) was weighed into a 16 mL vial containing a magnetic stir bar. Bis(pinacolato)boron (B_2Pin_2) (150 mg, 0.55 mmol, 0.5 equiv) and the substrate (1 mmol) were weighed into two test tubes separately, each being diluted with 0.5 mL of solvent. The B_2Pin_2 solution was transferred into the 16 mL vial containing the black solid. Next the solution containing the substrate was transferred into the vial. The reaction mixture was stirred for 24 h at 60 °C. Finally, the

substrate (1.0 mmol) was added to the vial with the remaining solvent (0.5 mL). Next the vial was closed and stirred for 24 h at 60 °C

After 24 h, the reaction mixture was filtered through a plastic disposable filter cone inside the glove-box and the black solid obtained was washed twice with 10 mL hexane. The solid obtained from this filtration was used for the next cycle of CHBs.

The filtrate was take out from the glove box and excess solvent was removed using the rotary evaporator. The oncentrated sample was passed through a plug of silica (BD 60 mL Syringe/Luer-Lok Tip-silica up to 50 mL mark) eluting with a 10:1 hexane/ethyl acetate solution (200 mL). The volatiles were removed by rotary evaporation to give the borylated product.

REFERENCES

REFERENCES

- (1) Cho, J.-Y.; Iverson, C. N.; Smith, M. R. Steric and Chelate Directing Effects in Aromatic Borylation. *J. Am. Chem. Soc.* **2000**, *122*, 12868–12869.
- (2) Yinghuai, Z.; Chenyan, K.; Peng, A. T.; Emi, A.; Monalisa, W.; Kui-Jin Louis, L.; Hosmane, N. S.; Maguire, J. A. Catalytic Phenylborylation Reaction by iridium(0) Nanoparticles Produced from Hydrido-iridium Carborane. *Inorg. Chem.* **2008**, *47*, 5756–5761.
- (3) Yinghuai, Z.; Yan, K. C.; Jizhong, L.; Hwei, C. S.; Hon, Y. C.; Emi, A.; Zhenshun, S.; Winata, M.; Hosmane, N. S.; Maguire, J. A. Iridium(I)-Salicylaldiminato-Cyclooctadiene Complexes Used as Catalysts for Phenylborylation. *J. Organomet. Chem.* **2007**, *692*, 4244–4250.
- (4) Tagata, T.; Nishida, M.; Nishida, A. Development of Recyclable Iridium Catalyst for C–H Borylation. *Tetrahedron Lett.* **2009**, *50* (45), 6176–6179.
- (5) Tagata, T.; Nishida, M.; Nishida, A. Continuous-Flow C–H Borylation of Arene Derivatives. *Adv. Synth. Catal.* **2010**, *352*, 1662–1666.
- (6) Kawamorita, S.; Ohmiya, H.; Hara, K.; Fukuoka, A.; Sawamura, M. Directed Ortho Borylation of Functionalized Arenes Catalyzed by a Silica-Supported Compact Phosphine-Iridium System. *J. Am. Chem. Soc.* **2009**, *131*, 5058–5059.
- (7) Kawamorita, S.; Ohmiya, H.; Sawamura, M. Ester-Directed Regioselective Borylation of Heteroarenes Catalyzed by a Silica-Supported Iridium Complex. *J. Org. Chem.* **2010**, *75*, 3855–3858.
- (8) Wu, F.; Feng, Y.; Jones, C. W. Recyclable Silica-Supported Iridium Bipyridine Catalyst for Aromatic C–H Borylation. *ACS Catal.* **2014**, *4* (5), 1365–1375.
- (9) Ishiyama, T.; Takagi, J.; Ishida, K.; Miyaura, N.; Anastasi, N. R.; Hartwig, J. F. Mild Iridium-Catalyzed Borylation of Arenes. High Turnover Numbers, Room Temperature Reactions, and Isolation of a Potential Intermediate. *J. Am. Chem. Soc.* **2002**, *124* (3),

390–391.

- (10) Preshlock, S. M.; Ghaffari, B.; Maligres, P. E.; Krska, S. W.; Maleczka, R. E., Jr; Smith, M. R., 3rd. High-Throughput Optimization of Ir-Catalyzed C-H Borylation: A Tutorial for Practical Applications. *J. Am. Chem. Soc.* **2013**, *135* (20), 7572–7582.

Chapter 8. Selective *para*-CH Activation Borylations

8.1 Introduction

Numerous C–H bond borylation and silylation methods are currently available. Although many methods have been developed for the *ortho*-borylation^{1–6} of arenes, remote C–H bond (*meta* and *para*) borylation remains difficult. Smith, Maleczka, Hartwig and co-workers reported exclusive *meta*-borylations/silylations from 1,3-disubstituted arenes and this regiochemistry results essentially from sterics.^{7–9} Recently, *meta*-selective borylation have been developed using the concept of noncovalent interaction^{10–12} between the substrate and ligand.^{13,14}

However, there was no general method for the *para* selective borylation until 2015, when Itami and Segawa reported selective *para*-borylation by use of a bulky diphosphine ligand.^{15,16} The basis behind this *para* borylation is the use of a bulky ligand that sterically blocks the *ortho* and *meta* positions resulting, a *para* selectivity. Very Recently, Nakao and co-workers reported a novel concept for *para*-borylation of benzamides and pyridines via a cooperative Ir/Al catalysis.¹⁷ The *para*-selectivity was controlled by a bulky aluminum-based Lewis acid catalyst. Also, in 2017 Chattopadhyay and co-workers introduced a L-shaped ligand for *para* selective borylations of aromatic esters.¹⁸ A noncovalent interaction between the substrate and a L-shaped ligand facilitate the Ir-catalyzed *para* C–H borylation of aromatic esters (Figure 52).

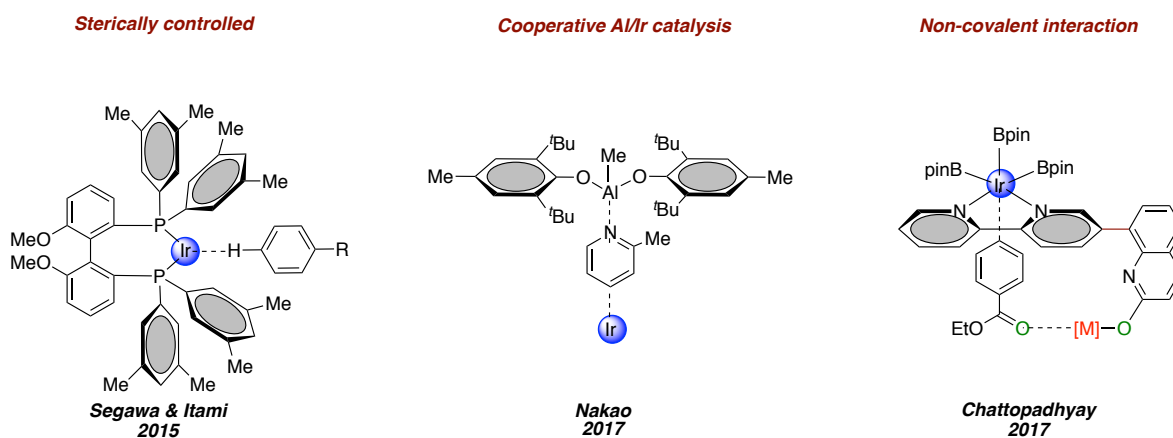


Figure 52. Discovery of selective *para* borylations

8.2 Sterically bulk ligand synthesis

Similar to Itami and Segawa's bulky diphosphine ligand, we envisioned that a ligand-controlled, *para*-selective C–H borylation could be achieved by iridium catalysis with sterically hindered ligands. Generally, in C–H borylations,^{19,20} arenes approach from the top side of square pyramidal iridium triboryl complex (Figure 53, left). In theory, bulky substituents on bipyridine ligands would restrict the upper hemisphere around the iridium center so that the *para*-C–H bond reacts preferentially over those in meta-positions (Figure 53, right). Because the boryl group can be easily converted into various functional groups,^{21,22} *para*-selective C–H borylation would be an extremely powerful method in organic synthesis.

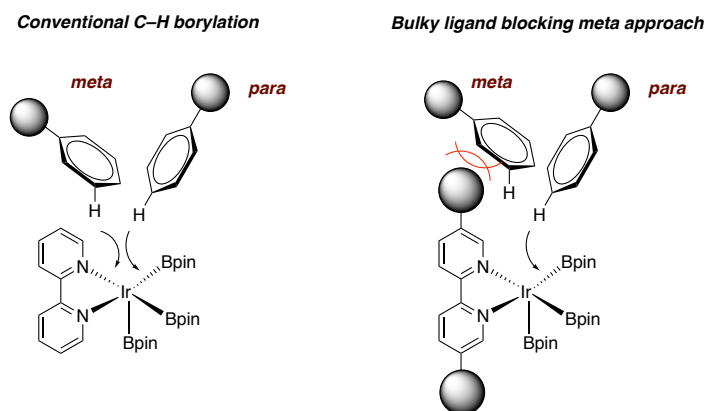


Figure 53. Selective iridium catalyzed C–H borylations

8.3 Ligand synthesis for *para* selective C–H borylations

In 2014, we designed a bulky ligand (**L2**) that was a modified bipyridine. The synthesis ligand (**L2**) consists of two parts (**Part-A** and **Part-B**) (Figure 54). **Part-A** is a borylated bipyridine unit and **Part-B** is a terphenyl moiety. We hypothesized that this bulky ligand (**L2**) would be suitable for the *para* C–H activation due to the following two considerations. First, in the presence of $[\text{Ir}(\text{COD})(\text{OMe})]_2$ and B_2pin_2 , **L2** would form the standard tris(boryl)iridium complex, which would facilitate the C–H borylation. Second, the terphenyl moiety will disfavor *meta* C–H activation due to steric hindrance. The designed ligand (**L2**) was synthesized using Suzuki cross coupling of **part A** and **part B**.

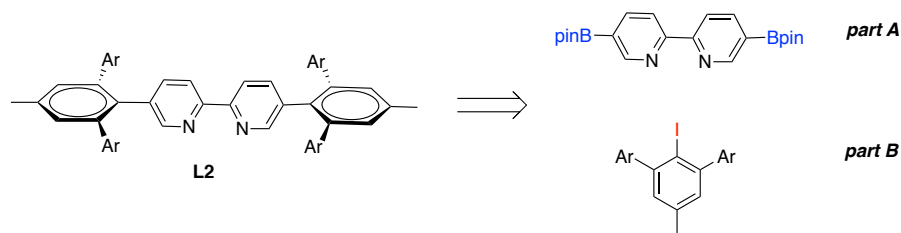
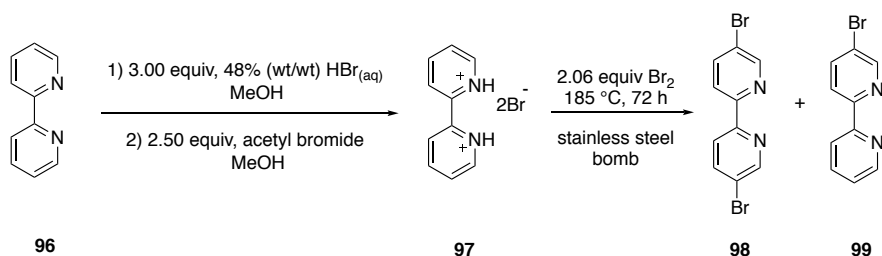


Figure 54. Sterically bulky ligand

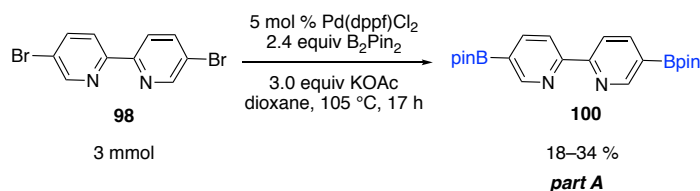
8.4 Synthesis of part A

In 2012, Woltering and co-workers reported a scalable, inexpensive synthetic route for versatile building block 5,5'-dibromo-2,2'-bipyridine (**98**)²³ that was based off the study by Romero and Ziesse.²⁴ Synthesis of 5,5'-dibromo-2,2'-bipyridine begins with reacting 48% (wt/wt) aqueous HBr with 2,2'-bipyridine (**96**) in methanol at 0 °C to obtain 2,2'-bipyridine dihydrobromide (**97**) (Scheme 86). Next, 2,2'-bipyridine dihydrobromide (**97**) is reacted with bromine under pressure to yield a mixture of 5,5'-dibromo-2,2'-bipyridine (**98**) and 5-bromo-2,2'-bipyridine (**99**). After column chromatography 5,5'-dibromo-2,2'-bipyridine (**98**) was isolated.



Scheme 86. Synthesis of 5,5'-dibromo-2,2'-bipyridine

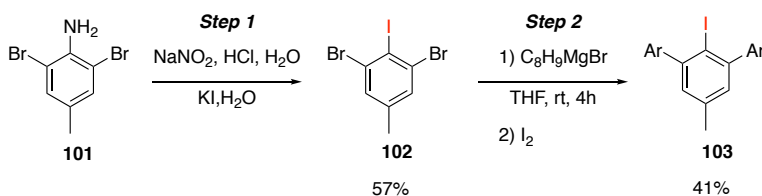
Pure 5,5'-dibromo-2,2'-bipyridine (**98**) was subjected for Miyaura coupling conditions to give the desired diborylated bipyridine 5,5'-bis(4,4,5,5-tetramethyl-1,3,2-dioxaborolan-2-yl)-2,2'-bipyridine (**100**) in 18–34% yield (Scheme 87).



Scheme 87. Miyaura coupling of 5,5'-dibromo-2,2'-bipyridine

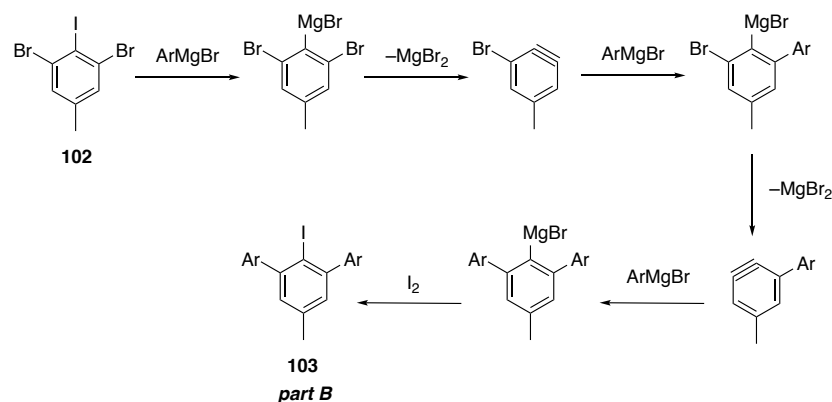
8.5 Synthesis of part B

Power and co-workers did pioneering work on synthesis of sterically encumbered aryl groups.²⁵ We were interested in a terphenyl moiety featuring two phenyls, or substituted phenyl, rings at the ortho positions of a central aryl ring. The most common synthetic route to these compounds begins with terphenyl halides, which are typically made from aniline derivatives. It has been shown that it is possible to synthesize iodo compounds like 2,6-diphenyl-4-methyliodobenzene (**103**) through a five-step route commencing with commercially available 2,6-dibromo-4-methylaniline (**101**) (Scheme 88).²⁶



Scheme 88. Synthesis of terphenyl halides

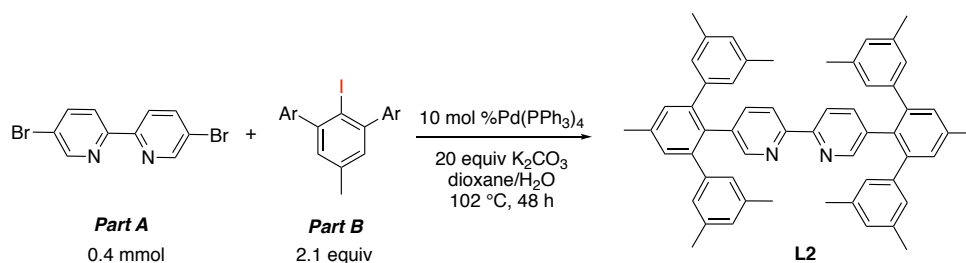
1,3-Dibromo-2-iodo-5-methylbenzene (**102**) was synthesized via diazotization and treatment with potassium iodide of commercially available 2,6-dibromo-4-methylaniline (**101**) (Step 1) (Scheme 88). Terphenyl was synthesized by a one pot reaction of a 1,2,3-trihalobenzene (**102**) with excess of a arylGrignard reagent. The mechanism involves Grignard exchange at the central halogen, followed by two cycles of magnesium halide loss and regioselective capture of the resulting aryne by the aryl-Grignard reagent (Scheme 89).²⁷ Finally, quenching by I_2 gives the desired 2,6-diphenyl-4-methyliodobenzene (**103**) in 41% yield.



Scheme 89. Mechanism for synthesis of terphenyl halides

8.5 Synthesis of the bulky ligand

Finally, by combining part A and part B through a Suzuki reaction would afford the desired bulky ligand (**L2**) (Scheme 90). The challenge was to successfully couple the sterically encumber terphenyl with the 5,5'-diBpin-2,2'-bipyridine. Since synthesizing parts A and B are time consuming and low yielding, we avoided extensive screening of Suzuki conditions. Instead, we chose the most frequently used Suzuki conditions (Scheme 90).



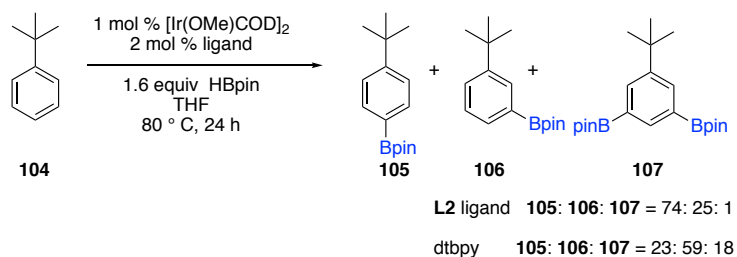
Scheme 90. Synthesis of bulky ligand

LCMS indicated the major Suzuki product to be the mono coupled product, with the product minor being **L2**. After column chromatography, the sterically hindered ligand

(L2) was isolated in 15%. With only few milligrams in hand, we moved to the next step, that is iridium catalyzed C–H borylation.

8.6 Iridium catalyzed selective para borylations

tert-Butylbenzene was chosen as the substrate to test ligand (L2). C–H borylation was carried out on this substrate with 1 mol % [Ir(OMe)COD]₂, 2 mol % ligand and 1.6 equiv of HBpin in THF at 80 °C for 24 h (Scheme 91). This resulted in borylations at the *para*, *meta* and di-*meta* positions in a ratio of 74: 25: 1.



Scheme 91. C–H activation borylation

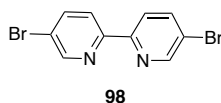
CHBs of **104** with dtbpy ligand favors the *meta* (**106**) regioisomer over *para* (**105**) and considerable amount of di-borylation (**107**) is also formed. Therefore, this indicates a promising result for selective *para* C-H borylations using terphenyl moieties with bipyridine ligands, but more work is needed in modifying new sterically hindered ligand systems.

8.7 Experimental

Unless indicated otherwise all reactions were carried out in oven-dried glassware under an atmosphere of argon, with magnetic stirring, and monitored by GC-MS or ¹H-NMR. Tetrahydrofuran was freshly distilled from sodium/benzophenone under nitrogen.

Standard Schlenk techniques on a double manifold vacuum line were used in the manipulation of air and moisture sensitive compounds.

Compound 98



Carry out Steps 1–14 of the described reaction in a well-vented fume hood and keep the sash down during the entire course of the reaction.

Have a $\text{Na}_2\text{S}_2\text{O}_3$ solution at hand in case of bromine spillages. Wipe all equipment and the fume hood surface thoroughly using $\text{Na}_2\text{S}_2\text{O}_3$ solution.

1) Charge a mortar with 12.0 g of 2,2'-bipyridine dihydrobromide **97** (1.00 equiv.). Take up 4.00 ml of bromine (2.06 equiv.) in a 5-ml disposable plastic syringe with a long needle. Slowly add the bromine, making sure that the tip of the needle is digging into **97**. From time to time, mix and grind the solids using the pestle.

Caution Slowly inject the bromine to minimize evaporation. This ensures reproducibility and prevents the release of bromine vapor.

2) Grind the mixture until a homogenous non fuming orange powder is obtained.

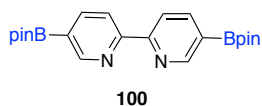
Critical step Grinding until a fine powder is obtained is crucial to ensure reproducibility.

3) Transfer the reaction mixture into a 15-ml sample vial using a plastic funnel and compress it using a spatula.

- 4) Transfer the sample vial into the stainless steel bomb using tweezers and seal the steel bomb in the fume hood using adjustable wrenches.
- 5) Place the stainless steel bomb in an insulated oil bath with a thermocouple temperature sensor. Cover the apparatus with a blast shield and heat the oil bath to 185 °C for 72 h.
- 6) Switch off the heating and allow the apparatus to cool to room temperature. Remove the blast shield and open the stainless steel bomb in the fume hood using adjustable wrenches.
- 7) Place the sample vial into a mortar and carefully smash the vial using the pestle; remove pieces of glass with the tweezers. Pestle the reaction cake until a fine powder is obtained.
- 8) Transfer the crude product into a large conical ask with a teflon-coated magnetic stirrer bar and add 200 ml of 2 M NaOH solution.
- 9) Add 10 g of EDTA tetrasodium salt, 10 g of Na₂SO₃ and 200 ml of CH₂Cl₂. Cover the conical ask with a watch glass and stir the mixture at 1,250 r.p.m. for 2 h at room temperature.
- 10) Separate the organic phase and extract the aqueous phase five times with 200 ml of CH₂Cl₂ using a separatory funnel.
- 11) Combine the organic phases in a conical ask, add 120 g of anhydrous Na₂SO₄ and stir for 15 min; next, filter the mixture and transfer it to a round-bottom ask.
- 12) Add silica (20 g for 1 g of crude) and remove the solvents using a rotary evaporator.
- 13) Purify the crude product by flash chromatography on silica gel using CH₂Cl₂.

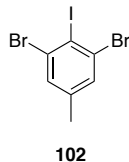
14) Collect the product containing fractions in a round-bottom ask and remove the solvents using a rotary evaporator. Order of elution: 5,5'-dibromo-2,2'-bipyridine **98** → 5-bromo-2,2'-bipyridine **99** → 2,2'-bipyridine **96**. 2.680 g of a colorless crystalline powder was obtained. ¹H NMR (500 MHz, CDCl₃) δ 8.71 (d, *J* = 2.3 Hz, 2H), 8.40 – 8.16 (m, 2H), 7.94 (dd, *J* = 8.5, 2.3 Hz, 2H). ¹³C NMR (126 MHz, CDCl₃) δ 153.6, 150.3, 139.6, 122.2, 121.4. The spectral data were in accordance with those reported in the literature.²³ MS EI+ *m/z* calculated for (M+H)⁺ C₁₀H₇Br₂N₂ 312.8976, found 312.9032.

Compound 100



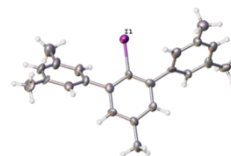
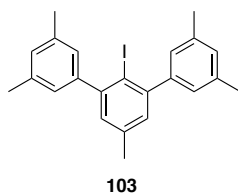
Pd(dppf)Cl₂ (0.122 g, 0.15 mmol, 5.0 mol%), KOAc (0.883 g, 9.0 mmol, 3.0 equiv), and bis(pinacolato)diboron (1.82 g, 7.16 mmol, 2.4 equiv) were added to a flask equipped with a magnetic stirring bar, a septum inlet, and a condenser. The flask was flushed with argon and then charged with degassed dioxane (10 mL) and 5,5'-dibromo-2,2'-bipyridine (0.942 g, 3.0 mmol). The mixture was then stirred at 105 °C for 17 h. Then, excess dioxane was pumped off and purify the crude product by flash chromatography on silica gel using EtOAc/CH₂Cl₂. After purification 0.298–0.414 g of **100** was isolated as a light pink solid in 18–34% yield. ¹H NMR (500 MHz, CDCl₃) δ 9.01 (d, *J* = 1.5 Hz, 2H), 8.42 (d, *J* = 7.9 Hz, 2H), 8.19 (d, *J* = 7.8 Hz, 2H), 1.37 (s, 24H). ¹¹B NMR (160 MHz, CDCl₃) δ 30.0 (brs). ¹³C NMR (126 MHz, CDCl₃) δ 157.9, 155.1, 143.3, 120.6, 84.2, 24.9. MS EI+ *m/z* calculated for (M+H)⁺ C₂₂H₃₁B₂N₂O₄ 409.2469, found 409.2542.

Compound 102²⁸



A solution of 2,6-dibromo-4-methylaniline (7.0 g, 26.4 mmol) in CH₃COOH (80 mL) was added dropwise into a solution of NaNO₂ (2.0 g, 28.8 mmol) in conc. H₂SO₄ (16 mL) keeping the temperature of the solution below 20 °C using an ice bath. The mixture was stirred for 4 h at rt. After addition of a solution of KI (31.8 g, 192 mmol) and I₂ (6.6 g, 26 mmol) in H₂O (60 mL), the resulting mixture was stirred for 12 h at rt. 15% NaOH aq (1200 mL) was added. The resulting material was extracted with EtOAc (150 mL x 3). The combined organic phase was washed with H₂O (150 mL x 2) and brine (150 mL) and dried over Na₂SO₄. The solvents were evaporated and recrystallization/sublimation gave 5.620 g of **102** as a white solid (mp 66–67 °C, lit 52–54 °C²⁹) in 57% yield. ¹H NMR (500 MHz, CDCl₃) δ 7.39 (d, *J* = 0.7 Hz, 2H), 2.26 (d, *J* = 0.8 Hz, 3H). ¹³C NMR (126 MHz, CDCl₃) δ 141.0, 131.9, 130.8, 104.9, 20.4. The spectral data were in accordance with those reported in the literature.²⁸ MS EI+ *m/z* calculated for (M+NH₄)⁺ C₇H₉NBr₂I 391.8146, found 391.8290.

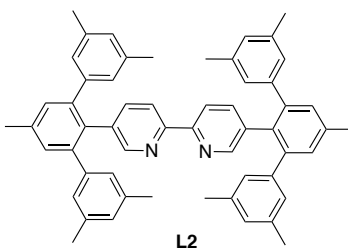
Compound 103²⁶



CCDC 1850721

To a suspension of 2.00 g (5.30 mmol) of 2,6-dibromo-4-methyliodobenzene 12 ml of THF (purge 1 hr with Ar), 32 ml (15.9 mmol, 3.0 equiv) of 0.5 M (3,5-dimethylphenyl)magnesium bromide (Aldrich) was added drop-wise and stirred for 4 h at room temperature. Iodine (2.600 g, 10.60 mmol) was added to the reaction mixture and stirred overnight. A solution of ca. 30 ml of 1 N Na₂SO₃ was added to the reaction mixture and the slurry was extracted with ether. The organic layer was sequentially washed with water and aqueous saturated NaCl and dried over anhydrous MgSO₄. After purification by column chromatography 0.922 g of **103** was isolated as a white solid (mp 111–113 °C) in 41% yield. ¹H NMR (500 MHz, CDCl₃) δ 7.06 (dd, *J* = 0.7, 0.7 Hz, 2H), 7.04 – 7.01 (m, 2H), 6.98 (dd, *J* = 1.4, 0.8 Hz, 4H), 2.37 (s, 12H), 2.34 (s, 3H). ¹³C NMR (126 MHz, CDCl₃) δ 147.9, 145.6, 137.3, 137.2, 129.4, 128.9, 127.2, 99.5, 21.4, 20.7. MS EI+ *m/z* calculated for (M+H)⁺ C₂₃H₂₄I 427.0923, found 427.0996.

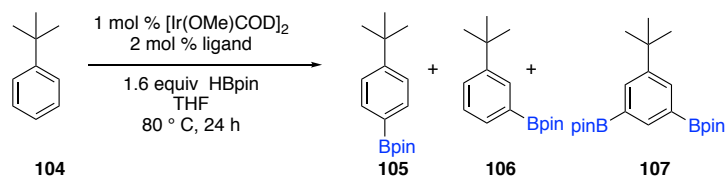
Compound L2



100 (0.163 g, 0.4 mmol) and **103** (0.366 g, 0.86 mmol, 2.1 equiv) were added to a schlenk flask equipped with a magnetic stirring bar, a septum inlet, and a condenser. The flask was under vacuum for 1 h. Then K₂CO₃ (2.378 g, 17.2 mmol), 20 mL of dioxane and water (460 μL) were added and performed freeze-pump thaw for 2 times. Finally, introduced Pd(PPh₃)₄ (0.086 mmol, 10.0 mol%) under argon and 3 more freeze-pump

thaws were performed. Reaction mixture was reflux at 102 °C for 48 h. Then, excess dioxane was pumped off and purify the crude product by flash chromatography on silica gel using EtOAc/CH₂Cl₂. After purification 0.019 g of **L2** was isolated as a off-white solid in 6% yield. ¹H NMR (500 MHz, CDCl₃) δ 8.05 (s, 2H), 7.88 (d, *J* = 8.3 Hz, 2H), 7.25 (d, *J* = 0.8 Hz, 4H), 7.23 – 7.19 (m, 2H), 6.77 (s, 4H), 6.67 (s, 8H), 2.46 (s, 6H), 2.13 (s, 24H). ¹³C NMR (126 MHz, CDCl₃) δ 151.3, 149.0, 142.4, 141.2, 137.6, 137.2, 130.3, 128.2, 127.9, 123.4, 120.9, 119.4, 34.7, 21.2, 21.2. MS EI+ *m/z* calculated for (M+H)⁺ C₅₆H₅₃N₂ 753.4209, found 753.4357.

CHBs of *tert*-butylbenzene (**104**)



In a nitrogen atmosphere glove box, [Ir(OMe)COD]₂ (6.6 mg, 0.001 mmol, 1.0 mol %) was weighed into a 10 mL pressure tube containing a magnetic stir bar. Add HBpin (250 μL) and 0.5 mL of THF and stir until clear orange/yellow color solution was observed. Next, **L2** ligand (15 mg, 0.020 mmol, 2.0 mol %) was weighed into a test tube. Transfer the ligand into the tube and use 0.5 mL THF to wash and transfer remaining ligand in the test tube. Finally, the substrate (1.0 mmol) was added to the tube with 1 mL of THF, which was then sealed and was taken out of the glove box. The reaction mixture was stirred for 24 h at 80 °C. After 24 h crude reaction was sampled using NMR.

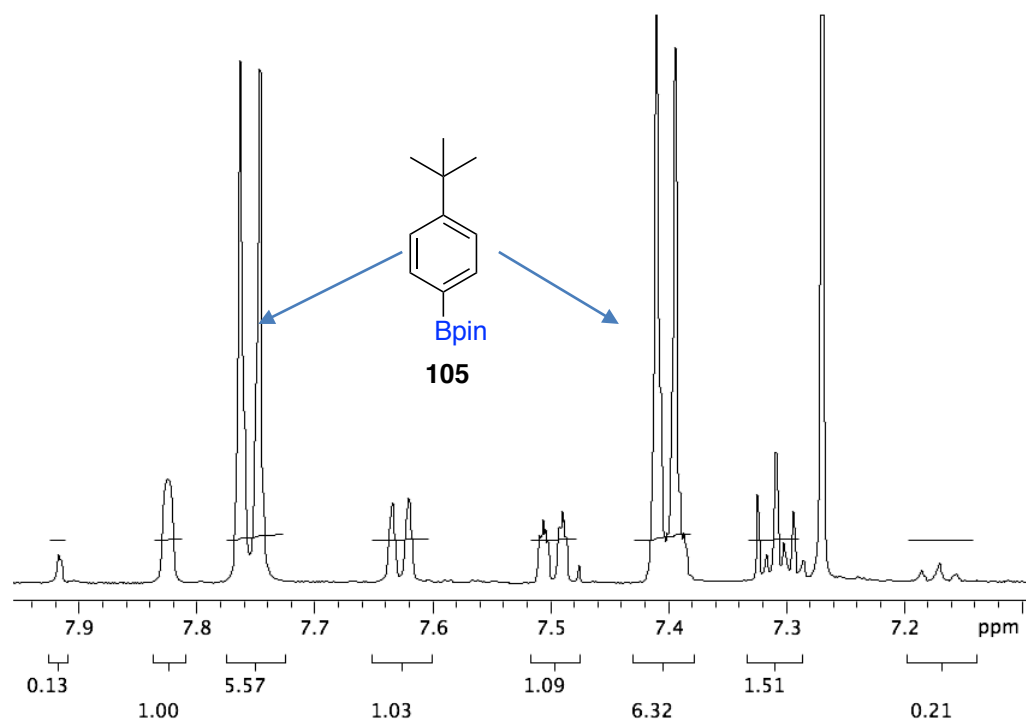


Figure 55. Crude ^1H NMR of the CHBs with 104

REFERENCES

REFERENCES

- (1) Boebel, T. A.; Hartwig, J. F. Silyl-Directed, Iridium-Catalyzed Ortho-Borylation of Arenes. A One-Pot Ortho-Borylation of Phenols, Arylamines, and Alkylarenes. *J. Am. Chem. Soc.* **2008**, *130*, 7534–7535.
- (2) Kawamorita, S.; Ohmiya, H.; Hara, K.; Fukuoka, A.; Sawamura, M. Directed Ortho Borylation of Functionalized Arenes Catalyzed by a Silica-Supported Compact Phosphine-Iridium System. *J. Am. Chem. Soc.* **2009**, *131*, 5058–5059.
- (3) Kawamorita, S.; Ohmiya, H.; Sawamura, M. Ester-Directed Regioselective Borylation of Heteroarenes Catalyzed by a Silica-Supported Iridium Complex. *J. Org. Chem.* **2010**, *75*, 3855–3858.
- (4) Yamazaki, K.; Kawamorita, S.; Ohmiya, H.; Sawamura, M. Directed Ortho Borylation of Phenol Derivatives Catalyzed by a Silica-Supported Iridium Complex. *Org. Lett.* **2010**, *12*, 3978–3981.
- (5) Ishiyama, T.; Isou, H.; Kikuchi, T.; Miyaura, N. Ortho-C–H Borylation of Benzoate Esters with Bis(pinacolato)diboron Catalyzed by Iridium–phosphine Complexes. *Chem. Commun.* **2010**, *46*, 159–161.
- (6) Dai, H.-X.; Yu, J.-Q. Pd-Catalyzed Oxidative Ortho-C-H Borylation of Arenes. *J. Am. Chem. Soc.* **2012**, *134*, 134–137.
- (7) Maleczka, R. E., Jr; Shi, F.; Holmes, D.; Smith, M. R., 3rd. C-H Activation/borylation/oxidation: A One-Pot Unified Route to Meta-Substituted Phenols Bearing Ortho-/para-Directing Groups. *J. Am. Chem. Soc.* **2003**, *125*, 7792–7793.
- (8) Murphy, J. M.; Liao, X.; Hartwig, J. F. Meta Halogenation of 1,3-Disubstituted Arenes via Iridium-Catalyzed Arene Borylation. *J. Am. Chem. Soc.* **2007**, *129*, 15434–15435.
- (9) Cheng, C.; Hartwig, J. F. Rhodium-Catalyzed Intermolecular C-H Silylation of Arenes with High Steric Regiocontrol. *Science* **2014**, *343*, 853–857.

- (10) Preshlock, S. M.; Plattner, D. L.; Maligres, P. E.; Krska, S. W.; Maleczka, R. E.; Smith, M. R. A Traceless Directing Group for C–H Borylation. *Angew. Chem. Int. Ed Engl.* **2013**, *125*, 13153–13157.
- (11) Chattopadhyay, B.; Dannatt, J. E.; Andujar-De Sanctis, I. L.; Gore, K. A.; Maleczka, R. E., Jr; Singleton, D. A.; Smith, M. R., 3rd. Ir-Catalyzed Ortho-Borylation of Phenols Directed by Substrate-Ligand Electrostatic Interactions: A Combined Experimental/in Silico Strategy for Optimizing Weak Interactions. *J. Am. Chem. Soc.* **2017**, *139*, 7864–7871.
- (12) Roosen, P. C.; Kallepalli, V. A.; Chattopadhyay, B.; Singleton, D. A.; Maleczka, R. E., Jr; Smith, M. R., 3rd. Outer-Sphere Direction in Iridium C-H Borylation. *J. Am. Chem. Soc.* **2012**, *134*, 11350–11353.
- (13) Bisht, R.; Chattopadhyay, B. Formal Ir-Catalyzed Ligand-Enabled Ortho and Meta Borylation of Aromatic Aldehydes via in Situ-Generated Imines. *J. Am. Chem. Soc.* **2016**, *138*, 84–87.
- (14) Davis, H. J.; Mihai, M. T.; Phipps, R. J. Ion Pair-Directed Regiocontrol in Transition-Metal Catalysis: A Meta-Selective C-H Borylation of Aromatic Quaternary Ammonium Salts. *J. Am. Chem. Soc.* **2016**, *138*, 12759–12762.
- (15) Saito, Y.; Segawa, Y.; Itami, K. Para-C-H Borylation of Benzene Derivatives by a Bulky Iridium Catalyst. *J. Am. Chem. Soc.* **2015**, *137*, 5193–5198.
- (16) Haines, B. E.; Saito, Y.; Segawa, Y.; Itami, K.; Musaev, D. G. Flexible Reaction Pocket on Bulky Diphosphine–Ir Complex Controls Regioselectivity in Para-Selective C–H Borylation of Arenes. *ACS Catal.* **2016**, *6*, 7536–7546.
- (17) Yang, L.; Semba, K.; Nakao, Y. Para -Selective C–H Borylation of (Hetero)Arenes by Cooperative Iridium/Aluminum Catalysis. *Angew. Chem. Int. Ed.* **2017**, *56*, 4853–4857.
- (18) Hoque, M. E.; Bisht, R.; Haldar, C.; Chattopadhyay, B. Noncovalent Interactions in Ir-Catalyzed C-H Activation: L-Shaped Ligand for Para-Selective Borylation of Aromatic Esters. *J. Am. Chem. Soc.* **2017**, *139*, 7745–7748.

- (19) Boller, T. M.; Murphy, J. M.; Hapke, M.; Ishiyama, T.; Miyaura, N.; Hartwig, J. F. Mechanism of the Mild Functionalization of Arenes by Diboron Reagents Catalyzed by Iridium Complexes. Intermediacy and Chemistry of Bipyridine-Ligated Iridium Trisboryl Complexes. *J. Am. Chem. Soc.* **2005**, *127*, 14263–14278.
- (20) Tamura, H.; Yamazaki, H.; Sato, H.; Sakaki, S. Iridium-Catalyzed Borylation of Benzene with Diboron. Theoretical Elucidation of Catalytic Cycle Including Unusual Iridium(v) Intermediate. *J. Am. Chem. Soc.* **2003**, *125*, 16114–16126.
- (21) Hartwig, J. F. Borylation and Silylation of C-H Bonds: A Platform for Diverse C-H Bond Functionalizations. *Acc. Chem. Res.* **2012**, *45*, 864–873.
- (22) Qiao, J.; Lam, P. Copper-Promoted Carbon-Heteroatom Bond Cross-Coupling with Boronic Acids and Derivatives. *Synthesis* **2011**, *2011*, 829–856.
- (23) D'Souza, D. M.; Leigh, D. A.; Pappmeyer, M.; Woltering, S. L. A Scalable Synthesis of 5,5'-Dibromo-2,2'-Bipyridine and Its Stepwise Functionalization via Stille Couplings. *Nat. Protoc.* **2012**, *7*, 2022–2028.
- (24) Romero, F. M.; Ziesel, R. A Straightforward Synthesis of 5-Bromo and 5,5'-Dibromo-2,2'-Bipyridines. *Tetrahedron Lett.* **1995**, *36*, 6471–6474.
- (25) Schiemenz, B.; Power, P. P. Synthesis of Sterically Encumbered Terphenyls and Characterization of Their Metal Derivatives Et₂OLiC₆H₃-2,6-Trip₂ and Me₂SCuC₆H₃-2,6-Trip₂ (Trip = 2,4,6-I-Pr₃C₆H₂-). *Organometallics* **1996**, *15*, 958–964.
- (26) Dickie, D. A.; Abeysekera, D.; McKenzie, I. D.; Jenkins, H. A.; Clyburne, J. A. C. Crystallographic Studies on Substituted M-Terphenyls: Identification of Weak [CH₃⋯I] Interactions. *Cryst. Eng.* **2003**, *6*, 79–86.
- (27) Du, C. J. F.; Hart, H.; Ng, K. K. D. A One-Pot Synthesis of M-Terphenyls, via a Two-Aryne Sequence. *J. Org. Chem.* **1986**, *51*, 3162–3165.
- (28) Osako, T.; Uozumi, Y. Enantioselective Copper-Catalyzed Azide-Alkyne Cycloaddition for Construction of Chiral Biaryl Derivatives. *Org. Lett.* **2014**, *16*, 5866–5869.

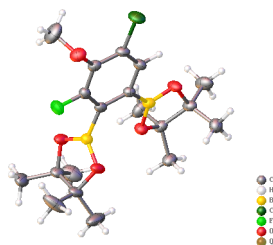
- (29) Stanciu, C.; Fox, A. R.; Richards, A. F.; Fetting, J. C.; Power, P. P. Ipso-and Para-Functionalization of Meta-Terphenyl Ligands with Substituted Methyl Groups: Unusual Head-to-Tail Coupling of Terphenyl Moieties. *J. Organomet. Chem.* **2006**, *691*, 2546–2553.

APPENDICES

APPENDIX A

Crystal Structures

Compound 67c



Compound	67c (CCDC 1851790)
Formula	C ₁₉ H ₂₈ B ₂ ClF ₅ O ₅
<i>D</i> _{calc.} / g cm ⁻³	1.258
μ /mm ⁻¹	1.849
Formula Weight	412.48
Colour	colourless
Shape	chunk
Size/mm ³	0.26×0.20×0.17
<i>T</i> /K	173(2)
Crystal System	monoclinic
Space Group	P2 ₁ /c
<i>a</i> /Å	12.39890(10)
<i>b</i> /Å	10.69680(10)
<i>c</i> /Å	17.1694(2)
α /°	90
β /°	106.9840(10)
γ /°	90
<i>V</i> /Å ³	2177.84(4)
<i>Z</i>	4
<i>Z</i> '	1
Wavelength/Å	1.541838
Radiation type	CuK α
θ _{min} /°	3.727
θ _{max} /°	72.029
Measured Refl.	24237
Independent Refl.	4268
Reflections Used	3577
<i>R</i> _{int}	0.0412
Parameters	262
Restraints	0
Largest Peak	0.325
Deepest Hole	-0.255
GooF	1.043
<i>wR</i> ₂ (all data)	0.1085
<i>wR</i> ₂	0.1029
<i>R</i> ₁ (all data)	0.0495
<i>R</i> ₁	0.0400

Table 26. Fractional Atomic Coordinates ($\times 10^4$) and Equivalent Isotropic Displacement Parameters ($\text{\AA}^2 \times 10^3$) for **67c**.

Atom	x	y	z	U_{eq}
C11	9069.6(4)	7340.9(4)	5235.5(3)	44.35(15)
F1	6250.1(9)	3830.8(10)	4875.5(6)	39.1(3)
O1	7267.4(11)	5881.8(12)	5679.2(7)	39.2(3)
O2	5644.2(10)	2592.8(10)	3056.9(8)	36.4(3)
O3	7160.2(10)	1453.9(10)	3774.9(8)	36.3(3)
O4	8095.6(10)	3000.1(10)	2475.1(7)	30.3(3)
O5	9313.3(11)	4655.0(11)	2678.8(7)	34.3(3)
C1	8398.6(14)	6004.9(14)	4751(1)	29.2(3)
C2	7555.4(14)	5458.6(14)	5014.3(9)	27.8(3)
C3	7059.7(13)	4382.8(14)	4602.5(9)	26.5(3)
C4	7337.0(13)	3842.2(13)	3960.5(9)	24.5(3)
C5	8191.7(13)	4436.3(14)	3703.9(9)	25.7(3)
C6	8711.0(14)	5507.5(15)	4108(1)	29.0(3)
C7	6369(2)	6719(3)	5513.3(15)	65.6(7)
C8	5392.6(14)	1303.7(15)	2769.7(11)	33.5(4)
C9	6280.4(15)	534.8(15)	3419.7(11)	37.0(4)
C10	4177.1(16)	1013(2)	2719.3(16)	54.1(6)
C11	5543(2)	1258(2)	1927.8(13)	60.1(6)
C12	5856(2)	83(2)	4116.6(15)	73.1(8)
C13	6799(2)	-532(2)	3071.8(19)	72.0(8)
C14	8459.5(14)	3099.8(15)	1736.2(9)	29.6(4)
C15	9554.4(15)	3897.4(15)	2036.9(10)	31.7(4)
C16	8631.7(15)	1796.1(16)	1451.1(11)	36.4(4)
C17	7514.7(17)	3756(2)	1101.3(12)	46.8(5)
C18	10600.3(15)	3129.5(18)	2446.8(11)	38.3(4)
C19	9782(2)	4766.3(18)	1402.9(13)	48.1(5)
B1	6711.2(15)	2599.2(16)	3575.7(11)	26.2(4)
B2	8546.4(16)	4006.2(16)	2945.0(11)	27.8(4)

Table 27. Anisotropic Displacement Parameters ($\times 10^4$) **67c**.

Atom	U_{11}	U_{22}	U_{33}	U_{23}	U_{13}	U_{12}
C11	59.0(3)	30.4(2)	44.0(3)	-16.51(18)	15.5(2)	-16.29(19)
F1	39.9(6)	40.5(6)	41.9(6)	-3.5(4)	19.7(5)	-10.7(4)
O1	53.4(8)	37.7(7)	28.2(6)	-6.1(5)	14.6(6)	3.7(6)
O2	30.9(6)	22.3(6)	46.8(7)	-5.9(5)	-3.0(5)	-2.9(4)
O3	31.1(6)	21.3(5)	47.6(7)	-0.9(5)	-2.6(5)	-5.0(5)
O4	35.4(6)	27.4(6)	28.8(6)	-7.2(4)	10.4(5)	-5.3(5)
O5	48.5(7)	24.3(6)	36.7(6)	-8.9(5)	22.7(6)	-8.0(5)
C1	36.6(9)	20.1(7)	27.6(8)	-3.6(6)	4.2(7)	-3.2(6)
C2	34.5(8)	24.5(7)	22.9(7)	-0.7(6)	6.2(6)	3.3(6)
C3	26.8(8)	25.7(7)	26.5(8)	2.8(6)	6.8(6)	-0.8(6)
C4	26.8(7)	19.9(7)	23.2(7)	0.8(5)	1.7(6)	0.3(6)
C5	29.4(8)	21.5(7)	25.0(7)	-1.1(6)	5.9(6)	-0.7(6)
C6	33.9(8)	24.2(8)	29.2(8)	-1.9(6)	9.7(7)	-6.5(6)
C7	68.4(15)	80.9(17)	56.5(14)	-4.1(12)	32.1(12)	25.3(13)
C8	32.5(9)	23.5(8)	40.2(9)	-9.0(7)	3.8(7)	-5.9(6)
C9	35.9(9)	21.8(8)	46.4(10)	-3.6(7)	1.2(8)	-7.8(7)
C10	31.8(10)	37.9(10)	85.0(16)	-16.7(10)	5.1(10)	-9.4(8)
C11	79.3(16)	56.1(13)	39.6(11)	-12.1(10)	9.0(11)	-20.3(12)
C12	91.2(19)	64.1(15)	51.2(13)	12.8(11)	0.9(13)	-46.5(14)

Table 27 (cont'd)

Atom	U_{11}	U_{22}	U_{33}	U_{23}	U_{13}	U_{12}
C13	50.9(13)	34.8(11)	112(2)	-26.0(12)	-5.3(13)	8.3(9)
C14	35.9(9)	29.0(8)	24.0(8)	-2.3(6)	8.8(7)	5.5(7)
C15	44.2(10)	24.0(8)	30.5(8)	-3.3(6)	16.5(7)	-0.2(7)
C16	38.3(9)	32.2(9)	36.6(9)	-12.1(7)	7.7(8)	1.5(7)
C17	48.1(11)	52.9(12)	34.7(10)	-0.8(8)	4.8(8)	19.9(9)
C18	34.5(9)	40.1(10)	39.7(10)	-7.0(8)	9.6(8)	-3.2(7)
C19	73.8(14)	34.4(10)	46.8(11)	3.9(8)	34.2(11)	0.5(9)
B1	27.2(9)	24.1(8)	26.8(8)	-1.4(7)	7.0(7)	-2.8(7)

Table 28. Bond Lengths in Å for 67c.

Atom	Atom	Length/Å
C11	C1	1.7384(15)
F1	C3	1.3604(18)
O1	C2	1.3690(19)
O1	C7	1.392(3)
O2	C8	1.4669(18)
O2	B1	1.362(2)
O3	C9	1.4628(19)
O3	B1	1.348(2)
O4	C14	1.469(2)
O4	B2	1.363(2)
O5	C15	1.4674(19)
O5	B2	1.360(2)
C1	C2	1.384(2)
C1	C6	1.379(2)
C2	C3	1.396(2)
C3	C4	1.374(2)
C4	C5	1.412(2)
C4	B1	1.583(2)
C5	C6	1.396(2)
C5	B2	1.561(2)
C8	C9	1.554(2)
C8	C10	1.516(3)
C8	C11	1.511(3)
C9	C12	1.520(3)
C9	C13	1.516(3)
C14	C15	1.558(2)
C14	C16	1.514(2)
C14	C17	1.519(2)
C15	C18	1.523(2)
C15	C19	1.519(2)

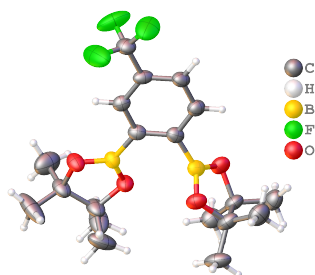
Table 29. Bond Angles in ° for **67c**.

Atom	Atom	Atom	Angle/°
C2	O1	C7	115.48(15)
B1	O2	C8	107.16(12)
B1	O3	C9	107.62(13)
B2	O4	C14	106.11(13)
B2	O5	C15	106.65(12)
C2	C1	C11	119.50(12)
C6	C1	C11	119.55(13)
C6	C1	C2	120.95(14)
O1	C2	C1	122.60(14)
O1	C2	C3	120.76(15)
C1	C2	C3	116.47(14)
F1	C3	C2	116.33(14)
F1	C3	C4	118.44(13)
C4	C3	C2	125.22(15)
C3	C4	C5	116.57(14)
C3	C4	B1	118.75(14)
C5	C4	B1	124.66(14)
C4	C5	B2	123.22(14)
C6	C5	C4	119.58(14)
C6	C5	B2	117.08(14)
C1	C6	C5	121.20(15)
O2	C8	C9	102.69(12)
O2	C8	C10	108.81(14)
O2	C8	C11	106.16(15)
C10	C8	C9	114.58(16)
C11	C8	C9	114.23(17)
C11	C8	C10	109.68(17)
O3	C9	C8	103.24(12)
O3	C9	C12	105.84(15)
O3	C9	C13	108.66(16)
C12	C9	C8	113.45(18)
C13	C9	C8	114.11(17)
C13	C9	C12	110.8(2)
O4	C14	C15	102.19(12)
O4	C14	C16	108.68(14)
O4	C14	C17	106.63(14)
C16	C14	C15	114.85(14)
C16	C14	C17	110.21(14)
C17	C14	C15	113.56(15)
O5	C15	C14	101.67(13)
O5	C15	C18	106.47(13)
O5	C15	C19	108.75(13)
C18	C15	C14	113.56(14)
C19	C15	C14	115.06(15)
C19	C15	C18	110.50(16)
O2	B1	C4	122.76(14)
O3	B1	O2	114.31(14)
O3	B1	C4	122.80(14)
O4	B2	C5	124.05(15)
O5	B2	O4	114.21(15)
O5	B2	C5	121.69(14)

Table 30. Hydrogen Fractional Atomic Coordinates ($\times 10^4$) and Equivalent Isotropic Displacement Parameters ($\text{\AA}^2 \times 10^3$) for **67c**.

Atom	x	y	z	U_{eq}
H6	9290	5901	3937	35
H7A	5731	6374	5086	98
H7B	6600	7515	5329	98
H7C	6143	6856	6008	98
H10A	4043	1213	3240	81
H10B	4029	123	2599	81
H10C	3673	1514	2286	81
H11A	5035	1864	1575	90
H11B	5366	417	1701	90
H11C	6325	1465	1961	90
H12A	6491	-238	4556	110
H12B	5301	-584	3922	110
H12C	5503	781	4321	110
H13A	7208	-197	2708	108
H13B	6202	-1095	2765	108
H13C	7323	-995	3517	108
H16A	9199	1358	1883	55
H16B	8889	1850	964	55
H16C	7918	1336	1321	55
H17A	6809	3295	1028	70
H17B	7696	3786	583	70
H17C	7429	4608	1284	70
H18A	11206	3687	2749	57
H18B	10845	2677	2032	57
H18C	10423	2530	2824	57
H19A	9142	5336	1201	72
H19B	9883	4272	949	72
H19C	10467	5251	1650	72

Compound 68c



Compound	68c (CCDC 1838224)
Formula	C ₁₉ H ₂₇ B ₂ F ₃ O ₄
<i>D</i> _{calc.} / g cm ⁻³	1.245
μ /mm ⁻¹	0.851
Formula Weight	398.02
Colour	colourless
Shape	chunk
Size/mm ³	0.18×0.14×0.07
<i>T</i> /K	173(2)
Crystal System	orthorhombic
Flack Parameter	-1.3(5)
Hooft Parameter	-0.9(4)
Space Group	<i>P</i> 2 ₁ 2 ₁ 2 ₁
<i>a</i> /Å	10.5055(7)
<i>b</i> /Å	11.7536(8)
<i>c</i> /Å	17.1954(11)
α /°	90
β /°	90
γ /°	90
<i>V</i> /Å ³	2123.2(2)
<i>Z</i>	4
<i>Z</i> '	1
Wavelength/Å	1.541838
Radiation type	CuK α
θ _{min} /°	4.557
θ _{max} /°	71.472
Measured Refl.	8302
Independent Refl.	3858
Reflections Used	2108
<i>R</i> _{int}	0.0979
Parameters	261
Restraints	0
Largest Peak	0.425
Deepest Hole	-0.265
GooF	0.973
<i>wR</i> ₂ (all data)	0.2515
<i>wR</i> ₂	0.2107
<i>R</i> ₁ (all data)	0.1427
<i>R</i> ₁	0.0880

Table 31. Fractional Atomic Coordinates ($\times 10^4$) and Equivalent Isotropic Displacement Parameters ($\text{\AA}^2 \times 10^3$) for **68c**.

Atom	x	y	z	U_{eq}
F1	2838(7)	4246(6)	5874(5)	104(3)
F2	2605(6)	3404(7)	4814(4)	104(3)
F3	3707(6)	2681(5)	5726(5)	93(2)
O1	4187(5)	6834(5)	3218(4)	48.9(14)
O2	6235(5)	7410(5)	3425(4)	48.0(14)
O3	8408(5)	5533(5)	3373(3)	49.7(14)
O4	8878(5)	6400(5)	4534(3)	48.7(14)
C1	4596(8)	4224(6)	5040(5)	42.4(19)
C2	4456(8)	5080(6)	4484(5)	39.4(17)
C3	5508(7)	5659(6)	4187(5)	39.1(17)
C4	6729(8)	5352(6)	4454(5)	41.0(18)
C5	6842(8)	4511(7)	5023(5)	45.9(19)
C6	5808(8)	3944(7)	5317(5)	45.4(19)
C7	3470(9)	3630(7)	5353(5)	51(2)
C8	4335(9)	7912(7)	2795(6)	54(2)
C9	5770(9)	8085(8)	2784(6)	61(3)
C10	3714(11)	8819(9)	3351(8)	91(4)
C11	3639(15)	7854(11)	2069(8)	114(6)
C12	6314(10)	9224(9)	2813(8)	84(4)
C13	6330(14)	7510(11)	2050(6)	94(4)
C14	9779(7)	5791(8)	3343(6)	52(2)
C15	9917(7)	6682(8)	3987(5)	48(2)
C16	10089(11)	6163(10)	2540(6)	72(3)
C17	10449(10)	4663(8)	3546(7)	69(3)
C18	9675(9)	7898(7)	3714(6)	58(2)
C19	11160(8)	6637(9)	4429(6)	61(3)
B1	5305(8)	6641(7)	3597(5)	37.9(19)
B2	7991(9)	5813(7)	4097(6)	42(2)

Table 32. Anisotropic Displacement Parameters ($\times 10^4$) **68c**.

Atom	U_{11}	U_{22}	U_{33}	U_{23}	U_{13}	U_{12}
F1	104(5)	91(5)	119(6)	-23(5)	71(5)	-17(4)
F2	89(4)	141(7)	81(5)	25(5)	-15(4)	-67(5)
F3	82(4)	65(4)	132(6)	50(4)	17(4)	-8(3)
O1	51(3)	41(3)	54(3)	13(3)	-10(3)	-16(2)
O2	43(3)	46(3)	55(4)	16(3)	0(3)	-8(2)
O3	54(3)	51(3)	44(3)	-10(3)	10(3)	-9(3)
O4	47(3)	50(3)	49(3)	-12(3)	7(3)	1(3)
C1	55(5)	28(3)	45(4)	2(3)	18(4)	-2(3)
C2	45(4)	32(3)	42(4)	-6(3)	5(4)	-3(3)
C3	49(4)	28(3)	40(4)	-2(3)	4(4)	-7(3)
C4	51(4)	33(4)	39(4)	-1(3)	3(4)	3(3)
C5	46(4)	43(4)	49(5)	2(4)	8(4)	4(4)
C6	53(5)	40(4)	43(5)	10(4)	8(4)	6(3)
C7	57(5)	47(5)	49(5)	9(4)	5(4)	-9(4)
C8	61(5)	47(5)	54(5)	21(4)	-12(5)	-14(4)
C9	60(5)	63(5)	61(6)	31(5)	-9(5)	-17(4)
C10	93(8)	62(6)	118(11)	15(7)	34(8)	21(6)
C11	152(13)	85(8)	105(10)	59(8)	-79(10)	-59(8)

Table 32 (cont'd)

Atom	U_{11}	U_{22}	U_{33}	U_{23}	U_{13}	U_{12}
C12	67(6)	61(6)	125(11)	46(7)	-27(7)	-25(5)
C13	146(12)	83(8)	52(6)	26(6)	25(8)	22(8)
C14	43(4)	56(5)	58(5)	-13(4)	16(4)	-9(4)
C15	39(4)	52(5)	52(5)	-2(4)	13(4)	-4(4)
C16	83(7)	82(7)	51(6)	-9(5)	27(5)	-23(6)
C17	63(6)	62(6)	83(8)	-10(6)	10(6)	9(5)
C18	61(5)	45(5)	68(6)	1(5)	6(5)	-2(4)
C19	47(5)	71(6)	66(6)	-9(5)	-1(5)	-3(4)
B1	41(4)	33(4)	39(5)	-2(4)	-6(4)	-3(3)
B2	49(5)	31(4)	45(5)	3(4)	5(4)	6(4)

Table 33. Bond Lengths in Å for **68c**.

Atom	Atom	Length/Å
F1	C7	1.330(10)
F2	C7	1.325(10)
F3	C7	1.310(10)
O1	C8	1.468(9)
O1	B1	1.362(10)
O2	C9	1.443(10)
O2	B1	1.363(10)
O3	C14	1.473(9)
O3	B2	1.359(11)
O4	C15	1.478(10)
O4	B2	1.382(11)
C1	C2	1.395(11)
C1	C6	1.399(11)
C1	C7	1.476(11)
C2	C3	1.395(10)
C3	C4	1.410(11)
C3	B1	1.552(11)
C4	C5	1.396(11)
C4	B2	1.559(12)
C5	C6	1.371(11)
C8	C9	1.522(13)
C8	C10	1.573(15)
C8	C11	1.448(13)
C9	C12	1.456(13)
C9	C13	1.549(15)
C14	C15	1.532(12)
C14	C16	1.485(13)
C14	C17	1.541(13)
C15	C18	1.525(12)
C15	C19	1.512(12)

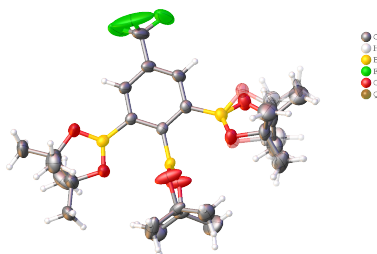
Table 34. Bond Angles in ° for **68c**

Atom	Atom	Atom	Angle/°
B1	O1	C8	106.8(6)
B1	O2	C9	106.7(6)
B2	O3	C14	107.3(7)
B2	O4	C15	105.3(6)
C2	C1	C6	119.9(7)
C2	C1	C7	120.5(8)
C6	C1	C7	119.6(7)
C3	C2	C1	121.3(8)
C2	C3	C4	118.5(7)
C2	C3	B1	119.6(7)
C4	C3	B1	121.9(7)
C3	C4	B2	123.8(7)
C5	C4	C3	119.2(7)
C5	C4	B2	116.7(7)
C6	C5	C4	122.3(8)
C5	C6	C1	118.8(7)
F1	C7	C1	112.8(7)
F2	C7	F1	103.7(8)
F2	C7	C1	112.9(8)
F3	C7	F1	103.3(8)
F3	C7	F2	107.6(8)
F3	C7	C1	115.4(8)
O1	C8	C9	103.1(7)
O1	C8	C10	103.9(7)
C9	C8	C10	109.2(9)
C11	C8	O1	109.4(7)
C11	C8	C9	119.7(10)
C11	C8	C10	110.3(10)
O2	C9	C8	104.6(7)
O2	C9	C12	110.3(8)
O2	C9	C13	104.7(8)
C8	C9	C13	109.2(9)
C12	C9	C8	120.7(9)
C12	C9	C13	106.2(10)
O3	C14	C15	102.0(6)
O3	C14	C16	107.9(8)
O3	C14	C17	105.2(7)
C15	C14	C17	112.5(8)
C16	C14	C15	116.7(8)
C16	C14	C17	111.3(9)
O4	C15	C14	103.7(6)
O4	C15	C18	106.5(7)
O4	C15	C19	108.1(7)
C18	C15	C14	113.7(8)
C19	C15	C14	114.9(7)
C19	C15	C18	109.4(8)
O1	B1	O2	113.8(7)
O1	B1	C3	123.7(7)
O2	B1	C3	122.4(7)
O3	B2	O4	113.7(7)
O3	B2	C4	123.5(8)
O4	B2	C4	122.2(8)

Table 35. Hydrogen Fractional Atomic Coordinates ($\times 10^4$) and Equivalent Isotropic Displacement Parameters ($\text{\AA}^2 \times 10^3$) for **68c**.

Atom	x	y	z	U_{eq}
H2	3628	5272	4305	47
H5	7665	4324	5213	55
H6	5913	3373	5702	55
H10A	2909	8521	3556	137
H10B	3550	9521	3061	137
H10C	4294	8980	3783	137
H11A	3921	7187	1773	171
H11B	3801	8544	1765	171
H11C	2726	7790	2178	171
H12A	6014	9615	3282	127
H12B	6049	9652	2352	127
H12C	7245	9171	2825	127
H13A	7257	7452	2102	141
H13B	6121	7966	1590	141
H13C	5967	6746	1993	141
H16A	9901	5546	2175	108
H16B	10995	6357	2509	108
H16C	9577	6832	2407	108
H17A	10225	4438	4078	104
H17B	11373	4763	3508	104
H17C	10175	4070	3182	104
H18A	8908	7917	3389	87
H18B	10406	8165	3410	87
H18C	9555	8394	4166	87
H19A	11144	7197	4851	92
H19B	11865	6811	4074	92
H19C	11278	5874	4647	92

Compound 68*



Compound	68* (CCDC 1838225)
Formula	C ₂₅ H ₃₈ B ₃ F ₃ O ₆
$D_{calc.}/\text{g cm}^{-3}$	1.214
μ/mm^{-1}	0.798
Formula Weight	523.98
Colour	colourless
Shape	block
Size/mm ³	0.45×0.35×0.18
T/K	173(2)
Crystal System	orthorhombic
Flack Parameter	0.1(4)
Hooft Parameter	0.13(5)
Space Group	$P2_12_12_1$
$a/\text{Å}$	11.6356(2)
$b/\text{Å}$	12.0322(3)
$c/\text{Å}$	20.4719(4)
$\alpha/^\circ$	90
$\beta/^\circ$	90
$\gamma/^\circ$	90
$V/\text{Å}^3$	2866.10(10)
Z	4
Z'	1
Wavelength/Å	1.541838
Radiation type	CuK α
$\theta_{min}/^\circ$	4.262
$\theta_{max}/^\circ$	72.173
Measured Refl.	18600
Independent Refl.	5516
Reflections Used	5174
R_{int}	0.0305
Parameters	376
Restraints	0
Largest Peak	0.834
Deepest Hole	-0.577
Goof	1.064
wR_2 (all data)	0.2069
wR_2	0.2026
R_1 (all data)	0.0879
R_1	0.0834

Table 36. Fractional Atomic Coordinates ($\times 10^4$) and Equivalent Isotropic Displacement Parameters ($\text{\AA}^2 \times 10^3$) for **68***.

Atom	x	y	z	U_{eq}
F1	8733(8)	6410(6)	4807(4)	196(4)
F2	8572(6)	7481(4)	5596(2)	140(3)
F3	7296(6)	7365(5)	4898(3)	133(3)
O1	9454(4)	4297(5)	7132(3)	103(2)
O2	7999(4)	3361(5)	7530(2)	79.7(16)
O3	6166(4)	2079(3)	6639(2)	78.7(16)
O4	5163(4)	3303(3)	7215(2)	68.6(13)
O5	4338(8)	3117(7)	5597(5)	49(2)
O5A	4012(8)	3482(10)	5858(5)	55(2)
O6	3820(8)	4886(7)	5365(5)	52(2)
O6A	4207(9)	4715(9)	5020(5)	60(2)
C1	7477(5)	5860(4)	5624(2)	45.3(12)
C2	8080(4)	5355(4)	6124(2)	40.1(11)
C3	7602(4)	4506(4)	6495(2)	33.1(9)
C4	6487(4)	4115(3)	6338(2)	30.1(9)
C5	5879(4)	4618(4)	5822(2)	34.9(9)
C6	6382(5)	5493(4)	5477(2)	44.4(11)
C7	8025(7)	6773(6)	5247(3)	73(2)
C8	9922(7)	3557(8)	7637(4)	97(3)
C9	8911(6)	3358(7)	8034(4)	85(3)
C10	10921(6)	4192(6)	7950(4)	78(2)
C11	10313(6)	2427(6)	7320(3)	67.5(15)
C12	8756(8)	4431(6)	8517(3)	80(2)
C13	8834(5)	2272(5)	8404(3)	61.2(16)
C14	5495(4)	1384(4)	7084(3)	46.4(12)
C15	4882(4)	2256(4)	7532(3)	44.3(12)
C16	6315(5)	625(5)	7436(5)	81(2)
C17	4694(6)	693(5)	6667(3)	66.5(15)
C18	5339(7)	2336(8)	8218(3)	83(2)
C19	3586(6)	2167(8)	7550(5)	89(2)
C20	3285(10)	3059(10)	5191(6)	50.4(18)
C20A	2880(10)	3533(12)	5531(6)	54(3)
C21	2805(9)	4239(12)	5254(7)	51(3)
C21A	3197(10)	4000(10)	4880(6)	50.4(18)
C22	2350(12)	2412(12)	5544(11)	81(2)
C22A	2552(15)	2099(11)	5413(8)	66.5(15)
C23	3718(18)	2736(17)	4530(8)	83(2)
C23A	2067(16)	4517(14)	5849(9)	67.5(15)
C24	2167(16)	4173(14)	5955(9)	67.5(15)
C24A	3646(15)	3130(11)	4371(8)	66.5(15)
C25	2120(20)	4720(30)	4718(9)	83(2)
C25A	2329(12)	4657(17)	4508(6)	65(5)
B1	8347(4)	4039(4)	7072(3)	34.6(10)
B2	5924(4)	3136(4)	6746(2)	29.9(9)
B3	4655(5)	4225(5)	5589(3)	39.8(12)

Table 37. Anisotropic Displacement Parameters ($\times 10^4$) **68***.

Atom	U_{11}	U_{22}	U_{33}	U_{23}	U_{13}	U_{12}
F1	262(10)	123(5)	203(7)	48(5)	163(7)	-30(6)
F2	201(6)	118(4)	102(3)	65(3)	-81(4)	-122(4)
F3	161(5)	113(4)	126(4)	84(4)	-79(4)	-75(4)
O1	59(3)	127(5)	123(4)	86(4)	-51(3)	-53(3)
O2	56(2)	103(4)	80(3)	56(3)	-35(2)	-39(2)
O3	98(3)	27.3(17)	111(4)	-2.7(19)	72(3)	-2(2)
O4	96(3)	30.7(18)	79(3)	10.6(18)	53(3)	7(2)
O5	45(5)	40(5)	62(6)	3(4)	-18(4)	-12(4)
O5A	41(5)	77(7)	48(5)	20(5)	-9(4)	-22(5)
O6	51(5)	37(4)	68(6)	-2(4)	-21(4)	-1(3)
O6A	57(6)	66(6)	56(5)	17(5)	-23(4)	-27(5)
C1	62(3)	42(3)	32(2)	2.2(19)	-7(2)	-22(2)
C2	45(3)	43(3)	33(2)	-0.8(19)	-6.3(19)	-17(2)
C3	36(2)	31(2)	32(2)	-3.9(17)	-0.8(17)	-7.2(18)
C4	30(2)	30(2)	31(2)	-6.6(16)	2.1(16)	-1.2(17)
C5	38(2)	31(2)	36(2)	-4.6(17)	-4.5(18)	-2.8(18)
C6	56(3)	41(2)	36(2)	5(2)	-14(2)	-14(2)
C7	97(5)	80(4)	43(3)	27(3)	-23(3)	-48(4)
C8	71(5)	111(6)	109(6)	62(5)	-45(5)	-47(5)
C9	70(4)	103(5)	83(5)	47(4)	-38(4)	-32(4)
C10	57(4)	89(5)	89(5)	26(4)	-39(4)	-22(4)
C11	53(3)	69(4)	81(4)	-11(3)	-6(3)	16(3)
C12	108(6)	90(5)	43(3)	-2(3)	-2(3)	40(5)
C13	50(3)	72(4)	61(3)	27(3)	-21(3)	-8(3)
C14	36(2)	28(2)	75(3)	7(2)	15(2)	-2.3(19)
C15	43(3)	35(2)	55(3)	14(2)	12(2)	-3(2)
C16	43(3)	44(3)	155(7)	4(4)	-23(4)	-1(2)
C17	72(4)	51(3)	77(4)	-2(3)	-11(3)	-12(3)
C18	89(4)	103(5)	57(3)	-8(3)	6(3)	-12(4)
C19	47(4)	106(6)	114(6)	14(5)	29(4)	14(4)
C20	44(4)	58(5)	49(5)	-8(4)	-19(4)	-9(4)
C20A	38(6)	68(8)	55(7)	3(7)	-8(5)	-16(5)
C21	34(5)	65(8)	55(7)	-21(6)	-18(5)	1(5)
C21A	44(4)	58(5)	49(5)	-8(4)	-19(4)	-9(4)
C22	43(3)	44(3)	155(7)	4(4)	-23(4)	-1(2)
C22A	72(4)	51(3)	77(4)	-2(3)	-11(3)	-12(3)
C23	89(4)	103(5)	57(3)	-8(3)	6(3)	-12(4)
C23A	53(3)	69(4)	81(4)	-11(3)	-6(3)	16(3)
C24	53(3)	69(4)	81(4)	-11(3)	-6(3)	16(3)
C24A	72(4)	51(3)	77(4)	-2(3)	-11(3)	-12(3)
C25	89(4)	103(5)	57(3)	-8(3)	6(3)	-12(4)
C25A	51(8)	85(10)	59(9)	16(9)	-40(7)	-14(8)
B1	34(2)	35(2)	35(2)	-2(2)	3(2)	-5(2)
B2	23(2)	29(2)	38(2)	-0.1(19)	-0.2(19)	-2.5(18)
B3	43(3)	38(3)	38(3)	-3(2)	-8(2)	-2(2)

Table 38. Bond Lengths in Å for **68***.

Atom	Atom	Length/Å
F1	C7	1.297(10)
F2	C7	1.282(7)
F3	C7	1.318(9)
O1	C8	1.469(8)
O1	B1	1.331(7)
O2	C9	1.479(7)
O2	B1	1.307(6)
O3	C14	1.462(6)
O3	B2	1.320(6)
O4	C15	1.454(6)
O4	B2	1.322(6)
O5	C20	1.482(13)
O5	B3	1.384(11)
O5A	C20A	1.479(15)
O5A	B3	1.290(11)
O6	C21	1.433(14)
O6	B3	1.336(10)
O6A	C21A	1.484(13)
O6A	B3	1.406(10)
C1	C2	1.382(7)
C1	C6	1.382(7)
C1	C7	1.486(7)
C2	C3	1.389(6)
C3	C4	1.417(6)
C3	B1	1.570(7)
C4	C5	1.408(6)
C4	B2	1.586(6)
C5	C6	1.396(7)
C5	B3	1.575(7)
C8	C9	1.449(12)
C8	C10	1.531(9)
C8	C11	1.575(13)
C9	C12	1.636(12)
C9	C13	1.514(9)
C14	C15	1.565(7)
C14	C16	1.504(8)
C14	C17	1.513(8)
C15	C18	1.505(9)
C15	C19	1.512(8)
C20	C21	1.531(18)
C20	C22	1.52(2)
C20	C23	1.50(2)
C20A	C21A	1.494(18)
C20A	C22A	1.784(19)
C20A	C23A	1.65(2)
C21	C24	1.62(2)
C21	C25	1.47(3)
C21A	C24A	1.57(2)
C21A	C25A	1.490(19)

Table 39. Bond Angles in ° for **68***.

Atom	Atom	Atom	Angle/°
B1	O1	C8	106.4(5)
B1	O2	C9	106.2(4)
B2	O3	C14	109.5(4)
B2	O4	C15	110.0(4)
B3	O5	C20	105.0(8)
B3	O5A	C20A	107.1(8)
B3	O6	C21	109.3(8)
B3	O6A	C21A	102.2(8)
C2	C1	C7	119.5(5)
C6	C1	C2	119.3(4)
C6	C1	C7	121.2(5)
C1	C2	C3	121.6(4)
C2	C3	C4	119.1(4)
C2	C3	B1	117.0(4)
C4	C3	B1	123.9(4)
C3	C4	B2	120.4(4)
C5	C4	C3	119.2(4)
C5	C4	B2	120.5(4)
C4	C5	B3	123.5(4)
C6	C5	C4	119.6(4)
C6	C5	B3	116.9(4)
C1	C6	C5	121.1(4)
F1	C7	F3	102.4(7)
F1	C7	C1	112.6(7)
F2	C7	F1	107.2(8)
F2	C7	F3	105.3(7)
F2	C7	C1	114.5(5)
F3	C7	C1	113.9(6)
O1	C8	C10	105.9(6)
O1	C8	C11	109.9(7)
C9	C8	O1	101.2(6)
C9	C8	C10	117.7(8)
C9	C8	C11	108.8(7)
C10	C8	C11	112.6(7)
O2	C9	C12	109.9(6)
O2	C9	C13	108.0(5)
C8	C9	O2	101.1(6)
C8	C9	C12	107.3(7)
C8	C9	C13	118.1(8)
C13	C9	C12	111.9(6)
O3	C14	C15	102.9(4)
O3	C14	C16	107.9(5)
O3	C14	C17	107.0(5)
C16	C14	C15	114.6(6)
C16	C14	C17	109.1(5)
C17	C14	C15	114.8(5)
O4	C15	C14	102.6(4)
O4	C15	C18	106.3(5)
O4	C15	C19	107.2(5)
C18	C15	C14	115.4(5)
C18	C15	C19	109.5(6)
C19	C15	C14	114.9(5)

Table 39 (cont'd)

Atom	Atom	Atom	Angle/°
O5	C20	C21	102.2(8)
O5	C20	C22	110.5(11)
O5	C20	C23	104.0(12)
C22	C20	C21	100.0(11)
C23	C20	C21	116.1(13)
C23	C20	C22	122.5(13)
O5A	C20A	C21A	101.5(9)
O5A	C20A	C22A	102.2(11)
O5A	C20A	C23A	111.2(11)
C21A	C20A	C22A	107.2(11)
C21A	C20A	C23A	103.0(12)
C23A	C20A	C22A	128.7(12)
O6	C21	C20	102.5(8)
O6	C21	C24	105.4(11)
O6	C21	C25	110.6(16)
C20	C21	C24	101.3(12)
C25	C21	C20	119.8(14)
C25	C21	C24	115.6(12)
O6A	C21A	C20A	103.9(9)
O6A	C21A	C24A	104.6(11)
O6A	C21A	C25A	109.1(11)
C20A	C21A	C24A	115.1(11)
C25A	C21A	C20A	119.2(12)
C25A	C21A	C24A	104.0(11)
O1	B1	C3	121.4(4)
O2	B1	O1	112.3(5)
O2	B1	C3	126.3(4)
O3	B2	O4	114.2(4)
O3	B2	C4	122.7(4)
O4	B2	C4	123.1(4)
O5	B3	C5	121.8(6)
O5A	B3	O6A	115.5(7)
O5A	B3	C5	127.1(6)
O6	B3	O5	112.6(7)
O6	B3	C5	125.7(6)
O6A	B3	C5	117.4(5)

Table 40. Hydrogen Fractional Atomic Coordinates ($\times 10^4$) and Equivalent Isotropic Displacement Parameters ($\text{\AA}^2 \times 10^3$) for **68***

Atom	x	y	z	U_{eq}
H2	8842	5593	6216	48
H6	5964	5841	5135	53
H10A	11545	4271	7632	117
H10B	11200	3782	8332	117
H10C	10657	4930	8086	117
H11A	9634	1978	7216	101
H11B	10801	2020	7628	101
H11C	10746	2578	6919	101
H12A	8879	5116	8268	120
H12B	9318	4388	8872	120

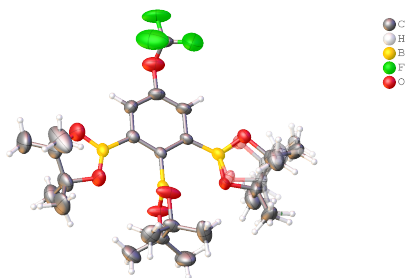
Table 40 (cont'd)

Atom	x	y	z	U_{eq}
H12C	7978	4432	8700	120
H13A	8074	2208	8607	92
H13B	9427	2253	8743	92
H13C	8950	1651	8101	92
H16A	6747	186	7117	121
H16B	5882	125	7723	121
H16C	6849	1070	7698	121
H17A	4214	1185	6401	100
H17B	4203	237	6949	100
H17C	5147	208	6381	100
H18A	5114	1672	8464	124
H18B	5022	2998	8431	124
H18C	6179	2390	8206	124
H19A	3264	2836	7753	134
H19B	3363	1512	7804	134
H19C	3290	2097	7103	134
H22A	2651	1688	5679	121
H22B	1695	2303	5249	121
H22C	2099	2829	5929	121
H22D	2398	1750	5837	100
H22E	3207	1728	5205	100
H22F	1873	2030	5133	100
H23A	4343	2196	4577	124
H23B	4003	3397	4303	124
H23C	3091	2403	4278	124
H23D	1300	4487	5652	101
H23E	2414	5244	5763	101
H23F	2004	4403	6322	101
H24A	2705	3891	6284	101
H24B	1505	3671	5924	101
H24C	1904	4916	6082	101
H24D	3980	2494	4602	100
H24E	4234	3475	4095	100
H24F	3006	2877	4098	100
H25A	1587	5274	4894	124
H25B	1679	4126	4503	124
H25C	2632	5069	4400	124
H25D	1593	4261	4509	98
H25E	2592	4756	4057	98
H25F	2232	5386	4714	98

Table 41. Atomic Occupancies for all atoms that are not fully occupied in **68***.

Atom	Occupancy
O5	0.5
O5A	0.5
O6	0.5
O6A	0.5
C20	0.5
C20A	0.5
C21	0.5
C21A	0.5
C22	0.5
H22A	0.5
H22B	0.5
H22C	0.5
C22A	0.5
H22D	0.5
H22E	0.5
H22F	0.5
C23	0.5
H23A	0.5
H23B	0.5
H23C	0.5
C23A	0.5
H23D	0.5
H23E	0.5
H23F	0.5
C24	0.5
H24A	0.5
H24B	0.5
H24C	0.5
C24A	0.5
H24D	0.5
H24E	0.5
H24F	0.5
C25	0.5
H25A	0.5
H25B	0.5
H25C	0.5
C25A	0.5
H25D	0.5
H25E	0.5
H25F	0.5

Compound 69*



Compound	69* (CCDC 1819547)
Formula	C ₂₅ H ₃₈ B ₃ F ₃ O ₇
<i>D</i> _{calc.} / g cm ⁻³	1.236
μ /mm ⁻¹	0.829
Formula Weight	539.98
Colour	colourless
Shape	chunk
Size/mm ³	0.21×0.20×0.19
<i>T</i> /K	173(2)
Crystal System	orthorhombic
Flack Parameter	0.0(2)
Hooft Parameter	-0.13(12)
Space Group	<i>P</i> 2 ₁ 2 ₁ 2 ₁
<i>a</i> /Å	11.5779(3)
<i>b</i> /Å	11.9042(3)
<i>c</i> /Å	21.0598(6)
α /°	90
β /°	90
γ /°	90
<i>V</i> /Å ³	2902.58(13)
<i>Z</i>	4
<i>Z</i> '	1
Wavelength/Å	1.541838
Radiation type	CuK α
θ _{min} /°	4.198
θ _{max} /°	72.355
Measured Refl.	21149
Independent Refl.	5615
Reflections Used	4195
<i>R</i> _{int}	0.0604
Parameters	389
Restraints	0
Largest Peak	0.808
Deepest Hole	-0.372
GooF	1.271
<i>wR</i> ₂ (all data)	0.3245
<i>wR</i> ₂	0.2936
<i>R</i> ₁ (all data)	0.1244
<i>R</i> ₁	0.1021

Table 42. Fractional Atomic Coordinates ($\times 10^4$) and Equivalent Isotropic Displacement Parameters ($\text{\AA}^2 \times 10^3$) for **69***.

Atom	x	y	z	U_{eq}
F1	8491(9)	5983(8)	5452(4)	139(4)
F2	9706(7)	6203(11)	4795(5)	154(4)
F3	9034(8)	7626(6)	5301(4)	113(3)
O1	4244(6)	4673(6)	4971(3)	76.8(18)
O2	4027(5)	3432(5)	4178(3)	72.0(18)
O3	5987(6)	2029(4)	3457(3)	73.3(19)
O4	5236(5)	3238(4)	2763(3)	63.3(16)
O5	7873(10)	3462(12)	2398(7)	47(3)
O5A	8095(16)	3063(12)	2586(9)	60(4)
O6	9458(8)	4178(10)	2879(5)	44(2)
O6A	9176(11)	4653(11)	2650(6)	56(3)
O7	7963(6)	6843(5)	4610(4)	78.8(19)
C1	7490(6)	5861(6)	4298(4)	54.1(16)
C2	6429(6)	5480(6)	4506(3)	47.8(14)
C3	5914(5)	4570(5)	4184(3)	38.0(12)
C4	6465(4)	4091(4)	3650(3)	32.0(11)
C5	7561(5)	4507(4)	3459(3)	36.0(12)
C6	8059(6)	5413(6)	3801(4)	51.6(16)
C7	3217(8)	4033(10)	5134(5)	77(3)
C8	2881(7)	3533(9)	4489(5)	75(3)
C9	2354(10)	4750(13)	5426(6)	102(4)
C10	3630(11)	3083(15)	5595(6)	125(6)
C11	2146(8)	4324(10)	4098(6)	84(2)
C12	2362(9)	2344(11)	4499(7)	106(5)
C13	5432(6)	1307(5)	2984(4)	49.1(16)
C14	4808(5)	2165(5)	2539(3)	44.4(14)
C15	4622(9)	542(6)	3350(5)	69(2)
C16	6361(7)	603(6)	2676(7)	82(3)
C17	3517(7)	2207(9)	2592(6)	80(3)
C18	5134(9)	2065(11)	1844(5)	88(3)
C19	8774(13)	3360(15)	1912(8)	57(3)
C19A	9141(13)	2910(15)	2194(8)	57(3)
C20	9866(11)	3481(13)	2346(7)	49(2)
C20A	9537(11)	4078(13)	2053(7)	49(2)
C21	8430(20)	4200(20)	1445(13)	84(2)
C21A	8790(19)	2340(20)	1579(14)	61(4)
C22	8710(30)	1990(30)	1696(19)	87(7)
C22A	10290(20)	2430(40)	2670(20)	84(2)
C23	10780(30)	4030(40)	1945(18)	87(7)
C23A	8872(14)	4580(16)	1498(8)	57(4)
C24	10050(20)	2320(30)	2630(20)	84(2)
C24A	10890(18)	4240(30)	2074(13)	61(4)
C25	8771(9)	6712(11)	5004(4)	86(3)
B1	4696(6)	4184(6)	4433(3)	39.3(13)
B2	5894(5)	3084(5)	3268(3)	34.4(12)
B3	8267(6)	4049(6)	2886(4)	39.5(14)

Table 43. Anisotropic Displacement Parameters ($\times 10^4$) **69***.

Atom	U_{11}	U_{22}	U_{33}	U_{23}	U_{13}	U_{12}
F1	179(8)	156(7)	82(5)	37(5)	-38(5)	-69(7)
F2	80(4)	251(12)	133(7)	-85(8)	-23(5)	8(6)
F3	146(6)	83(4)	109(5)	-33(4)	-43(5)	-43(4)
O1	64(3)	92(4)	75(4)	-11(3)	22(3)	-18(3)
O2	54(3)	84(4)	78(4)	-24(3)	28(3)	-27(3)
O3	87(4)	33(2)	100(5)	-1(3)	-56(4)	-4(2)
O4	91(4)	34(2)	64(3)	-1(2)	-44(3)	-4(2)
O5	25(4)	60(9)	56(8)	-23(6)	5(5)	-8(5)
O5A	72(10)	40(7)	69(11)	-14(6)	37(8)	-15(6)
O6	37(5)	49(5)	45(6)	1(5)	1(4)	-6(4)
O6A	53(6)	60(7)	55(7)	-14(6)	21(6)	-27(5)
O7	90(4)	63(3)	84(5)	-12(3)	-24(4)	-15(3)
C1	56(4)	52(3)	54(4)	-13(3)	-10(3)	-13(3)
C2	46(3)	55(3)	43(3)	-9(3)	4(3)	-5(3)
C3	36(3)	40(3)	38(3)	6(2)	-2(2)	-5(2)
C4	30(2)	33(2)	32(3)	6(2)	0(2)	-4.9(19)
C5	31(2)	38(3)	39(3)	0(2)	-3(2)	-11(2)
C6	43(3)	59(4)	53(4)	-10(3)	-3(3)	-21(3)
C7	57(5)	112(7)	62(5)	-1(5)	21(4)	-13(5)
C8	47(4)	103(7)	77(6)	6(5)	14(4)	-18(4)
C9	72(6)	147(11)	86(8)	-9(7)	35(6)	-3(7)
C10	83(7)	205(16)	86(8)	90(10)	-5(6)	-22(8)
C11	58(4)	110(6)	84(5)	14(4)	1(4)	18(4)
C12	70(6)	121(9)	127(11)	-22(8)	47(7)	-48(6)
C13	48(3)	31(3)	69(4)	-1(3)	-14(3)	-6(2)
C14	43(3)	37(3)	53(4)	-8(3)	-9(3)	-7(2)
C15	90(6)	42(4)	75(5)	7(4)	9(5)	-9(4)
C16	54(4)	43(4)	148(10)	-6(5)	25(5)	-2(3)
C17	47(4)	98(7)	96(7)	9(6)	-23(5)	-1(4)
C18	81(6)	130(9)	53(5)	-7(5)	-15(5)	-19(6)
C19	40(6)	80(8)	50(7)	-15(5)	9(5)	4(5)
C19A	40(6)	80(8)	50(7)	-15(5)	9(5)	4(5)
C20	38(5)	59(6)	52(6)	-6(4)	13(4)	-10(4)
C20A	38(5)	59(6)	52(6)	-6(4)	13(4)	-10(4)
C21	58(4)	110(6)	84(5)	14(4)	1(4)	18(4)
C21A	43(6)	75(11)	65(9)	-33(6)	24(5)	-28(6)
C22	76(11)	97(16)	89(14)	-54(9)	34(8)	-43(10)
C22A	58(4)	110(6)	84(5)	14(4)	1(4)	18(4)
C23	76(11)	97(16)	89(14)	-54(9)	34(8)	-43(10)
C23A	41(7)	84(10)	44(7)	-2(7)	-11(6)	1(7)
C24	58(4)	110(6)	84(5)	14(4)	1(4)	18(4)
C24A	43(6)	75(11)	65(9)	-33(6)	24(5)	-28(6)
C25	71(5)	134(9)	52(4)	-31(5)	4(4)	-51(6)
B1	34(3)	52(3)	32(3)	6(3)	4(3)	1(2)
B2	26(2)	36(3)	41(3)	4(2)	1(2)	-1(2)
B3	33(3)	42(3)	43(4)	2(3)	1(3)	-8(2)

Table 44. Bond Lengths in Å for **69***.

Atom	Atom	Length/Å
F1	C25	1.322(13)
F2	C25	1.317(15)
F3	C25	1.291(11)
O1	C7	1.454(10)
O1	B1	1.376(10)
O2	C8	1.485(9)
O2	B1	1.301(9)
O3	C13	1.464(8)
O3	B2	1.321(8)
O4	C14	1.449(7)
O4	B2	1.321(8)
O5	C19	1.47(2)
O5	B3	1.323(16)
O5A	C19A	1.48(2)
O5A	B3	1.348(18)
O6	C20	1.473(18)
O6	B3	1.388(12)
O6A	C20A	1.491(17)
O6A	B3	1.368(12)
O7	C1	1.448(8)
O7	C25	1.261(13)
C1	C2	1.380(10)
C1	C6	1.347(11)
C2	C3	1.411(9)
C3	C4	1.412(8)
C3	B1	1.574(8)
C4	C5	1.419(7)
C4	B2	1.589(8)
C5	C6	1.419(8)
C5	B3	1.557(9)
C7	C8	1.533(14)
C7	C9	1.452(15)
C7	C10	1.565(16)
C8	C11	1.513(14)
C8	C12	1.537(15)
C13	C14	1.564(9)
C13	C15	1.517(11)
C13	C16	1.509(11)
C14	C17	1.499(10)
C14	C18	1.516(13)
C19	C20	1.57(2)
C19	C21	1.46(3)
C19	C22	1.69(3)
C19A	C20A	1.49(2)
C19A	C21A	1.52(3)
C19A	C22A	1.76(3)
C20	C23	1.51(4)
C20	C24	1.52(4)
C20A	C23A	1.52(2)
C20A	C24A	1.58(2)

Table 45. Bond Angles in ° for **69***.

Atom	Atom	Atom	Angle/°
B1	O1	C7	106.5(7)
B1	O2	C8	107.1(6)
B2	O3	C13	108.6(5)
B2	O4	C14	109.7(5)
B3	O5	C19	109.9(11)
B3	O5A	C19A	104.3(13)
B3	O6	C20	105.3(9)
B3	O6A	C20A	106.3(9)
C25	O7	C1	118.7(8)
C2	C1	O7	117.2(7)
C6	C1	O7	119.2(7)
C6	C1	C2	123.5(6)
C1	C2	C3	118.4(6)
C2	C3	C4	120.1(5)
C2	C3	B1	116.2(6)
C4	C3	B1	123.6(5)
C3	C4	C5	119.3(5)
C3	C4	B2	121.3(4)
C5	C4	B2	119.4(5)
C4	C5	B3	124.6(5)
C6	C5	C4	118.9(6)
C6	C5	B3	116.5(5)
C1	C6	C5	119.8(6)
O1	C7	C8	101.7(7)
O1	C7	C10	106.0(8)
C8	C7	C10	110.3(11)
C9	C7	O1	110.8(10)
C9	C7	C8	115.4(10)
C9	C7	C10	111.8(10)
O2	C8	C7	101.2(7)
O2	C8	C11	108.2(8)
O2	C8	C12	106.4(8)
C7	C8	C12	116.4(10)
C11	C8	C7	112.5(10)
C11	C8	C12	111.2(10)
O3	C13	C14	103.1(5)
O3	C13	C15	106.2(7)
O3	C13	C16	107.8(7)
C15	C13	C14	114.3(6)
C16	C13	C14	115.8(8)
C16	C13	C15	109.0(6)
O4	C14	C13	102.9(5)
O4	C14	C17	106.7(7)
O4	C14	C18	107.4(7)
C17	C14	C13	115.9(7)
C17	C14	C18	108.8(8)
C18	C14	C13	114.4(7)
O5	C19	C20	99.1(12)
O5	C19	C22	103.5(14)
C20	C19	C22	106.4(18)
C21	C19	O5	102.7(15)
C21	C19	C20	123.4(17)

Table 45 (cont'd)

Atom	Atom	Atom	Angle/°
C21	C19	C22	118(2)
O5A	C19A	C20A	104.4(12)
O5A	C19A	C21A	108.2(14)
O5A	C19A	C22A	109.8(18)
C20A	C19A	C21A	109.2(15)
C20A	C19A	C22A	100.5(17)
C21A	C19A	C22A	123(2)
O6	C20	C19	103.8(11)
O6	C20	C23	114.0(14)
O6	C20	C24	105(2)
C23	C20	C19	106.3(18)
C23	C20	C24	121(2)
C24	C20	C19	105.0(16)
O6A	C20A	C19A	100.0(11)
O6A	C20A	C23A	109.0(13)
O6A	C20A	C24A	101.5(13)
C19A	C20A	C23A	111.3(13)
C19A	C20A	C24A	114.4(17)
C23A	C20A	C24A	118.3(17)
F2	C25	F1	98.0(13)
F3	C25	F1	105.4(8)
F3	C25	F2	110.9(9)
O7	C25	F1	111.6(8)
O7	C25	F2	116.5(8)
O7	C25	F3	112.9(12)
O1	B1	C3	119.5(6)
O2	B1	O1	113.9(6)
O2	B1	C3	126.6(6)
O3	B2	O4	114.9(5)
O3	B2	C4	122.1(5)
O4	B2	C4	122.9(5)
O5	B3	O6	113.1(9)
O5	B3	C5	127.3(8)
O5A	B3	O6A	113.7(9)
O5A	B3	C5	126.2(8)
O6	B3	C5	119.5(7)
O6A	B3	C5	120.2(7)

Table 46. Hydrogen Fractional Atomic Coordinates ($\times 10^4$) and Equivalent Isotropic Displacement Parameters ($\text{\AA}^2 \times 10^3$) for **69***.

Atom	x	y	z	U_{eq}
H2	6056	5823	4858	57
H6	8791	5701	3680	62
H9A	2670	5080	5816	153
H9B	1668	4303	5530	153
H9C	2140	5351	5131	153
H10A	4145	2569	5368	187
H10B	2958	2667	5753	187
H10C	4044	3419	5954	187
H11A	2300	5101	4228	126

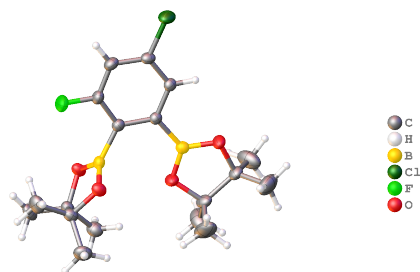
Table 46 (cont'd)

Atom	x	y	z	U_{eq}
H11B	1328	4151	4165	126
H11C	2335	4234	3647	126
H12A	2224	2091	4063	159
H12B	1629	2355	4733	159
H12C	2900	1829	4709	159
H15A	5074	34	3618	104
H15B	4159	101	3050	104
H15C	4110	997	3616	104
H16A	6992	1090	2534	123
H16B	6037	203	2311	123
H16C	6657	57	2985	123
H17A	3301	2425	3024	120
H17B	3196	1465	2496	120
H17C	3212	2759	2290	120
H18A	4757	2666	1602	132
H18B	4882	1334	1681	132
H18C	5973	2131	1799	132
H21A	7690	3985	1255	126
H21B	9020	4253	1113	126
H21C	8349	4933	1655	126
H21D	8580	1557	1666	91
H21E	9437	2359	1280	91
H21F	8126	2733	1395	91
H22A	8990	1521	2045	131
H22B	9189	1870	1320	131
H22C	7906	1791	1599	131
H22D	10350	2910	3051	126
H22E	11011	2468	2432	126
H22F	10141	1655	2803	126
H23A	10424	4593	1668	131
H23B	11170	3462	1686	131
H23C	11349	4399	2222	131
H23D	8077	4298	1502	85
H23E	9247	4365	1099	85
H23F	8866	5400	1536	85
H24A	10552	2373	3002	126
H24B	10420	1831	2310	126
H24C	9307	1995	2751	126
H24D	11082	5014	1955	91
H24E	11256	3719	1775	91
H24F	11173	4089	2504	91

Table 47. Atomic Occupancies for all atoms that are not fully occupied in **69***.

Atom	Occupancy
O5	0.5
O5A	0.5
O6	0.5
O6A	0.5
C19	0.5
C19A	0.5
C20	0.5
C20A	0.5
C21	0.5
H21A	0.5
H21B	0.5
H21C	0.5
C21A	0.5
H21D	0.5
H21E	0.5
H21F	0.5
C22	0.5
H22A	0.5
H22B	0.5
H22C	0.5
C22A	0.5
H22D	0.5
H22E	0.5
H22F	0.5
C23	0.5
H23A	0.5
H23B	0.5
H23C	0.5
C23A	0.5
H23D	0.5
H23E	0.5
H23F	0.5
C24	0.5
H24A	0.5
H24B	0.5
H24C	0.5
C24A	0.5
H24D	0.5
H24E	0.5
H24F	0.5

Compound 70c



Compound	70c (CCDC 1851809)
Formula	C ₁₈ H ₂₆ B ₂ ClFO ₄
<i>D</i> _{calc.} /g cm ⁻³	1.269
μ /mm ⁻¹	1.933
Formula Weight	382.46
Colour	colourless
Shape	chunk
Size/mm ³	0.24×0.18×0.15
<i>T</i> /K	173(2)
Crystal System	monoclinic
Space Group	<i>P</i> 2 ₁ / <i>n</i>
<i>a</i> /Å	10.5496(2)
<i>b</i> /Å	11.5620(2)
<i>c</i> /Å	16.4588(2)
α /°	90
β /°	94.4870(10)
γ /°	90
<i>V</i> /Å ³	2001.40(6)
<i>Z</i>	4
<i>Z</i> '	1
Wavelength/Å	1.541838
Radiation type	CuK α
θ _{min} /°	4.678
θ _{max} /°	71.956
Measured Refl.	16503
Independent Refl.	3891
Reflections Used	3282
<i>R</i> _{int}	0.0459
Parameters	243
Restraints	0
Largest Peak	0.606
Deepest Hole	-0.346
GooF	1.180
<i>wR</i> ₂ (all data)	0.1833
<i>wR</i> ₂	0.1783
<i>R</i> ₁ (all data)	0.0739
<i>R</i> ₁	0.0641

Table 48. Fractional Atomic Coordinates ($\times 10^4$) and Equivalent Isotropic Displacement Parameters ($\text{\AA}^2 \times 10^3$) for **70c**.

Atom	x	y	z	U_{eq}
C11	9082.4(9)	8861.0(9)	4481.6(6)	45.0(3)
F1	4355(2)	8619(2)	4712.5(14)	47.6(6)
O1	3964(2)	7279(2)	6555.8(14)	31.5(5)
O2	3481(2)	6119(2)	5447.5(13)	29.9(5)
O3	6120(2)	5210(2)	6653.3(15)	37.7(6)
O4	8253(2)	5494(2)	6626.2(16)	38.7(6)
C1	7746(3)	8243(3)	4853.1(19)	28.7(7)
C2	6558(3)	8691(3)	4608(2)	31.5(7)
C3	5529(3)	8177(3)	4939(2)	30.4(7)
C4	5599(3)	7255(3)	5478.1(18)	25.4(7)
C5	6831(3)	6832(3)	5713.4(18)	23.9(6)
C6	7890(3)	7328(3)	5392.5(18)	25.6(6)
C7	2618(3)	6975(3)	6581(2)	30.6(7)
C8	2496(3)	5905(3)	6012(2)	29.0(7)
C9	2356(4)	6733(4)	7460(2)	42.6(9)
C10	1873(4)	8021(4)	6252(3)	44.6(9)
C11	2851(4)	4773(3)	6440(2)	39.0(8)
C12	1222(3)	5788(4)	5523(2)	40.1(9)
C13	6692(4)	4439(3)	7278(2)	35.4(8)
C14	8148(3)	4500(3)	7158(2)	32.3(7)
C15	6102(5)	3267(4)	7181(4)	66.6(15)
C16	6350(6)	4971(5)	8082(3)	73.2(17)
C17	8641(5)	3481(4)	6707(4)	65.1(14)
C18	9001(5)	4704(5)	7924(3)	71.3(16)
B1	4339(4)	6841(3)	5841(2)	26.6(7)
B2	7065(4)	5817(3)	6340(2)	26.1(7)

Table 49. Anisotropic Displacement Parameters ($\times 10^4$) **70c**.

Atom	U_{11}	U_{22}	U_{33}	U_{23}	U_{13}	U_{12}
C11	38.9(5)	51.8(6)	44.2(5)	17.1(4)	3.6(4)	-17.3(4)
F1	35.2(12)	53.1(14)	54.1(13)	20.9(11)	0.2(10)	10.8(10)
O1	28.3(12)	36.3(13)	30.0(11)	-4.6(10)	3.4(9)	-5.3(10)
O2	25.0(12)	38.5(13)	26.6(11)	-6.3(10)	4.5(9)	-3.1(10)
O3	29.8(13)	42.2(14)	41.7(13)	21.0(11)	6.3(10)	1.6(11)
O4	28.9(13)	40.3(14)	46.7(14)	22.2(12)	1.9(10)	0.8(11)
C1	30.6(17)	29.6(17)	26.1(15)	1.3(13)	4.0(13)	-7.4(14)
C2	37.2(19)	29.2(17)	28.0(16)	6.3(13)	1.0(14)	-2.7(14)
C3	28.9(17)	32.5(17)	29.4(16)	5.2(13)	0.8(13)	6.4(14)
C4	27.6(16)	25.1(15)	23.5(14)	-0.1(12)	1.3(12)	0.0(13)
C5	25.7(16)	23.3(15)	22.6(14)	-1.0(12)	0.8(12)	-1.3(12)
C6	26.1(16)	25.4(15)	24.8(15)	-0.7(12)	-1.2(12)	-3.2(13)
C7	27.6(17)	34.1(18)	30.9(17)	-3.4(14)	6.6(13)	-2.7(14)
C8	23.3(16)	34.5(18)	29.3(16)	-4.0(14)	3.2(12)	-1.2(14)
C9	47(2)	50(2)	32.1(18)	-7.6(16)	12.0(16)	-3.6(19)
C10	37(2)	43(2)	54(2)	-3.6(18)	6.6(17)	10.8(18)
C11	38(2)	33.7(19)	46(2)	0.3(16)	8.2(16)	-2.6(16)
C12	23.7(17)	57(2)	39.1(19)	-11.1(17)	-0.1(14)	-5.7(16)
C13	42(2)	29.0(17)	36.1(18)	12.1(14)	9.0(15)	6.4(16)
C14	36.7(19)	26.4(16)	33.6(17)	10.3(14)	1.5(14)	1.8(15)

Table 49 (cont'd)

Atom	U_{11}	U_{22}	U_{33}	U_{23}	U_{13}	U_{12}
C15	49(3)	40(2)	110(4)	18(3)	5(3)	-7(2)
C16	91(4)	90(4)	43(2)	14(3)	32(3)	34(3)
C17	61(3)	45(2)	95(4)	3(3)	38(3)	10(2)
C18	73(3)	85(4)	52(3)	21(3)	-23(2)	-19(3)
B1	24.2(18)	28.3(18)	27.1(17)	3.2(14)	-0.1(14)	3.3(15)
B2	28.1(19)	25.1(17)	25.3(17)	-0.7(14)	4.1(14)	-0.6(14)

Table 50. Bond Lengths in Å for **70c**.

Atom	Atom	Length/Å
C11	C1	1.734(3)
F1	C3	1.365(4)
O1	C7	1.466(4)
O1	B1	1.368(4)
O2	C8	1.468(4)
O2	B1	1.358(4)
O3	C13	1.455(4)
O3	B2	1.354(4)
O4	C14	1.455(4)
O4	B2	1.357(4)
C1	C2	1.386(5)
C1	C6	1.382(5)
C2	C3	1.386(5)
C3	C4	1.385(4)
C4	C5	1.415(4)
C4	B1	1.573(5)
C5	C6	1.396(4)
C5	B2	1.569(5)
C7	C8	1.550(5)
C7	C9	1.520(5)
C7	C10	1.519(5)
C8	C11	1.519(5)
C8	C12	1.518(5)
C13	C14	1.565(5)
C13	C15	1.494(6)
C13	C16	1.529(6)
C14	C17	1.507(6)
C14	C18	1.509(6)

Table 51. Bond Angles in ° for **70c**.

Atom	Atom	Atom	Angle/°
B1	O1	C7	106.3(3)
B1	O2	C8	106.3(2)
B2	O3	C13	108.0(3)
B2	O4	C14	108.3(3)
C2	C1	C11	119.0(3)
C6	C1	C11	119.3(3)
C6	C1	C2	121.6(3)
C3	C2	C1	116.4(3)

Table 51 (cont'd)

Atom	Atom	Atom	Angle/°
F1	C3	C2	117.0(3)
F1	C3	C4	117.7(3)
C4	C3	C2	125.3(3)
C3	C4	C5	116.3(3)
C3	C4	B1	118.3(3)
C5	C4	B1	125.2(3)
C4	C5	B2	122.2(3)
C6	C5	C4	120.0(3)
C6	C5	B2	117.8(3)
C1	C6	C5	120.4(3)
O1	C7	C8	102.1(2)
O1	C7	C9	108.6(3)
O1	C7	C10	105.9(3)
C9	C7	C8	114.5(3)
C10	C7	C8	113.8(3)
C10	C7	C9	111.0(3)
O2	C8	C7	102.6(3)
O2	C8	C11	106.1(3)
O2	C8	C12	108.7(3)
C11	C8	C7	113.7(3)
C12	C8	C7	114.8(3)
C12	C8	C11	110.2(3)
O3	C13	C14	103.9(3)
O3	C13	C15	109.5(4)
O3	C13	C16	104.6(3)
C15	C13	C14	115.6(3)
C15	C13	C16	109.5(4)
C16	C13	C14	113.0(4)
O4	C14	C13	103.5(3)
O4	C14	C17	106.0(3)
O4	C14	C18	108.1(3)
C17	C14	C13	114.0(3)
C17	C14	C18	109.1(4)
C18	C14	C13	115.4(4)
O1	B1	C4	121.6(3)
O2	B1	O1	114.2(3)
O2	B1	C4	123.9(3)
O3	B2	O4	114.4(3)
O3	B2	C5	123.8(3)
O4	B2	C5	121.8(3)

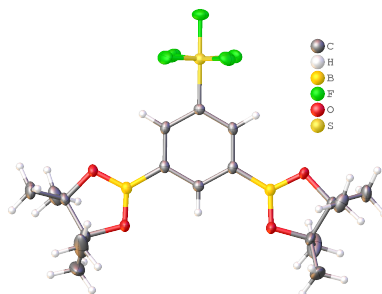
Table 52. Hydrogen Fractional Atomic Coordinates ($\times 10^4$) and Equivalent Isotropic Displacement Parameters ($\text{\AA}^2 \times 10^3$) for **70c**.

Atom	x	y	z	U_{eq}
H2	6456	9316	4234	38
H6	8716	7035	5546	31
H9A	2950	6144	7687	64
H9B	1482	6454	7479	64
H9C	2467	7446	7780	64
H10A	2140	8706	6572	67

Table 52 (cont'd)

Atom	x	y	z	U_{eq}
H10B	963	7888	6292	67
H10C	2037	8145	5681	67
H11A	2914	4161	6033	58
H11B	2196	4568	6806	58
H11C	3671	4860	6757	58
H12A	1048	6491	5200	60
H12B	550	5677	5894	60
H12C	1244	5120	5157	60
H15A	5196	3317	7267	100
H15B	6522	2737	7581	100
H15C	6203	2978	6630	100
H16A	6695	5757	8131	110
H16B	6712	4499	8537	110
H16C	5423	4999	8094	110
H17A	8078	3331	6216	98
H17B	8667	2797	7060	98
H17C	9499	3651	6552	98
H18A	9890	4701	7792	107
H18B	8868	4088	8318	107
H18C	8797	5453	8159	107

Compound 71c'



Compound	71c' (CCDC 1818920)
Formula	C ₁₈ H ₂₇ B ₂ F ₅ O ₄ S
$D_{calc.}/\text{g cm}^{-3}$	1.398
μ/mm^{-1}	1.919
Formula Weight	456.07
Colour	colourless
Shape	plate
Size/ mm^3	0.35×0.31×0.16
T/K	173(2)
Crystal System	orthorhombic
Space Group	<i>Pbcn</i>
$a/\text{Å}$	14.6808(2)
$b/\text{Å}$	13.28800(10)
$c/\text{Å}$	11.10730(10)
$\alpha/^\circ$	90
$\beta/^\circ$	90
$\gamma/^\circ$	90
$V/\text{Å}^3$	2166.80(4)
Z	4
Z'	0.5
Wavelength/Å	1.541838
Radiation type	CuK α
$\theta_{min}/^\circ$	6.004
$\theta_{max}/^\circ$	70.063
Measured Refl.	12825
Independent Refl.	2059
Reflections Used	1888
R_{int}	0.0298
Parameters	143
Restraints	0
Largest Peak	0.464
Deepest Hole	-0.426
GooF	1.045
wR_2 (all data)	0.0956
wR_2	0.0933
R_1 (all data)	0.0365
R_1	0.0338

Table 53. Fractional Atomic Coordinates ($\times 10^4$) and Equivalent Isotropic Displacement Parameters ($\text{\AA}^2 \times 10^3$) for **71c'**.

Atom	x	y	z	U_{eq}
S1	5000	5576.7(3)	7500	21.48(17)
F1	5000	6770.1(10)	7500	36.0(3)
F2	5043.1(6)	5630.2(7)	8922.2(8)	34.1(3)
F3	6081.4(6)	5624.3(7)	7440.5(8)	34.6(3)
O1	6600.7(6)	2525.0(7)	4823.6(9)	25.0(3)
O2	6150.2(8)	1047.6(8)	5680.7(9)	30.5(3)
C1	5000	4215.9(15)	7500	17.7(4)
C2	5517.7(8)	3705.2(11)	6649.7(11)	18.9(3)
C3	5523.3(8)	2657.5(11)	6641.9(11)	19.0(3)
C4	5000	2146.3(15)	7500	19.3(4)
C5	7133.5(9)	1740.1(11)	4221.9(12)	22.9(3)
C6	6601.5(11)	766.0(12)	4552.9(14)	32.8(4)
C7	7170.2(11)	1985.4(14)	2889.6(14)	35.5(4)
C8	8086.2(11)	1788.6(15)	4752.0(15)	39.9(4)
C9	5842.8(16)	530.4(19)	3664.8(19)	65.6(8)
C10	7191.5(19)	-145.0(15)	4802(2)	69.6(8)
B1	6103.1(10)	2066.7(12)	5693.3(13)	20.4(3)

Table 54. Anisotropic Displacement Parameters ($\times 10^4$) **71c'**.

Atom	U_{11}	U_{22}	U_{33}	U_{23}	U_{13}	U_{12}
S1	25.3(3)	19.8(3)	19.4(3)	0	-0.41(15)	0
F1	50.4(8)	18.4(7)	39.4(7)	0	0.9(6)	0
F2	54.9(6)	27.5(5)	20.0(5)	-5.5(3)	-1.7(3)	-4.5(4)
F3	26.7(5)	28.5(5)	48.8(6)	2.4(4)	1.1(4)	-8.1(3)
O1	27.7(5)	22.3(5)	25.1(5)	1.0(4)	11.4(4)	4.4(4)
O2	42.5(6)	22.3(6)	26.8(5)	-1.5(4)	17.7(4)	-1.0(4)
C1	18.1(9)	18.4(9)	16.6(8)	0	-3.0(6)	0
C2	15.4(6)	25.5(7)	15.7(6)	2.4(5)	0.6(5)	-0.6(5)
C3	16.0(6)	24.4(8)	16.5(6)	-0.6(5)	0.0(5)	0.8(5)
C4	18.7(9)	20.1(10)	19.2(9)	0	-0.7(6)	0
C5	23.1(7)	24.3(8)	21.3(6)	-2.4(5)	6.6(5)	4.1(5)
C6	42.4(9)	26.3(8)	29.8(8)	-7.8(6)	18.8(7)	-2.6(6)
C7	36.5(8)	46.1(10)	24.0(8)	3.8(7)	10.8(6)	7.1(7)
C8	26.7(8)	55.5(11)	37.3(9)	-11.6(8)	1.8(7)	6.8(7)
C9	62.8(13)	85.8(18)	48.3(12)	-39.4(11)	22.3(10)	-42.9(12)
C10	105(2)	28.6(11)	75.5(15)	7.2(10)	52.5(14)	21.7(11)
B1	18.8(7)	23.6(8)	18.7(7)	-0.4(6)	0.3(5)	0.9(6)

Table 55. Bond Lengths in \AA for **71c'**.

Atom	Atom	Length/ \AA
S1	F1	1.5857(14)
S1	F2 ¹	1.5826(9)
S1	F2	1.5826(9)
S1	F3 ¹	1.5902(10)

Table 55 (cont'd)

Atom	Atom	Length/Å
S1	F3	1.5902(10)
S1	C1	1.808(2)
O1	C5	1.4651(16)
O1	B1	1.3556(17)
O2	C6	1.4657(16)
O2	B1	1.3560(19)
C1	C2	1.3894(16)
C1	C2 ¹	1.3894(16)
C2	C3	1.392(2)
C3	C4	1.3999(16)
C3	B1	1.5657(19)
C4	C3 ¹	1.3999(16)
C5	C6	1.556(2)
C5	C7	1.5162(19)
C5	C8	1.519(2)
C6	C9	1.520(3)
C6	C10	1.514(3)

Table 56. Bond Angles in ° for **71c'**.

Atom	Atom	Atom	Angle/°
F1	S1	F3	87.72(4)
F1	S1	F3 ¹	87.72(4)
F1	S1	C1	180.0
F2	S1	F1	87.42(4)
F2 ¹	S1	F1	87.42(4)
F2 ¹	S1	F2	174.85(7)
F2 ¹	S1	F3 ¹	89.99(5)
F2 ¹	S1	F3	89.81(5)
F2	S1	F3 ¹	89.81(5)
F2	S1	F3	89.99(5)
F2 ¹	S1	C1	92.58(4)
F2	S1	C1	92.58(4)
F3 ¹	S1	F3	175.44(7)
F3 ¹	S1	C1	92.28(4)
F3	S1	C1	92.28(4)
B1	O1	C5	107.03(11)
B1	O2	C6	106.66(11)
C2	C1	S1	119.24(9)
C2 ¹	C1	S1	119.24(9)
C2	C1	C2 ¹	121.52(19)
C1	C2	C3	119.73(12)
C2	C3	C4	118.54(12)
C2	C3	B1	120.58(11)
C4	C3	B1	120.88(14)
C3 ¹	C4	C3	121.96(18)
O1	C5	C6	102.50(10)
O1	C5	C7	108.13(11)
O1	C5	C8	106.53(11)
C7	C5	C6	115.30(13)
C7	C5	C8	109.66(13)
C8	C5	C6	113.95(13)

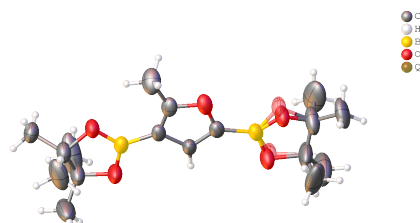
Table 56 (cont'd)

Atom	Atom	Atom	Angle/°
O2	C6	C5	102.51(11)
O2	C6	C9	106.02(13)
O2	C6	C10	107.86(14)
C9	C6	C5	112.69(15)
C10	C6	C5	114.90(15)
C10	C6	C9	111.90(19)
O1	B1	O2	114.45(12)
O1	B1	C3	123.18(13)
O2	B1	C3	122.37(12)

Table 57. Hydrogen Fractional Atomic Coordinates ($\times 10^4$) and Equivalent Isotropic Displacement Parameters ($\text{\AA}^2 \times 10^3$) for **71c'**.

Atom	x	y	z	U_{eq}
H2	5867	4069	6076	23
H4	5000	1431	7500	23
H7A	6549	2056	2577	53
H7B	7483	1442	2460	53
H7C	7502	2618	2771	53
H8A	8332	2469	4649	60
H8B	8480	1305	4337	60
H8C	8061	1624	5611	60
H9A	5466	-18	3982	98
H9B	6108	327	2893	98
H9C	5465	1131	3547	98
H10A	7615	8	5459	104
H10B	7537	-318	4076	104
H10C	6805	-714	5032	104

Compound 72c'



Compound	72c' (CCDC 1843466)
Formula	C _{8.5} H ₁₄ BO _{2.5}
$D_{calc.}/\text{g cm}^{-3}$	1.100
μ/mm^{-1}	0.625
Formula Weight	167.01
Colour	colourless
Shape	needle
Size/mm ³	0.31×0.14×0.05
T/K	173(2)
Crystal System	monoclinic
Space Group	$P2_1/c$
$a/\text{Å}$	13.567(2)
$b/\text{Å}$	12.3554(18)
$c/\text{Å}$	12.677(2)
$\alpha/^\circ$	90
$\beta/^\circ$	108.348(12)
$\gamma/^\circ$	90
$V/\text{Å}^3$	2017.0(6)
Z	8
Z'	2
Wavelength/Å	1.541838
Radiation type	CuK α
$\theta_{min}/^\circ$	3.432
$\theta_{max}/^\circ$	72.426
Measured Refl.	16929
Independent Refl.	3701
Reflections Used	2206
R_{int}	0.0606
Parameters	232
Restraints	0
Largest Peak	0.436
Deepest Hole	-0.345
GooF	1.052
wR_2 (all data)	0.2775
wR_2	0.2365
R_1 (all data)	0.1364
R_1	0.0878

Table 58. Fractional Atomic Coordinates ($\times 10^4$) and Equivalent Isotropic Displacement Parameters ($\text{\AA}^2 \times 10^3$) for **72c'**.

Atom	x	y	z	U_{eq}
O1	8377(2)	5170.8(19)	8762(2)	56.2(7)
O5	6564(2)	8221(2)	8834(2)	59.2(8)
O4	5876(2)	7846(2)	7000(2)	76.0(10)
C4	7894(3)	6068(3)	9016(3)	53.0(9)
C1	8046(3)	5083(3)	7618(3)	52.1(9)
C2	7367(3)	5896(3)	7186(4)	55.7(10)
C3	7257(3)	6538(3)	8075(3)	48.9(9)
C13	5661(4)	8927(4)	8404(4)	67.8(12)
C16	5848(4)	9983(4)	8999(4)	77.0(14)
C12	5460(4)	8901(4)	7180(4)	77.6(15)
B2	6561(3)	7555(3)	7981(4)	49.5(10)
B1	8493(3)	4181(3)	7053(4)	53.8(11)
C6A	9491(5)	2864(4)	6719(5)	95.3(19)
C5	8174(4)	6307(4)	10235(4)	83.1(15)
C17	4732(4)	8353(5)	8673(6)	114(2)
C15	4409(5)	9045(6)	6407(5)	145(3)
C8A	10447(5)	3539(6)	6486(7)	142(3)
C14	6221(7)	9778(5)	6901(7)	159(4)
O3B	8328(8)	4191(7)	5835(9)	65.1(18)
O3A	8040(8)	3963(7)	6060(9)	61.2(16)
C7	8619(6)	3048(5)	5736(5)	122(3)
C9A	9864(5)	1768(4)	7100(5)	110(2)
C10A	8683(7)	3042(7)	4607(6)	161(4)
C11A	7792(6)	2077(6)	5870(9)	177(5)
O2A	9111(12)	3380(11)	7460(11)	61.2(16)
O2B	9311(13)	3521(12)	7694(11)	65.1(18)

Table 59. Anisotropic Displacement Parameters ($\times 10^4$) **72c'**.

Atom	U_{11}	U_{22}	U_{33}	U_{23}	U_{13}	U_{12}
O1	56.1(16)	44.1(14)	76.0(19)	3.3(12)	31.5(13)	7.1(11)
O5	59.7(16)	55.1(15)	60.7(16)	-10.9(12)	15.8(13)	17.7(12)
O4	76(2)	75(2)	65.7(19)	-24.9(15)	7.7(15)	31.2(16)
C4	50(2)	48(2)	71(3)	-6.2(18)	32.5(19)	-3.9(16)
C1	40.9(19)	42.5(19)	73(3)	-9.7(17)	18.4(17)	-1.7(14)
C2	40.9(19)	47(2)	73(3)	-19.3(18)	9.0(17)	5.5(15)
C3	38.4(18)	38.0(17)	73(2)	-10.9(16)	20.4(17)	-2.5(14)
C13	71(3)	60(2)	70(3)	-10(2)	19(2)	24(2)
C16	80(3)	60(3)	83(3)	-23(2)	15(2)	18(2)
C12	83(3)	74(3)	68(3)	-16(2)	12(2)	37(2)
B2	42(2)	43(2)	67(3)	-12.4(19)	23(2)	-1.7(16)
B1	42(2)	42(2)	75(3)	-8(2)	16(2)	5.0(17)
C6A	124(5)	82(4)	88(4)	4(3)	45(3)	58(3)
C5	113(4)	76(3)	72(3)	8(2)	48(3)	23(3)
C17	86(4)	84(4)	204(8)	8(4)	92(5)	15(3)
C15	127(5)	164(7)	100(5)	-51(4)	-28(4)	92(5)
C8A	103(5)	136(6)	227(9)	-61(6)	109(6)	-22(4)
C14	222(9)	89(4)	238(10)	66(5)	177(8)	67(5)
O3B	81(6)	63(4)	50(4)	-6(2)	18(2)	31(4)
O3A	70(5)	62(4)	57(4)	-2(2)	27(2)	26(3)

Table 59 (cont'd)

Atom	U_{11}	U_{22}	U_{33}	U_{23}	U_{13}	U_{12}
C7	137(5)	111(5)	97(4)	-48(4)	5(4)	70(4)
C9A	130(5)	75(3)	137(5)	9(3)	59(4)	59(3)
C10A	220(9)	162(7)	89(5)	-24(5)	30(5)	107(7)
C11A	117(6)	108(5)	323(13)	-134(7)	93(7)	-43(4)
O2A	70(5)	62(4)	57(4)	-2(2)	27(2)	26(3)
O2B	81(6)	63(4)	50(4)	-6(2)	18(2)	31(4)

Table 60. Bond Lengths in Å for 72c'.

Atom	Atom	Length/Å
O1	C4	1.377(4)
O1	C1	1.381(5)
O5	C13	1.463(5)
O5	B2	1.358(5)
O4	C12	1.467(5)
O4	B2	1.346(5)
C4	C3	1.362(5)
C4	C5	1.500(6)
C1	C2	1.356(5)
C1	B1	1.549(5)
C2	C3	1.424(5)
C3	B2	1.554(5)
C13	C16	1.488(6)
C13	C12	1.489(6)
C13	C17	1.574(7)
C12	C15	1.463(7)
C12	C14	1.610(9)
B1	O3B	1.488(11)
B1	O3A	1.244(13)
B1	O2A	1.295(11)
B1	O2B	1.411(10)
C6A	C8A	1.644(9)
C6A	C7	1.441(8)
C6A	C9A	1.473(6)
C6A	O2A	1.364(15)
C6A	O2B	1.560(14)
O3B	C7	1.481(9)
O3A	C7	1.506(8)
C7	C10A	1.462(9)
C7	C11A	1.687(10)

Table 61. Bond Angles in ° for 72c'.

Atom	Atom	Atom	Angle/°
C4	O1	C1	106.7(3)
B2	O5	C13	105.8(3)
B2	O4	C12	106.4(3)
O1	C4	C5	114.5(4)
C3	C4	O1	110.8(3)
C3	C4	C5	134.7(4)

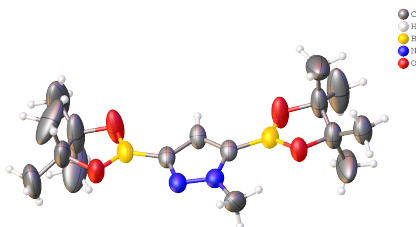
Table 61 (cont'd)

Atom	Atom	Atom	Angle/°
O1	C1	B1	119.8(3)
C2	C1	O1	108.8(3)
C2	C1	B1	131.4(4)
C1	C2	C3	108.6(4)
C4	C3	C2	105.1(3)
C4	C3	B2	127.9(4)
C2	C3	B2	127.0(4)
O5	C13	C16	110.2(4)
O5	C13	C12	103.4(3)
O5	C13	C17	106.5(4)
C16	C13	C12	119.6(4)
C16	C13	C17	107.8(4)
C12	C13	C17	108.6(5)
O4	C12	C13	103.2(4)
O4	C12	C14	105.0(4)
C13	C12	C14	107.1(5)
C15	C12	O4	110.2(4)
C15	C12	C13	121.0(5)
C15	C12	C14	109.1(6)
O5	B2	C3	125.4(4)
O4	B2	O5	113.7(3)
O4	B2	C3	120.9(3)
O3B	B1	C1	121.4(4)
O3A	B1	C1	118.9(4)
O3A	B1	O2A	106.9(6)
O2A	B1	C1	131.6(7)
O2B	B1	C1	120.1(6)
O2B	B1	O3B	115.9(9)
C7	C6A	C8A	104.1(6)
C7	C6A	C9A	122.2(6)
C7	C6A	O2B	108.2(5)
C9A	C6A	C8A	108.4(5)
C9A	C6A	O2B	110.0(7)
O2A	C6A	C8A	112.2(10)
O2A	C6A	C7	97.8(5)
O2A	C6A	C9A	111.6(8)
O2B	C6A	C8A	102.0(10)
C7	O3B	B1	97.1(5)
B1	O3A	C7	107.7(7)
C6A	C7	O3B	104.2(6)
C6A	C7	O3A	103.9(6)
C6A	C7	C10A	124.0(7)
C6A	C7	C11A	101.1(6)
O3B	C7	C11A	117.8(6)
O3A	C7	C11A	95.0(6)
C10A	C7	O3B	100.8(6)
C10A	C7	O3A	117.9(6)
C10A	C7	C11A	110.0(7)
B1	O2A	C6A	114.8(12)
B1	O2B	C6A	97.8(7)

Table 62. Hydrogen Fractional Atomic Coordinates ($\times 10^4$) and Equivalent Isotropic Displacement Parameters ($\text{\AA}^2 \times 10^3$) for **72c'**.

Atom	x	y	z	U_{eq}
H2	7022	6017	6418	67
H16A	5871	9874	9772	115
H16B	5286	10486	8634	115
H16C	6512	10284	8983	115
H5A	7939	5712	10607	125
H5B	7837	6981	10343	125
H5C	8929	6385	10550	125
H17A	4973	8067	9432	171
H17B	4472	7758	8148	171
H17C	4174	8877	8606	171
H15A	3942	8516	6576	218
H15B	4417	8938	5644	218
H15C	4166	9779	6485	218
H8AA	10680	3153	5933	213
H8AB	11025	3602	7180	213
H8AC	10204	4263	6208	213
H14A	6870	9816	7521	238
H14B	5884	10489	6790	238
H14C	6370	9562	6224	238
H9AA	9996	1369	6491	165
H9AB	9335	1387	7337	165
H9AC	10507	1818	7727	165
H10A	9105	3655	4512	242
H10B	7984	3101	4072	242
H10C	9004	2364	4479	242
H11A	8024	1372	5682	266
H11B	7094	2231	5367	266
H11C	7779	2063	6638	266

Compound 73c'



Compound	73c' (CCDC 1840217)
Formula	C ₁₆ H ₂₈ B ₂ N ₂ O ₄
$D_{calc.}/\text{g cm}^{-3}$	1.110
μ/mm^{-1}	0.621
Formula Weight	334.02
Colour	colourless
Shape	chunk
Size/mm ³	0.32×0.24×0.14
T/K	213(2)
Crystal System	monoclinic
Space Group	$P2_1/c$
$a/\text{Å}$	13.5810(3)
$b/\text{Å}$	12.1863(2)
$c/\text{Å}$	12.7568(3)
$\alpha/^\circ$	90
$\beta/^\circ$	108.8070(10)
$\gamma/^\circ$	90
$V/\text{Å}^3$	1998.56(7)
Z	4
Z'	1
Wavelength/Å	1.541838
Radiation type	CuK α
$\theta_{min}/^\circ$	3.438
$\theta_{max}/^\circ$	72.168
Measured Refl.	18729
Independent Refl.	3904
Reflections Used	2909
R_{int}	0.0366
Parameters	230
Restraints	0
Largest Peak	0.539
Deepest Hole	-0.362
GooF	1.085
wR_2 (all data)	0.2799
wR_2	0.2575
R_1 (all data)	0.1107
R_1	0.0904

Table 63. Fractional Atomic Coordinates ($\times 10^4$) and Equivalent Isotropic Displacement Parameters ($\text{\AA}^2 \times 10^3$) for **73c'**.

Atom	x	y	z	U_{eq}
O1	3427.3(18)	1821.8(18)	1140.5(18)	67.9(7)
O2	4076(2)	2150(2)	2967(2)	89.8(9)
O3	804(2)	6653(2)	2385(2)	89.7(9)
O4	1837(3)	5970(2)	3970(2)	106.5(12)
N1	2099(2)	3992(2)	966(2)	58.0(6)
N2	1609(2)	4882(2)	1172(2)	60.3(7)
C1	2733(2)	3506(2)	1909(3)	52.5(7)
C2	2623(2)	4137(2)	2757(3)	56.6(7)
C3	1920(2)	4979(2)	2274(3)	53.9(7)
C4	1887(4)	3646(3)	-180(3)	86.1(12)
C5	4323(3)	1088(3)	1575(3)	77.5(10)
C6	4484(3)	1085(4)	2783(3)	91.9(14)
C7	4126(3)	44(3)	951(3)	86.3(12)
C8	5280(4)	1661(5)	1374(7)	146(3)
C9	3682(7)	178(5)	2974(8)	191(4)
C10	5523(5)	903(6)	3587(5)	167(4)
C11	567(4)	7252(4)	3259(4)	101.7(16)
C12	1429(5)	6999(5)	4231(4)	131(2)
C13	-429(5)	6617(7)	3435(7)	171(4)
C14	235(5)	8367(5)	2910(5)	141(2)
C15	1361(7)	6982(6)	5343(5)	174(4)
C16	2264(5)	7979(5)	4126(8)	186(4)
B1	3411(3)	2469(3)	1987(3)	53.7(8)
B2	1507(2)	5889(3)	2876(3)	55.1(8)

Table 64. Anisotropic Displacement Parameters ($\times 10^4$) **73c'**.

Atom	U_{11}	U_{22}	U_{33}	U_{23}	U_{13}	U_{12}
O1	77.4(14)	62.4(13)	63.5(13)	-8.6(10)	21.9(11)	22.2(11)
O2	94.7(18)	91.4(19)	68.8(15)	-29.1(13)	6.4(13)	40.7(15)
O3	115(2)	84.1(17)	83.2(17)	11.6(13)	49.9(16)	50.2(16)
O4	126(2)	93(2)	76.2(17)	-25.6(14)	-0.2(15)	61.2(18)
N1	66.1(15)	47.6(13)	70.1(15)	-0.1(11)	35.7(13)	0.6(11)
N2	65.1(15)	46.7(13)	78.6(17)	3.5(11)	36.5(13)	4.9(11)
C1	43.5(13)	45.2(14)	70.6(17)	-9.4(12)	21.0(12)	-3.6(11)
C2	43.8(14)	49.9(15)	72.3(19)	-16.9(14)	13.2(13)	2.0(11)
C3	45.5(14)	43.5(14)	77.2(19)	-9.2(13)	25.9(13)	-3.5(11)
C4	127(3)	75(2)	69(2)	5.1(18)	49(2)	18(2)
C5	81(2)	71(2)	79(2)	-12.0(17)	23.1(18)	25.2(18)
C6	98(3)	93(3)	74(2)	-17(2)	12(2)	51(2)
C7	95(3)	72(2)	85(2)	-22.1(19)	20(2)	23(2)
C8	117(4)	91(3)	283(9)	13(4)	137(5)	18(3)
C9	261(9)	102(4)	311(11)	87(5)	230(9)	71(5)
C10	157(5)	193(7)	99(4)	-50(4)	-29(3)	109(5)
C11	137(4)	91(3)	91(3)	2(2)	55(3)	59(3)
C12	143(4)	124(4)	102(3)	-49(3)	6(3)	73(4)
C13	100(4)	228(8)	223(8)	-113(6)	104(5)	-34(4)
C14	169(6)	105(4)	157(5)	4(4)	62(5)	81(4)
C15	266(9)	163(6)	85(3)	-20(4)	46(4)	110(6)
C16	127(5)	125(5)	325(11)	-138(6)	100(6)	-50(4)

Table 64 (cont'd)

Atom	U_{11}	U_{22}	U_{33}	U_{23}	U_{13}	U_{12}
B1	48.7(16)	48.9(17)	65.9(19)	-11.3(14)	22.0(15)	-2.3(13)
B2	44.6(15)	45.8(16)	77(2)	-5.7(15)	21.8(15)	2.1(13)

Table 65. Bond Lengths in Å for 73c'.

Atom	Atom	Length/Å
O1	C5	1.467(4)
O1	B1	1.344(4)
O2	C6	1.460(4)
O2	B1	1.342(4)
O3	C11	1.452(4)
O3	B2	1.337(4)
O4	C12	1.453(5)
O4	B2	1.324(5)
N1	N2	1.342(3)
N1	C1	1.368(4)
N1	C4	1.459(4)
N2	C3	1.337(4)
C1	C2	1.374(4)
C1	B1	1.548(4)
C2	C3	1.402(4)
C3	B2	1.552(4)
C5	C6	1.485(5)
C5	C7	1.479(5)
C5	C8	1.567(6)
C6	C9	1.625(8)
C6	C10	1.469(6)
C11	C12	1.438(7)
C11	C13	1.636(8)
C11	C14	1.456(6)
C12	C15	1.450(8)
C12	C16	1.682(9)

Table 66. Bond Angles in ° for 73c'.

Atom	Atom	Atom	Angle/°
B1	O1	C5	106.3(3)
B1	O2	C6	106.5(3)
B2	O3	C11	107.0(3)
B2	O4	C12	106.4(3)
N2	N1	C1	112.9(2)
N2	N1	C4	118.7(3)
C1	N1	C4	128.4(3)
C3	N2	N1	105.6(2)
N1	C1	C2	104.6(2)
N1	C1	B1	127.1(3)
C2	C1	B1	128.3(3)
C1	C2	C3	107.2(3)
N2	C3	C2	109.7(2)

Table 66 (cont'd)

Atom	Atom	Atom	Angle/°
N2	C3	B2	122.8(3)
C2	C3	B2	127.5(3)
O1	C5	C6	102.7(3)
O1	C5	C7	109.7(3)
O1	C5	C8	107.3(3)
C6	C5	C8	108.5(4)
C7	C5	C6	119.8(4)
C7	C5	C8	108.2(4)
O2	C6	C5	103.2(3)
O2	C6	C9	105.8(4)
O2	C6	C10	110.5(4)
C5	C6	C9	106.0(5)
C10	C6	C5	120.8(4)
C10	C6	C9	109.4(5)
O3	C11	C13	105.4(4)
O3	C11	C14	111.0(4)
C12	C11	O3	103.5(3)
C12	C11	C13	105.0(5)
C12	C11	C14	123.4(5)
C14	C11	C13	107.2(5)
O4	C12	C15	111.2(5)
O4	C12	C16	106.2(4)
C11	C12	O4	104.6(3)
C11	C12	C15	123.8(6)
C11	C12	C16	99.3(6)
C15	C12	C16	110.1(6)
O1	B1	C1	126.2(3)
O2	B1	O1	113.5(3)
O2	B1	C1	120.3(3)
O3	B2	C3	125.7(3)
O4	B2	O3	112.9(3)
O4	B2	C3	121.4(3)

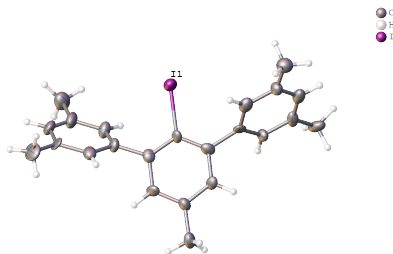
Table 67. Hydrogen Fractional Atomic Coordinates ($\times 10^4$) and Equivalent Isotropic Displacement Parameters ($\text{\AA}^2 \times 10^3$) for **73c'**.

Atom	x	y	z	U_{eq}
H2	2920(30)	4000(30)	3520(30)	71(10)
H4A	1153	3742	-584	129
H4B	2071	2878	-198	129
H4C	2296	4086	-521	129
H7A	3479	-273	978	130
H7B	4693	-462	1280	130
H7C	4075	182	187	130
H8A	5050	2063	682	220
H8B	5783	1109	1339	220
H8C	5599	2164	1978	220
H9A	3534	345	3652	287
H9B	3993	-545	3032	287
H9C	3041	194	2354	287
H10A	6009	1426	3455	250
H10B	5750	163	3506	250
H10C	5494	1001	4332	250
H13A	-785	7106	3793	257

Table 67 (cont'd)

Atom	x	y	z	U_{eq}
H13B	-188	5974	3896	257
H13C	-904	6392	2722	257
H14A	793	8754	2748	212
H14B	64	8744	3498	212
H14C	-373	8346	2251	212
H15A	956	6352	5424	260
H15B	1028	7649	5471	260
H15C	2055	6933	5876	260
H16A	2933	7863	4689	278
H16B	1995	8694	4232	278
H16C	2344	7946	3399	278

Compound 103



Compound	103 (CCDC 1850721)
Formula	C ₂₃ H ₂₃ I
<i>D</i> _{calc.} / g cm ⁻³	1.446
μ /mm ⁻¹	12.821
Formula Weight	426.31
Colour	colourless
Shape	chunk
Size/mm ³	0.41×0.18×0.05
<i>T</i> /K	173(2)
Crystal System	monoclinic
Space Group	<i>P</i> 2 ₁ / <i>c</i>
<i>a</i> /Å	24.3583(9)
<i>b</i> /Å	10.6108(3)
<i>c</i> /Å	15.9920(6)
α /°	90
β /°	108.596(2)
γ /°	90
<i>V</i> /Å ³	3917.5(2)
<i>Z</i>	8
<i>Z</i> '	2
Wavelength/Å	1.541838
Radiation type	CuK α
θ _{min} /°	4.586
θ _{max} /°	72.506
Measured Refl.	6301
Independent Refl.	6301
Reflections with <i>I</i> > 2(<i>I</i>)	4823
<i>R</i> _{int}	.
Parameters	444
Restraints	0
Largest Peak	1.954
Deepest Hole	-1.796
GooF	1.041
<i>wR</i> ₂ (all data)	0.2410
<i>wR</i> ₂	0.2192
<i>R</i> ₁ (all data)	0.1075
<i>R</i> ₁	0.0845

Table 68. Fractional Atomic Coordinates ($\times 10^4$) and Equivalent Isotropic Displacement Parameters ($\text{\AA}^2 \times 10^3$) for **103**.

Atom	x	y	z	U_{eq}
I1	4277.7(5)	237.1(9)	1162.3(7)	44.7(3)
C1	3516(5)	-574(11)	278(10)	27(3)
C2	3358(6)	-1763(14)	433(9)	31(3)
C3	2840(5)	-2267(11)	-134(10)	28(3)
C4	2498(6)	-1586(13)	-860(9)	32(3)
C5	2681(6)	-381(12)	-1018(10)	32(3)
C6	3207(6)	145(12)	-426(9)	31(3)
C7	3691(5)	-2609(14)	1182(10)	33(3)
C8	3754(6)	-2278(14)	2070(11)	39(3)
C9	4038(6)	-3138(12)	2735(10)	34(3)
C10	4240(6)	-4245(14)	2509(11)	41(4)
C11	4194(6)	-4568(13)	1647(10)	34(3)
C12	3920(5)	-3734(11)	984(9)	29(3)
C13	4073(7)	-2857(16)	3653(12)	48(4)
C14	4437(6)	-5762(16)	1407(12)	45(4)
C15	1943(6)	-2147(14)	-1445(10)	39(3)
C16	3351(6)	1424(12)	-675(10)	32(3)
C17	2929(7)	2410(14)	-783(10)	39(3)
C18	3051(7)	3624(11)	-1034(11)	41(4)
C19	3588(7)	3771(14)	-1188(11)	46(4)
C20	3973(8)	2879(14)	-1085(11)	47(4)
C21	3853(7)	1666(13)	-853(11)	41(3)
C22	2608(10)	4615(14)	-1104(14)	63(6)
C23	4570(7)	3129(18)	-1228(14)	57(4)
I1A	601.4(4)	5228.0(8)	1828.9(6)	34.2(3)
C1A	1408(5)	4607(11)	1746(8)	24(2)
C2A	1598(6)	3415(12)	2068(9)	32(3)
C3A	2150(6)	3003(12)	2027(9)	33(3)
C4A	2480(6)	3702(12)	1650(9)	32(3)
C5A	2260(6)	4901(12)	1317(10)	30(3)
C6A	1730(7)	5374(11)	1351(10)	34(3)
C7A	1295(5)	2530(11)	2504(9)	26(3)
C8A	1246(7)	2784(13)	3330(10)	39(3)
C9A	1020(6)	1915(13)	3804(10)	35(3)
C10A	858(6)	753(12)	3379(10)	32(3)
C11A	911(7)	445(11)	2556(11)	35(3)
C12A	1123(5)	1339(10)	2117(10)	27(3)
C13A	951(8)	2167(17)	4668(11)	55(5)
C14A	725(7)	-849(13)	2149(12)	47(4)
C15A	3048(6)	3236(14)	1602(12)	45(4)
C16A	1550(6)	6631(11)	947(9)	29(3)
C17A	1033(6)	6841(13)	295(10)	37(3)
C18A	897(7)	8004(13)	-100(11)	37(3)
C19A	1274(7)	8981(11)	179(11)	41(4)
C20A	1805(6)	8828(12)	811(10)	33(3)
C21A	1942(6)	7638(12)	1218(10)	31(3)
C22A	310(7)	8230(16)	-827(11)	53(4)
C23A	2248(8)	9918(14)	1107(12)	45(4)

Table 69. Anisotropic Displacement Parameters ($\times 10^4$) **103.**

Atom	U_{11}	U_{22}	U_{33}	U_{23}	U_{13}	U_{12}
I1	40.8(6)	34.3(6)	47.6(6)	5.1(4)	-2.0(4)	-9.8(4)
C1	18(6)	22(6)	39(7)	8(5)	7(5)	7(5)
C2	20(6)	42(8)	31(7)	2(6)	7(5)	0(6)
C3	21(6)	22(6)	42(8)	2(5)	11(6)	5(5)
C4	27(7)	33(7)	33(8)	8(5)	4(5)	5(6)
C5	16(7)	28(7)	43(8)	-2(5)	-2(5)	6(5)
C6	38(8)	31(7)	27(7)	1(5)	14(5)	3(6)
C7	18(6)	33(7)	37(8)	1(6)	-7(5)	-11(5)
C8	27(7)	33(8)	58(11)	2(7)	14(7)	-2(6)
C9	34(7)	28(7)	37(8)	2(6)	6(6)	5(6)
C10	26(7)	29(7)	63(11)	7(7)	7(7)	-1(6)
C11	19(7)	30(7)	54(9)	14(6)	15(6)	4(5)
C12	29(7)	22(6)	32(7)	1(5)	3(5)	8(5)
C13	47(9)	50(9)	44(10)	-3(8)	10(7)	-1(7)
C14	28(8)	40(9)	57(10)	-16(8)	-2(6)	-3(6)
C15	35(8)	35(8)	47(9)	15(6)	16(6)	2(6)
C16	37(7)	18(6)	41(8)	3(5)	11(6)	4(6)
C17	55(10)	30(7)	28(8)	-3(5)	7(6)	0(7)
C18	43(9)	7(6)	59(10)	-7(5)	-3(7)	-4(6)
C19	55(10)	23(7)	52(10)	1(6)	7(7)	-14(7)
C20	66(11)	28(8)	45(10)	6(6)	16(8)	-10(8)
C21	50(9)	25(7)	51(10)	3(6)	22(7)	0(6)
C22	89(15)	24(8)	65(12)	-17(7)	9(10)	11(8)
C23	48(10)	59(11)	65(12)	17(9)	19(9)	-6(9)
I1A	30.5(5)	27.3(5)	46.4(6)	3.6(3)	14.5(4)	1.5(3)
C1A	20(6)	29(6)	23(6)	-8(5)	7(5)	4(5)
C2A	31(7)	20(6)	32(7)	5(5)	-7(5)	-9(5)
C3A	43(8)	22(6)	31(7)	2(5)	7(6)	-3(6)
C4A	27(7)	27(6)	34(7)	-8(5)	-4(5)	-9(6)
C5A	28(7)	23(6)	43(8)	8(5)	14(6)	-3(5)
C6A	49(9)	14(6)	44(8)	4(5)	23(7)	-14(6)
C7A	19(6)	18(6)	35(8)	0(5)	2(5)	-1(5)
C8A	58(10)	31(7)	30(8)	8(6)	18(7)	-3(7)
C9A	35(7)	34(7)	39(8)	10(6)	15(6)	-1(6)
C10A	25(6)	24(6)	49(8)	9(6)	14(6)	2(6)
C11A	37(8)	9(5)	56(9)	2(5)	9(6)	-2(5)
C12A	24(6)	15(6)	45(8)	1(5)	14(5)	0(5)
C13A	81(13)	51(10)	34(10)	5(7)	18(8)	-24(9)
C14A	56(10)	18(7)	76(12)	-10(7)	34(8)	-7(6)
C15A	30(8)	35(8)	72(12)	6(7)	18(7)	0(7)
C16A	34(7)	14(5)	42(8)	-3(5)	17(6)	-9(5)
C17A	32(8)	37(8)	43(9)	-3(6)	16(6)	-9(6)
C18A	37(8)	32(7)	49(9)	12(6)	25(7)	7(7)
C19A	65(10)	9(6)	67(11)	1(6)	47(9)	8(6)
C20A	41(8)	21(6)	50(9)	-2(5)	30(7)	4(6)
C21A	29(7)	19(6)	40(9)	-2(5)	4(6)	-10(5)

Table 69 (cont'd)

Atom	U_{11}	U_{22}	U_{33}	U_{23}	U_{13}	U_{12}
C22A	54(10)	50(9)	44(9)	28(8)	0(7)	-1(8)
C23A	52(10)	34(7)	49(9)	-2(6)	17(7)	-3(7)

Table 70. Bond Lengths in Å for 103.

Atom	Atom	Length/Å
I1	C1	2.123(13)
C1	C2	1.365(19)
C1	C6	1.370(19)
C2	C3	1.404(18)
C2	C7	1.509(19)
C3	C4	1.397(18)
C4	C5	1.404(19)
C4	C15	1.50(2)
C5	C6	1.44(2)
C6	C16	1.487(19)
C7	C8	1.42(2)
C7	C12	1.40(2)
C8	C9	1.40(2)
C9	C10	1.37(2)
C9	C13	1.47(2)
C10	C11	1.39(2)
C11	C12	1.379(18)
C11	C14	1.50(2)
C16	C17	1.44(2)
C16	C21	1.37(2)
C17	C18	1.41(2)
C18	C19	1.41(2)
C18	C22	1.49(2)
C19	C20	1.31(2)
C20	C21	1.40(2)
C20	C23	1.56(2)
I1A	C1A	2.117(12)
C1A	C2A	1.388(18)
C1A	C6A	1.411(18)
C2A	C3A	1.44(2)
C2A	C7A	1.497(18)
C3A	C4A	1.37(2)
C4A	C5A	1.418(18)
C4A	C15A	1.49(2)
C5A	C6A	1.40(2)
C6A	C16A	1.487(18)
C7A	C8A	1.39(2)
C7A	C12A	1.410(17)
C8A	C9A	1.412(19)
C9A	C10A	1.40(2)
C9A	C13A	1.47(2)
C10A	C11A	1.40(2)
C11A	C12A	1.373(19)
C11A	C14A	1.526(18)

Table 70 (cont'd)

Atom	Atom	Length/Å
C16A	C17A	1.37(2)
C16A	C21A	1.406(17)
C17A	C18A	1.38(2)
C18A	C19A	1.36(2)
C18A	C22A	1.55(2)
C19A	C20A	1.37(2)
C20A	C21A	1.411(19)
C20A	C23A	1.55(2)

Table 71. Bond Angles in ° for 103.

Atom	Atom	Atom	Angle/°
C2	C1	I1	119.4(10)
C2	C1	C6	123.4(13)
C6	C1	I1	117.2(9)
C1	C2	C3	118.9(13)
C1	C2	C7	125.6(12)
C3	C2	C7	115.5(12)
C4	C3	C2	121.0(12)
C3	C4	C5	118.8(12)
C3	C4	C15	119.6(12)
C5	C4	C15	121.7(12)
C4	C5	C6	120.1(12)
C1	C6	C5	117.7(12)
C1	C6	C16	127.8(13)
C5	C6	C16	114.4(13)
C8	C7	C2	120.3(13)
C12	C7	C2	118.8(13)
C12	C7	C8	120.8(13)
C9	C8	C7	117.8(14)
C8	C9	C13	118.8(14)
C10	C9	C8	119.4(15)
C10	C9	C13	121.7(14)
C9	C10	C11	123.5(14)
C10	C11	C14	123.3(14)
C12	C11	C10	118.1(13)
C12	C11	C14	118.6(15)
C11	C12	C7	120.4(14)
C17	C16	C6	118.5(13)
C21	C16	C6	122.1(12)
C21	C16	C17	119.4(13)
C18	C17	C16	119.5(15)
C17	C18	C19	116.2(14)
C17	C18	C22	117.0(16)
C19	C18	C22	126.8(15)
C20	C19	C18	124.4(14)
C19	C20	C21	119.9(17)
C19	C20	C23	121.5(14)
C21	C20	C23	118.6(15)
C16	C21	C20	120.4(15)
C2A	C1A	I1A	117.8(10)
C2A	C1A	C6A	121.7(12)

Table 71 (cont'd)

Atom	Atom	Atom	Angle/°
C6A	C1A	I1A	120.5(9)
C1A	C2A	C3A	117.7(12)
C1A	C2A	C7A	126.2(13)
C3A	C2A	C7A	116.0(11)
C4A	C3A	C2A	123.2(12)
C3A	C4A	C5A	116.5(13)
C3A	C4A	C15A	121.8(12)
C5A	C4A	C15A	121.6(13)
C6A	C5A	C4A	123.4(12)
C1A	C6A	C16A	125.7(13)
C5A	C6A	C1A	117.4(11)
C5A	C6A	C16A	116.9(11)
C8A	C7A	C2A	121.7(12)
C8A	C7A	C12A	119.1(12)
C12A	C7A	C2A	118.7(12)
C7A	C8A	C9A	123.3(13)
C8A	C9A	C13A	124.5(14)
C10A	C9A	C8A	114.4(14)
C10A	C9A	C13A	121.2(13)
C9A	C10A	C11A	124.3(12)
C10A	C11A	C14A	120.4(13)
C12A	C11A	C10A	118.8(12)
C12A	C11A	C14A	120.9(14)
C11A	C12A	C7A	120.1(14)
C17A	C16A	C6A	123.3(12)
C17A	C16A	C21A	118.6(12)
C21A	C16A	C6A	118.0(12)
C16A	C17A	C18A	121.5(13)
C17A	C18A	C22A	120.9(14)
C19A	C18A	C17A	119.5(15)
C19A	C18A	C22A	119.6(13)
C18A	C19A	C20A	122.0(13)
C19A	C20A	C21A	118.2(12)
C19A	C20A	C23A	122.5(13)
C21A	C20A	C23A	119.2(14)
C16A	C21A	C20A	120.1(13)

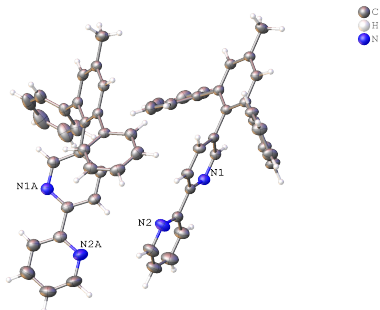
Table 72. Hydrogen Fractional Atomic Coordinates ($\times 10^4$) and Equivalent Isotropic Displacement Parameters ($\text{\AA}^2 \times 10^3$) for **103**.

Atom	x	y	z	U_{eq}
H3	2721.01	-3085.05	-21.7	34
H5	2457.84	89.17	-1516.17	38
H8	3609.41	-1501.63	2208.03	47
H10	4421.45	-4825.63	2966.16	50
H12	3887.31	-3926.05	390.23	35
H13A	4403.66	-2299.89	3919.66	72
H13B	4123.37	-3643.46	3990.8	72
H13C	3715.45	-2440.44	3660.44	72
H14A	4122.53	-6364.76	1159.16	68
H14B	4717.39	-6123.65	1936.32	68
H14C	4630.77	-5577.45	969.89	68

Table 72 (cont'd)

Atom	x	y	z	<i>U_{eq}</i>
H15A	2025.25	-2941.65	-1694.01	58
H15B	1757.17	-1559	-1924.34	58
H15C	1682.55	-2308.32	-1098.83	58
H17	2570.79	2244.88	-686.23	47
H19	3674.33	4572.88	-1378.97	55
H21	4122.31	1004.98	-819.36	49
H22A	2617.95	4874.77	-510.89	95
H22B	2223.77	4281.05	-1425.13	95
H22C	2690.8	5343.96	-1420.72	95
H23A	4526.69	3043.48	-1855.39	86
H23B	4854.8	2517.1	-886.65	86
H23C	4700.88	3984.02	-1030.01	86
H3A	2293.37	2207.34	2273.12	40
H5A	2481.88	5410.1	1056.22	36
H8A	1369.93	3583.91	3588.15	47
H10A	701.73	133.41	3668.18	38
H12A	1153.34	1154.41	1552.43	33
H13D	609.8	1719.61	4712.1	83
H13E	902.02	3074.95	4732.51	83
H13F	1296.43	1876.25	5135.36	83
H14D	320.98	-811.86	1765.91	71
H14E	760.94	-1466.78	2619.28	71
H14F	972.79	-1100.51	1800.86	71
H15D	3023.84	3124.97	983.39	68
H15E	3140.99	2427.08	1911.15	68
H15F	3351.6	3850.17	1881.51	68
H17A	763.12	6169.98	112.81	44
H19A	1165.84	9792.32	-70.22	49
H21A	2298.75	7517.19	1675.36	37
H22D	152.02	7422.49	-1095.23	79
H22E	367.22	8788.4	-1279.74	79
H22F	38.12	8621.15	-565.87	79
H23D	2504.31	9757.76	1708.53	67
H23E	2041.46	10714.04	1093.37	67
H23F	2479.51	9972.52	706.62	67

Compound L2*



Compound	L2* (CCDC 1851547)
Formula	C ₂₉ H ₂₂ N ₂
<i>D</i> _{calc.} / g cm ⁻³	1.203
μ /mm ⁻¹	0.540
Formula Weight	398.48
Colour	colourless
Shape	plate
Size/mm ³	0.28×0.28×0.09
<i>T</i> /K	173(2)
Crystal System	monoclinic
Space Group	<i>P</i> 2 ₁ / <i>n</i>
<i>a</i> /Å	9.92670(10)
<i>b</i> /Å	10.3265(2)
<i>c</i> /Å	42.9795(5)
α /°	90
β /°	93.1340(10)
γ /°	90
<i>V</i> /Å ³	4399.16(11)
<i>Z</i>	8
<i>Z</i> '	2
Wavelength/Å	1.541838
Radiation type	CuK α
θ _{min} /°	2.059
θ _{max} /°	73.064
Measured Refl.	25709
Independent Refl.	8557
Reflections with <i>I</i> > 2(<i>I</i>)	6629
<i>R</i> _{int}	0.0390
Parameters	561
Restraints	0
Largest Peak	0.218
Deepest Hole	-0.213
GooF	1.021
<i>wR</i> ₂ (all data)	0.1276
<i>wR</i> ₂	0.1153
<i>R</i> ₁ (all data)	0.0625
<i>R</i> ₁	0.0461

Table 73. Fractional Atomic Coordinates ($\times 10^4$) and Equivalent Isotropic Displacement Parameters ($\text{\AA}^2 \times 10^3$) for L2*.

Atom	x	y	z	U_{eq}
N1	10598.3(15)	5968.8(15)	7132.5(3)	41.7(3)
N2	8337.5(19)	3741(2)	7490.5(4)	62.7(5)
C1	9829.4(15)	7345.2(15)	6331.0(4)	32.1(3)
C2	9651.8(15)	6629.9(15)	6052.1(4)	32.3(3)
C3	9778.6(16)	7240.1(16)	5765.8(4)	34.6(3)
C4	10136.2(16)	8539.1(16)	5746.8(4)	35.7(3)
C5	10355.0(16)	9221.5(16)	6022.8(4)	36.6(4)
C6	10189.9(15)	8661.0(16)	6314.6(4)	34.1(3)
C7	9643.8(16)	6681.8(15)	6633.5(4)	33.9(3)
C8	10659.7(18)	6657.1(17)	6868.7(4)	39.8(4)
C9	8479.1(17)	5972.4(17)	6686.6(4)	38.2(4)
C10	8401.0(17)	5269.6(17)	6954.9(4)	38.8(4)
C11	9479.7(17)	5264.3(16)	7171.7(4)	36.7(4)
C12	9444.7(18)	4464.6(17)	7458.5(4)	39.8(4)
C13	10512(2)	4453(2)	7676.4(4)	50.7(5)
C14	10443(3)	3673(2)	7936.0(5)	63.1(6)
C15	9321(2)	2926(2)	7971.6(5)	63.7(6)
C16	8301(3)	2989(3)	7744.3(5)	72.8(7)
C17	9369.8(16)	5208.2(15)	6054.2(3)	32.1(3)
C18	10216.9(18)	4355.4(17)	6222.4(4)	39.1(4)
C19	9915(2)	3042.1(18)	6230.6(4)	45.0(4)
C20	8774(2)	2569.3(17)	6071.0(4)	45.7(4)
C21	7950.7(19)	3404.0(17)	5897.6(4)	44.7(4)
C22	8247.9(17)	4712.8(17)	5886.9(4)	39.2(4)
C23	10305.5(19)	9166.2(19)	5435.6(4)	46.5(4)
C24	10376.2(18)	9519.4(16)	6592.5(4)	39.7(4)
C25	11560(2)	10235.9(18)	6638.2(5)	50.8(5)
C26	11720(3)	11103(2)	6883.3(6)	67.8(7)
C27	10704(3)	11277(2)	7084.6(6)	75.0(8)
C28	9532(3)	10564(2)	7044.7(5)	69.1(7)
C29	9367(2)	9691(2)	6801.3(4)	51.8(5)
N1A	3460.8(14)	6067.4(14)	6365.1(3)	36.2(3)
N2A	5273.6(18)	3314.2(16)	6702.6(4)	50.2(4)
C1A	3637.4(15)	6975.1(15)	5518.2(3)	29.7(3)
C2A	3096.9(16)	6366.5(15)	5244.8(3)	31.5(3)
C3A	2910.0(16)	7084.9(15)	4971.8(4)	33.6(3)
C4A	3244.5(16)	8391.0(15)	4956.3(4)	33.0(3)
C5A	3784.7(16)	8975.6(15)	5225.7(4)	32.3(3)
C6A	3990.0(15)	8292.2(15)	5505.0(4)	30.7(3)
C7A	3849.2(15)	6240.0(15)	5816.5(3)	30.9(3)
C8A	3283.3(16)	6663.2(16)	6088.1(3)	33.3(3)
C9A	4633.7(17)	5131.2(16)	5840.4(4)	35.0(3)
C10A	4836.9(16)	4506.9(16)	6121.3(4)	35.1(3)
C11A	4241.3(16)	4996.2(15)	6379.6(4)	32.4(3)
C12A	4435.8(17)	4335.6(16)	6687.2(4)	35.8(4)
C13A	3771(2)	4753(2)	6939.4(4)	53.2(5)
C14A	3981(3)	4106(2)	7220.9(5)	64.8(6)
C15A	4834(2)	3080(2)	7240.3(4)	56.6(5)
C16A	5465(2)	2718(2)	6979.0(5)	57.3(5)
C17A	2721.7(16)	4969.6(15)	5232.9(3)	32.0(3)
C18A	1841.8(18)	4417.6(17)	5435.7(4)	39.5(4)

Table 73 (cont'd)

Atom	x	y	z	U_{eq}
C19A	1510(2)	3118.5(18)	5414.7(4)	46.6(4)
C20A	2069(2)	2343.5(17)	5192.3(4)	48.1(4)
C21A	2944(2)	2877.0(18)	4989.2(4)	46.3(4)
C22A	3261.0(18)	4177.2(16)	5008.2(4)	38.0(4)
C23A	3037.6(19)	9134.6(16)	4656.0(4)	40.5(4)
C24A	4634.3(16)	8996.1(16)	5777.5(4)	33.2(3)
C25A	4070.8(18)	10138.7(17)	5882.9(4)	40.0(4)
C26A	4689(2)	10826.0(19)	6128.7(4)	49.1(5)
C27A	5889(2)	10383(2)	6270.1(4)	54.0(5)
C28A	6463(2)	9260(2)	6164.9(4)	51.3(5)
C29A	5842.7(17)	8564.9(18)	5922.4(4)	40.4(4)

Table 74. Anisotropic Displacement Parameters ($\times 10^4$) L2*.

Atom	U_{11}	U_{22}	U_{33}	U_{23}	U_{13}	U_{12}
N1	48.4(8)	40.1(8)	36.5(7)	-3.4(6)	2.6(6)	-2.9(6)
N2	59.9(11)	76.1(13)	52.5(10)	19.3(9)	5.7(8)	-17.6(9)
C1	30.2(7)	30.4(8)	36.0(8)	-2.1(6)	4.6(6)	1.3(6)
C2	31.9(8)	29.5(8)	35.9(8)	-1.4(6)	4.6(6)	0.3(6)
C3	36.1(8)	34.3(9)	33.8(8)	-1.7(7)	4.7(6)	1.0(6)
C4	32.0(8)	34.3(8)	41.2(9)	4.5(7)	5.8(6)	3.6(6)
C5	33.2(8)	26.3(8)	50.7(10)	2.0(7)	4.4(7)	-0.1(6)
C6	30.4(8)	30.5(8)	41.4(9)	-3.1(7)	2.8(6)	1.3(6)
C7	40.1(8)	29.6(8)	32.6(8)	-4.8(6)	6.9(6)	2.6(6)
C8	43.6(9)	37.3(9)	38.8(9)	-1.9(7)	3.9(7)	-3.8(7)
C9	37.2(8)	42.0(9)	36.1(8)	-3.9(7)	7.6(6)	-0.3(7)
C10	38.6(9)	41.7(10)	37.0(8)	-3.9(7)	11.2(7)	-4.0(7)
C11	42.8(9)	34.3(9)	33.9(8)	-5.8(7)	10.0(6)	-0.4(7)
C12	48.6(10)	36.7(9)	35.1(8)	-4.8(7)	10.7(7)	-1.3(7)
C13	57.2(12)	49.1(11)	45.7(10)	3.6(9)	2.0(8)	-8.9(9)
C14	72.4(15)	63.0(14)	53.0(12)	10.8(10)	-5.4(10)	-2.1(11)
C15	77.2(15)	65.5(14)	49.4(12)	17.2(10)	11.4(10)	-3.5(12)
C16	69.6(15)	88.1(18)	61.0(13)	28.9(13)	6.8(11)	-23.8(13)
C17	37.7(8)	28.7(8)	30.5(7)	-2.4(6)	8.3(6)	-1.5(6)
C18	43.2(9)	35.8(9)	38.4(9)	-2.9(7)	3.3(7)	-0.1(7)
C19	57.0(11)	33.5(9)	45.0(10)	3.0(7)	6.4(8)	5.6(8)
C20	59.3(11)	26.6(8)	52.6(11)	-3.7(8)	15.6(8)	-6.6(8)
C21	46.7(10)	36.9(10)	50.6(10)	-10.1(8)	4.4(8)	-7.5(8)
C22	42.9(9)	35.7(9)	38.9(9)	-3.5(7)	0.8(7)	0.8(7)
C23	47.2(10)	43.2(10)	49.6(10)	12.0(8)	5.8(8)	-1.0(8)
C24	43.6(9)	28.5(8)	46.1(9)	-2.9(7)	-6.6(7)	4.0(7)
C25	54.8(11)	37.9(10)	57.9(11)	3.7(9)	-14.6(9)	-5.3(8)
C26	83.5(17)	40.0(11)	75.3(15)	-0.7(11)	-37.5(13)	-13.2(11)
C27	107(2)	48.1(13)	66.1(15)	-23.6(11)	-32.7(15)	12.9(13)
C28	79.4(16)	70.4(15)	56.1(13)	-25.7(11)	-9.6(11)	21.4(13)
C29	50.3(11)	54.7(12)	49.6(11)	-17.3(9)	-3.6(8)	8.1(9)
N1A	41.1(7)	36.8(7)	31.2(7)	0.1(6)	4.8(5)	-0.3(6)
N2A	67.0(10)	42.8(9)	40.3(8)	6.7(7)	-0.6(7)	7.8(8)
C1A	32.2(7)	26.8(7)	30.8(7)	0.1(6)	6.5(6)	1.8(6)
C2A	35.2(8)	28.8(8)	31.2(7)	-1.2(6)	7.3(6)	-0.6(6)
C3A	41.1(9)	29.3(8)	30.6(8)	-3.3(6)	3.7(6)	-3.3(6)

Table 74 (cont'd)

Atom	U_{11}	U_{22}	U_{33}	U_{23}	U_{13}	U_{12}
C4A	36.7(8)	30.6(8)	32.0(8)	2.3(6)	4.6(6)	0.4(6)
C5A	37.2(8)	23.6(7)	36.2(8)	0.3(6)	4.4(6)	-1.2(6)
C6A	32.1(7)	27.2(8)	33.0(8)	0.2(6)	3.8(6)	-0.5(6)
C7A	33.7(8)	28.0(8)	31.3(8)	0.5(6)	3.4(6)	-4.4(6)
C8A	34.9(8)	32.4(8)	32.7(8)	-1.7(6)	4.2(6)	0.7(6)
C9A	43.2(9)	31.8(8)	30.8(8)	0.0(6)	10.0(6)	2.3(7)
C10A	40.3(9)	29.3(8)	36.1(8)	3.2(6)	6.9(6)	4.1(6)
C11A	34.4(8)	31.1(8)	31.6(8)	1.0(6)	2.4(6)	-4.1(6)
C12A	39.3(9)	33.5(8)	34.1(8)	2.1(7)	-1.7(6)	-5.6(7)
C13A	64.5(12)	55.7(12)	40.3(10)	6.8(9)	11.6(8)	11.2(10)
C14A	87.8(17)	68.7(15)	38.9(10)	4.3(10)	12.3(10)	3.6(13)
C15A	78.7(14)	53.9(12)	35.9(10)	11.4(9)	-7.7(9)	-8.0(11)
C16A	79.1(14)	46.6(11)	45.4(11)	11.9(9)	-5.3(10)	9.0(10)
C17A	38.3(8)	27.8(8)	30.1(7)	-0.1(6)	3.1(6)	-1.4(6)
C18A	45.8(9)	34.5(9)	39.5(9)	-2.8(7)	12.9(7)	-3.5(7)
C19A	54.5(11)	39.4(10)	47.3(10)	3.9(8)	14.5(8)	-11.9(8)
C20A	67.1(12)	26.6(9)	50.9(11)	-1.0(8)	5.4(9)	-9.4(8)
C21A	63.5(12)	34.0(9)	42.3(10)	-8.6(7)	12.6(8)	-1.7(8)
C22A	48.8(9)	33.6(9)	32.7(8)	-0.6(7)	11.1(7)	-4.5(7)
C23A	55.2(10)	30.3(8)	35.5(9)	4.3(7)	-1.9(7)	-4.6(7)
C24A	37.9(8)	29.9(8)	32.2(8)	0.7(6)	5.3(6)	-6.6(6)
C25A	43.6(9)	34.2(9)	42.6(9)	-5.3(7)	5.0(7)	-3.8(7)
C26A	60.0(12)	40.1(10)	48.4(10)	-15.0(8)	13.7(8)	-12.5(9)
C27A	58.0(12)	61.3(13)	42.5(10)	-12.9(9)	2.3(8)	-23.1(10)
C28A	44.6(10)	62.5(13)	45.9(10)	1.9(9)	-6.4(8)	-11.2(9)
C29A	41.5(9)	39.2(9)	40.5(9)	1.0(7)	1.4(7)	-3.0(7)

Table 75. Bond Lengths in Å for L2*.

Atom	Atom	Length/Å
N1	C8	1.343(2)
N1	C11	1.346(2)
N2	C12	1.342(2)
N2	C16	1.341(3)
C1	C2	1.411(2)
C1	C6	1.408(2)
C1	C7	1.490(2)
C2	C3	1.394(2)
C2	C17	1.495(2)
C3	C4	1.391(2)
C4	C5	1.387(2)
C4	C23	1.504(2)
C5	C6	1.399(2)
C6	C24	1.491(2)
C7	C8	1.389(2)
C7	C9	1.398(2)
C9	C10	1.368(2)
C10	C11	1.381(2)
C11	C12	1.486(2)
C12	C13	1.375(3)
C13	C14	1.381(3)

Table 75 (cont'd)

Atom	Atom	Length/Å
C14	C15	1.371(3)
C15	C16	1.370(3)
C17	C18	1.392(2)
C17	C22	1.390(2)
C18	C19	1.390(2)
C19	C20	1.381(3)
C20	C21	1.378(3)
C21	C22	1.385(2)
C24	C25	1.393(3)
C24	C29	1.392(3)
C25	C26	1.385(3)
C26	C27	1.376(4)
C27	C28	1.380(4)
C28	C29	1.384(3)
N1A	C8A	1.343(2)
N1A	C11A	1.350(2)
N2A	C12A	1.343(2)
N2A	C16A	1.342(2)
C1A	C2A	1.412(2)
C1A	C6A	1.406(2)
C1A	C7A	1.495(2)
C2A	C3A	1.392(2)
C2A	C17A	1.490(2)
C3A	C4A	1.392(2)
C4A	C5A	1.387(2)
C4A	C23A	1.506(2)
C5A	C6A	1.398(2)
C6A	C24A	1.492(2)
C7A	C8A	1.393(2)
C7A	C9A	1.385(2)
C9A	C10A	1.374(2)
C10A	C11A	1.382(2)
C11A	C12A	1.491(2)
C12A	C13A	1.369(3)
C13A	C14A	1.388(3)
C14A	C15A	1.355(3)
C15A	C16A	1.368(3)
C17A	C18A	1.389(2)
C17A	C22A	1.395(2)
C18A	C19A	1.383(2)
C19A	C20A	1.386(3)
C20A	C21A	1.380(3)
C21A	C22A	1.380(2)
C24A	C25A	1.392(2)
C24A	C29A	1.394(2)
C25A	C26A	1.388(2)
C26A	C27A	1.385(3)
C27A	C28A	1.379(3)
C28A	C29A	1.382(2)

Table 76. Bond Angles in ° for L2*.

Atom	Atom	Atom	Angle/°
C8	N1	C11	117.89(15)
C16	N2	C12	117.67(19)
C2	C1	C7	119.01(14)
C6	C1	C2	118.87(14)
C6	C1	C7	122.11(14)
C1	C2	C17	121.58(14)
C3	C2	C1	120.01(15)
C3	C2	C17	118.39(14)
C4	C3	C2	121.55(15)
C3	C4	C23	120.59(15)
C5	C4	C3	117.92(15)
C5	C4	C23	121.49(16)
C4	C5	C6	122.42(15)
C1	C6	C24	123.67(15)
C5	C6	C1	119.14(15)
C5	C6	C24	117.17(15)
C8	C7	C1	121.61(15)
C8	C7	C9	116.47(15)
C9	C7	C1	121.76(15)
N1	C8	C7	124.04(16)
C10	C9	C7	120.07(16)
C9	C10	C11	119.56(16)
N1	C11	C10	121.89(16)
N1	C11	C12	117.46(15)
C10	C11	C12	120.65(15)
N2	C12	C11	116.81(16)
N2	C12	C13	122.00(17)
C13	C12	C11	121.18(16)
C12	C13	C14	119.02(19)
C15	C14	C13	119.7(2)
C16	C15	C14	117.8(2)
N2	C16	C15	123.8(2)
C18	C17	C2	121.10(15)
C22	C17	C2	120.22(15)
C22	C17	C18	118.68(15)
C19	C18	C17	120.37(17)
C20	C19	C18	120.29(17)
C21	C20	C19	119.56(17)
C20	C21	C22	120.49(17)
C21	C22	C17	120.54(16)
C25	C24	C6	119.70(17)
C29	C24	C6	122.02(16)
C29	C24	C25	118.18(18)
C26	C25	C24	120.7(2)
C27	C26	C25	120.4(2)
C26	C27	C28	119.6(2)
C27	C28	C29	120.4(2)
C28	C29	C24	120.7(2)
C8A	N1A	C11A	117.62(14)
C16A	N2A	C12A	117.46(17)
C2A	C1A	C7A	121.12(14)

Table 76 (cont'd)

Atom	Atom	Atom	Angle/°
C6A	C1A	C2A	118.75(14)
C6A	C1A	C7A	120.13(13)
C1A	C2A	C17A	122.83(14)
C3A	C2A	C1A	119.42(14)
C3A	C2A	C17A	117.75(14)
C4A	C3A	C2A	122.41(14)
C3A	C4A	C23A	120.90(14)
C5A	C4A	C3A	117.65(14)
C5A	C4A	C23A	121.45(14)
C4A	C5A	C6A	121.91(14)
C1A	C6A	C24A	122.45(14)
C5A	C6A	C1A	119.86(14)
C5A	C6A	C24A	117.65(14)
C8A	C7A	C1A	121.00(14)
C9A	C7A	C1A	122.37(14)
C9A	C7A	C8A	116.61(14)
N1A	C8A	C7A	124.03(15)
C10A	C9A	C7A	120.52(15)
C9A	C10A	C11A	119.06(15)
N1A	C11A	C10A	122.16(14)
N1A	C11A	C12A	117.53(14)
C10A	C11A	C12A	120.31(15)
N2A	C12A	C11A	116.94(15)
N2A	C12A	C13A	122.17(16)
C13A	C12A	C11A	120.88(16)
C12A	C13A	C14A	118.9(2)
C15A	C14A	C13A	119.6(2)
C14A	C15A	C16A	118.39(18)
N2A	C16A	C15A	123.5(2)
C18A	C17A	C2A	122.70(14)
C18A	C17A	C22A	118.16(15)
C22A	C17A	C2A	119.14(14)
C19A	C18A	C17A	120.84(16)
C18A	C19A	C20A	120.15(16)
C21A	C20A	C19A	119.71(16)
C20A	C21A	C22A	120.02(17)
C21A	C22A	C17A	121.12(16)
C25A	C24A	C6A	120.38(15)
C25A	C24A	C29A	118.45(15)
C29A	C24A	C6A	121.10(15)
C26A	C25A	C24A	120.82(17)
C27A	C26A	C25A	119.96(18)
C28A	C27A	C26A	119.64(17)
C27A	C28A	C29A	120.59(18)
C28A	C29A	C24A	120.53(18)

Table 77. Hydrogen Fractional Atomic Coordinates ($\times 10^4$) and Equivalent Isotropic Displacement Parameters ($\text{\AA}^2 \times 10^3$) for **L2***.

Atom	x	y	z	U_{eq}
H3	9620.5	6767.54	5583.23	42
H5	10621.24	10083.47	6013.62	44
H8	11430.34	7147.75	6841.8	48
H9	7756.65	5978.21	6539.46	46
H10	7626.36	4798.55	6990.94	47
H13	11268.53	4963.26	7649.3	61
H14	11155.26	3654.11	8085.84	76
H15	9253.89	2392.81	8144.57	76
H16	7538.44	2482.38	7767.4	87
H18	10988.91	4666.35	6329.81	47
H19	10484.17	2479.14	6344.09	54
H20	8561.79	1693.37	6080.44	55
H21	7190.16	3085.84	5786.89	54
H22	7692.24	5264.98	5766.7	47
H23A	11138.83	8885.23	5354.45	70
H23B	10318.15	10090.39	5459.74	70
H23C	9567.62	8923.36	5293.87	70
H25	12250.36	10131	6502.59	61
H26	12518.16	11569.27	6912.06	81
H27	10806.85	11872.11	7246.6	90
H28	8848.66	10670	7182.18	83
H29	8574.14	9213.74	6776.95	62
H3A	2548.36	6677.01	4793.32	40
H5A	4017.06	9847.47	5220.27	39
H8A	2749.85	7403.85	6076.93	40
H9A	5025.93	4806.97	5664.89	42
H10A	5367.94	3765.45	6137.44	42
H13A	3189.6	5458.86	6922.43	64
H14A	3539.51	4373.95	7395.07	78
H15A	4986.01	2633.79	7426.85	68
H16A	6058.7	2021.68	6993.58	69
H18A	1471.32	4928.07	5587.48	47
H19A	910.4	2764.38	5550.19	56
H20A	1854.82	1467.61	5179.94	58
H21A	3321.07	2360.47	4839.47	56
H22A	3843.77	4530.81	4868.81	46
H23D	3050.23	10046.45	4699.52	61
H23E	2183.39	8903.24	4555.78	61
H23F	3747.2	8927.93	4521.28	61
H25A	3269.83	10445.18	5787.5	48
H26A	4298.28	11583.35	6198.47	59
H27A	6305.69	10840.99	6435.07	65
H28A	7274.85	8968.02	6257.91	62
H29A	6234.53	7803.33	5855.45	48

APPENDIX B

NMR

^1H NMR in CDCl_3 (500 MHz)

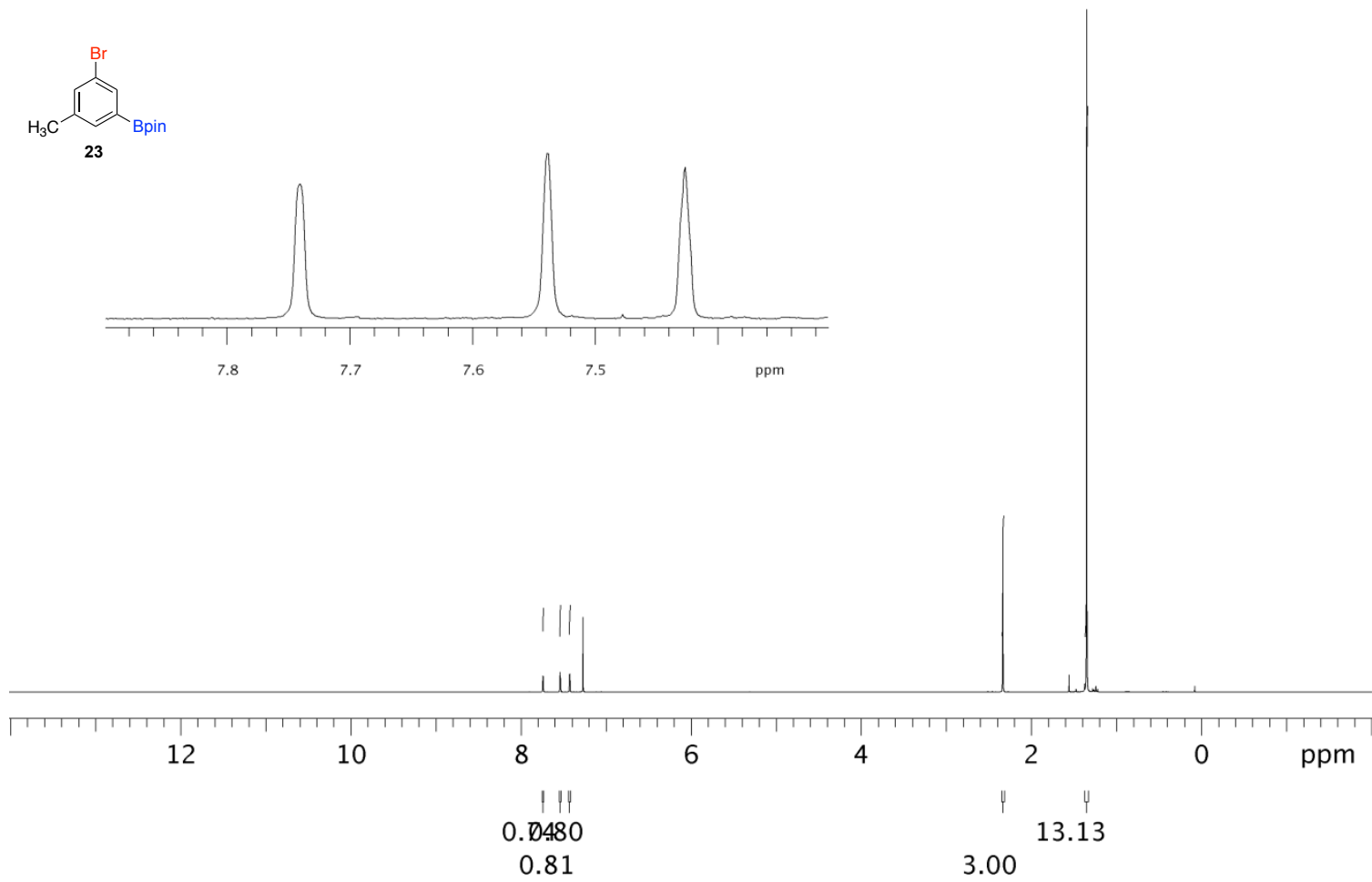


Figure 56. ^1H NMR of **23**

^{13}C NMR in CDCl_3 (125 MHz)

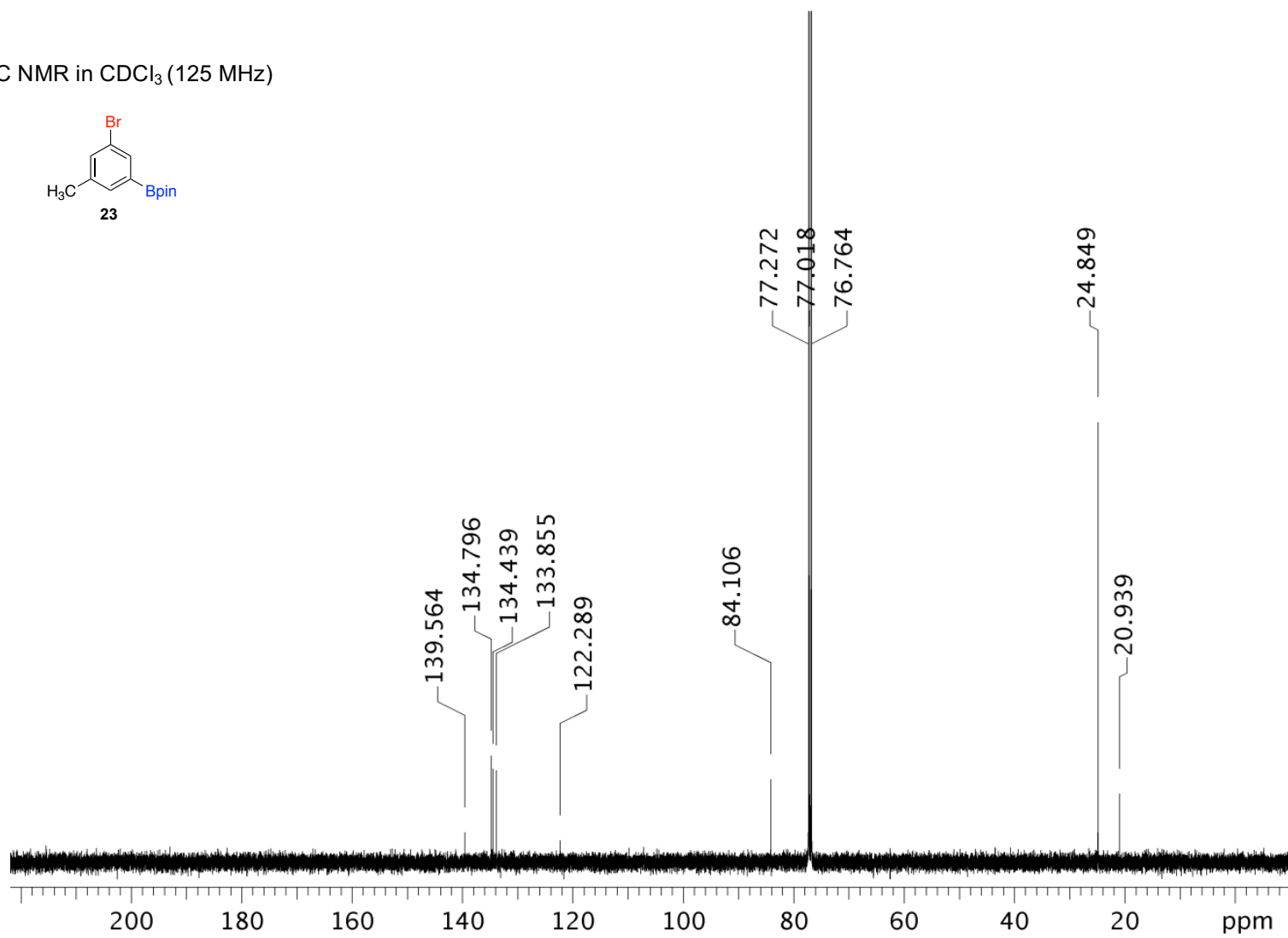
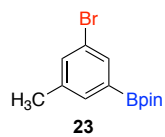


Figure 57. ^{13}C NMR of 23

^1H NMR in CDCl_3 (500 MHz)

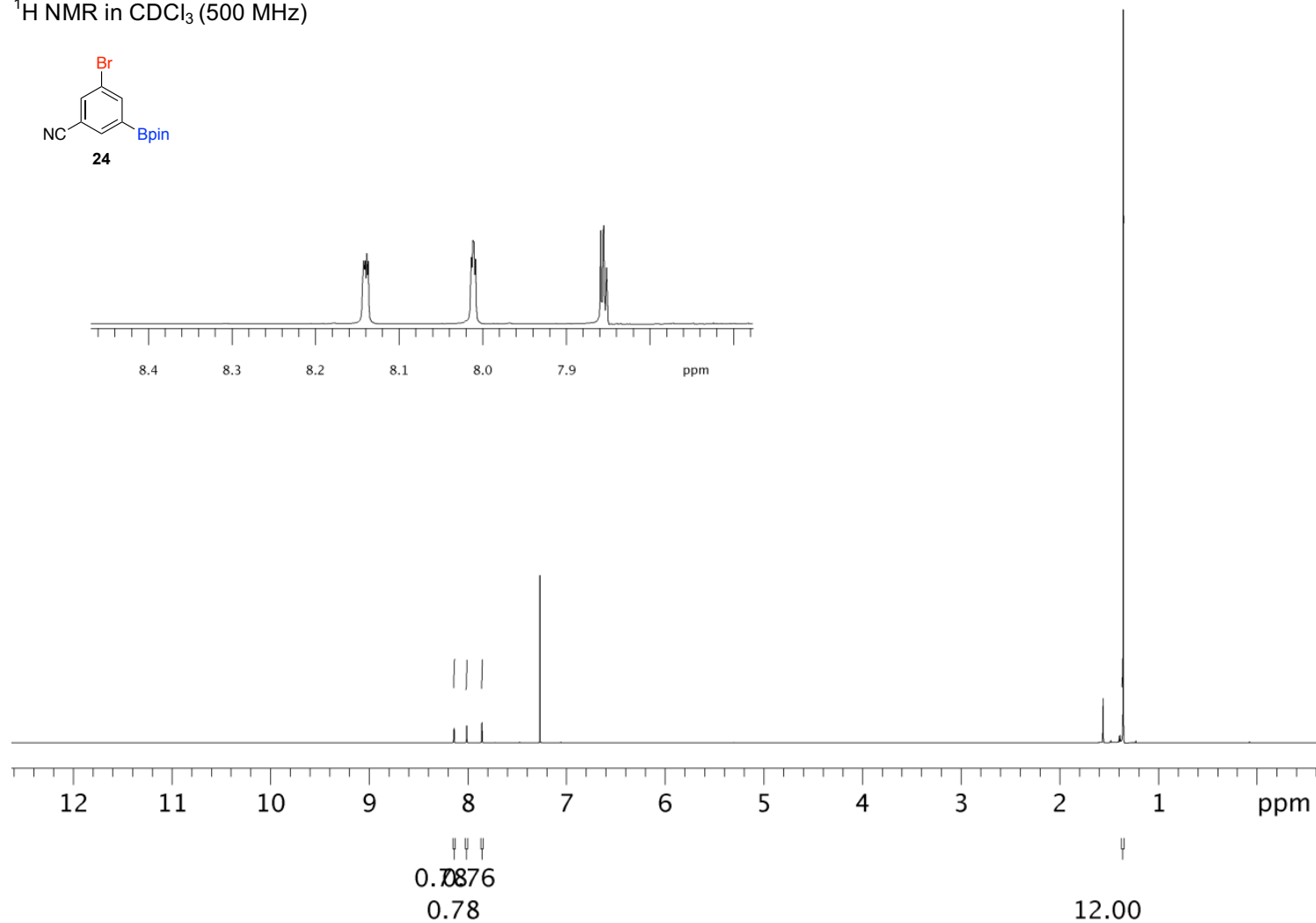
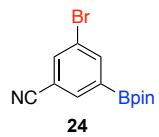


Figure 58. ^1H NMR of **24**

^{13}C NMR in CDCl_3 (125 MHz)

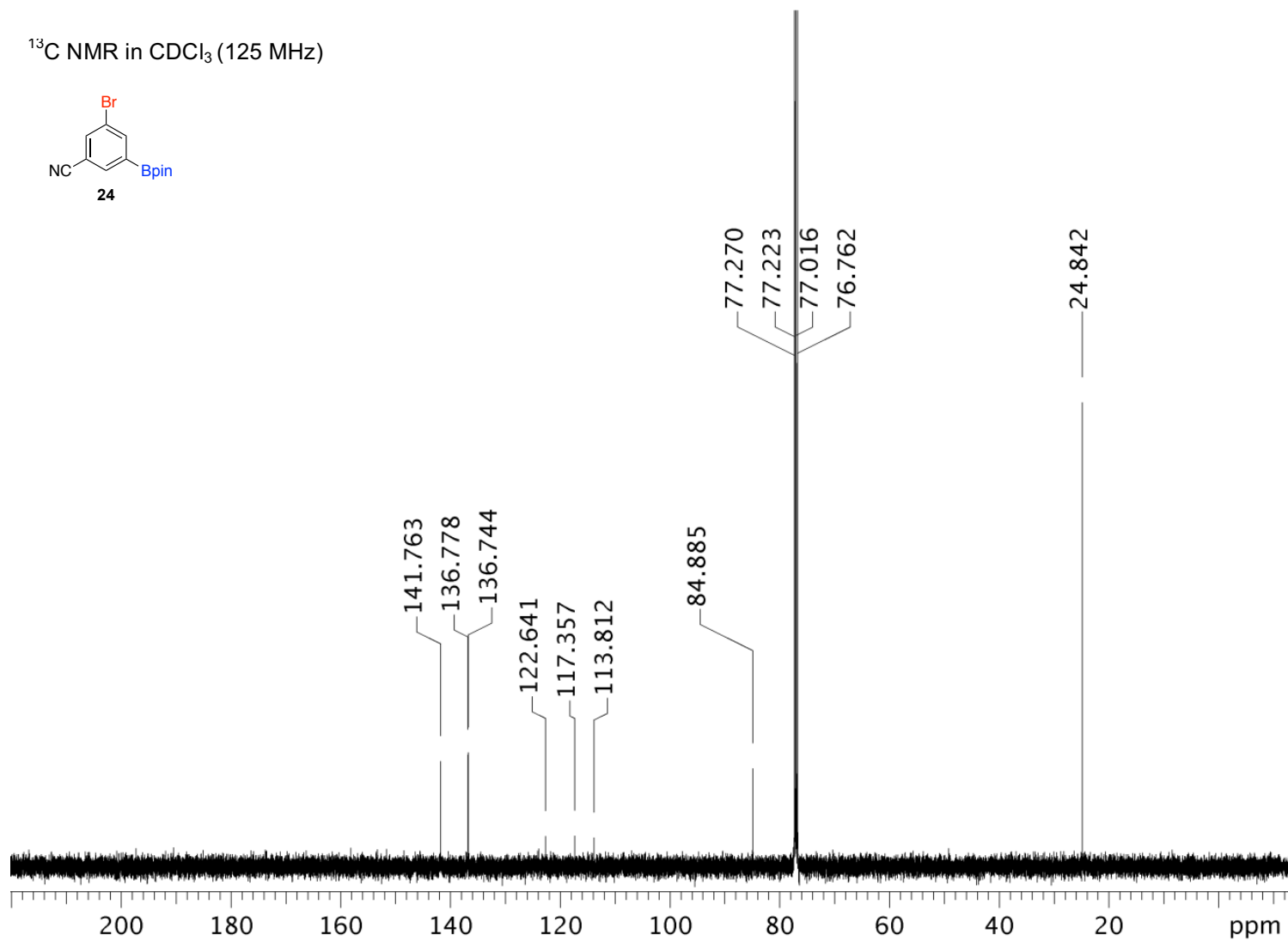
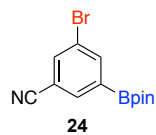


Figure 59. ^{13}C NMR of 24

^1H NMR in CDCl_3 (500 MHz)

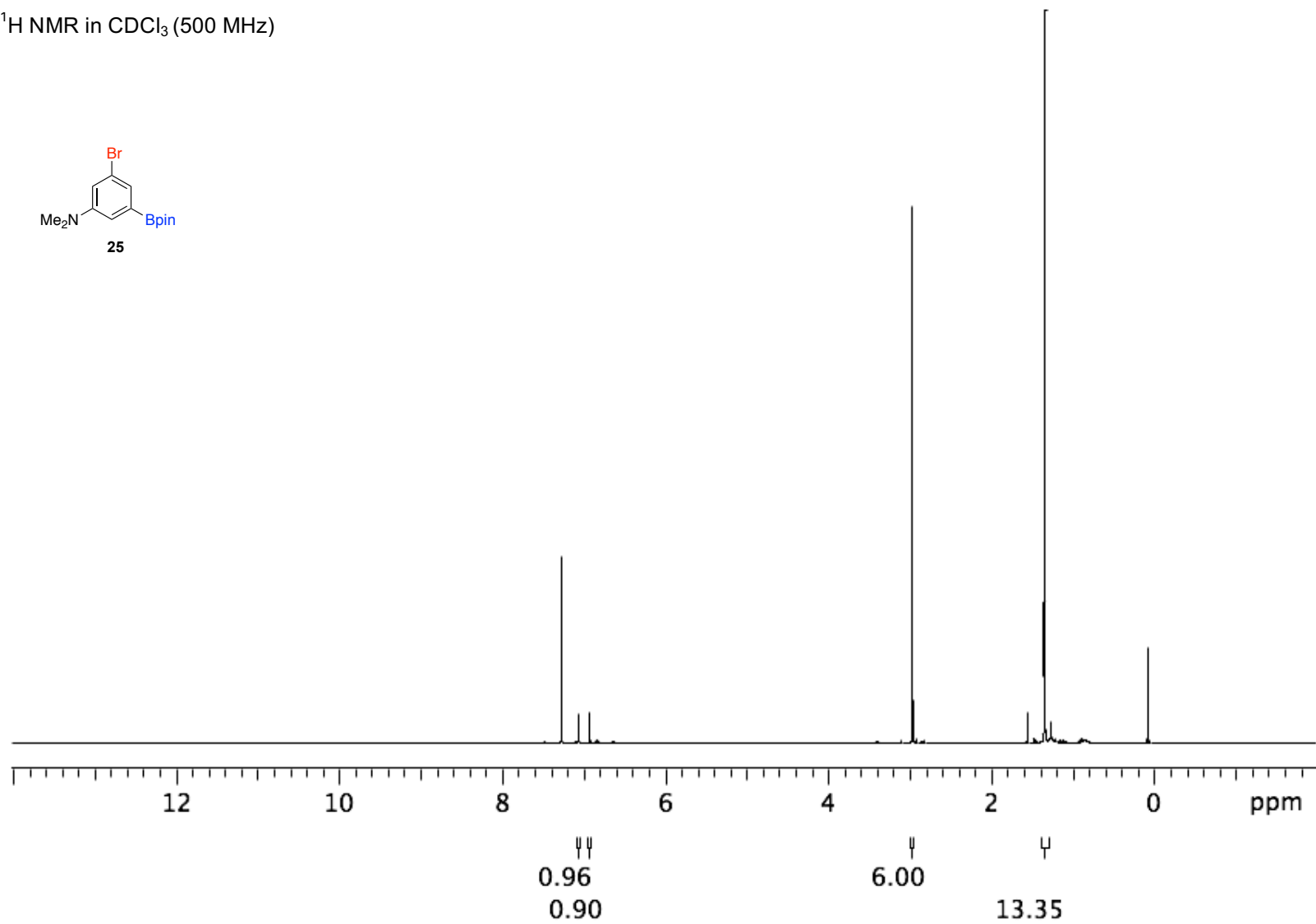
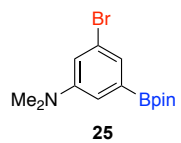


Figure 60. ^1H NMR of 25

^{13}C NMR in CDCl_3 (125 MHz)

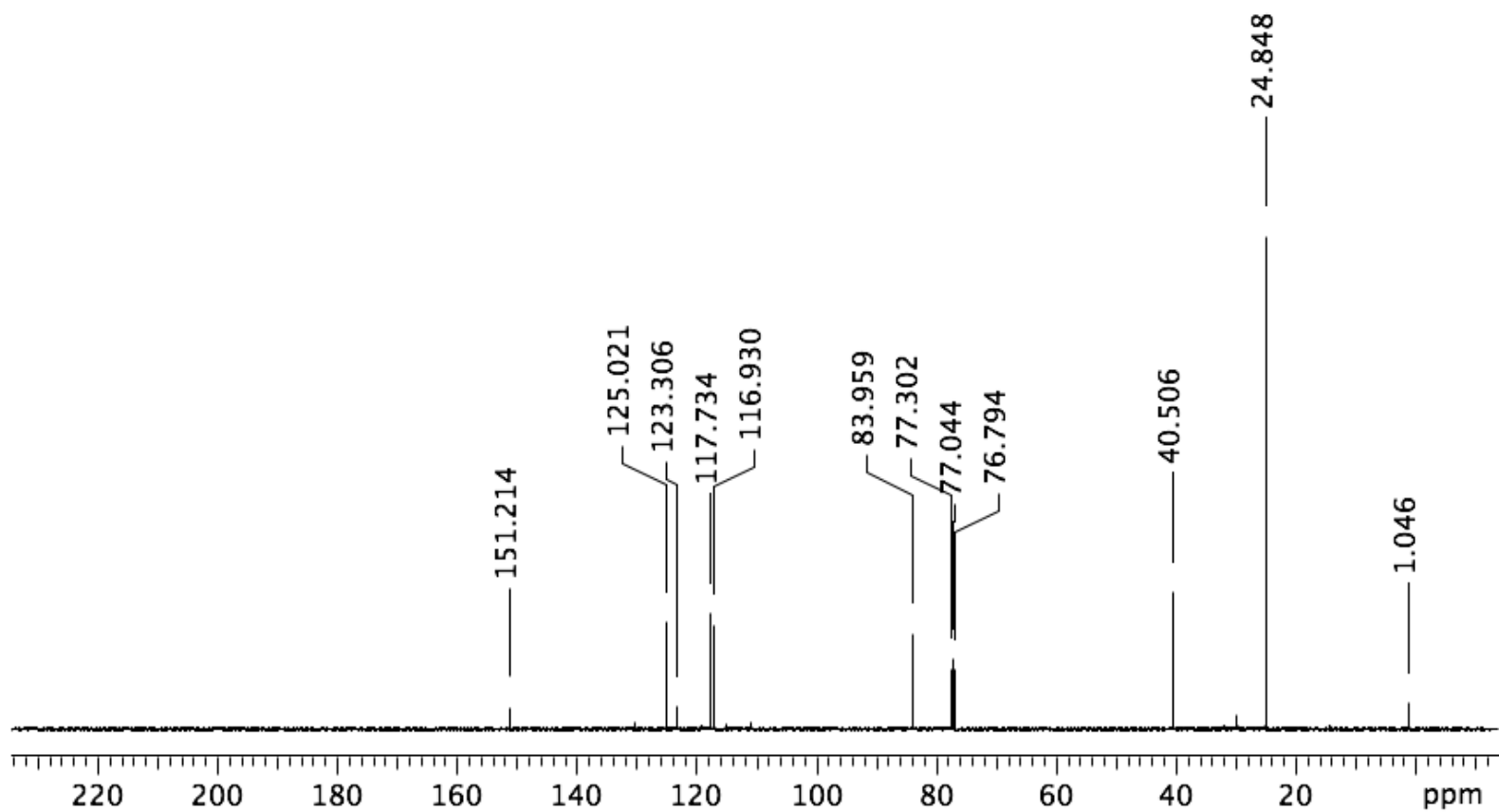
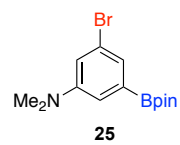


Figure 61. ^{13}C NMR of 25

^1H NMR in CDCl_3 (500 MHz)

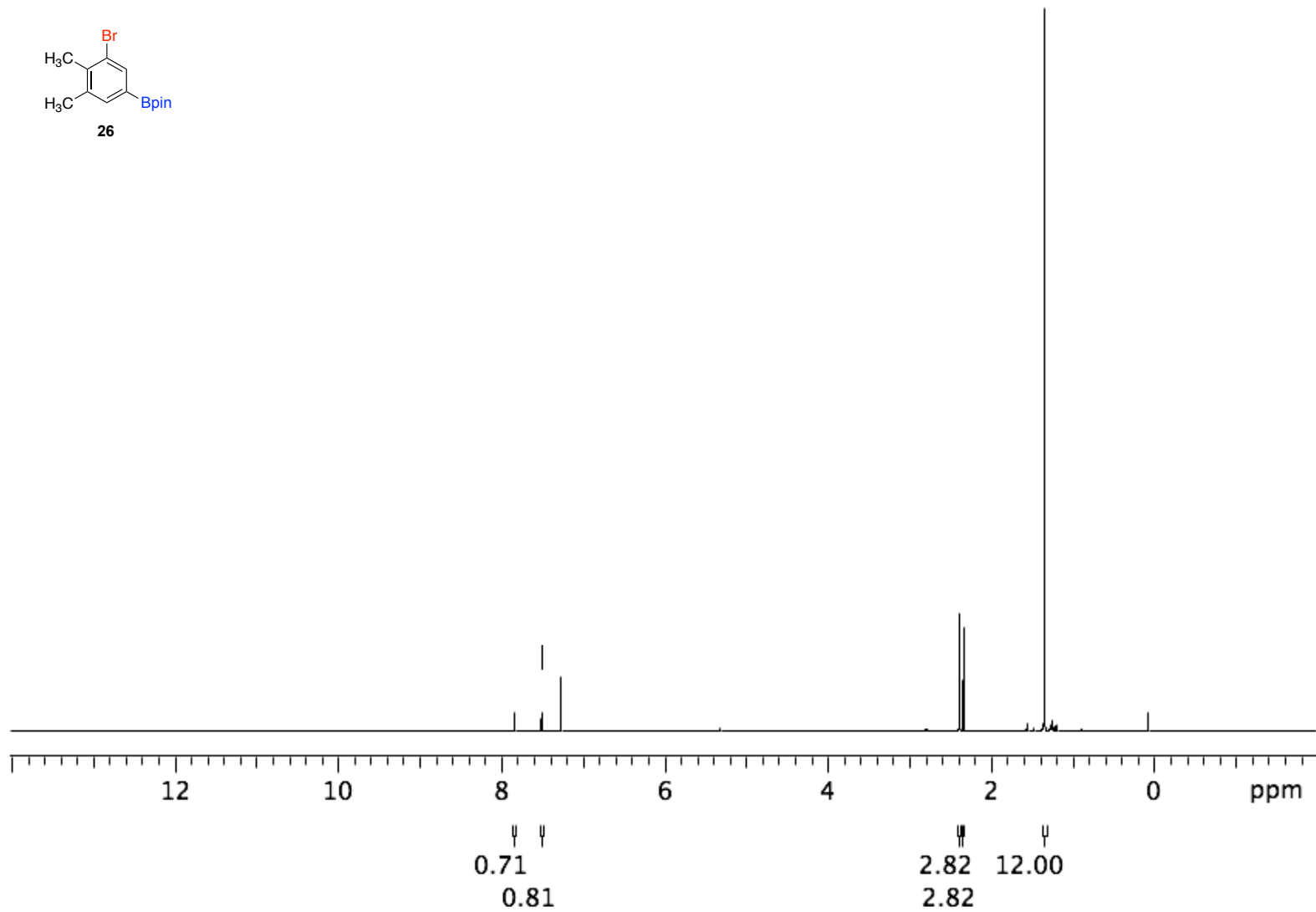
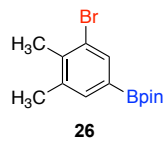


Figure 62. ^1H NMR of 26

^{13}C NMR in CDCl_3 (125 MHz)

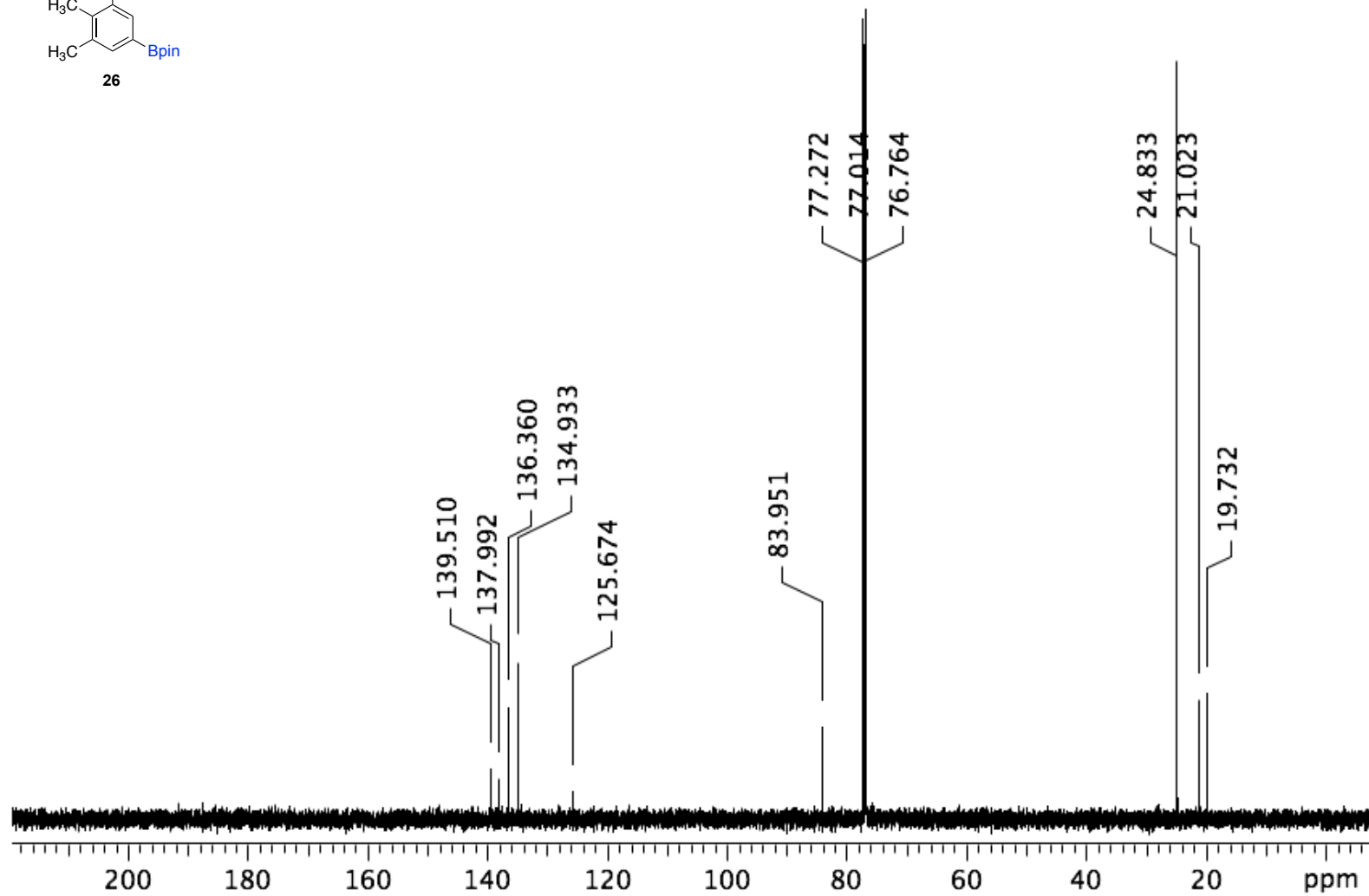
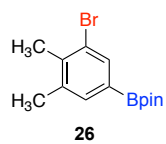


Figure 63. ^{13}C NMR of 26

^1H NMR in CDCl_3 (500 MHz)

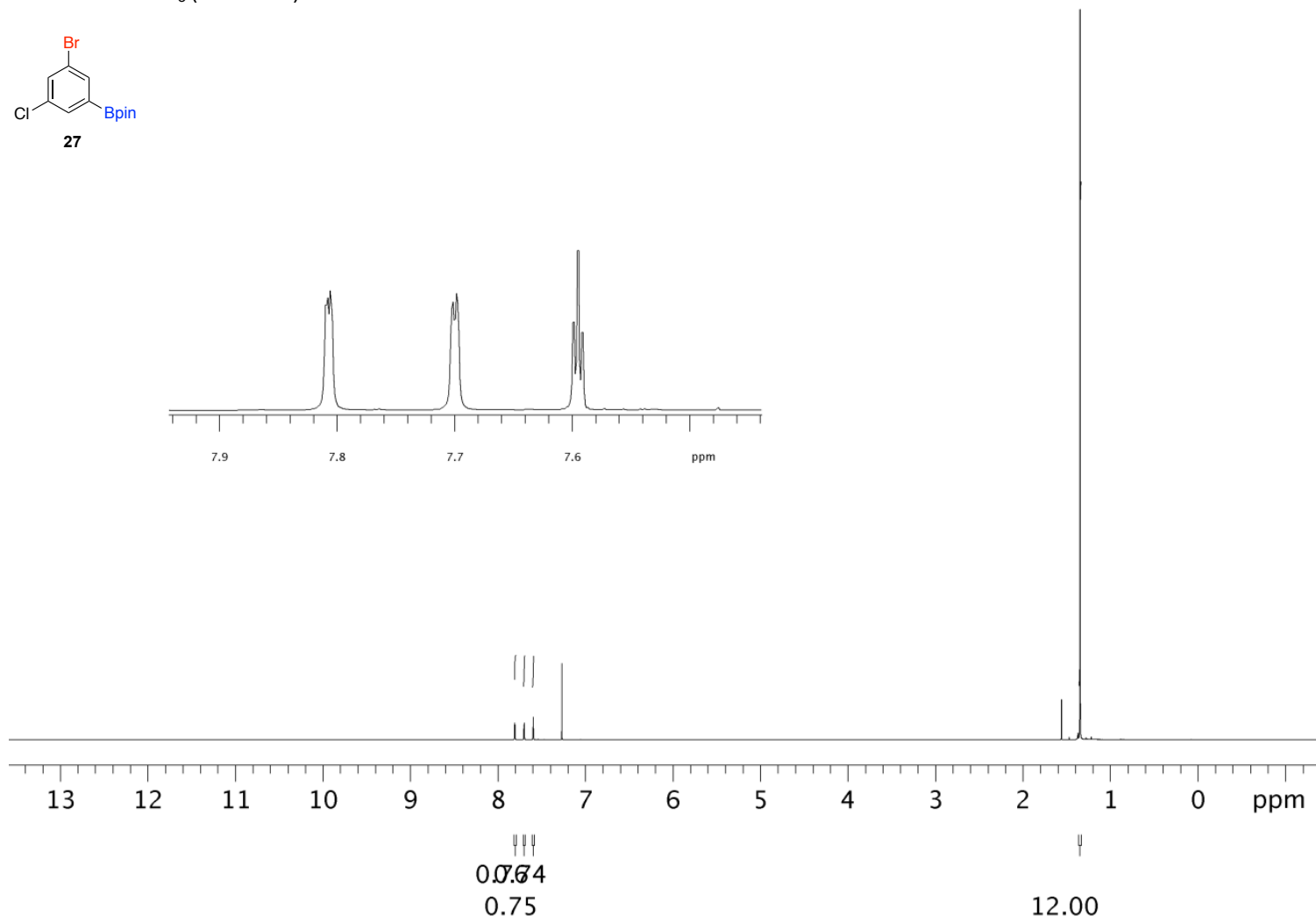
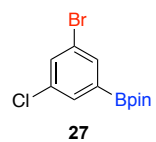


Figure 64. ^1H NMR of **27**

^{13}C NMR in CDCl_3 (125 MHz)

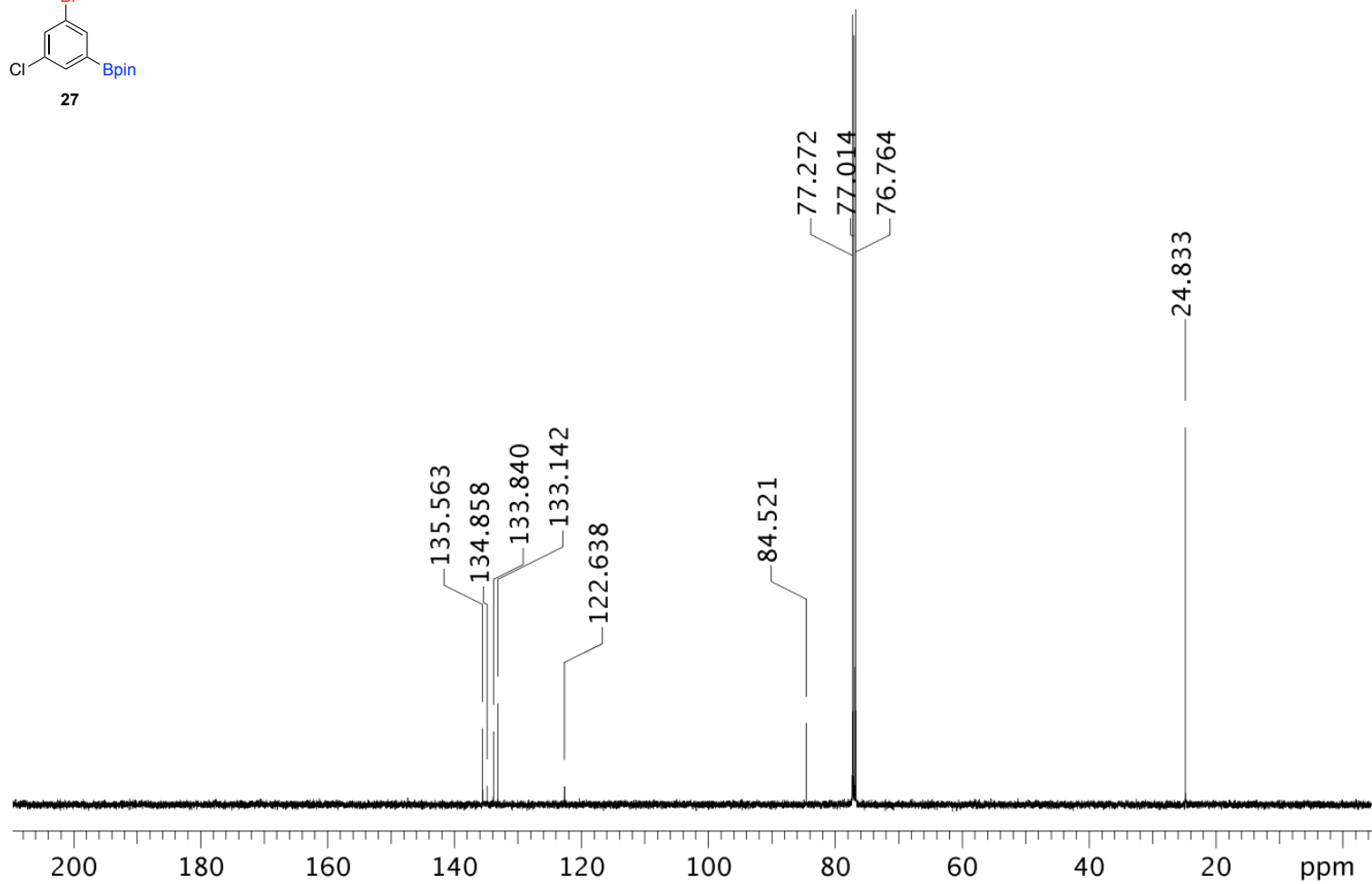
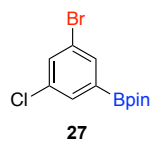


Figure 65. ^{13}C NMR of 27

^1H NMR in CDCl_3 (500 MHz)

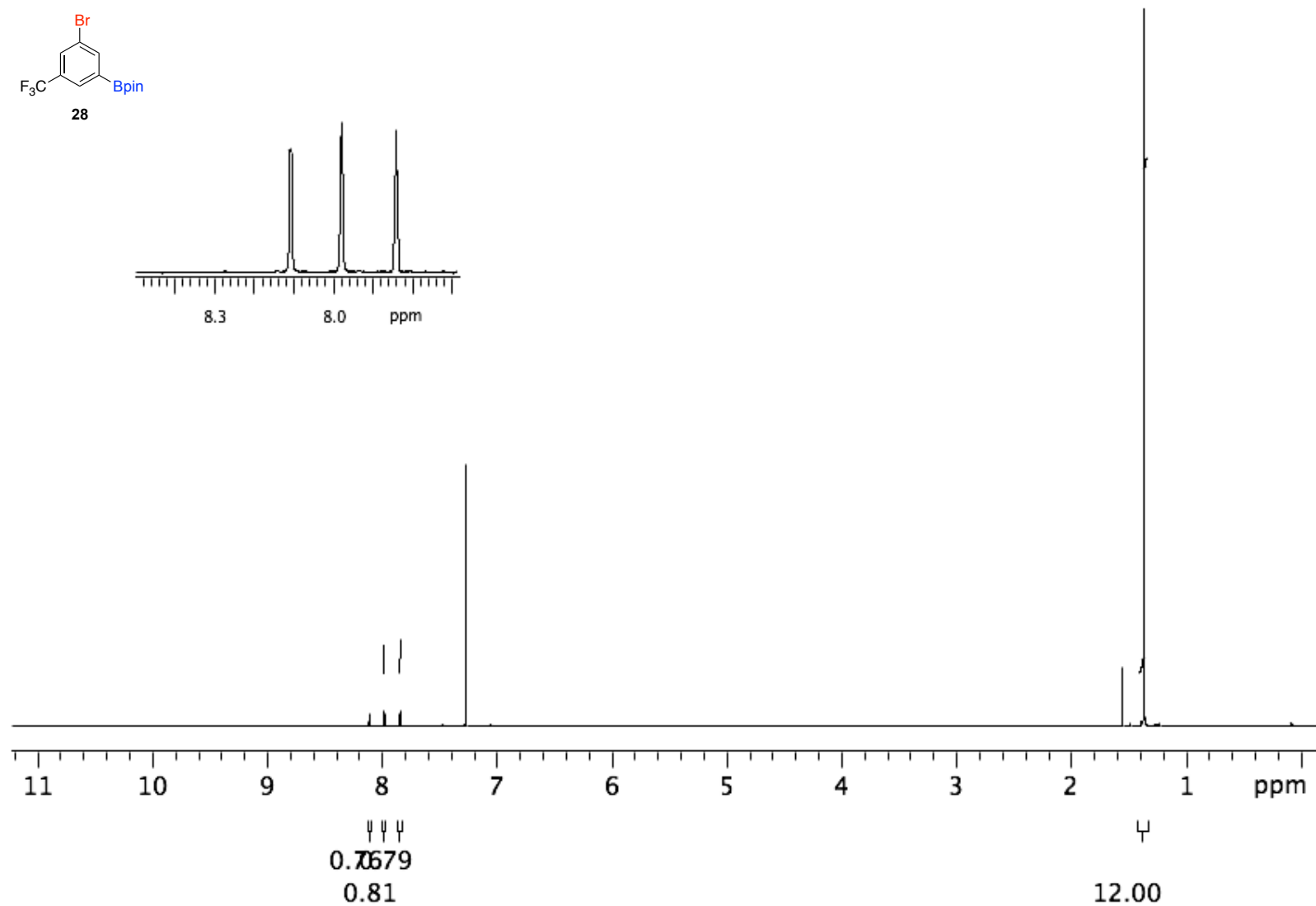
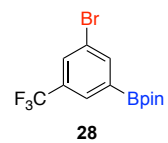


Figure 66. ^1H NMR of 28

^{13}C NMR in CDCl_3 (125 MHz)

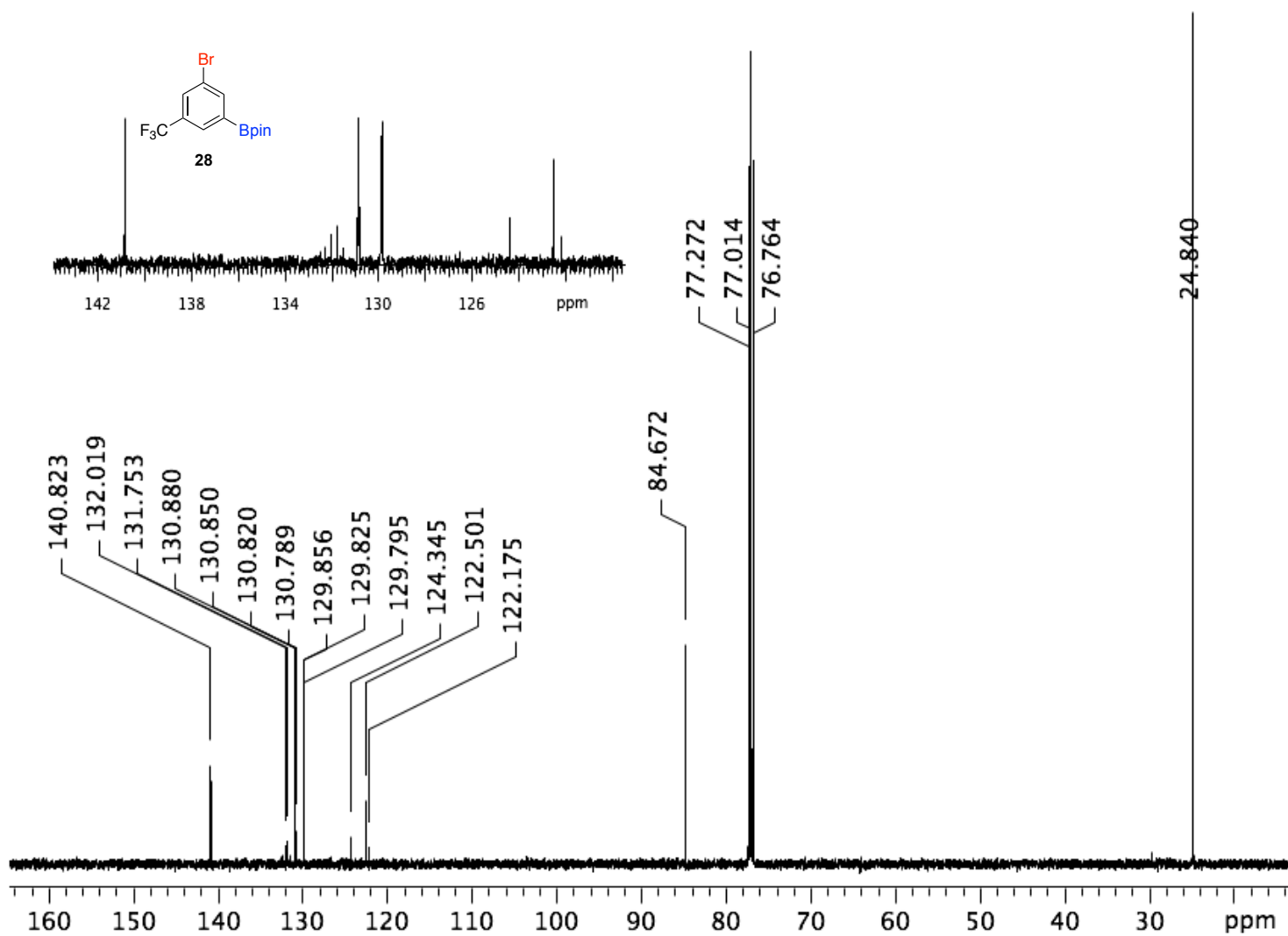


Figure 67. ^{13}C NMR of 28

^1H NMR in CDCl_3 (500 MHz)

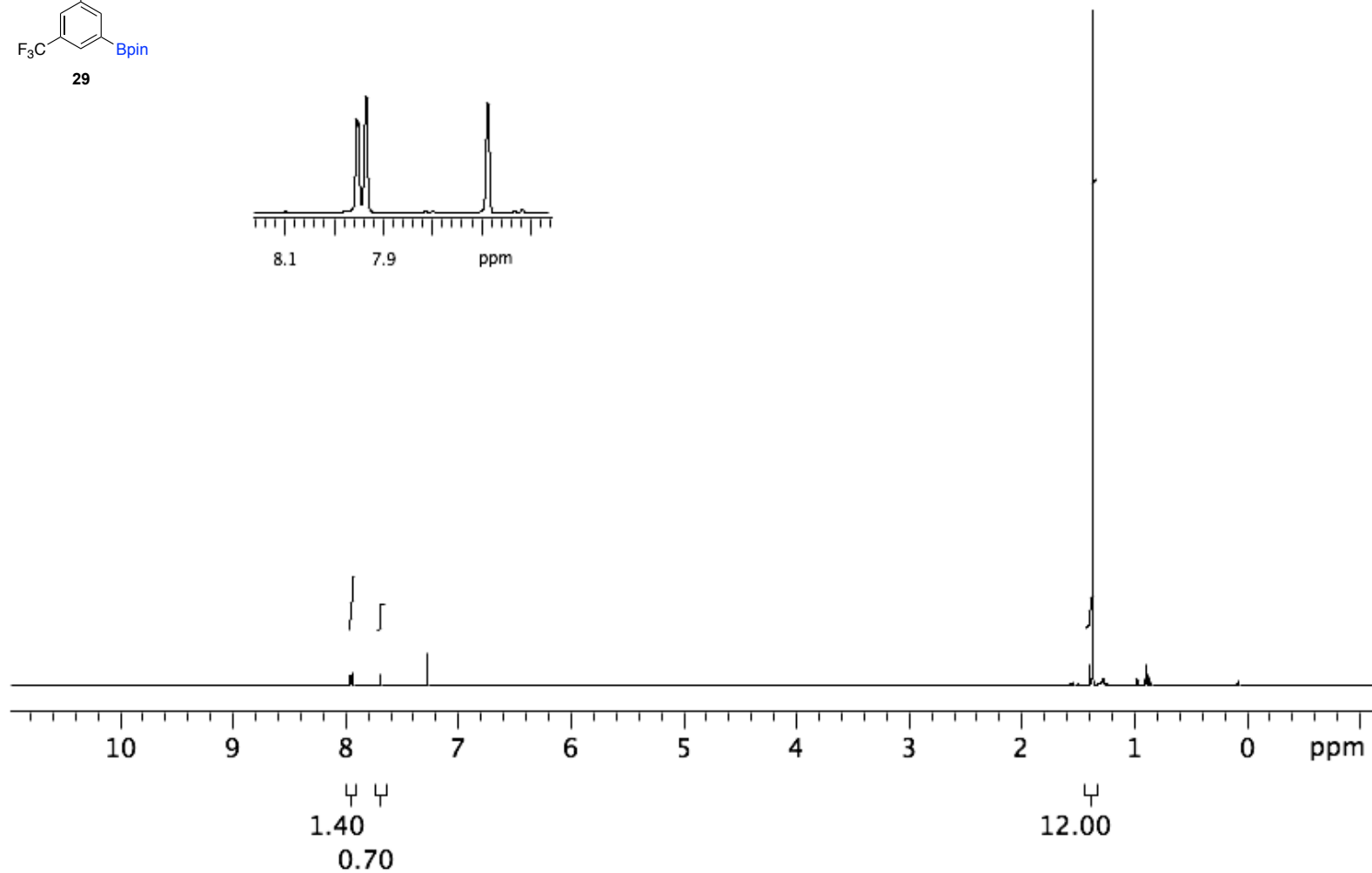
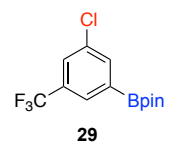


Figure 68. ^1H NMR of 29

^{13}C NMR in CDCl_3 (125 MHz)

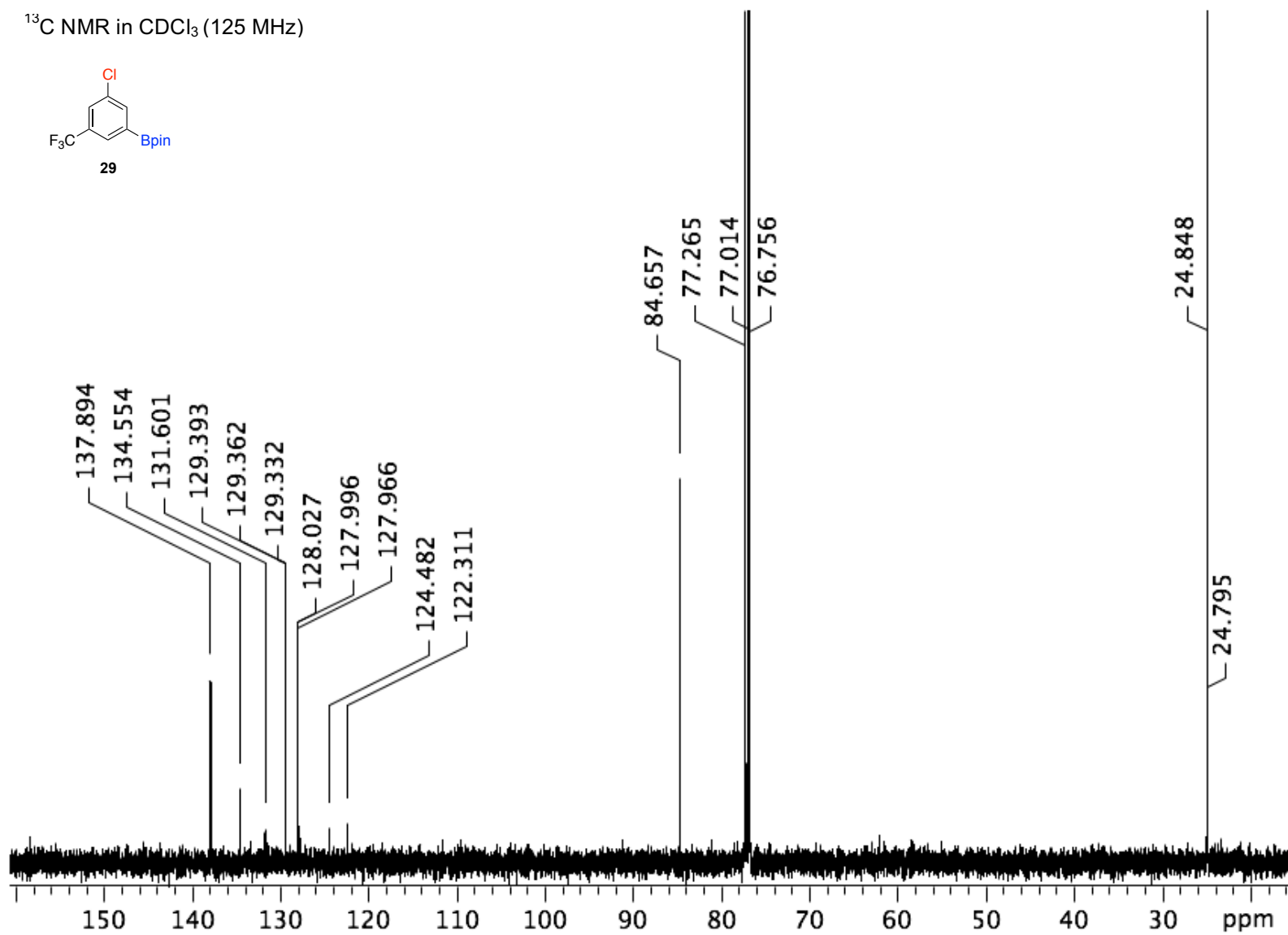
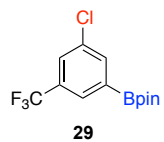


Figure 69. ^{13}C NMR of 29

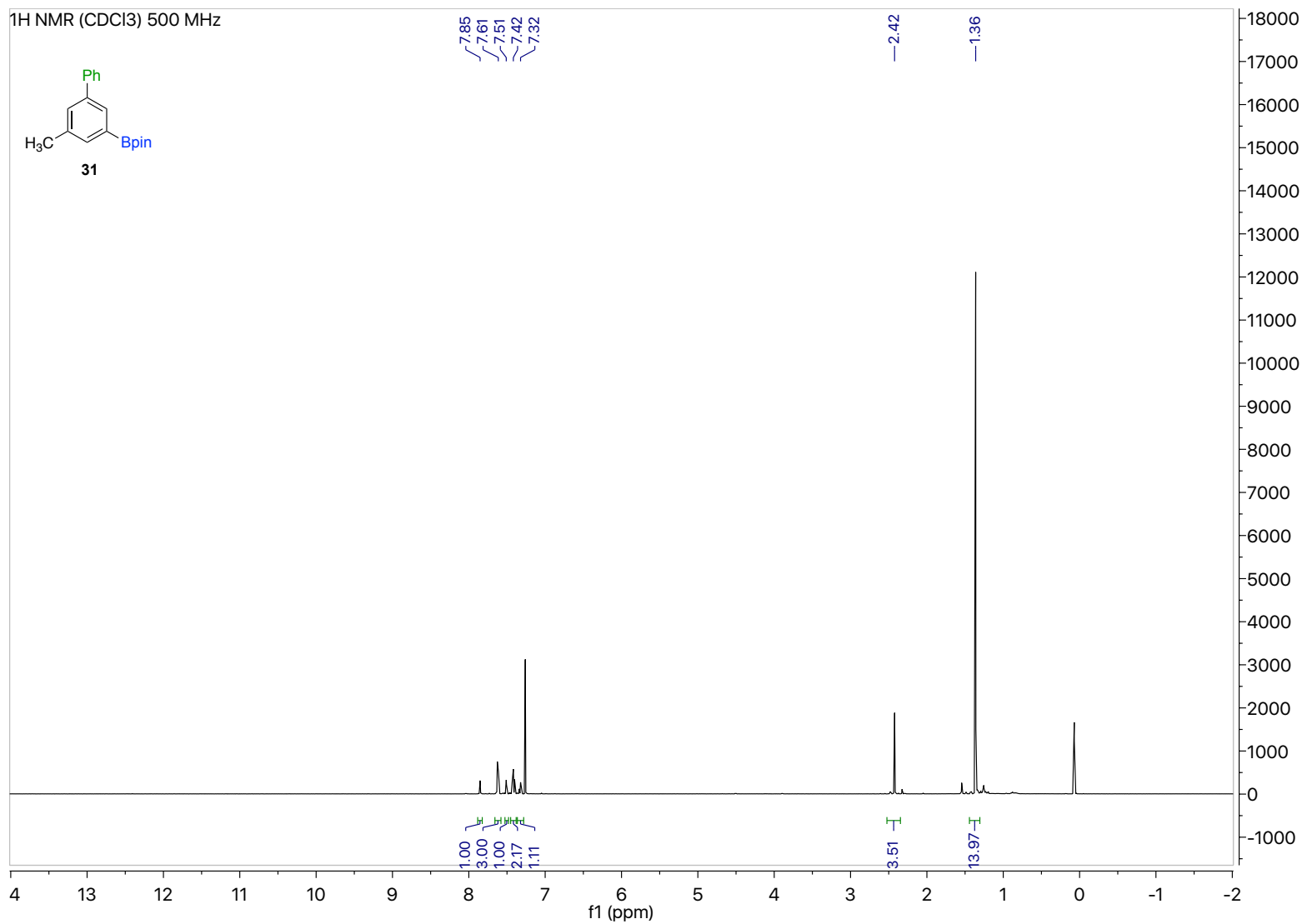


Figure 70. ¹H NMR of **31**

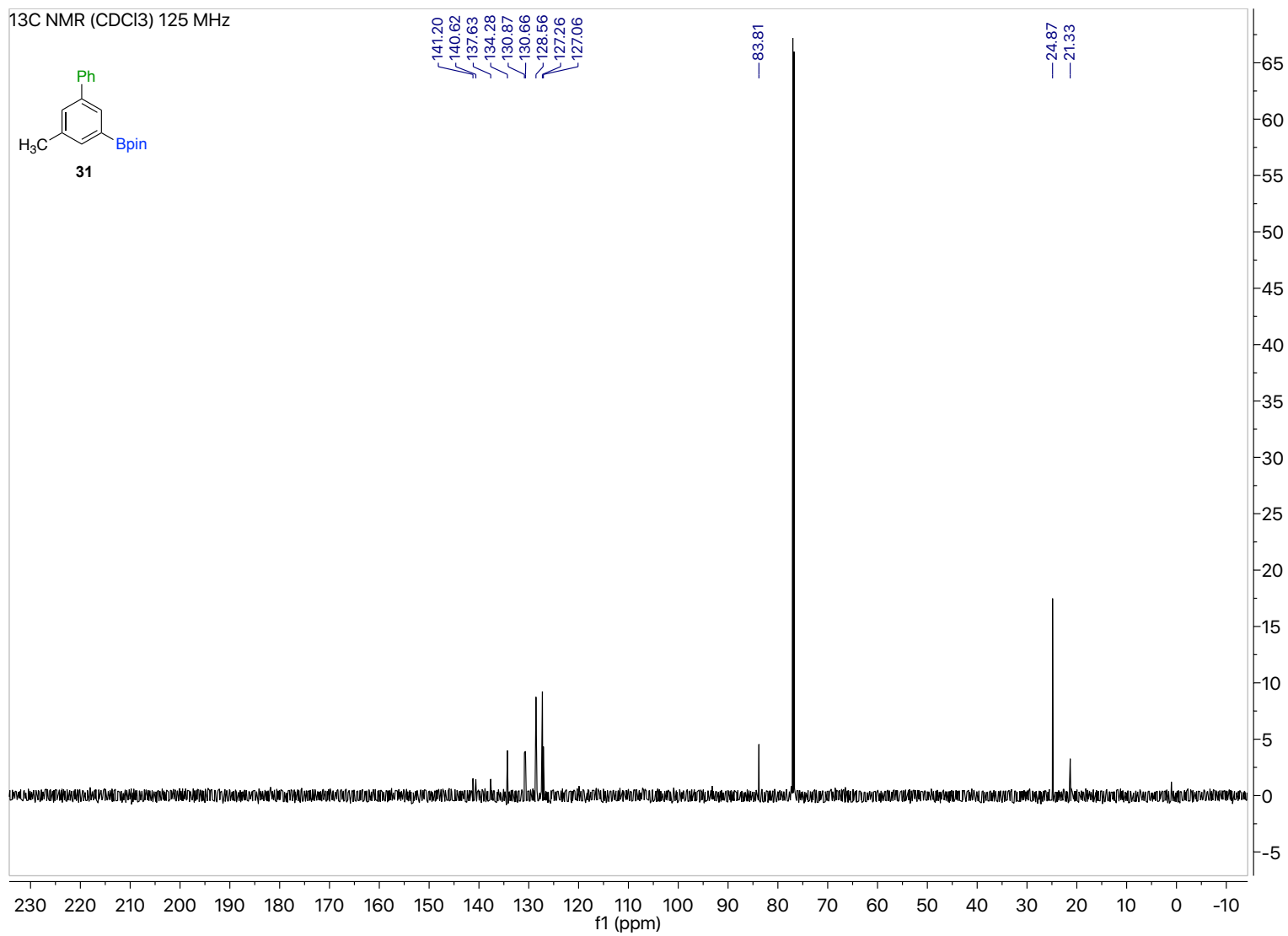


Figure 71. ¹³C NMR of **31**

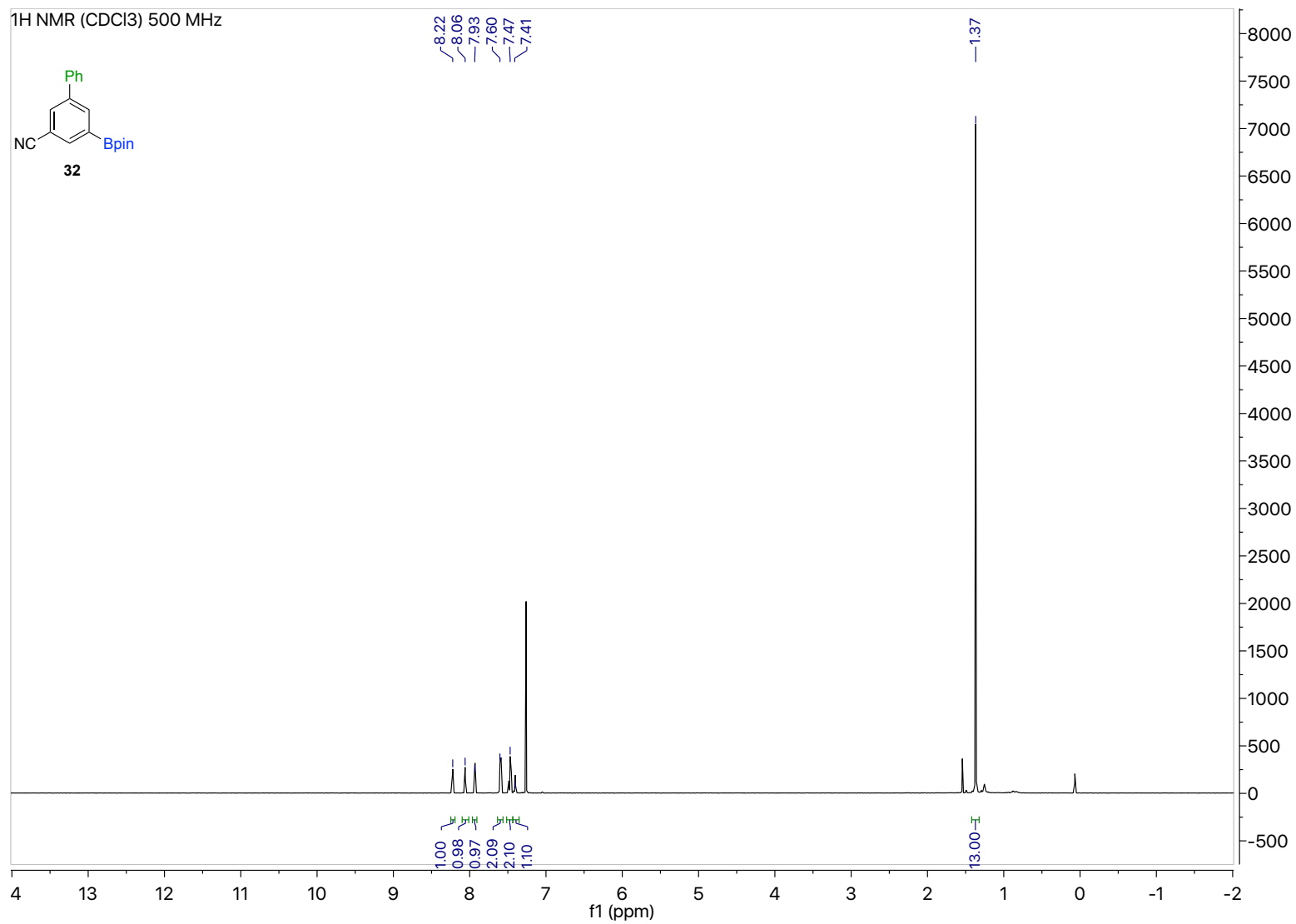


Figure 72. ¹H NMR of 32

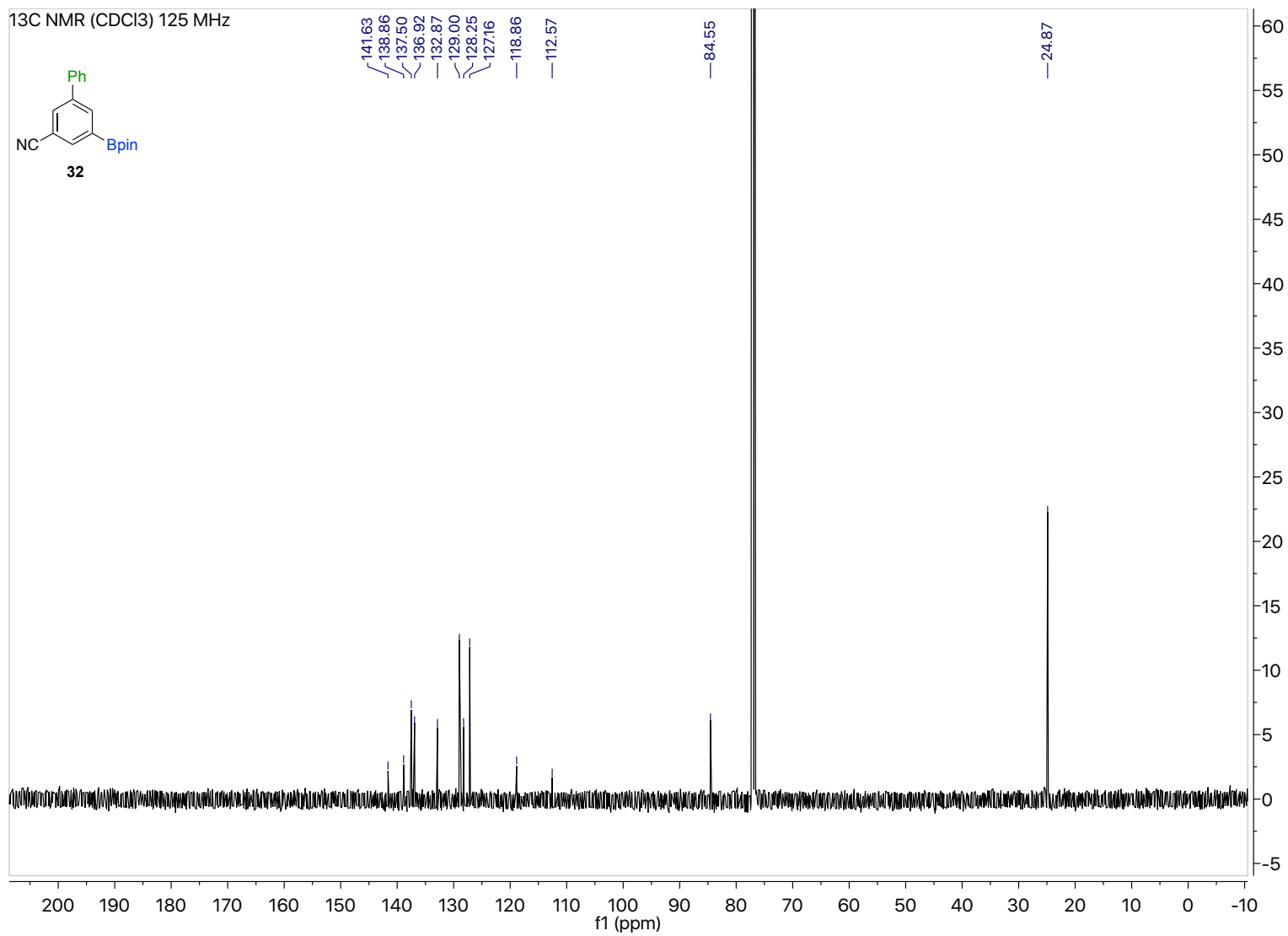


Figure 73. ¹³C NMR of **32**

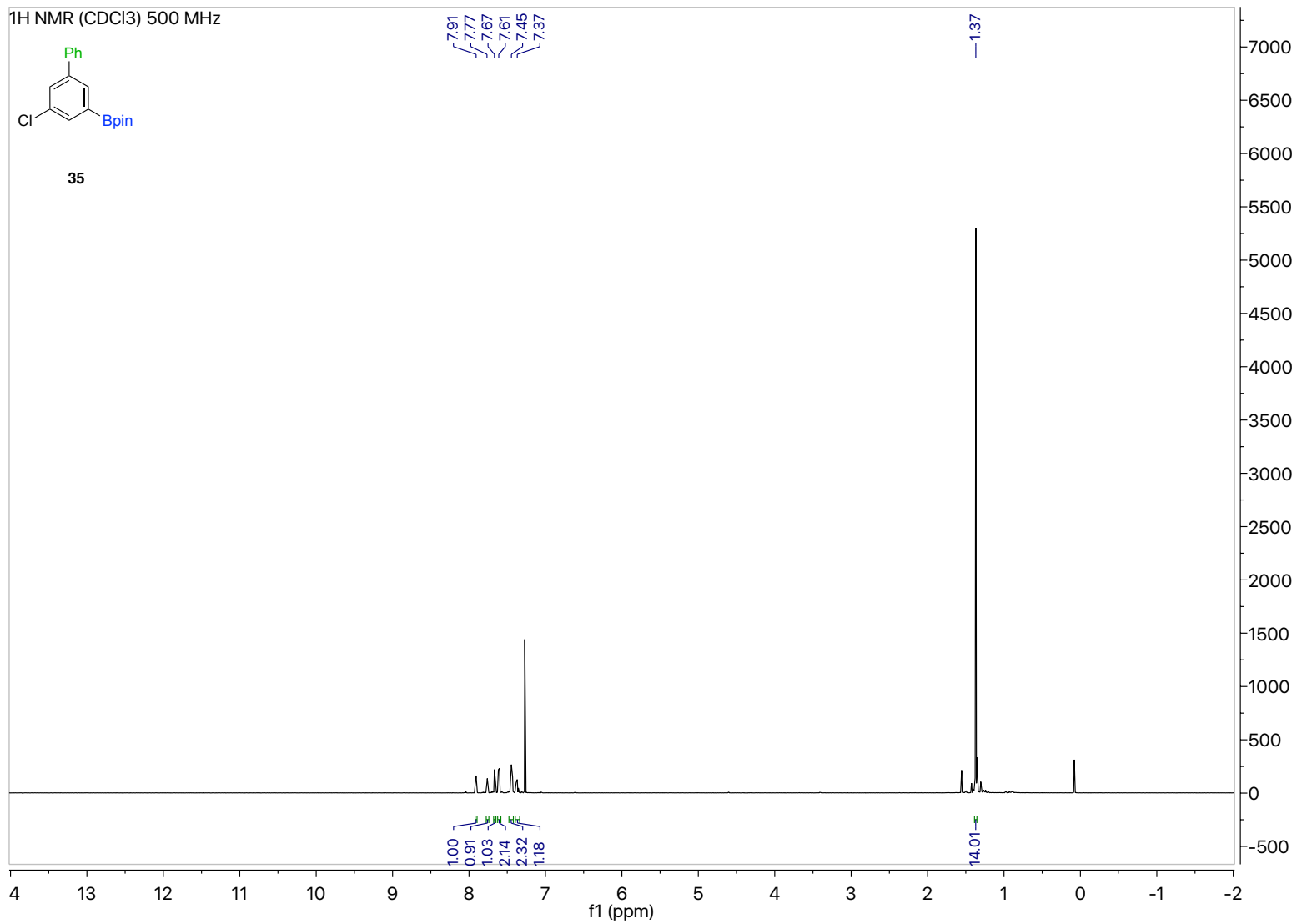


Figure 74. ¹H NMR of **35**

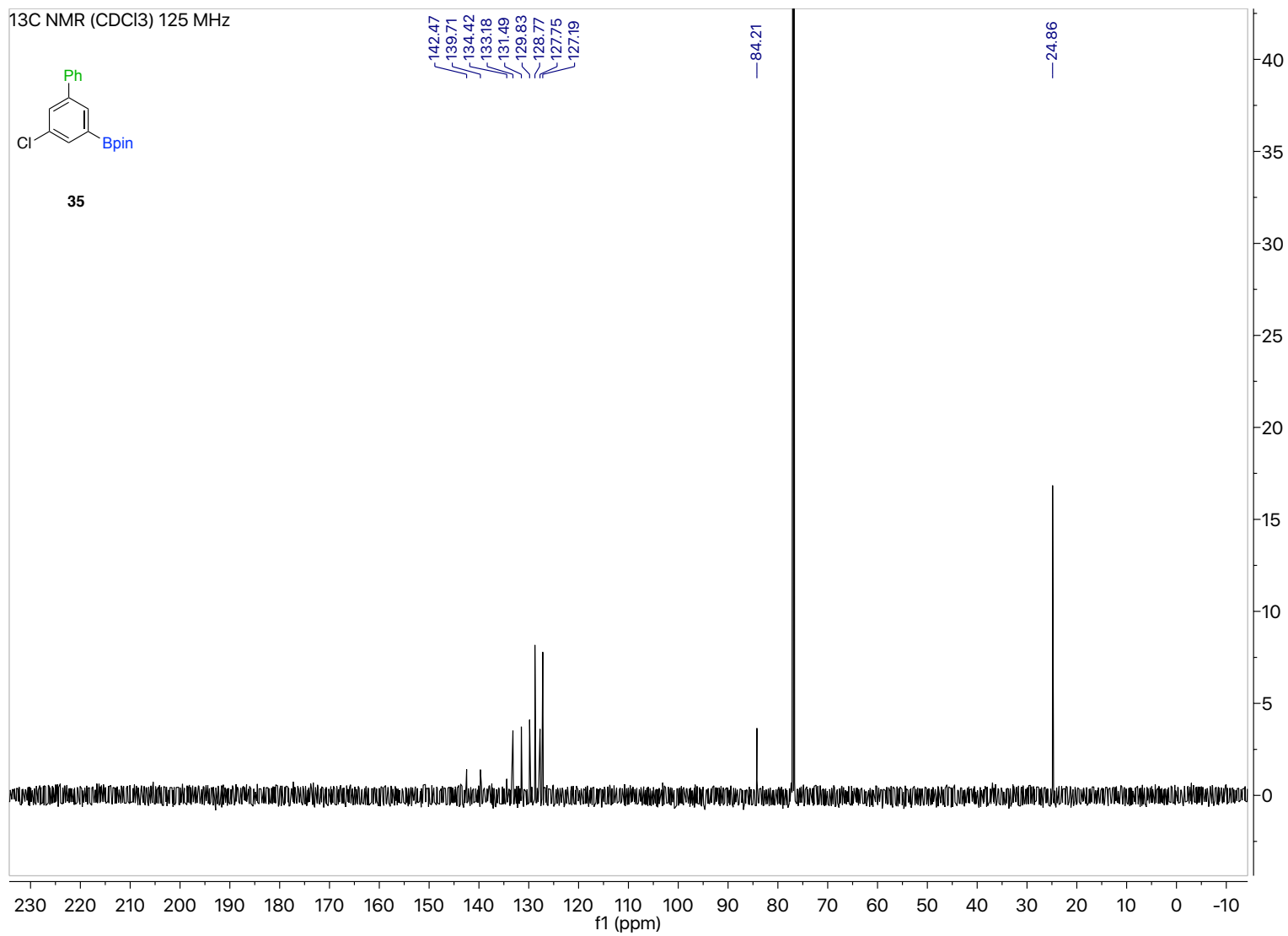


Figure 75. ¹³C NMR of 35

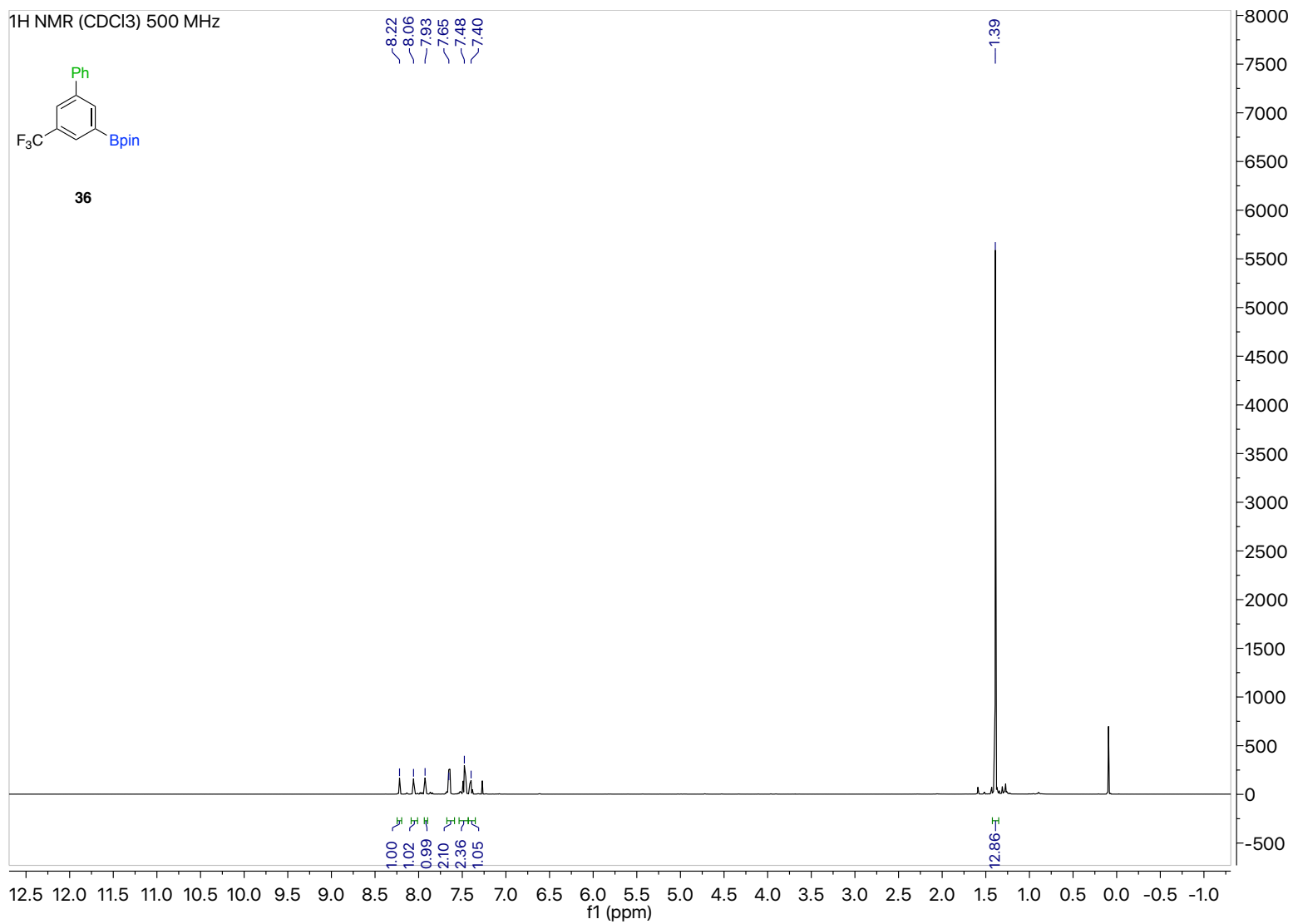


Figure 76. ¹H NMR of **36**

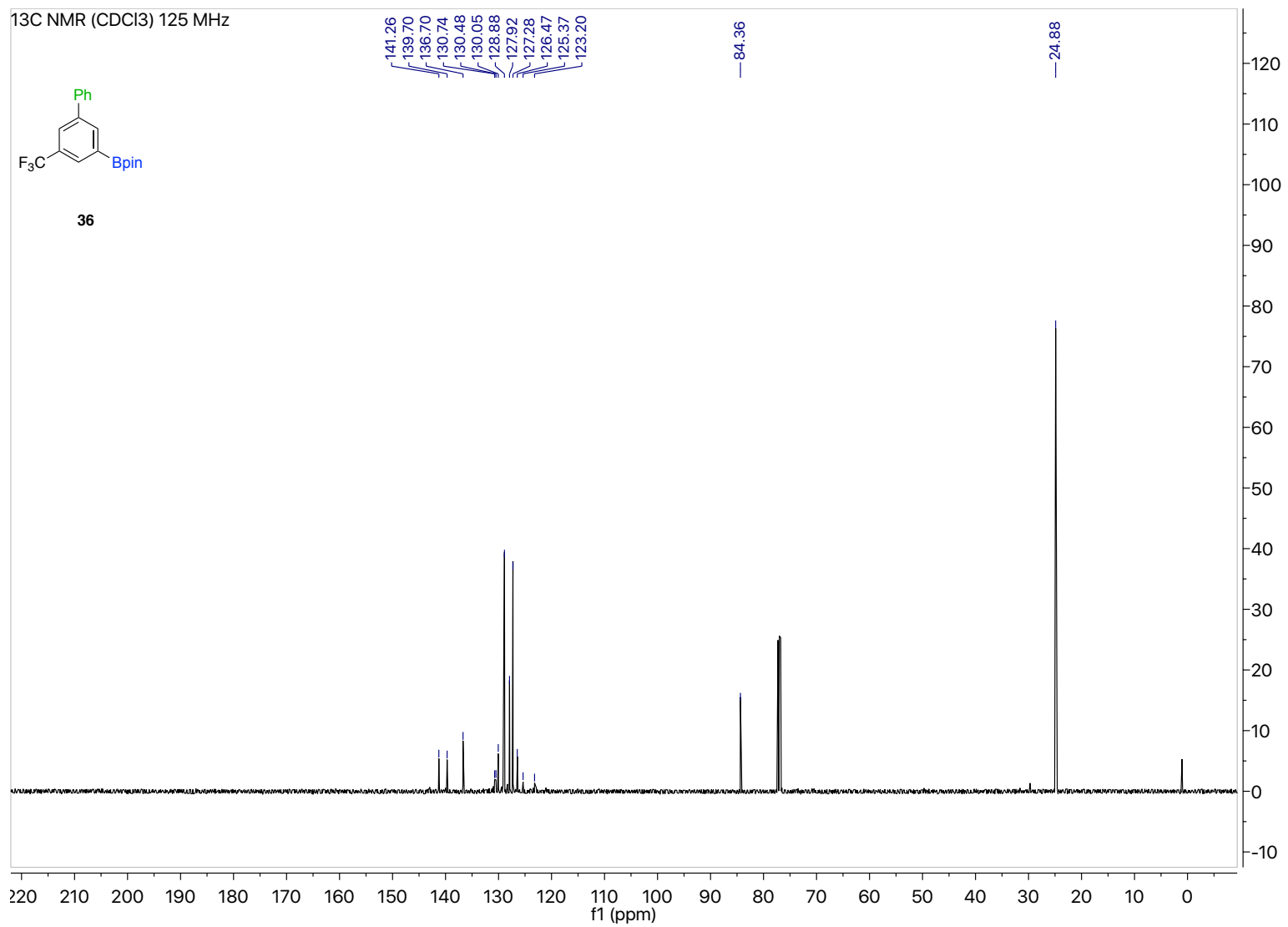


Figure 77. ¹³C NMR of 36

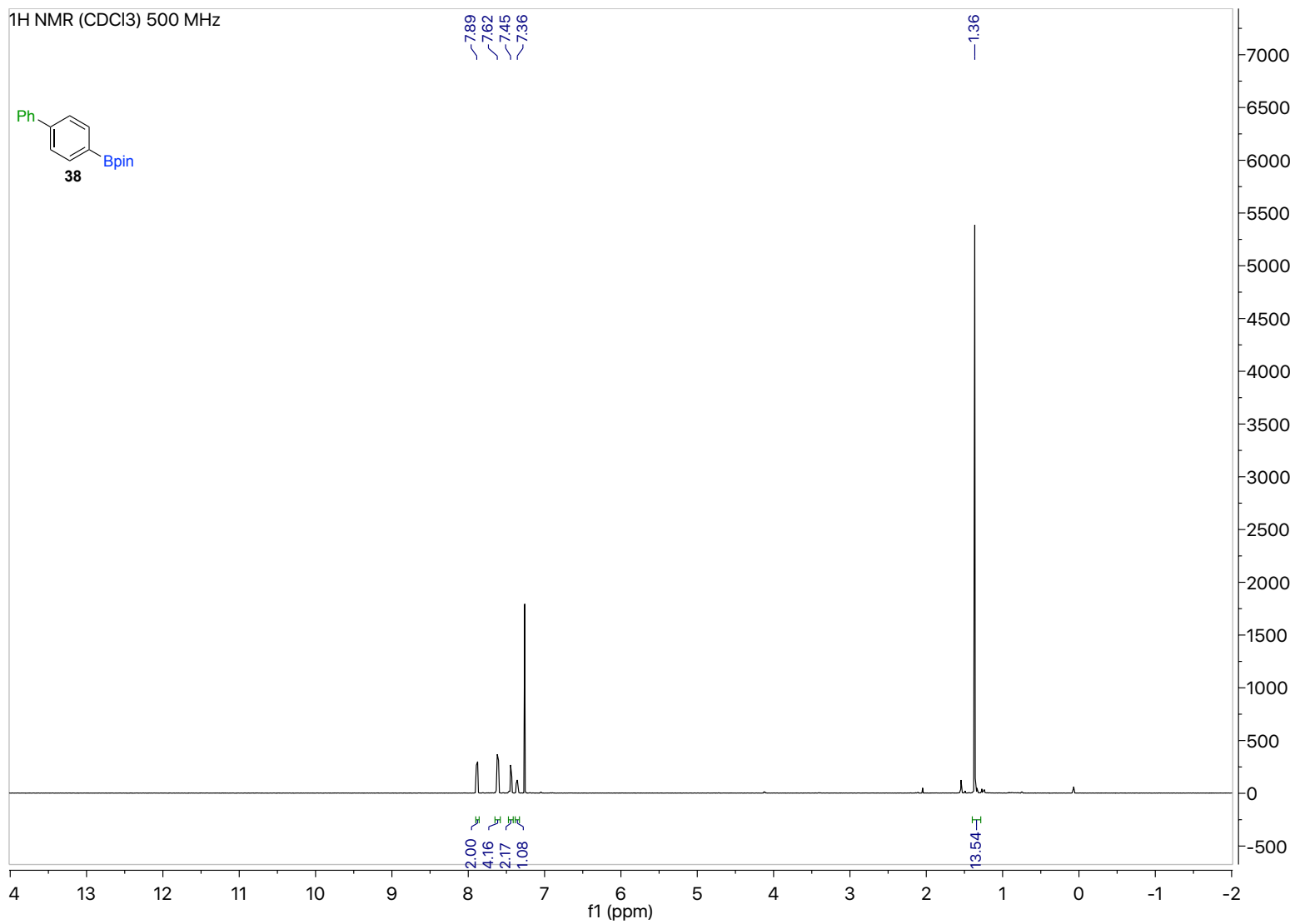


Figure 78. ¹H NMR of **38**

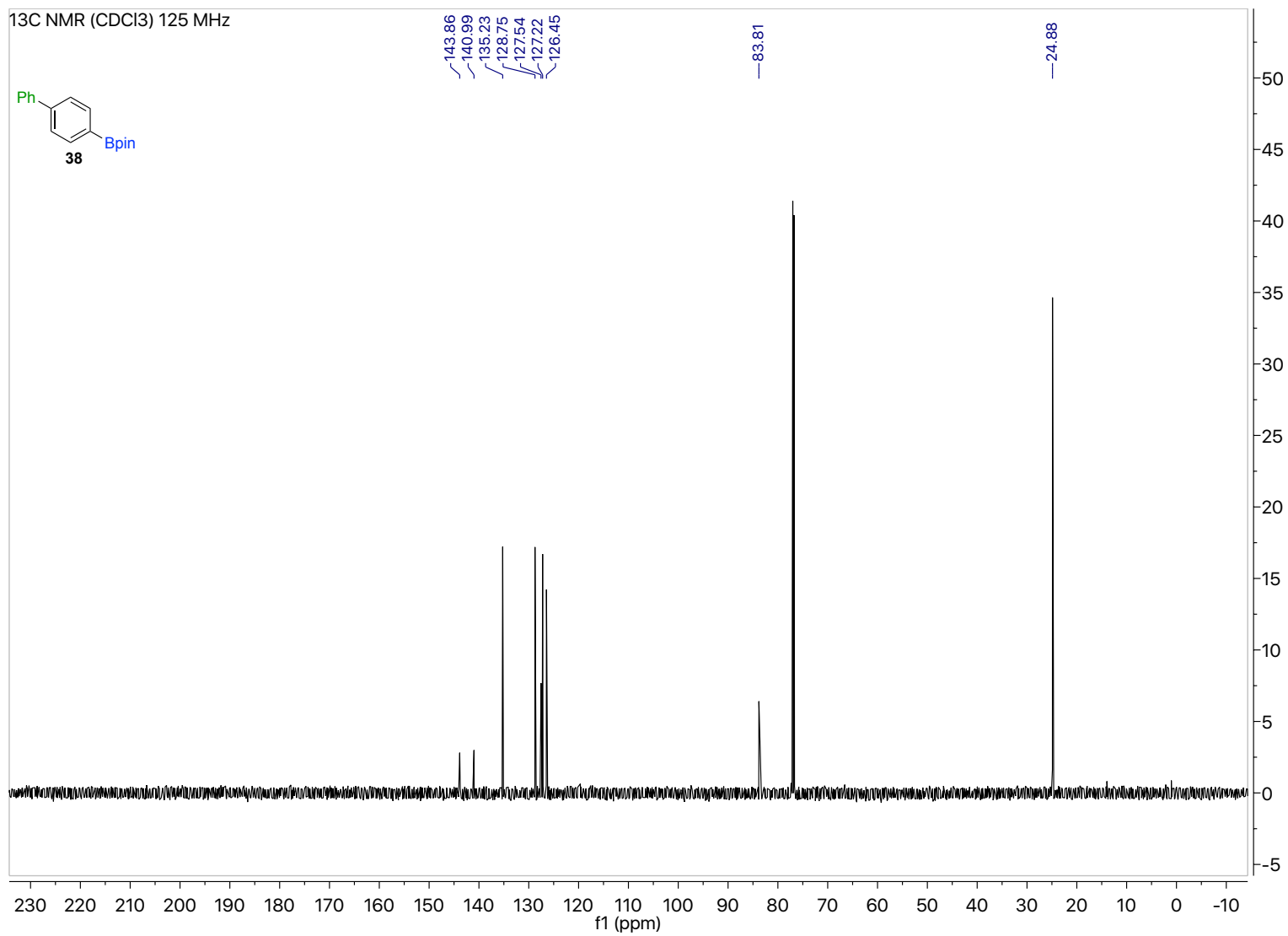


Figure 79. ¹³C NMR of 38

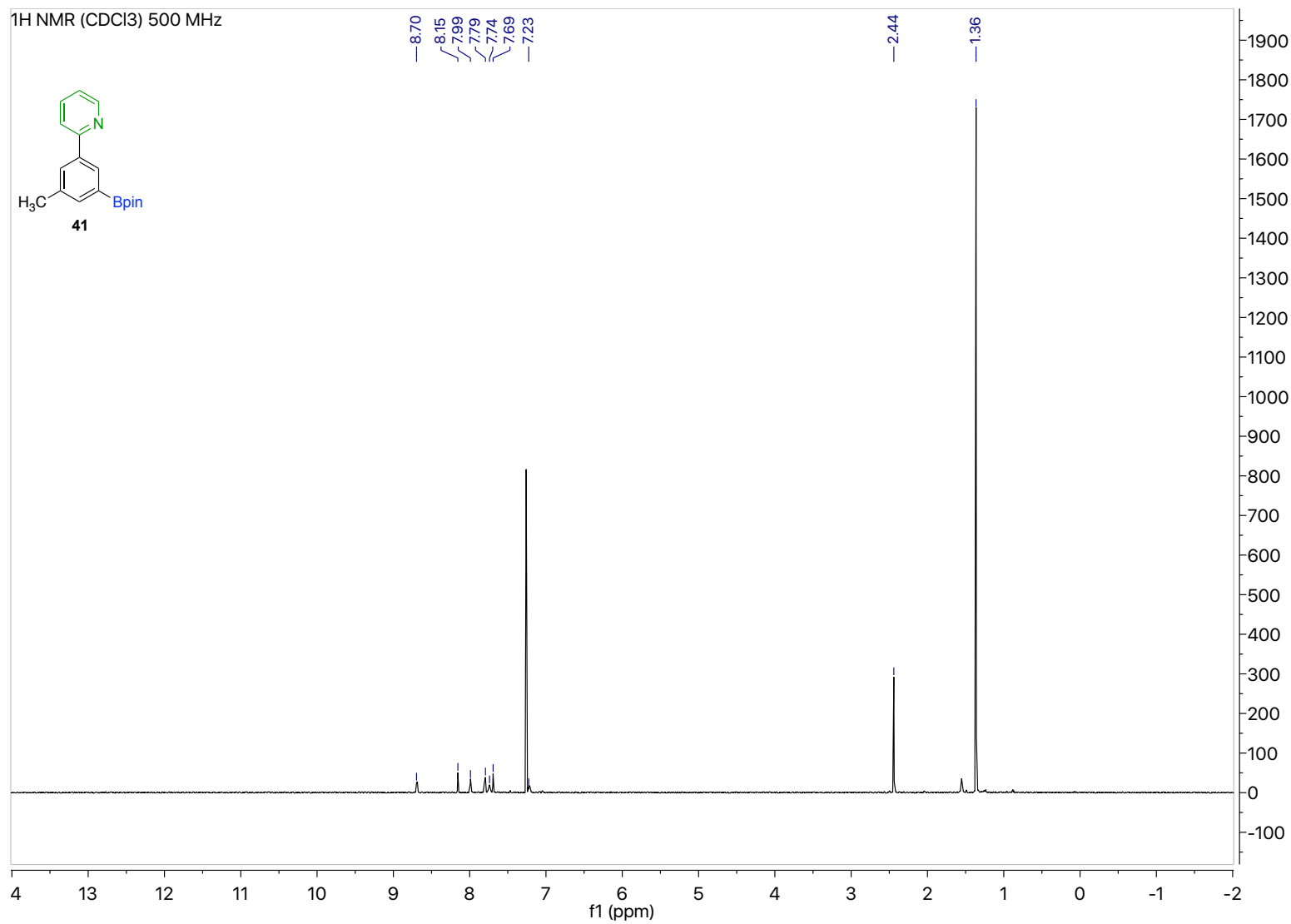


Figure 80. ¹H NMR of **41**

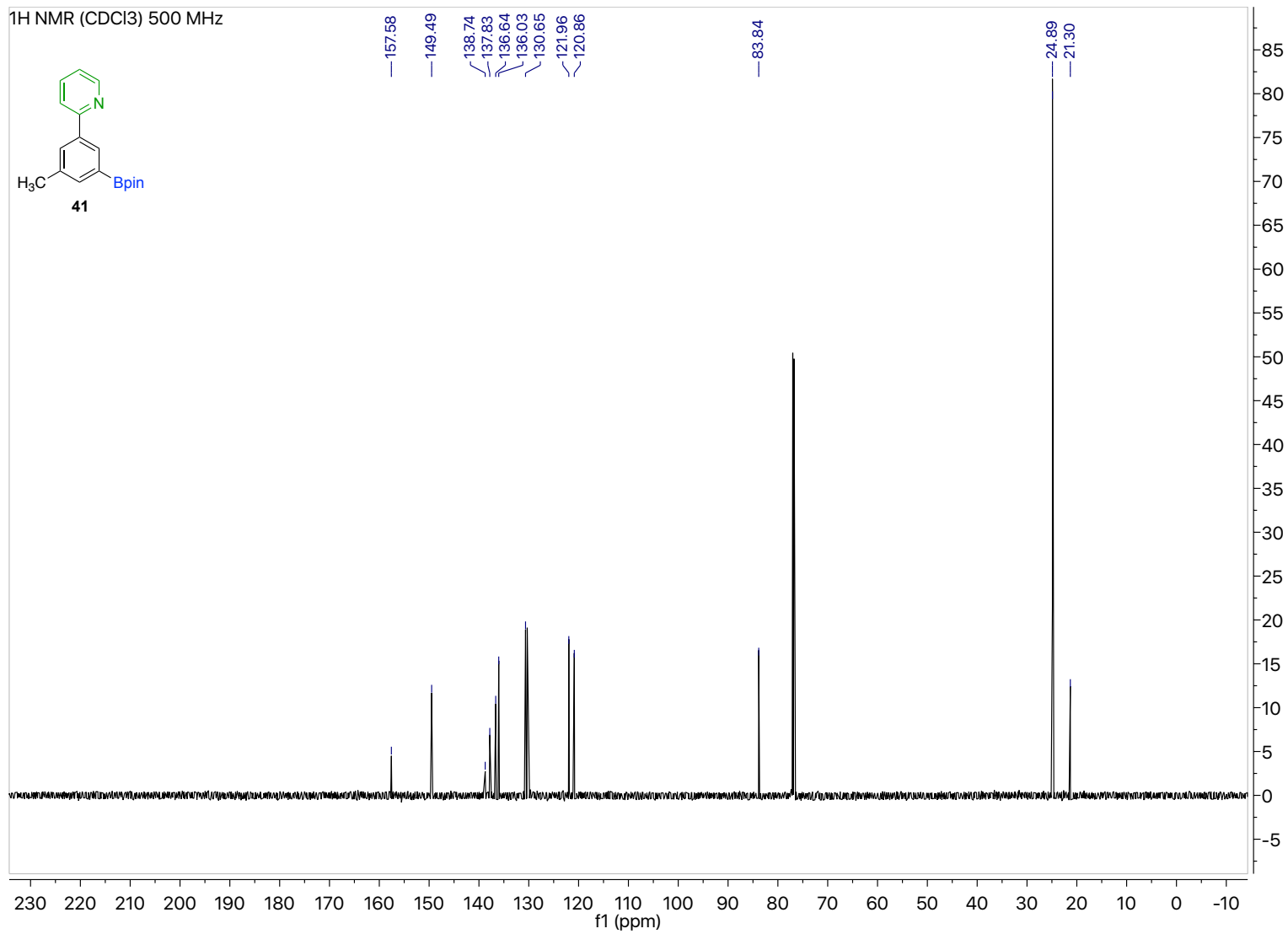


Figure 81. ¹³C NMR of 41

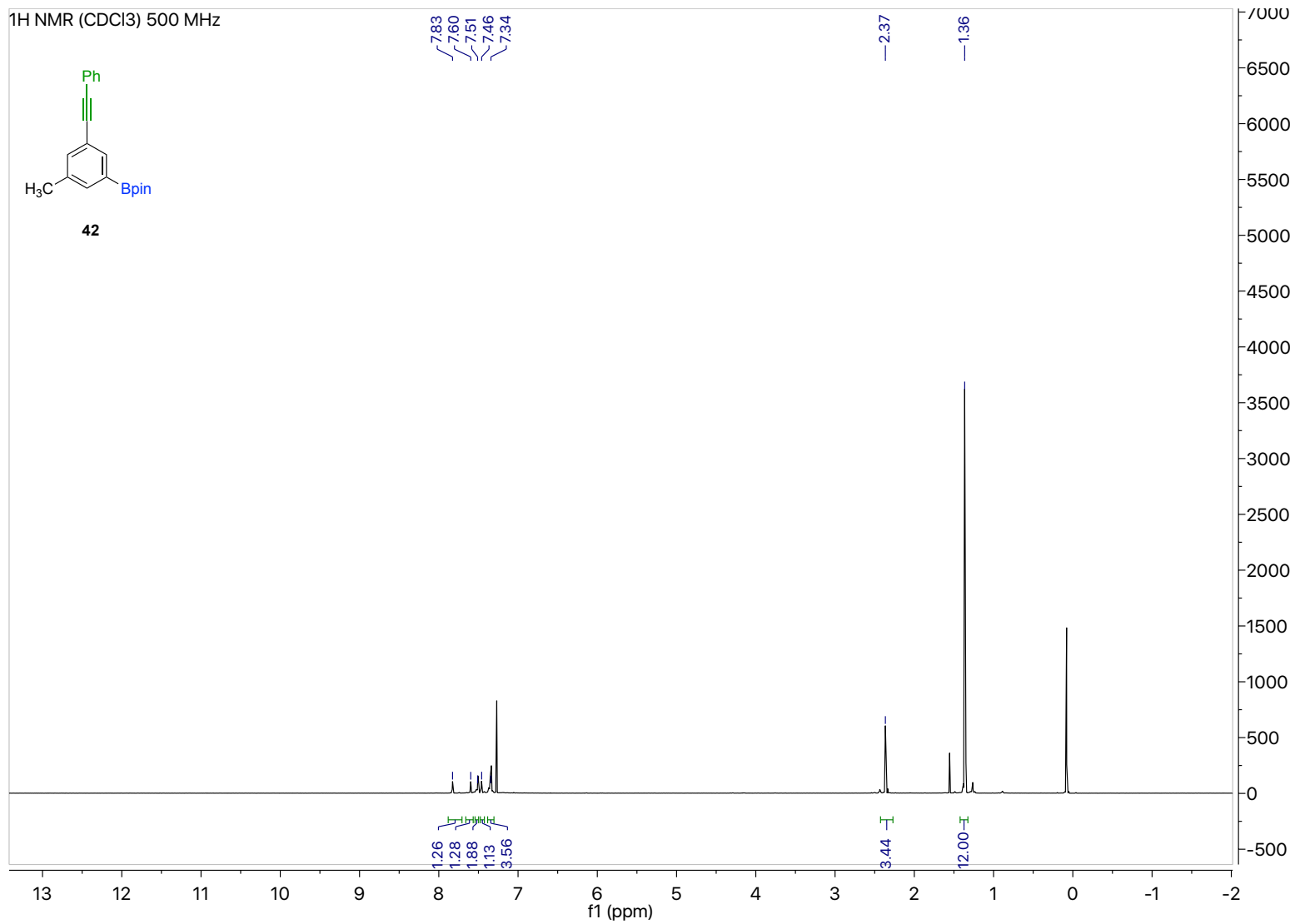


Figure 82. ¹H NMR of **42**

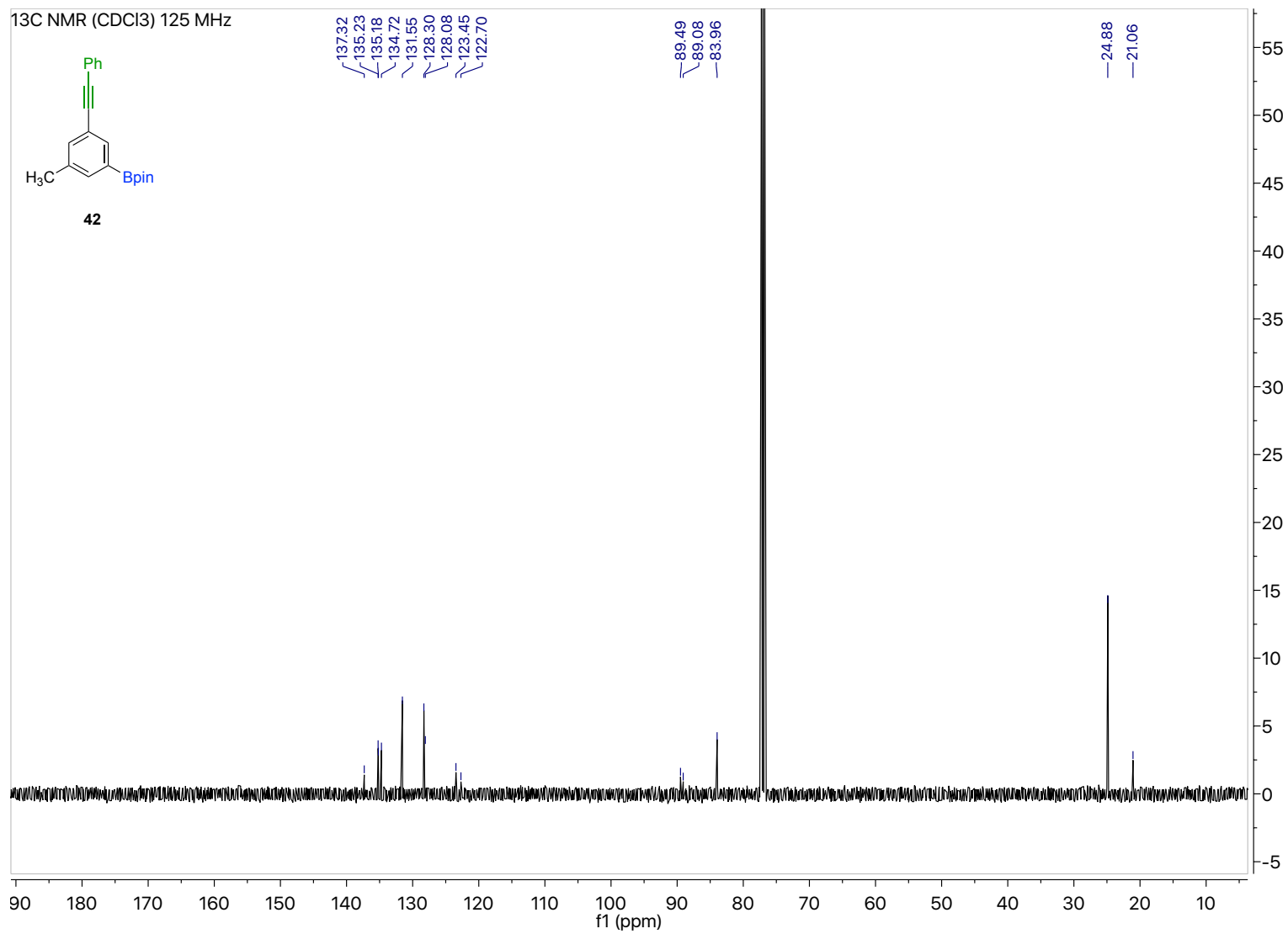


Figure 83. ¹³C NMR of 42

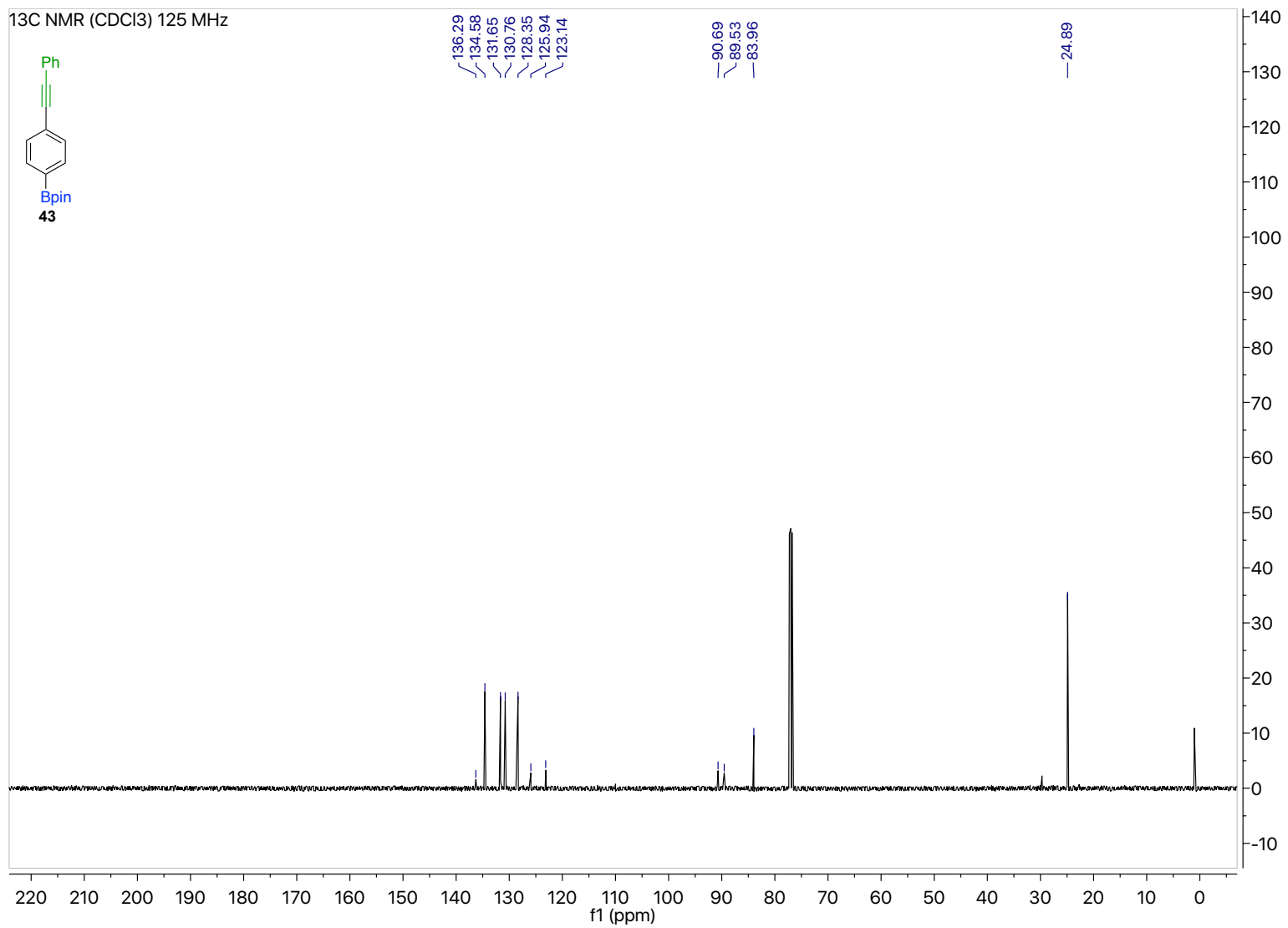


Figure 85. ¹³C NMR of 43

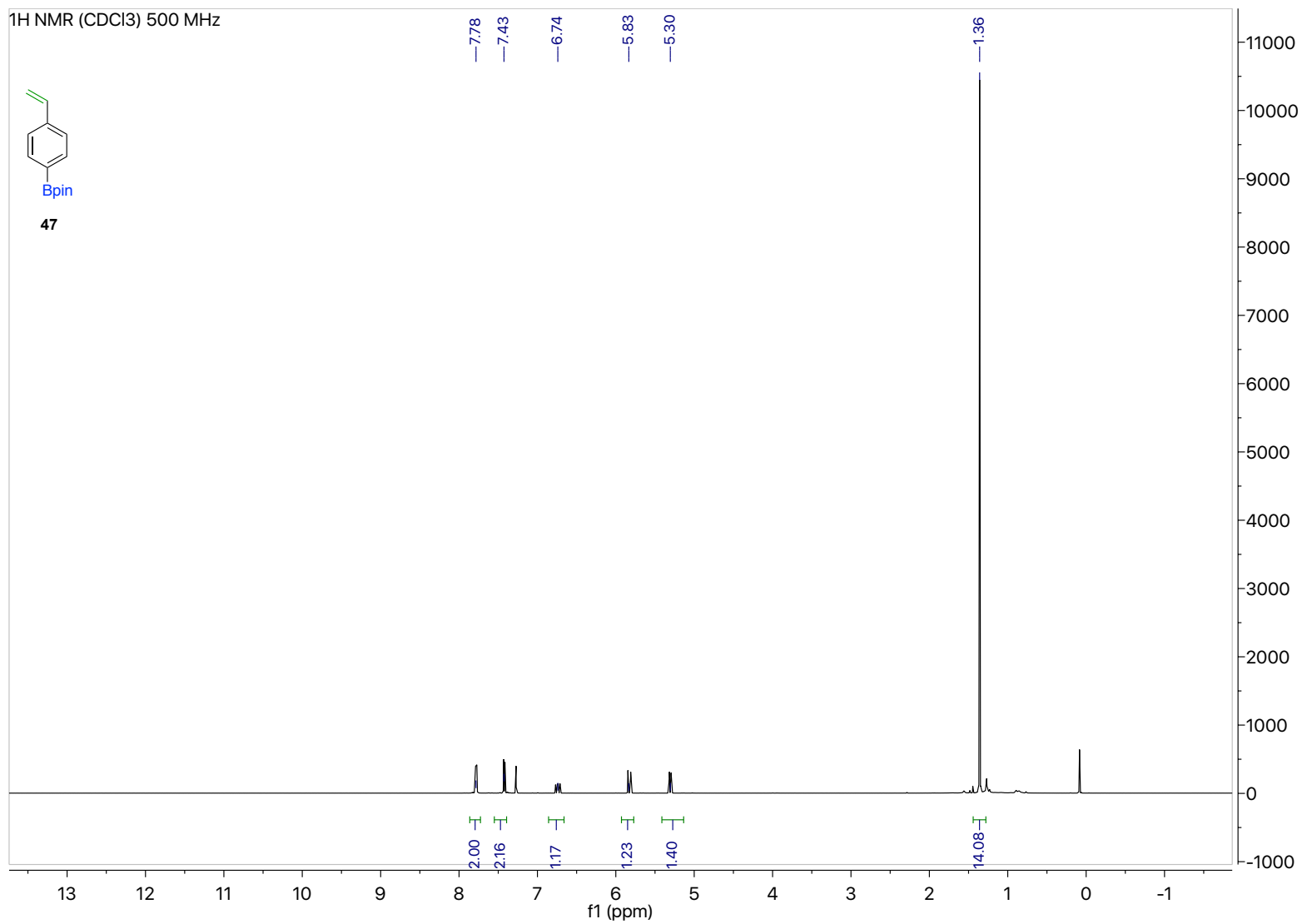


Figure 86. ¹H NMR of 47

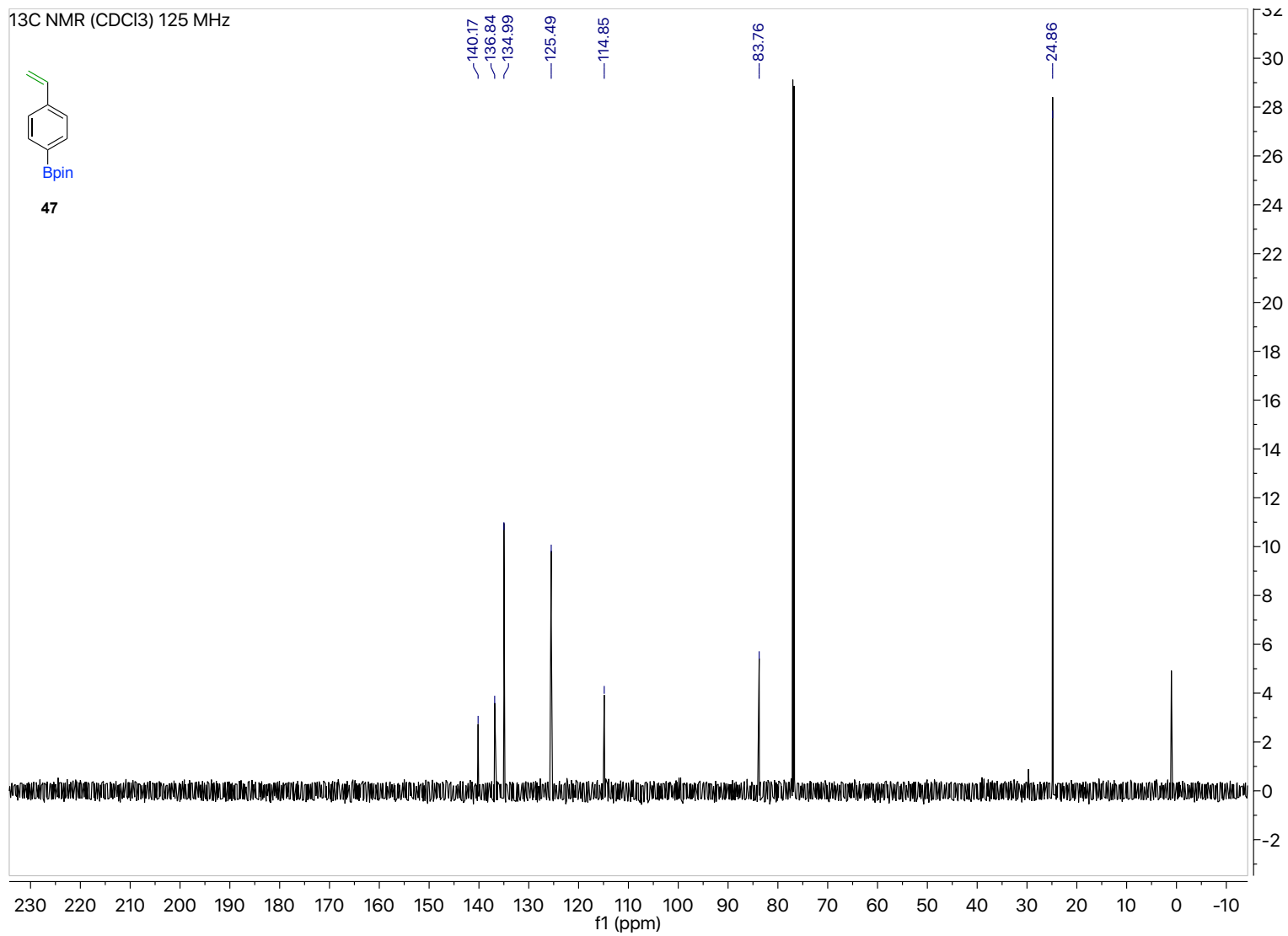


Figure 87. ¹³C NMR of 47

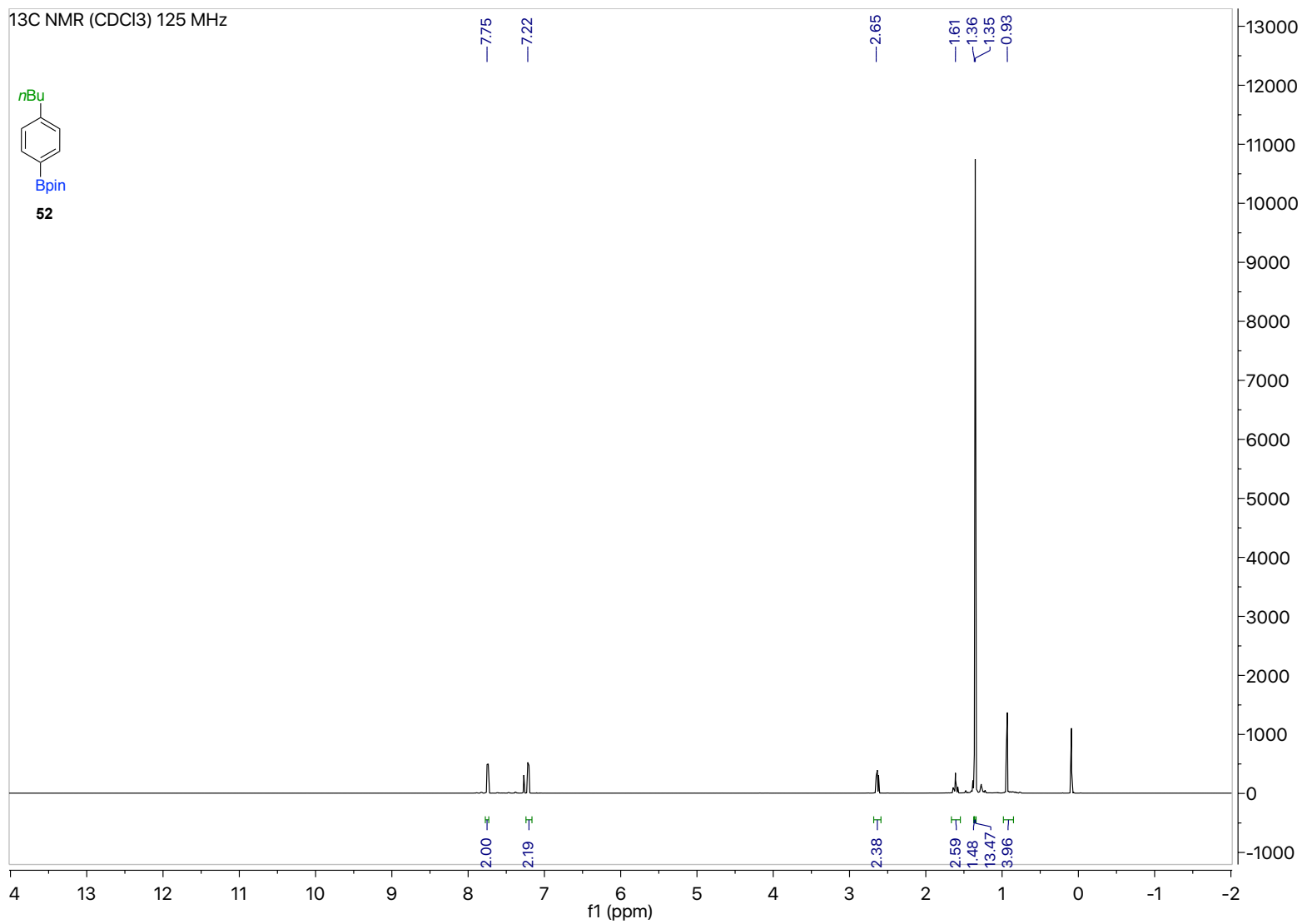


Figure 88. ¹H NMR of **52**

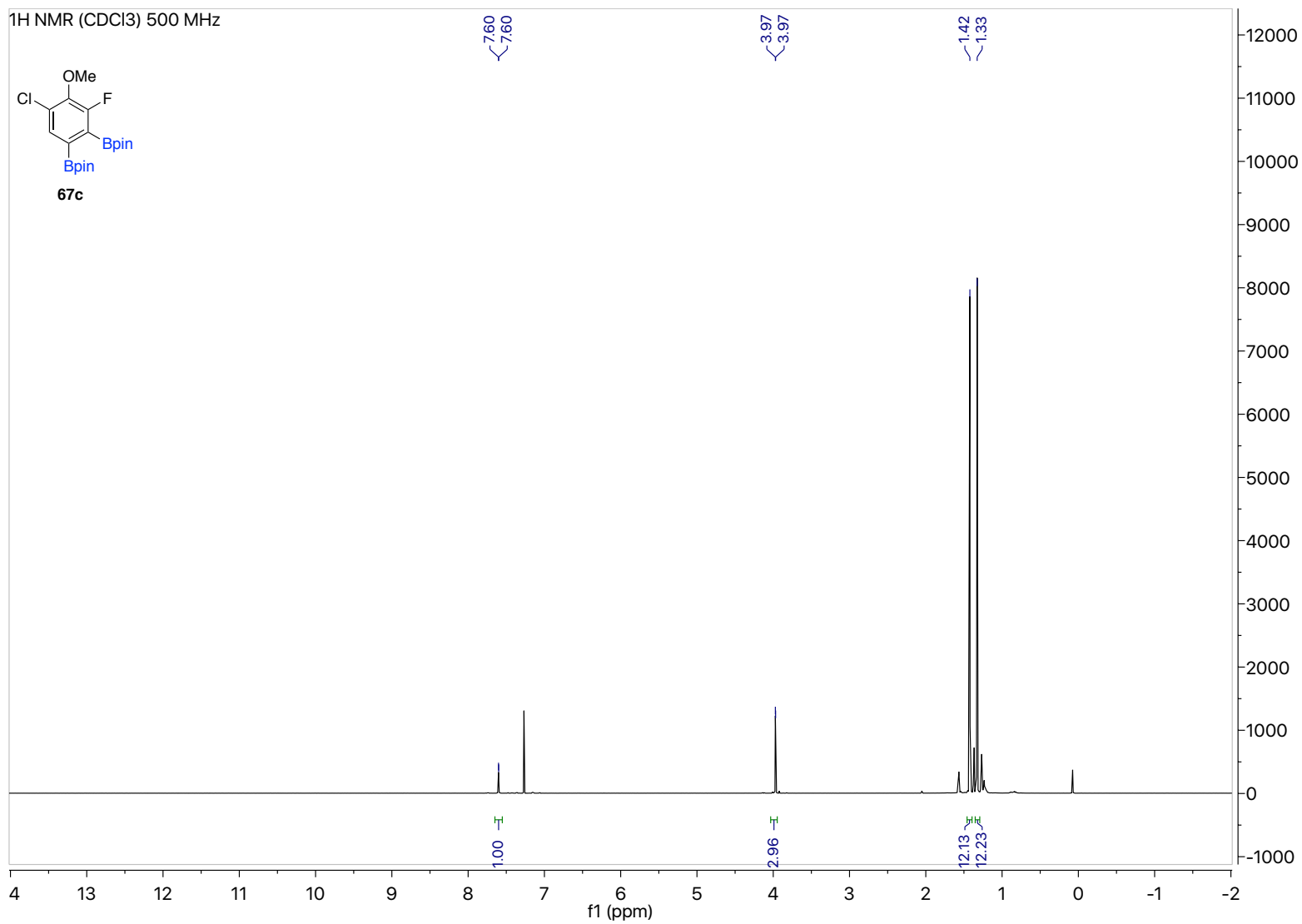


Figure 90. ¹H NMR of 67c

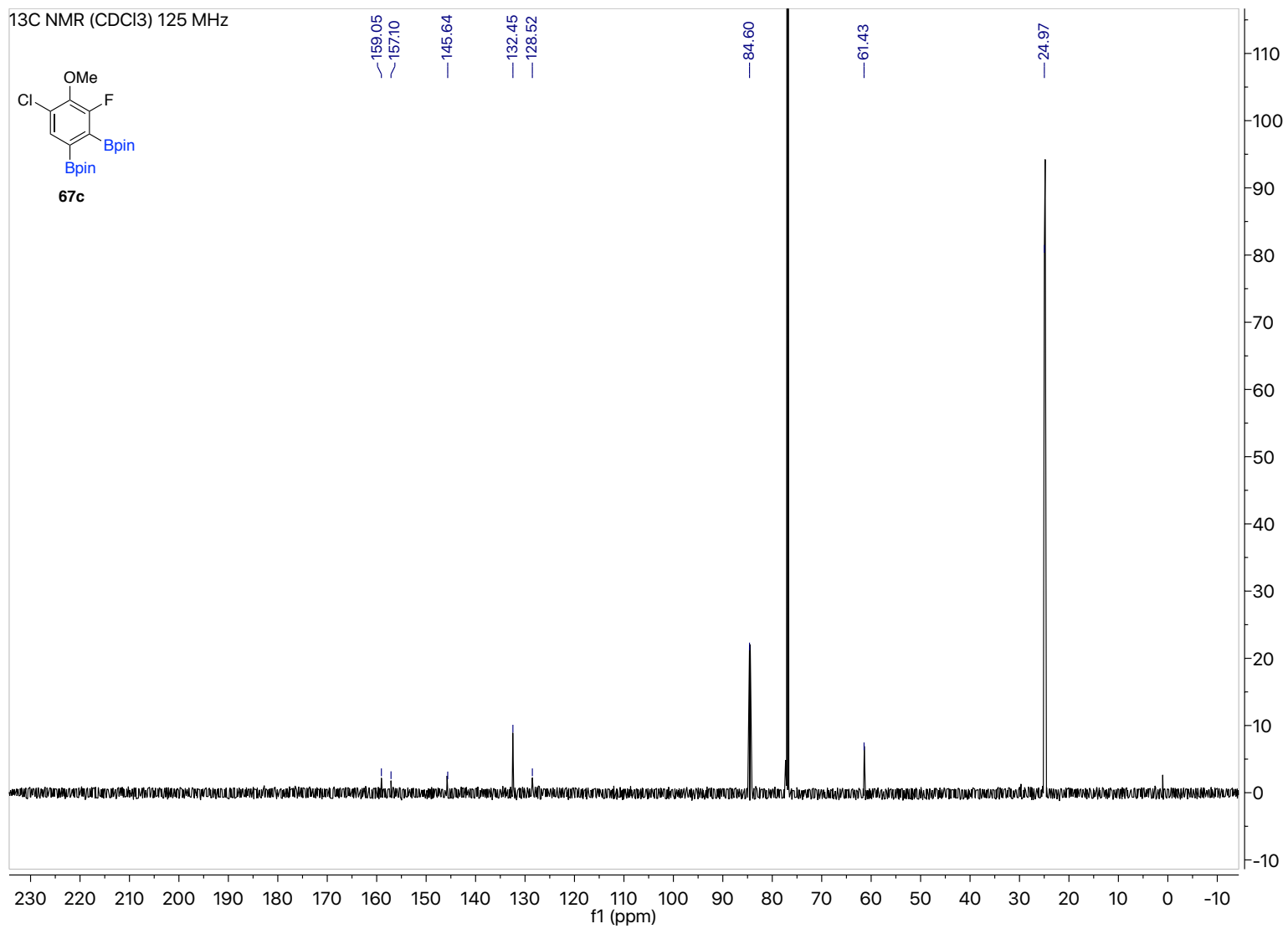


Figure 91. ¹³C NMR of 67c

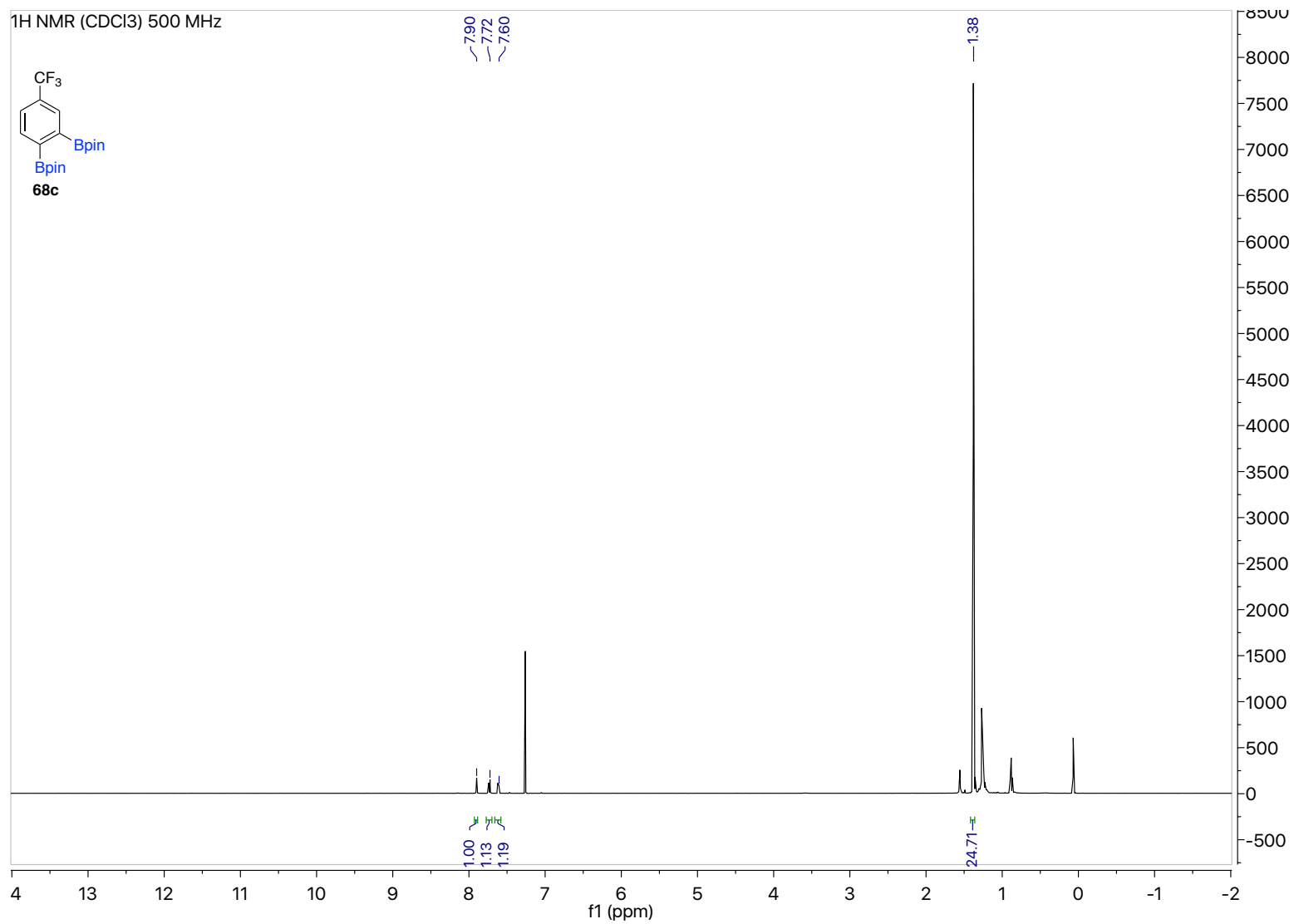


Figure 92. ¹H NMR of **68c**

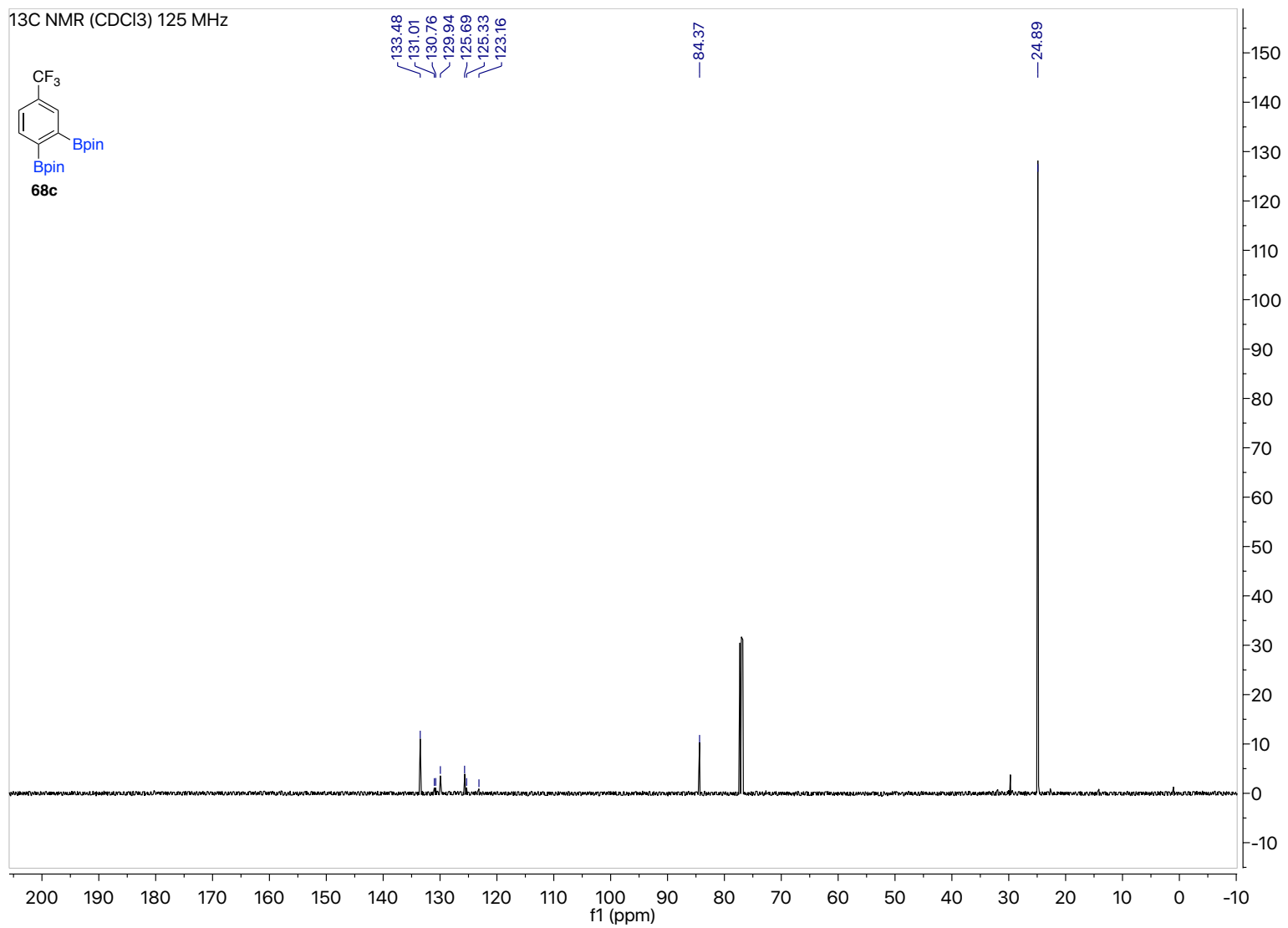


Figure 93. ¹³C NMR of 68c

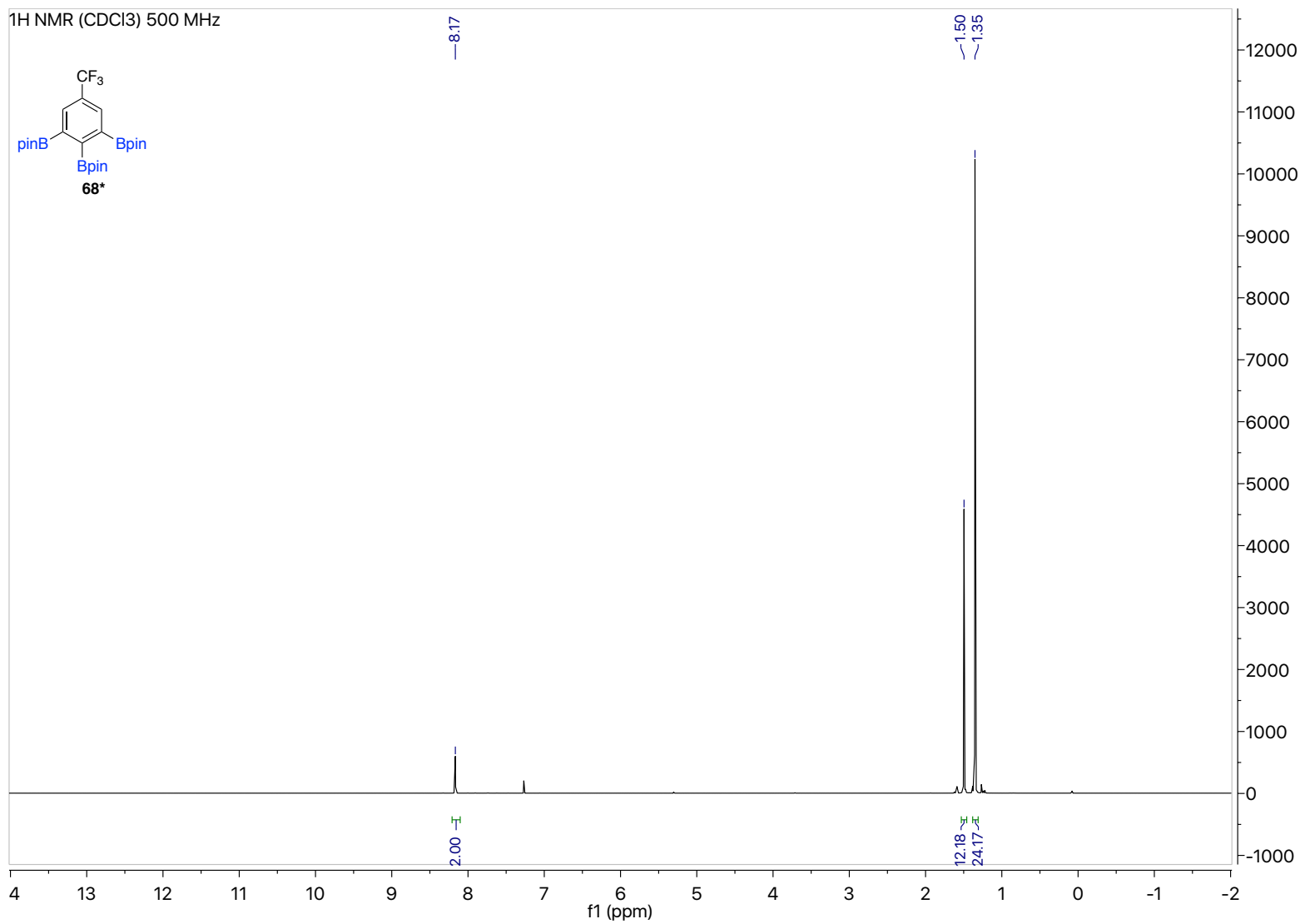


Figure 94. ¹H NMR of 68*

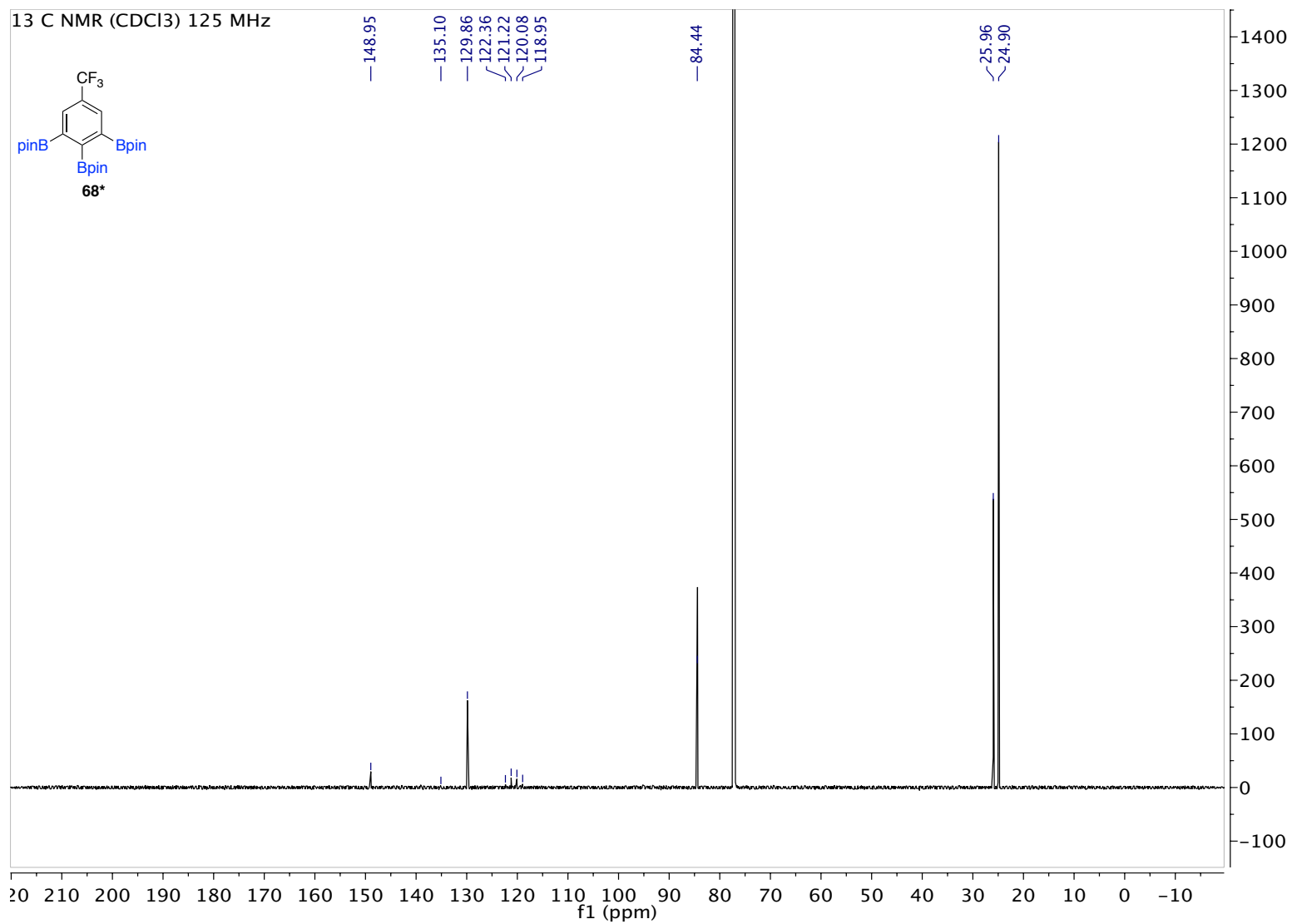


Figure 95. ¹³C NMR of 68*

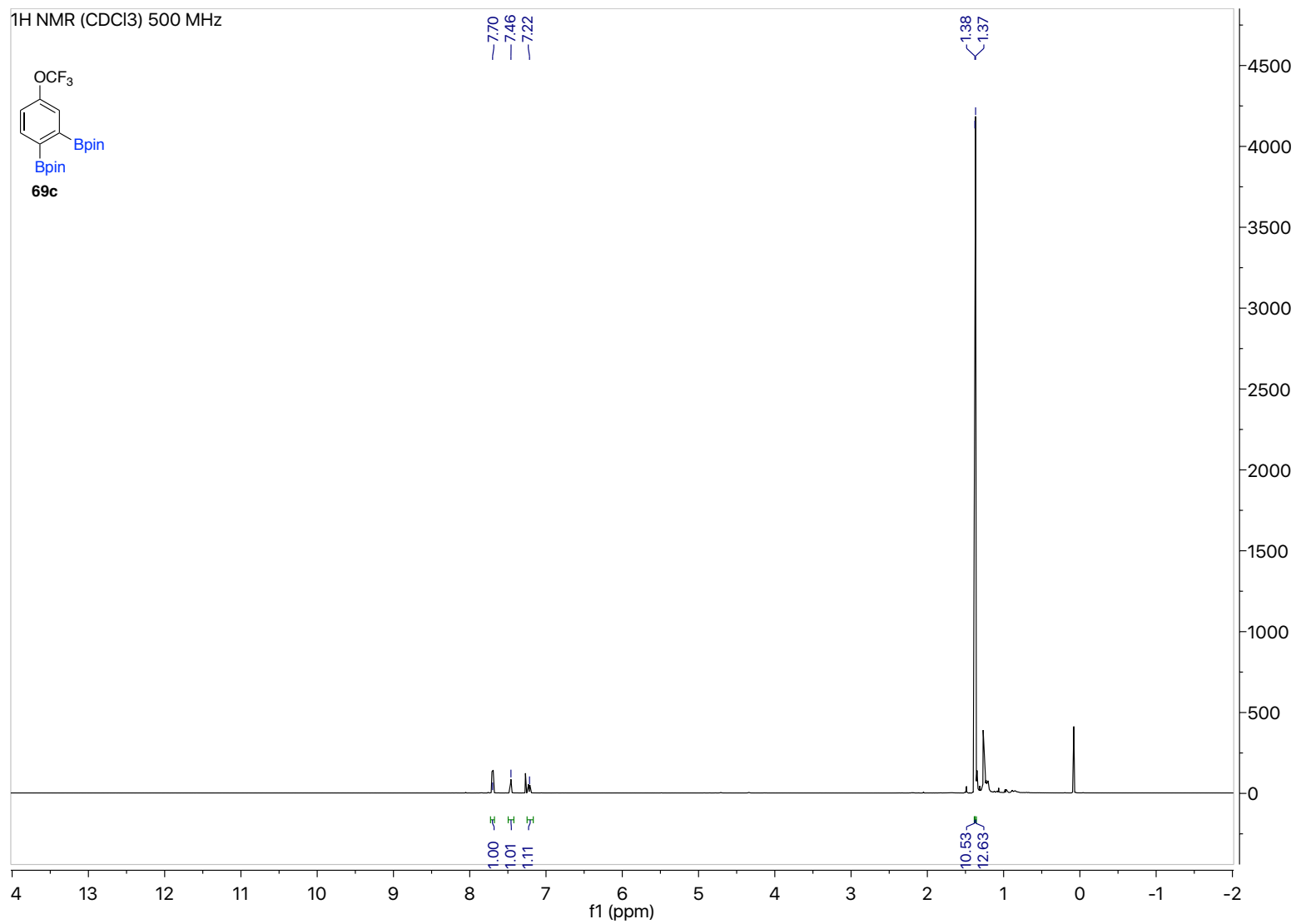


Figure 96. ¹H NMR of 69c

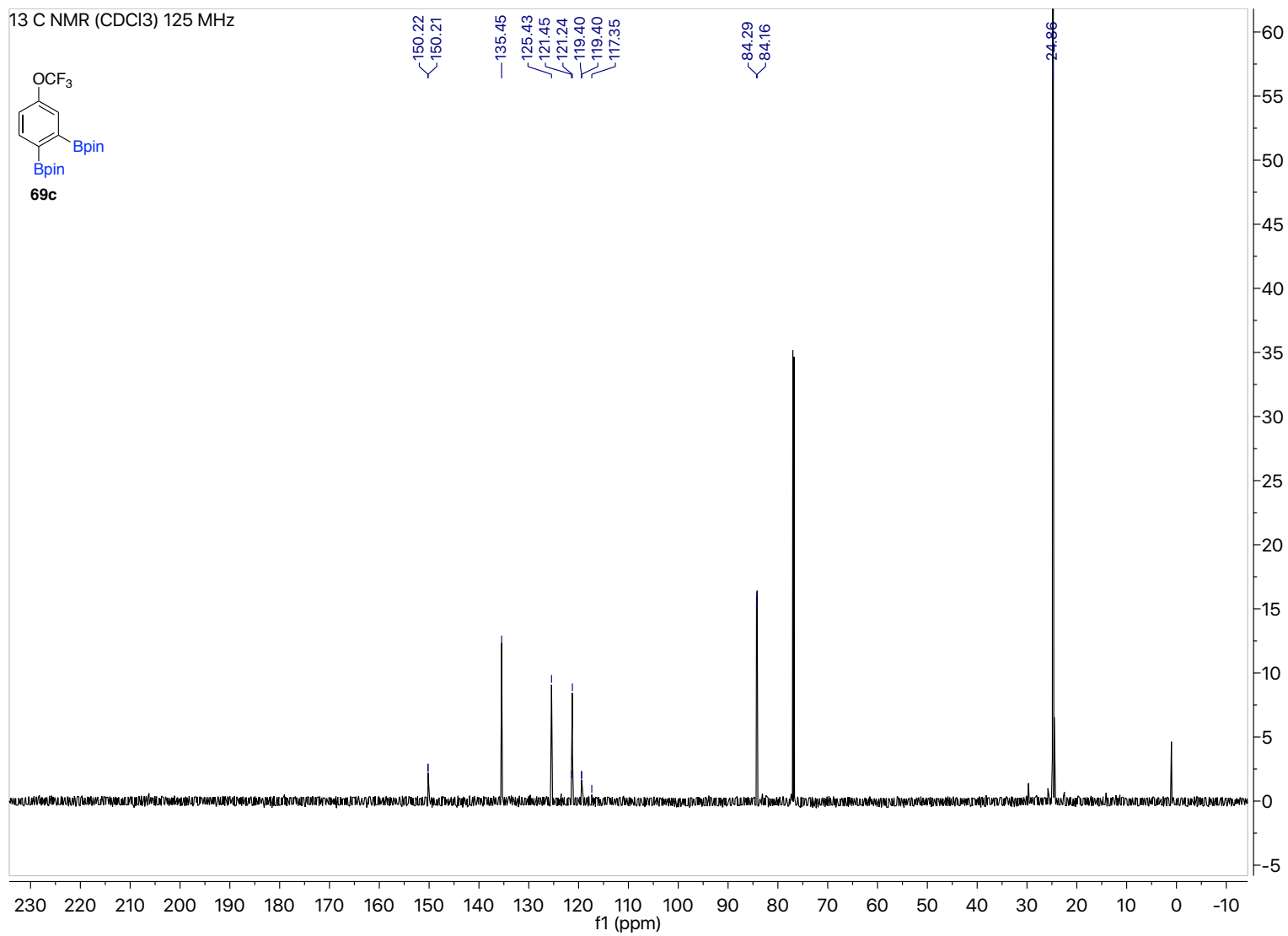


Figure 97. ¹³C NMR of 69c

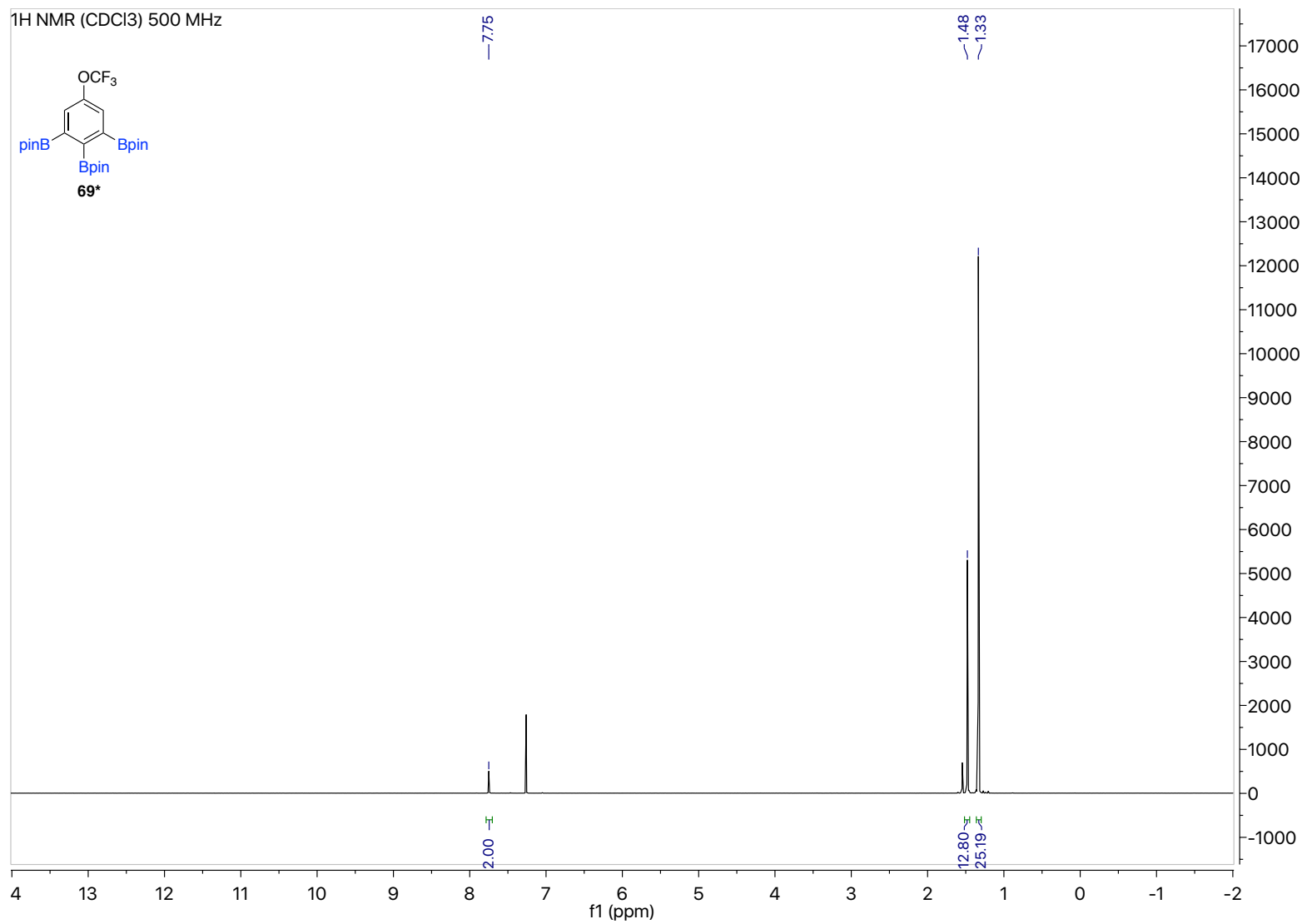


Figure 98. ¹H NMR of 69*

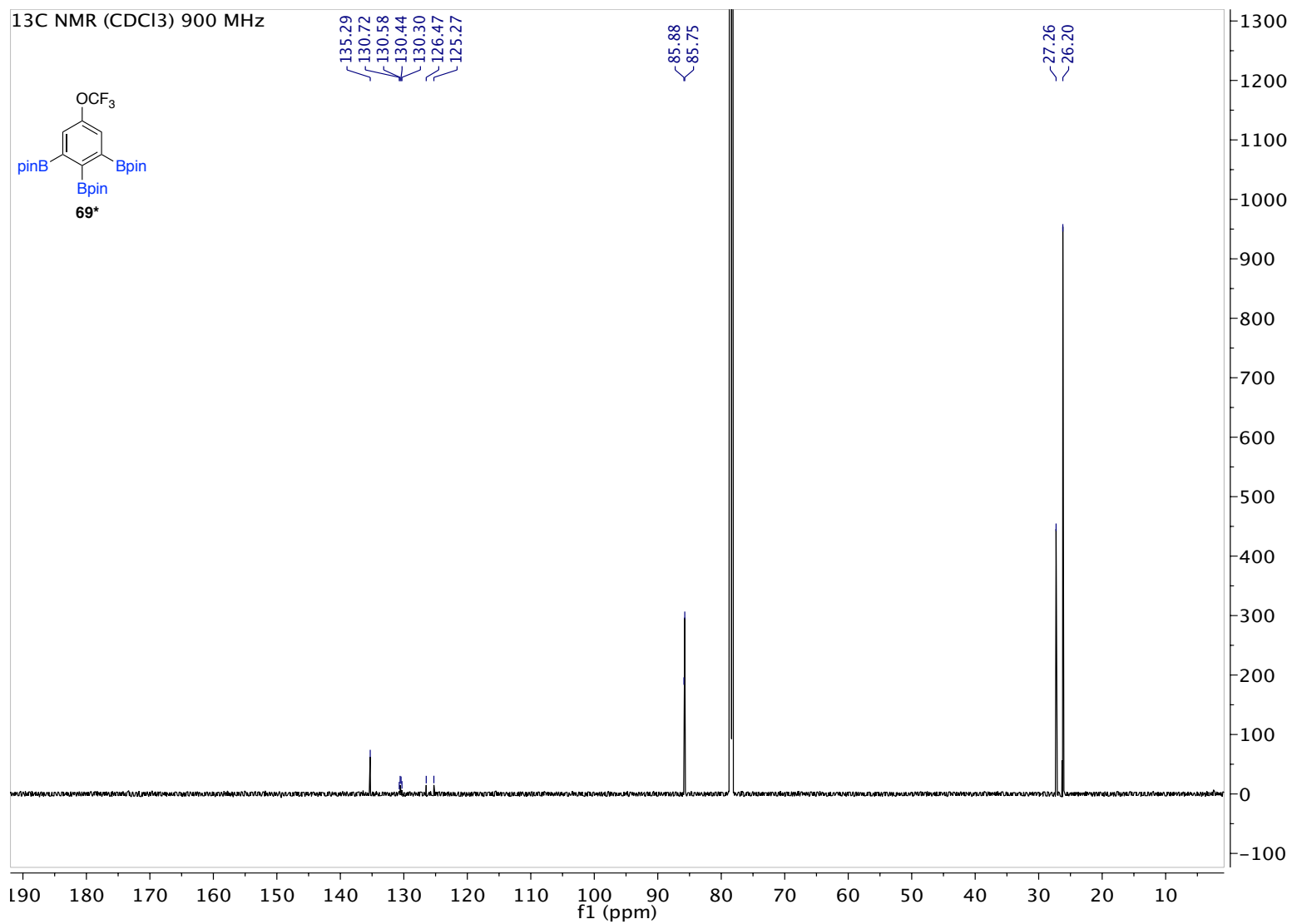


Figure 99. ¹³C NMR of **69***

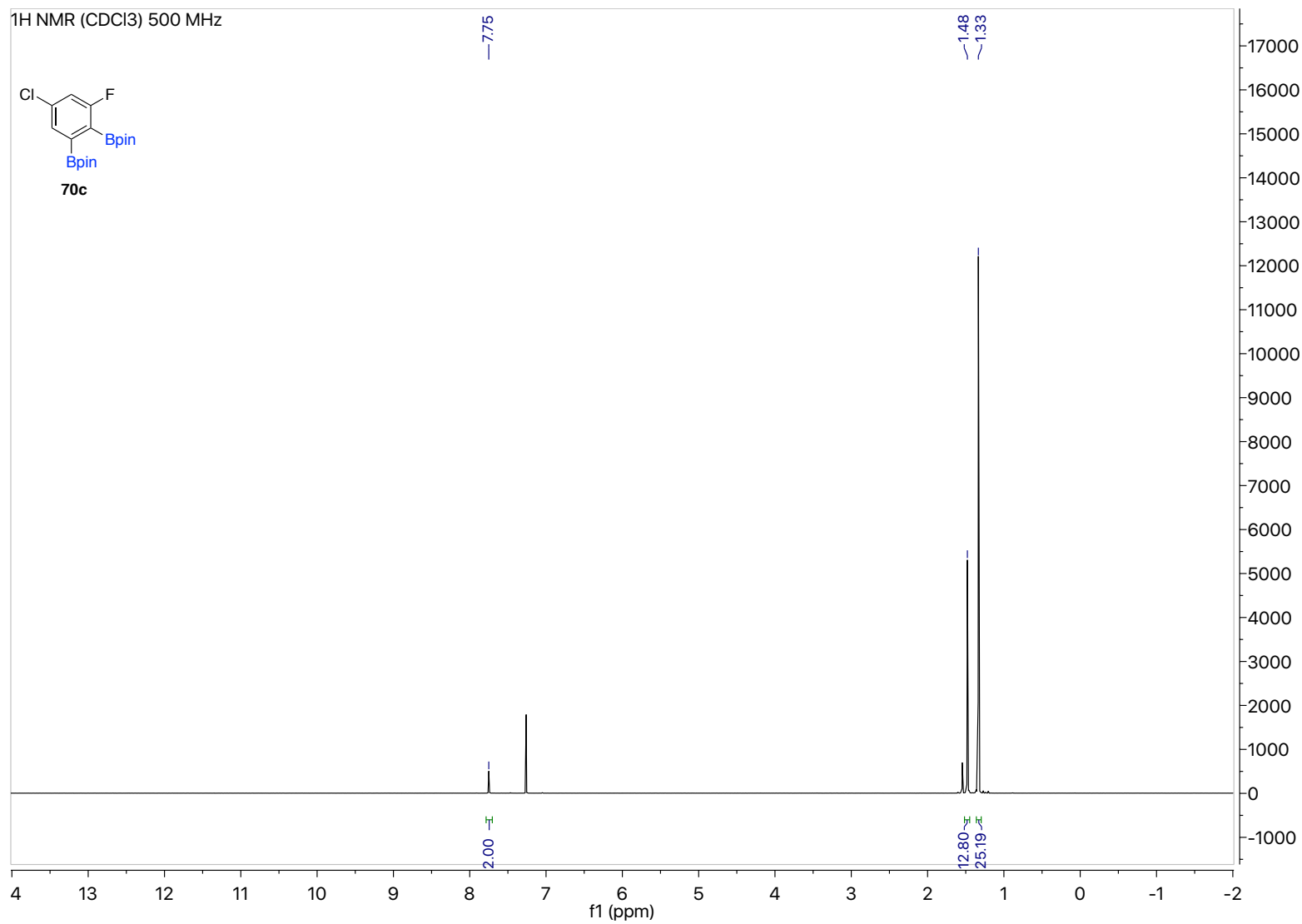


Figure 100. ¹H NMR of **70c**

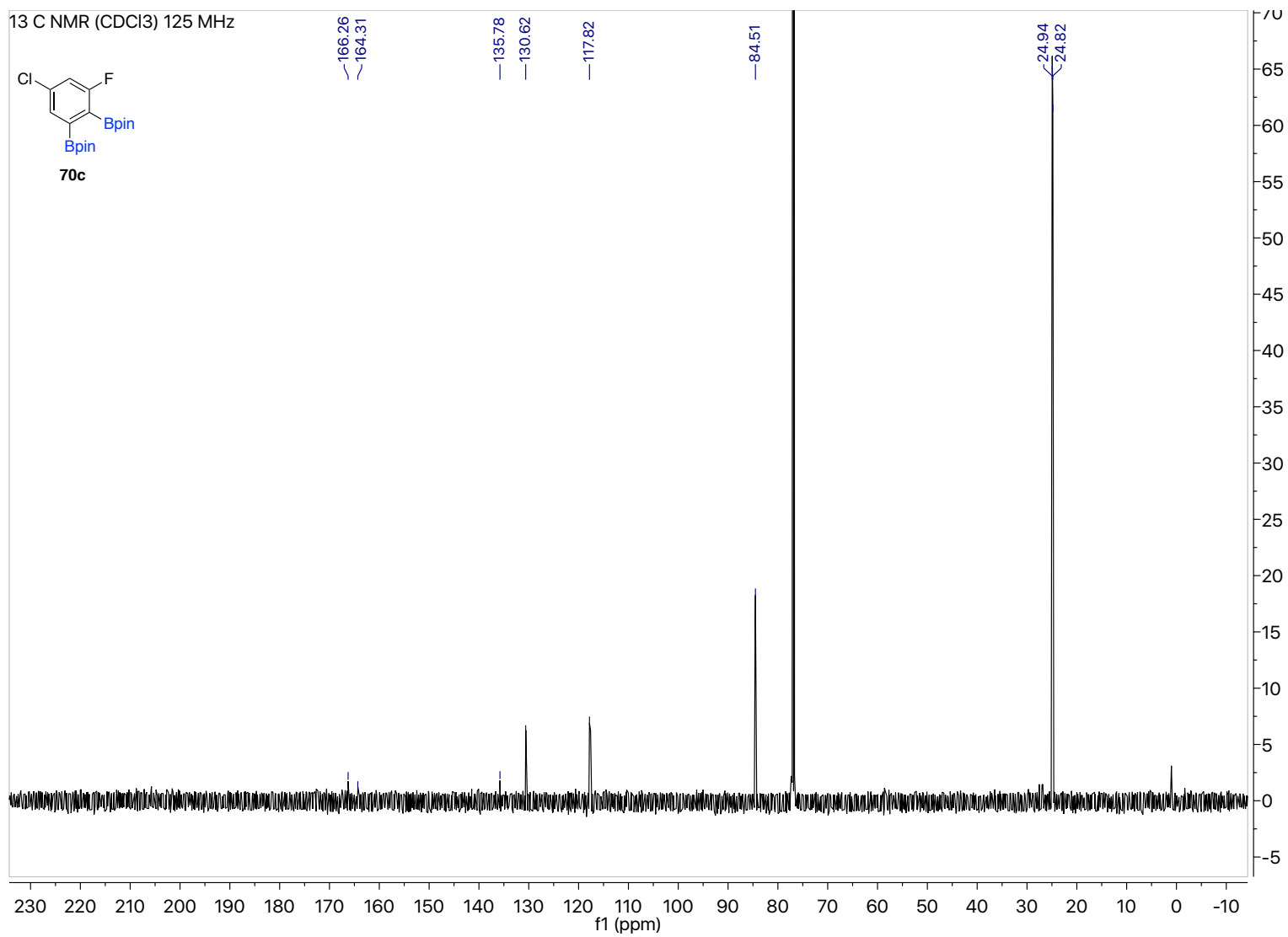


Figure 101. ¹³C NMR of **70c**

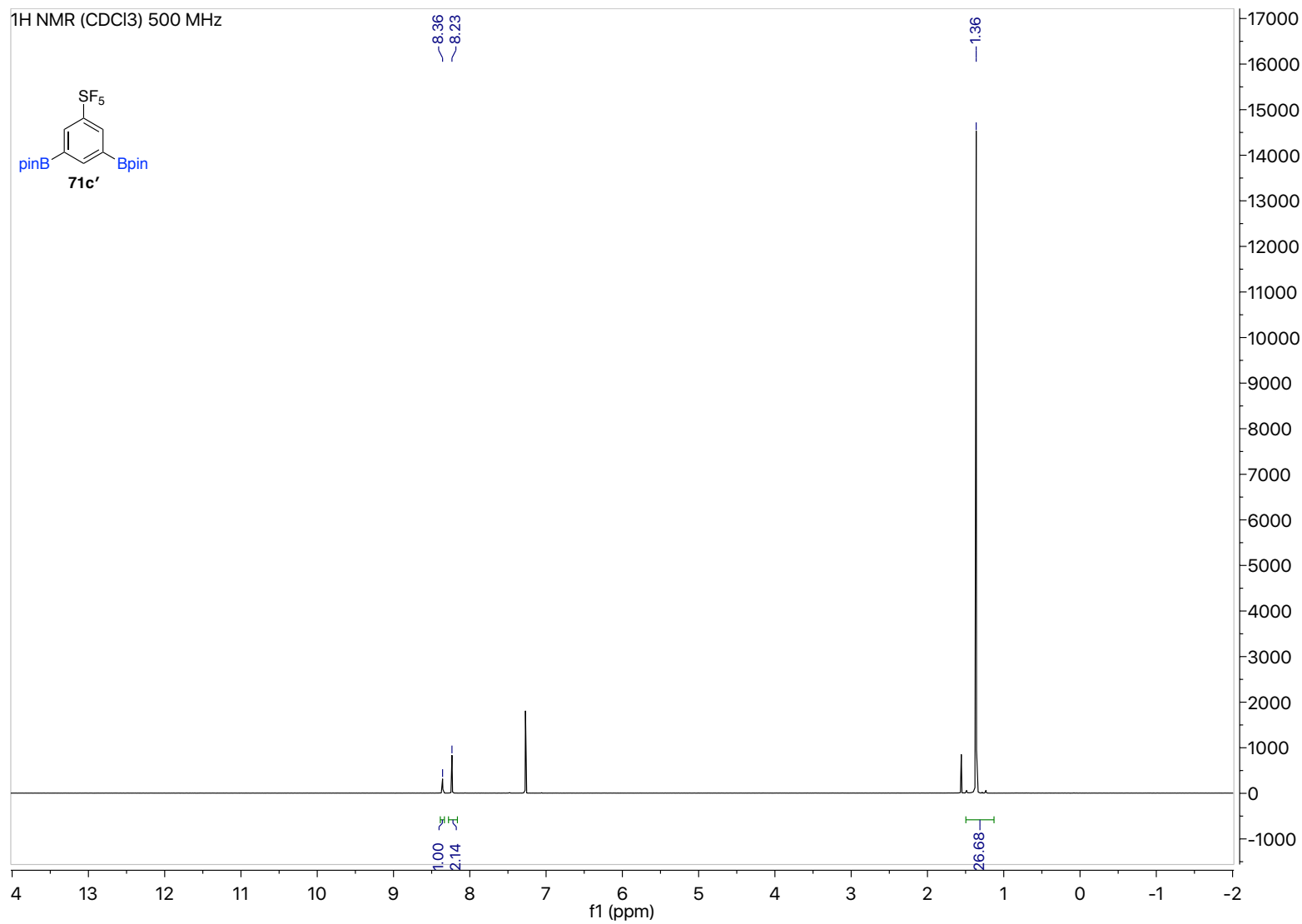


Figure 102. ¹H NMR of 71c'

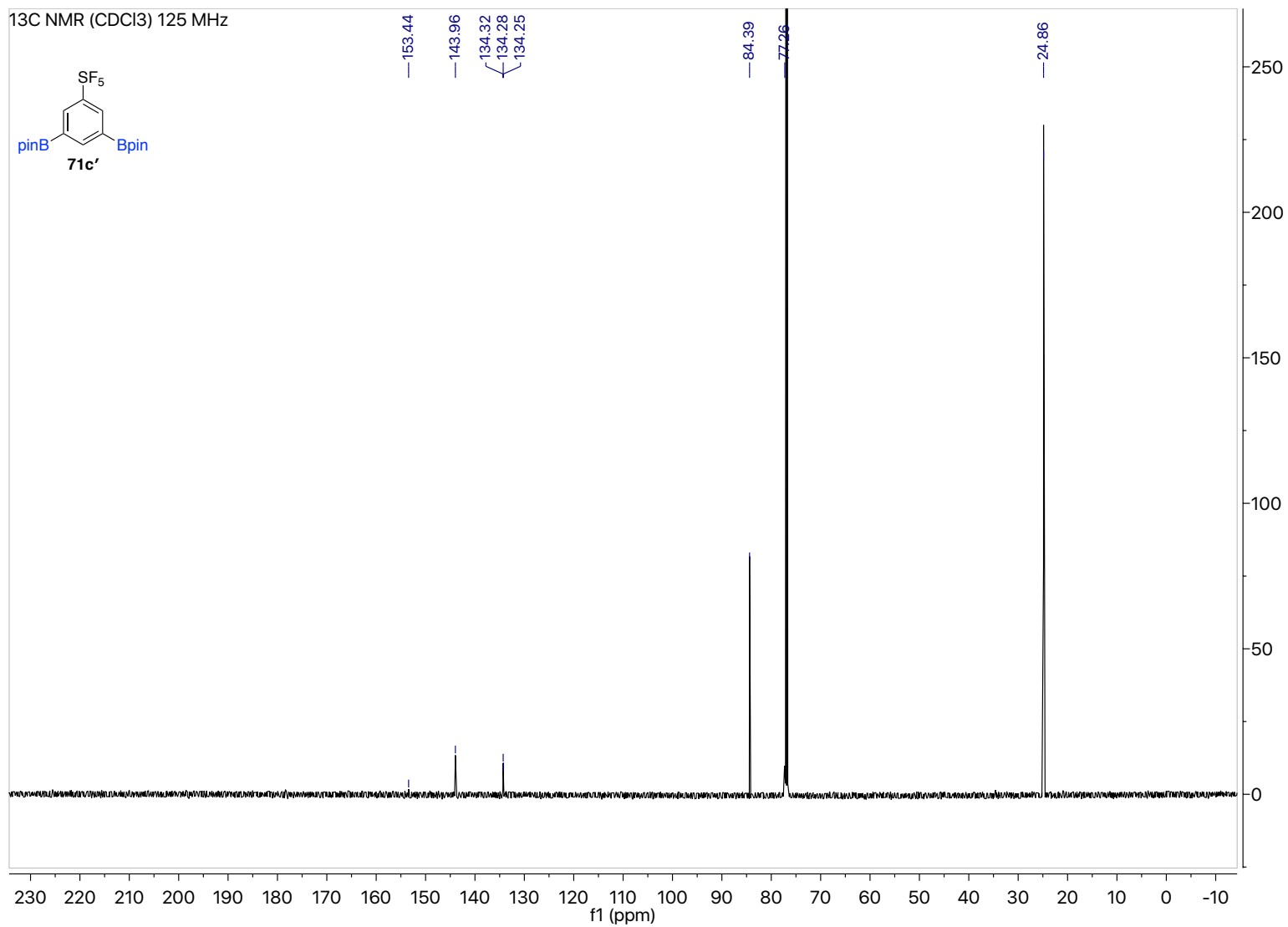


Figure 103. ¹³C NMR of 71c'

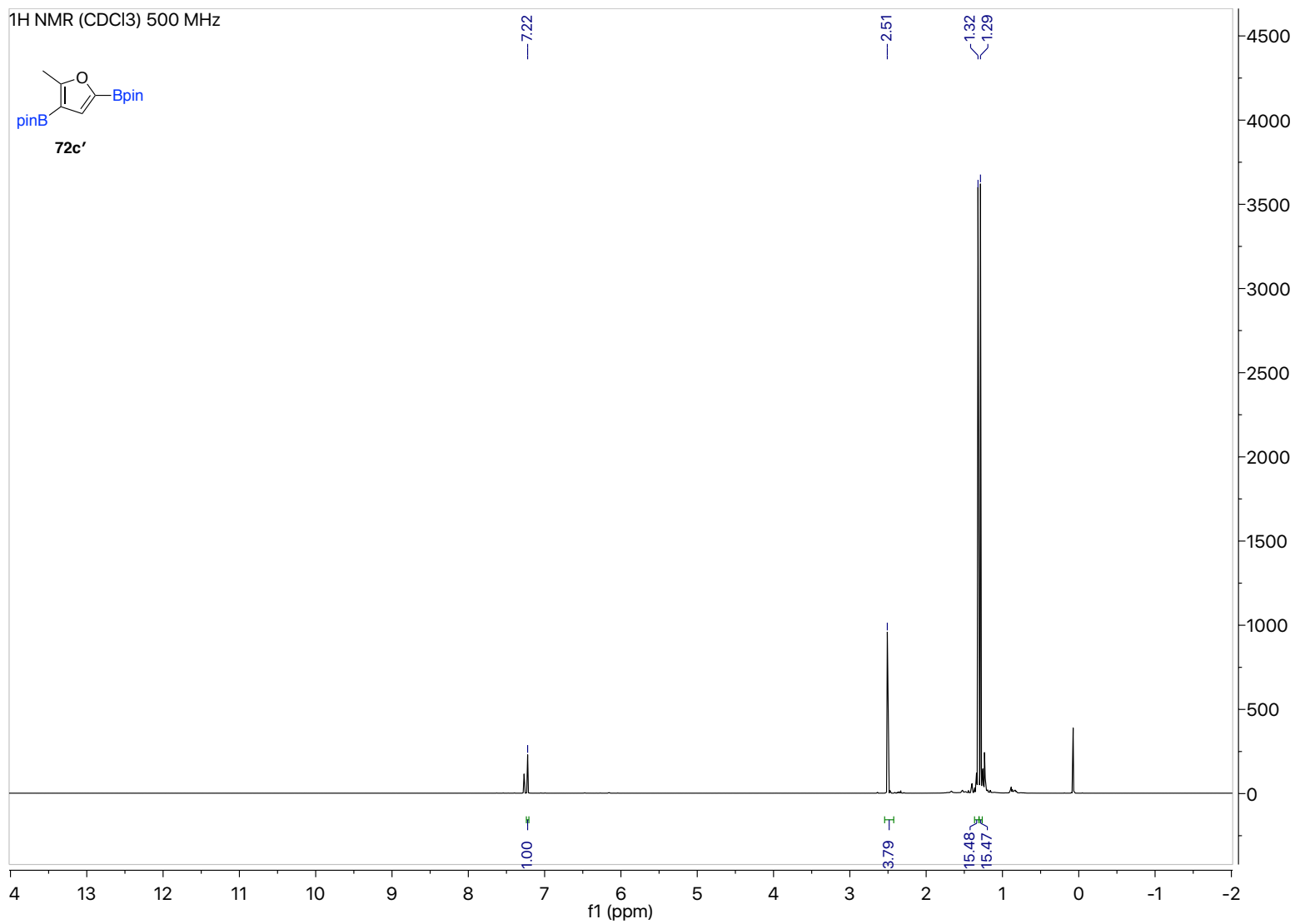


Figure 104. ¹H NMR of 72c'

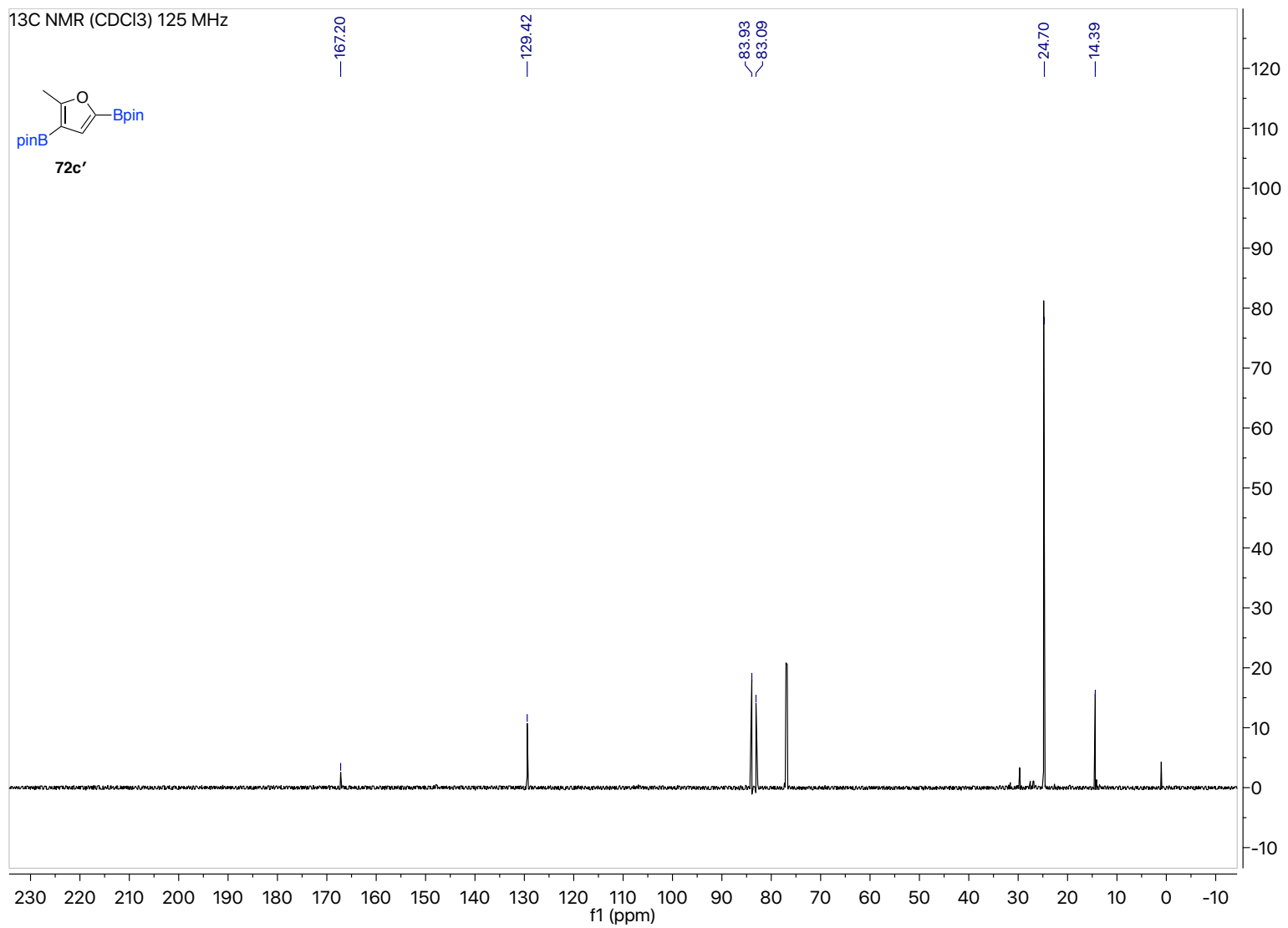


Figure 105. ¹³C NMR of 72c'

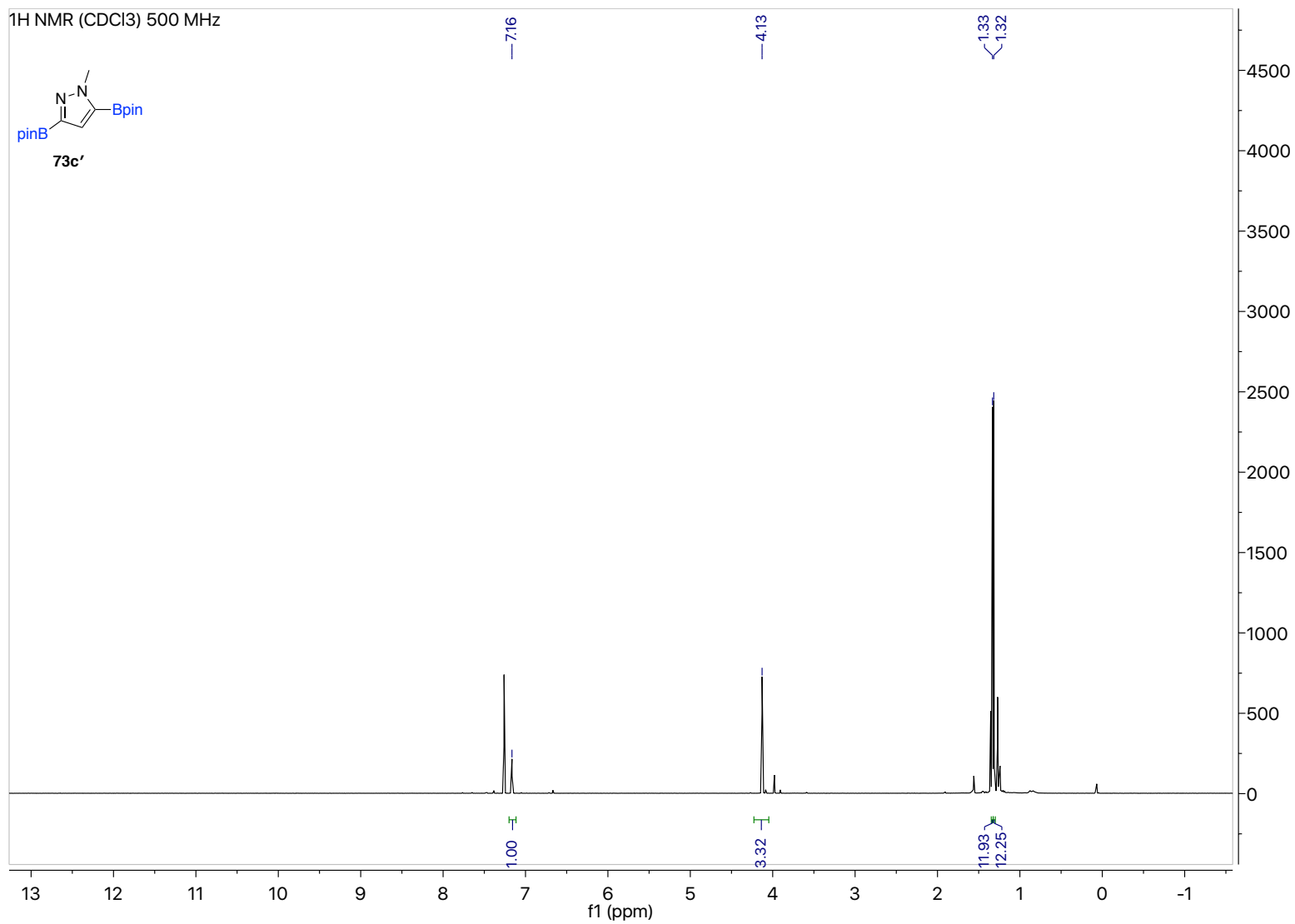


Figure 106. ¹H NMR of 73c'

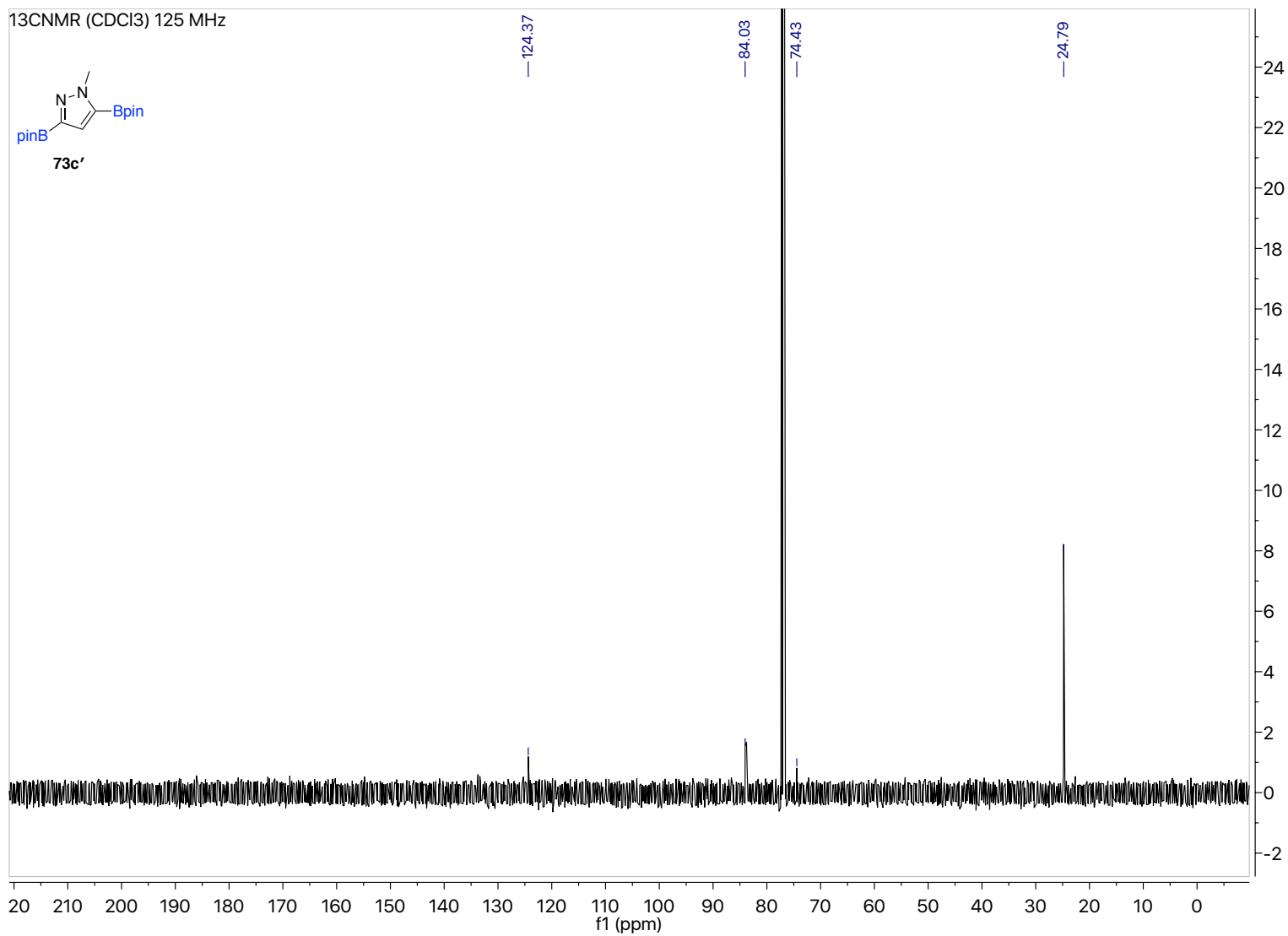


Figure 107. ¹³C NMR of **73c'**

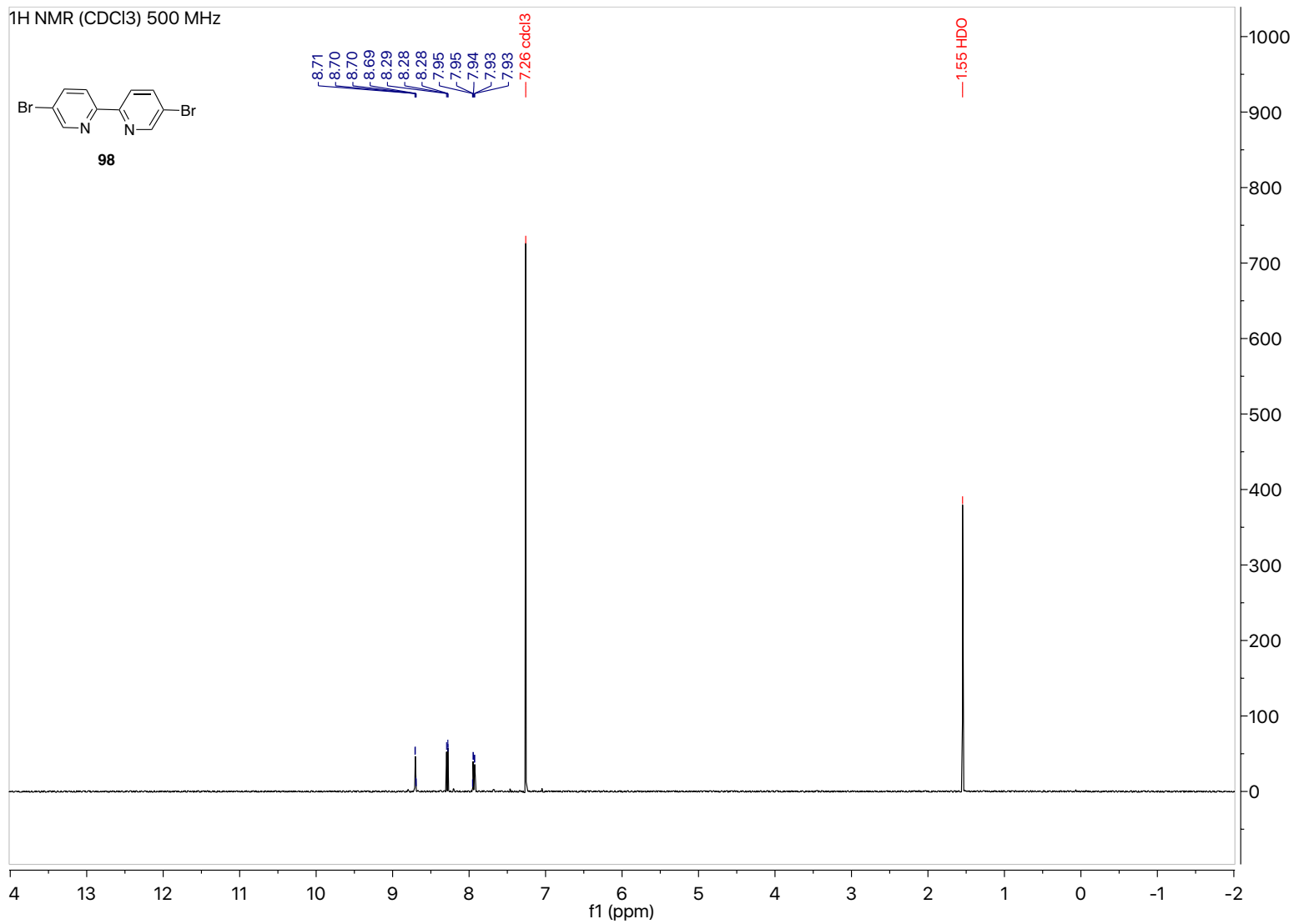


Figure 108. ¹H NMR of 98

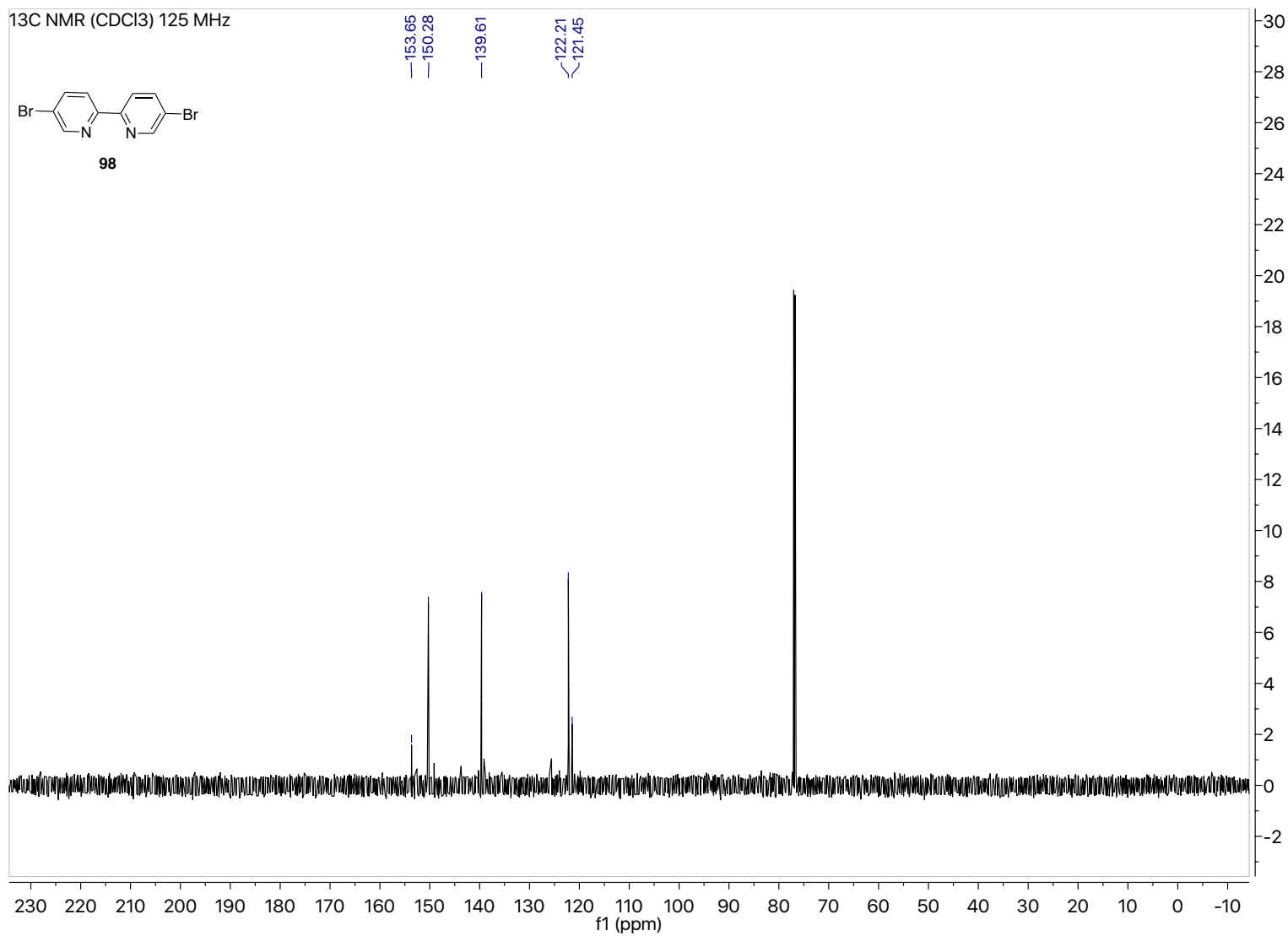


Figure 109. ¹³C NMR of 98

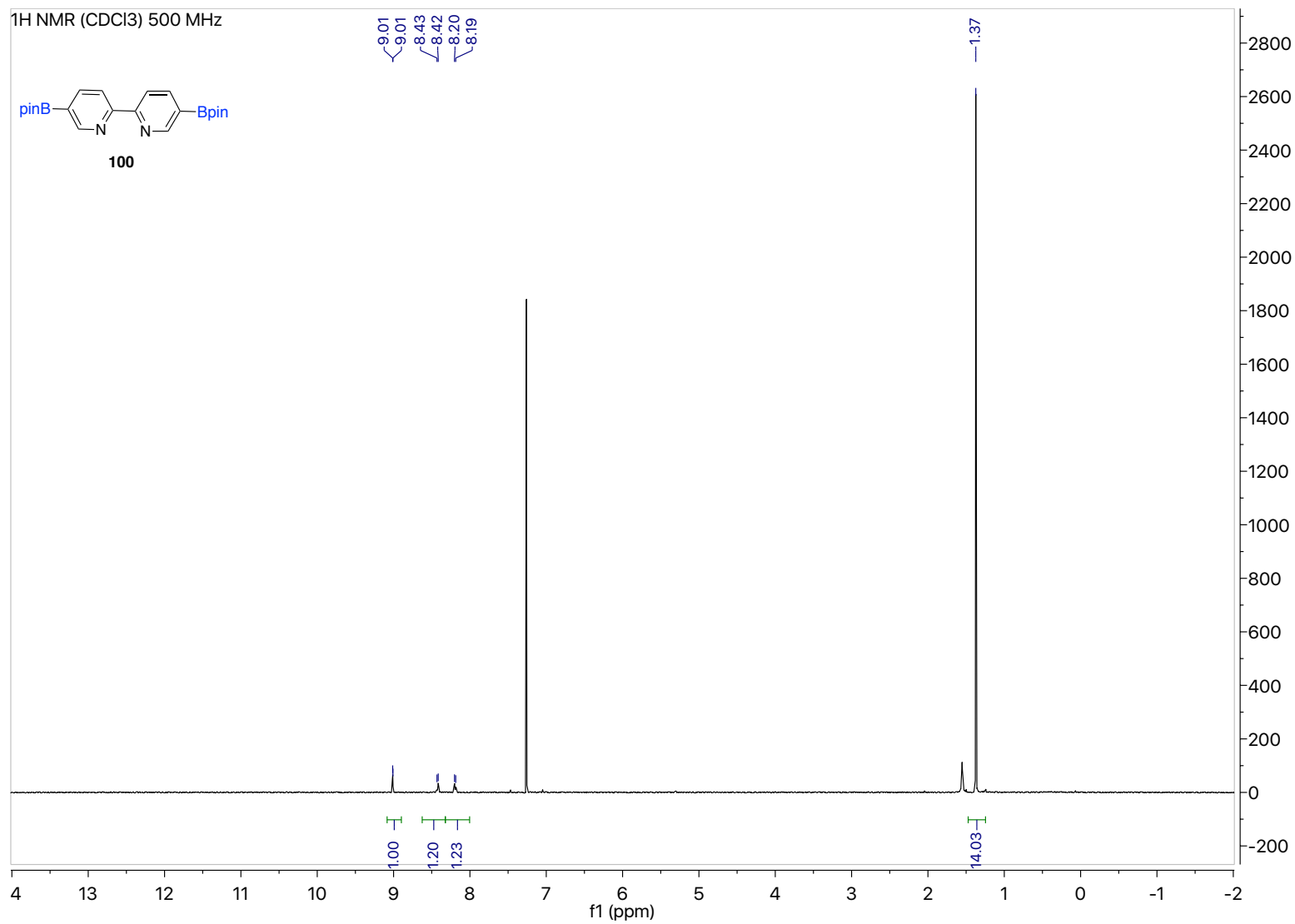


Figure 110. ¹H NMR of **100**

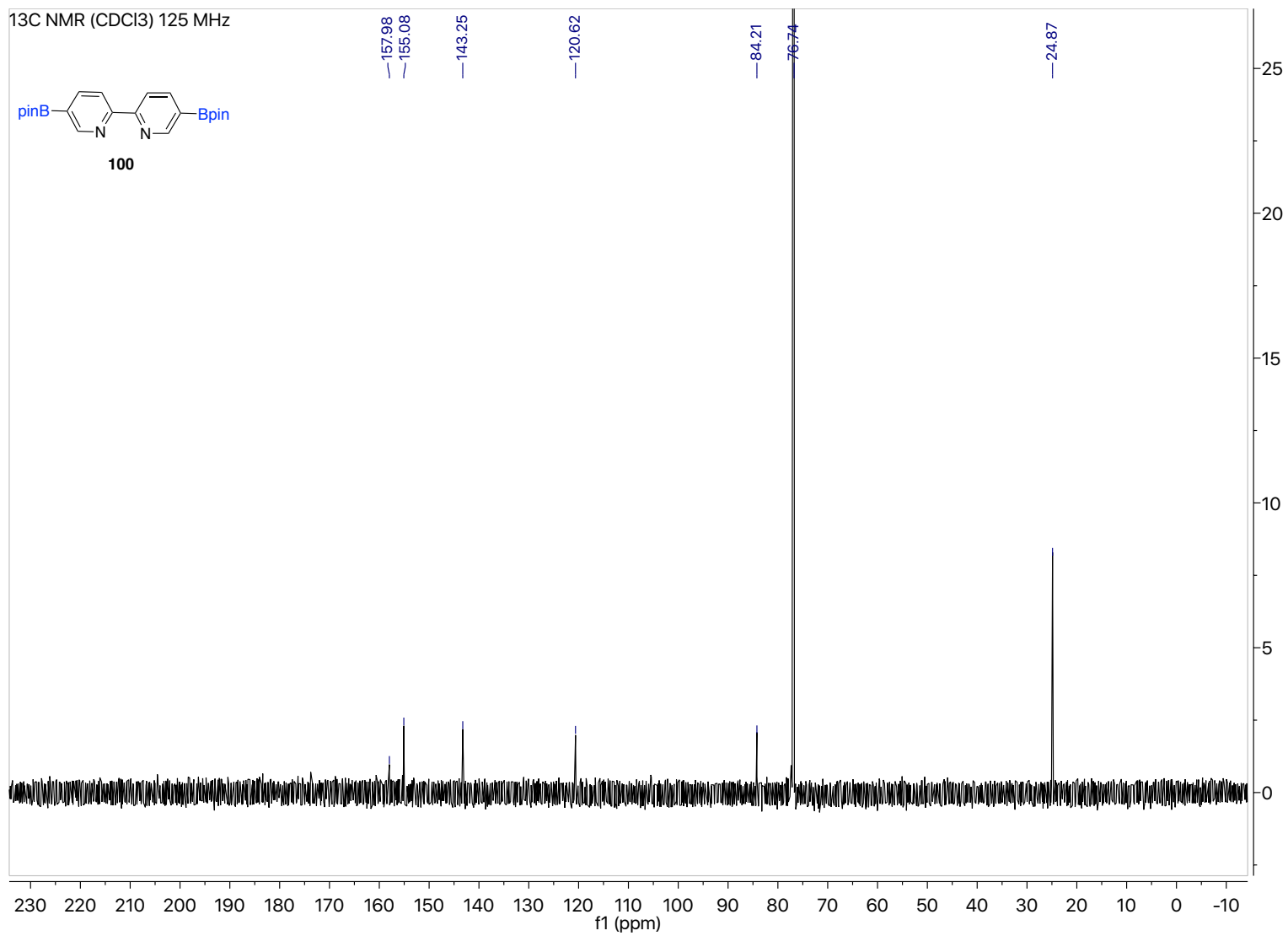


Figure 111. ¹³C NMR of 100

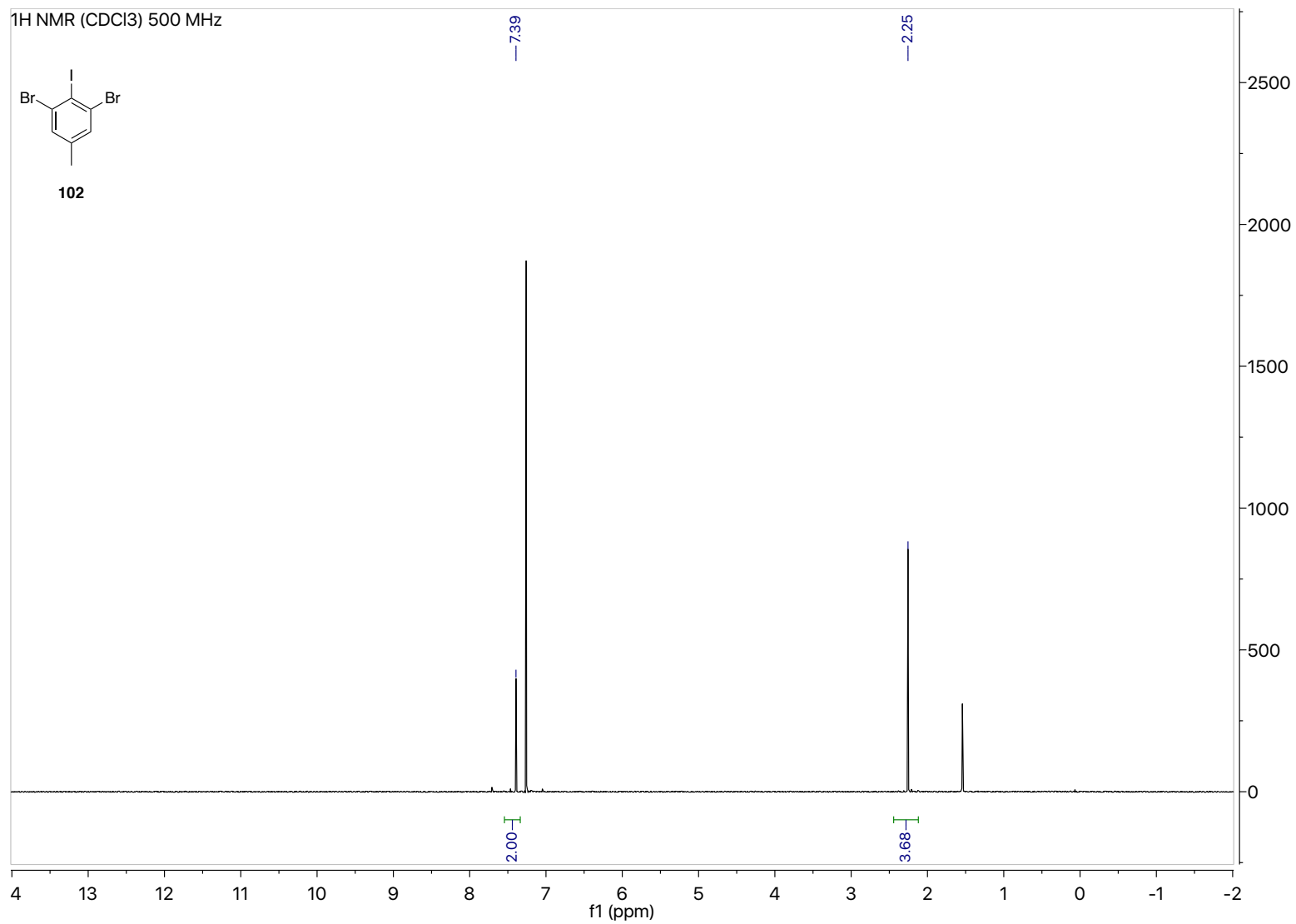


Figure 112. ¹H NMR of 102

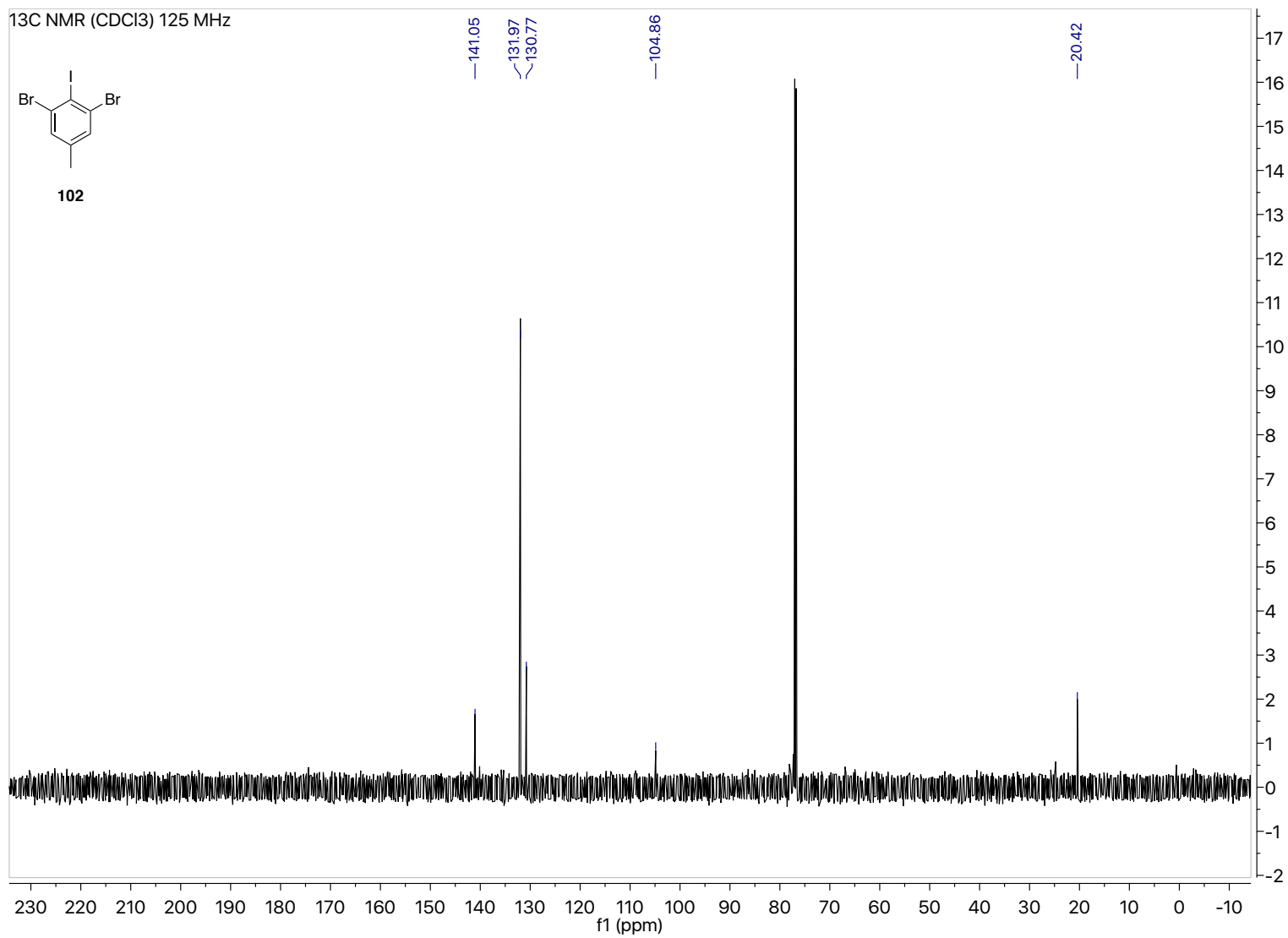


Figure 113. ¹³C NMR of 102

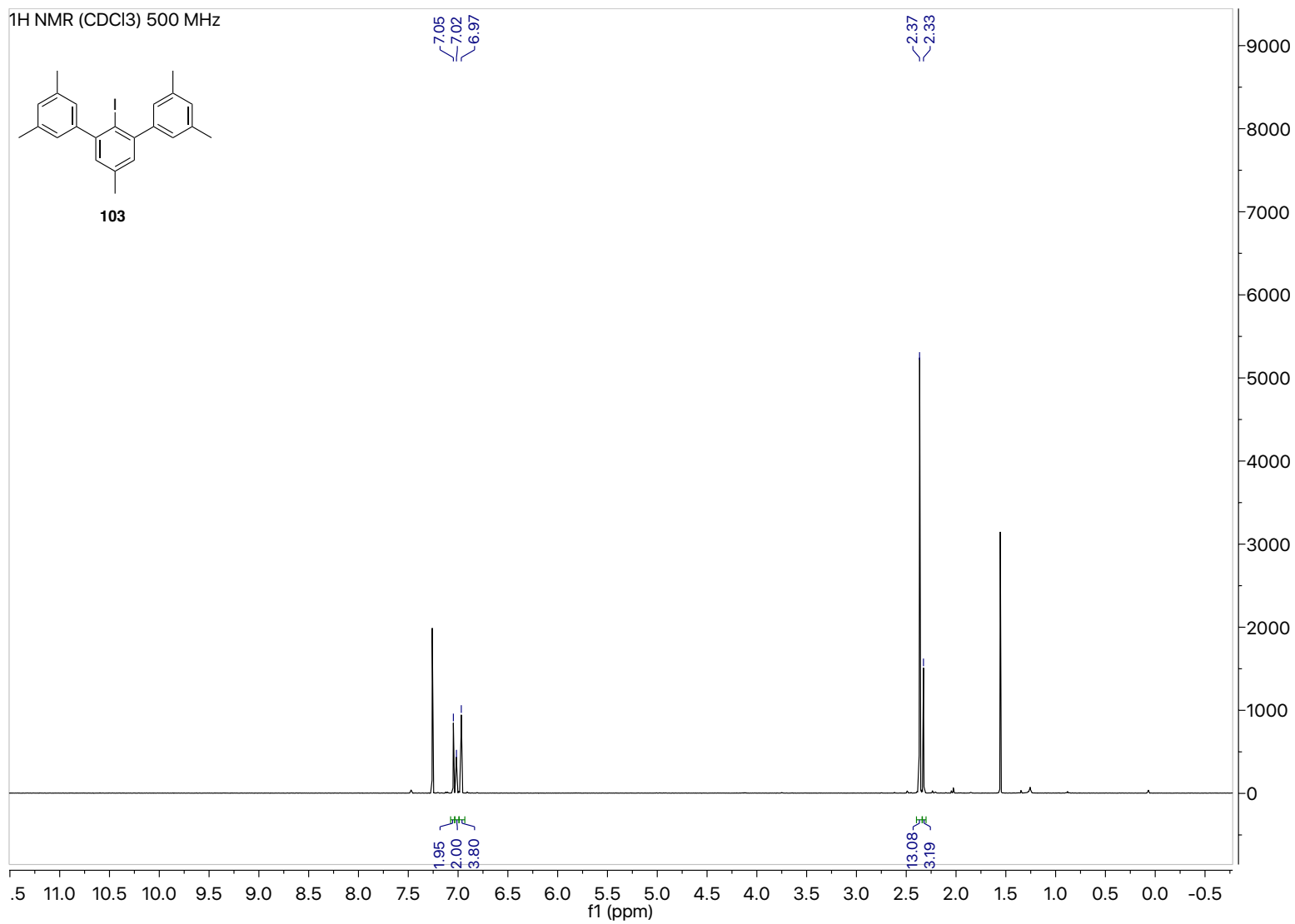


Figure 114. ¹H NMR of 103

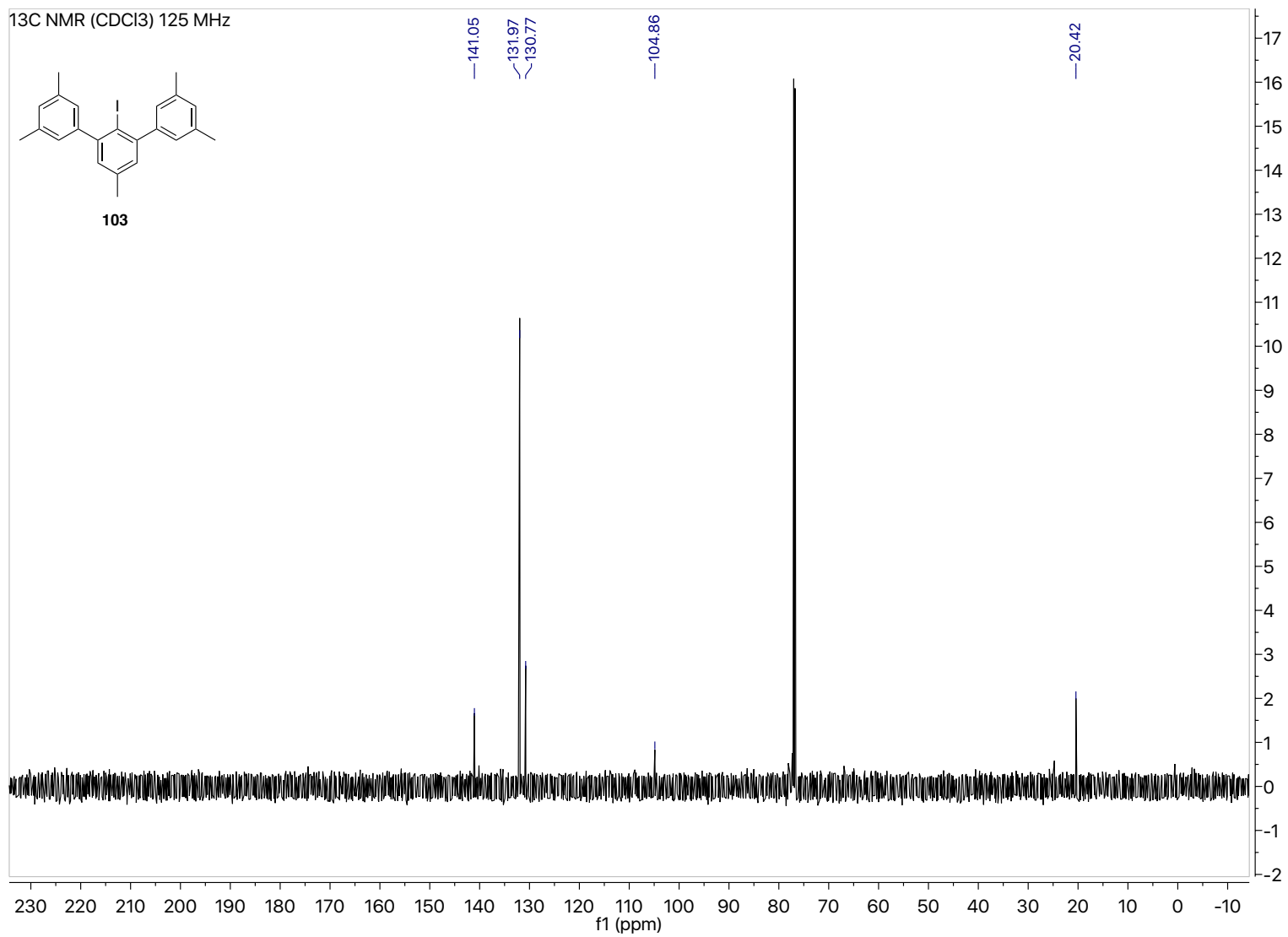


Figure 115. ¹³C NMR of 103

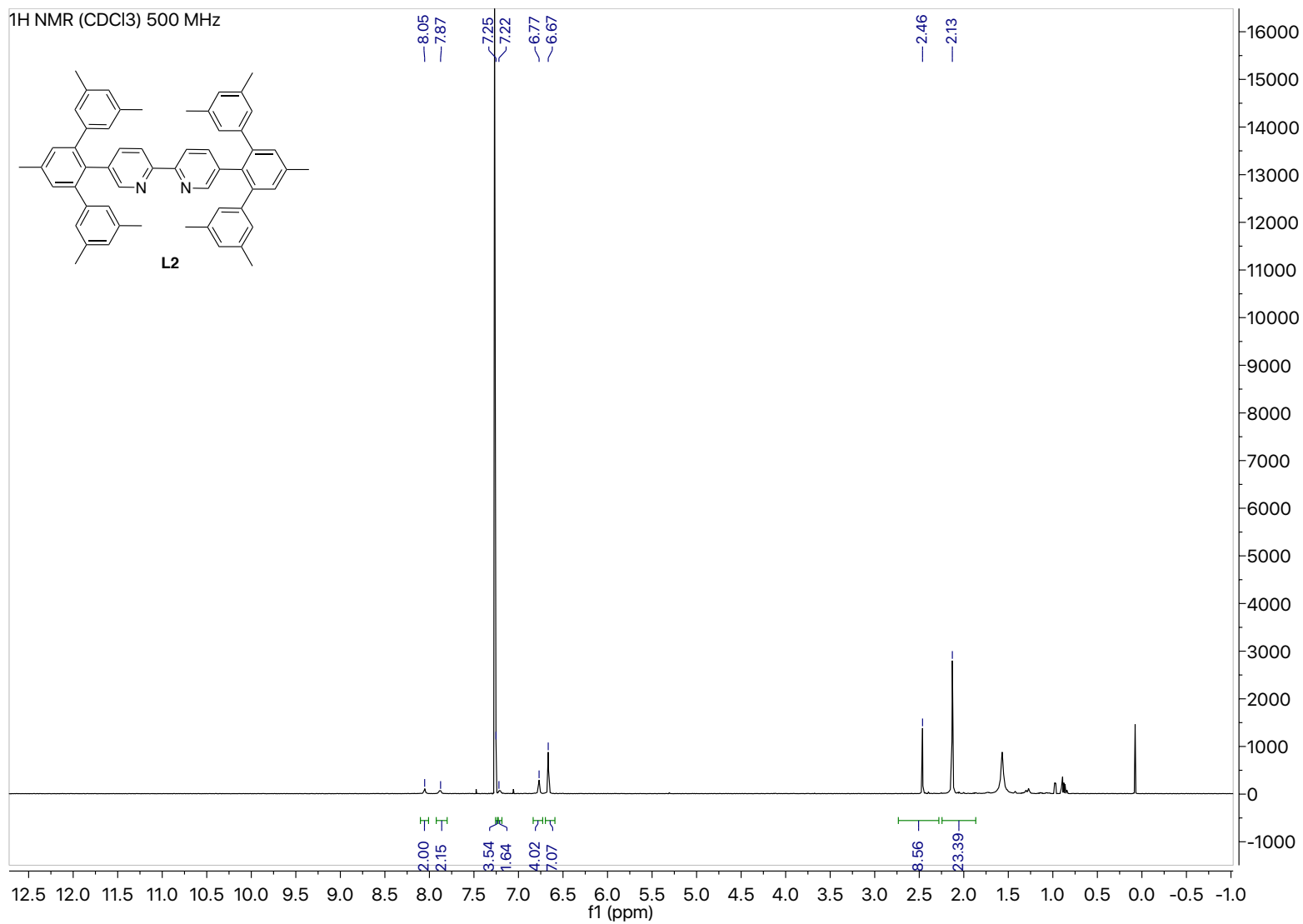


Figure 116. ¹H NMR of L2

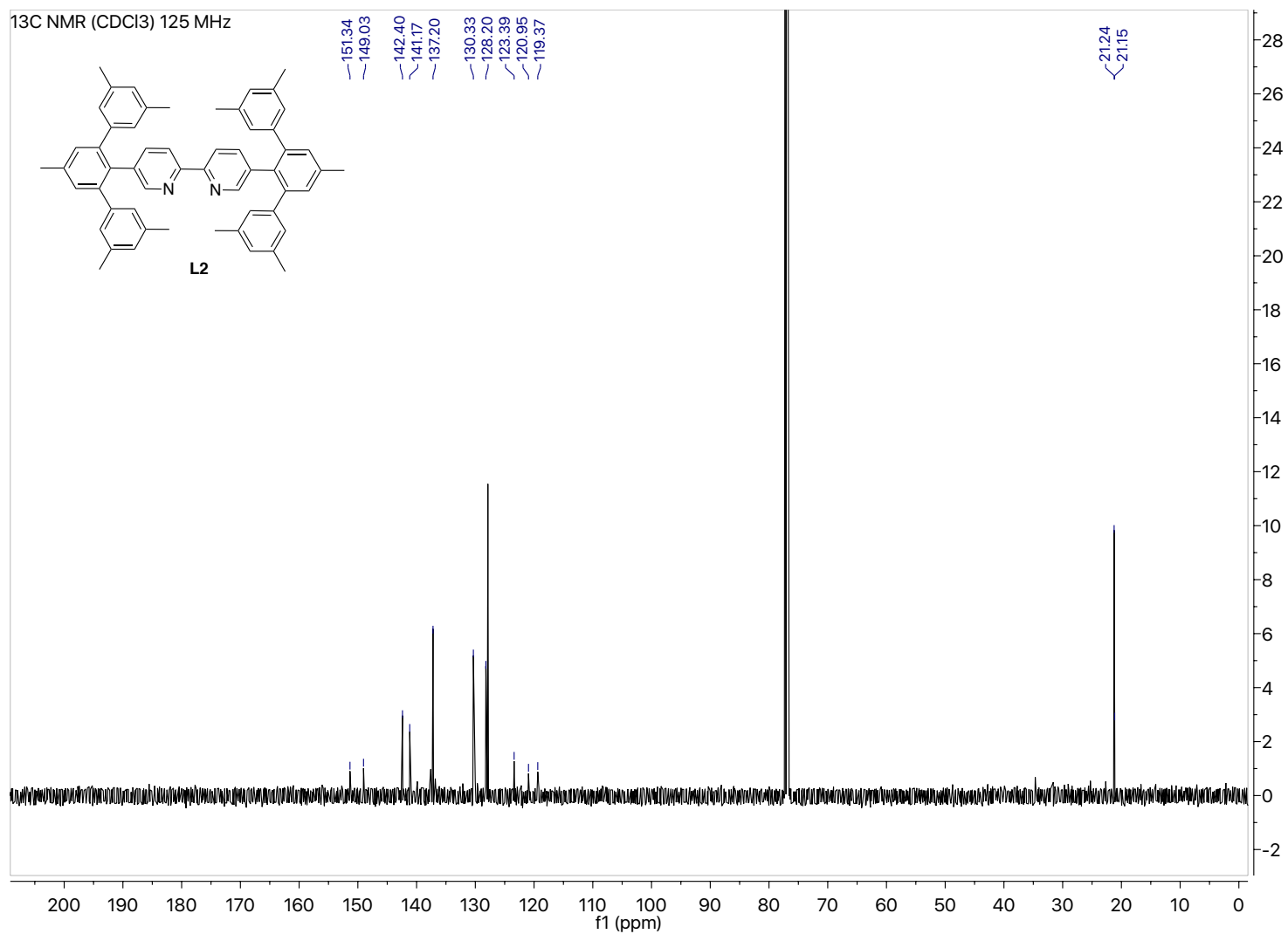


Figure 117. ¹³C NMR of L2